Probabilistic Approach for Design Optimization of Prestressed Girder Bridges Using Multi-Purpose Computer-Aided Model

By:

Yassin Taha Mashal Al-Delaimi

Thesis Submitted to the
Faculty of Graduate and Postdoctoral Studies
in Partial Fulfilment of the Requirements
for the Doctor in Philosophy degree in Civil Engineering

Department of Civil Engineering
Faculty of Engineering
University of Ottawa

Abstract

Prestressed girder bridges are a very common type of bridges constructed all over the world. The girder bridges are ideal as short to medium spans (15 m to 60 m) structures, due to their moderate self-weight, structural efficiency, ease of fabrication, fast construction, low initial cost, long life expectancy, low maintenance, simple deck removal, and replacement process. Thus, the vast applicability of prestressed girder bridges provides the motivation to develop optimization methodologies, techniques, and models to optimize the design of these widely-used types of bridges, in order to achieve cost-effective design solutions.

Most real-world structural engineering problems involve several elements of uncertainty (e.g. uncertainty in loading conditions, in material characteristics, in analysis/simulation model accuracy, in geometric properties, in manufacturing precision, etc). Such uncertainties need to be taken into consideration in the design process in order to achieve uniform levels of safety and consistent reliability in the structural systems. Consideration of uncertainties and variation of design parameters is made through probabilistic calibration of the design codes and specifications. For all current bridge design codes (e.g. AASHTO LRFD, CHBDC, or European code) no calibration is yet made to the Serviceability Limit State or Fatigue Limit State. Eventually, to date only Strength I limit state has been formally calibrated with reliability basis.

Optimum designs developed without consideration of uncertainty associated with the design parameters can lead to non-robust designs, ones for which even slight changes in design variables and uncertain parameters can result in substantial performance degradation and localized damages. The accumulated damage may result in serviceability limitations or even collapse, although the structural design meets all code requirements for ultimate flexural and shear capacity.

In order to search for the best optimization solution between cost reduction and satisfactory safety levels, probabilistic approaches of design optimization were applied to control the structural uncertainties throughout the design process, which cannot be achieved by deterministic optimization. To perform probabilistic design optimization, the basic design parameters were treated as random variables. For each random variable, the statistical distribution type was properly defined and the statistical parameters were accurately derived. After characterizing the random variables, in the current research, all the limit state functions were formulated and a comprehensive reliability analysis has been conducted to evaluate the bridge's safely level (reliability index) with respect to every design limit state. For that purpose, a computer-aided model has been developed using Visual Basic Application (VBA). The probabilities of failure and corresponding reliability indexes determined by using the newly developed model, with respect to limit state functions considered, were obtained by the First-Order Reliability Method (FORM) and/or by Monte Carlo Simulation MCS technique. For the overall structural system reliability, a comprehensive Failure Mode Analysis (FMA) has been conducted to determine the failure probability with respect to each possible mode of failure. The Improved Reliability Bounds (IRB) method was applied to obtain the upper and lower bounds of the system reliability.

The proposed model also provides two methods of probabilistic design optimization. In the first method, a reliability-based design optimization of prestressed girder bridges has been formulated and developed, in which the calculated failure probabilities and corresponding reliability indexes have been treated as probabilistic constraints. The second method provides a quality-controlled optimization approach applied to the design of prestressed girder bridges where the Six Sigma quality concept has been utilized. For both methods, the proposed model conducts simulation-based optimization technique. The simulation engine performs Monte Carlo Simulation while the optimization engine performs metaheuristic scatter search with neural network accelerator.

The feasibility of any bridge design is very sensitive to the bridge superstructure type. Failing to choose the most suitable bridge type will never help achieving cost-effective design alternatives. In addition to the span length, many other factors (e.g. client's requirements, design requirements, project's conditions, etc.) affect the selection of bridge type. The current research focusses on prestressed girder bridge type. However, in order to verify whether selecting the prestressed girder bridge type, in a specific project, is the right choice, a tool for selecting the optimum bridge type was needed. Hence, the current research provides a new model for selecting the most suitable bridge type, by integrating the experts' decision analysis, decision tree analysis and sensitivity analysis. Experts' opinions and decisions form essential tool in developing decision-making models. However the uncertainties associated with expert's decisions need to be properly incorporated and statistically modelled. This was uniquely addressed in the current study.

Dedication

To my parents, my beloved wife, and my sweet kids

Acknowledgement

In the name of Allah, the Most Gracious Most Merciful. First, I would like to praise God Almighty for His uncountable bounties, strength, inspiration, and blessings which helped me greatly to finish this work, and without which I could not achieve completion of this thesis.

My sincere appreciation and deepest thankfulness are due to my research supervisor Dr. Elena Dragomirescu. Her deep knowledge, continuous encouragement, inspiring ideas and keen supervision tremendously helped me achieve this work. Besides her academic distinction, her kindness was a great stress relief to me.

I would like to express my sincere love and warmest gratitude to my beloved wife, Hadeel, for her love and never-ending support she gave me throughout all these years, which were not always so easy.
Finally, my love is always due to my sweet kids, Tabarak, Obaida, Ahmed and Noor.

Table of Contents

LIST OF TABLES

LIST OF FIGURES

Chapter 1

Introduction

1.1 Background

Prestressed girder bridges are very common types of bridges constructed all over the world. According to the Federal Highway Administration (FHWA 2000), almost one-quarter of the bridges in United States, which total more than half a million, are designed as a prestressed girder bridge system (Sirca and Adeli, 2005). This bridge system also represents 40% of the short and medium span bridges built in the United States and Canada (Lounis and Cohn, 1993). As an efficient structural system with moderate self-weight and low initial cost, prestressed girder bridges are ideal for short to medium spans (15 m to 60 m). Prestressed girder bridges are also attractive for their ease of fabrication, fast construction, high sustainability, low maintenance, simple deck removal, and replacement process (Precast/Prestressed Concrete Institute PCI, 2003).

Unlike steel bridges or reinforced concrete bridges, the design of prestressed girder bridges is usually governed by serviceability limit states SLS. In other words, prestressed girder bridges are designed to satisfy the requirements of SLS and fatigue; then, the design adequacy with respect to ultimate limit state ULS is checked.

As a matter of fact, most of the structural engineering problems involve several elements of uncertainty, such as: uncertainties in loading conditions, in material characteristics, in analysis/simulation model accuracy, in geometric properties, in manufacturing precision, etc. (Nowak and Collins 2000). These uncertainties need to be taken into consideration in the design process if uniform levels of safety and consistent reliability indexes in the structural systems are required. Estimation of uncertainties and their effect on the design parameters is performed through probabilistic calibration of the design codes and specifications. For all current bridge design codes (e.g. AASHTO LRFD 7th Edition 2014, CHBDC 2010, or Eurocode EN1999) no calibration was made until today for the Serviceability Limit State or for the Fatigue Limit State. Eventually, to date only Strength I limit state has been formally calibrated with reliability analysis basis (Barker R. M. and

Puckett 2013). In other words, all limit states, other than Strength I, are still deterministically formulated in the current bridge design codes.

During the last three decades, much work has been done in structural optimization, as a result of considerable developments in mathematical optimization techniques, advances in computer's technologies, and the need to perform cost-effective designs (Ahsan et al, 2012). This motivated researchers worldwide to apply optimization processes to the design of bridge structures, and to develop cost-effective design alternatives. A number of researchers contributed in performing deterministic design optimization of prestressed girder bridges, revealing smaller sections, longer spans, and higher slenderness ratios. As a result of such optimization solutions, bridge structural systems have become highly sensitive, due to repeated applications of heavy loads (trucks), to cracks, deflections, vibrations, or fatigue failure at service load levels (Beck and Gomes 2012). Eventually, the optimum bridge designs developed without considering the uncertainty associated with the design parameters, can lead to non-robust designs of bridges, for which even slight changes in design variables and uncertain parameters can result in substantial performance degradation and localized damages (Ahsan et al. 2012). The accumulated damage may result in serviceability limitations or even collapse, although the structural design meets all code requirements for ultimate flexural and shear capacity (Nilson et al. 2010). Every year significant investments of the order of millions of dollars are spent for maintenance of girder bridges. Such maintenance procedures are conducted to rectify problems, most of which are serviceability and/or fatigue consequent (Hassanain and Loov 2003).

In order to achieve the best compromise between cost reduction and satisfactory safety levels, probabilistic approaches for bridge design optimization should be applied to control the structural uncertainties throughout the design process, which cannot be achieved by performing deterministic design optimization (Chateauneuf, 2007). Hence, safety constraints with respect to every possible mode of failure need to be imposed on the design optimization process.

Until present, no probabilistic design optimization approach, methodology or model has been applied to prestressed girder bridges. Therefore, as a new contribution, the main aim of the current research is to develop a unique and efficient computer-aided model that performs probabilistic multi-objective design optimization of prestressed girder bridges. The application of the proposed model will reveal cost-effective design solutions of prestressed girder bridges that guarantee satisfactory safety levels reserved in the optimized structural configuration.

1.2 Problem Statement and Research Significance

In bridge engineering, many design factors play an essential role in deciding the members' dimensions, geometry, weight, and cost. This reflects the importance of developing optimization tools that provide cost-effective design by determining certain design variables to achieve the best measurable objective function under given constraints (Rana and Ihsan 2010). From the studied literature, attempts have been made to perform design optimization applied to prestressed girder bridges. However, such attempts were made deterministically, i.e., they did not consider the variability and uncertainties involved with the basic design variables.

Deterministic design optimization could achieve considerable cost saving but, very possibly, could lead to unsafe structural configuration. In order to maintain satisfactory safety levels while performing the optimization process, it becomes necessary to adopt a probabilistic approach that consider the uncertainties associated with the basic design variables. This can only be achieved through reliability analysis and probabilistic assessment of the bridge performance. In other words, the optimization process should be controlled by imposing probabilistic constraints in addition to the deterministic ones.

As a new contribution, the current research provides a model that performs probabilistic design optimization of prestressed girder bridges in order to minimize the bridge cost and, at the same time, to guarantee satisfactory safety levels reserved in the optimized bridge configuration. Two different probabilistic methods have been implemented in the proposed model. The first method is the reliability-based design optimization, where the failure probabilities with respect to all possible limit states are incorporated as optimization constraints. In the second method, a quality-controlled optimization approach is developed by applying the six sigma quality concept to achieve robust design solutions. Such approach ensures not only that the design performs as desired but also that the design consistently performs as desired.

The cornerstone in the probabilistic optimization model is its ability to perform reliability (probabilistic) analysis with respect to every limit state function (individual component reliability) as well as with respect to the overall structural performance (system reliability). Previous researches mainly focused on performing reliability analysis with respect to ultimate strength (load carrying capacity) of the bridge (Nowak et al., 1991;

Nowak and Szersszen, 2000; Nowak et al. 2001; Du and Au 2004). Such reliability analysis could help in evaluating the load carrying capacity of existing bridges. However, for the sake of reliability-based design and design optimization of a new bridge, the reliability of the structure with respect to all limit states (Serviciability Limit States, Fatigue Limit States, and Ultimate Limit States); besides, the system redundancy need to be investigated and evaluated. Having such comprehensive analyses incorporated in the proposed optimization model forms another target of the current research.

In addition to the above, another important and sensitive issue related to the optimization of bridge design exists. As there are many different types of bridge superstructures, the bridge designer should pay careful attention and effort to successfully select the most appropriate bridge type with respect to the specific project's conditions, data and information. If the designer failed to choose the most suitable bridge superstructure type, then no efficient optimization solution could ever be achieved, no matter how efficient optimization model has been used. In other words, efficient optimization solution can only be achieved when an efficient methodology is applied on properly selecting the bridge type. For that reason, the current research provide a new model for bridge type selection. This model will be used to verify whether prestressed girder bridge type is the most suitable bridge type, with respect to a specific project, before starting the design optimization process. It was noticed from the thoroughly reviewed literature that some models and methods were proposed by a number of researchers to help selecting the most appropriate bridge superstructure type. These models and methods mainly depend on the subjective judgement of the experts. However, the uncertainties associated with experts' judgments were not considered in the previous researches. This is a drawback because an engineering decision which accounts for experts' judgement with high level of uncertainty should be treated probabilistically rather than deterministically. The proposed model, of the current research, uniquely, incorporates the uncertainties associated with experts' decisions and integrates them to a decision tree analysis and sensitivity analysis (Al-Delaimi and Dragomirescu 2015).

1.3 Research Objectives

The current research proposes an efficient computer-aided multi-objective model that performs probabilistic-based design optimization of prestressed girder bridges. The proposed model aims to provide cost-effective design alternatives with guaranteed safety levels in the optimized bridge configuration. Two different probabilistic optimization methodologies are suggested: 1- reliability-based design optimization, and 2- six sigma robust design optimization. The proposed model is capable of performing comprehensive reliability analysis both on the individual component level and the entire structural system level. Different reliability methods have been incorporated. As another important objective, the current research also proposes a new method (as part of the integrated model) for choosing the optimum bridge superstructure type by modelling the experts' decisions probabilistically and integrating them with decision tree analysis and sensitivity analysis.

1.4 Scope

To achieve the proposed objectives, the following tasks were completed:

- Thorough review of the broader literature to identify the propagation of uncertainties and associated statistical parameters, statistical distribution type, load models, resistance model, reliability investigation and assessment, design advances and design optimization of prestressed girder bridges.
- Review of developments of reliability computational methods corresponding to individual structural components (elements) and overall structural system.
- Review of developments of calibration of LRFD Bridge Design Codes (AASHTO, Ontario Bridge Design code, and CHBDC).
- Deriving new statistical parameters of the random variables related to the load effects (bending, shear, fatigue stress range) and resistance (section properties, allowable stresses, flexural resistance, and shear resistance).
- Conducting deterministic analysis and design of prestressed girder bridges, according to AASHTO LRFD 7th Edition 2014, in order to determine the baseline of bridge configuration with nominal values of the basic design variables and parameters.
- Using Visual Basic Application VBA integrated with Spreadsheets, developing an integrated model BREL (Bridge RELiability) that: (1) estimates the component's failure probabilities and corresponding reliability indexes by the First-Order Reliability Method FORM, (2) estimates the overall system's reliability by conducting nonlinear failure mode analysis FMA and, then, utilizing the method of Improved Reliability Bounds IRB. For that purpose, a 2-D nonlinear grillage analogy GRANAL (Grillage ANALogy) algorithm has been coded with VBA, (3) alternatively, evaluates the probability of failure and corresponding reliability

indexes by the Monte Carlo Simulation MCS technique, (4) performs probabilistic design optimization of prestressed girder bridges with reliability-based design optimization approach in which the failure probabilities are utilized as probabilistic constraints, (5) conducts a quality-control design optimization through implementing the six sigma quality concept in order to achieve robust structural configuration, (6) as a new contribution, the proposed model incorporates the Copula method in order to precisely quantify the dependency (correlation) among random variables and investigate its effect on the reliability indexes, and (7) provides a decision-making tool to select the most appropriate bridge superstructure type by integrating expert decision analysis, decision tree analysis, and sensitivity analysis.

- Developing a cost model and integrating it to the optimization engine in order to evaluate the objective function (bridge cost) in every optimization cycle. For that purpose, the proposed model performs work breakdown structure WBS to classify, in detail, the bridge elements according to ASTM UNIFORMAT II Standard. A unit cost database has been developed and added to the model. The unit cost would, then, be adjusted according to location and inflation rates.
- The proposed probabilistic model incorporates the most popular and common types of standard precast girders; namely: AASHTO Girders, CPCI Girders, Bulb-T Girders, and NU Girders. However the user can use any other shape/type of girders provided that he/she stores the dimensions of the girder in the database of the model.
- Performing model validation to investigate the applicability and accuracy of the proposed model.

Figure 1.1 illustrates the flowchart of the proposed research methodology.

1.5 Manuscript Organization

This thesis is organized in eight chapters and six appendices. Chapter 1 states the background, problem statement, objectives, and scope. Chapter 2 highlights key research efforts conducted with respect to: (i) load and resistance models (ii) reliability assessment of prestressed girder bridges, (iii) design optimization of prestressed girder bridges, (iv) cost model, and (v) selecting the most appropriate bridge type. In Chapter 3, the derivation of current (new) statistical parameters of random variables associated with load effects and resistance is presented. Chapter 4 demonstrates the reliability analysis and assessment of prestressed girder bridges. Both the components' and system's reliability indexes have been estimated. Different reliability methods have been utilized. In Chapter 5, the methodology of performing the reliability-based design optimization of prestressed girder bridges is defined, formulated and applied. In Chapter 6, the methodology of performing the six sigma-based robust design optimization of prestressed girder bridges is defined, formulated and applied. Chapter 7 proposes a new method, as a decision-making tool, to help choosing the most appropriate bridge superstructure type. The final summary, conclusions and recommendations for future work are presented in Chapter 8. Appendix A illustrates the development of the reliability methods used in the current research. Appendix B demonstrates the Simplified Modified Compression Field Theory that was utilised in deriving the statistical parameters of the shear resistance. Appendix C presents the detailed design calculations of the bridge related to the case study adopted in Chapters 5 and 6. Appendix D provides a sample of the VBA macro of the proposed model for the components' reliability assessment. A sample of The VBA code for evaluating the system reliability is presented in Appendix E. Appendix F presents the mathematical formulations and details of the Copula functions used in Chapter 4 to quantify the dependency (correlation) among random variables.

1.6 Novelty and new contributions of the current research

In this section the new contributions of the current research are listed, as follows:

- Derivation of new statistical parameters of random variables related to the load effects and resistance with respect to the most popular and common standard precast girders (AASHTO Girders, CPCI Girders, Bulb-T Girders, and NU Girders).
- A new model for comprehensive reliability analysis of prestressed girder bridges to evaluate the probability of failure and corresponding reliability index with respect to every possible limit state function as well as the overall structural system (bridge redundancy). The analyses are performed with different reliability methods.
- For the first time, the Copula method is applied to precisely quantify the dependency (correlation) among the random variables and to investigate its effect on reliability index.

- A new 2-D grillage analogy model for 2-D linear and nonlinear bridge analysis. This model was utilized to evaluate the redundancy (system reliability) of prestressed girder bridges.
- A new model to define, formulate and apply the reliability-based optimization approach on the design of prestressed girder bridges.
- A new model to define, formulate and apply the six sigma-based robust design optimization of prestressed girder bridges.
- A new model to select the optimum bridge type by integrating expert decision analysis, decision tress analysis, and sensitivity analysis.

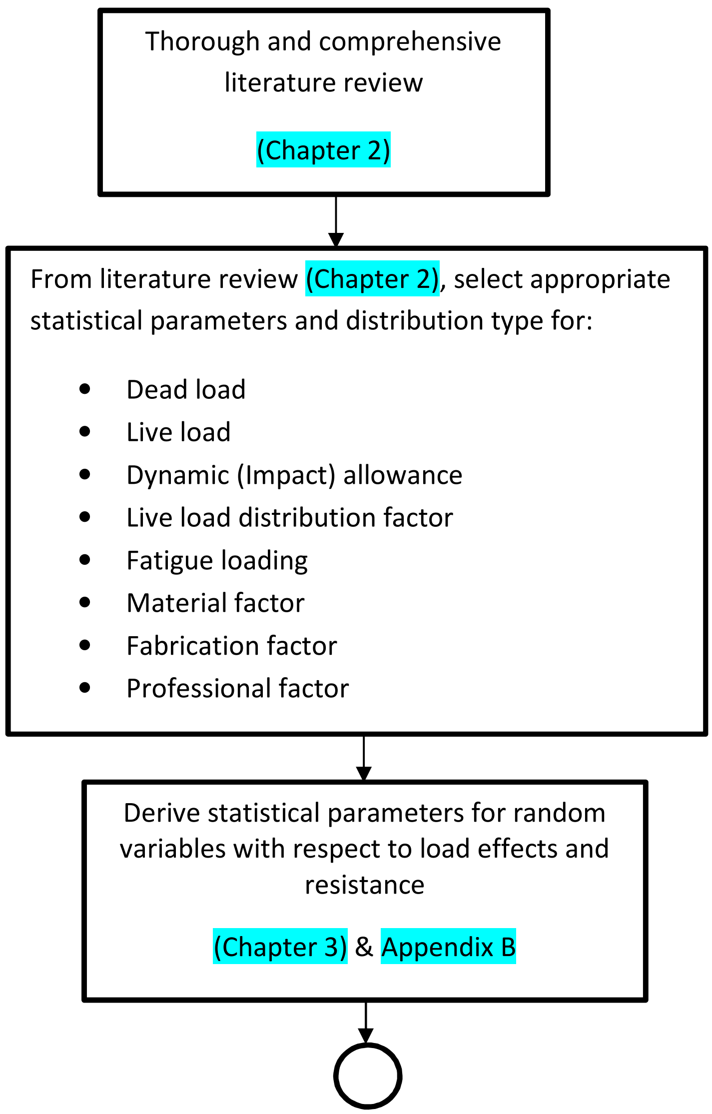

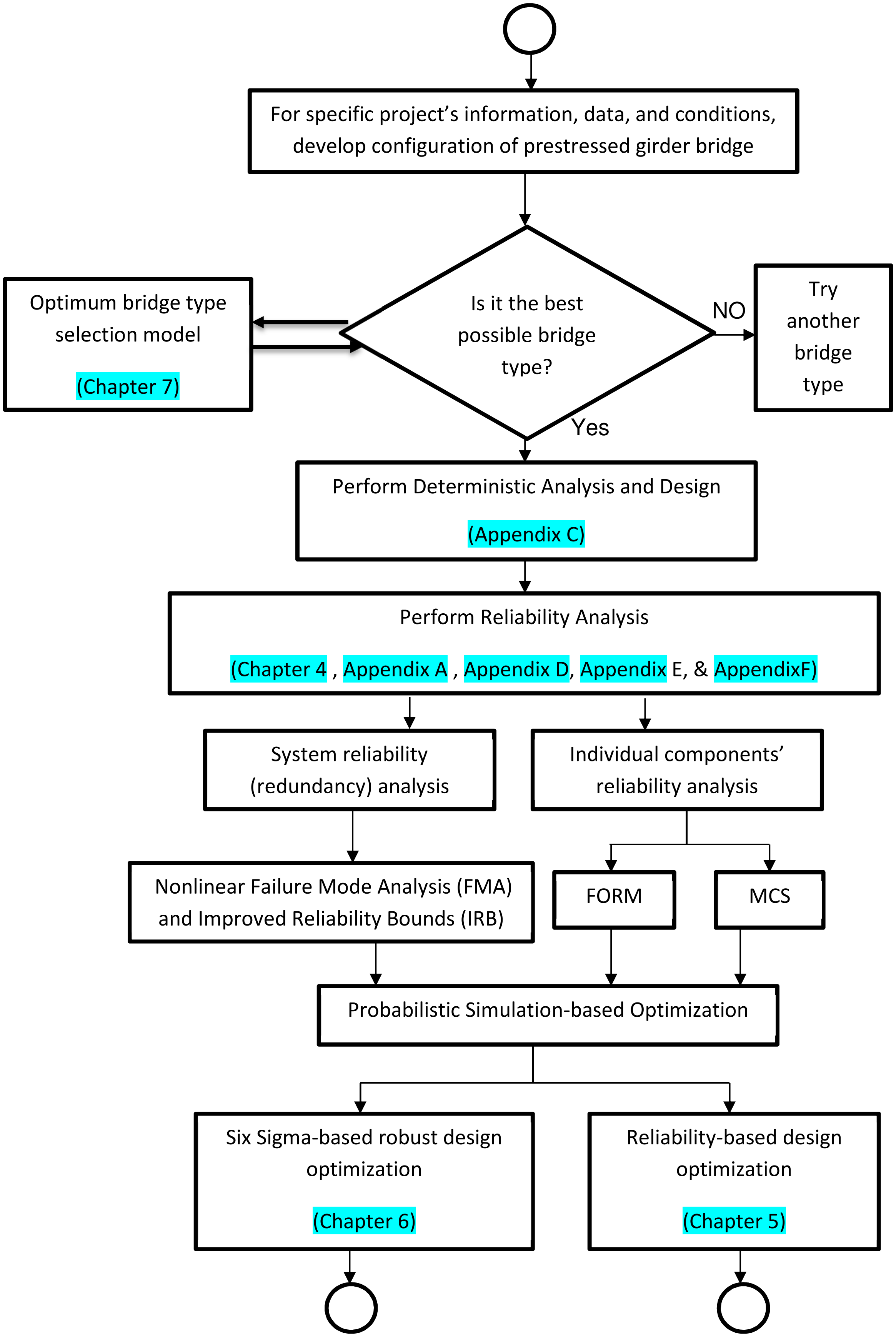
For specific project's information, data, and conditions, develop configuration of prestressed girder bridge
Is it the best possible bridge type?
NO
Try another bridge type
Optimum bridge type selection model
(Chapter 7)
Yes
Perform Deterministic Analysis and Design
(Appendix C)
Perform Reliability Analysis
(Chapter 4 , Appendix A , Appendix D, Appendix E, & AppendixF)
System reliability (redundancy) analysis
Individual components' reliability analysis
Nonlinear Failure Mode Analysis (FMA) and Improved Reliability Bounds (IRB)
FORM
MCS
Probabilistic Simulation-based Optimization
Six Sigma-based robust design optimization
(Chapter 6)
Reliability-based design optimization
(Chapter 5)

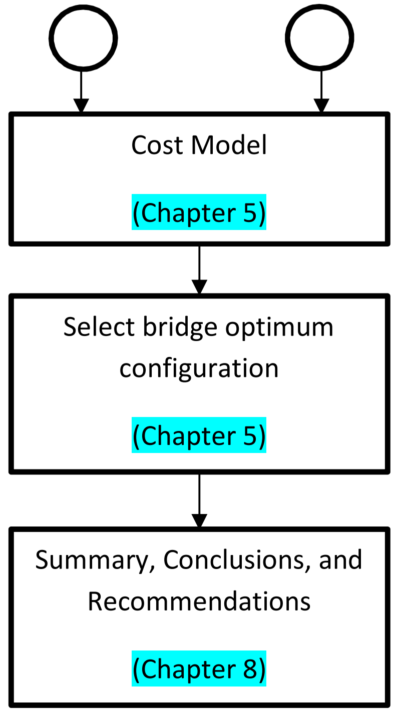

Figure 1.1: Flowchart of the proposed research methodology

Chapter 2

Literature Review

2.1 Load and Resistance Models

2.1.1 Load Models

Bridges are subjected to different types of loads (e.g. permanent loads, transient loads, and special loads). Permanent loads include dead load of structural components (DC), wearing service (DW), and earth pressure. Transient loads include vehicle live load (LL), vehicular dynamic load allowance (IM), friction (FR) and environmental loads such as earthquake (EQ), ice load (IC), wind loads on structure (WS), and temperature. Special loads include collision and breaking force (AASHTO LRFD 2010).

The critical loads mainly depend on the bridge span length. For long span bridges, the critical loads are winds, earthquakes, and dead load while in short and medium spans (up to 60 m), the most significant loads are live load and dead load (Czarnecki 2006). Also the truck weight and truck configuration (number of axels, distance between axles, and weight of each axle) have considerable effects on the analysis and design of bridges.

In probabilistic analysis, load models are usually developed to define different load components as random variables by considering the uncertainties associated with these variables. In order to quantify such uncertainties, the statistical distribution type and the statistical parameters of the random variables should be properly defined and evaluated. The main components, that need to be statistically defined, in any load model are: dead load, live load, dynamic (impact) factor, distribution of load to individual members, the transverse position of the trucks on the bridge, and the probability of occurrence of one truck or two trucks side by side in one lane.

In reliability analysis, the general model of load (Q_i) can be expressed as per Equation 2.1 (Nowak and Collin 2013).

[2.1] $$Q_i = A_i \, B_i \, C_i$$

where,

A_i = the load itself (nominal value).

B_i = a variation results from the mode in which the load is assumed to act (such as idealization with perfectly uniformly distributed load)

C_i = variation due to the method of analysis (such as two-dimensional idealization of three dimensional modelling).

2.1.1.1 Dead Load Model

Dead load is the weight of structural and non-structural members. Because of the differences in the statistical parameters, Tabsh and Nowak (1991) advised to distinguish between factory-made members (e.g. precast girders), cast-in-situ members (e.g. deck slab), and wearing surface (asphalt).

The variability in the dead load of factory-made members (precast girders) are given in Table 2.1. While, Table 2.2 summarizes the variability of cast-in-situ dead load considered by several researchers. The variability is represented by the bias factor (mean to nominal dead load) and the coefficient of variation (standard deviation to mean).

For asphalt surface, Tabsh and Nowak (1991) considered the mean thickness equals 3.5 in (90 mm) and coefficient of variation as 0.25. While, Nowak (1993) considered the mean asphalt thickness equals 3.0 in (75 mm) and coefficient of variation as 0.25.

In the current research, the mean-to-nominal ratio is taken to be 1.03 for factory-made members and 1.05 for cast-in-situ members, with coefficient of variation equal to 0.08 and 0.10, respectively. This study also considered the mean thickness of asphalt equals 3.0 in (75 mm) and coefficient of variation as 0.25.

Table 2.1: Statistical parameters of dead load for factory-made members

Bias Facor	Coefficient of Variation	Reference
1.03	0.08	Tabsh and Nowak (1991)
1.03	0.08	Nowak (1995)

Table 2.2: Statistical parameters of dead load for cast-in-situ members

Bias Factor	Coefficient of Variation	Reference
1.00	0.08	Galambos and Ravindra (1973)
1.00	0.108	Ravindra, Lind and Siu (1974)
1.00	0.13	Ellingwood and Ang (1974)
1.00	0.07	Siuet. Al., (1975)
1.00	0.10	Allen (1976)
1.00	0.10	Ellingwood (1977, 1978, 1979)
1.00	0.07	MacGregor (1976)
1.05	0.10	Ellingwood et al., (1980)
1.05	0.10	Galambos, et al., (1982)
1.05	0.10	Tabsh and Nowak (1991)
1.05	0.10	Nowak (1995)

2.1.1.2 Live Load Model

Bridges are subjected to a variety of movable loads, including those due to vehicles, motorcycles, bicycles, and pedestrians. Live loads refer to loads due to moving vehicles that change their positions with respect to time. The live load on bridges is divided into two categories: static load (truck weight, braking force, etc.) and dynamic load (impact). Due to the variation of vehicles on bridges, defined by the Federal Highway Administration (FHWA 2013), presented in Figure 2.1, live load effect is different. Live load effect depends on truck weight, axel configuration, wheel force, wheel geometry, transverse and longitudinal position of vehicle, multiple presence of vehicles, deck stiffness, girders stiffness, and road surface roughness.

Design codes define and formulate live load based on truck survey and calibration. The first calibration of AASHTO LRFD Code was based on the truck survey conducted by the Ontario Ministry of Transportation in 1975 as there was lack of reliable data for the United States (Kozikowski 2009). The data collected in the mid-1970s at different locations in the Province of Ontario, Canada, include 9,250 vehicles. The average age of 75 years for bridges was considered in load calculations. The estimated average daily truck traffic (ADTT) was 1,000 trucks in one direction. For longer spans, three cases of correlated multiple presence of trucks in one lane was considered. These cases are: i- no correlation, ii- partial correlation, and iii- full correlation.

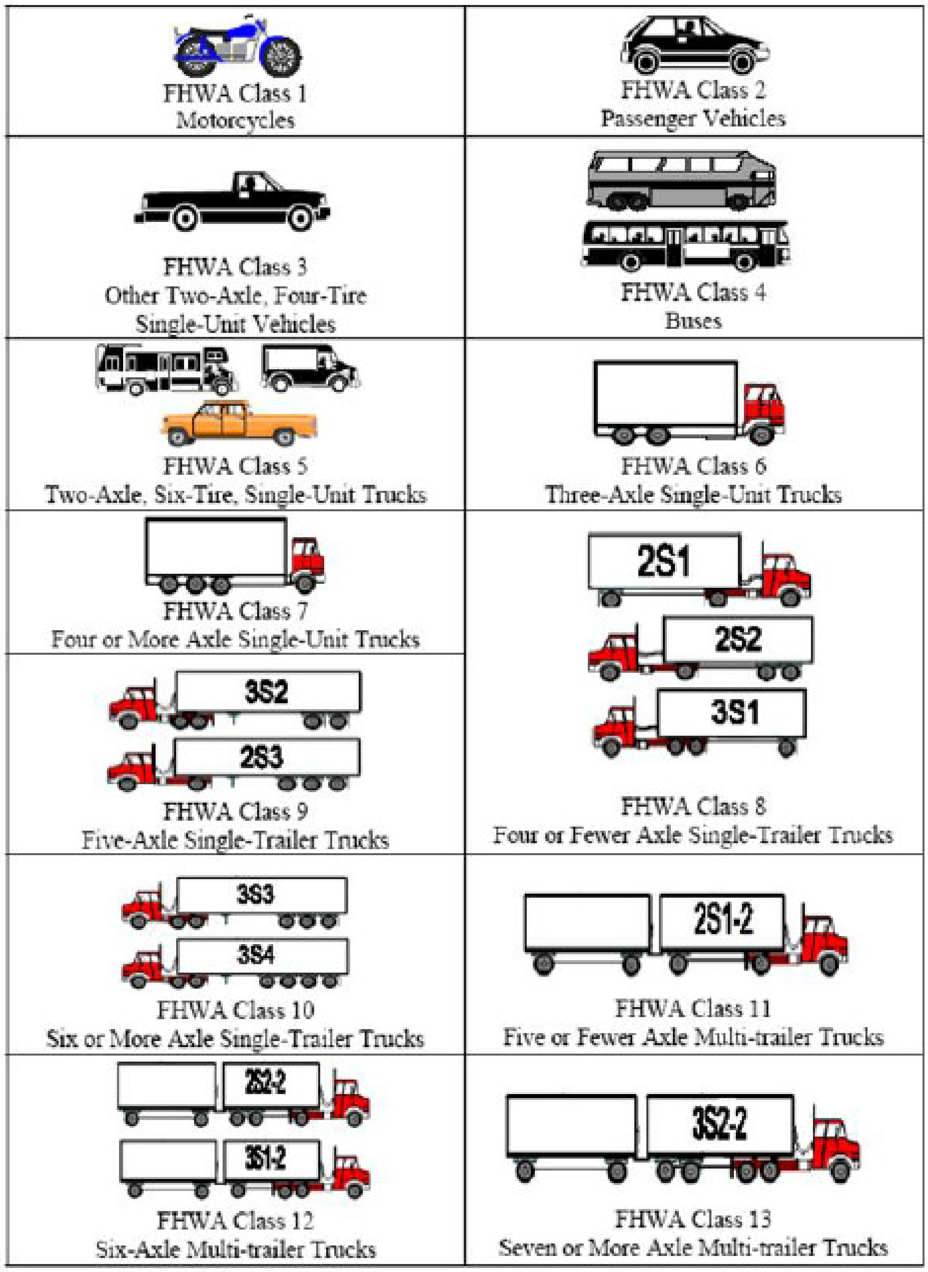

Figure 2.1: FHWA Vehicle Categories (2013)

The live load calibration for AASHTO LRFD revealed the HL-93 (Design Live Load) shown in Figure 2.2. Figures 2.2a and 2.2b present the HL93, HS20 + LL or tandem + LL for simple beam, which give the extreme bending moment. Figure 2.2c presents the HL93 for continuous beam.

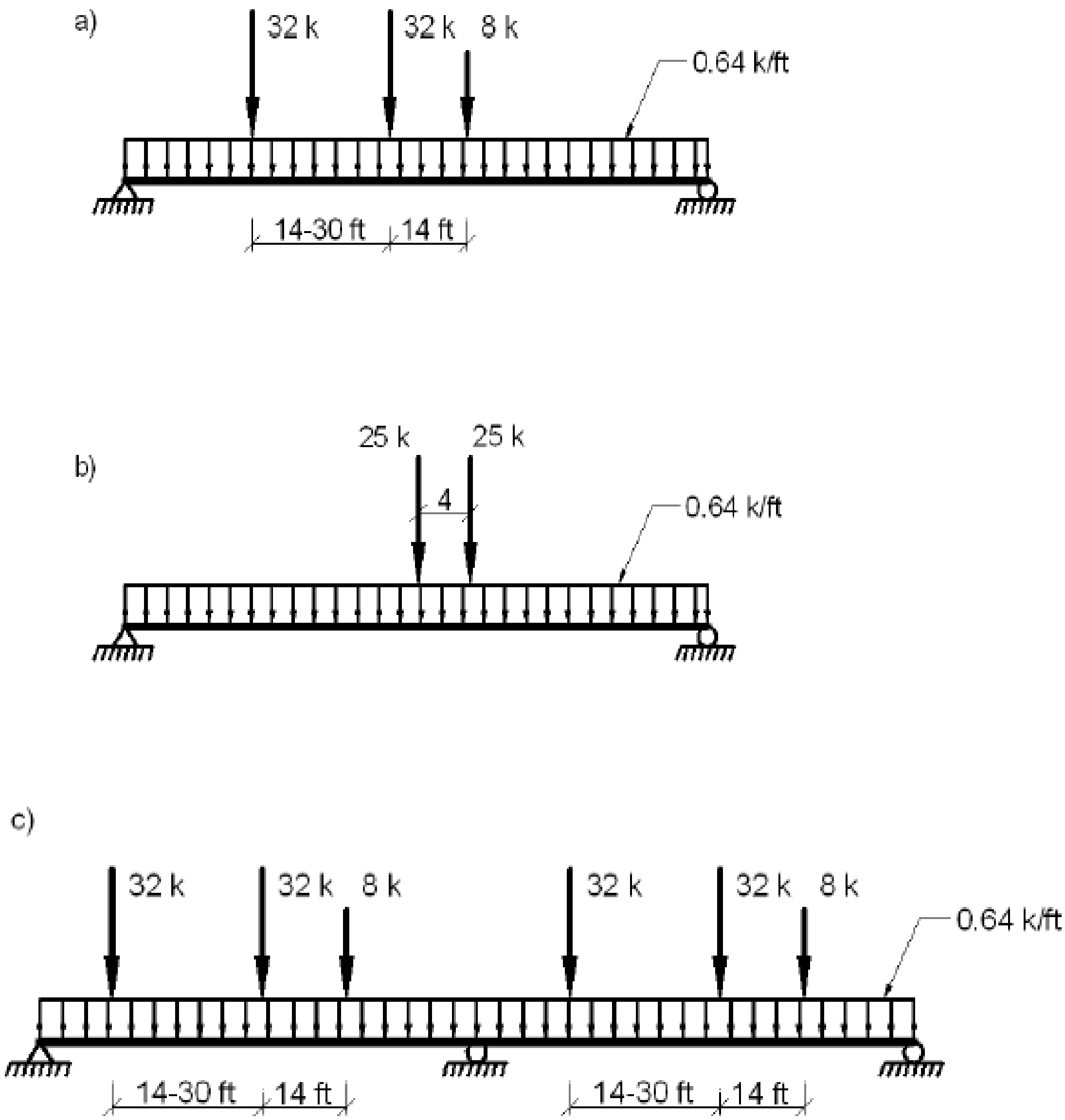

Figure 2.2: HL93 a, b for Simple Beam and c for Continuous Beam

The collected number of 9,250 vehicles in the Ontario data survey was assumed to represent two weeks of heavy traffic illustrated in Figure 2.3. This amount of data corresponds to the probability of 1/9250, which corresponds to inverse normal standard distribution function (Φ^{-1}) equal to 3.71. Similarly the probability and corresponding inverse normal standard distribution function (Φ^{-1}) for other truck volume over various time periods is calculated as presented in Table 2.3.

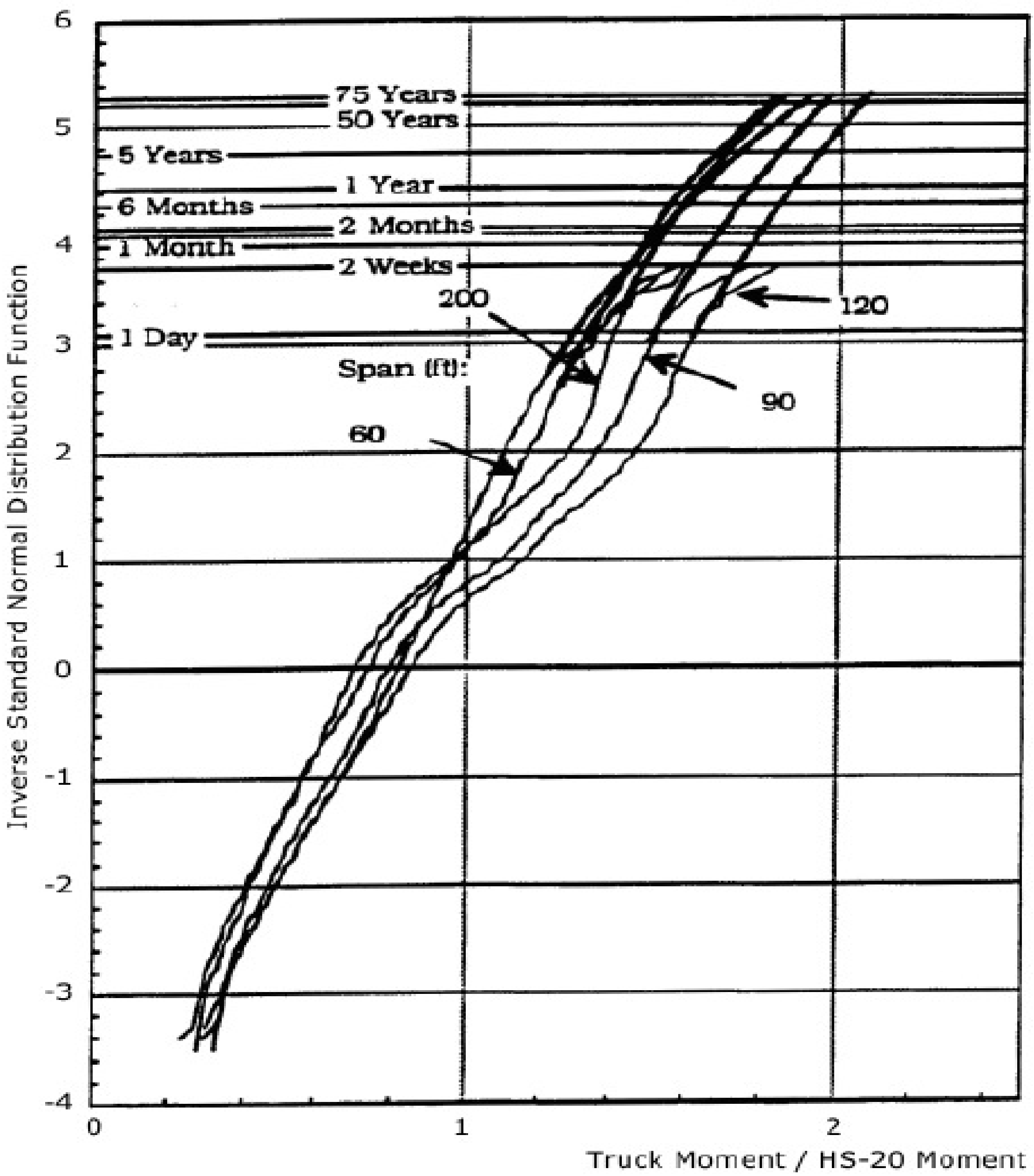

Figure 2.3: Extrapolated Moments for Simple Spans by: Nowak (1999)

The HL-93 live load model was based on following assumptions (Nowak 1999):

- multiple lane - every 500th truck is fully correlated,
- one lane - every 100th truck is fully correlated,
- two trucks have to have the same number of axles,
- gross vehicle weight (GVW) of the trucks has to be within the ± 5% limit,
- spacing between each axle has to be within the 10% limit.

Table 2.3: Number of Trucks versus Time Period and Probability

Time Period (*T*)	Number of Trucks (*N*)	Probability (1/*N*)	Inverse Normal (*z*)
75 years	20,000,000	5.00E-08	5.33
50 years	15,000,000	6.67E-08	5.27
5 years	1,500,000	6.67E-07	4.83
1 year	300,000	3.33E-06	4.50
6 months	150,000	6.67E-06	4.35
2 months	50,000	2.00E-05	4.11
1 month	30,000	3.33E-05	3.99
2 weeks	10,000	1.00E-04	3.27
1 day	1,000	1.00E-03	3.09

Due to different categories of real live load, several live load models were developed by researchers (Nowak and Zhou 1985, Elingwood 1982, Ghosn and Moses 1984, Nowak and Hong 1991, Nowak 1999).

HL93 design truck loading, specified by the SSHTO LRFD code is a combination of the HS20 design truck and uniformly distributed load of 9.3 kN/m (0.64 kip/ft). For each design lane, the live load model, consisting of either a truck or tandem coincident with lane load, was developed as a notional representation of shear and moment produced by a group of vehicles routinely permitted on highways of various states.

The design truck HS20, weights and spacing are shown in Figure 2.4, where the spacing between the two 32.0 kips axles shall be varied between 14.0 ft. and 30 ft. to produce extreme force effects. The design tandem consists of a pair of 25.0 kip axles spaced 4.0 ft. apart as specified in Figure 2.5. Transverse spacing between wheels is 6.0 ft. The design lane load consists of a uniformly distributed load (0.64 k/ft.) in the longitudinal direction. Transversely, the design lane load is assumed to be uniformly distributed over a 10.0 ft. width as presented in Figure 2.5.

For simply supported bridge, 14' spacing produces greatest design truck load moment, shear and deflection as per AASHTO LRFD clause (S3.6.1.2.2).

A dynamic load effect is considered as an equivalent static load added to design truck HS20 or tandem as specified in AASHTO LRFD cluase (3.6.2). The lane load is not subject to a dynamic load allowance.

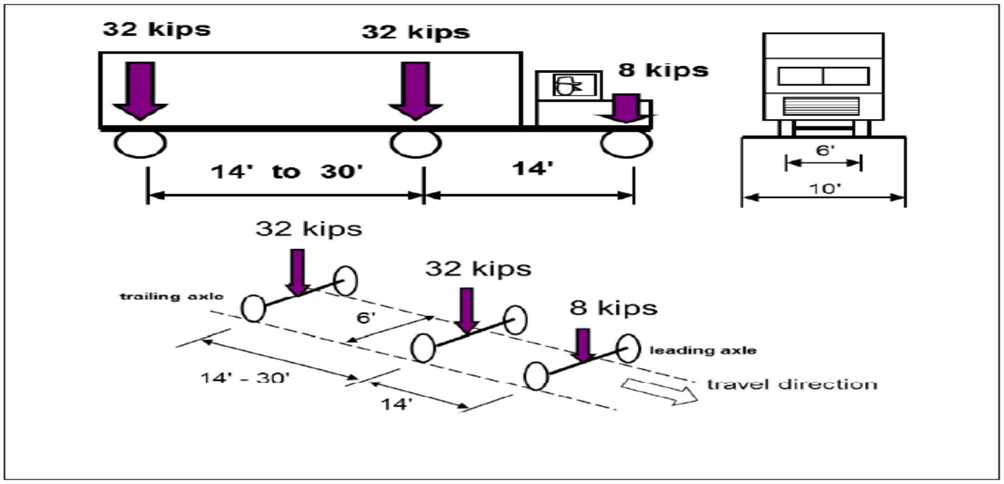

Figure 2.4: Characteristic of the Design Truck, HS20

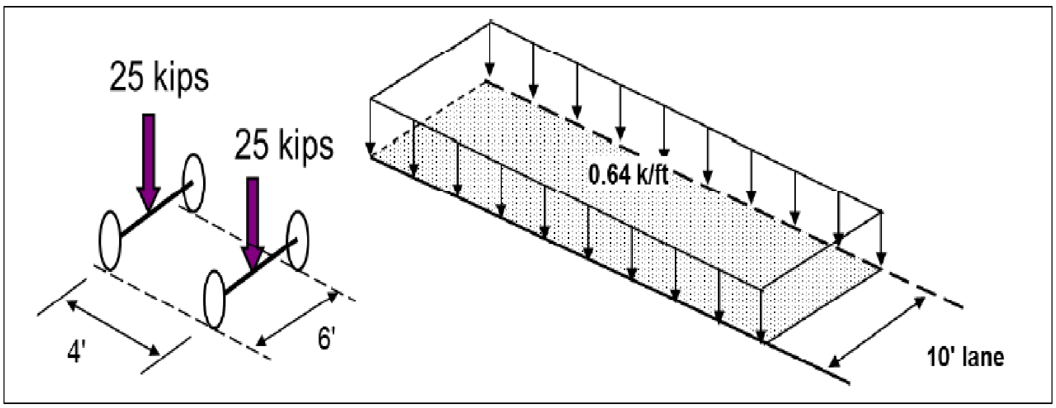

Figure 2.5: Characteristics of Tandem and Lane Load

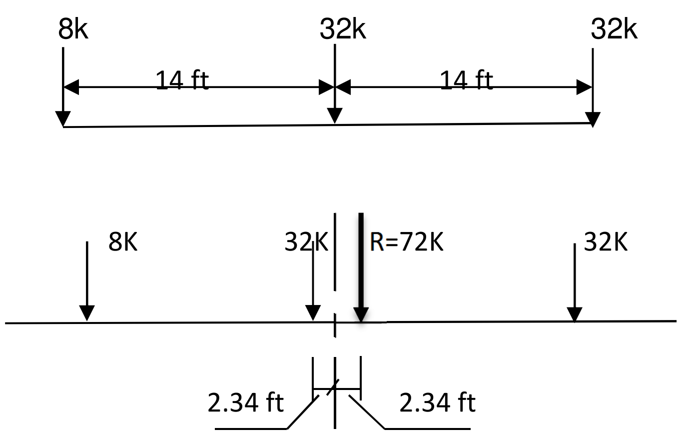

Figure 2.6: Position of HL93 that provide maximum moment in simple span

For simple span bridges, a maximum live load moment occurred in the mid-span. The critical section should be placed bisecting the distance between the truck loading resultant and middle load and calculated as indicated in Figure 2.6.

Rakoczy (2011) developed the statistical parameters (mean, coefficient of variation, and bias factor) of live load for highway bridges using the available weight-in motion (WIM) data. The WIM data includes about 35 million trucks (32 WIM locations) were considered as representative for the truck traffic in the United States. The cumulative distribution functions were plotted on the normal probability paper for both growth vehicle weight (GVW), and moment (Figure 2.7). The WIM truck moments were calculated for spans from 30 to 300 for time periods from 1 day to 10 years. CDF's plotted on the normal probability paper and the bias factors were obtained (Figure 2.8). The cumulative distribution functions indicate a complex shape for both gross vehicle weight and load effects (moments). A range of records for average daily truck traffic (ADTT) from 100 to 10,000 can be obtained from Nowak and Rakocy (2012).

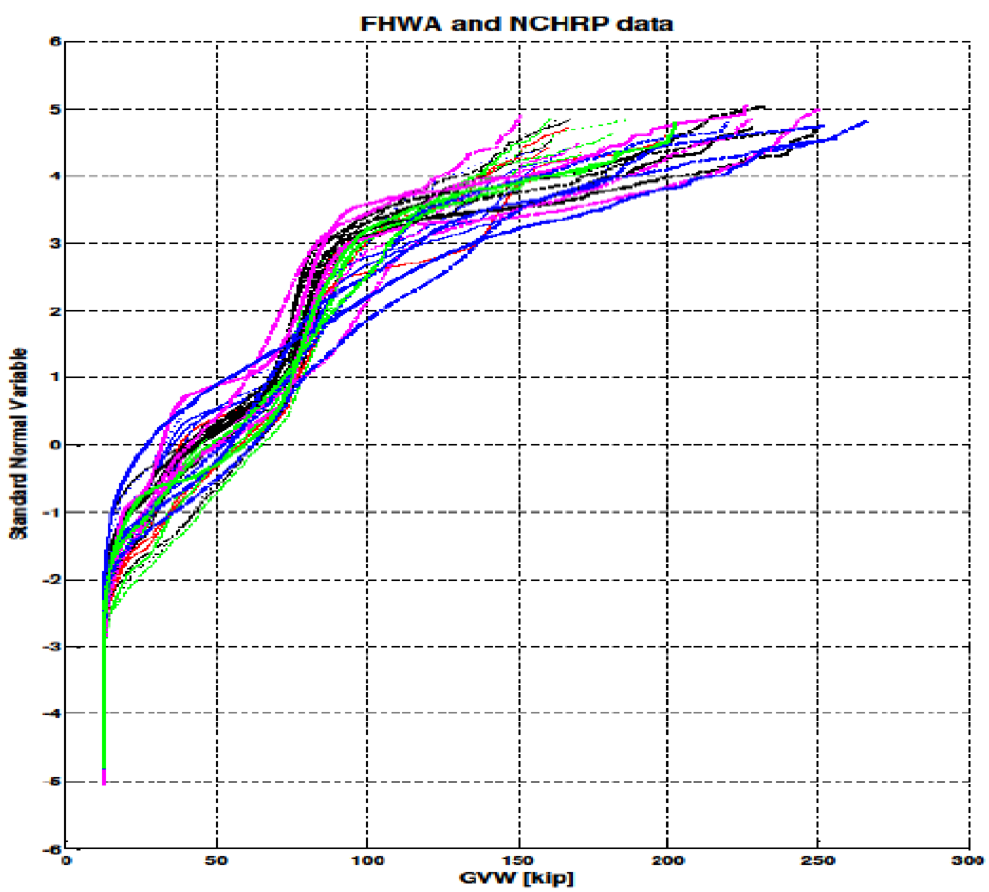

Figure 2.7: Moment Ratio, Span=90 ft. by: Rakoczy (2011)

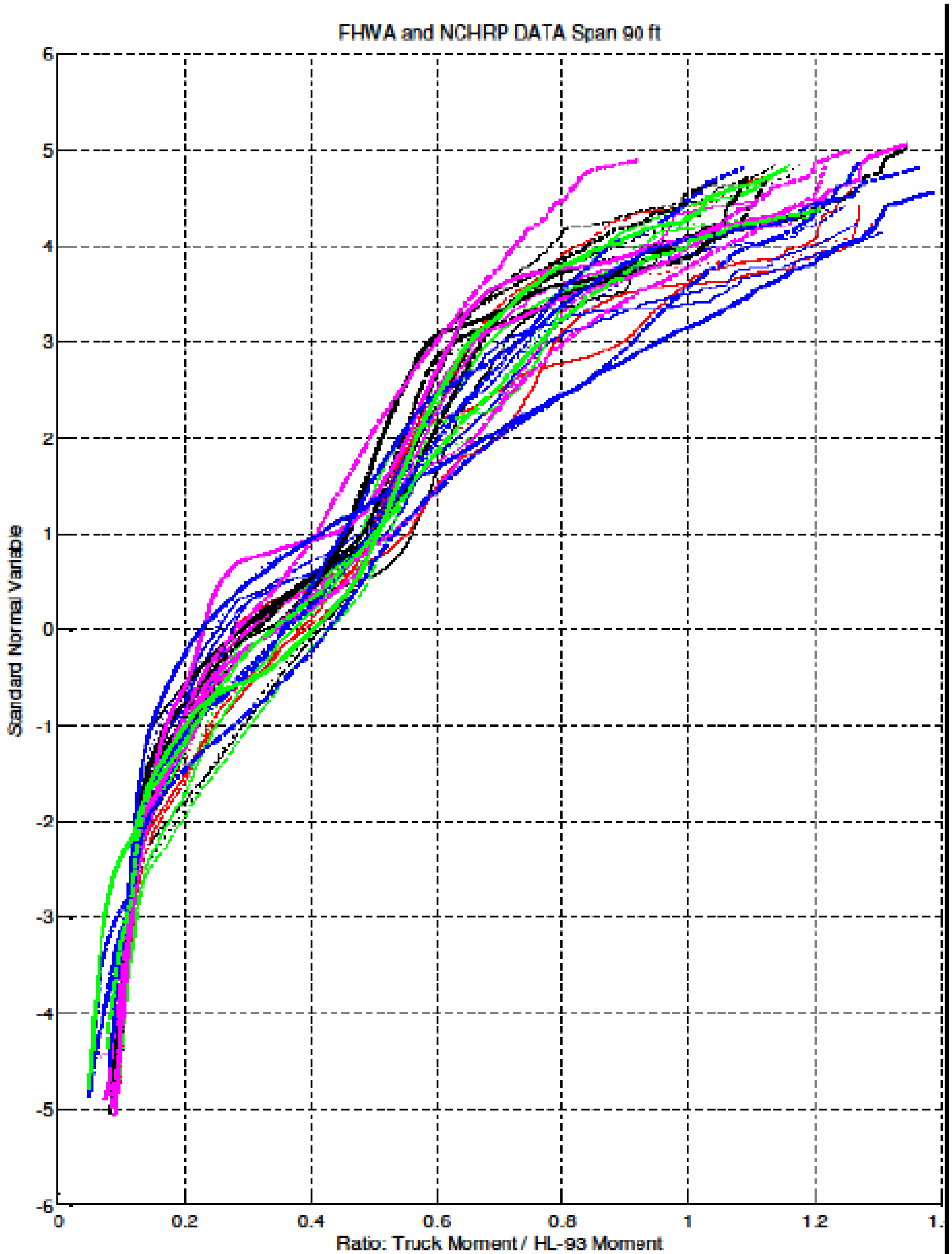

Figure 2.8: CDF of Gross Vehicle Weight (GVW) (Rakoczy 2011)

Depending on the ADTT, the span, and time, Tables 2.4 and 2.5 (Rakoczy 2011) show the statistical parameters for live considering 5000 and 10000 ADTT, respectively. The statistical parameters for a specific span, ADTT and time can be obtained by extrapolation. The statistical parameters for reliability analysis of AASHTO Girders at design are extrapolated from Tables 2.4 and 2.5 (Rakoczy 2011).

Table 2.4: Statistical Parameters for Live Load for ADDT 5000 by: Rakozy (2011)

Span (ft)	Statistical Parameter	Time Period (*T*), where: D= Day, Mn=Month, Yr=Year									
		1 Day	2 Week	1 Month	2 Month	6 Month	1 Year	5 Year	50 Year	75 Year	100 Year
30	$\mu+1.5\boldsymbol{\sigma}$	1.25	1.42	1.46	1.48	1.51	1.54	1.58	1.62	1.63	1.63
	μ	1.05	1.19	1.22	1.24	1.27	1.28	1.32	1.36	1.37	1.38
	V	0.12	0.13	0.13	0.13	0.13	0.13	0.13	0.13	0.12	0.12
60	$\mu+1.5\boldsymbol{\sigma}$	1.09	1.30	1.34	1.36	1.39	1.41	1.48	1.53	1.54	1.55
	μ	0.94	1.10	1.13	1.15	1.18	1.20	1.25	1.29	1.30	1.31
	V	0.11	0.12	0.12	0.12	0.12	0.12	0.12	0.12	0.12	0.12
90	$\mu+1.5\boldsymbol{\sigma}$	1.14	1.36	1.39	1.43	1.47	1.50	1.54	1.59	1.60	1.61
	μ	0.96	1.13	1.16	1.20	1.23	1.26	1.30	1.35	1.36	1.37
	V	0.13	0.13	0.13	0.13	0.13	0.13	0.12	0.12	0.12	0.12
120	$\mu+1.5\boldsymbol{\sigma}$	1.12	1.36	1.40	1.44	1.48	1.51	1.56	1.61	1.62	1.62
	μ	0.94	1.13	1.17	1.20	1.24	1.27	1.30	1.35	1.36	1.37
	V	0.13	0.13	0.13	0.13	0.13	0.13	0.13	0.13	0.13	0.13
200	$\mu+1.5\boldsymbol{\sigma}$	1.02	1.26	1.30	1.33	1.39	1.41	1.46	1.52	1.53	1.53
	μ	0.84	1.03	1.06	1.09	1.13	1.15	1.19	1.23	1.24	1.25
	V	0.14	0.15	0.15	0.15	0.15	0.15	0.15	0.15	0.15	0.15

Table 2.5: Statistical Parameters for Live Load for ADDT 10000 by: Rakozy (2011)

Span (ft)	Statistical Parameter	Time Period (*T*)									
		1 Day	2 Weak	1 Month	2 Month	6 Month	1 Year	5 Year	50 Year	75 Year	100 Year
30	$\mu+1.5\boldsymbol{\sigma}$	1.31	1.45	1.48	1.50	1.52	1.55	1.60	1.64	1.65	1.66
	μ	1.10	1.21	1.24	1.26	1.28	1.29	1.34	1.37	1.38	1.39
	V	0.13	0.13	0.13	0.13	0.13	0.13	0.13	0.13	0.13	0.13
60	$\mu+1.5\boldsymbol{\sigma}$	1.20	1.35	1.39	1.42	1.45	1.46	1.50	1.56	1.57	1.57
	μ	1.00	1.12	1.16	1.19	1.21	1.22	1.26	1.30	1.31	1.32
	V	0.13	0.13	0.13	0.13	0.13	0.13	0.13	0.13	0.13	0.13
90	$\mu+1.5\boldsymbol{\sigma}$	1.23	1.40	1.43	1.46	1.48	1.51	1.55	1.62	1.63	1.63
	μ	1.03	1.17	1.20	1.23	1.25	1.28	1.31	1.36	1.37	1.38
	V	0.13	0.13	0.13	0.12	0.12	0.12	0.12	0.13	0.12	0.12
120	$\mu+1.5\boldsymbol{\sigma}$	1.21	1.41	1.45	1.48	1.52	1.54	1.59	1.62	1.63	1.64
	μ	1.01	1.18	1.21	1.24	1.26	1.28	1.33	1.35	1.36	1.37
	V	0.13	0.13	0.13	0.13	0.13	0.13	0.13	0.13	0.13	0.13
200	$\mu+1.5\boldsymbol{\sigma}$	1.11	1.31	1.36	1.39	1.41	1.44	1.49	1.54	1.55	1.55
	μ	0.91	1.07	1.10	1.13	1.15	1.17	1.22	1.25	1.26	1.27
	V	0.14	0.15	0.15	0.15	0.15	0.15	0.15	0.15	0.15	0.15

As a continuation to their work, Nowak and Rackoczy (2013) made a comprehensive review and analysis of the available data obtained from the Weigh-In-Motion (WIM) technology. About 32 WIM locations have been considered to represent the truck traffic in the United States. Data obtained from 35 million trucks were utilized to determine the statistical parameters of an updated live load model. The statistical parameters calculations were carried out for all considered cases of ADTT (Average Daily Total Traffic) and span length. A value of 0.12 is recommended for the coefficient of variation. The variation of the bias factor with span length considering different ADTT is presented in Table 2.6.

Table 2.6: Bias factor of maximum moment due to live load in 75 years (Nowak and Rakoczy, 2013)

Span (ft)	Bias factor, λ				
	ADTT 250	ADTT 1000	ADTT 2500	ADTT 5000	ADTT 10,000
200	1.34	1.36	1.37	1.4	1.4
190	1.35	1.37	1.38	1.41	1.41
180	1.35	1.37	1.39	1.42	1.42
170	1.36	1.38	1.4	1.42	1.43
160	1.37	1.39	1.41	1.43	1.44
150	1.37	1.39	1.41	1.44	1.44
140	1.38	1.4	1.42	1.45	1.45
130	1.38	1.4	1.43	1.45	1.46
120	1.39	1.41	1.44	1.46	1.47
110	1.4	1.41	1.44	1.46	1.47
100	1.4	1.42	1.43	1.45	1.47
90	1.41	1.42	1.43	1.45	1.47
80	1.41	1.42	1.43	1.45	1.47

2.1.1.2.1 Statistical parameters of live load effect

The statistical parameters of the live load effect (moment and shear) were first investigated by Nowak (1993) according to both AASHTO LRFD and the previous methodology of AASHTO (*allowable stress method*) as illustrated in Figures 2.9, 2.10, and 2.11 for simple span moment, shear and for continuous negative moment, respectively. Those figures clearly show uniform distribution of the bias factor when calculated based on AASHTO LRFD procedure as a result of the calibration process. A value of 0.12 for the corresponding coefficient of variation was also recommended.

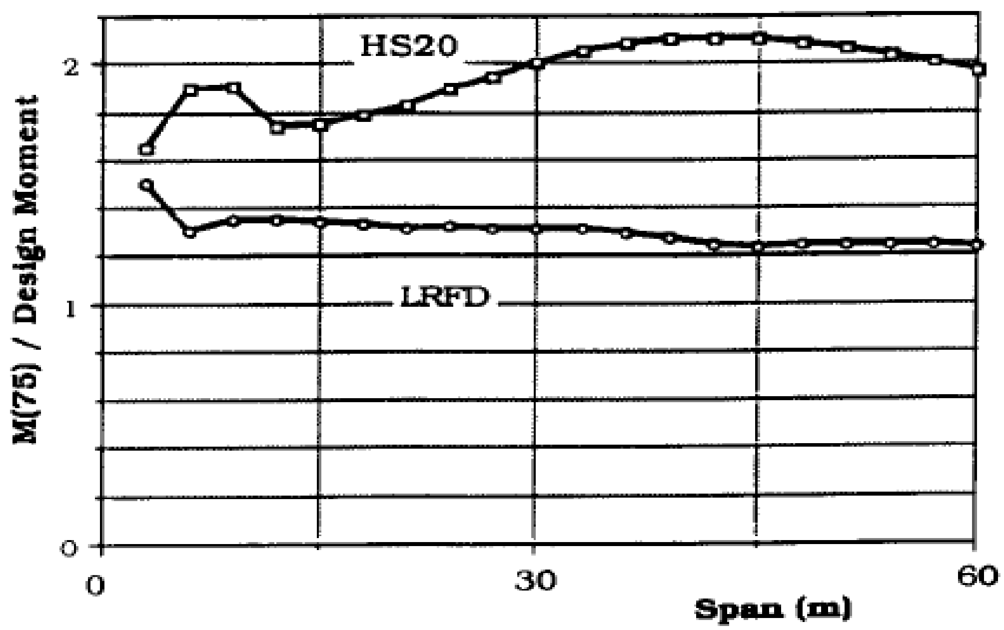

Figure 2.9: Bias factors for simple span moments: HS20 and LRFD (Nowak, 1993)

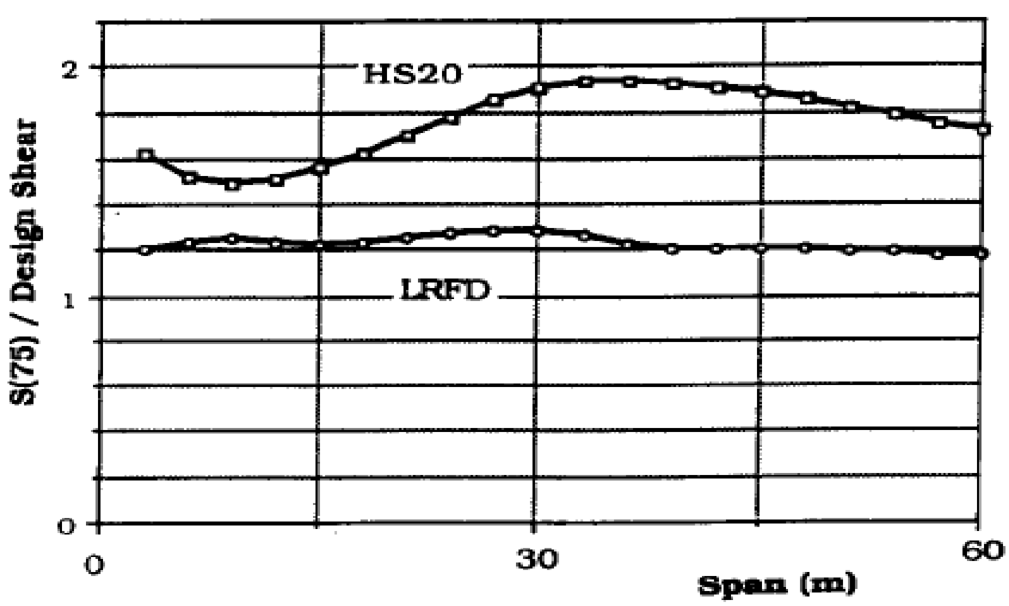

Figure 2.10: Bias factors for shears: HS20 and LRFD (Nowak, 1993)

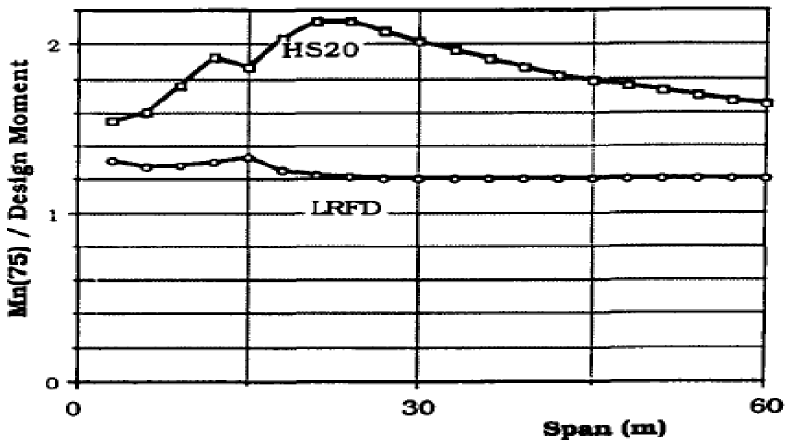

Figure 2.11: Bias factors for negative moments : HS20 and LRFD (Nowak, 1993)

This work was further continued by Nowak and Szerszen (1998) considering the truck survey already conducted, in Ontario, by the Ministry of Transportation MTO. The study covered about 10,000 selected trucks (only trucks which appeared to be heavily loaded were measured and included in the database). Different cases of truck positioning with different level of correlation between trucks were investigated. For different span lengths, the bias factor for moment and shear is shown in Figure 2.12; while, the coefficient of variation was considered as constant value of 0.12.

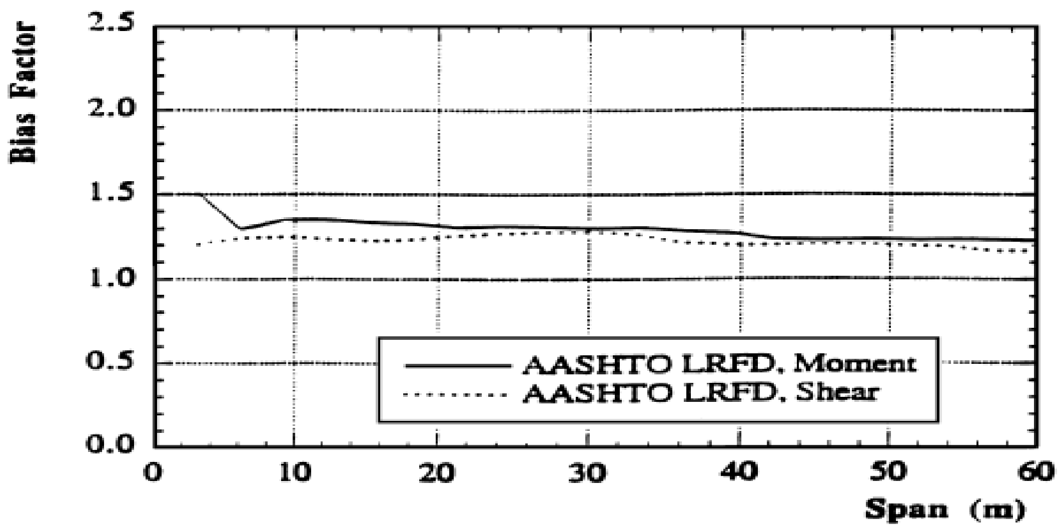

Figure 2.12: Bias factors for live load effects (Nowak and Szerszen 1998).

However, the statistical parameters of the load effects (moment and shear) have not been updated based on the new statistical parameters, of the live load itself, as developed by Nowak and Rakoczy (2011 and 2013). This will be addressed in Chapter Three of the current research.

2.1.1.2.2 Statistical parameters of live load distribution factor

The transverse distribution of live load among girders can be obtained using the girder distribution factors GDFs. As illustrated in Figure 2.13, the GDFs in old AASHTO (*allowable stress approach*) are too conservative in comparison with those derived from the LRFD methodology (Nowak, 1993). However, Nowak et al., (2001) investigated the effect of analysis method on the statistical parameters of the GDFs. The results, based on simplified methods, indicated that the bias factor $\lambda=0.93$ and the coefficient of variation $V=0.15$ while using sophisticated methods (e.g., finite element analysis), the bias factor $\lambda=0.98$ and the coefficient of variation $V=0.07$.

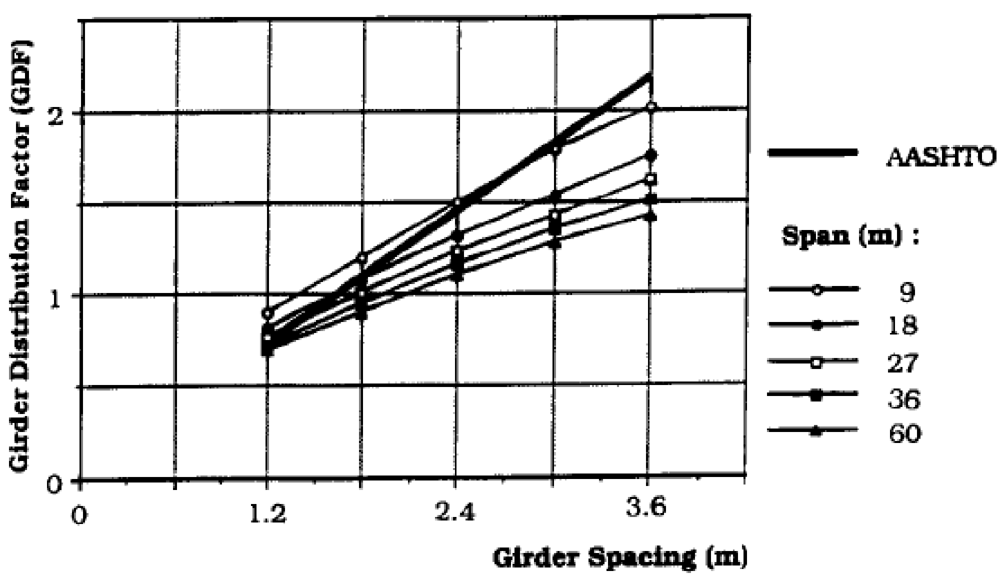

Figure 2.13: Girders distribution factors (Nowak, 1993)

2.1.1.2.3 Dynamic Load Effect

There are analytical and experimental field studies presented to provide a general outline for the study of dynamic load effect (DLF), but do not provide uniform conclusions concerning the value of DLF or the variables influencing this value.

The derivation of the statistical model for the dynamic behavior of bridges was presented by Hwang and Nowak (1991). For all spans, the simulations indicated that the mean dynamic load is less than 0.17 for a single truck and less than 0.12 for two trucks. The coefficient of variation of a joint effect of the live load and dynamic load is 0.18. This was further verified by Kim and Nowak (1997).

The dynamic load is time-variant, random in nature, and it depends on the vehicle type, vehicle weight, axle configuration, bridge span length, road roughness, and transverse position of the truck on the bridge as defined by Nassif and Nowak (1995). The dynamic impact, IM, is essentially the percent difference between the maximum dynamic and static responses as defined by Billing (1984), Paultre (1991), Laman (1999), Ashebo (2006), and Moghimi (2007).

Some measurements of dynamic loads were taken from the Ontario Ministry of Transportation. Billing (1984) and Billing and Green (1984) conducted a test on 27 bridges (prestressed and steel girders, trusses, and rigid frames) to obtain data to support the Ontario Highway Bridge Design (OHBDC 1979). Mean values are about 0.05 to 0.1 for prestressed AASHTO Girders and about 0.08 to 0.2. Cantienti (1983) tested 226 bridges (205 were prestressed concrete) in Switzerland. All bridges were loaded with the same vehicle and with the same tire pressure to minimize the variability due to truck dynamics. The results indicated that the dynamic fraction of the load was as high as 0.7 for bridges with fundamental natural frequency between 2 and 4 Hz. O'Connor and Pritchard (1985) tested short span composite steel and concrete bridges in Australia. The results indicated that the dynamic load is vehicle dependent and it varies with the suspension geometry. Also, the results indicated that the dynamic load decreases as the weight of the vehicle increases. O'Connor and Chan (1988) collected strain data and found that the extreme values are associated with light trucks.

Field measurements were performed to determine the actual variation of the dynamic load factor (DLF). The results indicated that the dynamic deflection was almost constant and does not depend on the vehicle weight, and then DLF was smaller for heavier trucks, because static deflection increases.

Dynamic force effect acting on the bridge can be estimated by a difference between the dynamic strain or deflection (at normal speed) and static strain or deflection (at crawling speed). The dynamic load factor (DLF) is defined as the ratio of the dynamic load effect to the static load effect. Hwang and Nowak (1989, 1991) and Nowak et al. (1990) developed procedures for calculating the statistical parameters for dynamic loads on highway bridges, and the results indicated that a uniform dynamic load factor of 0.25 was recommended for all spans greater than 6 m.

Kim and Nowak (1997) conducted load distribution and impact factor testing on two simply supported I-girder bridges in Michigan to assess impact factors. The findings of this test that, the impact factor decreases as the peak static strain increases. The results obtained for statistical parameters for dynamic impact are: mean of 0.12, standard deviation of 0.15, and a maximum value of 0.6 obtained from loading corresponding to low static strain. These values result in DLFs of 1.12, 1.15, and 1.6, respectively. Test results that DLF is less than 0.10 for two trucks traveling side-by-side and is less than 0.15 of the mean live load for a single truck. Therefore, the mean DLF is taken as 0.10, and the coefficient of variation is 0.80.The authors noted that the average values are lower than the AASHTO values.

AASHTO LRFD (2010) simplified the DLF as a constant factor that can be applied to all bridges of all makes, lengths, and materials. AASHTO LRFD, Article (3.6.2.1) simply sets three constant impact factors (*IM*) as shown in Table 2.7. These values were obtained through field testing, resulted in a maximum *IM* factor of 25% for most highway bridges applied to the design truck only, and were reported to be 33% as indicated below.

Table 2.7: Dynamic Load Allowance, IM (Table 3.6.2.1-1 AASHTO LRFD 2012).

Component	IM
Deck Joints – All Limit States	75 %
All Other Components • Fatigue and Fracture Limit State • All Other Limit States	 15 % 33 %

The Total Live load is calculated as defined by Equation 2.2.

[2.2] $$M_{LL} = D.F.(M_{lane} + IM\ M_{truck})$$

where, D.F. is AASHTO live load distribution factor.

2.1.1.2.4 Fatigue Model

Jeffrey et al. (1996) developed fatigue live load model in order to establish an equivalent fatigue truck that will cause the same cumulative fatigue damage as the normal traffic distribution. This fatigue-load model has been developed from the weigh-in-motion (WIM) measurements (Laman, 1995). The developed fatigue live load model has been verified using fatigue-damage analysis to compare the model with the measured results. A smooth curve has been fit to the data relating average number of cycles per truck n_{avg}.The calculated and measured average stress cycles per vehicle are presented in Figure 2.14.

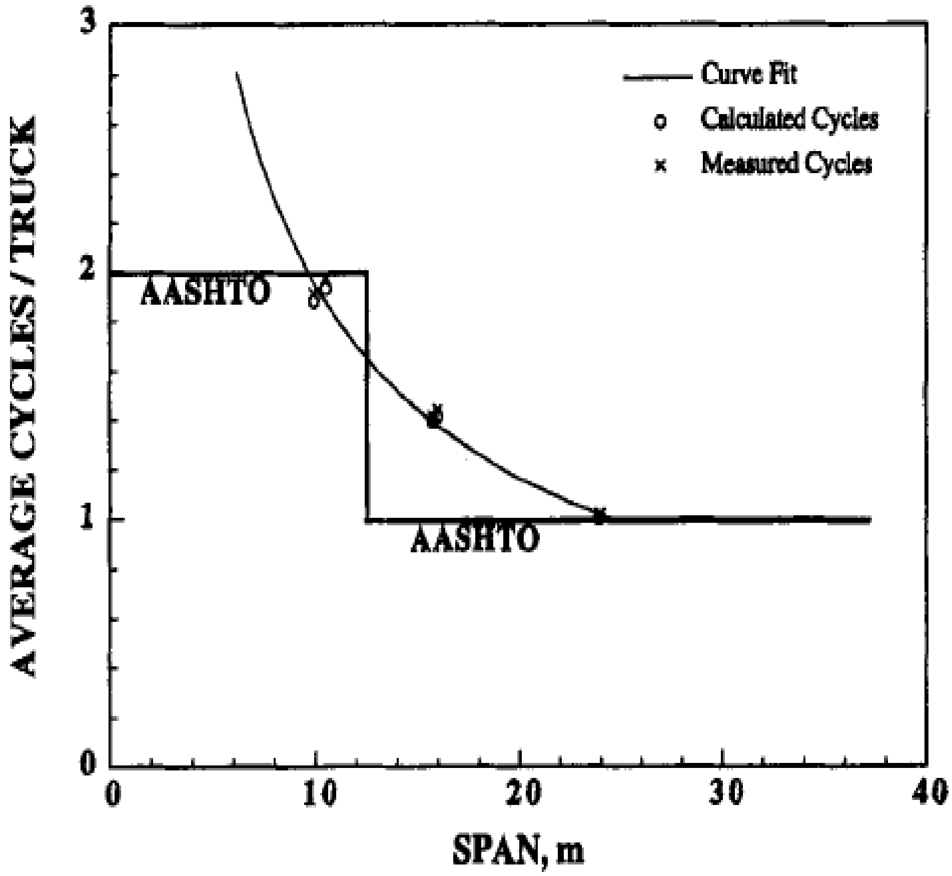

Figure 2.14: Calculated and measured average stress cycles per truck (Jeffrey et al., 1996).

2.1.1.2.5 Live load model for system reliability:

Traditionally, structural design is based on design of individual components (e.g. beams, columns, connections, etc.). The design codes specify nominal values of loads, and the objective of the design is to determine the required value of nominal resistance with predetermined safety factors. The resistance of a component is expressed in terms of geometry and materials characteristics. In most cases, component-based design is conservative because of redundancy and ductility. In a redundant structure, when an individual component reaches its ultimate load carrying capacity, other components can take additional loads to prevent a failure. However, the quantification of this load sharing requires a special approach using the system reliability models.

Nowak (2004) developed a load model for system reliability assessment. This model consists of a 3-axle vehicle (denoted by S) and a 5-axle vehicle (denoted by T), as shown in Figure 2.15. The gross vehicle weight (GVW) was considered as a random variable. The transverse position of the truck within the roadway (curb distance) is also a random variable. The probability density functions (PDF) of the curb distance are shown in Figure 2.16, for two traffic lanes. Each PDF represents a curb distance for a line of wheels, spaced at 1.80 m for a truck. Different possible load cases and probabilities of occurrence, including simultaneous presence with two trucks (side-by-side) in the same lane, are shown in Figure 2.17.

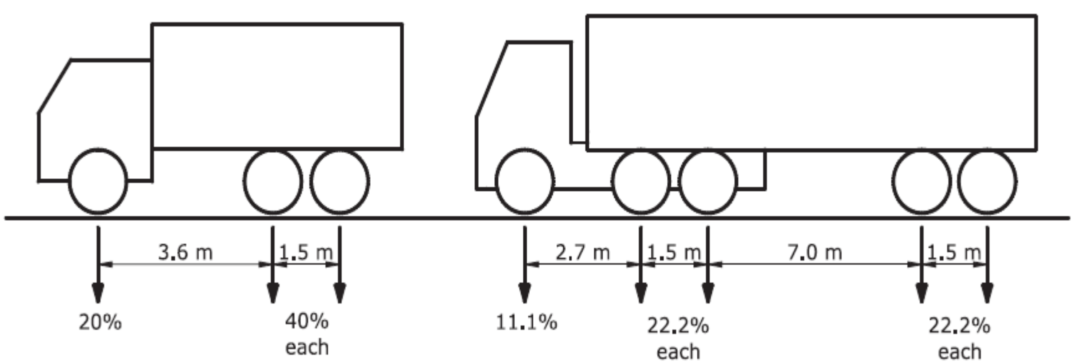

Figure 2.15: Truck configurations considered in the project (Nowak 2004).

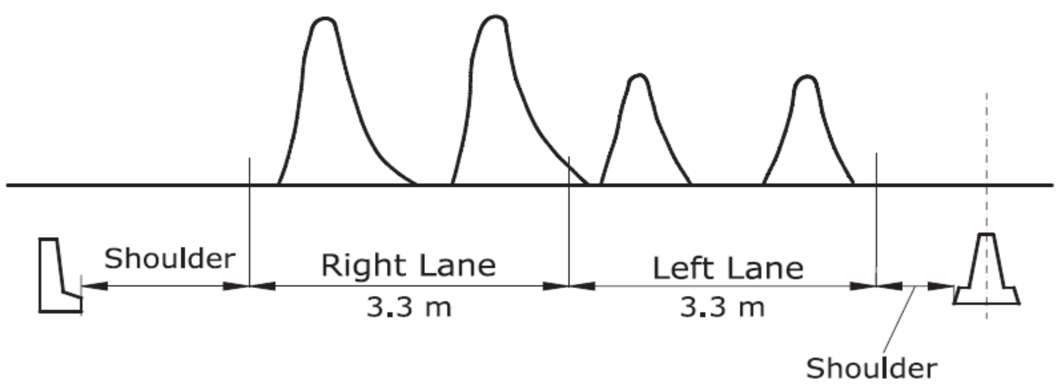

Figure 2.16: Example of the Probability Density Functions (PDF) of the Curb Distance. Each PDF Represents a Line of Truck Wheels (Nowak 2004).

One Lane Loaded		Two Lanes Loaded	
Truck Placement	Probability of Occurrence	Truck Placement	Probability of Occurrence
S	0.133	S T	0.2
T	0.533	T S	0.3
S	0.067	S S	0.1
T	0.267	T T	0.4

Figure 2.17: Considered Truck Positions and Probabilities of Occurrence (Nowak 2004).

In his study, Nowak (2004) investigated two extreme cases of correlation between the two trucks (side-by-side): no correlation, with the coefficient of correlation, $\rho = 0$, and full correlation, with the coefficient of correlation, $\rho = 1$.

For traffic with three lanes, Khorasani (2010) suggested a truck positioning patters with seven possible load cases as shown in Figure 2.18.

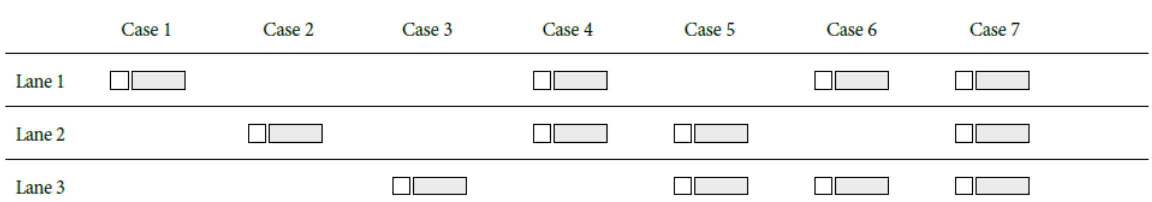

Figure 2.18: Possible truck positions on a bridge with three lanes of traffic (Khorasani 2010).

2.1.2 Resistance Model

The capacity of a bridge depends on the resistance of its components and connections. The resistance (R) of the structural system or its components is determined mostly by material strength and dimensions. In design, the resistance of structure elements is often considered deterministic; in reality, there is some uncertainty associated with each element. Because of the uncertainty of the resistance components, the resistance is treated as random variables in reliability analysis. The uncertainty in resistance may depend on many factors, which can be categorized with three major parameters: material, fabrication, and analysis (Nowak and Szerszen 2003).

The major parameters of resistance that affect the nature of the element strength are:

- Material properties: The material parameter reflects the uncertainty in the strength of material which is presented in the modulus of elasticity, cracking stresses, and chemical composition.
- Fabrication: The fabrication parameter reflects the uncertainty in the overall dimensions of the component that can affect the cross-section area, moment of inertia, and section modulus.
- Analysis: The analysis parameter presents the uncertainty resulting from approximate methods of analysis, idealized stress/strain distribution models, and the engineering judgment.

The variability in resistance has been modeled by tests and observation of existing structures by engineering judgment. The resistance models can be developed based on the available test data that was collected for basic and common materials. However, structural systems are more complicated and consist of composite members which are often made of several materials. Therefore, special methods of analysis are required to obtain the resistance variability for composite members combined of several materials. Since information on the variability of the resistance of such members is not always available, it is often necessary to develop resistance models using the available material test data and numerical simulations (Nowak 1993 and Tabsh and Nowak 1991). The resistance (R) can be modeled in the analysis using the model presented by Nowak and Szerszen (2003). This model considers R as a product of the nominal resistance (R_n) used in the design and three parameters that account for some of the sources of uncertainty mentioned above as expressed in Equation [2.3].

[2.3] $$R = R_n \, M \, F \, P$$

where,

R_n = nominal value of resistance specified in the code, usually in the form of design equation.

M = materials property factor.

F = fabrication factor.

P = professional factor.

The mean value of resistance (μ_R), coefficient of variation (V_R), and bias factor (λ_R) can be calculated by Equations 2.4, 2.5, and 2.6:

[2.4] $$\mu_R = R_n \, \mu_M \, \mu_F \, \mu_F$$

[2.5] $$V_R = \sqrt{(V_M)^2 (V_F)^2 (V_P)^2}$$

[2.6] $$\lambda_R = \lambda_M \, \lambda_F \, \lambda_P$$

The statistical parameters for R can also be calculated as presented in Equations 2.7 and 2.8.

[2.7] $$\lambda_R = \lambda_{FM} \, \lambda_P$$

[2.8] $$V_R = \sqrt{(V_{FM})^2 (V_P)^2}$$

where,

λ_{FM} = the bias factor of FM

λ_P = the bias factor of P

V_{FM} = the coefficient of variation of FM

V_P = the coefficient of variation of professional factor P.

Resistance is treated as random variables and is described by bias factors (ratio of mean to nominal), denoted by λ, and by coefficient of variation denoted by V (Nowak 1993).

2.1.2.1 Statistical Parameters of Materials

2.1.2.1.1 Statistical Parameters of Compressive Strength of Concrete

Concrete properties usually show the highest variability due to various sources of uncertainties, like material properties, curing and placing methods (Nowak and Szerszen

2008). Many factors like the strain rate and duration of loading, casting direction, and effect of creep, shrinkage and confinement affect the mean strength in the actual structure (Ahmed et al. 2014). The variability of concrete strength depends also on the quality control of concreting operation (Al-Harthy and Fragopol 1994).

From field-cast laboratory-cured cylinders using exponential quality control method, 0.07 to 0.1 coefficients of variation were obtained, and a reasonable maximum value of 0.20 for average control (Mirza et al. 1996).

Grant et al. (1978) suggested a number of equations for the statistical parameters of concrete compressive strength. For loading rate R in *psi/sec*, the mean value of compressive strength for in-situ-cast concrete $\overline{f'_{cstrR}}$ and its coefficient of variation V_{cstrR} can be determined as follows:

[2.9] $$\overline{f'_{cstrR}} = \overline{f'_{cstr35}}\,[0.89(1+0.08 \log R)]$$

[2.10] $$V_{cstrR} = \sqrt{{V_{cyl}}^{2} + 0.084}$$

Where $\overline{f'_{cstr35}}$ is the mean compressive strength corresponding to loading rate of 35 *psi/sec*. V_{cstrR} denotes the coefficient of variation of cylinder compressive strength.

Some researchers investigated the effect of method of curing and quality of workmanship on the statistical parameters of concrete compressive strength. Table 2.8 summarizes their results (Al-Harthy and Frangopol 1994).

It was observed that the quality of materials has been improved over the last 3 decades and this was reflected in reduced coefficients of variation and increased bias factors (Nowak and Szerszen 2003). The statistical parameters have been updated based on new material test data including compressive strength of concrete (Nowak and Racoczy 2010). It is a convenient way to present cumulative distribution functions (CDFs) as it allows for an easy evaluation of the most important statistical parameters as well as type of the distribution function (Nowak et al. 2011).
As part of the probabilistic calibration process of the *Design Code for Concrete Structures* (ACI 318), Nowak and Rakoczy (2012) obtained compressive strength tests data and

plotted them on the normal probability paper. The construction and use of the normal probability paper is described in the textbook (Nowak and Collins 2000). The CDFs of concrete compressive strength, f'_c , of normal weight concrete, high strength concrete, and lightweight concrete are shown in Figures 2.19, 2.20, and 2.21, respectively. The values of bias factor and coefficient of variation of compressive strength corresponding to different nominal values are presented in Table 2.9 (Nowak and Rakoczy 2012).

Table 2.8: Statistical properties of concrete compressive strength f'_c (Al-Harthy and Frangopol 1994).

Nominal f'c (ksi)	Distribution Type	Mean	Coefficient of variation (c.o.v)	Remarks
		$K\ f'_c$	0.174-0.207	Ellingwood (1978) K =0.8 for poor field cure K =1.01 for good field cure
3.0		$1.17f'_c$		Ellingwood and Ang (1974)
3.0	Normal	$1.17f'_c$	0.10 0.15 0.25	Ellingwood (1977) The 3 c.o.v, are for good, average, and poor workmanship
	Normal	$Kf'_c + K_0$		Allen (1970) K =0.74, $K_0 = 0.64$(ksi) for 4 hours duration of loading K =0.94, $K_0 = 0.80$(ksi) for 1 second duration of loading For good workmanship $\overline{f'_c}$ increases by 10% and V decreases to 0.15

As an alternative to the conventional direct experemental testing, often performed as compression test on cub or cylider specimens, Lehky et al. (2012) suggested a new methodology to obtain the statistical parameters of concrete using experimental data of three-point bending tests used in inverse analysis based on combination of artificial networks and stochastic analysis (Novak and Lehky 2006).

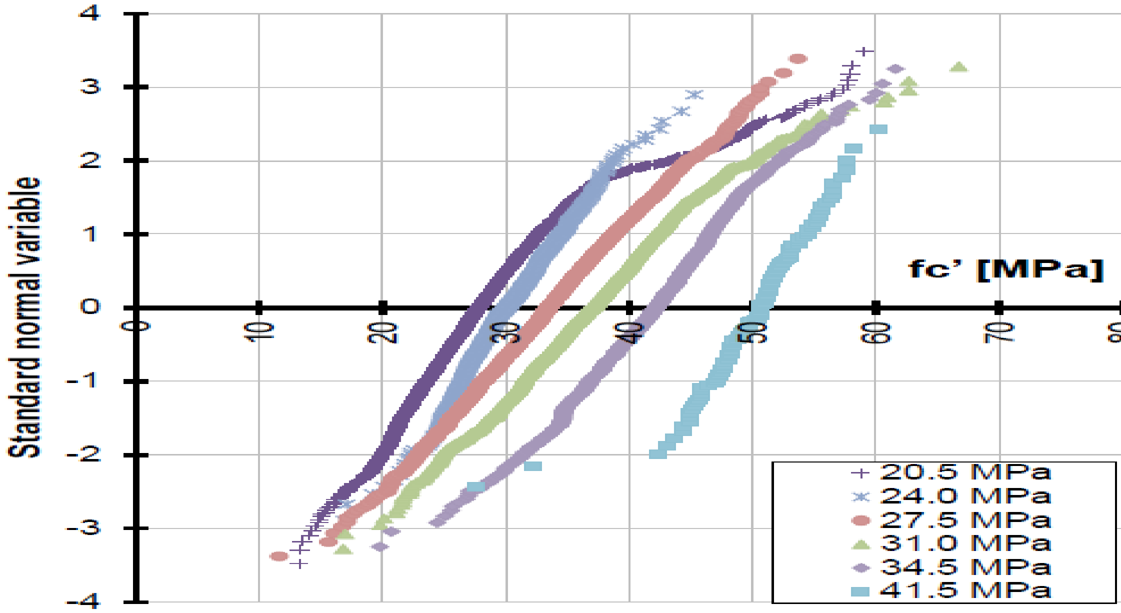

Figure 2.19: CDFs of f'_c for normal weight concrete (Rakoczy and Nowak, 2012).

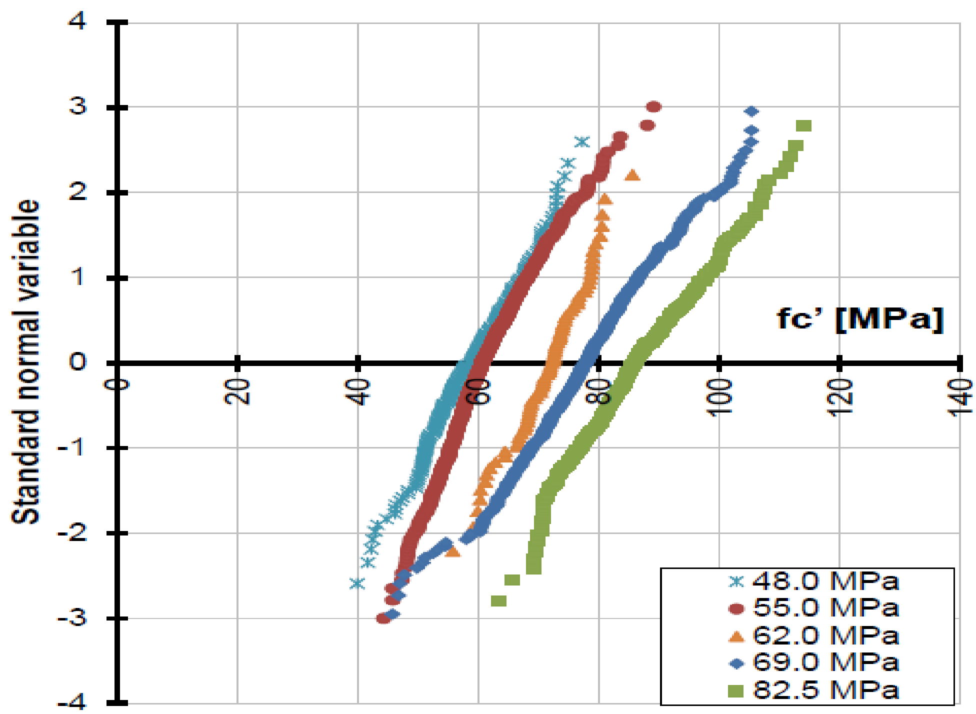

Figure 4.20: CDFs of f'_c for high strength concrete (Rakoczy and Nowak, 2012)

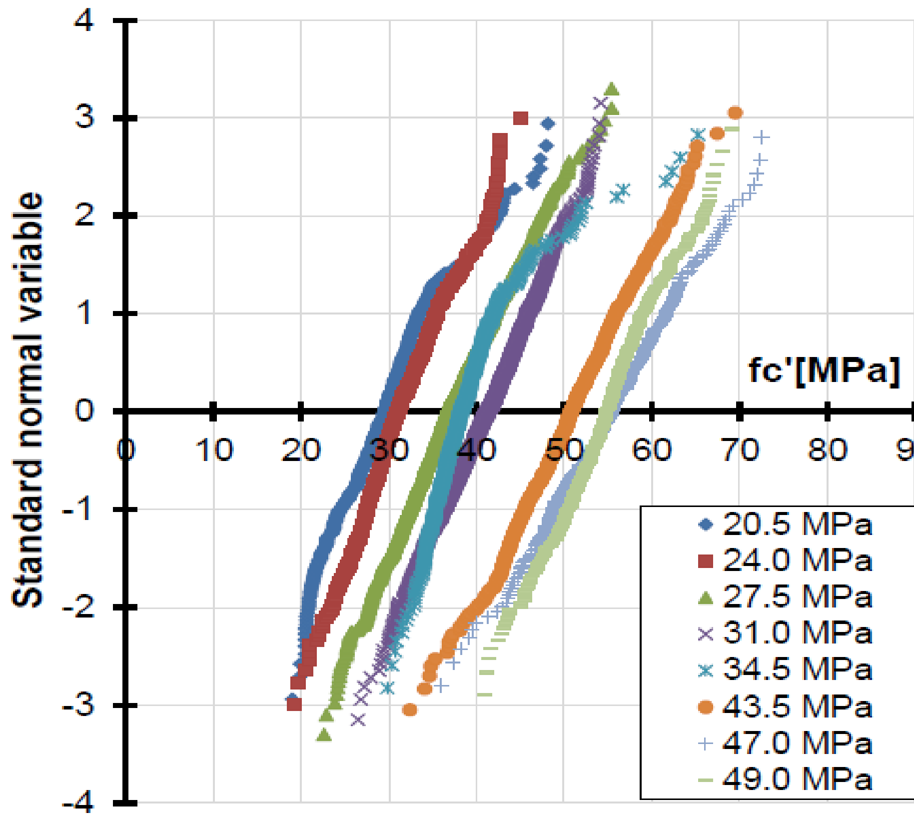

Figure 4.21: CDFs of f'_c for light weight concrete (Rakoczy and Nowak, 2012)

Table 2.9: Statistical parameters for compressive strength of concrete (Nowak and Rakoczy, 2012).

Compressive strength of concrete f'_c (psi)	Statistical parameters	
	Bias factor	Coefficient of variation V
4000	1.24	0.15
5000	1.19	0.135
6000	1.15	0.125
7000	1.13	0.115
8000	1.11	0.110
9000	1.1	0.110
10,000	1.09	0.110
12,000	1.08	0.110

Accordingly, the obtained results of statistical parameter of concrete compressive strength for different types of concrete, comforming to Eurocode, are presented in Table 2.10.

Table 2.10: Statistical parameters of compressive strength (Lehky et al., 2012)

Concrete Type	Statistical Parameters	
	Mean "Mpa"	COV %
C30/37 H	58.5	8.0
C25/30 B3	47.3	5.4
C25/30 XCI GK16	53.4	5.2
C20/25 XCI GK16	39.8	5.4

The statistical parameters for compressive strength of concrete were obtained from the data provided by ready mix companies and precasting plants. The cumulative distribution functions (CDF) of compressive strength of concrete (ordinary, highstrength, and light-weight) were plotted on the normal probability paper (Nowak and Szerszen 2001). CDFs for ordinary ready-mix concrete are presented in Figure 2.22. Statistical parameters for ordinary and high-performance concrete are presented in Table 2.11.

2.1.2.1.2 Statistical Parameters of Tensile Strength of Concrete

It has long been known that concrete has a low tensile strength compared to its compressive strength. Although concrete has been used as compressive member material, its tensile behavior has been carefully investigated by many researchers; Raphel (1984), Nonaka et al. (1996), Lorifice et al. (2008), and Wu (2012).

Many test results were analyzed (Mirza et al, 1996) to develop equations for the strength of concrete in flexural tension (f_r) and compared with other developed equations. The following equation was found appropriate to represent the data:

[2.11] $$f_r = 8.3\sqrt{f'_c}$$

Like the compressive strength, tensile strength is also affected by the rate of loading. Mirza et al. (1996) derived Equations 2.12, 2.13, and 2.14 for the mean and the coefficient of variation of the flexural tension strength of in-situ concrete:

Table 2.11: Recommended Statisticals Parameters for Ordinary Ready-mix Concrete by: Nowak and Szerszen (2001)

f'c (psi)	Compressive Strength		Shear Strength	
	λ	CoV	λ	CoV
3000	1.31	0.17	1.31	0.205
3500	1.27	0.16	1.27	0.19
4000	1.24	0.15	1.24	0.18
4500	1.21	0.14	1.21	0.17
5000	1.19	0.135	1.19	0.16
5500	1.17	0.13	1.17	0.155
6000	1.15	0.125	1.15	0.15
6500	1.14	0.12	1.14	0.145
7000	1.13	0.115	1.13	0.14
8000	1.11	0.11	1.11	0.135
9000	1.1	0.11	1.1	0.135
10000	1.09	0.11	1.09	0.135
12000	1.08	0.11	1.08	0.135

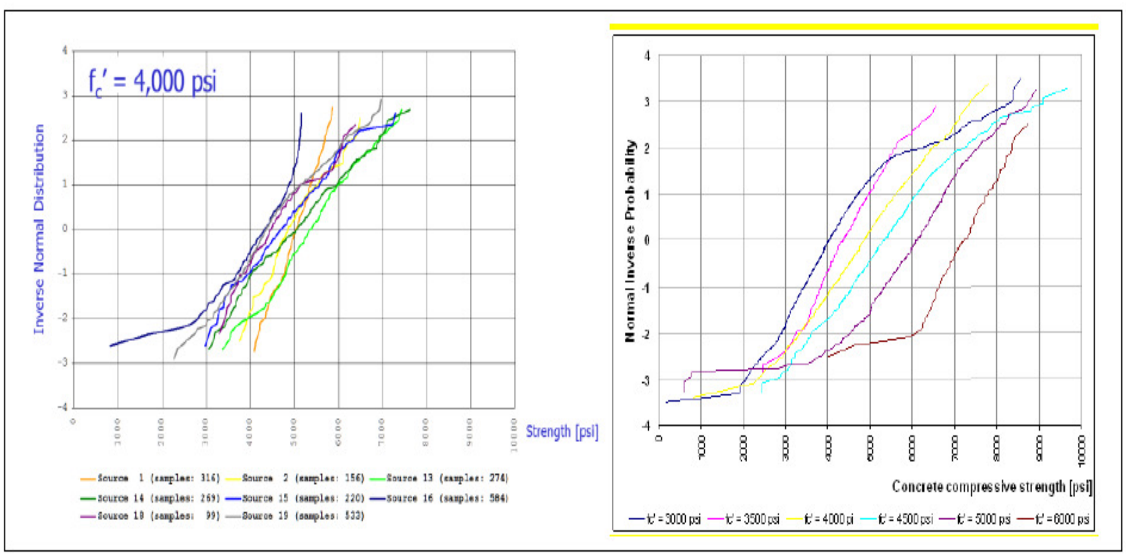

Figure 2.22: CDFs for Ordinary Ready-Mix Concrete by: Nowak and Szerszen (2001)

[2.12] $\overline{f'_{rstrR}} = 8.3\sqrt{\overline{f'_c}}\,[0.96(1+0.11 \log R)]$

[2.13] $V_{f'_r} = \sqrt{(V_{cyl}{}^2/4) + 0.0421}$

Where;

[2.14] $\overline{f'_c} = (0.675\, f'_c + 1100)\ psi \leq 1.15\, f'_c$

It was also observed that the dispersion of tensile strength tests tend to be slightly higher than the dispersion in compressive strength tests. Ellingwood (1978) suggested a coefficient of variation for the tensile strength ranging from 0.174 to 0.207.

In their study, Mirza et al. (1996) used a mean value for the modulus of rupture f_r equal to 485 psi for a nominal concrete strength of 5000 psi and a standard deviation of 105 psi for average control and 100 psi for excellent control of concrete. MacGregor et al. (1983) used the statistical parameters shown in Table 2.12.

Table 2.12: Uncertainty in concrete tensile strength (MacGregor et al 1983)

Property	Mean (Ksi)	Coefficient of Variation
Concrete under normal control Tensile strength in structure loaded to failure in one hour:		
f= 3.0 ksi	0.306	0.18
f= 4.0 ksi	0.339	0.18
f= 5.0 ksi	0.366	0.18

Using experimental data of three-point bending tests used in inverse analysis based on combination of artificial networks and stochastic analysis (Novak and Lehky 2006), Lehky et al. (2012) suggested the statistical parameters presented in Table 2.13 for the tensile strength of different types of concrete comforming to Eurocode.

Table 2.13: Statistical parameters of tensile strength (Lehky et al. 2012)

Concrete Type	Statistical Parameters	
	Mean "MPa"	COV %
C30/37 H	5.0	14.3
C25/30 B3	4.1	17.2
C25/30 XCI GK16	4.2	12.1
C20/25 XCI GK16	3.1	15.6

2.1.2.1.3 Statistical Parameters of Prestressing Steel

Mirza et al. (1980) have analyzed data from 200 samples of grade 270 strands of 7/16 and 1/2 in. diameter, half of them stress relieved and the other half stabilized. The elastic limit stress f_{el} and the stress at 1% strain were taken as $0.7f_{pu}$ and $0.89f_{pu}$ for stress relieved strands, and $0.75f_{pu}$ and $0.90f_{pu}$ for stabilized strands. The probability distribution of modulus of elasticity, ultimate tensile strength and ultimate tensile strain of grade 270 strands were assumed to be Gaussian with mean values equal to 28,400 ksi, 281 ksi, and 0.05, respectively. Very little difference was observed between the statistical values for the stress relieved strands and stabilized strands. It was assumed that the mean stress at transfer was equal to its nominal value (189 ksi for grade 270 strands) with over-tensioning of strands to jacking force to account for losses that occur before transfer. The standard deviation of stress at transfer was taken as 2.8 ksi and 3.8 ksi for pre-tensioned and post-tensioned beams, respectively. A comparison of post-transfer losses showed that there was essentially no difference between the losses for pre-tensioned and post-tensioned beams (Al-Harthy and Frangopol 1994). The mean values of these losses for grade 270 strands were taken as 36 ksi and 26.5 ksi for stress relieved and stabilized strands, respectively, and the corresponding standard deviation equal to 5.75 ksi and 5.3 ksi. The probability models of the stress at transfer and post-transfer losses were arbitrarily assumed to follow normal distribution (Al-Harthy and Frangopol 1994). These results were used by Elligwood et al. (1980) in their development of a probability-based load criteria for the American National Standard A58. Similar values reported by Al-Harthy and Frangopol (1994) are shown in Table 2.14.

Table 2.14: Uncertainty in Prestressing steel properties (Al-Harthy and Frangopol 1994)

Variable	Nominal	Maximum	Minimum	Mean	Coefficient of Variation
$A_{ps}\ in^2$	0.153	0.158	0.153	0.1548	0.0125
$f_{pu}\ ksi$	270	284.6	276.9	280.46	0.0142
$f_{py}\ ksi$		252.1	237.5	246.5	0.022
$E_{ps}\ ksi$	29000	29800	28500	29320	0.01

Based on reliability-based sensitivity, Rakoczy and Nowak (2012), suggested a bias factor of 1.04 and coefficient of variation of 0.017 for the statistical parameters of 0.5 in. diameter strands, while for 0.6 in diameter strands, the values of bias factor and coefficient of variation are 1.02 and 0.015, respectively.

Statistical parameters for prestressing steel were obtained based on test data collected for prestressing steel Grades 250 ksi and 270 ksi. The cumulative distribution functions (CDF) of prestressing steel strengths were plotted on the normal probability paper for tested steel. The statistical parameters of prestressing steel (7-wire strands) strengths were obtained (Nowak and Szerszen 2001). CDF for prestressing steel (0.6-in Grade270 ksi strands), is shown in Figure 2.23. Statistical parameters recommended for prestressing steel are presented in Table 2.15.

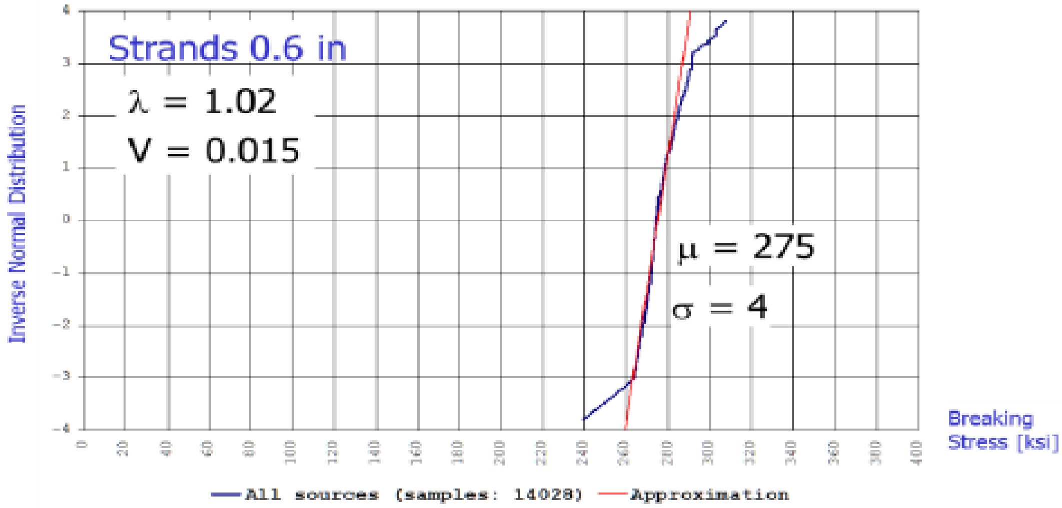

Figure 2.23: CDF for Prestressing Steel (7-Wire Strands) – 270 ksi by: Nowak and Szerszen (2001).

Table 2.15: Statistical Parameters of Prestressing Steel (7-WIRE STRAND) by: Nowak and Szerszen (2001)

Grade	Size	Number of Samples	λ	CoV
250 Ksi	1/4 in (6.25 mm)	22	1.07	0.01
	3/8 in (9.5 mm)	83	1.11	0.025
	7/16 in (11 mm)	114	1.11	0.01
	1/2 in (12.5 mm)	66	1.12	0.02
270 Ksi	3/8 in (9.5 mm)	54	1.04	0.02
	7/16 in (11 mm)	16	1.07	0.02
	1/2 in (12.5 mm)	33570	1.04	0.015
	0.6 in (15 mm)	14028	1.02	0.015

2.1.2.1.4 Statistical Parameters of Reinforcing Steel (Rebars)

Tests were performed by the industry to determine the variation in yield strength for reinforcing steel (grade 60). The CDFs of yield strength (fy) for different numbers of bar diameters were plotted on the normal probability paper. The results showed that there was no substational difference in distributions between diameters of a rebar and fy (Nowak and Szerszen 2001). CDFs for reinforcing steel (grade 60) are presented in Figure 2.24. Statistical parameters, λ and V, recommended for reinforcing steel (grade 60) are presented in Table 2.16.

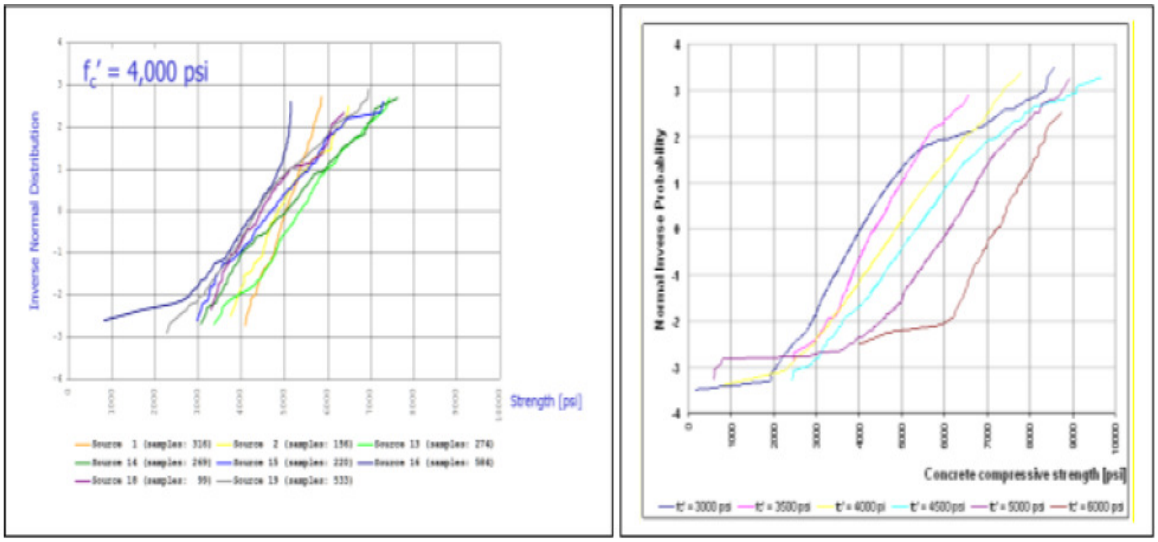

Figure 2.24: CDF for Reinforcing Steel (Grade 60) by: Nowak and Szerszen (2001)

Table 2.16: Statistical Parameters for the Reinforcing Steel (Grade 60) by: Nowak and Szerszen (2001)

Size	Number of Samples	Mean Yeild Strength, f_y (Ksi)	λ	CoV
No. 3 (9.5 mm)	864	71	1.18	0.04
No. 4 (12.5 mm)	2685	67.5	1.13	0.03
No. 5 (15.5 mm)	3722	67	1.12	0.02
No. 6 (19.0 mm)	1455	67	1.12	0.02
No. 7 (22.0 mm)	1607	68.5	1.14	0.03
No. 8 (25.0 mm)	1446	68	1.13	0.025
No. 9 (28.0 mm)	1573	68.5	1.14	0.02
No. 10 (31 mm)	1080	68	1.13	0.02
No. 11 (34.5 mm)	1318	68	1.13	0.02
No. 14 (44.5 mm)	12	68.5	1.14	0.02

2.1.2.2 Statistical Parameters of Fabrication Factor

The second factor affects the resistance is the fabrication factor (F) as explained by Nowak and Szerszen (2003). The fabrication factor reflects the variation in geometry and dimensions of cross section and section properties (area, cover of reinforcement, and moment of inertia).

Al-Harthy and Frangopol (1994) have compiled measurements of concrete member dimensions by other researchers. Much of the data reported come From Mirza and Macgregor (1979a). Their recommended statistical parameters for beams are shown in Table 2.17. Table 2.18 summarizes some of the statistical parameters for slab dimensions.

Table 2.17: Uncertainty in dimensions for beams (Al-Harthy and Frangopol 1994)

Dimension Description	In-Situ (in)			Precast (in)		
	Nominal Range	Mean Deviation from Nominal	Standard Deviation	Nominal Range	Mean Deviation from Nominal	Standard Deviation
Width:						
Rib b_w	11-12	+3/32	3/16	14	0	3/16
Flane b				19-24	+5/32	1/4
Overall Depth	18-27	-1/8	1/4	21-39	+1/8	5/32
Concrete Cover:						
Top reinf.	1-1/2	+1/8	5/8	2-2 1/2	0	5/16
Bottom reinf.	3/4 -1	+1/16	7/16	3/4	0	5/16
Effective Depth:						
Top reinf.		-1/4	11/16		+1/8	11/32
Bottom reinf.		-3/16	1/2		+1/8	11/32
Beam spacing		0	11/16		0	11/32
Span		0	11/16		0	11/32
Note: All distributions assumed normal						

Siriakson (1980) assumed means and coefficient of variation for dimensions of partially prestressed concrete beams in Table 2.19. Tabsh and Nowak (1991) suggested a bias factor of 1.0 and coefficient of variation of 0.028 for dimensions of concrete members.

Table 2.18: Uncertainty in dimensions of slabs (Al-Harthy and Frangopol 1994)

Variable	Nominal Value (in)	Mean Deviation from Nominal (in)	Standard Deviation (in)
h	5-8	+0.05	0.30
d (pos. region)		-0.25	0.30
d (neg. region)		-0.75	0.50
h, d (precast)		0.00	0.15
h (in-situ)	3.94-7.87	+0.04	0.458
h (precast)	5.98-8.66	0.00	0.178
d (pos. region)	4.80-7.17	-0.31	0.594
d (neg. region)	4.96-7.28	-0.77	0.630

Table 2.19: Statistical properties of dimensions for beams (Siriakson, 1983)

Variable	Distribution Type	Mean Deviation from Nominal (in)	Coefficient of Variation
Beam width b	Normal	0 to 5/32	0.0 to 0.045
Web width bw			
Overall depth h	Normal	-1/8 to +1/8	$(1/6.4\mu)$ to 0.045
Flange thickness h_f			
Depth to reinf. d_p	Normal	0 to 1/16	0.04 to $(0.64/h_n)$
Cable eccent. e			
Span	Normal	0	$(11/32\mu)$ to $(11/16\mu)$

Nowak and Szerszen (2001) recommended values of statistical parameters, λ and V, for geometry and dimensions of cross section which are based on previous studies by

Ellingwood (1980). The statistical parameters, λ and V, for fabrication are presented in Table 2.20.

Table 2.20: Statistical Parameters for Fabrication by: Nowak and Szerszen (2001).

Item	λ	CoV
Width of beam, cast - in - place	1.01	0.04
Effective depth of a reinforced concrete beam	0.99	0.04
Effective depth of prestressed concrete beam	1.00	0.025
Effective depth of slab, cast-in-place	0.92	0.12
Effective depth of slab, plant cast	1.00	0.06
Effective depth of slab, post-tensioned	0.96	0.08
Column width and breadth	1.005	0.4

2.1.2.3 Statistical Parameters of Professional Factor

The third factor that affects the resistance is the professional factor (P) (Nowak and Szerszen 2003). The professional factor accounts for the variation between the actual in situ performances compared to the value predicted by used model. The data comes from the previous study by Ellingwood (1980), and confirmed recently by Nowak and Szeszen (2001); while the data for shear in slabs without reinforcement was obtained from Reineck (2003). The recommended values of statistical parameters for professional factor are presented in Table 2.21.

Table 2.21: Statistical Parameters for Professional Factor by: Nowak and Szerszen (2011)

Item	λ	CoV
Beam, flexure	1.02	0.06
Beam, shear	1.075	0.1
Slab, flexure and shear with shear reinforcement	1.02	0.06
Column, tied	1.00	0.08
Column, spiral	1.02	0.06
Plain concrete	1.02	0.06

2.1.2.4 Statistical Parameters of Resistance

The statistical parameters for resistance were obtained by implementing Monte Carlo simulation in the resistance model defined in Equation 2.3 and applying the statistical parameters of its components (M, F, P). The statistical parameters (λ, V) for resistance were developed in Chapter 3 using the explained procedures for resistance.

2.2 Reliability Assessment of Prestressed Girder Bridges

Structural reliability is employed for estimating the safety levels of a structure, in the design or maintenance phase, considering the probabilistic description of the variables composing the respective limit states. Reliability analysis has received the attention of several researchers and, consequently, it has been introduced into almost all recent structural codes worldwide. For any structure, two types of reliability exist:

- The individual (component) reliability index related to every limit state function. The component reliability index depends on different factors, such as the number of basic random variables, their statistical parameters, the statistical distribution type, the probability of failure, the correlation between random variables, and the reliability prediction method.
- The overall system reliability which depends on the individual component's reliabilities, the sequence of failure occurrence, the dependency (correlation) between different modes of failure, and the method of estimating the system reliability.

Different methods are available for determining the individual components' reliability indices such as the First-Order Reliability Method FORM, the Second-Order Reliability Method SORM, Direct integration method, and Monte Carlo Simulation technique. The overall system's reliability can be obtained using different methods such as the narrow bounds approach, linear programming, or the Monte Carlo simulation.

A number of researchers performed probabilistic (reliability) analysis for the purpose of code calibration (Nowak and Zhou 1990), evaluation of design codes (Bartlett et al. 1992), or evaluation of existing bridges (Panesar and Bartlett 2006). The reliability of prestressed girder bridges has been investigated by a number of researchers. Nowak and Zhou (1990) investigated the reliability of girder bridges (steel and prestressed girders). They used the old approach of AAHSTO code (allowable stress design approach). For prestressed girder bridges, they did not consider the serviceability limit states corresponding to the tensile and compressive stresses in the initial and final stages. The overall system reliability was estimated considering the ultimate flexure limit state. For the girder reliability, Nowak and Zhou (1990) used incremental load approach to develop the moment-curvature relations, while for the system reliability, they developed load-deflection curves and determined the formation of plastic hinges till the total failure of the bridge (mechanism). As a case study, Nowak and Zhou investigated the girder and system reliabilities of a 27 ft simple span bridge with the cross section shown in Figure 2.25. As no accurate data on correlation, of random variables, was available, an assumption was made to consider either no correlation or full correlation exist. Such assumption reflects a lack of accuracy of the calculated reliability indices. The overall system reliability index varied from 5.00 (perfect correlation) to 5.25 (no correlation). While the reliability index for individual girder was 4.85.

Nowak et al.(2001) performed reliability analysis for prestressed concrete bridge girders design according to three codes: Spanish Norma IAP-98, Eurocode, and AASHTO LRFD. Typical Spanish precast girders were considered. Five prestressed girder bridges were selected with spans varying from 20 to 40m and girder spacing varied from 1.3 to 3.4m. The reliability analysis considered only the ultimate strength limit state despite the fact that the serviceability limit state (tension stress in concrete) governs the design. The correlation (dependency) of random variables was considered. It was concluded that the Eurocode is the most conservative and AAHSTO LRFD is the most permissive code.

The first-order reliability method (FORM) was used to estimate the reliability index. The calculated reliability index $\boldsymbol{\beta}$ = 5.1-6.8 for Eurocode, $\boldsymbol{\beta}$ = 5.1-6.8 for Spanish code, and $\boldsymbol{\beta}$ = 4.5-4.9 for AASHTO. For the Eurocode and Spanish code, the largest value of $\boldsymbol{\beta}$ are for span of 35 m, and $\boldsymbol{\beta}$ decreases for shorter span lengths. It was also concluded that AASHTO LRFD provides the most uniform reliability level. However, the behaviour of a prestressed girder bridge is governed by different limit state functions both at initial (at transfer) phase and final phase (after losses). A comprehensive reliability assessment needs to take those limit state functions into consideration as will be addressed in Chapter Four.

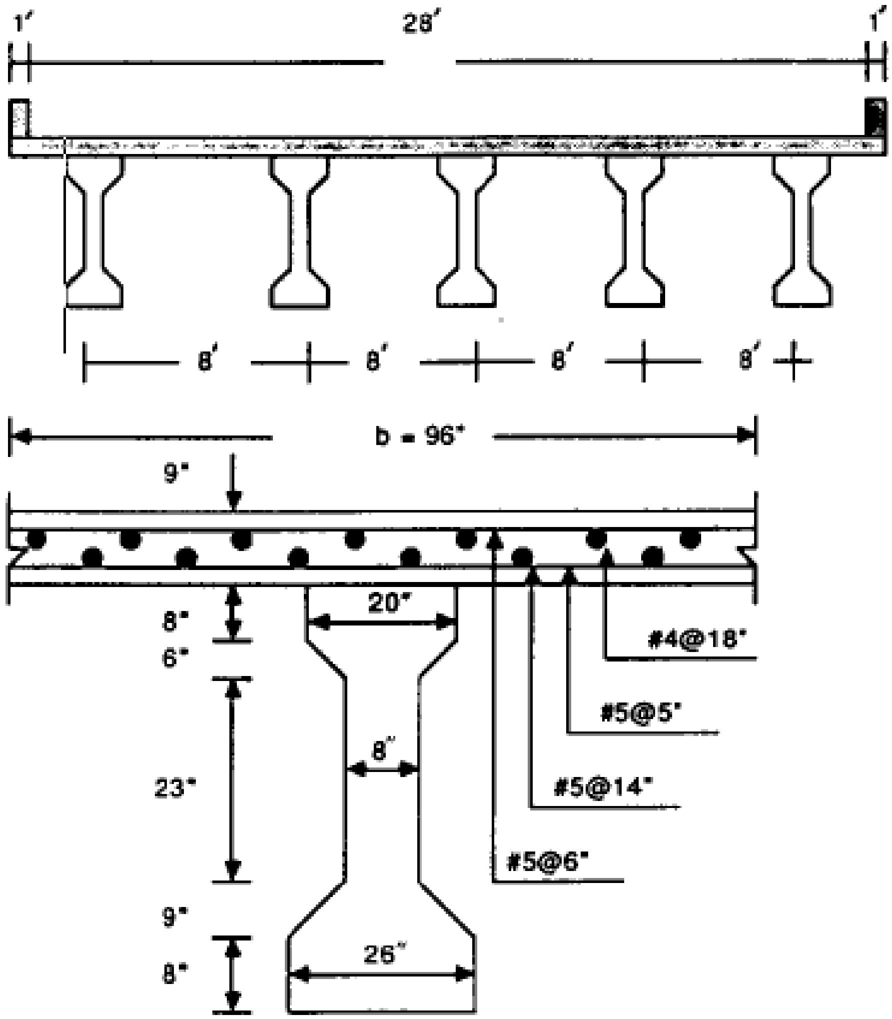

Figure 2.25: Prestressed girder bridge considered (Nowak and Zhou 1990)

Another comparison made by Du and Au (2005) for the deterministic and reliability analysis of prestressed girder bridges using three codes: the Chinese code, the Hong Kong code, and the AASHTO LRFD code. Post-tensioned concrete girders of spans ranging from 25 to 40m were considered. The First-Order Reliability Method (FORM) was used to estimate the reliability index. The comparison between the three codes was made by evaluating the capacity of sections with the amount of prestressing strands. The results obtained from the three different codes revealed that the AASHTO LRFD provides the most consistent level of reliability. Figure 2.26 shows the required number of strands with respect to different span length. Figure 2.27 shows the variability of reliability index with span length.

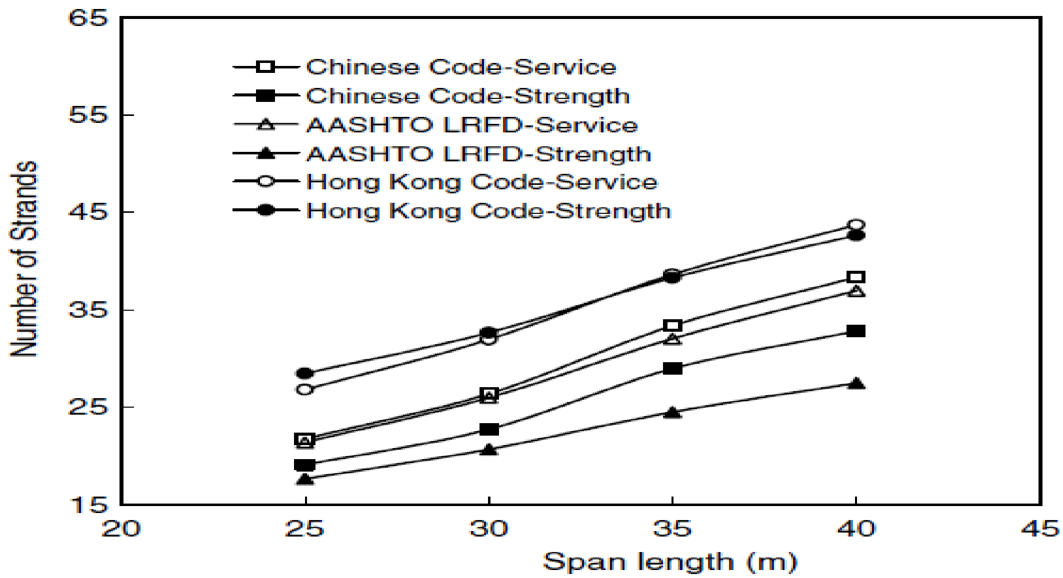

Figure 2.26: Reliability index for flexural capacity in strength limit state (Du and AU, 2005).

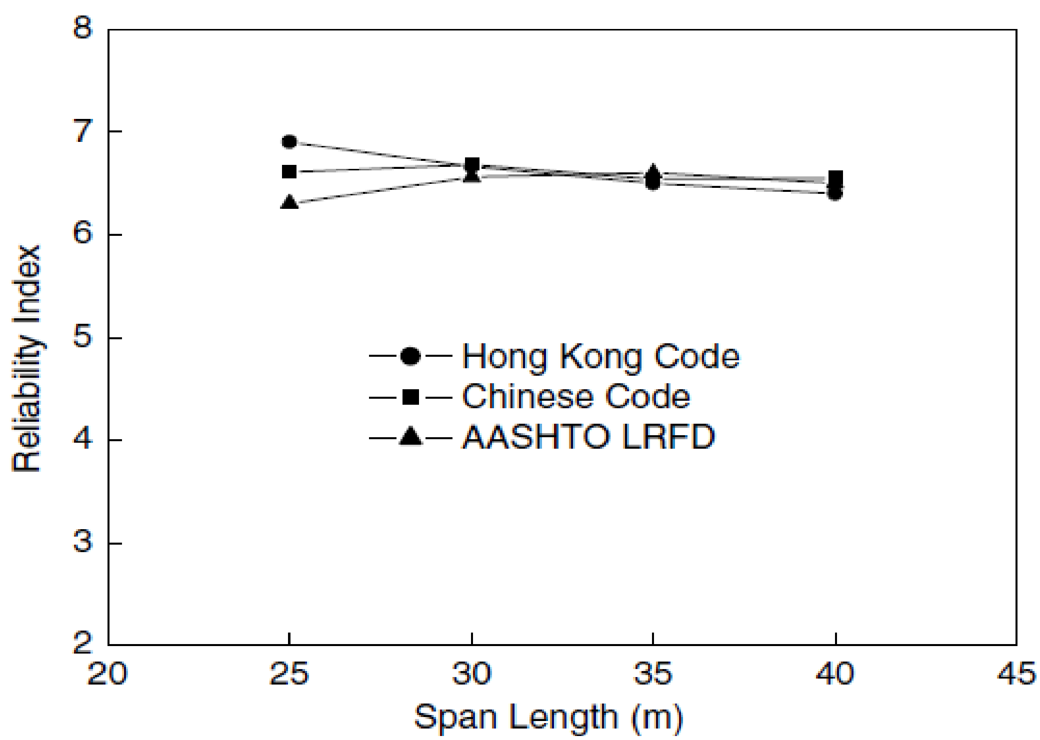

Figure 2.27: Reliability index for flexural capacity in serviceability limit state in the three codes (Du and AU 2005).

The reliability of the standard NU-Girder (sometimes known as the University of Nebraska's I-girders) has been investigated by Morcous et al. (2007). The NU girder type is unique and its shape and dimensions are shown in Figure 2.28. The reliability analysis was performed for the flexural and shear capacity considering Strength I limit state of the AASHTO LRFD code. Other limit states have not been considered. The overall bridge system reliability was not considered too. Out of the six types of NU girders, only three types were considered (NU1600, NU1800, and NU2000) with span lengths varying from 120 to 200 ft. No correlation (dependency) of random variables was considered. Figures 2.29 and 2.30 show the variation of the calculated flexural reliability index of different NU girders with span and girder spacing, respectively. Similarly, Figures 2.31 and 2.32 show the variation of the calculated shear reliability index of different NU girders with span and girder spacing, respectively. Although the area of prestreesing steel is one of the most sensitive and decisive variable in the design of prestressed girders and has its own statistical parameters, Mocous et al. (2007) considered it as a deterministic variable; and this will affect the accuracy of the results.

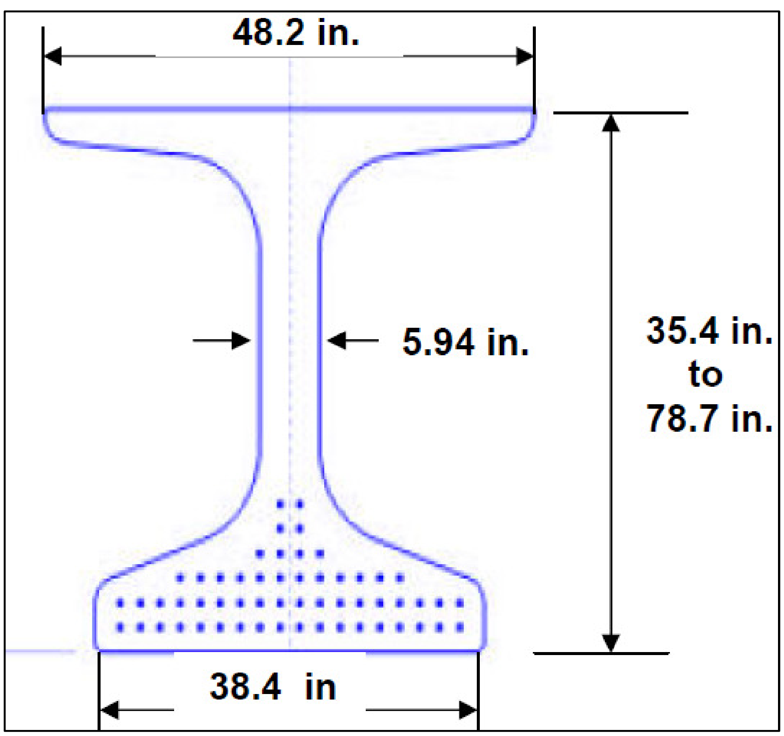

Figure 2.28: the cross section of NU girder (Morcous et al., 2007).

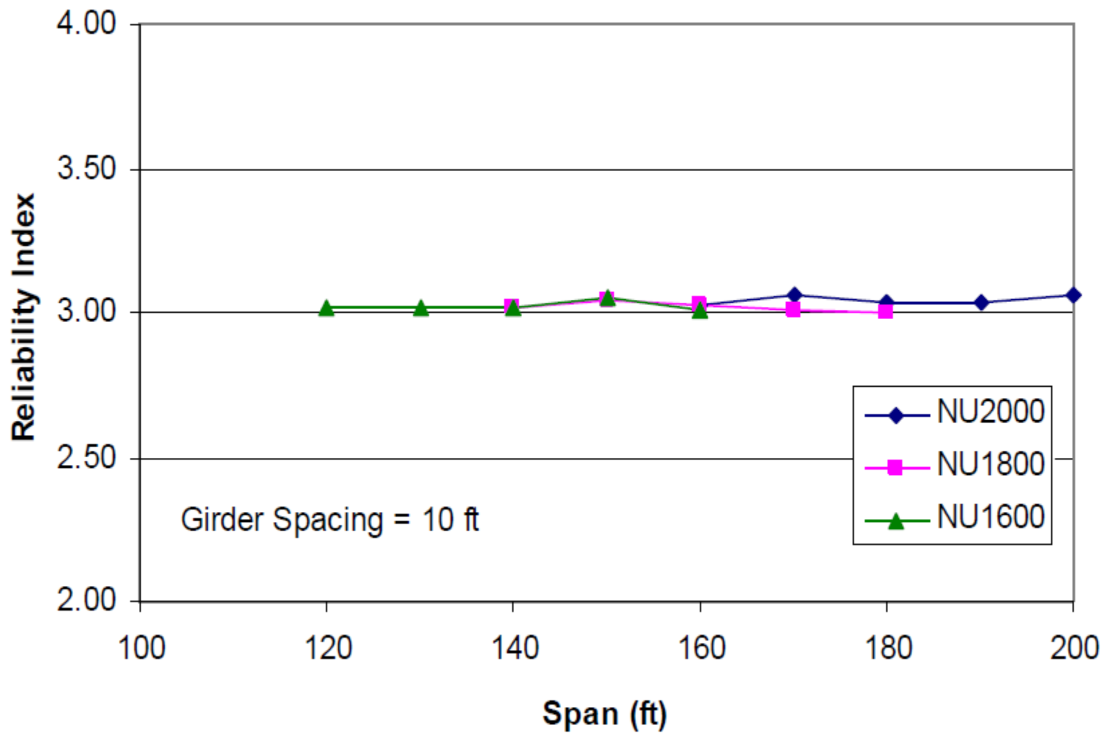

Figure 2.29: Flexural reliability index of NU girder at different spans (Morcous et al, 2007).

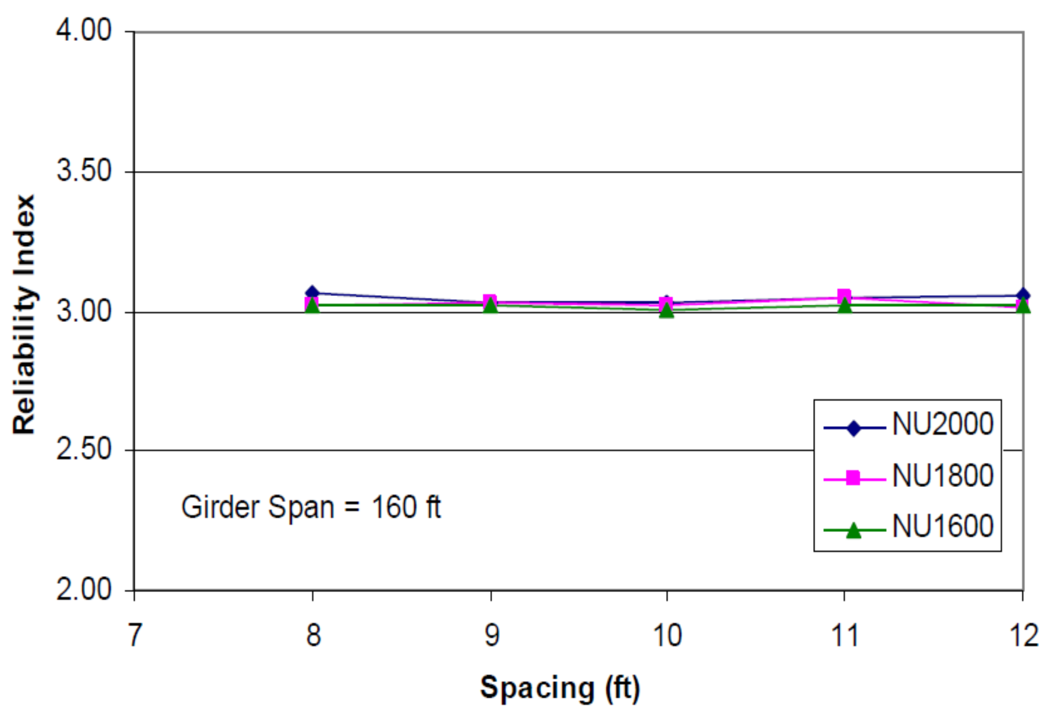

Figure 2.30: Flexural reliability index of NU girder at different girder spacing (Morcous et al., 2007).

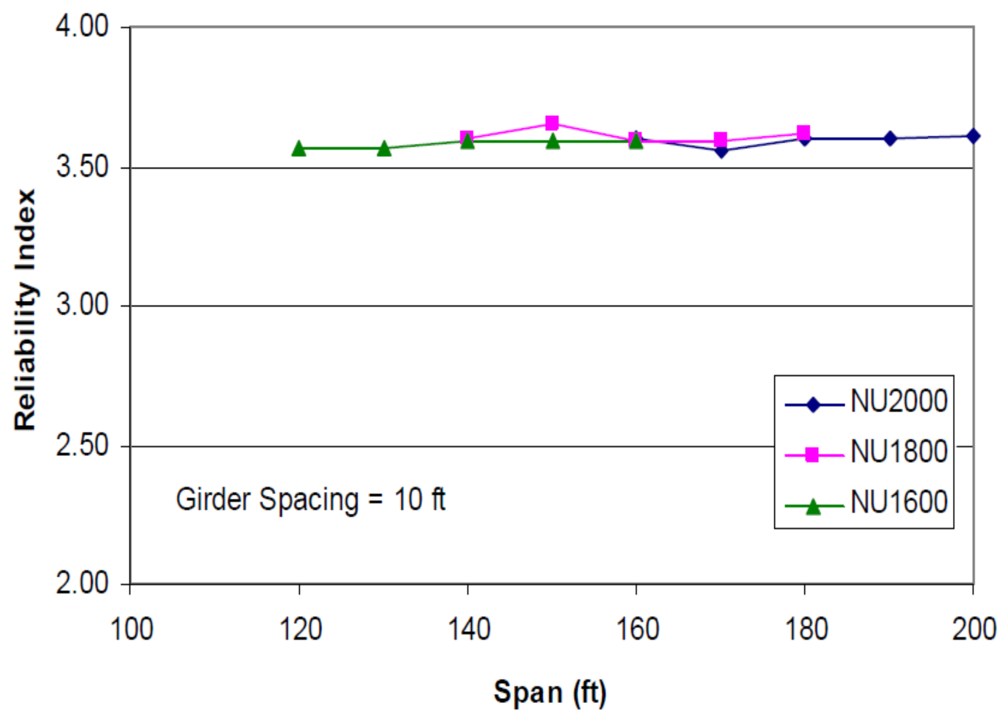

Figure 2.31: Shear reliability index of NU girder at different spans (Morcous et al. 2007).

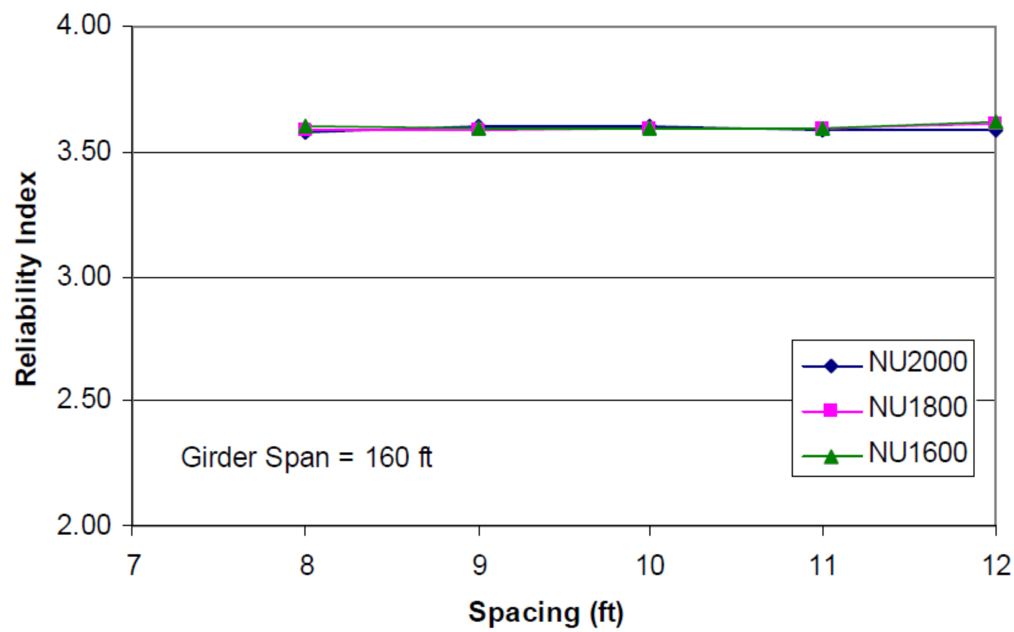

Figure 2.32: Shear reliability index of NU girder at different girder spacing (Morcous, et al. 2007).

The reliability of girder bridges using special type of concrete (ultra performance concrete UHPC) was investigated by some researches, like Stienberg (2010), Graybeal (2006), Imani and Frangopol (2002), and Reeves (2004). The results of reliability analyses show that the AASHTO LRFD code provides the most consistent level of reliability.

Cheng (2013) presented a new methodology for serviceability reliability analysis of prestressed concrete bridges. The method integrates the advantages of the Artificial Neural Network (ANN) method, First Order Reliability Method (FORM) and the importance sampling updating method. As a new feature included in the method was the introduction of an explicit approximate limit state function. The explicit formulation of the approximate limit state function is derived by using the parameters of the developed ANN model. Once the explicit limit state function is obtained, the failure probability can be easily estimated by using a hybrid reliability method consisting of the FORM and the importance sampling updating method. However, the method focused only on the serviceability performance of the prestressed girder bridges, specifically deflection and cracking control. Their results highlighted that the reliability indices are very sensitivity to live load and initial stress in prestressing tendon. As shown in Figure 2.33, the method converges quickly since, with 2,000 samples, the coefficient of variation of the probability of failure is less than 5%. It can be learned from Figure 2.34 that the reliability of the prestresed girder bridges bridges is highly influenced by the initial stress in prestressing tendon. As the initial stress in prestressing tendon increases, the estimated reliability index increase. This means that accurate determination of the initial stress in prestressing tendon is very important in obtaining reliable probabilistic results.

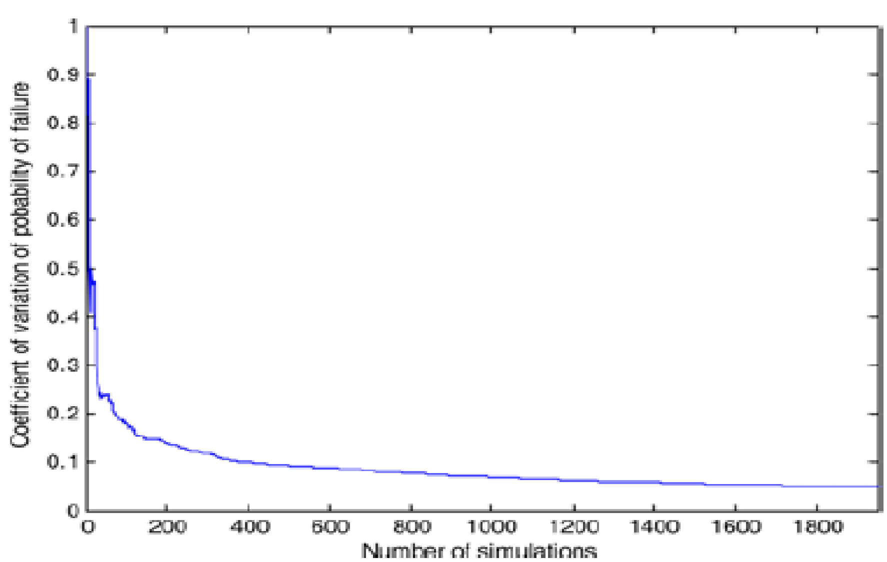

Figure 2.33: Coefficient of Variation of Probability of Failure versus Number of Simulations (Cheng 2013)

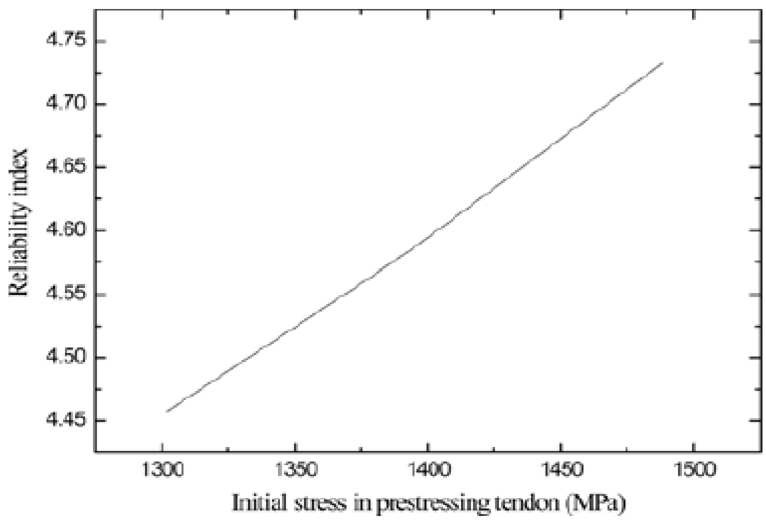

Figure 2.34: Reliability index for various initial stress in prestressing tendon (Cheng, 2013).

2.3 Design Optimization of Prestressed Girder Bridges

Traditionally, the process of design in structural engineering has relied mainly on the designer's experience, intuition, and ingenuity. Although this process has worked well, as evidenced by the existence of many fine structures, it has led to a less than rigorous approach to design optimization. It has generally revealed conservative designs that were not the best possible (Hassanain and Loov 2003).

As the prestressed girder bridges are very popular and widely used all over the world, particularly in the North America, much work has been done during the last three decades in optimizing the design of this type of bridges (Sirca and Adeli, 2005).

Yu et al. (1986) utilized the generalized geometric programming to the optimal design of a prestressed concrete bridge girder. The actual cost of construction consisting of prestressing, formwork and concrete was minimized. Constraints were formulated as stipulated by the British Code of Practice CP110. The constraints of the geometric program related to bending and shear stresses. A sample design was presented and sensitivity studies were performed to test the influence of major design parameters on cost factors. All design variables were deterministic. The uncertainty involved in the design variables, loads, and resistance has not been considered. Such optimization process could achieve cost saving but may, very possibly, be unsafe.

Lounis and Cohn (1993) presented a methodology to transform the multi-objective optimization into equivalent single-objective optimization problem by applying the $\boldsymbol{\varepsilon}$-constraint (trade-off) approach. As case studies, Lounis and Chon applied their methodology to optimize the prestressed girder bridge with different span length and bridge width. Figure 2.35 shows the bridge cross section used in one of the case studies considered. The constraints included in the serviceability and ultimate limit states requirements of the Ontario Highway Bridge Design Code OHBDC: *Ontario* 1983) were adopted. Some of the case studies were made according to AASHTO specifications. The design variables were the girder spacing S, deck overhang $S^{/}$, prestressing force P , and tendon eccentricities e_e and e_c at end and midspan, respectively. The optimization process performed deterministically.

The application of discretized continuum-type optimality criteria (DCOC) has been presented by Adamu and Karihaloo (1995) to obtain the minimum cost design of prestressed concrete girders. The design variables included the cross sectional area of the girder, the area of prestressing strands, the area of the normal reinforcements, and the surface area of the formwork. The constraints were those included in the Australian Standards AS 3600-1986. No uncertainty consideration was made to control the safety level reserved in the final optimized configuration.

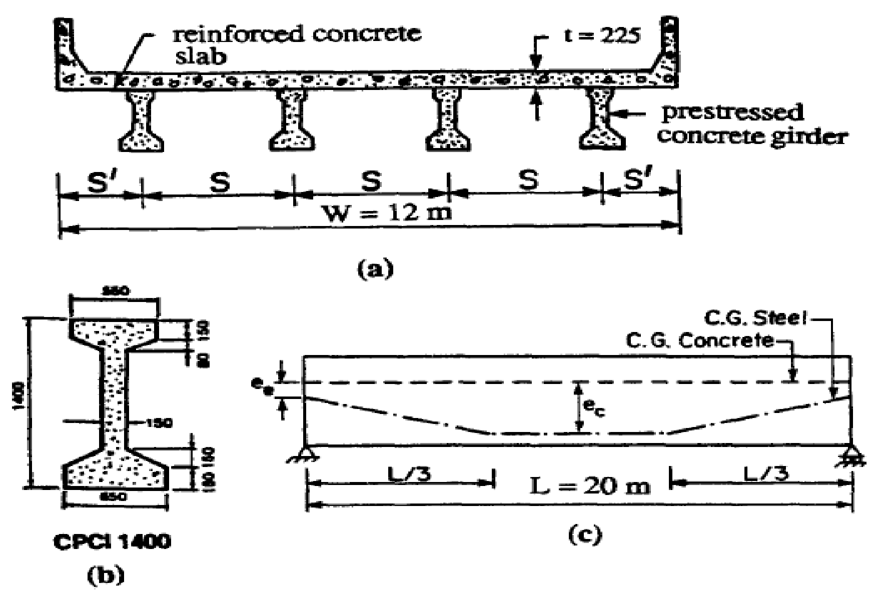

Figure 2.35: Case study considered by Lounis and Chon, (1993) : (a) Bridge cross section; (b) Girder cross section; (c) Tendon Layout.

A methodology for deterministic design optimization of simply supported prestressed girder bridges has been presented by Barakat et al.(2002). As an optimization technique, the method of Feasible Directions (FD) was adopted. This method finds the minimum of a constrained function by first finding bound on the solution and then using polynomial interpolation. The old AASHTO Standard (allowable stress design approach 1989) was used to define the constraint functions.

Sirca and Adeli (2005) presented an optimization method for minimizing the total cost of the prestressed girder bridge system. The problem was deterministically characterized by both discrete real and integer variables. A total cost function is defined to include the cost of deck concrete, prestressed concrete, normal reinforcement, prestressing strands, and formwork. The design variables considered included the number of beams, the cross-sectional area of the precast girder, the area of prestressing strands, the deck thickness, the area of normal reinforcement, and the surface area of the formwork. The constraints were derived from the requirement of the AASHTO specifications. In order to generate the parameters used in the constraint equations, a counterpropagation neural CPN network was developed to obtain the average flange thickness, the distance from the top of the member to the centroids of the pre stressing steel, the thickness of the web, and the width of the flange of the I-beams used in the bridge design for a given cross-sectional area. The topology of the CPN network, presented in Fig.2.36, consists of an input layer with one node, a competition layer with six layers (equal to the number of standard I-beam shapes), an interpolation layer, and an output layer, each with four nodes. The prestress losses were not considered which can be considered as a serious drawback.

By integrating the genetic algorithm (GA) technique and the artificial neural networks (ANN), Srinivas and Ramanjaneyulu (2007) developed a model for cost optimization of bridge deck configuration. Their method utilized ANN to evaluate the fitness and constraint violations in GA optimization process. Grillage analysis was used to model the bridge deck configurations. The study also considered the correlation between sectional parameters and design responses.

Rana and Ihsan (2010) studied the optimization of the total cost, in the design process, of prestressed I-Girders for bridges with span lengths varies from 20 to 50m. An optimization algorithm called Evolutionary Operation (EVOP) was used. The objective was to minimize the total cost in the design process of the bridge system considering the cost of materials, fabrication and installation. The design variables considered were girder spacing, various cross sectional dimensions of the girder, number of strands per tendon, number of tendons, tendons configuration, slab thickness and ordinary reinforcement for deck slab and girder. Design constraints for the optimization are considered according to AASHTO Standard Specifications. The method was applied to a real life project and the optimized design revealed a total cost saving around 35%.

A topology and shape optimization of prestressed girder bridges was presented by Aydin and Ayvas (2010). An optimization design approach that uses a genetic algorithm GA has been utilized. The objective function was to minimize the cost of the girder. The design variables considered were the cross-sectional dimensions of the prestressed girders, the cross-sectional area of the prestressing steel and the number of beams in the bridge cross-section. The constraints considered were the limitations provided by AASHTO LRFD with respect to stresses and displacements. The solution obtained by the GA was up to 28% more economical than the real life project. Figure 2.37 illustrates the difference in cross section between the real life project and the optimized one

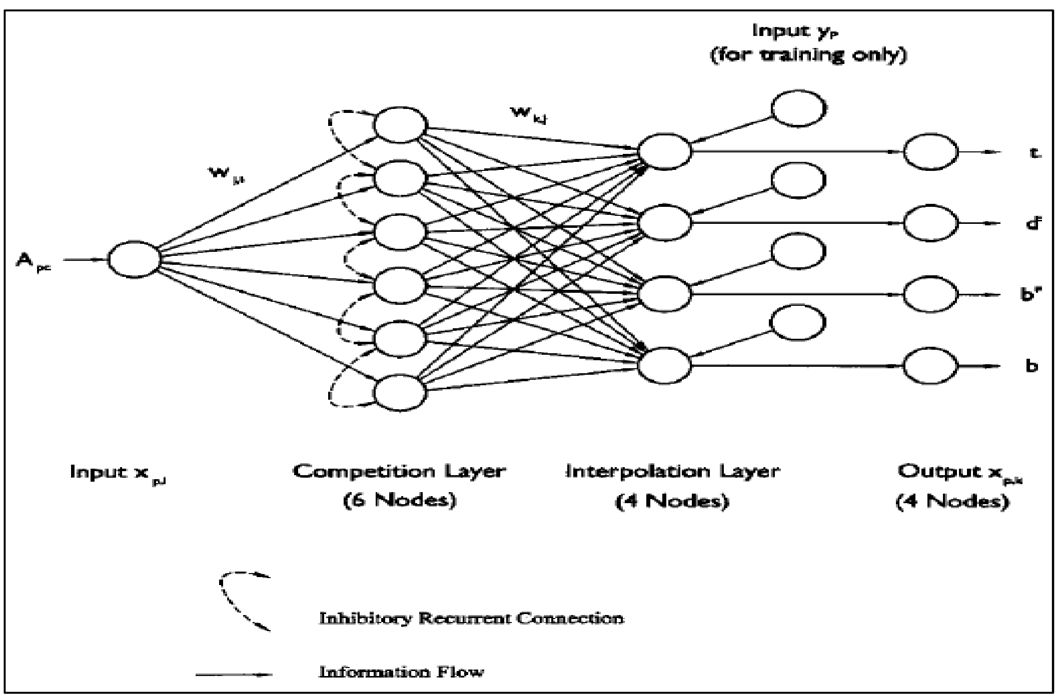

Figure 2.36: Counterpropagating neural model to determine precast prestressed concrete I-beam design parameters (Sirca and Adeli, 2005).

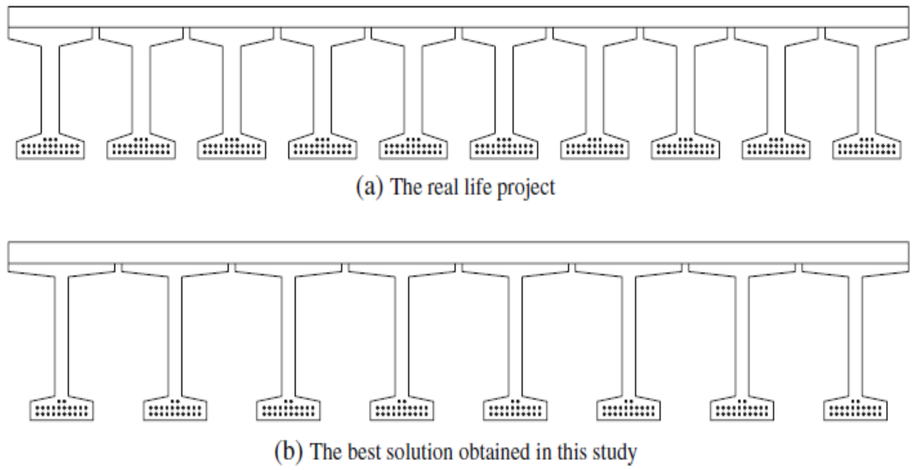

Figure 2.37 : Cross section before and after optimization (Aydin and Ayvas, 2010).

Ahsan et al., (2012) suggested a methodology for the cost optimization of prestressed I-girder bridges. The optimization problem was characterized by a combination of continuous, discrete and integer sets of design variables and multiple local minima. Their method was a continuation to the work done by Rana and Ahsan (2010). An optimization engine, based on updated evolutionary operation (EVOP) (Ghani, 2008), was utilized. The general outline of EVOP algorithm is illustrated in Figure 2.38. Different explicit and implicit constraints where considered. The requirements of AASHTO LRFD (2002) have been utilized. The methodology was used for a real-life bridge project and resulted in around 35% savings in cost per square meter of the deck area (Ahsan et al., 2012).

Similarly, Rana et al. (2013) applied the EVOP algorithm for the design optimization of two span continuous prestressed girder bridge. A cost saving of 36% per square meter of the deck area has been achieved. As shown in Figure 2.39, the minimum cost design problem is subjected to highly nonlinear, implicit and discontinuous constraints that have multiple local minima requiring an optimization method that seeks the global optimum.

A simulation-based design optimization method was suggested by Marti et al., (2013) and applied on the design of prestressed girder bridges. First, a cost sensitivity analysis has been performed. Then, a hybrid simulated annealing SA algorithm with a mutation operator (SAMO) was applied. Figure 2.40 illustrate the flowchart of the SA algorithm. SA was developed by Kirkpatrick et al. (1983) to find the best solution of a combinatorial optimization problem. The practical application of the algorithm is thoroughly described by

Dreo et al. (2006). The design was performed in accordance to the Spanish Code requirements. The parametric study showed a good correlation for the cost, geometric and reinforcement characteristics with the beam span length.

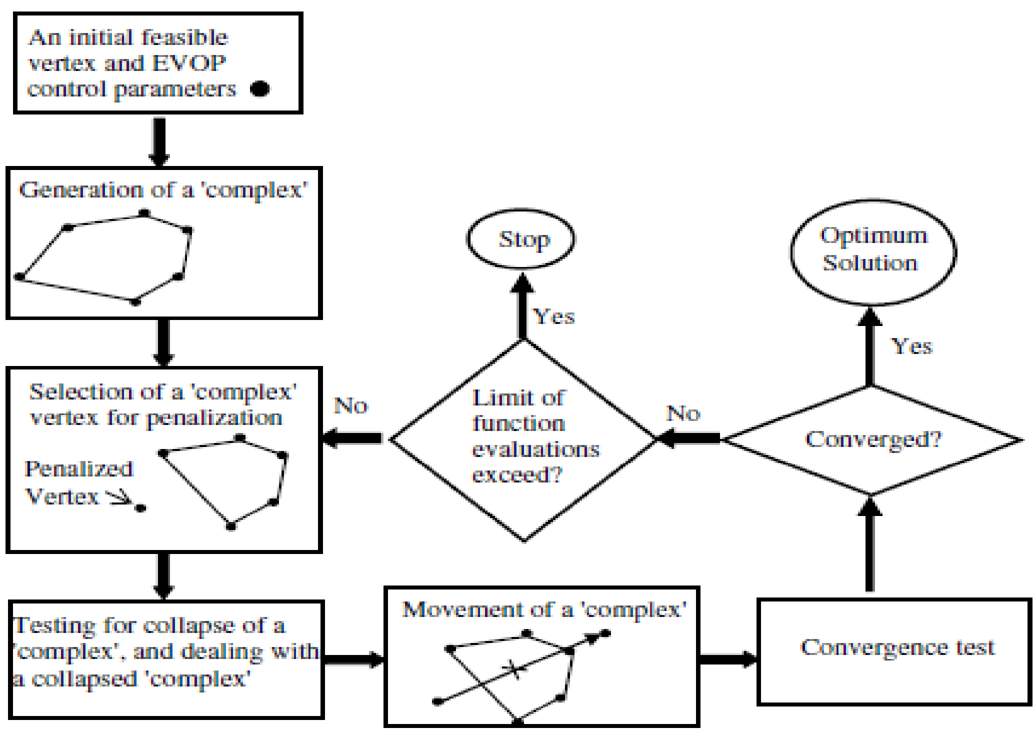

Figure 2.38: General outline of EVOP algorithm (Ghani, 2008)

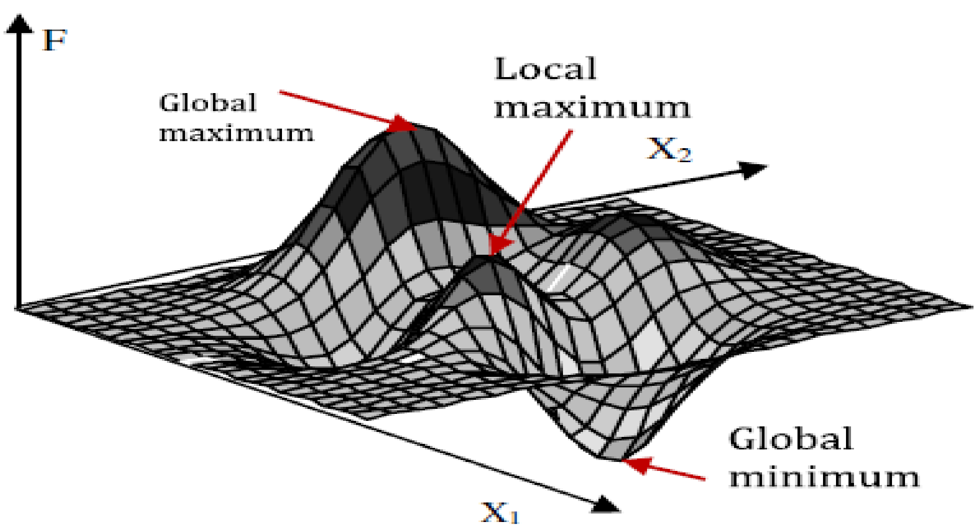

Figure 2.39: Global and local optima of a 2-D function (Rana et al., 2013)

In order to determine the optimum span number and optimum cross-sectional properties of multi-span bridges, the Genetic Algorithm (GA) approach was adopted by Aydin and Ayvaz (2013). The overall cost optimization of simply supported pre-tensioned I-girder bridges was investigated. Span number, cross-section dimensions of prestressed girders and the area of prestressing steel were considered as design variables. The bridge was designed according to AASHTO LRFD Standard Specifications for Highway Bridges. Working stress, ultimate strength, ductility limits, deflection, and geometry constraints are considered. Total cost of the bridge is taken as an objective function. The change of average of the penalized objective functions according to iteration number is demonstrated for the 10^{th} design in Figure 2.41 .The solution obtained by the proposed GA is up to 12.6% more economical than the considered application project.

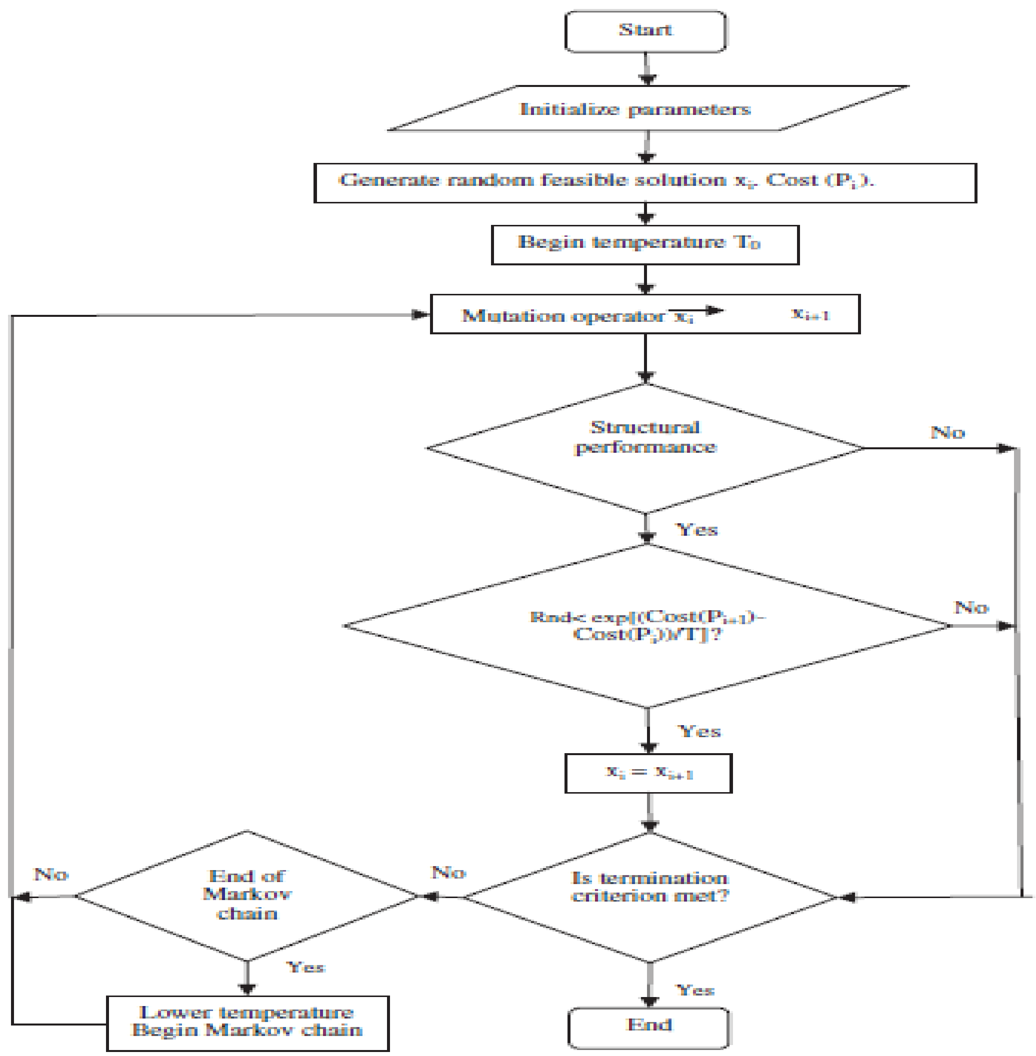

Figure 2.40: Flowchart of the hybrid simulated annealing process (Marti et al., 2013).

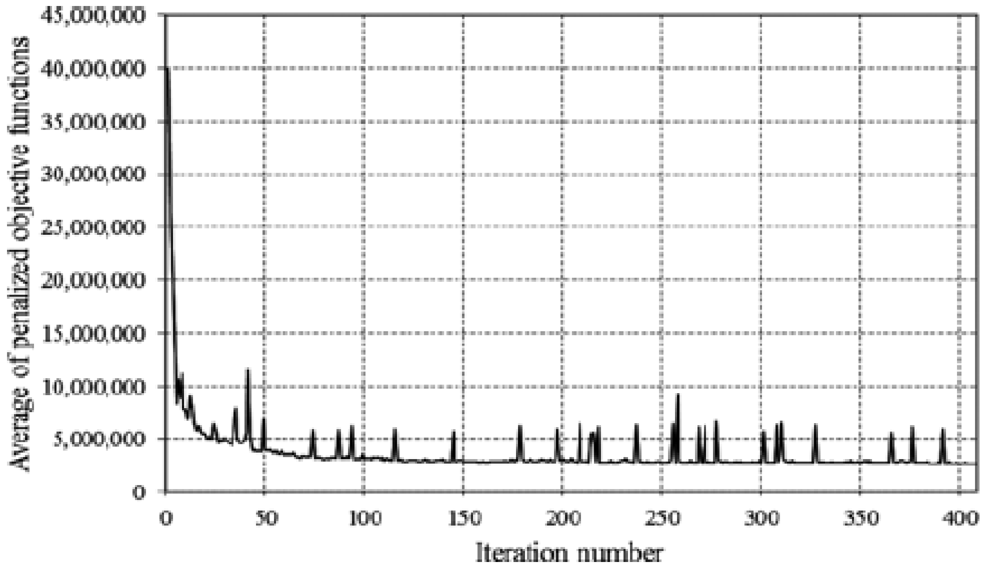

Figure 2.41 : Variation of Average of the Penalized Objective Functions for the10th Design (Aydin and Ayvaz, 2013).

The Feasible Direction (FD) method has been utilized by Madhkhan et al. (2013) to determine the optimum values of the design variables of simple and spliced pre-tensioned girder bridges. The life cycle cost of the whole structure was considered as the optimization objective function. AASHTO LRFD principles were used, assuming initial values for the design variables such as the dimensions of the girders and the deck, and the strands number. Then, using the analysis outcomes and considering the design criteria, the total cost of the structure, including that of the girders and slabs concreting, pre-tensioning cables performance, reinforcement and frameworks, were minimized as functions of the design variables.

2.4 Cost Estimation

2.4.1 Definition and purpose

Cost estimation is one of the most crucial and difficult tasks in project management. Cost estimating has influence on maintaining a contractor's success in insuring his/her profit. Cost estimating can be defined as a report of the approximate quantity of material, time and cost required to complete the construction of a project (Carr 1989). Rad (2001) define cost estimating as the art and science of using historical data and experience to forecast the duration total cost of a project.

Cost-estimating task is affected by different factors such as project site and environmental risk. The methods used to do cost estimates depend on the project stage; this is due to the change in the amount of information available from one stage to another. The main purpose of cost estimating is to provide detailed information that helps stakeholders to make major decisions related to the profitability of the project within a specified budget and the required time. The purposes of cost estimation summarized by Westeny (1997) as follows:

- Provides an evaluation and assessment of the capital cost for a specific work.
- Creates the basis for planning and monitoring project progress.
- Provides necessary information required for the preparation of project schedule such as durations, resources and tasks.
- Gives financial input necessary to prepare cash flow.

2.4.2 Cost Estimation Types

According to Stewart (1982), cost estimates are divided into two major types, which are the approximate and the detailed estimates. Butcher and Demmers (2003) also divided project cost estimates into two types: approximated conceptual cost estimates, which are conducted in the predesign stage, as well as the detailed estimates, which are performed during the post-design stage. Peurifoy et al (2002), however, categorized project cost estimates into three types: back of the envelope estimates, preliminary or conceptual estimates, and full funding estimates. On the other hand, Halpin (1985) categorized cost estimates into four types, which are: the conceptual estimate, preliminary estimate, engineer's estimate, and bid estimate. Cost estimates were also classified by Holm et al (2005) into four types as follows: preliminary cost estimate, elemental cost estimate, unit price estimate, and detailed cost estimation. These four types represent the estimating process, which starts with the conceptual and ends with the bid estimate.

AACE International in 2005 classified cost estimates into five classes. Each estimate class is identified by the project stage, purpose, preparation effort and level of accuracy. Table 2.22 illustrates the five classes of estimate.

Table 2.22: Cost Estimation Matrix for Process Industries (AACE International 2005)

	Primary Characteristic	*Secondary Characteristic*			
ESTIMATE CLASS	**MATURITY LEVEL OF PROJECT DEFINITION DELIVERABLES** Expressed as % of complete definition	**END USAGE** Typical purpose of estimate	**METHODOLOGY** Typical estimating method	**EXPECTED ACCURACY RANGE** Typical +/- range relative to index of 1 (i.e. Class 1 estimate) [a]	**PREPARATION EFFORT** Typical degree of effort relative to least cost index of 1 [b]
Class 5	0% to 2%	Screening or feasibility	Stochastic (factors and/or models) or judgment	4 to 20	1
Class 4	1% to 15%	Concept study or feasibility	Primarily stochastic	3 to 12	2 to 4
Class 3	10% to 40%	Budget authorization or control	Mixed but primarily stochastic	2 to 6	3 to 10
Class 2	30% to 75%	Control or bid/tender	Primarily deterministic	1 to 3	5 to 20
Class 1	65% to 100%	Check estimate or bid/tender	Deterministic	1	10 to 100

As shown in Figure 2.38, the accuracy of conceptual cost estimate ranges between 3 to 12. Expected accuracy range of 1 means the estimate has the highest level of accuracy, while expected accuracy range of 20 means the estimate has the lowest level of accuracy. Preparation effort value of 1 represents the typical degree of effort relative to the lowest effort needed in preparing the cost estimate, while preparation effort of 100 represents the highest degree of effort required to prepare the estimate.

2.4.3 Definition and Importance of the Conceptual Cost Estimation

Usually, the amount of information available prior to any design is limited. However, it is very important to the owner to assess the economic feasibility of proposed project before continuing with it. Thus it is crucial to prepare and use an approximate cost estimate during the feasibility study. The first effort made to predict the cost of the project is a conceptual cost estimate. It is always performed at the beginning of the project, where significant experience and judgment are required to prepare a reliable conceptual cost estimate. Conceptual cost estimation is defined as the prediction of project costs that is performed before the availability of a significant amount of information and the completion of the work scope definition with the purpose of using it as the basis for important project decisions such as budget setting, allotment of funds and project continuity decisions. The importance of the conceptual cost estimate is that it helps controlling the project cost by providing the first check against the budget (Pratt, 2004). It also indicates cost overruns at the early stages of the project, which assists in reviewing the design for different alternatives. Adrian (1993) listed the purposes of conceptual cost estimates as follows:

- Provides help to owners during the economic feasibility study,
- Assists designers in controlling the budget of the design, and
- Helps the owner in establishing the funding of the project.

2.4.4 Characteristics of the Conceptual Cost Estimation

Each type of cost estimate has some unique characteristics due to the time needed in process, data available and time required by the process. Peurifoy et al (2002) identified three characteristics of the conceptual cost estimate. The first characteristic is that conceptual cost estimation is a mixture of art, visualizing the project and the construction detailed sequence and adjusting them into new conditions, and science, making use of the costs of past works. The second characteristic is that the accuracy of the estimate is highly related to the level of the information available by the scope of the project. The third characteristic is that it is limited to its resources, which are available information, time and cost. The information is restricted in detail and precision due to the fact that the estimate is developed in the early stage of the project. Time and cost are also restricted due to the need to screen several alternative designs and to define the feasibility of the project as quickly as possible.

2.4.5 Preparation of the Conceptual Cost Estimate

Generally, preparation of a conceptual cost estimate involves a sequence of activities (Peurifoy et al, 2002). The first activity that needs to be achieved is to study the scope of the project and to produce an estimating plan. The estimating plan contains information about cost analysis of previous similar projects, sketch plans of the proposed project and brief specifications of services for the proposed project. Next, historical data of similar past projects is to be collected. This activity is very critical because availability of any unsuitable selected data will undesirably affect the estimate. After that, adjustments are applied to the selected data to be suitable and compatible to the scope of the project. The consequential cost estimate is then submitted, describing in detail all the information, assumptions, procedures, and adjustments to management for decision-making. Figure 2.42 illustrates the conceptual cost estimation process.

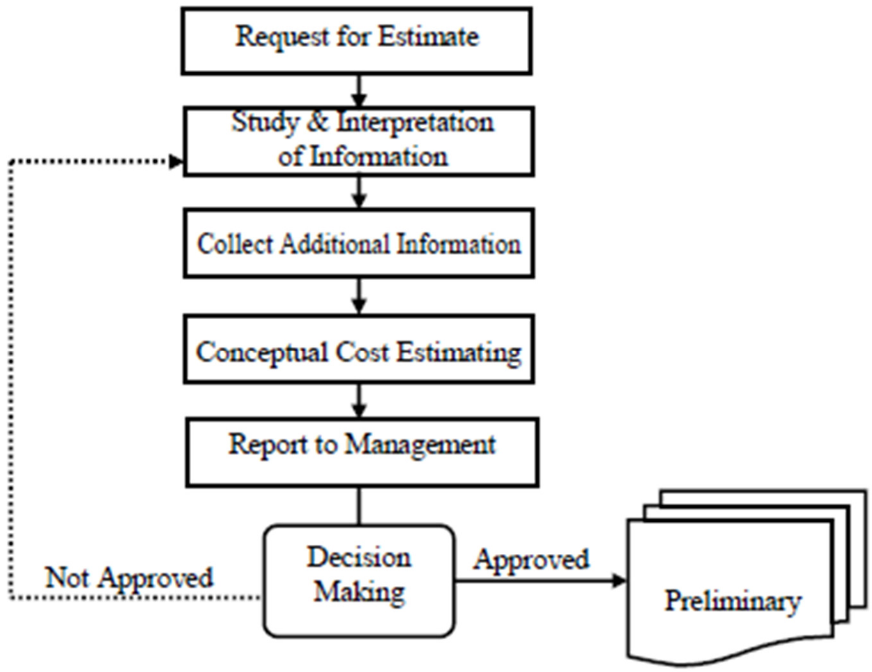

Figure 2.42 Conceptual Cost Estimation Process (Peurifoy et al 2002).

2.4.6 Conceptual Cost Estimate Adjustments

It is important to adjust the cost of similar previous projects to be suitable for the proposed project. There are two types of cost adjustments: time adjustment and location adjustment.

To have a reliable cost estimate it is important to have no difference in time between the historical project data and the proposed project. In the case of a time difference, it is necessary to adjust the cost data in order to have no time difference between the two projects. The time adjustment should represent the inflation or deflation of cost with respect to time. The inflation and deflation are due to differences in labor rates, material costs and interest rates (Peurifoy et al, 2002). In order to measure the difference, data index numbers are used as a means of expressing the difference. The index can be used to adjust previous cost information, calculate an equivalent compound interest rate and to forecast future projects. Various organizations publish indices that show the economic trends of the construction industry with respect to time. Using time adjustment indices, similar types of work from the past to the present or future period can be forecasted (Adrian, 1993).

Similarly to the time adjustment, cost estimation reliability will not be available if there is a difference in location between the past project and the proposed project, unless location adjustment is applied. The reason is that price levels differ from one region of the country to another. The factors affecting the variation in construction cost according to location are the construction cost of labor, material, and equipment in addition to other factors such as weather, climate, mobilization, labor availability, and productivity. Indices that measure the difference in cost with respect to geographical location are published by many organizations (Migiliaccio et al, 2013).

2.5 Selecting the Optimum Bridge Superstructure Type

The disposition of bridges involves obvious economical and safety implications (Nowak 2004). Several researchers invested valuable efforts towards optimizing the bridge design processes (Hong, 2002, Siriniva and Ramanjaneyulu, 2007). From their investigations it can be concluded that planning and designing bridges are partly art and partly compromise for the most significant aspects of structural engineering (Malekly et al, 2010).

Selecting the bridge superstructure type is a sensitive and important step in the conceptual phase of bridge planning and design process particularly for short and medium span bridges. Although it takes up to 10-15% of the design process, the conceptual phase influences the entire design output and quality (Wood and Agogino, 1996). Inefficient conceptual design concept will lead to design shortcomings that will be difficult to rectify in the detailed design stage (Xu et al , 2005).

The superstructure represents about 70% of the total bridge cost (Menn, 1990); therefore, an improper superstructure selection may lead to uneconomical project results besides reducing the quality of the structure.

Many factors must be considered and evaluated in terms of different conflicting criteria in the conceptual design of a bridge, leading to a large set of subjective or ambiguous data. Subjectivity can be considered as the main factor that affects the selection process of a bridge type at the conceptual design stage (Malekly, 2010).

A knowledge-based expert system was utilized by Burgoyne and Sham (1987) to develop a model for selecting the appropriate type of bridge structure. A backward chaining strategy, first suggested by Winston (1984), was adopted as a selection technique.
Choi and Choi (1993) developed an expert system SUPEREX that serves to select the best type of bridge superstructure based on experience and knowledge of the domain experts. The system was mainly composed of a working memory, knowledge base, and a database as shown in Figure 2.43. Different types of reinforced concrete, prestressed concrete, and steel bridges were considered. Five main stages govern the selection of bridge superstructure type by SUPEREX system as illustrated in Figure 2.44.

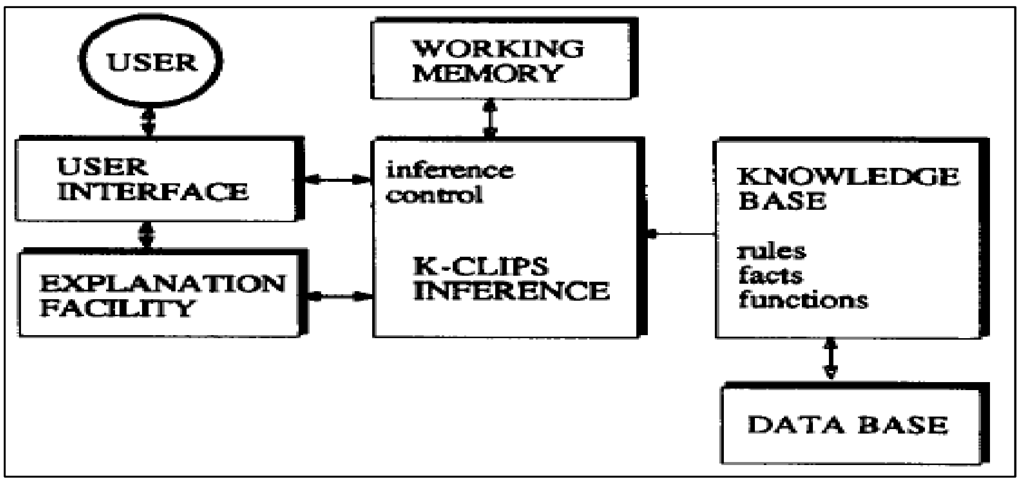

Figure 2.43: Model of SUPEREX (Choi and Choi, 1993).

Hammad and Itoh (1993) applied the object-oriented approach to develop an expert system model to help selecting the most appropriate bridge type. The bridge was broken down into group types: Section_Type, Deck_Type, Deck_Material, Structural_Type, etc. as shown in Figure 2.45. A number of sub-classes might be generated automatically. This action of generating new classes is called *expanding a class according to a classifier*.

Based on genetic algorithm (GA) optimization technique and computer graphics (CG), Furuta et al. (1995) developed a decision making support system to select the best bridge type from the aesthetic point of view. Different alternatives of bridge types were investigated. In order to evaluate the alternatives, the concept of psychovector is used to quantify the aesthetic factors of bridge structures. It was considered that the aesthetic of bridge structures consist of three basic items: 1) the structural configuration, 2) the functional factors, and 3) the harmony with surrounding environment. The methodology is illustrated in Figure 2.46.

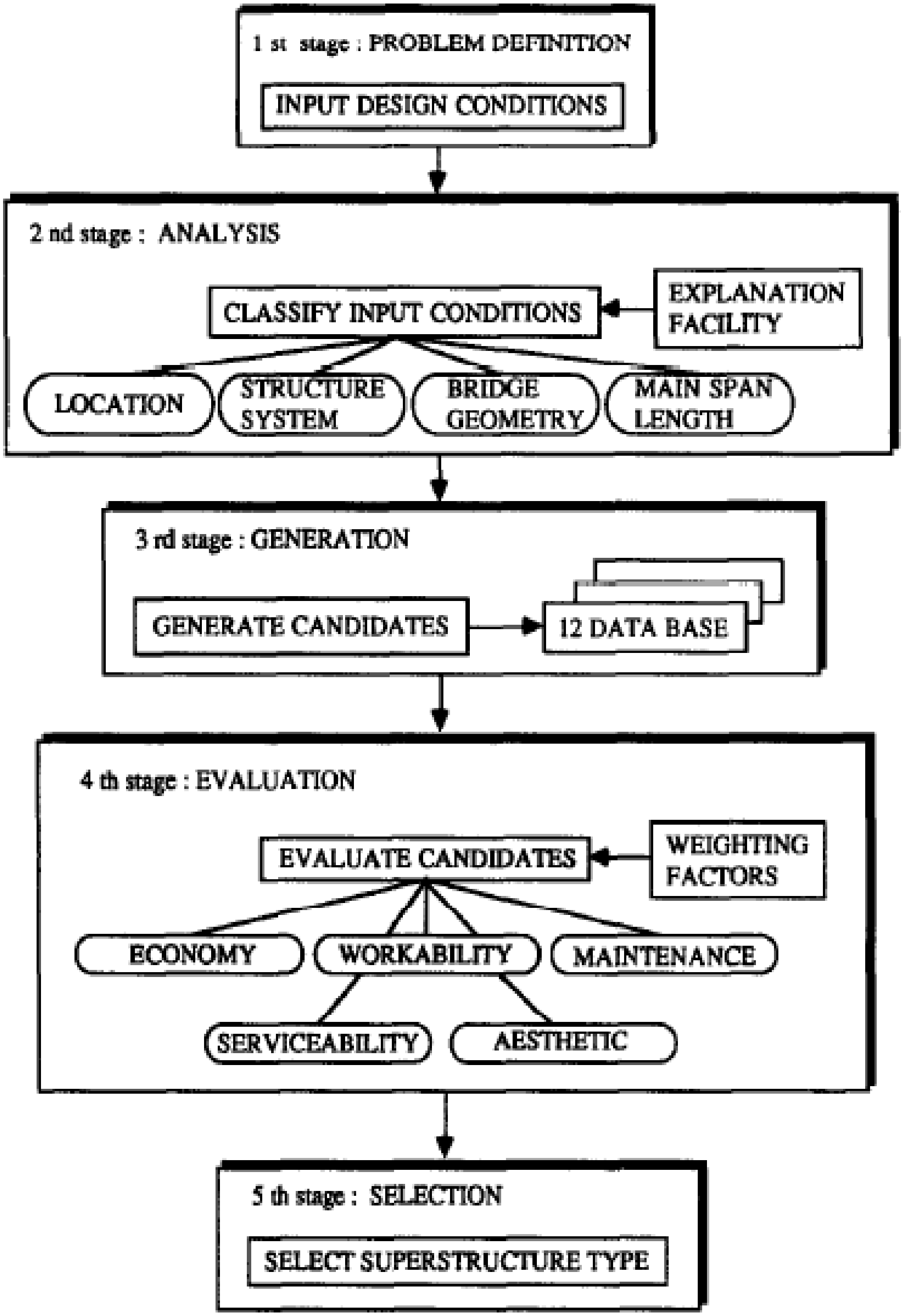

Figure 2.44: Selecting stages of SUPEREX (Choi and Choi, 1993)

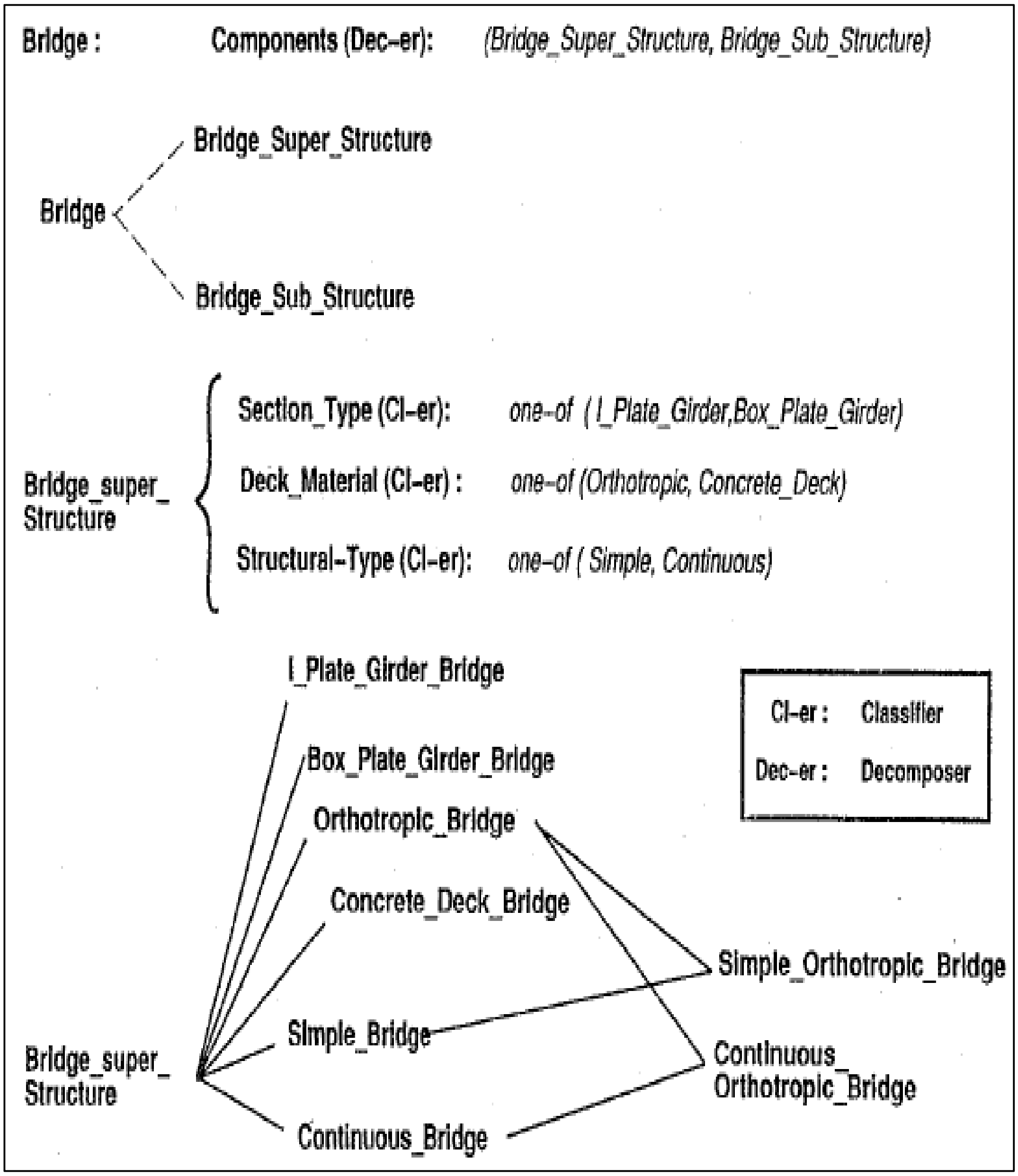

Figure 2.45: Usage of classifiers and decomposers (Hammad and Itoh 1993).

An integrated optimization-based methodology to select the best type of bridge superstructure was proposed by Malekly et al. (2010). The projects requirements were transformed to design requirements by the application of Quality Function Deployment (QFD). Then, Technique for Order Performance by Similarity to Ideal Solution (TOPSIS) was utilized to select the best superstructure. Fuzzy linguistic variables were applied to evaluate each alternative. The flowchart shown in Figure 2.47 illustrates that methodology.

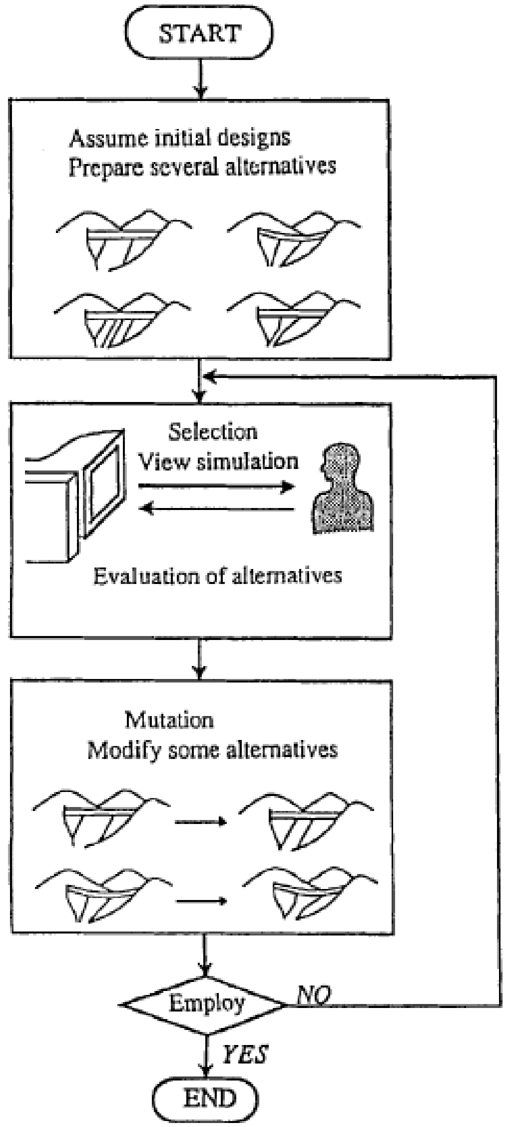

Figure 2.46: Flowchart of GA optimization of bridge type (Furuta et al. 1995)

A hierarchy process (AHP) integrated with a specific mathematical simulation software, originally called Kane simulation (KSIM), was utilized by Farkas (2011) to develop a model to select the most appropriate bridge type. The AHP consists usually of three levels: the goal of the decision at the top level, followed by a second level containing the criteria by which the alternatives, located in the third level, will be evaluated. The relevant variables governing the bridge type selection were, first, defined and listed. Then the evaluation of those variables was made by a team of a decision makers (experts). After that, a matrix $M = [m_{ij}]$ was developed, called a *cross-impact matrix*. The entries m_{ij} of this matrix M were elicited from subjective judgements made by the group of experts. M Summarized

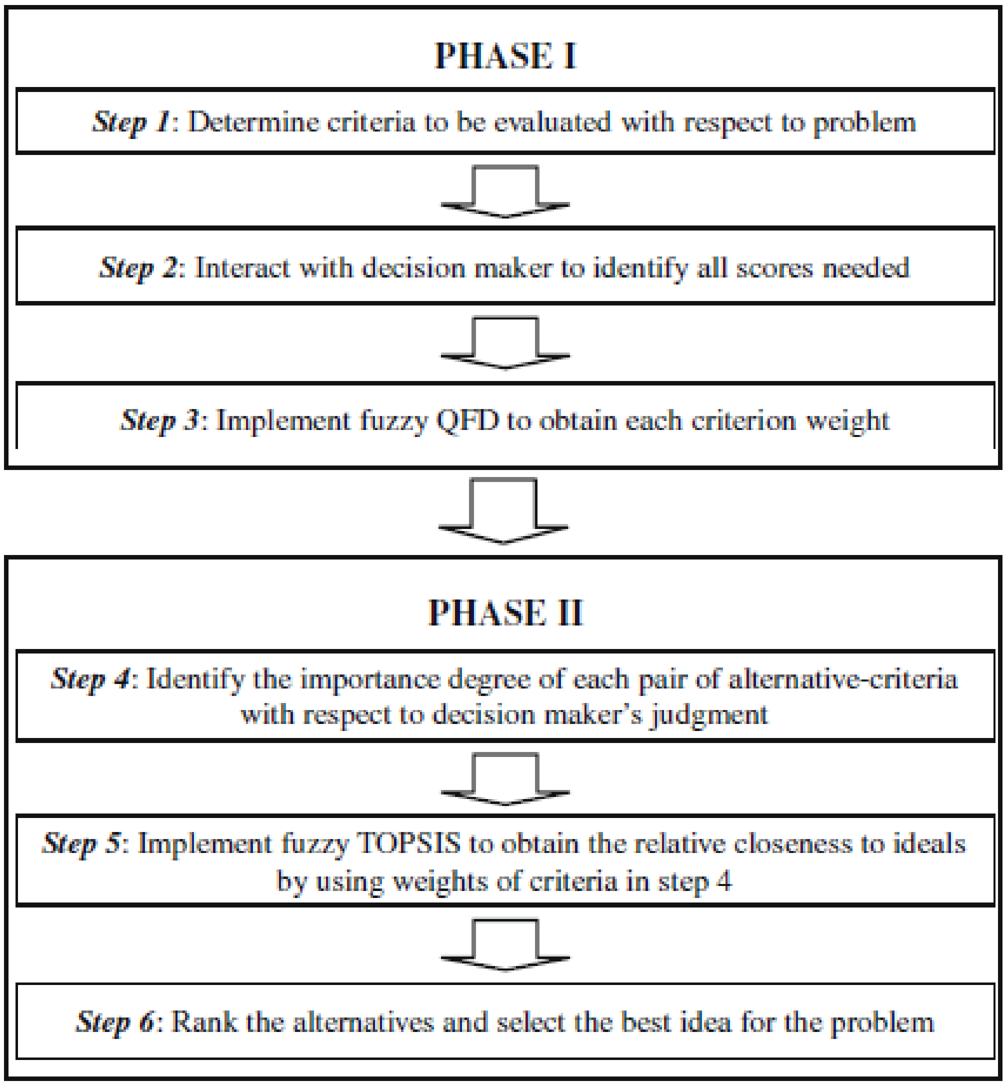

Figure 2.47: The methodology proposed by Malekly et al., (2010).

the interaction (correlation) between the variables. The variables considered were: Engineering Feasibility (EF), Capital Cost (CC), Maintenance (MA), Aesthetic (AE), Environmental Impact (EI), and Durability (DU). Different types of bridge superstructure have been investigated. Once the model's configuration has been agreed upon, the simulation engine will function to revel the best bridge type.

Bitarafan et al.,(2013) developed a methodology for selecting the best design scenario for bridges including most appropriate type of bridge structure. Their methodology integrated the analytical hierarchy process (AHP) with decisions from a team of experts. In order to determine the best-case alternative, the following criteria were considered: casualty and vulnerability reduction, possibility of localization of sensor technology, performance costs, performance speed and maintenance. Pairwise comparison technique was adopted.

As presented above, the experts' judgments have been utilized by almost all the research efforts to choose the most appropriate type of bridge structure. However, no researcher has considered or incorporated the uncertainty associated with the expert judgement. This would, with high possibility, lead to erroneous results. Based on that and as a new contribution, Al-Delaimi and Dragomirescu (2015) developed a new methodology for choosing the optimum type of bridge superstructure. The methodology, which is presented in detail in chapter seven of this proposal, probabilistically models the experts' decisions by appropriate statistical distributions, then, combines the experts' decisions with, decision tree analysis and sensitivity analysis to reveal the most appropriate type of bridge superstructure. Both the design requirements and the client's requirements are defined and treated as variables. Due to different sources of uncertainties, the expert's decision is treated as a random variable with PERT statistical distribution. Then, a combined probability distribution function representing the expert team is allocated to each variable used in the model. The possible dependency (correlation) between the statistical distributions related to design requirements and the client's requirements is also considered. For that purpose, a Monte Carlo simulation is utilized to generate random numbers from the combined distributions. Using those random numbers, a correlation matrix can be built. A decision tree analysis is then performed to obtain the best type of bridge superstructure. In order to investigate the influence of the independent variables on the dependent variables, a sensitivity analysis is suggested.

2.6 Summary

A comprehensive literature review was conducted to investigate the available literature and the contribution of previous researches on reliability analysis and design optimization of prestressed girder bridges.

The literature on bridge reliability focused on derivation of the statistical parameters of the load and resistance models as well as on the assessment of the reliability of prestressed girder bridges.

The derivation of the statistical parameters of load and resistance models started in the mid 1970s. The LRFD bridge design codes' calibration (AASHTO and OBDC) was made based on the load and resistance models developed in early 1990s. Based on those models, the reliability evaluation of prestressed girder bridge was made accordingly. However, due to recent experimental and analytical work, the statistical parameters of Live load model was updated (Rakoczy 2011, Nowak and Rakoczy 2012, and Nowak and Rakoczy 2013). Based on these updates, the statistical parameters of the load effects (bending, shear, and fatigue) need to be derived. This will be made in the next chapter. Also, both the statistical parameters of the material coefficient M and fabrication coefficient F were recently updated (Nowak and Szerszen 2011, and Nowak and Rakoczy 2012). Based on the updated M and F factors, the statistical parameters of the random variables corresponding to resistance (allowable stresses, flexural resistance, and shear resistance) need to be derived. This will be addressed in Chapter Three.

The reliability of prestressed girder bridges was assessed by some researchers focusing, mainly, on the ultimate strength (load carrying capacity) of the bridge. Based on the above mentioned updates in load and resistance models, the reliability of prestressed girder bridges need to be re-evaluated and updated. This will be made in Chapter Four using the statistical parameters derived in Chapter Three. Focusing on ultimate strength limit state, in evaluating bridge reliability, helps in rating existing bridges. However, for the sake of reliability-based design and/or design optimization, an all-in-one reliability model is required to estimate the reliability index with respect to all limit state functions as well as the overall system reliability. A comprehensive bridge reliability model (BREL) is provided by the current research.

Several researchers invested efforts and made contributions, during the last three decades, in the area of Deterministic Design Optimization (DDO) of prestressed girder bridges. The DDO treats the basic variables involved in the optimization problem as fixed values (uncertainty-free variables) (Beck and Gomes 2012). DDO could reveal considerable cost savings, however, the optimized structural configuration might not be safe, particularly with respect with serviceability and fatigue limit states. Alternatively, probabilistic approaches for design optimization aim at searching cost-effective solutions with assuring satisfactory safety levels by properly modelling and incorporating the uncertainties associated with the basic design variables (Chteauneuf, 2008). Such probabilistic approaches have not yet been applied to the design optimization of prestressed girder bridges. To bridge this gap, the current research provides, as a new contribution, two methodologies. The first one is the reliability-based design optimization which incorporates the failure probability and corresponding reliability index, with respect to every limit state function and mode of failure, as constraints in the optimization process. The details, formulation and application of this method are presented in Chapter Five. The second methodology of probabilistic optimization is the six sigma-based robust design optimization which is a quality approach that intends to ensure not only that the design performs as desired but also that the design consistently performs as desired. The details, formulation, and application of this methodology are illustrated in Chapter Six.

As presented in the previous section, the experts' judgments have been utilized by almost all the research efforts in choosing the most appropriate type of bridge structure. However, no researcher has considered or incorporated the uncertainty associated with the expert judgement. Based on that, the current research will continue the approach and methodology suggested by Al-Delaimi and Dragomirescu (2015) to develop a model that serves choosing the optimum type of bridge superstructure.

Chapter 3

Current Statistical Parameters of Random Variables Related to Load Effects and Resistance

3.1 Background

In structural reliability analysis, any limit state function, $g(R, Q)$, consists of two main parts: the resistance, R, and the load effect, Q, which are treated as random variables. The determination of the load effect is usually made according to pre-defined load model. Similarly, the resistance is obtained using pre-defined resistance model.

As explained in Chapter Two, most of the statistical parameters of the load models and resistance models were derived in the 1980s and 1990s (e.g. Ellingwood et al. 1980, Galambos, et al. 1982, Nowak 1995, and Nowak 1999). Then, those models were used to evaluate the reliability of prestressed girder bridges (e.g. Nowak and Zhou 1990, and Nowak et al.2001). However, new statistical parameters were derived for the live load models (Rakoczy 2011, and Nowak and Rakoczy, 2013). Also, new statistical parameters for material factors and fabrication factors have been derived (Rakoczy 2011, and Rakoczy and Nowak 2012). This means that the old load models and resistance models are no longer valid to provide accurate reliability analysis. Based on that, it becomes necessary to derive new statistical parameters for the random variables related to the load effects and to the resistance. This will be addressed in this Chapter. Also, the reliability analysis of prestressed girder bridges should be revised and updated, accordingly; this will be conducted in Chapter Four.

The reliability analysis of prestressed girder bridges is highly dependant to the type of the prestressed girders used in the design. Different types of standard prestressed girders exist all over the world. However, The most popular and comon types (families) of standard prestressed girders, used in the design of prestressed bridges, particularly in North America, are:

- AASHTO Girders: Type I, Type II, Type III, Type IV, Type V, and Type VI.

- CPCI Girders: CPCI 900, CPCI 1200, CPCI 1400, CPCI 1500, CPCI 1600, CPCI 1900, and CPCI 2300.
- Bulb T-Girders: NEBT1000, NEBT1200, NEBT1400, NEBT1600, and NEBT1800.
- NU Girders: NU 900, NU 1100, NU 1350, NU 1600, NU 1800, and NU 2000.

The current research proposes a probabilistic-based optimization model that utilizes the above mentioned types of standard girders. In the following sections, the nominal properties of those girders and their statistical parameters with respect to load and resistance models are presented. However, the proposed model is also flexible to utilize any other type/shape of girder that might be suggested by the user. To do so, the nominal dimensions of the new girder type/shape need to be added to the database spreadsheet of the proposed model; then the statistical parameters of the random variables related to the load and resistance models can be obtained as explained in following sections.

3.2 Nominal dimensions and properties of the standard girders

In this section, the shape, nominal dimensions, and nominal properties of AASHTO Girders, CPCI Girders, Bulb-T Girders, and NU Girders are presented.

3.2.1 AASHTO Girders

The AASHTO Standard girders have the shapes and nominal dimensions illustrated in figure 3.1. The nominal properties are shown in Table 3.1.

Table: 3.1 Nominal properties of AASHTO Girders.

Girder Type	Area (mm^2)	$I\ (mm^4)$	$Z_b(mm^3)$	$Z_t\ (mm^3)$
AASHTO I	214193	11028231598	33848279	28616041
AASHTO II	238064	21218955250	52775146	41416045
AASHTO III	360967	52191403453	101353189	83100164
AASHTO IV	509031	108528434340	172750085	145997051
AASHTO V	653547	216924247324	267247897	275108879
AASHTO VI	699999	305230951205	330312080	337371820

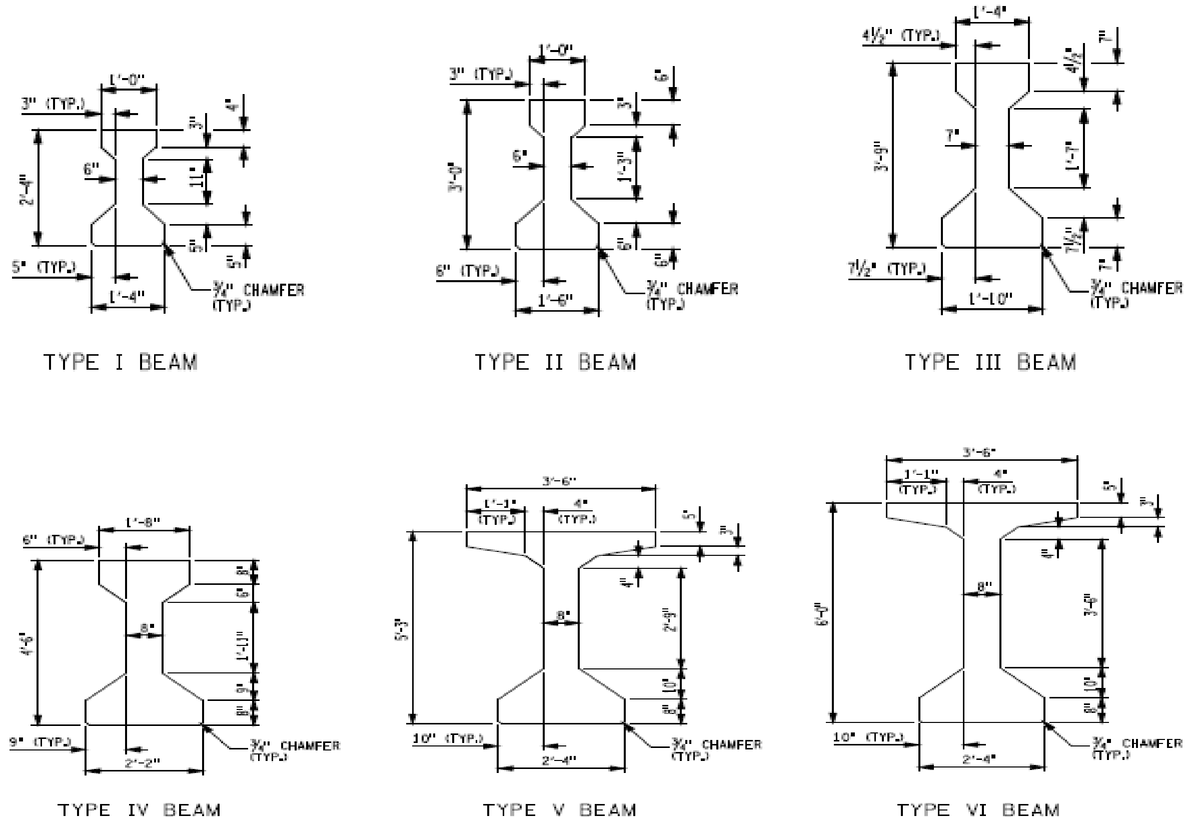

Figure 3.1: Shapes and nominal dimensions of AASHTO Girders.

3.2.2 CPCI Girders

The Canadian Precast Institute CPCI developed the CPCI Standard girders that have the shapes and nominal dimensions illustrated in figure 3.2. The nominal properties are shown in Table 3.2.

Table 3.2: Nominal properties of CPCI Girders.

Girder Type	Area (mm^2)	I (mm^4)	$Z_b(mm^3)$	Z_t (mm^3)
CPCI 900	227,250	19,943,417,450	49,895,595	3,986,3154
CPCI 1200	331,750	55,370,372,721	104,604,277	82,560,012
CPCI 1400	427,500	104,925,478,015	164,548,482	137,635,509
CPCI 1500	499,375	151,383,499,801	203,243,716	200,464,746
CPCI 1600	515,375	178,128,870,775	224,490,210	220,861,533
CPCI 1900	563,375	274,136,159,686	291,672,422	285,521,875
CPCI 2300	627,375	441,936,751,353	389,053,327	379,647,419

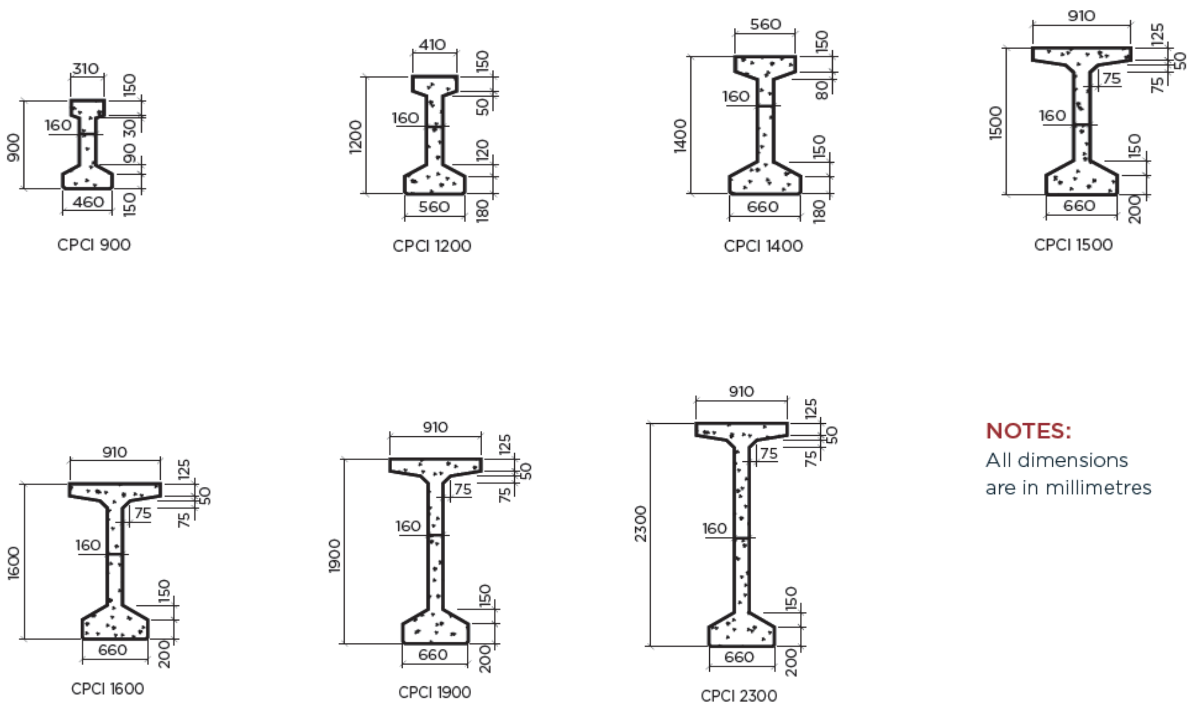

Figure 3.2: Shapes and nominal dimensions of CPCI Girders.

3.2.3 Bulb-T (NEBT) Girders

The Bulb T-Girders (sometimes referred to as New England Bulb-Tee NEBT Girders) have the shapes and nominal dimensions illustrated in figure 3.3. The nominal properties are shown in Table 3.3.

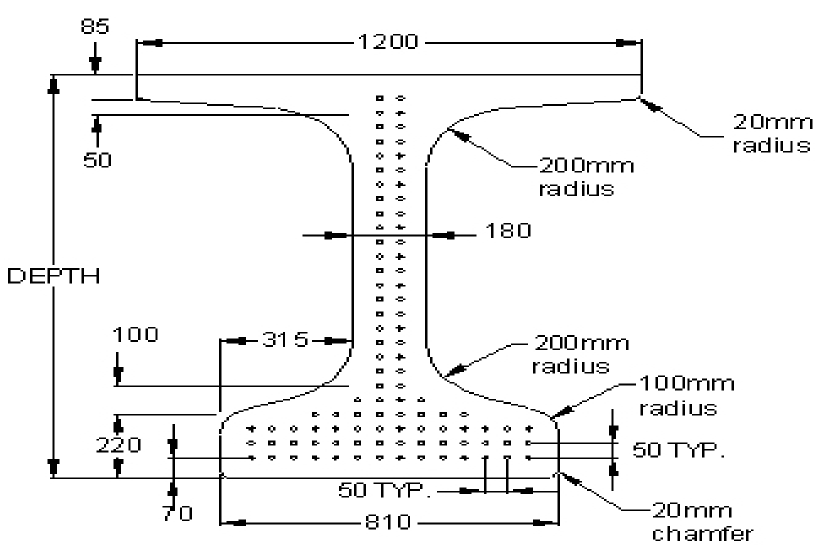

Figure 3.3: Shape and nominal dimensions of Bulb-T (NEBT) Girders.

Table 3.3: Nominal properties of Bulb-T (NEBT) Girders.

Girder Type	Area (mm^2)	$I\ (mm^4)$	$Z_b(mm^3)$	$Z_t\ (mm^3)$
NEBT 1000	462300	60511294056	593574	534980
NEBT 1200	498300	96259978109	793218	704117
NEBT 1400	534300	141892790084	1006004	886671
NEBT 1600	570300	198145234424	1230967	1082062
NEBT 1800	606300	265749133172	1467608	1289921

3.2.4 NU Girders

The NU Girders (sometimes referred to as the University of Nebraska Girders) have the shapes and nominal dimensions illustrated in figure 3.4. The wide top flange of this type of girders offers excellent work platform and, also, helps reducing the required structural thickness of the deck. The nominal properties are shown in Table 3.4.

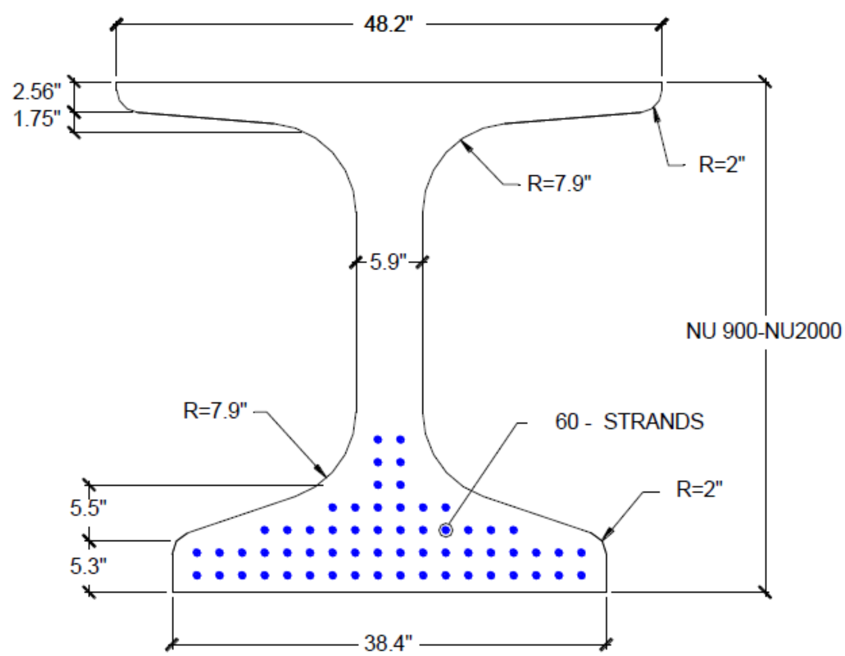

Figure 3.4: Shape and nominal dimensions of NU Girders.

Table 3.4: Nominal properties of NU Girders.

Girder Type	Area (mm^2)	$I\ (mm^4)$	$Z_b (mm^3)$	$Z_t\ (mm^3)$
NU 900	397280	44139954792	110553917	88297885
NU 1100	427351	72799662035	149943693	118507036
NU 1350	464654	120174530183	201960005	159446366
NU 1600	502338	182474168505	257754264	204507501
NU 1800	532409	243420209564	304529760	243048694
NU 2000	562099	314033620666	352646418	283302555

The statistical parameters of the random variables related to the load effects and resistance models will be obtained in the following sections.

3.3 Statistical parameters of the random variables with respect to the load effects

In this section the statistical parameters (bias factor and coefficient of variation) of the load effects (bending moment, shear, cracking moment, and fatigue stress range) are derived. The following steps have been followed, in the current study, in order to determine the statistical parameters of the random variables related to the load effects:

- For different span lengths (from 15 m to 60 m) and different girder spacing (from 1m to 3.25m), the nominal values of load effect were calculated, at critical sections, as per AASHTO LTFD (7th Edition 2014) code. Bending moment and shear were calculated for Strength I Limit State. Service I Limit State was considered for cracking moment, while Fatigue I Limit state has been followed to calculate the fatigue stress range.

- The bias factors and coefficients of variation of each load (dead load, live load, and dynamic impact load) were, then, applied to calculate the mean and standard deviation of the load effects using the *Central Limit Theorem CLT*, assuming that the probability density function PDF of each load has a normal distribution (Nowak and Collins 2000). According to the CLT, the sum of n independent random variables x_i, will asymptotically approach a normal distribution with known mean and standard deviation (Vose 2009):

[3.1] $$\sum_{x=1}^{n} x_i \approx Normal(n\mu\,, \sigma\sqrt{n}\,)$$

where, μ and σ are, respectively, the mean and standard deviation of the distribution from which the n samples are drawn.

For that purpose, Monte Carlo Simulation was performed with 25,000 cycles.

- Then, the bias factor and coefficient of variation of the load effect (bending, shear, cracking moment, and fatigue) are calculated using Equations 3.2 and 3.3, respectively.

[3.2] $$Bias\ factor = \frac{Mean\ value\ of\ load\ effect}{Nominal\ value\ of\ load\ effect}$$

[3.3] $$CoV = \frac{Standard\ deviation\ of\ the\ load\ effect}{Mean\ value\ of\ the\ load\ effect}$$

Table 3.5 shows the obtained statistical parameters related to AASHTO Girders, with respect to the load effects (i.e. ultimate bending moment, ultimate shear force, cracking moment, and fatigue stress range). Similarly, for CPCI Girders, the statistical parameters of load effects are shown in Table 3.6. While, Table 3.7 and Table 3.8 demonstrate the statistical parameters of the load effects with respect to Bulb-T (NEBT) Girders and NU Girders, respectively. As shown in those Tables, different span lengths were considered. These statistical parameters will be used to perform the reliability analysis of prestressed girder bridges in Chapter Four. However, to perform such reliability analysis, the statistical parameters of the random variables related to resistance model need to be derived. This will be conducted in the following section.

Table 3.5: Statistical parameters of load effects for AASHTO Girders.

Girder Type	Span (m)	Mu λ	Mu CoV	Vu λ	Vu CoV	Mcr Λ	Mcr CoV	Stress Range Fatigue I λ	Stress Range Fatigue I CoV
AASHTO I	10	1.246	0.080	1.196	0.100	1.056	0.067	1.156	0.108
	15	1.242	0.080	1.196	0.100	1.055	0.067	1.156	0.108
	Average	**1.244**	**0.080**	**1.196**	**0.100**	**1.056**	**0.067**	**1.156**	**0.108**
AASHTO II	15	1.240	0.080	1.194	0.090	1.054	0.059	1.155	0.108
	20	1.242	0.090	1.192	0.090	1.082	0.066	1.157	0.108
	25	1.240	0.090	1.194	0.090	1.083	0.078	1.157	0.108
	Average	**1.241**	**0.087**	**1.193**	**0.090**	**1.073**	**0.068**	**1.156**	**0.108**
AASHTO III	15	1.242	0.080	1.194	0.090	1.049	0.055	1.155	0.107
	20	1.238	0.080	1.192	0.090	1.072	0.059	1.153	0.110
	25	1.240	0.080	1.190	0.090	1.079	0.061	1.154	0.108
	Average	**1.240**	**0.080**	**1.192**	**0.090**	**1.067**	**0.058**	**1.154**	**0.108**
AASHTO IV	20	1.238	0.080	1.190	0.090	1.067	0.054	1.152	0.109
	25	1.238	0.0.80	1.192	0.090	1.072	0.059	1.152	0.109
	30	1.236	0.080	1.190	0.090	1.078	0.060	1.152	0.109
	35	1.220	0.090	1.190	0.090	1.086	0.061	1.152	0.109
	Average	**1.233**	**0.083**	**1.191**	**0.090**	**1.076**	**0.059**	**1.152**	**0.109**
AASHTO V	20	1.224	0.090	1.192	0.090	1.061	0.052	1.153	0.109
	25	1.222	0.090	1.192	0.090	1.067	0.052	1.152	0.109
	30	1.220	0.090	1.190	0.090	1.072	0.053	1.150	0.109
	35	1.222	0.090	1.190	0.088	1.079	0.053	1.150	0.109
	40	1.220	0.090	1.188	0.088	1.083	0.055	1.152	0.109
	Average	**1.222**	**0.090**	**1.190**	**0.089**	**1.072**	**0.053**	**1.151**	**0.109**
AASHTO VI	25	1.220	0.090	1.188	0.082	1.064	0.052	1.152	0.109
	30	1.186	0.090	1.187	0.080	1.069	0.052	1.150	0.109
	35	1.188	0.090	1.187	0.080	1.076	0.052	1.150	0.110
	40	1.188	0.090	1.186	0.080	1.080	0.053	1.150	0.109
	45	1.188	0.090	1.186	0.080	1.083	0.054	1.150	0.109
	Average	**1.198**	**0.090**	**1.187**	**0.081**	**1.072**	**0.053**	**1.151**	**0.109**

Table 3.6: Statistical parameters load effects for CPCI Girders

Girder Type	Span "m"	Mu		Vu		Mcr		Stress Range Fatigue I	
		λ	CoV	λ	CoV	λ	CoV	λ	CoV
CPCI 900	15	1.240	0.090	1.190	0.080	1.054	0.067	1.154	0.109
	20	1.240	0.090	1.190	0.080	1.054	0.067	1.154	0.109
	Average	**1.240**	**0.090**	**1.190**	**0.080**	**1.054**	**0.067**	**1.154**	**0.109**
CPCI 1200	15	1.238	0.090	1.190	0.080	1.054	0.059	1.154	0.108
	20	1.238	0.090	1.192	0.080	1.052	0.066	1.154	0.109
	25	1.238	0.090	1.190	0.080	1.052	0.078	1.153	0.108
	Average	**1.238**	**0.090**	**1.191**	**0.080**	**1.053**	**0.068**	**1.154**	**0.108**
CPCI 1400	15	1.238	0.090	1.190	0.080	1.048	0.055	1.153	0.106
	20	1.238	0.090	1.192	0.080	1.048	0.059	1.153	0.110
	25	1.238	0.090	1.190	0.080	1.043	0.061	1.153	0.109
	Average	**1.238**	**0.090**	**1.191**	**0.080**	**1.046**	**0.058**	**1.153**	**0.108**
CPCI 1500	20	1.238	0.090	1.190	0.080	1.056	0.054	1.152	0.109
	25	1.238	0.0.90	1.192	0.080	1.056	0.059	1.152	0.109
	30	1.236	0.090	1.190	0.080	1.050	0.0600	1.152	0.108
	35	1.218	0.090	1.190	0.080	1.048	0.061	1.152	0.108
	Average	**1.233**	**0.090**	**1.190**	**0.080**	**1.053**	**0.059**	**1.152**	**0.109**
CPCI 1600	20	1.218	0.090	1.190	0.080	1.048	0.052	1.155	0.109
	25	1.218	0.090	1.119	0.080	1.048	0.052	1.152	0.109
	30	1.218	0.090	1.119	0.080	1.050	0.053	1.152	0.109
	35	1.218	0.090	1.119	0.080	1.050	0.053	1.152	0.109
	40	1.218	0.090	1.188	0.080	1.050	0.055	1.152	0.109
	Average	**1.218**	**0.090**	**1.147**	**0.080**	**1.049**	**0.053**	**1.153**	**0.109**
CPCI 1900	25	1.218	0.090	1.188	0.080	1.050	0.052	1.152	0.109
	30	1.180	0.090	1.187	0.080	1.050	0.052	1.150	0.108
	35	1.180	0.090	1.186	0.080	1.050	0.052	1.150	0.111
	40	1.180	0.090	1.186	0.080	1.050	0.053	1.150	0.109
	45	1.180	0.090	1.182	0.080	1.050	0.054	1.150	0.109
	Average	**1.188**	**0.090**	**1.189**	**0.080**	**1.050**	**0.053**	**1.150**	**0.109**
CPCI 2300	35	1.180	0.090	1.180	0.080	1.050	0.053	1.150	0.109
	40	1.180	0.090	1.180	0.080	1.050	0.053	1.150	0.109
	45	1.180	0.090	1.180	0.080	1.050	0.053	1.150	0.108
	50	1.180	0.090	1.180	0.080	1.050	0.053	1.150	0.109
	55	1.180	0.090	1.180	0.080	1.050	0.052	1.150	0.108
	60	1.180	0.090	1.180	0.080	1.050	0.052	1.150	0.108
	Average	**1.180**	**0.090**	**1.180**	**0.080**	**1.050**	**0.053**	**1.150**	**0.108**

Table 3.7: Statistical parameters of load effects for Bulb-T (NEBT) Girders

Girder Type	Span "m"	Mu		Vu		Mcr		Stress Range Fatigue I	
		λ	CoV	λ	CoV	λ	CoV	λ	CoV
NEBT 1000	10	1.242	0.080	1.198	0.090	1.049	0.055	1.155	0.106
	15	1.238	0.080	1.198	0.090	1.072	0.059	1.154	0.106
	Average	**1.240**	**0.080**	**1.198**	**0.090**	**1.061**	**0.057**	**1.155**	**0.106**
NEBT 1200	10	1.240	0.080	1.198	0.090	1.079	0.061	1.154	0.106
	15	1.238	0.080	1.198	0.090	1.067	0.054	1.154	0.106
	20	1.238	0.0.80	1.196	0.090	1.072	0.059	1.152	0.106
	Average	**1.239**	**0.080**	**1.197**	**0.090**	**1.073**	**0.058**	**1.153**	**0.106**
NEBT 1400	10	1.236	0.080	1.196	0.090	1.078	0.060	1.152	0.106
	15	1.220	0.090	1.196	0.090	1.086	0.061	1.152	0.106
	20	1.224	0.090	1.196	0.090	1.061	0.052	1.153	0.106
	Average	**1.227**	**0.090**	**1.196**	**0.090**	**1.075**	**0.058**	**1.152**	**0.106**
NEBT 1600	20	1.222	0.090	1.196	0.090	1.067	0.052	1.152	0.105
	25	1.220	0.090	1.196	0.090	1.072	0.053	1.150	0.105
	30	1.222	0.090	1.195	0.090	1.079	0.053	1.150	0.106
	35	1.220	0.090	1.192	0.090	1.083	0.055	1.152	0.104
	Average	**1.221**	**0.090**	**1.195**	**0.090**	**1.075**	**0.053**	**1.151**	**0.105**
NEBT 1800	20	1.220	0.090	1.192	0.090	1.058	0.052	1.152	0.104
	25	1.220	0.090	1.92	0.090	1.064	0.052	1.152	0.104
	30	1.186	0.090	1.192	0.090	1.069	0.052	1.150	0.105
	35	1.188	0.090	1.191	0.090	1.076	0.052	1.150	0.104
	40	1.188	0.090	1.191	0.090	1.080	0.053	1.150	0.104
	Average	**1.200**	**0.090**	**1.192**	**0.090**	**1.069**	**0.052**	**1.151**	**0.104**

Table 3.8: Statistical parameters of load effects for NU Girders

Girder Type	Span "m"	Mu		Vu		Mcr		Stress Range Fatigue I	
		λ	CoV	λ	CoV	λ	CoV	λ	CoV
NU 900	15	1.238	0.090	1.190	0.080	1.043	0.061	1.153	0.109
	20	1.238	0.090	1.190	0.080	1.056	0.054	1.152	0.109
	Average	**1.238**	**0.090**	**1.190**	**0.080**	**1.050**	**0.058**	**1.153**	**0.109**
NU 1100	15	1.238	0.0.90	1.192	0.080	1.056	0.059	1.152	0.109
	20	1.236	0.090	1.190	0.080	1.050	0.060	1.152	0.108
	25	1.218	0.090	1.190	0.080	1.048	0.061	1.152	0.108
	Average	**1.231**	**0.090**	**1.191**	**0.080**	**1.051**	**0.060**	**1.152**	**0.108**
NU 1350	15	1.218	0.090	1.190	0.080	1.048	0.052	1.155	0.109
	20	1.218	0.090	1.119	0.080	1.048	0.052	1.152	0.109
	25	1.218	0.090	1.119	0.080	1.050	0.053	1.152	0.109
	Average	**1.218**	**0.090**	**1.143**	**0.080**	**1.049**	**0.052**	**1.153**	**0.109**
NU 1600	20	1.218	0.090	1.119	0.080	1.050	0.053	1.152	0.109
	25	1.218	0.090	1.188	0.080	1.050	0.055	1.152	0.109
	30	1.218	0.090	1.186	0.080	1.050	0.052	1.152	0.109
	35	1.218	0.090	1.188	0.080	1.050	0.052	1.152	0.109
	Average	**1.218**	**0.090**	**1.170**	**0.080**	**1.050**	**0.053**	**1.152**	**0.109**
NU 1800	20	1.222	0.090	1.195	0.090	1.079	0.053	1.150	0.106
	25	1.220	0.090	1.192	0.090	1.083	0.055	1.152	0.104
	30	1.220	0.090	1.192	0.090	1.058	0.052	1.152	0.104
	35	1.220	0.090	1.92	0.090	1.064	0.052	1.152	0.104
	40	1.189	0.090	1.187	0.080	1.069	0.052	1.150	0.109
	Average	**1.214**	**0.090**	**1.337**	**0.090**	**1.071**	**0.053**	**1.151**	**0.105**
NU 2000	20	1.189	0.090	1.187	0.080	1.076	0.052	1.150	0.110
	25	1.189	0.090	1.186	0.080	1.080	0.053	1.150	0.109
	30	1.189	0.090	1.186	0.080	1.083	0.054	1.150	0.109
	35	1.189	0.090	1.187	0.080	1.076	0.052	1.150	0.110
	40	1.188	0.090	1.186	0.080	1.080	0.053	1.150	0.109
	45	1.186	0.090	1.186	0.080	1.083	0.054	1.150	0.109
	Average	**1.188**	**0.090**	**1.186**	**0.080**	**1.080**	**0.053**	**1.150**	**0.109**

3.4 Statistical parameters of the random variables corresponding to the resistance model

3.4.1 Statistical parameters of section properties

As already mentioned in Chapter Two (clause 2.1.2.2), the statistical parameters (λ, CoV) of section properties are available as developed by some researchers; however, those parameters for area, inertia, and section modulus do not exist. In this section, the Monte Carlo Simulation (MCS) is utilized to develop the statistical parameters for girder properties by implementing the data available in Table 2.20. For this purpose, Monte Carlo Simulation was performed with 25,000 cycles.

The section properties are calculated in two different phases:

- At initial phase (at transfer)

In this phase, the girder gross section properties are used in calculating the stresses due to dead load and prestressing force. The stresses are calculated with respect to the top and bottom fibers of the girder. The section properties are: the girder's area, moment of inertia, and section modulus with respect to the top and bottom fibers. These properties are treated as random variables in calculating the reliability indices at this phase.

The procedure to calculate the statistical parameters of section properties is illustrated in the flow chart shown in Figure 3.1. The statistical parameters of the section properties, at initial phase, with respect to AASHTO Girders are shown in Figure 3.9. Similarly, Figure 3.10 shows the statistical parameters of CPCI Girders. The statistical parameters with respect to Bulb-T Girders and NU Girders are, respectively, shown in Tables 3.11 and 3.12.

- At service phase (after losses)

In this phase, the girder and the deck will be in composite action. The dead load, live load, dynamic (impact) allowance, and prestressing force will be applied to calculate the load effects. These load effects are: stress at the top fiber of the deck, stress at top fiber of the girder, stress at bottom fiber of the girder, fatigue stress range, cracking moment, and ultimate bending and shear. The properties of the composite section are treated as random variables in estimating the reliability indices at this phase. The procedure illustrated in Figure 3.5 is used to calculate the statistical parameters of the section properties at the service phase. The statistical parameters of the section properties, at service phase, with respect to AASHTO Girders are shown in Table 3.13. Similarly, Table 3.14 shows the statistical parameters of CPCI Girders. The statistical parameters with respect to Bulb-T Girders and NU Girders are, respectively, shown in Tables 3.15 and 3.16.

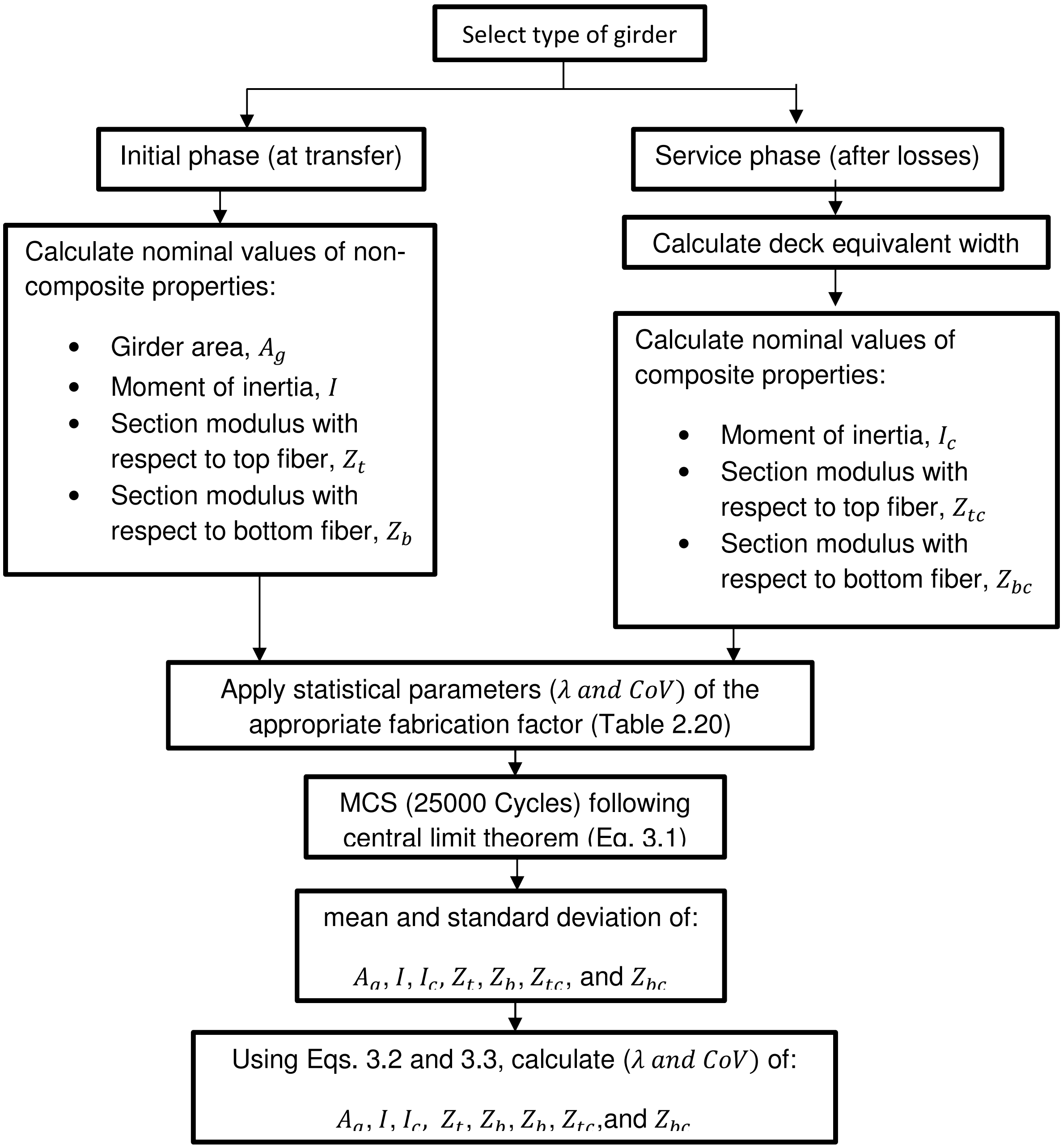

Figure 3.5: Procedure to determine the statistical parameters of variation of geometrical properties of standard girders.

Table 3.9: Statistical parameter of girder properties at transfer for AASHTO Girders.

Girder Type	Span "m"	Ag		Ig		Zb		Zt	
		λ	CoV	λ	CoV	λ	CoV	λ	CoV
AASHTO I	10	1.010	0.025	1.000	0.045	1.000	0.034	1.003	0.078
	15	1.010	0.026	1.000	0.045	0.999	0.035	1.003	0.077
	Average	**1.010**	**0.026**	**1.000**	**0.045**	**1.000**	**0.035**	**1.003**	**0.078**
AASHTO II	15	1.010	0.024	1.000	0.046	1.000	0.035	1.002	0.076
	20	1.010	0.024	0.999	0.047	0.999	0.036	1.003	0.077
	25	1.008	0.025	1.000	0.045	1.000	0.035	1.004	0.077
	Average	**1.009**	**0.024**	**1.000**	**0.046**	**1.000**	**0.035**	**1.003**	**0.077**
AASHTO III	15	1.008	0.024	1.001	0.045	1.000	0.034	1.004	0.076
	20	1.008	0.024	1.000	0.046	1.000	0.035	1.004	0.076
	25	1.006	0.023	1.001	0.045	1.000	0.035	1.005	0.078
	Average	**1.007**	**0.024**	**1.001**	**0.045**	**1.000**	**0.035**	**1.004**	**0.077**
AASHTO IV	20	1.010	0.023	1.000	0.045	1.000	0.035	1.003	0.078
	25	1.010	0.024	1.000	0.046	1.000	0.035	1.005	0.078
	30	1.011	0.023	1.000	0.046	1.000	0.035	1.005	0.077
	35	1.010	0.024	1.000	0.045	1.000	0.035	1.003	0.076
	Average	**1.010**	**0.024**	**1.000**	**0.046**	**1.000**	**0.035**	**1.004**	**0.077**
AASHTO V	20	1.007	0.023	1.000	0.047	1.000	0.036	1.004	0.077
	25	1.006	0.023	1.000	0.047	1.000	0.036	1.004	0.077
	30	1.008	0.023	1.000	0.048	1.008	0.036	1.004	0.078
	35	1.006	0.023	1.000	0.047	1.006	0.036	1.004	0.077
	40	1.005	0.023	1.000	0.048	1.008	0.036	1.004	0.076
	Average	**1.006**	**0.023**	**1.000**	**0.047**	**1.004**	**0.036**	**1.004**	**0.077**
AASHTO VI	25	1.011	0.023	1.000	0.050	1.008	0.037	1.003	0.077
	30	1.010	0.023	1.000	0.050	1.008	0.037	1.005	0.076
	35	1.009	0.023	0.998	0.048	1.002	0.038	1.005	0.076
	40	1.008	0.023	1.000	0.049	1.002	0.036	1.003	0.078
	45	1.004	0.023	1.000	0.049	1.002	0.036	1.001	0.078
	Average	**1.009**	**0.023**	**1.000**	**0.049**	**1.005**	**0.037**	**1.004**	**0.077**

Table 3.10: Statistical parameter of girder properties at transfer for CPCI Girders.

Girder Type	Span (m)	Ag		Ig		Zb		Zt	
		λ	CoV	λ	CoV	λ	CoV	λ	CoV
CPCI 900	15	1.020	0.025	1.010	0.050	1.014	0.037	1.002	0.081
	20	1.020	0.025	1.010	0.050	1.014	0.037	1.002	0.082
	Average	**1.020**	**0.025**	**1.010**	**0.050**	**1.014**	**0.037**	**1.002**	**0.082**
CPCI 1200	15	1.020	0.025	1.010	0.052	1.014	0.038	1.005	0.082
	10	1.020	0.024	1.010	0.052	1.014	0.038	1.006	0.083
	15	1.018	0.024	1.010	0.052	1.014	0.038	1.004	0.084
	Average	**1.019**	**0.024**	**1.010**	**0.052**	**1.014**	**0.038**	**1.005**	**0.083**
CPCI 1400	15	1.018	0.024	1.010	0.052	1.014	0.038	1.004	0.084
	20	1.020	0.023	1.010	0.051	1.013	0.037	1.003	0.084
	25	1.020	0.023	1.010	0.051	1.013	0.037	1.003	0.084
	Average	**1.019**	**0.023**	**1.010**	**0.051**	**1.013**	**0.037**	**1.003**	**0.084**
CPCI 1500	20	1.020	0.023	1.010	0.051	1.013	0.037	1.003	0.084
	25	1.020	0.023	1.010	0.051	1.013	0.037	1.003	0.084
	30	1.020	0.023	1.010	0.051	1.014	0.037	1.003	0.084
	35	1.020	0.023	1.010	0.051	1.014	0.037	1.003	0.084
	Average	**1.020**	**0.023**	**1.010**	**0.051**	**1.014**	**0.037**	**1.003**	**0.084**
CPCI 1600	20	1.018	0.023	1.010	0.052	1.013	0.038	1.002	0.088
	25	1.018	0.023	1.010	0.051	1.013	0.037	1.002	0.088
	30	1.016	0.023	1.010	0.052	1.013	0.038	1.005	0.088
	35	1.016	0.023	1.010	0.051	1.013	0.037	1.004	0.088
	40	1.016	0.023	1.009	0.051	1.014	0.037	1.003	0.088
	Average	**1.017**	**0.023**	**1.010**	**0.051**	**1.013**	**0.037**	**1.003**	**0.088**
CPCI 1900	20	1.016	0.023	1.009	0.056	1.014	0.039	1.003	0.093
	25	1.016	0.023	1.009	0.056	1.012	0.038	1.003	0.093
	30	1.016	0.023	1.009	0.056	1.012	0.039	1.003	0.093
	35	1.016	0.023	1.009	0.056	1.012	0.038	1.003	0.093
	40	1.015	0.023	1.009	0.055	1.012	0.039	1.003	0.091
	45	1.015	0.023	1.009	0.056	1.012	0.039	1.003	0.093
	Average	**1.016**	**0.023**	**1.009**	**0.056**	**1.012**	**0.039**	**1.003**	**0.093**
CPCI 2300	35	1.015	0.023	1.008	0.057	1.012	0.038	1.003	0.094
	40	1.015	0.023	1.009	0.057	1.012	0.039	1.003	0.093
	45	1.014	0.023	1.009	0.057	1.012	0.038	1.003	0.094
	50	1.014	0.023	1.008	0.057	1.012	0.039	1.003	0.094
	55	1.014	0.023	1.008	0.057	1.012	0.038	1.002	0.093
	60	1.014	0.023	1.007	0.058	1.012	0.039	1.002	0.093
	Average	**1.014**	**0.023**	**1.008**	**0.057**	**0.012**	**0.039**	**1.003**	**0.094**

Table 3.11: Statistical parameter of girder properties at transfer for Bulb-T (NEBT) Girders.

Girder Type	Span "m"	Ag		Ig		Zb		Zt	
		λ	CoV	λ	CoV	λ	CoV	λ	CoV
NEBT 1000	15	1.020	0.023	1.010	0.051	1.013	0.037	1.003	0.084
	20	1.020	0.023	1.010	0.051	1.013	0.037	1.003	0.084
	Average	**1.020**	**0.023**	**1.010**	**0.051**	**1.013**	**0.037**	**1.003**	**0.084**
NEBT 1200	15	1.020	0.023	1.010	0.051	1.013	0.037	1.003	0.084
	20	1.020	0.023	1.010	0.051	1.013	0.037	1.003	0.084
	25	1.020	0.023	1.010	0.051	1.014	0.037	1.003	0.084
	Average	**1.020**	**0.023**	**1.010**	**0.051**	**1.013**	**0.037**	**1.003**	**0.084**
NEBT 1400	15	1.020	0.023	1.010	0.051	1.014	0.037	1.003	0.084
	20	1.018	0.023	1.010	0.052	1.013	0.038	1.002	0.088
	25	1.018	0.023	1.010	0.051	1.013	0.037	1.002	0.088
	Average	**1.019**	**0.023**	**1.010**	**0.051**	**1.031**	**0.037**	**1.002**	**0.087**
NEBT 1600	20	1.016	0.023	1.010	0.052	1.013	0.038	1.005	0.088
	25	1.016	0.023	1.010	0.051	1.013	0.037	1.004	0.088
	30	1.016	0.023	1.009	0.051	1.014	0.037	1.003	0.088
	35	1.016	0.023	1.009	0.056	1.014	0.039	1.003	0.093
	Average	**1.016**	**0.023**	**1.010**	**0.053**	**1.014**	**0.038**	**1.004**	**0.089**
	25	1.016	0.023	1.009	0.056	1.013	0.039	1.003	0.093
	30	1.016	0.023	1.009	0.056	1.012	0.038	1.003	0.093
	35	1.014	0.023	1.009	0.055	1.012	0.039	1.003	0.091
	40	1.014	0.023	1.009	0.056	1.012	0.039	1.003	0.093
	Average	**1.015**	**0.023**	**1.009**	**0.056**	**1.012**	**0.039**	**1.003**	**0.093**

Table 3.12: Statistical parameter of girder properties at transfer for NU Girders.

Girder Type	Span "m"	Ag		Ig		Zb		Zt	
		λ	CoV	λ	CoV	λ	CoV	λ	CoV
NU 900	15	1.000	0.022	0.999	0.051	1.000	0.038	1.001	0.082
	20	1.000	0.022	0.999	0.046	0.999	0.036	1.002	0.077
	average	**1.000**	**0.022**	**0.999**	**0.049**	**1.000**	**0.037**	**1.002**	**0.080**
NU 1100	15	1.000	0.022	1.000	0.052	1.000	0.038	1.003	0.083
	20	1.000	0.22	1.002	0.053	1.001	0.039	1.006	0.083
	25	1.000	0.022	0.999	0.053	0.999	0.039	1.003	0.085
	Average	**1.000**	**0.022**	**1.000**	**0.053**	**1.000**	**0.039**	**1.004**	**0.084**
NU 1350	15	1.001	0.022	1.001	0.055	1.001	0.039	1.005	0.087
	20	1.000	0.022	1.001	0.055	1.000	0.040	1.005	0.089
	25	1.000	0.023	1.000	0.055	1.000	0.040	1.004	0.089
	Average	**1.000**	**0.022**	**1.001**	**0.055**	**1.000**	**0.040**	**1.005**	**0.088**
NU 1600	20	1.000	0.023	0.999	0.056	0.999	0.039	1.001	0.089
	25	1.000	0.023	1.001	0.058	1.000	0.040	1.006	0.090
	30	1.000	0.023	1.000	0.058	0.999	0.040	1.004	0.091
	35	1.000	0.023	1.001	0.057	1.000	0.040	1.005	0.089
	Average	**1.000**	**0.023**	**1.000**	**0.057**	**1.000**	**0.040**	**1.004**	**0.090**
NU 1800	20	1.000	0.024	0.999	0.058	0.999	0.040	1.002	0.091
	25	1.000	0.023	1.000	0.058	1.000	0.040	1.004	0.090
	30	1.001	0.024	1.001	0.058	1.000	0.040	1.004	0.092
	35	1.000	0.024	1.001	0.059	1.000	0.040	1.006	0.092
	40	1.000	0.023	1.000	0.059	1.000	0.040	1.004	0.093
	Average	**1.000**	**0.024**	**1.000**	**0.058**	**1.000**	**0.040**	**1.004**	**0.092**
NU 2000	20	1.000	0.024	1.000	0.060	1.000	0.040	1.005	0.093
	25	1.000	0.024	1.002	0.059	1.001	0.040	1.006	0.094
	30	1.000	0.024	1.000	0.059	1.000	0.040	1.003	0.093
	35	1.000	0.024	1.001	0.059	1.000	0.040	1.005	0.092
	40	1.000	0.024	1.000	0.060	0.999	0.041	1.004	0.095
	45	1.000	0.024	1.001	0.059	1.000	0.040	1.006	0.092
	Average	**1.000**	**0.024**	**1.001**	**0.059**	**1.000**	**0.040**	**1.005**	**0.093**

Table 3.13: Statistical parameter of girder properties at service phase for AASHTO Girders.

Girder Type	Span (m)	Ic		Zbc		Ztc	
		λ	CoV	λ	CoV	λ	CoV
AASHTO I	10	1.057	0.070	1.058	0.078	1.073	0.100
	15	1.058	0.070	1.059	0.079	1.073	0.104
	Average	**1.058**	**0.070**	**1.059**	**0.079**	**1.073**	**0.102**
AASHTO II	15	1.060	0.067	1.061	0.076	1.070	0.102
	20	1.059	0.069	1.060	0.079	1.070	0.102
	25	1.058	0.069	1.059	0.078	1.069	0.100
	Average	**1.059**	**0.068**	**1.060**	**0.078**	**1.070**	**0.101**
AASHTO III	15	1.065	0.067	1.066	0.076	1.072	0.100
	20	1.063	0.065	1.064	0.073	1.072	0.099
	25	1.063	0.064	1.064	0.073	1.069	0.101
	Average	**1.064**	**0.065**	**1.065**	**0.074**	**1.071**	**0.100**
AASHTO IV	20	1.065	0.059	1.067	0.069	1.073	0.100
	25	1.063	0.060	1.065	0.067	1.071	0.100
	30	1.063	0.059	1.064	0.067	1.073	0.102
	35	1.064	0.060	1.065	0.069	1.069	0.102
	Average	**1.064**	**0.060**	**1.065**	**0.068**	**1.072**	**0.101**
AASHTO V	20	1.057	0.054	1.057	0.063	1.063	0.100
	25	1.056	0.054	1.057	0.062	1.064	0.100
	30	1.057	0.053	1.058	0.061	1.066	0.099
	35	1.056	0.053	1.057	0.062	1.064	0.101
	40	1.056	0.054	1.057	0.062	1.062	0.100
	Average	**1.056**	**0.054**	**1.057**	**0.062**	**1.064**	**0.100**
AASHTO VI	25	1.057	0.053	1.058	0.061	1.065	0.100
	30	1.057	0.051	1.058	0.060	1.064	0.099
	35	1.056	0.052	1.057	0.061	1.062	0.099
	40	1.056	0.052	1.057	0.061	1.062	0.099
	45	1.058	0.052	1.058	0.061	1.064	0.099
	Average	**1.057**	**0.052**	**1.058**	**0.061**	**1.064**	**0.099**

Table 3.14: Statistical parameter of girder properties at service phase for CPCI Girders.

Girder Type	Span (m)	Ic		Zbc		Ztc	
		λ	CoV	λ	CoV	λ	CoV
CPCI 900	15	1.064	0.070	1.058	0.078	1.082	0.100
	20	1.064	0.070	1.059	0.079	1.083	0.104
	Average	**1.064**	**0.070**	**1.059**	**0.079**	**1.083**	**0.102**
CPCI 1200	15	1.063	0.067	1.061	0.076	1.082	0.102
	20	1.064	0.069	1.060	0.079	1.082	0.102
	25	1.062	0.069	1.059	0.078	1.082	0.100
	Average	**1.063**	**0.068**	**1.060**	**0.078**	**1.082**	**0.101**
CPCI 1400	15	1.065	0.067	1.066	0.076	1.082	0.100
	20	1.063	0.065	1.064	0.073	1.082	0.099
	25	1.060	0.070	1.058	0.078	1.082	0.100
	Average	**1.063**	**0.067**	**1.063**	**0.076**	**1.082**	**0.100**
CPCI 1500	20	1.060	0.070	1.059	0.079	1.082	0.104
	25	1.060	0.067	1.061	0.076	1.084	0.102
	30	1.059	0.069	1.060	0.079	1.082	0.102
	35	1.058	0.069	1.059	0.078	1.084	0.100
	Average	**1.059**	**0.069**	**1.060**	**0.078**	**1.083**	**0.102**
CPCI 1600	20	1.058	0.067	1.066	0.076	1.082	0.100
	25	1.058	0.065	1.064	0.073	1.083	0.099
	30	1.058	0.064	1.064	0.073	1.082	0.101
	35	1.058	0.059	1.067	0.069	1.082	0.100
	40	1.059	0.060	1.065	0.067	1.082	0.100
	Average	**1.058**	**0.063**	**1.065**	**0.072**	**1.082**	**0.100**
CPCI 1900	20	1.063	0.059	1.064	0.067	1.082	0.102
	25	1.064	0.060	1.065	0.069	1.082	0.102
	30	1.057	0.054	1.057	0.063	1.082	0.100
	35	1.056	0.054	1.057	0.062	1.082	0.100
	40	1.057	0.053	1.058	0.061	1.084	0.099
	45	1.056	0.053	1.057	0.062	1.082	0.101
	Average	**1.059**	**0.056**	**1.060**	**0.064**	**1.082**	**0.101**
CPCI 2300	35	1.056	0.054	1.057	0.062	1.084	0.100
	40	1.057	0.052	1.058	0.061	1.078	0.100
	45	1.057	0.053	1.058	0.061	1.078	0.100
	50	1.057	0.051	1.058	0.060	1.079	0.099
	55	1.056	0.052	1.057	0.061	1.079	0.099
	60	1.056	0.052	1.057	0.061	1.070	0.099
	Average	**1.057**	**0.052**	**1.058**	**0.061**	**1.078**	**0.100**

Table 3.15: Statistical parameter of girder properties at service phase for Bulb-T Girders.

Girder Type	Span "m"	Ic		Zbc		Ztc	
		λ	CoV	λ	CoV	λ	CoV
NEBT 1000	15	1.060	0.068	1.108	0.141	1.067	0.100
	20	1.063	0.068	1.106	0.144	1.067	0.100
	Average	**1.062**	**0.068**	**1.107**	**0.143**	**1.067**	**0.100**
NEBT 1200	15	1.061	0.069	1.106	0.140	1.068	1.020
	20	1.061	0.069	1.106	0.140	1.066	0.100
	25	1.063	0.068	1.113	0.141	1.064	0.100
	Average	**1.062**	**0.069**	**1.115**	**0.140**	**1.066**	**0.101**
NEBT 1400	15	1.063	0.068	1.113	0.141	1.065	0.100
	20	1.061	0.068	1.112	0.141	1.064	0.099
	25	1.062	0.068	1.112	0.141	1.064	0.098
	Average	**1.062**	**0.068**	**1.112**	**0.141**	**1.064**	**0.099**
NEBT 1600	20	1.064	0.068	1.112	0.140	1.064	0.098
	25	1.067	0.068	1.111	0.140	1.066	0.099
	30	1.067	0.068	1.110	0.140	1.063	0.098
	35	1.063	0.067	1.110	0.138	1.065	0.100
	Average	**1.065**	**0.068**	**0.111**	**0.140**	**1.065**	**0.099**
	25	1.063	0.067	1.110	0.138	1.066	0.098
	30	1.063	0.067	1.110	0.138	1.063	0.099
	35	1.063	0.068	1.114	0.141	1.065	0.097
	40	1.064	0.068	1.114	0.141	1.063	0.097
	Average	**1.063**	**0.067**	**1.112**	**0.139**	**1.064**	**0.097**

Table 3.16: Statistical parameter of girder properties at service phase for NU Girders.

Girder Type	Span "m"	Ic		Zbc		Ztc	
		λ	CoV	λ	CoV	λ	CoV
NU 900	15	1.058	0.055	1.061	0.065	1.065	0.099
	20	1.059	0.056	1.061	0.065	1.065	0.099
	Average	**1.059**	**0.056**	**1.061**	**0.065**	**1.065**	**0.099**
NU 1100	15	1.059	0.054	1.060	0.065	1.066	0.098
	20	1.059	0.056	1.061	0.065	1.065	0.098
	25	1.058	0.054	1.062	0.065	1.065	0.099
	Average	**1.059**	**0.055**	**1.061**	**0.065**	**1.065**	**0.098**
NU 1350	15	1.059	0.056	1.061	0.065	1.065	0.099
	20	1.060	0.057	1.061	0.066	1.066	0.100
	25	1.060	0.058	1.062	0.066	1.067	0.102
	Average	**1.060**	**0.057**	**1.061**	**0.066**	**1.066**	**0.100**
NU 1600	20	1.059	0.055	1.059	0.064	1.069	0.098
	25	1.058	0.056	1.058	0.065	1.064	0.101
	30	1.058	0.056	1.059	0.065	1.065	0.098
	35	1.059	0.056	1.059	0.066	1.068	0.100
	Average	**1.059**	**0.056**	**1.059**	**0.065**	**1.067**	**0.099**
NU 1800	20	1.059	0.056	1.060	0.065	1.066	0.100
	25	1.059	0.055	1.061	0.065	1.065	0.099
	30	1.060	0.055	1.062	0.064	1.068	0.101
	35	1.057	0.055	1.058	0.064	1.065	0.099
	40	1.059	0.059	1.060	0.064	1.064	0.098
	Average	**1.059**	**0.056**	**1.060**	**0.064**	**1.066**	**0.099**
NU 2000	20	1.057	0.055	1.059	0.064	1.063	0.097
	25	1.059	0.055	1.060	0.064	1.064	0.096
	30	1.058	0.055	1.060	0.065	1.064	0.097
	35	1.058	0.055	1.059	0.063	1.066	0.099
	40	1.058	0.055	1.058	0.064	1.066	0.097
	45	1.057	0.055	1.059	0.063	1.062	0.096
	Average	**1.058**	**0.055**	**1.059**	**0.064**	**1.064**	**0.097**

3.4.2 Statistical parameters of allowable stresses

According to AASHTO LRFD, clause [A5.9.4], both the allowable tensile and compressive stresses are functions of the 28-day concrete compressive strength f'_c. In reliability analyses, these allowable stresses are treated as random variables. To obtain the statistical parameters of those random variables, Monte Carlo Simulation technique has been applied (25000 cycles). Table 3.17 shows the calculated statistical parameters of the allowable stresses both at initial and service phases.

Table 3.17: Statistical parameter of allowable stresses.

Concrete Compressive Strength (MPa)	Initial Phase (at transfer)				Service phase (after losses)			
	Allowable tensile stress		Allowable compressive stress		Allowable tensile stress		Allowable compressive stress	
	λ	CoV	λ	CoV	λ	CoV	λ	CoV
20	1.139	0.087	1.307	0.172	1.139	0.087	1.307	0.172
25	1.125	0.080	1.27	0.158	1.125	0.080	1.27	0.158
27	1.110	0.077	1.24	0.151	1.112	0.077	1.24	0.151
30	1.097	0.071	1.208	0.139	1.097	0.071	1.208	0.139
35	1.090	0.067	1.193	0.133	1.090	0.067	1.193	0.133
38	1.078	0.067	1.167	0.133	1.078	0.067	1.167	0.133
40	1.070	0.063	1.150	0.125	1.071	0.063	1.150	0.125
45	1.065	0.059	1.137	0.117	1.065	0.059	1.137	0.117
50	1.061	0.058	1.129	0.115	1.061	0.058	1.129	0.115
55	1.051	0.056	1.107	0.112	1.051	0.056	1.107	0.112
60	1.049	0.055	1.104	0.109	1.050	0.055	1.104	0.109
70	1.043	0.054	1.092	0.108	1.04	0.054	1.092	0.108
80	1.039	0.055	1.082	0.108	1.039	0.055	1.082	0.108

3.4.3 Statistical parameters of flexural and shear resistance

Using strain incremental approach, the flexural capacity of prestressed girders can be evaluated by developing moment-curvature relationship. To avoid the complexity of the actual section, an equivalent simplified section, with the same properties, is generated by a set of uniform layers as illustrated in Figure 3.6 (PCI Design Manual 2003).

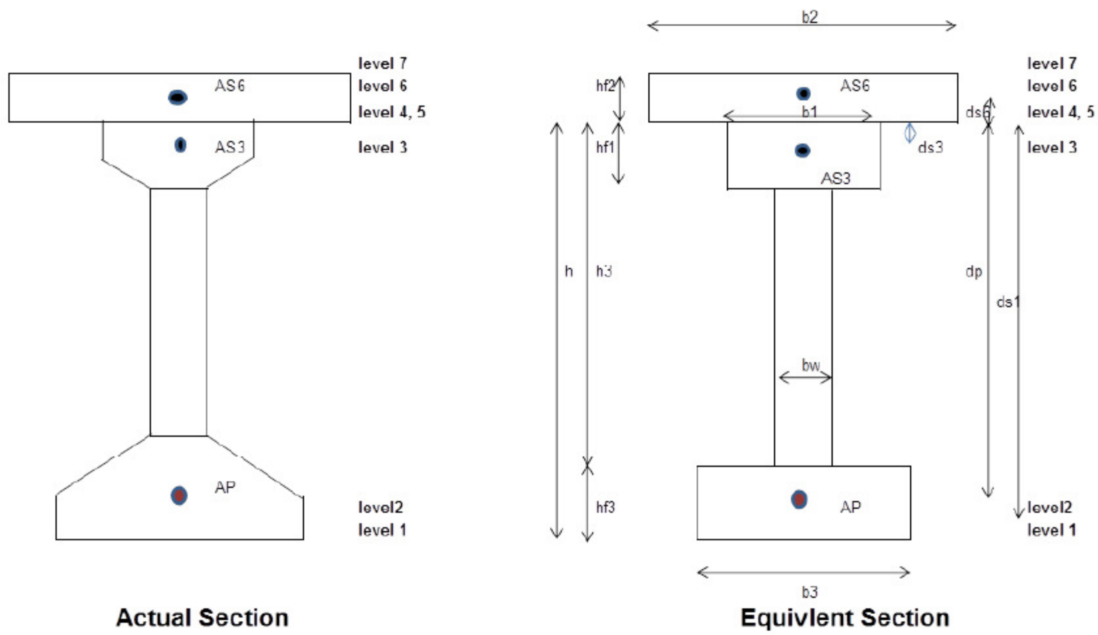

Figure 3.6: Schematic Present the Actual Section and Equivalent Section (PCI Design Manual 2003).

The following steps illustrate the application of the incremental strain compatibility approach to evaluate the flexural capacity of precast girders:

Step 1: Assume a neutral axis location with depth c.

Step 2: For an applied strain level, generate stress diagram using the nonlinear stress-strain relationships for the materials. Figures 3.7 to 3.9 show the stress-strain curves for concrete, reinforcement, and prestressing strands, respectively.

Step 3: Check the neutral axis depth using equilibrium of forces. Neglect tensile strength of concrete (below neutral axis).

Step 4: Increase strain incrementally and repeat steps 2, 3 and 4 until a maximum strain of 0.0035 is reached at the top fiber.

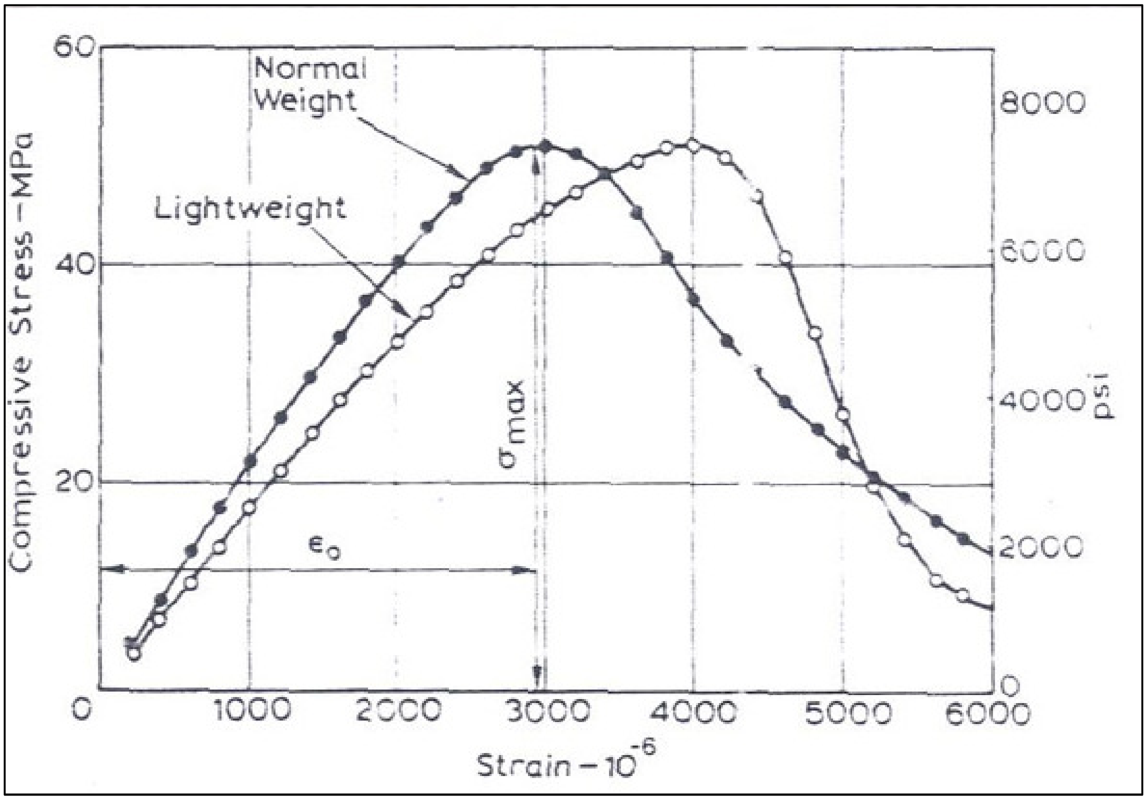

Figure 3.7: Stress-Strain curve for concrete (Ellingwood et al. 1980).

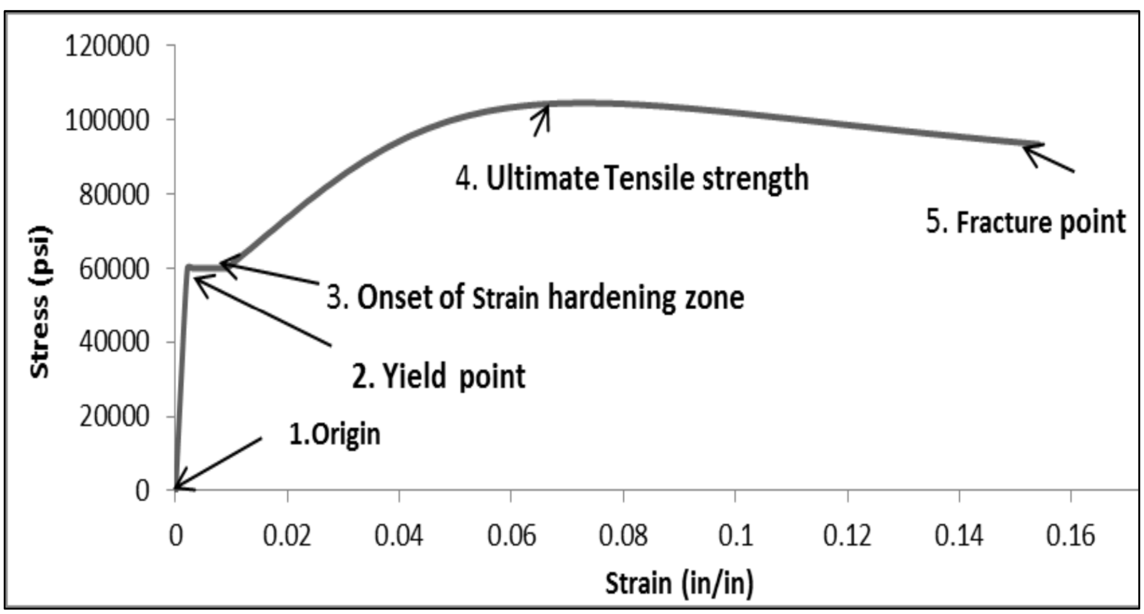

Figure 3.8: Stress-Strain curve for steel (Manzoor and Ahmed 2013).

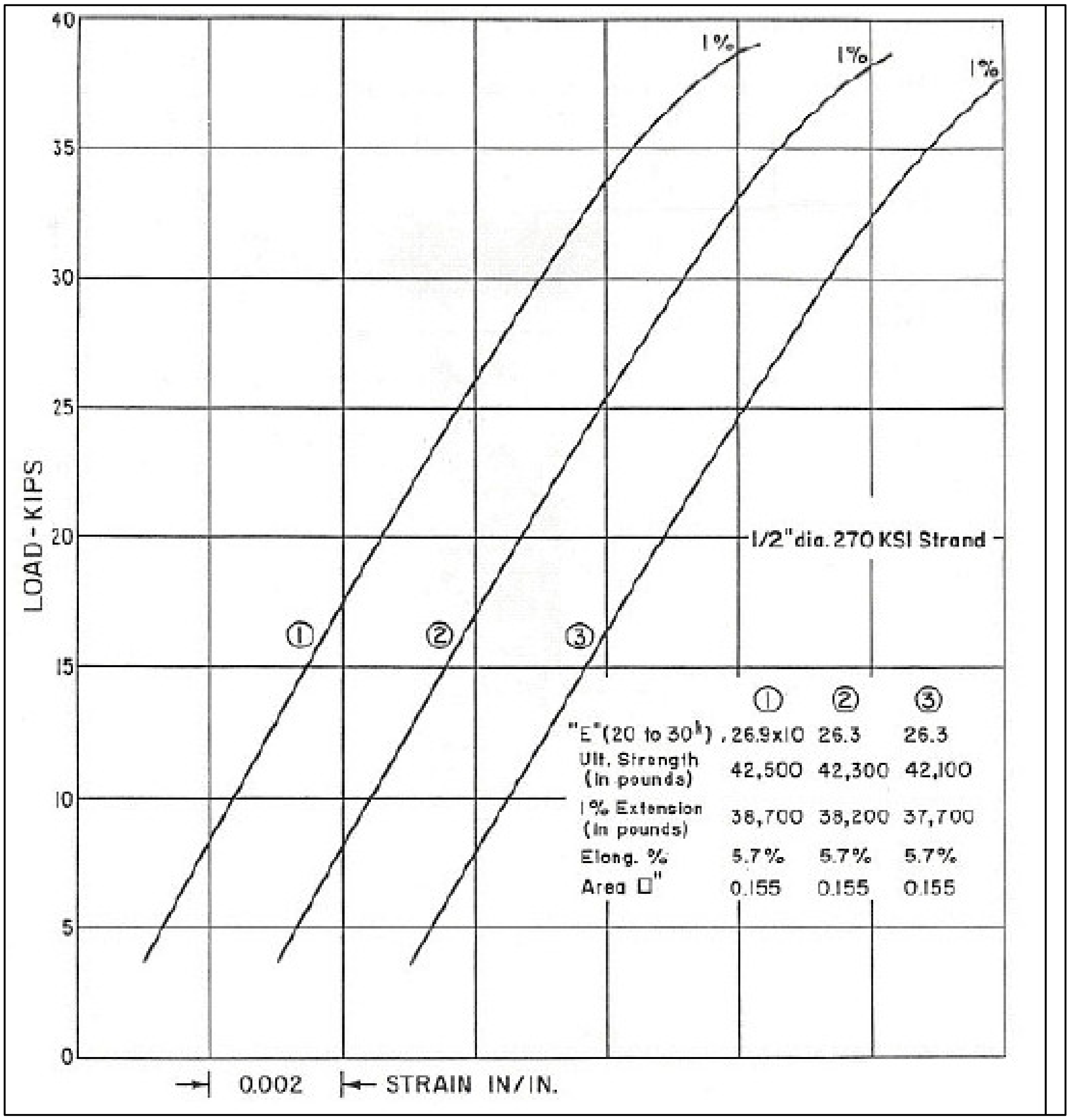

Figure 3.9: Typical Stress-Strain Curve for 0.5 inch (12.70 mm) 270 ksi (1860 MPa) Strand (Barker and Puckett 2013).

The development of moment versus curvature depends on geometry and material properties. Moment-curvature relationships were generated for the considered types of girders. Twenty five thousand cycles of Monte Carlo Simulation MCS were performed using the statistical parameters for material factor M, fabrication factor F, and professional factor P. (Table 1) (Tabsh 1990). The nominal moment carrying capacities are obtained from the AASHTO LRFD specifications (Sixth Edition 202). Different span lengths and girder spacing were considered to calculate the bias factor λ, and the coefficient of variation, CoV.

In order to evaluate the shear capacity (resistance) of prestressed girders, the Simplified Modified Compression Field Theory (Bentz et al. 2006) has been utilized assuming that the shear force is resisted only by the girder concrete and reinforcing steel (stirrups). The detailed procedure is illustrated in Appendix- A. Also, Monte Carlo Simulation technique, with 25000 cycles, has been applied considering different span lengths and girder spacing. Tables 3.18 to 3.21 show the statistical parameters for flexural resistance and shear for AASHTO Girders, CPCI Girders, Bulb-T (NEBT) Girders, and NU Girders, respectively.

Table 3.18: Statistical parameters of ultimate flexural resistance of AASHTO Girders.

Girder Type	Span (m)	Mr		Vr	
		λ	CoV	λ	CoV
AASHTO I	10	1.062	0.068	1.110	0.140
	15	1.063	0.068	1.111	0.142
	Average	**1.063**	**0.068**	**0.111**	**0.141**
AASHTO II	15	1.061	0.068	1.107	0.141
	20	1.064	0.069	1.112	0.140
	25	1.065	0.068	1.109	0.138
	Average	**1.063**	**0.068**	**1.109**	**0.140**
AASHTO III	15	1.062	0.066	1.109	0.142
	20	1.062	0.069	1.111	0.140
	25	1.064	0.067	1.108	0.142
	Average	**1.063**	**0.067**	**1.109**	**0.141**
AASHTO IV	20	1.065	0.068	1.109	0.138
	25	1.062	0.069	1.111	0.140
	30	1.063	0.068	1.111	0.142
	35	1.064	0.069	1.112	0.140
	Average	**1.064**	**0.069**	**1.111**	**0.140**
AASHTO V	20	1.064	0.069	1.112	0.140
	25	1.062	0.069	1.110	0.142
	30	1.064	0.069	1.112	0.140
	35	1.065	0.068	1.109	0.138
	40	1.062	0.066	1.111	0.142
	Average	**1.063**	**0.068**	**1.111**	**0.140**
AASHTO VI	20	1.061	0.067	1.110	0.141
	25	1.065	0.066	1.108	0.138
	30	1.064	0.069	1.112	0.140
	35	1.062	0.069	1.111	0.140
	40	1.061	0.068	1.107	0.141
	45	1.065	0.068	1.110	0.142
	Average	**1.063**	**0.068**	**1.110**	**0.140**

Table 3.19: Statistical parameters of ultimate resistance of CPCI Girders.

Girder Type	Span “m”	Mr		Vr	
		λ	CoV	λ	CoV
CPCI 900	15	1.063	0.069	1.112	0.143
	20	1.064	0.067	1.109	0.141
	Average	**1.064**	**0.068**	**1.111**	**0.142**
CPCI 1200	15	1.061	0.068	1.107	0.139
	20	1.062	0.069	1.111	0.141
	25	1.063	0.069	1.111	0.141
	Average	**1.062**	**0.069**	**1.110**	**0.140**
CPCI 1400	15	1.060	0.068	1.108	0.141
	20	1.060	0.068	1.108	0.141
	25	1.063	0.068	1.106	0.144
	Average	**1.061**	**0.068**	**1.107**	**0.142**
CPCI 1500	20	1.061	0.069	1.106	0.140
	25	1.061	0.069	1.106	0.140
	30	1.063	0.068	1.113	0.141
	35	1.063	0.068	1.113	0.141
	Average	**1.062**	**0.069**	**1.110**	**0.140**
CPCI 1600	20	1.061	0.068	1.112	0.141
	25	1.062	0.068	1.112	0.141
	30	1.064	0.068	1.112	0.140
	35	1.067	0.068	1.111	0.140
	40	1.067	0.068	1.110	0.140
	Average	**1.064**	**0.068**	**1.111**	**0.140**
CPCI 1900	20	1.063	0.067	1.110	0.138
	25	1.063	0.067	1.110	0.138
	30	1.063	0.067	1.110	0.138
	35	1.063	0.067	1.110	0.138
	40	1.063	0.068	1.114	0.141
	45	1.064	0.068	1.114	0.141
	Average	**1.063**	**0.067**	**1.111**	**0.139**
CPCI 2300	35	1.061	0.068	1.110	0.139
	40	1.064	0.068	1.110	0.139
	45	1.066	0.068	1.110	0.140
	50	1.066	0.068	1.110	0.140
	55	1.066	0.068	1.110	0.140
	60	1.066	0.068	1.110	0.140
	Average	**1.065**	**0.068**	**1.110**	**0.140**

Table 3.20: Statistical parameters of ultimate flexural resistance of Bulb-T (NEBT) Girders.

Girder Type	Span "m"	Mr		Vr	
		λ	CoV	λ	CoV
NEBT 1000	15	1.062	0.068	1.112	0.142
	20	1.063	0.068	1.110	0.142
	Average	**1.063**	**0.068**	**1.111**	**0.142**
NEBT 1200	15	1.063	0.067	1.105	0.140
	20	1.063	0.068	1.110	0.140
	25	1.064	0.069	1.111	0.142
	Average	**1.063**	**0.068**	**1.109**	**0.141**
NEBT 1400	15	1.061	0.068	1.109	0.140
	20	1.064	0.067	1.108	0.143
	25	1.065	0.068	1.114	0.140
	Average	**1.063**	**0.068**	**1.110**	**0.141**
NEBT 1600	20	1.062	0.068	1.112	0.141
	25	1.062	0.067	1.110	0.142
	30	1.063	0.068	1.111	0.140
	35	1.066	0.068	1.114	0.139
	Average	**1.063**	**0.068**	**1.112**	**0.141**
	25	1.060	0.068	1.111	0.141
	30	1.062	0.068	1.111	0.140
	35	1.064	0.068	1.107	0.141
	40	1.065	0.067	1.113	0.139
	Average	**1.063**	**0.068**	**1.110**	**0.140**

Table 3.21: Statistical parameters of ultimate resistance of NU Girders.

Girder Type	Span "m"	Mr		Vr	
		λ	CoV	λ	CoV
NU 900	15	1.062	0.068	1.109	0.139
	20	1.062	0.069	1.112	0.146
	Average	**1.062**	**0.069**	**1.111**	**0.143**
NU 1100	15	1.062	0.067	1.110	0.141
	20	1.063	0.068	1.107	0.138
	25	1.064	0.069	1.110	0.140
	Average	**1.063**	**0.068**	**1.109**	**0.140**
NU 1350	15	1.061	0.068	1.105	0.143
	20	1.061	0.068	1.105	0.141
	25	1.063	0.067	1.107	0.144
	Average	**1.062**	**0.068**	**1.106**	**0.143**
NU 1600	20	1.062	0.068	1.111	0.141
	25	1.062	0.068	1.109	0.139
	30	1.062	0.068	1.109	0.142
	35	1.064	0.068	1.110	0.141
	Average	**1.063**	**0.068**	**1.110**	**0.141**
NU 1800	20	1.062	0.068	1.112	0.141
	25	1.062	0.067	1.113	0.139
	30	1.062	0.068	1.113	0.141
	35	1.062	0.068	1.109	0.140
	40	1.064	0.069	1.109	0.140
	Average	**1.062**	**0.068**	**1.111**	**0.140**
NU 2000	20	1.062	0.068	1.117	0.141
	25	1.062	0.068	1.117	0.141
	30	1.062	0.067	1.111	0.142
	35	1.063	0.066	1.108	0.143
	40	1.063	0.068	1.111	0.139
	45	1.065	0.068	1.107	0.141
	Average	**1.063**	**0.068**	**1.112**	**0.141**

3.5 Summary

In this chapter, new statistical parameters (bias factor and coefficient of variation) of random variables related to the load effects (ultimate bending, ultimate shear, cracking moment, and fatigue stress range) were derived. These statistical parameters were derived for the most popular precast girders namely: AASHTO Girders, CPCI Girders, Bulb-T (NEBT) Girders, and NU Girders.

The Central Limit Theorem CLT has been applied in association with Monte Carlo Simulation MCS to derive the statistical parameters of sectional properties. To derive the statistical parameters of the ultimate flexural capacity, strain compatibility (incremental approach) was utilized. For shear resistance, the simplified equivalent compression field was applied (as detailed in Appendix B).

From large number of trials, it was found that 25000 cycles of MCS are sufficient to have satisfactory convergence for accurate results.

The statistical parameters derived in this chapter will be used to conduct comprehensive reliability analysis, of prestressed girder bridges, in the next chapter.

Chapter 4

Reliability Analysis and Assessment of Prestressed Girder Bridges

4.1 Introduction

When performing reliability-based structural design and/or design optimization, it becomes essential to consider the structural reliability with respect to all limit state functions, every possible mode of failure, and the overall structural system reliability.

In this Chapter, the reliability of prestressed girder bridges is investigated and estimated. The limit states were considered as per the AASHTO LRFD (Seventh Edition, 2014) code requirements. The individual components' reliabilities have been calculated using two different methods; namely: the *First-Order Reliability Method,* FORM and the Monte Carlo Simulation, MCS technique. Failure Mode Analysis, FMA and Improved Reliability Bounds, IRB method were utilized to evaluate the overall system reliability. The development of these reliability computational methods is demonstrated in Appendix A.

A computer algorithm, BREL (Bridge RELiability), has been coded, by Visual Basic Application VBA and Excel Worksheets, to calculate the components' and system's probability of failure and the corresponding reliability indices. To validate the proposed reliability model, the results were compared with those obtained from the finite element reliability analysis, performed using COSSAN-X Software (a comprehensive sophisticated Finite Element Probabilistic software) from the University of Liverpool-UK (2014). The results from the two models revealed a very good agreement.

4.2 Limit States and Limit State Functions Considered in the Current Research

Following the AASHTO LRFD requirements, the limit states considered for the design of prestressed girder bridges are as summarized in Table 4.1. These limit states have been investigated in different locations of the bridge as illustrated in Figure 4.1.

In general, any limit state function can be expressed as follows:

[4.1] $$g(R, Q) = R - Q$$

where, Q = Load effect

R = Resistance

Table 4.1 Limit states considered in the design of prestressed girder bridges

Phase	Limit State	Description
Initial Phase (at transfer)	Service I	Tensile stress at top fiber at end section
		Compressive stress at bottom fiber at end section
		Tensile stress at top fiber at transfer length section
		Compressive stress at bottom fiber at transfer length section
		Tensile stress at top fiber at harp point section
		Compressive stress at bottom fiber at harp point section
		Tensile stress at top fiber at midspan
		Compressive stress at bottom fiber at midspan
Service Phase (after losses)	Service I	Compressive stress at top fiber of girder at midspan, case 1: under effective prestress + permanent loads
		Compressive stress at top fiber of girder at midspan, case 2: under ½(Effective prestress + permanent loads) + transient loads.
		Compressive stress at top fiber of girder at midspan, case 3: under effective prestressing, permanent and transient loads
		Compressive stress at top fiber of deck at midspan, case 1: under permanent loads
		Compressive stress at top fiber of deck at midspan, case 2: under permanent and transient loads
	Service III	Tensile stress at bottom fiber of the girder at midspan
	Fatigue I	Fatigue limit state
	Service I	Cracking limit state
	Strength I	Ultimate strength limit state (flexure)
	Strength I	Ultimate strength limit state (shear)

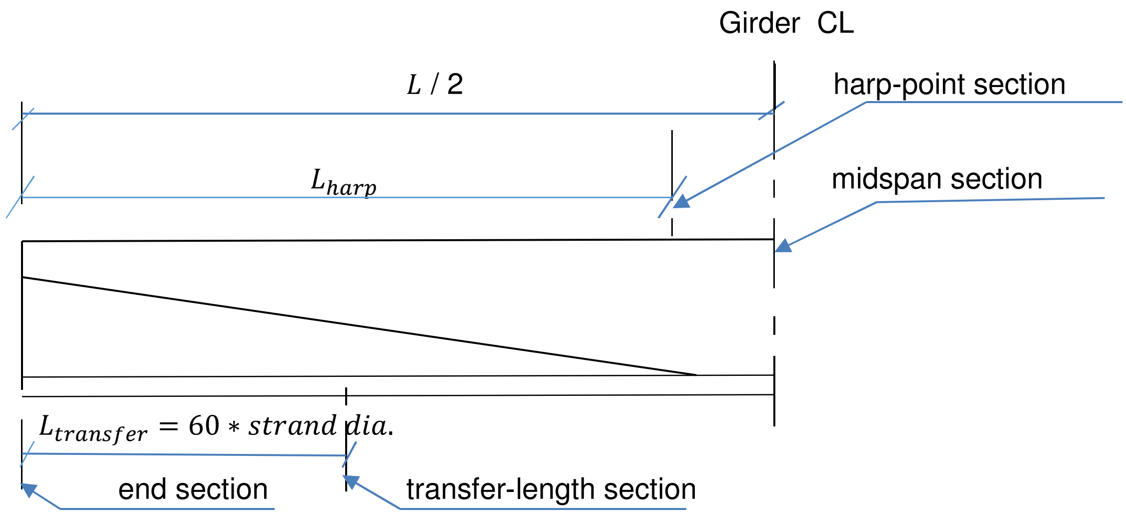

Figure 4.1: Locations considered for the possible modes of failure.

4.2.1 Limit State Functions at Initial Phase (at transfer)

The girder is subjected to selfweight and initial jacking force (prestressing) before time-dependent losses occur. The limit state functions at the top and bottom fibers of the girder are investigated at the considered locations shown in Figure 4.1. The tension at the top fiber at the end section is expressed by limit state function, g_1, formulated in Equation 4.2, while, the compression at the bottom fiber at the end section is governed by limit state function, g_2 , as in Equation 4.3. At the transfer length section, the limit state functions for tension at top fiber (g_3) and compression at the bottom fiber (g_4) are expressed by Equations 4.4 and 4.5, respectively. Similarly, Equations 4.6 and 4.7 express the limit state functions of the tension (g_5) and compression (g_6) at the harp-point section, respectively. For the midspan section, the tension at top fiber and the compression at bottom fiber are defined by the limit state functions (g_7 and g_8) as formulated in Equations 4.8 and 4.9, respectively.

[4.2] $$g_1 = 0.24\sqrt{f'_{ci}} + \frac{P_i}{A_g} - \frac{P_i\, e_{0i}}{Z_t}$$

[4.3] $$g_2 = 0.60\, f'_{ci} + \frac{P_i}{A_g} + \frac{P_i\, e_{0i}}{Z_b}$$

[4.4] $$g_3 = 0.24\sqrt{f'_{ci}} + \frac{P_i}{A_g} - \frac{P_i\, e_{ti}}{Z_t} + \frac{M_{transfer}}{Z_t}$$

where, $M_{transfer}$ is the moment due to dead load, *DC* at transfer length section.

[4.5] $$g_4 = 0.60\, f'_{ci} + \frac{P_i}{A_g} + \frac{P_i\, e_{ti}}{Z_b} - \frac{M_{transfer}}{Z_b}$$

[4.6] $$g_5 = 0.24\sqrt{f'_{ci}} + \frac{P_i}{A_g} - \frac{P_i\, e_{hi}}{Z_t} + \frac{M_{harp}}{Z_t}$$

where, M_{harp} is the moment due to dead load, *DC* at harp-point section.

[4.7] $$g_6 = 0.60\, f'_{ci} + \frac{P_i}{A_g} + \frac{P_i\, e_{hi}}{Z_b} - \frac{M_{harp}}{Z_b}$$

[4.8] $$g_7 = 0.60\, f'_{ci} + \frac{P_i}{A_g} - \frac{P_i\, e_{ci}}{Z_t} + \frac{M_{mid}}{Z_t}$$

where, M_{mid} is the moment due to dead load, *DC* at midspan section.

[4.9] $$g_8 = 0.60\, f'_{ci} + \frac{P_i}{A_g} + \frac{P_i\, e_{ci}}{Z_b} - \frac{M_{mid}}{Z_b}$$

where, A_g = cross sectional area of a girder (mm^2).

e_{0i} = eccentricity of strand at end section (at initial stage) (mm).

e_{ti} = eccentricity of strand at transfer length section (at initial stage) (mm).

e_{hi} = eccentricity of strand at harp point section (at initial stage) (mm).

e_{ci} = eccentricity of strand at centerline section (at initial stage) (mm).

f'_{ci} = compressive strength of concrete (at initial stage) (MPa).

Z_b = section modulus at bottom fiber (noncomposite section) (mm^3).

Z_t = section modulus at top fiber (noncomposite section) (mm^2).

P_i = jacking stress before time-dependent losses (MPa).

4.2.2 Limit State Functions at Service Phase (after losses)

In the service phase, after losses occur, the girder acts compositely with the deck. Hence, the properties of the composite section were applied.

For short and medium spans, the combination of dead load, live load, and dynamic (impact) effect of live load dominates the design of prestressed girder bridges (Nowak 2004 and Barker and Puckett 2013). For simply supported bridges, the midspan section is usually the critical section in final stage (service phase).

4.2.2.1 Compressive and Tensile Stresses at Top and Bottom Fibers

According to AASHTO LRFD [A.5.9.4.2.1-1], the compression at top fiber of girder is investigated under three load conditions (referred to, in Table 4.1, as load case1, load case2, and load case3). Hence, three limit state functions exist. Equation 4.10 defines the limit state function for the compression at the top fiber of the girder under effective prestress and permanent loads (Service I). For the same limit state function, but considering only half of the summation of effective prestress and permanent loads, plus the transient loads (Service I), Equation 4.11 is applied. Equation 4.12 expresses the same limit state function but for transient loads (Service I).

The compression at the top fiber of deck slab is investigated under two load conditions. Hence, two limit state functions exist Equation 4.13 applies for the compression at the top fiber of the deck under permanent loads (Service I). For the same limit state function but under permanent and transient loads (Service I), Equation 4.14 is applied.

The tension at the bottom fiber of the girder subjected to effective prestress, permanent and transient loads (Service III) is investigated by applying the limit state function formulated in Equation 4.15.

[4.10] $$g9 = 0.45\, f'_{ci} + \frac{P_e}{A_g} - \frac{P_e\, e_c}{Z_t} + \frac{M_{DC}}{Z_t} + \frac{M_W}{Z_{tg}}$$

[4.11] $$g10 = 0.40\, f'_{ci} + 0.5\left(\frac{P_e}{A_g} - \frac{P_e\, e_c}{Z_t} + \frac{M_{DC}}{Z_t} + \frac{M_W}{Z_{tg}}\right) + \frac{M_L}{Z_{tg}}$$

[4.12] $$g11 = 0.45\, f'_{ci} + \frac{P_e}{A_g} - \frac{P_e\, e_c}{Z_t} + \frac{M_{DC}}{Z_t} + \frac{M_{DW}}{Z_{tg}} + \frac{M_L}{Z_{tg}}$$

[4.13] $$g12 = 0.45\, f'_{ci} + \left(\frac{M_{DW}}{Z_{tc}}\right)/\, n$$

[4.14] $$g13 = 0.45\, f'_{ci} + \left(\frac{M_{DW}}{Z_{tc}} + \frac{M_L}{Z_{tc}}\right)/\, n$$

[4.15] $$g14 = 0.19\sqrt{f'_{ci}} + \frac{P_e}{A_g} + \frac{P_e\, e_c}{Z_b} - \frac{M_{DC}}{Z_b} - \frac{M_{DW}}{Z_{bc}} - 0.8\,\frac{M_L}{Z_{bc}}$$

where, e_c = eccentricity of strand at midspan section (mm).

M_{DC} = moment due to dead load ($kN\ m$).

M_{DW} = moment due to wearing surface and utilities ($kN\ m$).

M_L = moment due to live load ($kN\ m$).

Z_{tg} = section modulus of transformed section at top fiber of girder (mm^3).

Z_{tc} = section modulus of composite section at top fiber of girder (mm^3).

Z_{bc} = section modulus of composite section at bottom fiber of girder (mm^3).

n = E_d / E_g (i.e. modulus of elasticity of deck / modulus of elasticity of girder).

P_e = effective jacking stress (after losses) (MPa).

4.2.2.2 Fatigue limit state

AASHTO LRFD [A.3.4.1] defines two limit states for load-induced fatigue. However, only Fatigue I is related to infinite load-induced fatigue life, which is applicable to concrete elements (Barker and Puckett, 2013). For fatigue considerations, concrete members shall satisfy the requirements of AASHTO LRFD [A.5.5.3.1], that is: $\gamma(\Delta f) \leq (\Delta F)_{TH}$. Thus, the limit state function can be expressed as in Equation 4.16.

(4.16) $$g_{15} = (\Delta F)_{TH} - \gamma(\Delta f)$$

[4.17] $$\Delta f = f_{max} - f_{min}$$

where

$\gamma =$ load factor (AASHTO LRFD 5.5.3.1, Table 5.1, for the fatigue I load combination).

Δf = force effect, live-load stress range due to the passage of the fatigue load (AASHTO LRFD A3.6.1.4).

$(\Delta F)_{TH}$ =fatigue-amplitude threshold (AASHTO LRFD A5.5.3.2, A5.5.3.3, or A5.5.3.4, as appropriate). The nominal value of $(\Delta F)_{TH}$, varies with the radius of curvature of the tendon and shall not exceed:

- 125 MPa for radii of curvature in excess of 9000 mm.
- 70 MPa for radii of curvature not exceeding 3600 mm.

f_{min} = minimum stress due to permanent load which can be obtained as follows:

[4.18] $$f_{min} = \frac{E_p}{E_c}\,(f_{cgp} + f_{ccp,min})$$

where,

f_{ccp}= concrete stress at centre of gravity of prestress tendons due to fatigue moment. This stress can be calculated as follows:

[4.19] $$f_{ccp} = \frac{M_{fatigue}\ e_{pc}}{I_c}$$

and

f_{cgp} = concrete stress at centre of gravity of prestress tendons due to permanent load and prestress. This stress can be obtained as follows:

[4.20] $$f_{cgp} = -\frac{F_{eff}}{A_g} - \frac{F_{eff}\ e_m\ e_{pg}}{I_g} + \frac{M_{DC1}\ e_{pg}}{I_g} + \frac{(M_{DC2} + M_{DW})e_{pc}}{I_c}$$

where,

e_m = eccentricity of prestress tendon with respect to midspan section, mm.

e_{pc} = eccentricity of prestress tendon in composite section, mm.

e_{pg}= eccentricity of prestress tendon in girder, mm.

I_c= second moment of area (moment of inertia) of composite section, mm^4.

I_g= second moment of area (moment of inertia) of girder, mm^4.

M_{DC1} = moment due to self weight of girder, deck and diaphragm, $kN\ m$.

M_{DC2} = moment due to self weight of barriers and utilities, $kN\ m$.

M_{DW}= moment due to wearing surface (asphalt), $kN\ m$.

f_{max} = maximum stress due to permanent load plus transitory fatigue load. This maximum stress can be obtained as follows:

[4.21] $$f_{max} = \frac{E_p}{E_c}\,(f_{cgp} + f_{ccp,max})$$

where

E_p= modulus of elasticity of prestress steel, ksi.

E_c = modulus of elasticity of concrete, ksi.

According to AASHTO LRFD [A5.3.3.1], cracked section properties should be used for fatigue calculation, if the sum of stresses in concrete at the bottom fiber due to factored permanent loads and prestress plus $M_{\text{fatigue}-\text{I}}$, exceeds $0.095\sqrt{f'_c}$.
However, according to AASHTO LRFD [A5.3.3.1], if the section is in compression under dead load DL and fatigue I load, then verification for fatigue does not need to be performed. The fatigue load is the AASHTO LRFD design truck (HS20-44truck) but with a fixed rear-axle spacing of 30 feet.

4.2.2.3 Ultimate Strength Limit State Function - Flexure

The AASHTO LRFD bridge specifications provide unified design provisions that are applicable to concrete members reinforced with a combination of conventional reinforcement and prestressing strands (Barker and Pukett, 2013).
In general, the limit state function with respect to the ultimate flexural strength is expressed as follows:

[4.22] $$g_{16} = M_R - M_u$$

The factored flexural resistance, M_r, is expressed as follows:

[4.23] $$M_r = \emptyset\, M_n$$

where,

$\emptyset$ = resistance factor for flexure ; $\emptyset = 1.0$.

As per AASHTO LRFD [A5.7.3.1.1], the stress in prestressing Steel-Bonded Tendons is determined as:

[4.24] $$f_{ps} = f_{pu}(1 - k\frac{c}{d_p})$$

where,

[4.25] $$k = 2(1.04 - \frac{f_{py}}{f_{pu}})$$

d_p =effective depth to the centroid of the prestressing strands.

c =depth of compression stress block. From AASHTO LRFD (A.5.7.2.2);

[4.26] $$c = \frac{A_{ps}\, f_{pu} + A_s\, f_y - A'_s\, f'_y - 0.85\, f'_c\, (b - b_w) h_f}{0.85 \beta_1 f'_c b_w + k\, A_{ps}\, f_{pu}/d_p} \geq h_f$$

where,

$\beta_1 = 0.85$ for $f'_c \leq 27.6\ MPa$

$\beta_1 = 0.65$ for $f'_c \geq 55\ MPa$

$\beta_1 = 0.85 - 0.05(f'_c - 4)$ for $27.6 \leq f'_c \leq 55\ MPa$

$b =$ width of flange, mm.

$b_{w=}$width of web, mm.

$h_f =$ compression flange thickness, mm.

A_{ps} =area of prestressing steel, mm^2.

$A_s =$ area on nonprestressed tension reinforcement, mm^2.

$A'_s =$ area of compression nonprestressed reinforcement, mm^2.

f_{ps} =average stress in prestressing steel at nominal bending resistance of member, MPa.

$f_y =$ specified minimum yield strength of tension reinforcement, MPa.

$f'_y =$ absolute value of specified strength of nonprestressed compression reinforcement, MPa.

When $a = \beta_1 c$ is greater than the compression flange thickness h_f, then:

[4.27] $$M_n = A_{ps} f_{ps} \left(d_p - \frac{a}{2}\right) + A_s f_y (d_s - \frac{a}{2}) + A'_s f'_y \left(\frac{a}{2} - d'_s\right) + 0.85 f'_s (b - b_w) h_f (\frac{a}{2} - \frac{h_f}{2})$$

If $a \leq h_f$, or if the beam has no compression flange, then, by setting b_w equal b, the nominal flexural strength can be obtained as follows:

[4.28] $$\emptyset M_n = \emptyset [A_{ps} f_{ps} \left(d_p - \frac{a}{2}\right) + A_s f_y (d_s - \frac{a}{2})]$$

The ultimate factored moment, for Strength I limit state, is calculated as follows:

[4.29] $$M_u = 1.25\, M_{DC} + 1.50\, M_{DW} + 1.75 M_L$$

where;

M_{DC} = moment due to dead load (structural and non-structural components), $kN\ m$.

M_{DW} = moment due to wearing surface (asphalt), $kN\ m$.

L= moment due to live load effect, $kN\ m$.

However, AASHTO LRFD [A5.7.3.3.2] requires that the amount of prestressed and nonprestressed tensile reinforcement shall, at any section, be adequate to develop a factored flexural resistance M_r at least equal to the least of:

- 1.2 times the cracking moment M_{cr} determined on the basis of elastic stress distribution and the modulus of rupture f_r of concrete ($f_r = 0.37\sqrt{f'_c}$) , or
- 1.33 times the factored moment required by the applicable strength load combination.

This reveals another limit state function considered in this current research:

[4.30] $$g_{17} = M_R - (1.2\ or\ 1.3)\ M_{cr}$$

The cracking moment can be obtained according to AASHTO LRFD [A5.7.3.3.3-1] as follows:

[4.31] $$M_{cr} = Z_C(f_r + f_{cpe}) - M_{dnc}(\frac{Z_c}{Z_{nc}} - 1) \geq Z_c f_r$$

where

f_{cpe}= compressive stress in concrete due to effective prestress force F_{eff} only (after allowance for all prestress losses) at the extreme fiber of the section where tensile stress is caused by externally applied loads. This stress can be obtained as follows:

[4.32] $$f_{cpe} = -\frac{F_{eff}}{A_g} - \frac{F_{eff}\, e_m}{Z_{bg}}$$

M_{dnc} =total unfactored dead load moment acting on the noncomposite section, $kN\ m$.

Z_{nc}= section modulus for the extreme fiber of the noncomposite section where tensile stress is caused by externally applied loads, mm^3.

4.2.2.4 Ultimate Strength Limit State – Shear

The limit state function with respect to the ultimate shear, g_{18}, requires that the ultimate shear force V_u should not exceed the factored shear resistance V_R :

[4.33] $$g_{18} = V_R - V_u$$

[4.34] $$V_R = \emptyset\, V_n$$

$\emptyset$ = resistance factor for shear ; $\emptyset = 0.90$.

As per AASHTO LRFD [A.5.8.3.3], the nominal shear resistance V_n shall be the lesser of:

[4.35] $$V_n = V_c + V_s + V_p$$

and

[4.36] $$V_n = 0.25 f'_c b_v d_v + V_p$$

where

V_c =nominal concrete shear resistance:

[4.37] $$V_c = 0.0316 \beta \sqrt{f'_c}\, b_v d_v$$

V_s =nominal transverse reinforcement shear resistance:

[4.38] $$V_s = \frac{A_v\, f_y\, d_v\, (\cot\theta + \cot\alpha)\, sin\alpha}{s}$$

However, for vertical stirrups ($\alpha = 90^{\circ}$), then:

[4.39] $$V_s = \frac{A_v\, f_y\, d_v\, \cot\theta}{s}$$

where,

$b_v =$ minimum web width, measured parallel to the neutral axis, between the resultants of the tensile and compressive forces due to flexure, modified for the presence of the ducts (mm).

$d_v =$ effective shear depth taken as the distance, measured perpendicular to the neutral axis, between the resultants of the tensile and compressive forces due to flexure; it need not be taken less than the greater of $0.9d_c$ or $0.72h$ (mm).

$s =$ spacing of stirrups (mm).

$\beta =$ factor indicating ability of diagonally cracked concrete to transmit tension;

According to AASHTO LRFD [A5.8.3.4.1]:

$\beta = 2.0$

θ =angle of inclination of diagonal compressive stresses; traditionally:

$\theta = 45^{\circ}$

A_v =area of shear reinforcement within a distance s (mm^2)

V_p =component in the direction of the applied shear of the effective prestressing force; (positive if resisting the applied shear force) (kN).

The ultimate shear force, according to Strength I limit state, is obtained as follows:

[4.40] $$V_u = 1.25\, V_{DC} + 1.50\, V_{DW} + 1.75 V_L$$

where;

V_{DC} = shear due to dead load (structural and non-structural components), (kN).

V_{DW} = shear due to wearing surface and utilities, (kN).

V_L = shear due to live load effect, (kN).

4.3 Reliability Analysis and Prediction

4.3.1 Components Reliability Indexes

When applying the FORM method to evaluate the reliability indices corresponding to the limit state functions described above, only the first two statistical moments (mean and standard deviation) of each random variable are sufficient to calculate the probability of failure. In general, the basic variables are not normally distributed. All random variables are transformed into uncorrelated standard normal variables and the limit state function is then transformed into a corresponding limit state function in the reduced coordinates. Then, the gradients of the limit state function with respect to each variable in the reduced coordinates are derived. An initial failure point is assumed and the reliability index $\boldsymbol{\beta}$ is estimated. The reliability index $\boldsymbol{\beta}$ represents the distance from the origin, in the reduced coordinate space, to the failure point. By successive iterations, the failure point is calculated and a new value of reliability index is obtained. The process is repeated until convergence is achieved. As the probability of failure is well approximated in a standardized normal space, it becomes necessary to transform those non-normal random variables to equivalent normally distributed variables. The space transformation procedure is presented in details in Appendix A.

4.3.2 System Reliability

In a redundant structure, when an individual component reaches its ultimate load carrying capacity, other components can take additional loads to prevent a failure (Mahadevan and Halder 2000). However, the quantification of such redundancy requires a special approach using the system reliability models (Bhattacharya et al. 2009).
For two-lane bridges, the load patterns described in Section 2.1.1.2.5 are considered. For single truck loading events, 80% of trucks are assumed to drive in the right lane and 20% move in the left lane (Ressler 1991). Probability values for the multiple truck loading events are based on the study reported by Nowak (1999) and the assumptions described are summarized below and are illustrated in Figure 4.2.

a) Single truck – right lane: 0.8,

b) Single truck – left lane: 0.2,

c) Two trucks – every 15th truck passing on the bridge is simultaneous with another truck,

d) Two trucks – For each such occurrence it is assumed that every 10th time (correlation factor ρ =0.5), and

e) Two trucks – For each such occurrence it is assumed that every 30th time (full correlation ρ =1.0).

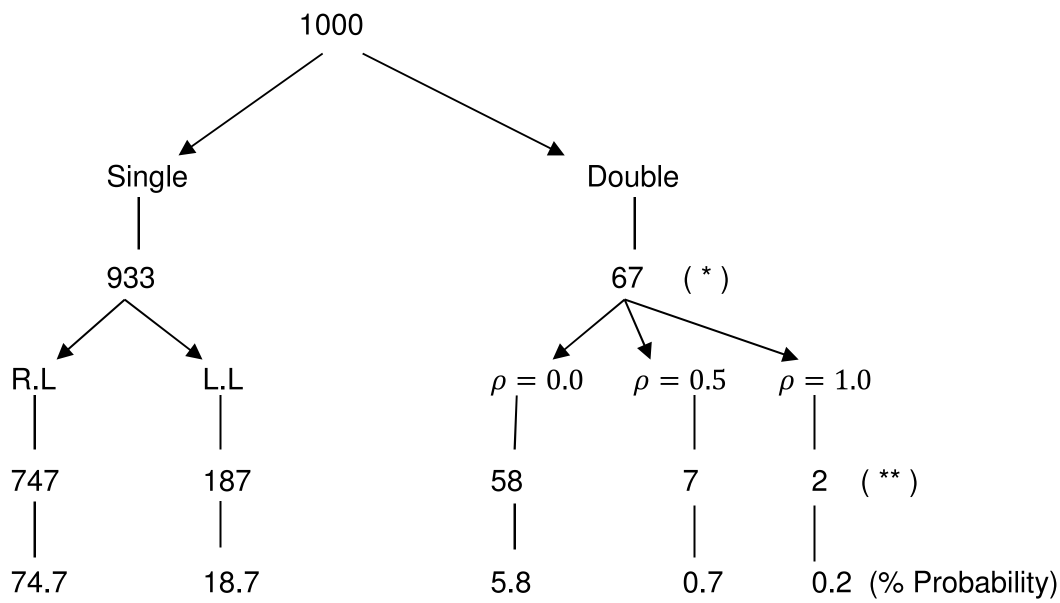

(*): assumption c mentioned above.

(**): assumption a, b, d, and e.

Figure 4.2: Different scenarios for truck positioning.

The model BREL, developed in the current study, provides an algorithm that performs Failure Mode Analysis FMA using 2-D nonlinear grillage analogy. The macro of this algorithm, named GRALAL (GRillage ANALogy), is presented in Appendix E. The following steps are followed to estimate the structural redundancy (system reliability):

Step 1: Generate a mesh that best represents the actual bridge configuration. Figure 4.3 gives an example of such idealization (Hambly 1991). While Figure 4.4 shows a snapshot from the proposed model to define the grillage configuration.

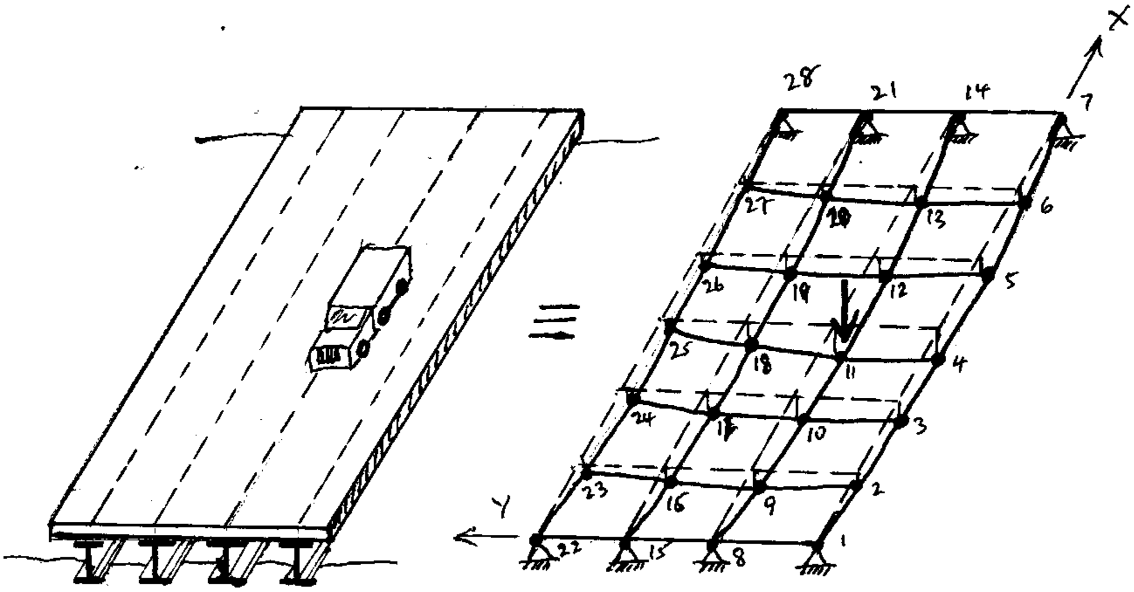

Figure 4.3: A grillage mesh to represent the actual bridge configuration (Hambly 1991).

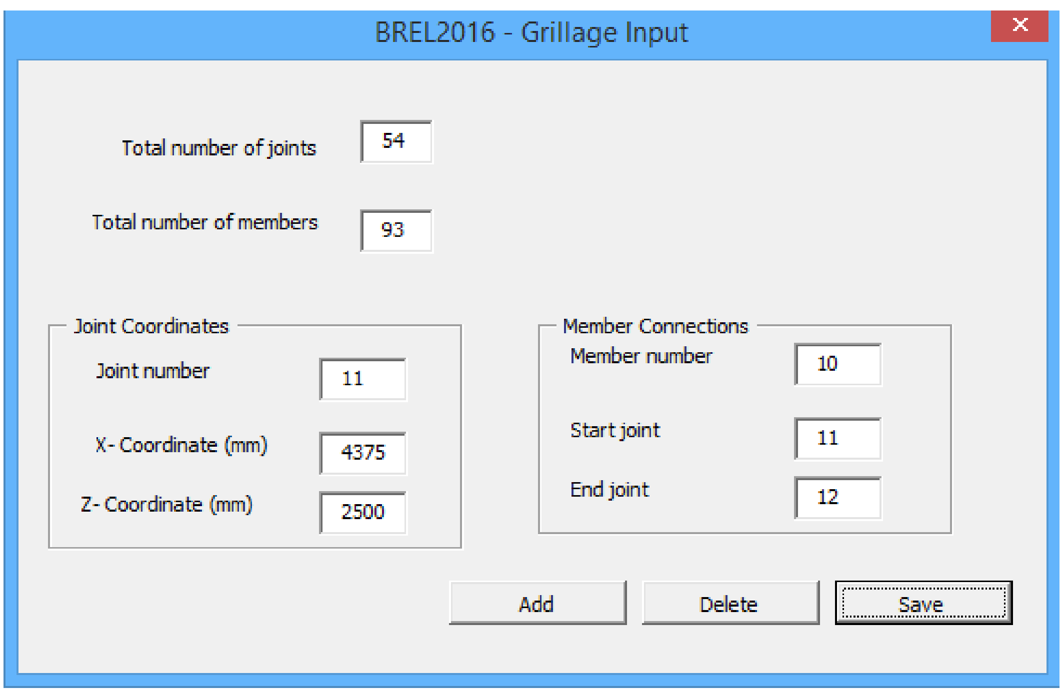

Figure 4.4: A snapshot from the proposed model to define the grillage configuration.

Step 2: Classify the grillage members into the following groups:

- Group A: External girders.
- Group B: Internal girders.
- Group C: Diaphragms.
- Group D: Deck slab.

Step 3: Calculate the member properties. In the grillage analysis, three member properties are required; the cross sectional area, the moment of inertia, and the torsional constant. To simplify the calculations, the actual section could be converted to an equivalent section that has the same properties of the original (actual) one, as illustrated in Figure 4.5. Then, the section properties are determined as follows:

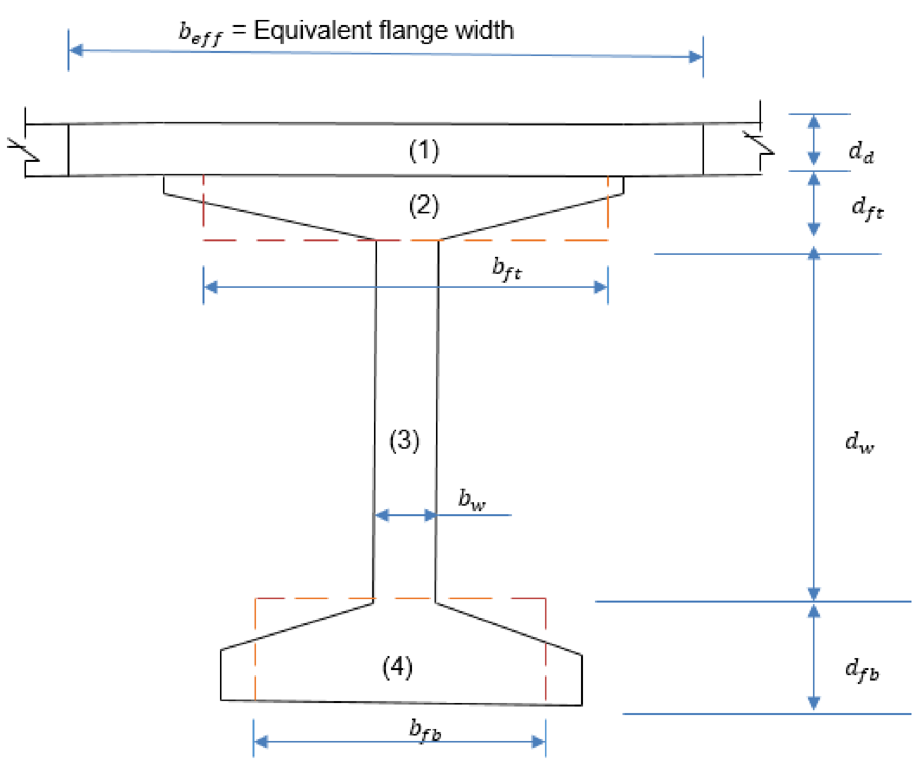

Figure 4.5: Converting actual composite section to equivalent section

[4.41] Area, $A = A_1 + A_2 + A_3 + A_4$

[4.42] $I_c = [b_{eff} {d_d}^3/12 + A_d(y_d - y_c)^2] + \sum[I_i + A_i(y_c - y_i)^2]$

For torsional constant J, the Saint-Venant expression (Equation 4.43), (Hambly 1991), was considered.

[4.43] $$J = \frac{A^4}{40I_p}$$

where, I_p is the polar moment of inertia. Equation 4.43 can be reduced, for rectangular sections of b width and d depth, as follows:

[4.44] $$J = \frac{3b^3d^3}{10(b^2+d^2)}$$

However, when b is greater than 5d, the section is considered thin. Thus:

[4.45] $$J = \frac{bd^3}{3}$$

Therefore, for the section shown in figure 4.3, the torsional constant can be calculated as follows:

[4.46] $$J = J_1 + (J_2 + J_3 + J_4)\frac{E_g}{E_d}$$

[4.47] $$J_1 = \frac{1}{2}(\frac{1}{3}b_{eff}{d_d}^3)$$

where, b_{eff} is the deck effective width and d_d is the deck thickness.

[4.48] $$J_2 = \frac{1}{3}{b_w}^3d_w$$

where, b_w is the web width and d_w is the web thickness.

[4.49] $$J_3 = \frac{3{b_{ft}}^3{d_{ft}}^3}{10({b_{ft}}^2{d_{ft}}^2)}$$

where, b_{ft} is the top flange width and d_{ft} is the top flange thickness.

[4.50] $$J_4 = \frac{3{b_{fb}}^3{d_{fb}}^3}{10({b_{fb}}^2{d_{fb}}^2)}$$

where, b_{ft} is the bottom flange width and d_{ft} is the bottom flange thickness.

Figure 4.6 shows a snapshot from the BREL model employed for defining the properties of the grillage members.

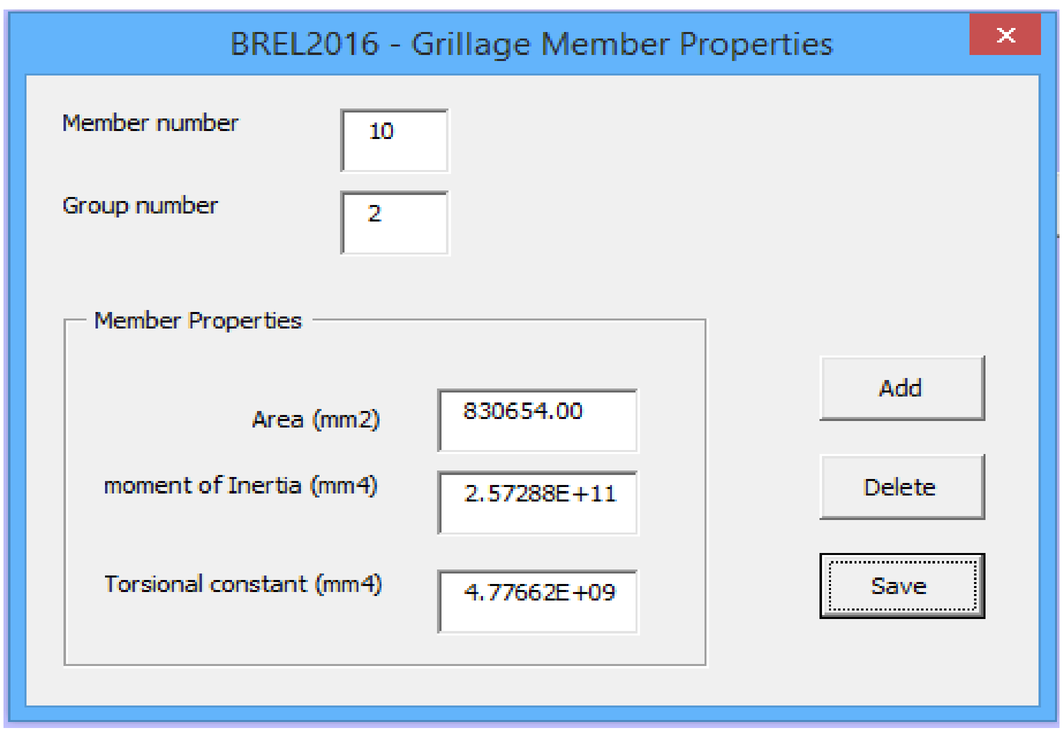

Figure 4.6: A snapshot from the proposed model defining the properties of the grillage members.

Step 4: Perform deterministic analysis using the proposed algorithm to obtain the nominal values of the basic variables.

Step 5: Apply the statistical parameters of dead load (Table 2.1).

Step 6: Utilize the live load model defined in section 2.1.1.2.5. To apply the live load, the user shall identify the number of loaded lanes and also shall consider the scenarios of the truck placement. This information needs to be provided as input data in the proposed model as illustrated in Figure 4.7.

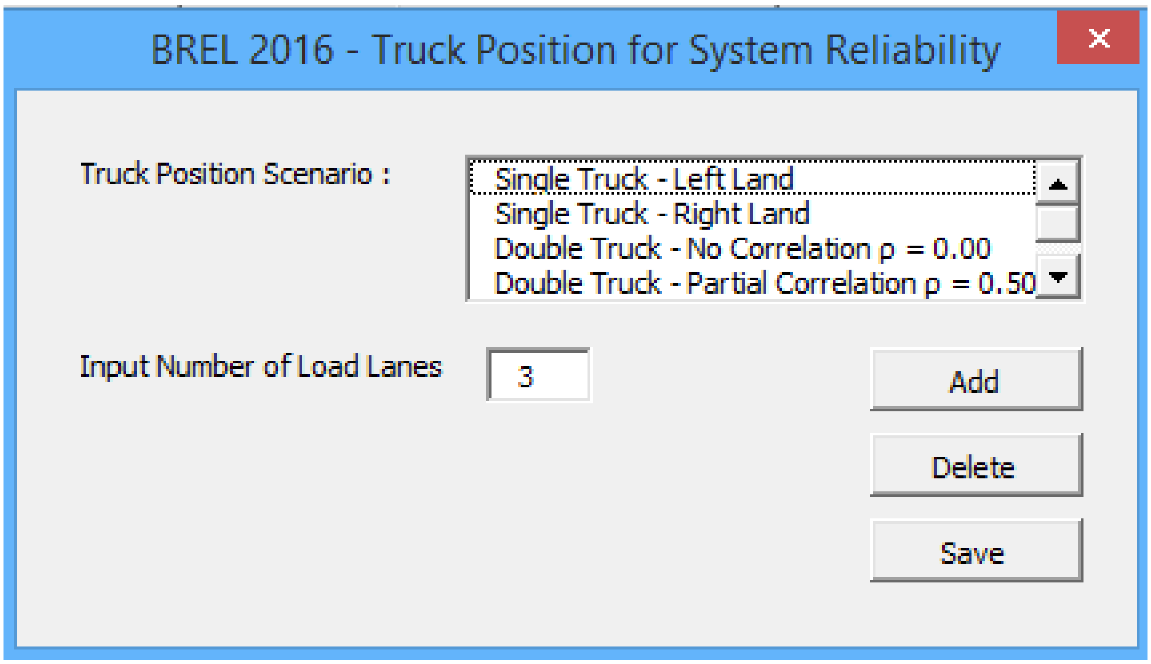

Figure 4.7: A snapshot from the proposed model to define the live load model.

Step 7: Calculate the load effects at the critical sections.

Step 8: Incrementally, increase the live load and calculate the bridge response. Record the load just before the formation of the first plastic hinge.

Step 9: Continue increasing the live load until the bridge is no more able to bear more load (mechanism or excessive deflection).

Step 10: Just before collapse, record the load (number of standard trucks) applied to the bridge. The difference between the two loads recorded in steps 8 and 10 indicates the structural redundancy for a specific truck positioning.

Step 11: calculate the probability of failure and the corresponding reliability index associated with every mode of failure (related to the load positioning scenario).

Step 12: Apply the Improved Reliability Bounds IRB approach to calculate the upper and lower bounds of the system reliability. The IRB approach assures providing the narrowest possible bounds of system reliability. The IRB method can be illustrated as follows:

A limit state function, F_k,with respect to a mode of failure, k , can be formulated as:

[4.51] $$F_k = \sum_{i=1}^{n} M_{ki} R_i - \sum_{j=1}^{m} S_{kj} Q_j$$

where,

M_{ki} = Resistance coefficient related to the k^{th} mode.

S_{kj} = Load coefficient related to the k^{th} mode.

R_i = Resistance considered as independent continuous random variable of at the i^{th} point in the system.

Q_j = Load effect considered as independent continuous random variable of at the j^{th} point in the system.

n = Number of random variables related to the resistance.

m = Number of random variables related to the load effect.

Assuming that the *Central Limit Theorem* is applicable, then F_k will have a normal distribution.

Equation 4.51 can be re-written in a compact form as follows:

[4.52] $$F_k = \sum_{i=1}^{r} C_{ki}\, x_i \qquad \begin{cases} > 0 & \mathit{Survaival\ mode} \\ \leq 0 & \mathit{Failure\ mode} \end{cases}$$

where C_{ki} replaces M_{ki} and S_{kj}; x_i replaces R_i and Q_j; and r is the sum of m and n.

The failure probability of the k^{th} mode can be obtained as follows:

[4.53] $$P(F_k \leq 0) = \Phi(-\beta_k)$$

in which Φ denotes the cumulative distribution function, and β_k is the reliability index with corresponding to the k^{th} mode.

For any dependent (correlated) modes of failure (k and l), the conditional mean, $\mu(Z_k|Z_l)$,and the standard deviation, $\sigma(Z_k|Z_l)$, can be calculated as per Equations 4.54 and 4.55, respectively (Stevenson 1968):

[4.54] $$\mu(Z_k|Z_l) = \mu_{zk} + \rho_{kl}(\frac{\sigma_{zk}}{\sigma_{zl}})(Z_l - \mu_{zj})$$

[4.55] $$\sigma(Z_k|Z_l) = \sigma_{zk}\sqrt{(1 - {\rho_{kl}}^2)}$$

where, ρ_{kl} is the correlation coefficient between Z_k and Z_l.

The probability of failure of the first and second modes can be expressed as:

[4.56] $$P(Z_1 < 0, Z_2 < 0) = \int_{\nu=-\infty}^{\nu=0}\int_{\mathcal{U}=-\infty}^{\mathcal{U}=0} P(Z_{1=\mathcal{U}}/Z_{2=\nu}).P(Z_{2=\nu})\, d_{\mathcal{U}}d_{\nu}$$

[4.57] $$P(Z_1 < 0, Z_2 < 0) = \int_{\nu=-\infty}^{\nu=0}\int_{\mathcal{U}=-\infty}^{\mathcal{U}=0} P(Z_{2=\mathcal{U}}/Z_{1=\nu}).P(Z_{2=\nu})\, d_{\nu}d_{\mathcal{U}}$$

If a polynomial expression is used, then the double integration in Equations (4.56 and 4.57) can equivalently be replaced by a single integration (Abramowitz and Stegun 1970). The joint failure probability can be calculated by selecting a suitable range of integration, e.g. -5σ_{z2} to 0. For almost all practical applications, the lower limit of -5σ_{z2} would yield nearly same results (Ahmed and Koo 1990). By substituting $Z_n = \nu$ in Eq. (4.54), $\mu_{(Z_1/Z_2)}$ is obtained. Then from Eq. (4.55), $\sigma_{(Z_1/Z_2)}$ can be calculated. Having the mean and standard deviation detarmined, the joint reliability can be estimated as per Equation 4.58 and the cumulative distribution function as in Equation 4.59:

[4.58] $$\beta_{(Z_1/Z_2)} = \mu_{(Z_1/Z_2)}/\sigma_{(Z_1/Z_2)}$$

[4.59] $$\phi_x(x) = \int_{-\infty}^{x} \frac{1}{\sqrt{2\pi}} \exp(\frac{t^2}{2})\, dt$$

Now, the probability density function $f_x(\nu)$ can be calculated as follows:

[4.60] $$f_x(\nu)=[\frac{1}{\sigma\sqrt{2\pi}}] \exp(\frac{-\frac{1}{2}(x-\mu)^2}{\sigma^2})$$

The joint probability can be obtained by applying a suitable numerical integration technique to integrate function $\phi(-\boldsymbol{\beta})$. $f_x(\nu)$ with respect to ν :

[4.61] $$P(m,n)= \int_{-5\sigma_n}^{0} \frac{1}{\sigma_n\sqrt{2\pi}} \exp[\frac{-(\nu-\mu_n{}^2)}{2\sigma_n{}^2}][\int_{-\infty}^{\beta} \frac{1}{\sqrt{2\pi}} \exp(\frac{t^2}{2})\, dt]\, d\nu$$

where,

[4.62] $$\boldsymbol{\beta}=\frac{\mu_m+r_{mn}(\frac{\sigma_m}{\sigma_n})\,(\nu-\mu_m)}{\sigma_m\sqrt{1-r_m{}^2}}$$

For a general solution with multiple failure modes, the probability of failure corresponding to a specific mode, with consideration to the dependency (correlation) among different modes, can be obtained as follows:

[4.63] $$C_k = P(F_k) - \sum_{i=1}^{k-1} P(F_k F_i) + \sum_{\substack{m=1,k-2 \\ n=2,k-1}}^{m<n} P(F_k F_m \cap F_k F_n), \qquad k > 2$$

As explained above, every scenario of live load (truck) positioning would reveal a possible failure mode. From Figure 4.2, five possible modes of failure were estimated as follows:

[4.64] $$C_5 = P(F_5) - \sum_{i-1}^{4} P(F_5 F_i) + \sum_{\substack{m=1,2,3 \;\; n=2,3,4 \\ n>m}} P(F_5 F_m \cap F_5 F_n)$$

[4.65] $$C_4 = P(F_4) - \sum_{i-1}^{3} P(F_4F_i) + \sum_{\substack{m=1,2 \\ n>m}} {}_{n=2,3} P(\, F_4F_m \cap\ F_4F_n)$$

[4.66] $$C_3 = P(F_3) - \sum_{i-1}^{2} P(F_3F_i) + P(F_5F_1 \cap\ F_3F_2)$$

[4.67] $$C_2 = P(F_2) - P(F_2F_1)$$

[4.68] $$C_1 = P(F_1)$$

From the basics of conditional probability, the following expression can be written as:

[4.69] $$P(A).P(B) \leq P(A \cap B) \leq \min[P(A), P(B)]$$

The limits refer to complete dependence or independence of A and B. Therefor,

[4.70] $$L_k \leq C_k \leq U_k$$

Where, L_k and U_k are the lower and upper bounds of the probability of failure with respect to the k^{th} mode. For the first and second modes:

[4.71] $$L_1 = U_1 = C_1$$

[4.72] $$L_2 = U_2 = C_2$$

The lower bound's general formula is described by Equation 4.73:

[4.73] $$L_k = P(F_k) - \sum_{i=1}^{k-1} P(F_kF_i) + \sum_{m=2}^{k-1}[P(F_kF_m) \sum_{n=1}^{m-1} P(F_kF_n)] \ ,$$

$$K > 2,\ L_k \geq 0$$

The upper bound formula is described by Equation 4.74:

[4.74] $U_k = \max[min(V_k, W_k)\,, 0] \qquad k > 2,$ in which:

[4.75] $V_k = P(F_k) - \sum_{i=1}^{k-1} P(F_k F_i) + \sum_{\substack{m=1,k-2 \\ n=2,k-1}}^{n>m} \max[P(F_k F_m), P(F_k F_n)]$

and

[4.76] $W_k = P(F_k) - \max[P(F_k F_i)]\,, \quad i = 1, k-1$

Thus, Equation 4.70 can be re-written as:

[4.77] $\sum_{i=1}^{k} L_i \leq P(F) \leq \sum_{i=1}^{k} U_i$

4.4 Bridge Reliability and Optimization Algorithm (BREL)

In the current research, a new and unique computer-aided algorithm for Bridge reliability analysis and design optimization is proposed (Figure 4.8). The required data, information, type of analysis, design and optimization can easily be provided through the main menu (Figure 4.9). As examples of the user-friendly entry of the input data, Figure 4.10 and Figure 4.11 show the interface for geometry and material input data, respectively. The model performs different methods of reliability analysis to obtain the failure probability and the corresponding reliability index with respect to every limit state function as well as the entire structural system. As will be demonstrated in the next chapter, the proposed model also performs different probabilistic optimization approaches.

Figure 4.8: A snapshot showing the start interface of the proposed model.

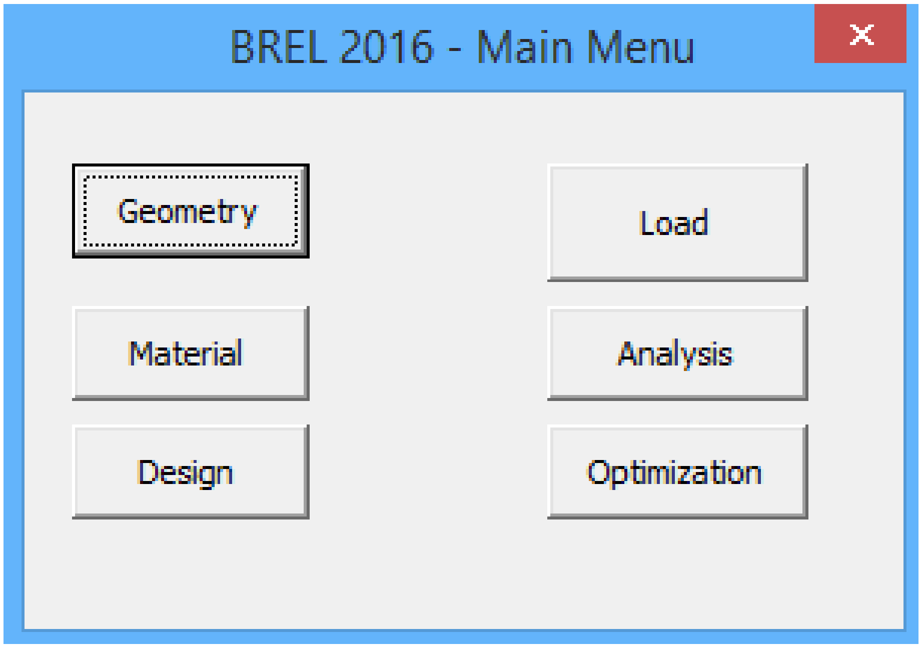

Figure 4.9: A snapshot demonstrates the main menu of the proposed model.

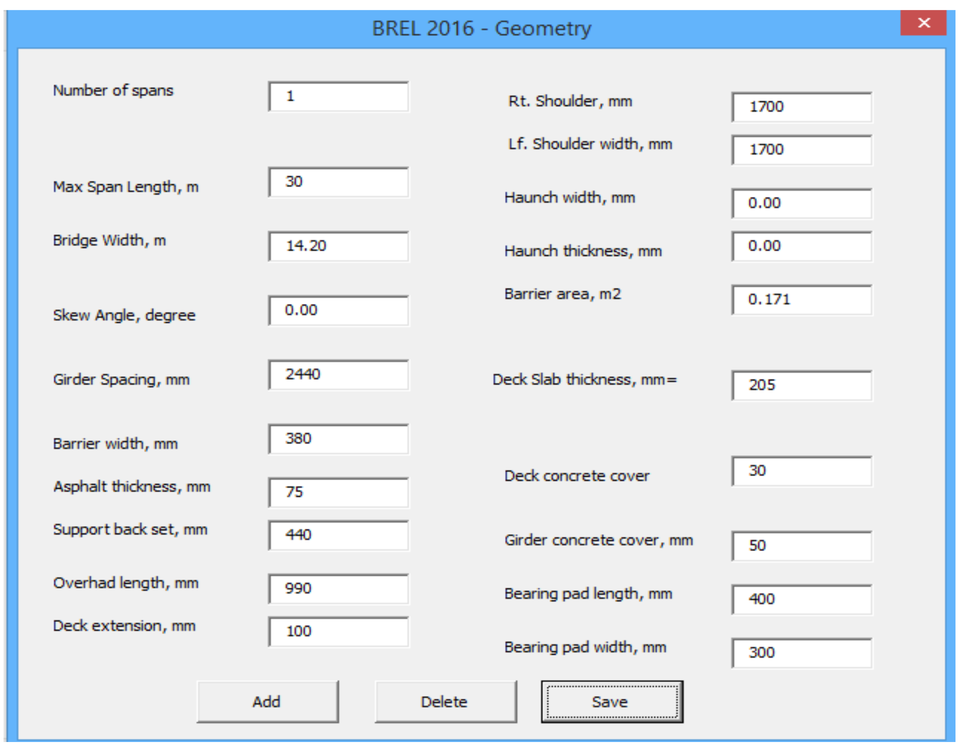

Figure 4.10: A snapshot for the geometry interface of the proposed model.

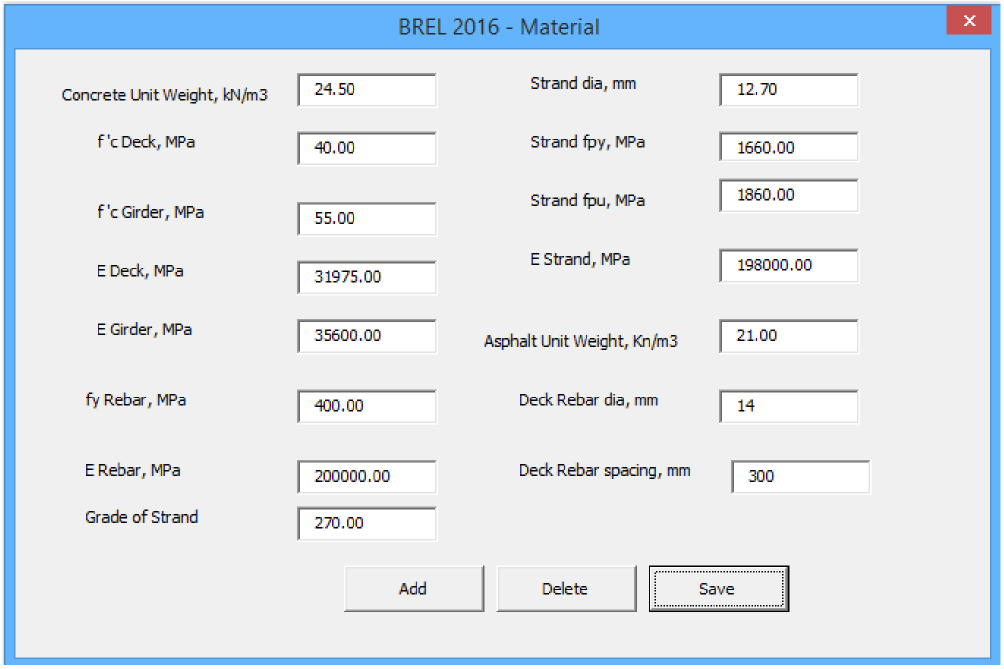

Figure 4.11: A snapshot for the material interface of the proposed model.

In addition to the deterministic analysis, the model performs probabilistic analysis using different approaches; the First-Order Reliability Method (FORM), the Monte Carlo Simulation (MCS) technique, and the Improved Reliability Bounds IRB (Figure 4.12).

BREL has been programmed with Visual Basic Application (VBA) code. This coded is presented in Appendix D. Different types of girder can be utilized by the proposed model (Figure 4.13). As illustrated in Figure 4.14, the proposed model defines all the random variables along with their statistical parameters and statistical distribution type.

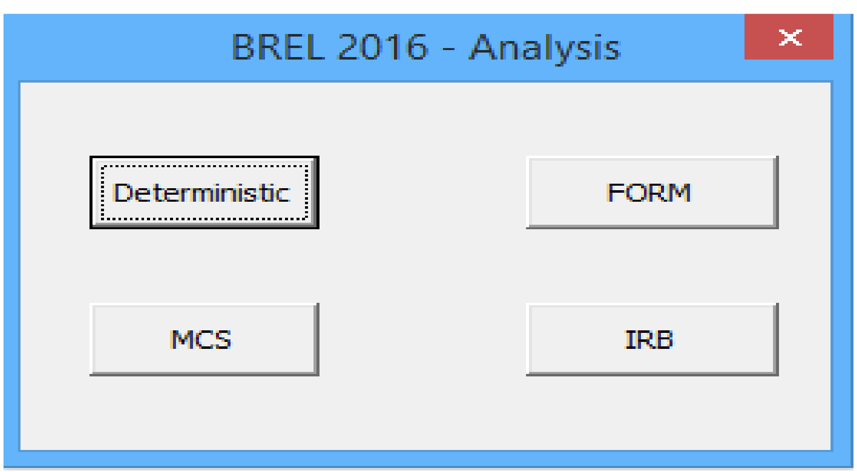

Figure 4.12: A snapshot from the proposed model showing types of analysis.

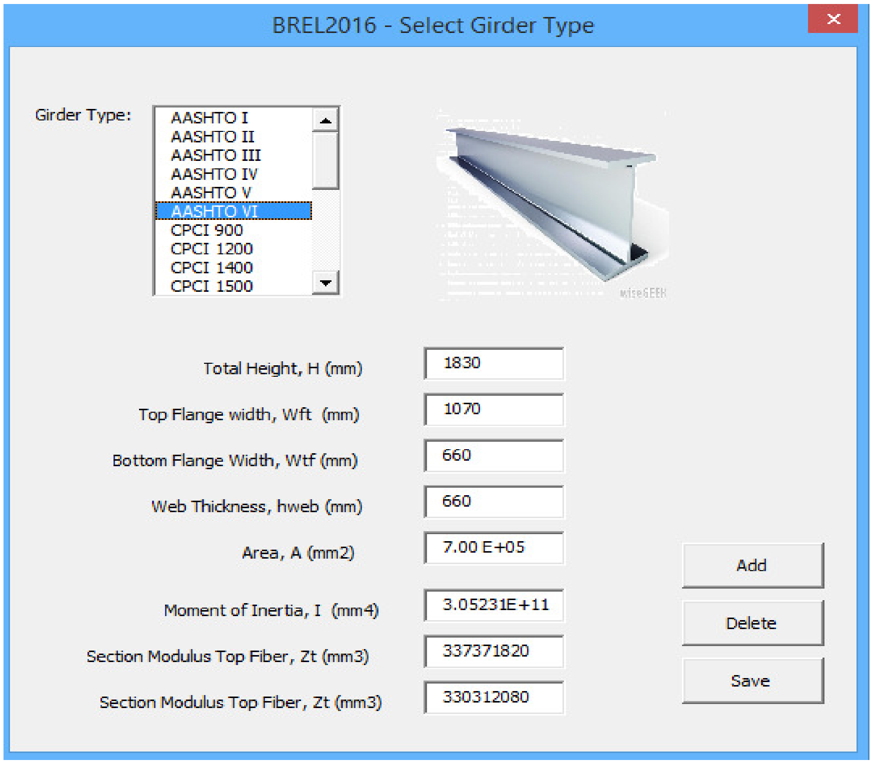

Figure 4.13: A snapshot from the proposed model showing different girder types.

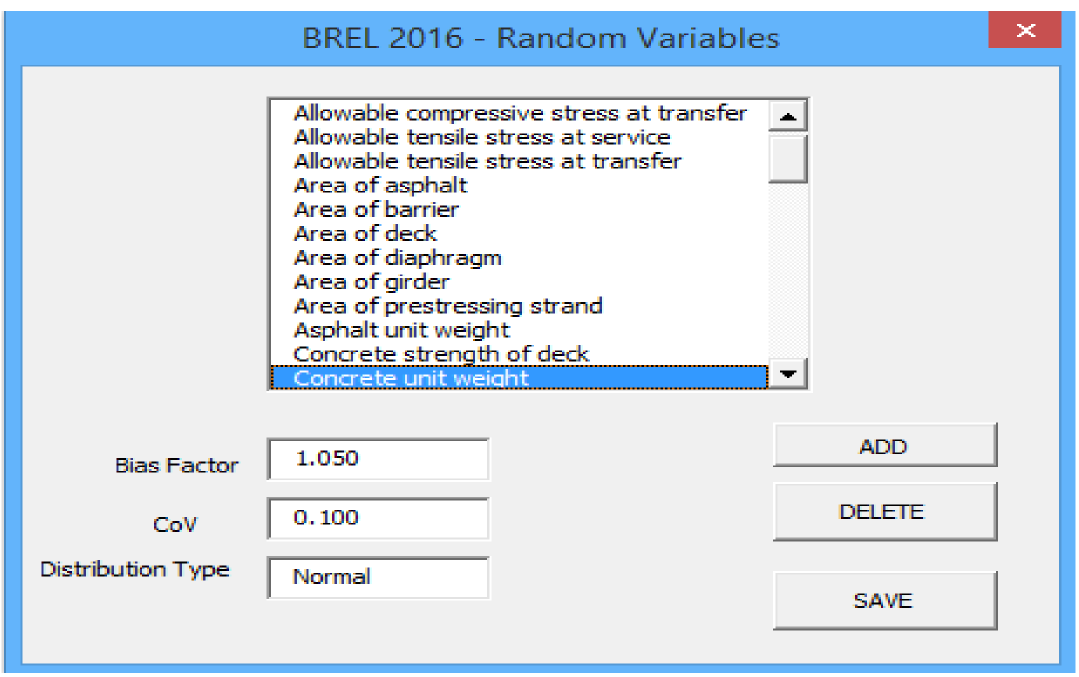

Figure 4.14: A snapshot from the proposed model defining the random variables, their statistical parameters and distribution type.

BREL has been programmed with Visual Basic Application (VBA) code. This code is presented in Appendix D. Different types of girders can be utilized by the proposed model (Figure 4.13).

As illustrated in Figure 4.14, the proposed model defines all the random variables along with their statistical parameters and statistical distribution type.

The applicability and accuracy of the proposed model will be exemplified in the following sections.

4.5 Case Study

In this section, the components' reliabilities and the overall system's reliability of a simple span prestressed girder bridge are investigated. The bridge has the cross section shown in Figure 4.15. Standard AASHTO IV precast girder type is used. Table 4.2 illustrates the random variables and the type of their statistical distributions. The statistical parameters of these random variables are as derived in Chapter Three.

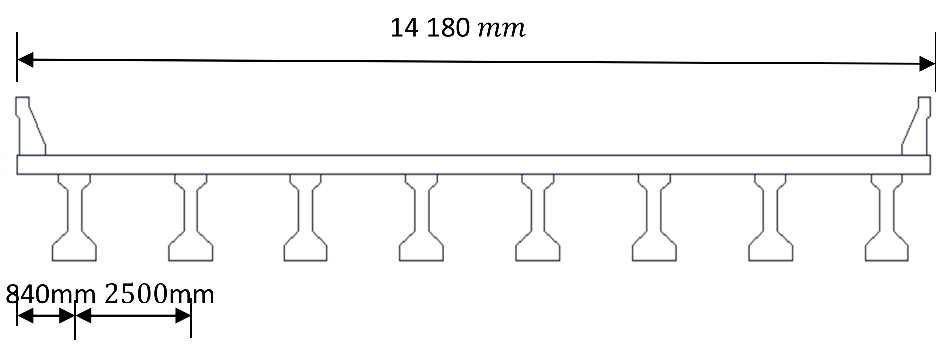

Figure 4.15: Cross section of prestressed girder bridge

The deck thickness is 205 mm and the barrier width is 380 mm. The concrete nominal strength of deck, f'_c =40 MPa. Initial and final nominal concrete strength of girder are f'_{ci}=40 MPa and f'_c =55 MPa, respectively. Low-relaxation 12.70 mm, seven wires strands are used. The yield strength of non-prestressing reinforcement, f_y =400 MPa. The thickness of asphalt layer is 75 mm.

Table 4.2: List of random variables.

Description	Distribution
Allowable compressive stress at service, MPa	Normal
Allowable compressive stress at transfer, MPa	Normal
Allowable tensile stress at service, MPa	Normal
Allowable tensile stress at transfer, MPa	Normal
Area of asphalt , mm^2	Normal
Area of barrier, mm^2	Normal
Area of deck, mm^2	Normal
Area of diaphragm, mm^2	Normal
Area of girder, mm^2	Normal
Area of prestressing strand area, mm^2	Normal
Asphalt unit weight, kN/m^3	Normal
Concrete strength of deck, f'_c , MPa	Normal
Concrete unit weight , kN/m^3	Normal
Dynamic load factor (Impact)	Normal
Eccentricity of strand at service, mm	Normal
Eccentricity of strand at transfer, mm	Normal
Fatigue truck bending moment , $kN\ m$	Normal
Final concrete strength of girder, f'_c MPa	Normal
Girder distribution factor	Normal
Initial concrete strength of girder, f'_{ci} MPa	Normal
Jacking stress at service, kN	Normal
Jacking stress at transfer, kN	Normal
Lane load bending moment, $kN\ m$	Normal
Lane load shear, kN	Normal
Moment resistance, $kN\ m$	Lognormal
Second moment of area (composite), I_c, mm^4	Normal
Second moment of area (noncomposite), I, mm^4	Normal
Section modulus (composite) bottom fiber,Z_{bc}, mm^3	Normal
Section modulus (composite) top fiber, Z_{tc}, mm^3	Normal
Section modulus (noncomposite) bottom fiber, Z_b, mm^3	Normal
Section modulus (noncomposite) top fiber, Z_t, mm^3	Normal
Shear resistance, kN	Lognormal
Truck load bending moment, $kN\ m$	Normal
Truck load shear, kN	Normal
Ultimate strength of prestressing strands, MPa	Normal

The variability of the components' and system's reliabilities with different values of span length are investigated.

Initially, deterministic analysis is performed to obtain the nominal values of the basic variables. Then, the probabilistic analysis was conducted by the proposed reliability model, BREL. The reliability analysis was conducted using the First-Order Reliability Method FORM at first. The results obtained by FORM will be presented and discussed herewith. Then, the Monte Carlo Simulation MCS analysis was also performed and the results comparison demonstrated the good agreement (convergence) between the reliability indexes obtained by FORM and MCS methods.

To obtain the system reliability, failure mode analysis FMA was performed to determine the probability of failure and corresponding reliability index with respect to every possible mode of failure. Thereafter, the Improved Reliability Bounds IRB approach will be applied to obtain the lower and upper bounds of the system reliability.

4.6 Results and Discussion

In this section, the results of the reliability analysis are demonstrated and discussed. First the components' reliability indexes will be presented.

4.6.1 At Initial Phase (at transfer)

4.6.1.1 Reliability with Respect to the Stress at Top Fiber of Girder

The stress at the top fiber of girder should not exceed the allowable tensile stress as defined by AASHTO LRFD code. Figure 4.16 shows the variation of reliability indexes, with different span lengths, with respect to the stress at the top fiber of girder. Usually, the top fibers are in tension; however due to the increase in number of strands (as a result of increase in span length), the full section could be in compression. The reliability index with respect to the allowable stress at the top fiber, usually, has a lower value (less than 3). The change in the stress at the top fiber from tension to compression explains the abrupt discontinuity (kinks) in the curves of the reliability indices shown in Figure 4.2.

The moment due to girder self-weight causes compressive stress at the top fiber of the girder. This moment has zero value at the end section and has maximum value at midspan section. Therefore, for different span lengths, the reliability indexes at mid span β_{tt_mid} and harp point, β_{tt_hrp}, were higher than those at end section, β_{tt_end}, and transfer length section, β_{tt_trns}.

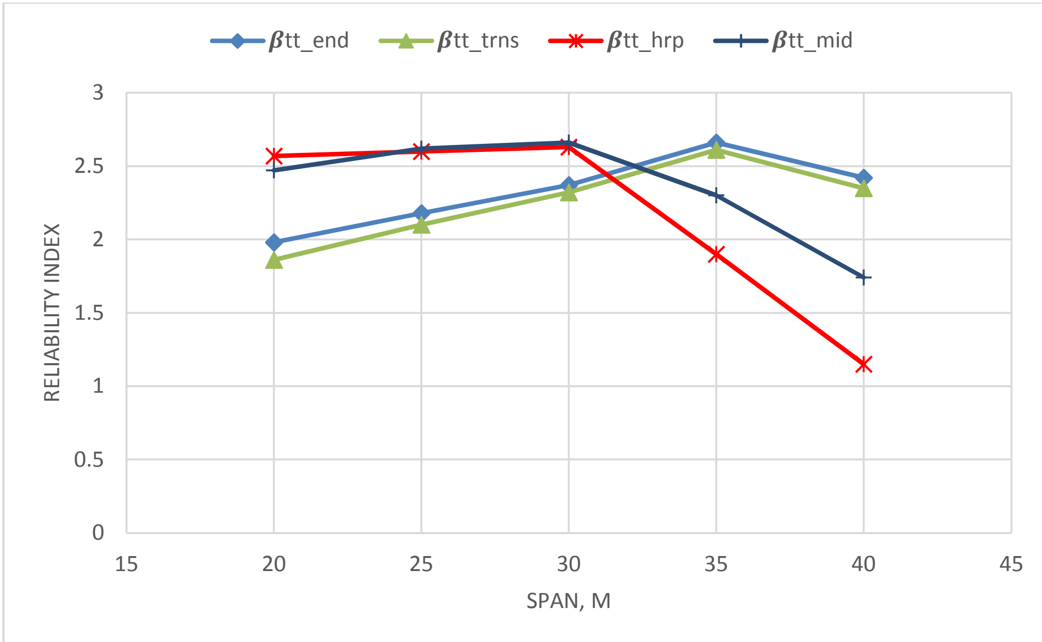

Figure 4.16: Variation of reliability indices (at transfer) related to stress at top fiber with span length.

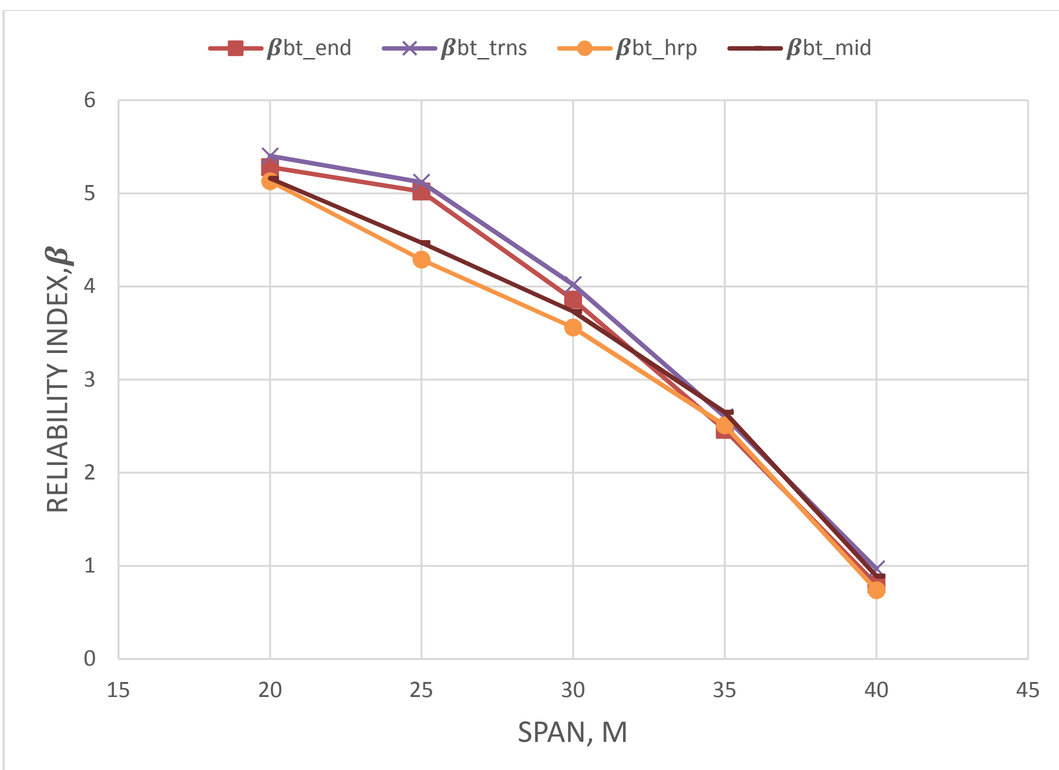

Figure 4.17: Variation of reliability indices (at transfer) related to stress at bottom fiber with span length.

4.6.1.2 Reliability with Respect to Stress at Bottom Fiber of Girder

The variability of the reliability indexes, related to the bottom fiber of the girder, with different span lengths is shown in Figure 4.17. The reliability index is evaluated at end section β_{bt_end}, at transfer length section β_{bt_trns}, at harp point β_{bt_hrp}, and at midspan section β_{bt_mid}.

At initial phase (at transfer), the bottom fibers are in compression and, usually, the reliability with respect to permissible stress takes high values (higher than 5) for shorter spans. With increased span lengths, the number of required strands increases; this would produce higher compressive stresses at the bottom fiber of the girder. This explains the gradual decrease in reliability index with the increase of the span length as shown in Figure 4.17.

4.6.2 At Service (after losses)

4.6.2.1 Reliability with Respect to Stress at Top Fiber of Deck

According to the AASHTO LRFD design code requirements, the limit state with respect to the stress at the top fiber of the deck was investigated under two load cases, Service I: (1) under permanent load, and (2) permanent and transient loads. The variability of the reliability indexes, related to the stress at top fiber of the deck, with span length is shown in Figure 4.18. The reliability index with respect to the first load case is denoted as βts_d1 and that for the second load case as βts_d2.

The top fiber of the deck is in compression at the final stage and has higher values of reliability (greater than 5.5) for shorter span lengths. However the reliability index decreases with longer span lengths. It can be seen that the reliability index corresponding to the second load case, βts_d2, is lower than that related to the first load case, βts_d1 . This is because of the effect of the transient loads.

4.6.2.2 Reliability with Respect to Stress at Top Fiber of Girder

As per AASHTO LRFD requirements, the limit state function with respect to the stress at the top fiber of the girder was investigated under three load cases: (1) under effective prestress plus permanent loads, and (2) under half the summation of the effective prestress and permanent loads plus transient loads, and (3) under effective prestress, permanent and transient loads.

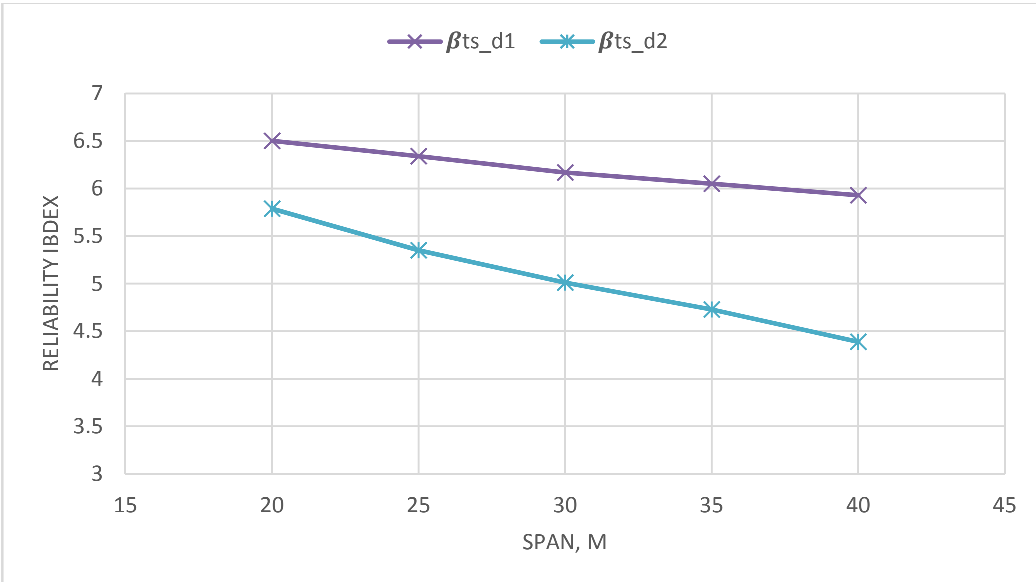

Figure 4.18: Variation of reliability indices (at service) related to stress at top fiber of deck with span length.

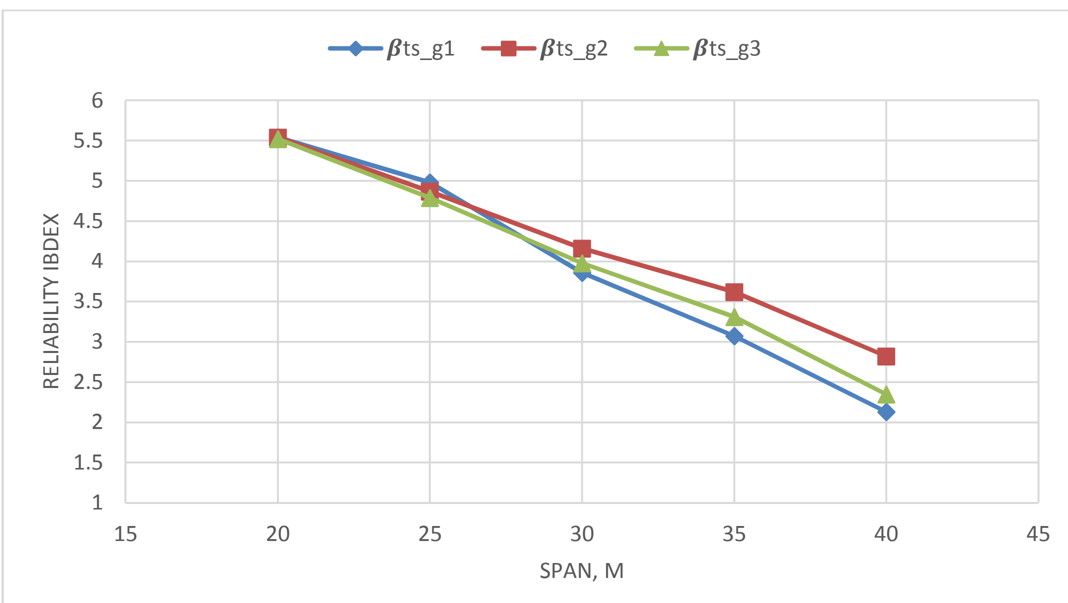

Figure 4.19: Variation of reliability indices (at service) related to stress at top fiber of girder with span length.

The reliability index corresponding to the first load case is denoted as βts_g1 and that related to the second load case is denoted as βts_g2; while, βts_g3 denotes the reliability index corresponding to the third load case.

The variation of reliability indexes, determined for the top fiber of girder, with different span length is shown in Figure 4.19.

The top fiber of girder, at service phase, is in compression, thus registering high values of reliability index (greater than 5.0) for shorter span lengths and gradually decreases for longer spans. This decrease is caused by the compressive stresses at the top fiber increases (with the increase in span length) occurring due to the effect of permanent and transient loads.

4.6.2.3 Reliability with Respect to Other Service I Limit State Functions and Fatigue I Limit State Function

In this section, three different reliability indexes are presented: the reliability with respect to the stress at the bottom fiber of the girder, βbs (Service III), the reliability with respect to the cracking moment, βcr (Service I), and the reliability with espect to Fatigue I Limit State βftg. The variation of these reliability indices with different span length is shown in Figure 4.20.

The stress at the bottom fiber should not exceed the allowable tensile stress, according to AASHTO LRFD. When the span length increases the load effect (mainly the dead load) increases the tensile stress and, thus, it reduces the reliability index.

From Figure 4.20, it can be noticed that the reliability index, βcr, increases with the increase in span length. To explain this increase, reference is made to Equations 4.27, 4.30 and 4.31. When the span increases the dead load increases as well and, consequently, the required number of prestressing strands will increase, accordingly. The increase in dead load has no effect on the resisting moment, M_r, but will reduce the cracking moment, M_{cr} as per Equation 4.31. The increase in the prestressing strands will increase both M_r and M_{cr}, as per Equations 4.27 and 4.31, respectively; but the rate of the increment in M_r is higher than that for M_{cr}. As a result, βcr will take higher values for longer spans (higher reliability) than for shorter spans.

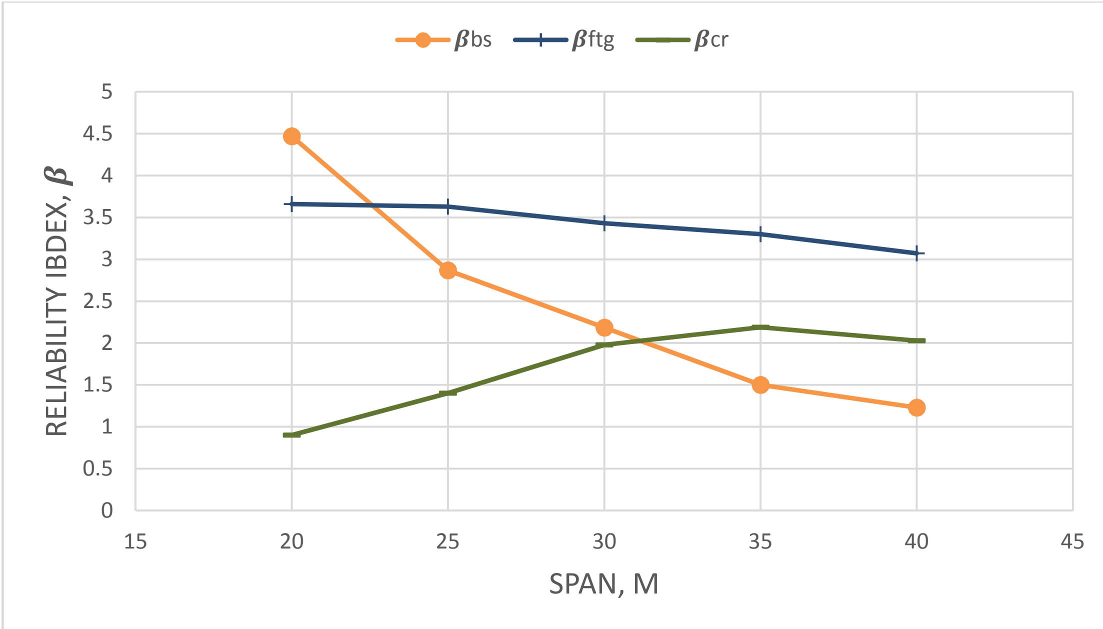

Figure 4.20: Variation of reliability indices (at service) related to stress at bottom fiber of girder, cracking moment, and fatigue vs. span length.

Usually, fatigue is not critical in prestressed girder bridges (Barker and Puckett 2013). However, the fatigue reliability index should always be maintained higher than a target reliability, which ranges between 1.00 and 2.00 (Nowak and Szerszen 2000). For the current case study, as shown in Figure 4.8, the fatigue reliability index varies between 3.20 and 3.70.

4.6.2.4 Ultimate Strength Limit State Functions

Ultimate bending moments and shear forces are calculated according to AASHTO LRFD, Strength I Limit State. Until Present, AASHTO LRFD code, has only been formally calibrated for Strength I Limit State (Nowak and Szerszen 2000, and Barker and Puckett 2013). This calibration, revealed consistency (uniform level) in reliability indexes with respect to ultimate bending moments and shear forces by imposing the load factors associated with Strength I Limit State.

Figures 4.21 to 4.24 show the variability of the reliability index related to ultimate bending, β_{ult} ,with span length for all types of AAHTO Girders, CPCI Girders, Bulb-T

(NEBT) Girders, and NU Girders, respectively. These reliability indices vary between 3.60 and 3.90 for the different types of precast girders considered in this study.

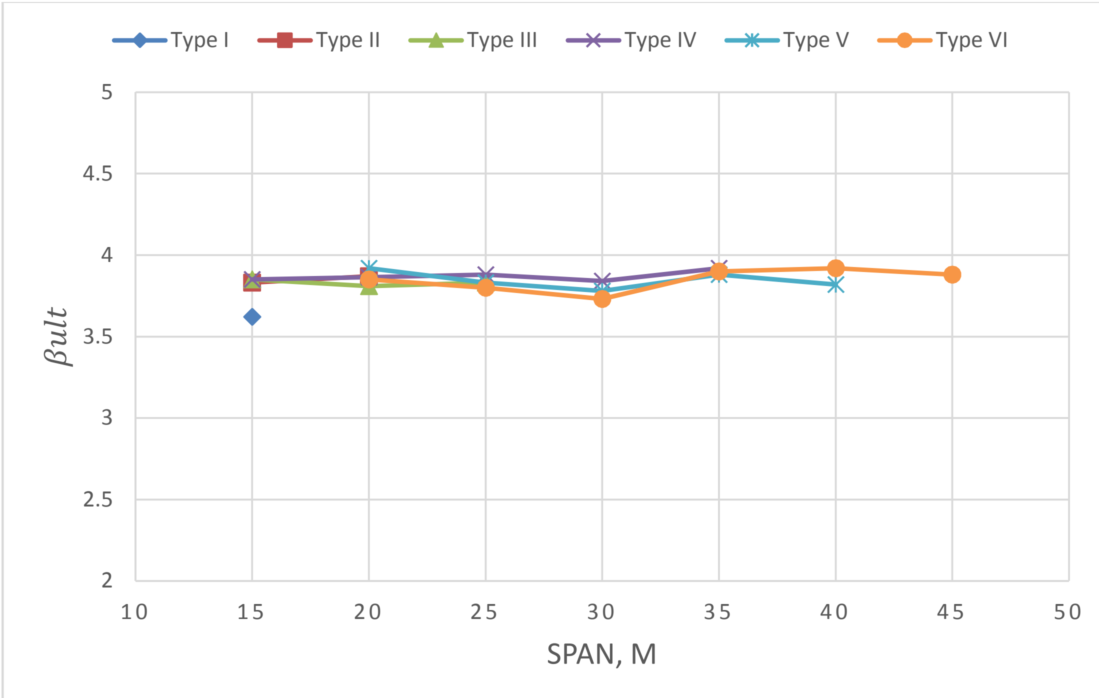

Figure 4.21: Variation of reliability indices related to ultimate bending with span length for AASHTO Girders.

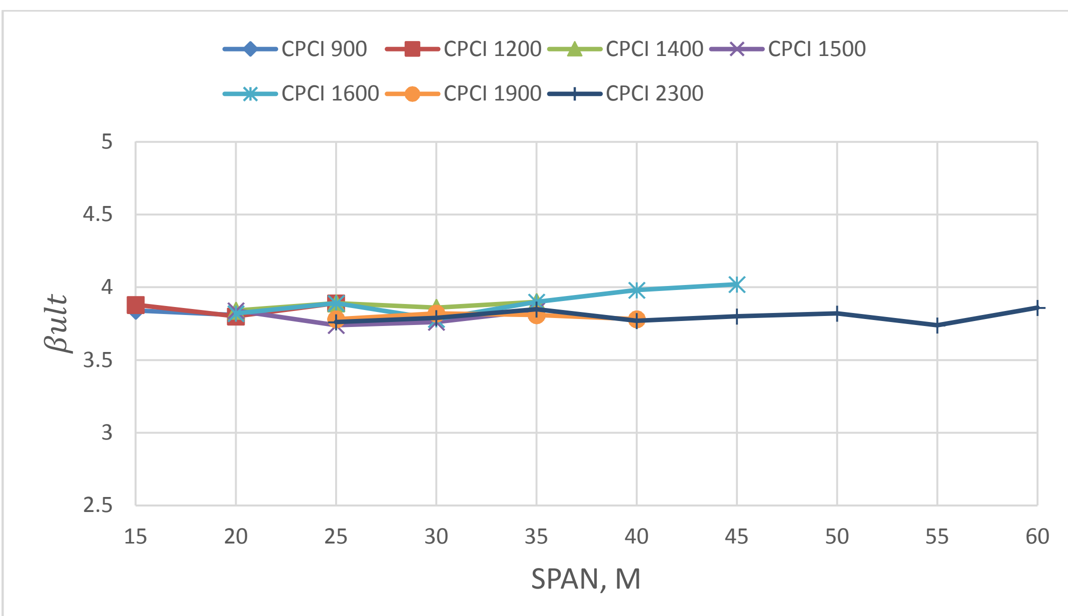

Figure 4.22: Variation of reliability indices related to ultimate bending with span length for CPCI Girders.

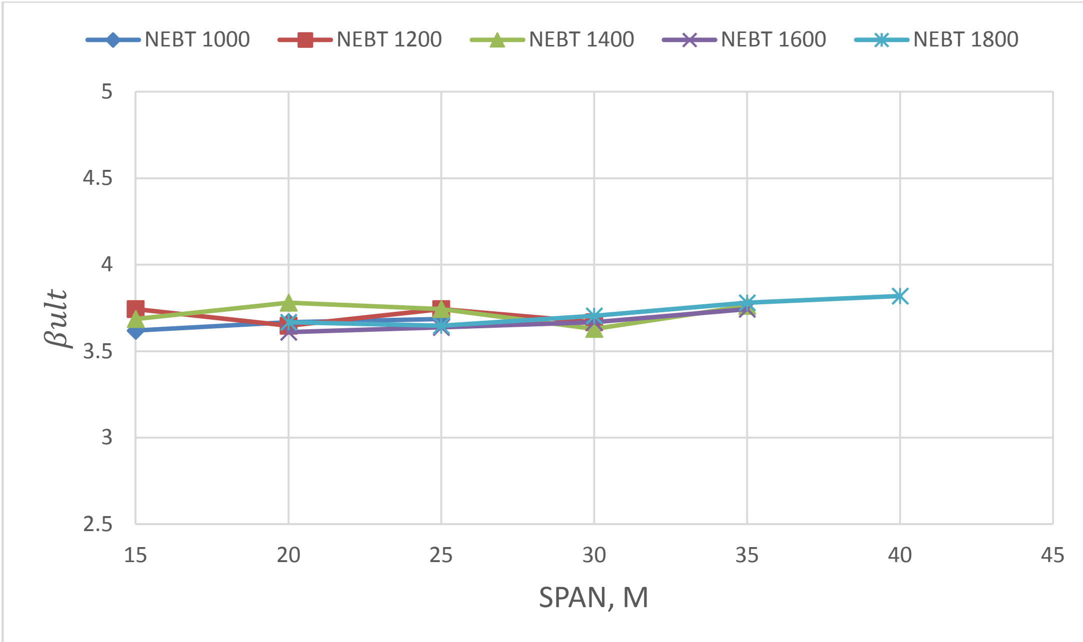

Figure 4.23: Variation of reliability indices related to ultimate bending with span length for Bulb-T (NEBT) Girders.

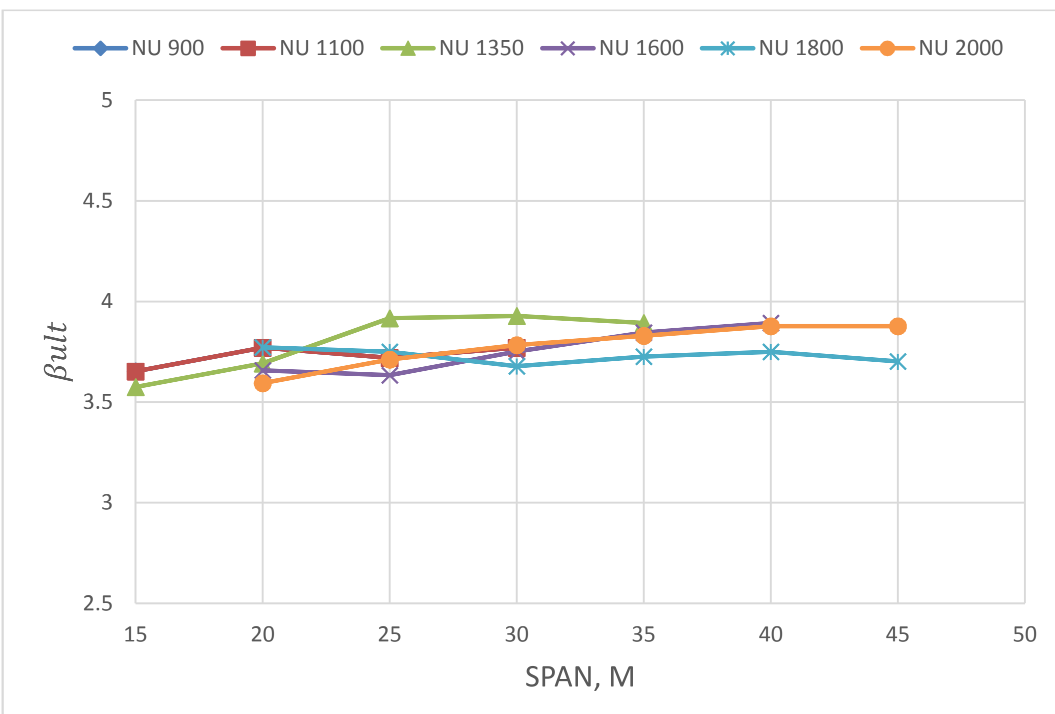

Figure 4.24: Variation of reliability indices related to ultimate bending with span length for NU Girders.

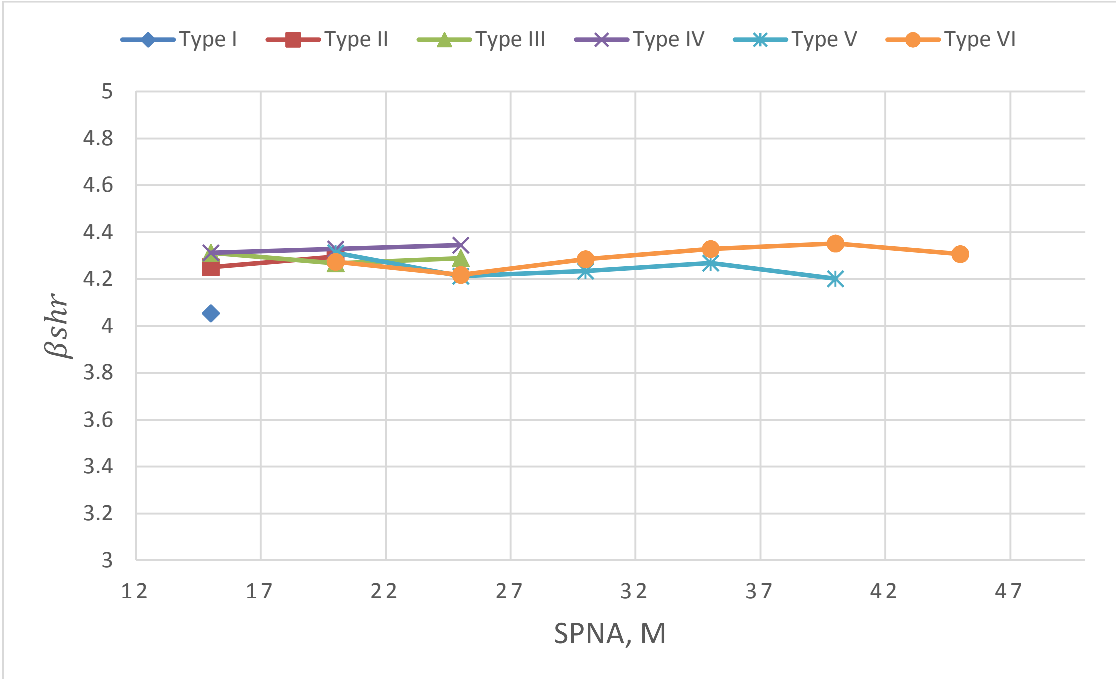

Figure 4.25: Variation of reliability indices related to ultimate shear with span length for AASHTO Girders.

Figures 4.25 to 4.28 show the variability of the reliability index related to ultimate shear, β_{shr} ,with span length for all types of AAHTO Girders, CPCI Girders, Bulb-T (NEBT) Girders, and NU Girders, respectively. These reliability indices vary between 4.00 and 4.90 for the different types of precast girders considered in this study.

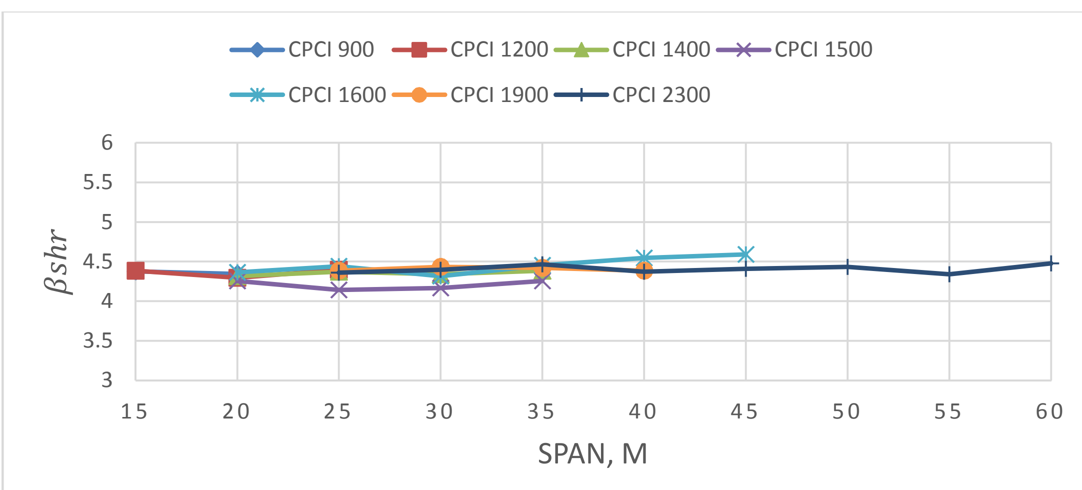

Figure 4.26: Variation of reliability indices related to ultimate shear with span length for CPCI Girders.

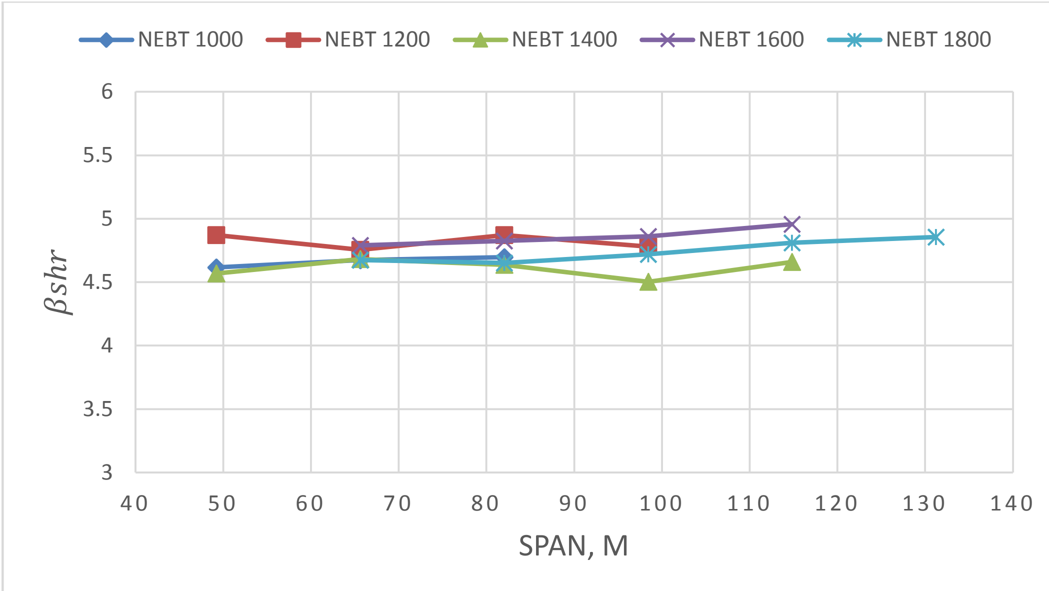

Figure 4.27: Variation of reliability indices related to ultimate shear with span length for Bulb-T (NEBT) Girders.

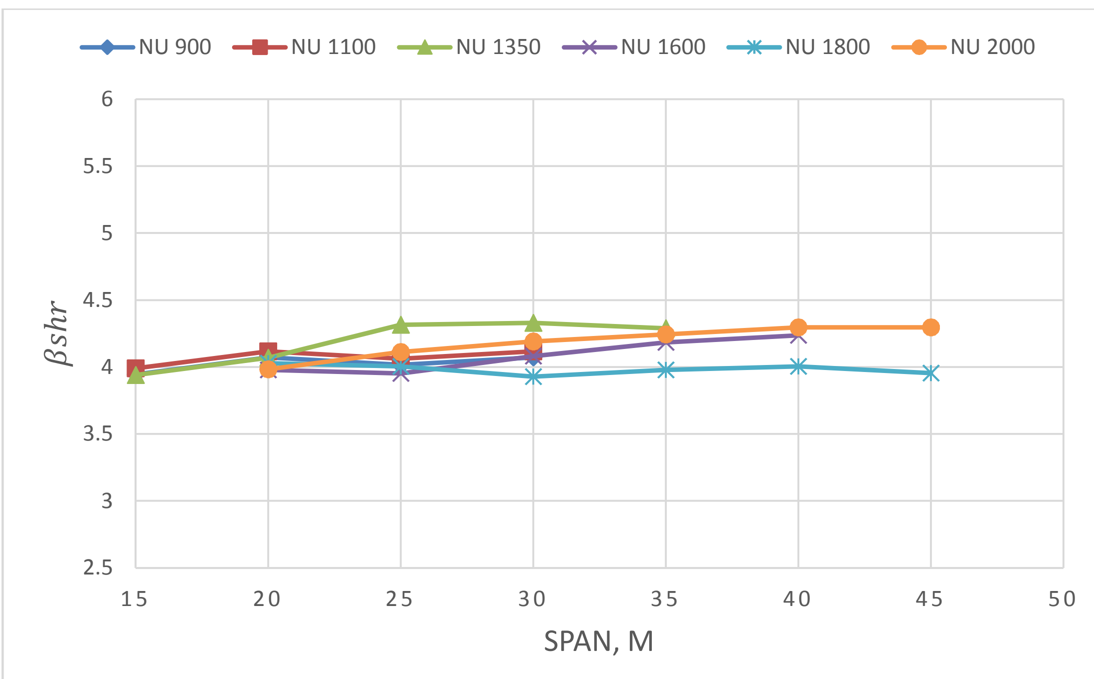

Figure 4.28: Variation of reliability indices related to ultimate shear with span length for NU Girders.

4.6.3 Effect of Correlation Among Random Variables on Reliability Indexes

Quantifying the dependency (correlation) between random variables has long been a major topic in risk analysis (Jiang et al. 2014). The conventional *Rank Order Correlation* employed by most probabilistic analysis is certainly a meaningful measure of dependence but is very limited in the patterns it can produce (Vose 2009).

In order to quantify precisely the dependency (correlation) between random variables and to assess its effect on the reliability index, the Copula approach offers a more flexible and accurate method to utilize. As a new contribution in this research, the Copula functions are applied, for the first time, to bridge reliability analysis. The word ‘‘copula’’ derives from the Latin term for a ‘‘link’’ or a ‘‘tie’’ that connects two different things (Jiang et al. 2014). The copula function is currently the most effective mathematical tool in correlation analyses of probabilistic methods (Vose 2009). Copula functions are capable of connecting the joint distribution $F(x_1, x_2, \ldots, x_n)$ of multiple random variables $x_1, x_2, \ldots, x_n$ and their respective marginal distributions $F(x_1), F(x_2), \ldots, F(x_n)$ (Salvadori and Michele 2007).

In probability theory and statistics, copula is a multivariate probability distribution for which the marginal probability distribution of each variable is uniform (Jiang et al. 2014).

Two main categories of copulas exist (Tang et. al. 2013):

- Archimedean copulas: this category has three copula types; namely: Clayton, Frank and Gumbel.
- Elliptical Copulas: this category has two types of copula: Normal and T.

In this section, the effect of the correlation between some of the random variables on reliability indexes has been investigated using these types of copulas mentioned above. The mathematical formulation and physical characteristics of every copula type is illustrated and well explained in Appendix F.

The following steps are employed to evaluate the level of correlation (dependency) among the random variables.

Step 1: Select the random variables that need to be correlated.

Step 2: Using the statistical parameters and the statistical distribution type, determine the probability density function PDF of each random variable.

Step 3: Using Monte Carlo Simulation MCS, generate a set of n random numbers from every PDF.

Step 4: Select a Copula Type (Figure 4.29).

Step 5: Calculate Kendall's Tau Coefficient, τ, (refer to Appendix F). Kendall's Tau τ is carried out on the ranks of the data. That is, for each variable separately the values are placed in order and numbered. An estimate of Kendall's tau for a sample of n observations is given by:

[4.78] $$\tau = \frac{C-D}{C+D} = \frac{C-D}{\binom{n}{2}}$$

where, C is the number of concordant pairs and D the number of discordant pairs. This can also be written as:

[4.79] $$\tau = \binom{2}{n}^{-1} \sum_{i>j} \sin[(X_i - X_j)(Y_i - Y_j)]$$

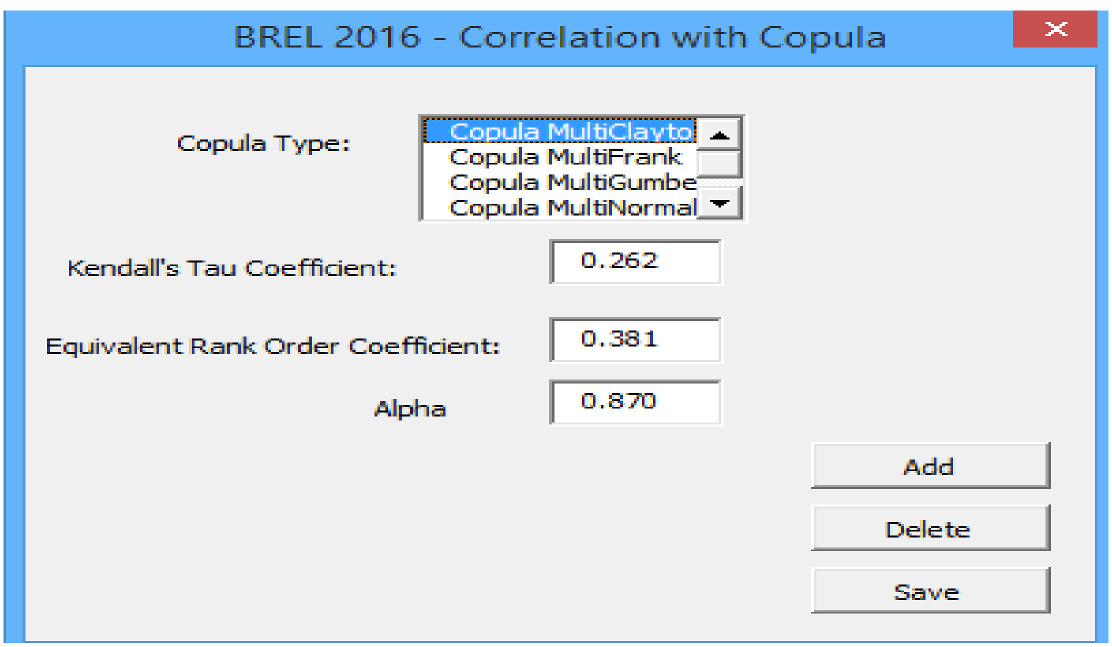

Figure 4.29: A snapshot from the proposed model showing the selection of Copula type.

Step 6: Use τ calculated in Step 5 to obtain the Copula parameter (alpha), α, (refer to Appendix F).

- For Multivariate Clayton copula:

[4.80] $$\propto = \frac{2\tau}{1-\tau}$$

- For Multivariate Frank copula:

[4.81] $$\frac{[D_1(\propto)-1]}{\propto} = \frac{1-\tau}{4}$$ where,

[4.82] $$D_1(\propto) = \frac{1}{\propto}\int_0^{\infty} \frac{t}{e^t - 1}\,dt$$

- For Multivariate Gumbel copula:

[4.83] $$\propto = \frac{1}{1-\tau}$$

- For Multivariate Normal copula:

[4.84] $$\rho(X,Y) = sin(\frac{\pi}{2}\tau)\ ,$$ where, $\rho(X,Y)$ is the linear correlation coefficient.

- For Multivariate T- copula:

[4.85] $$\rho(X,Y) = sin(\frac{\pi}{2}\tau)$$

Step 7: Use the copula parameter obtained in step 6 to determine the Multivariate Copula:

- For Multivariate Clayton copula:

[4.86] $$C_{\propto}(u,v) = \max([u^{-\propto} + v^{-} - 1]^{-\propto}, 0)$$

- For Multivariate Frank copula:

[4.87] $$C_{\propto}(u,v) = -\frac{1}{\propto} ln\left(1 + \frac{(e^{-\propto u}-1)(e^{-\propto v}-1)}{e^{-\propto}-1}\right)$$

- For Multivariate Gumbel copula:

[4.88] $$C_{\propto}(u,v) = \exp\{-[(-\ln u)^{\propto} + (-\ln v)^{\propto}]^{\frac{1}{\propto}}\}$$

- For Multivariate Normal copula:

[4.89] $$C_{\rho}(u,v) = \int_{-\infty}^{\Phi^{-1}(u)} \int_{-\infty}^{\Phi^{-1}(v)} \frac{1}{2\pi(\rho^2)^{1/2}} \exp\{-\frac{x^2-2\rho xy+y^2}{2(1-\rho^2}\} dxdy$$

- For Multivariate T- copula:

[4.90] $$C_{\rho}(u,v) = \int_{-\infty}^{\overset{-1}{t_v}(u)} \int_{-\infty}^{\overset{-1}{t_v}(v)} \frac{1}{2\pi(\rho^2)^{1/2}} \exp\{1 + \frac{x^2-2\rho xy+y^2}{v(1-\rho^2}\}^{-(v+2)/2} dxdy$$

To solve these equations, BREL model is interactively linked to an Excel Add-Inn ModelRisk (Figure 4.30).

In the current research, the correlation among the following random variables has been estimated:

- The jacking stress,
- The area of prestressing steel (strands),

- The eccentricity of strands,
- The cross sectional area of precast girder, and
- Span length.

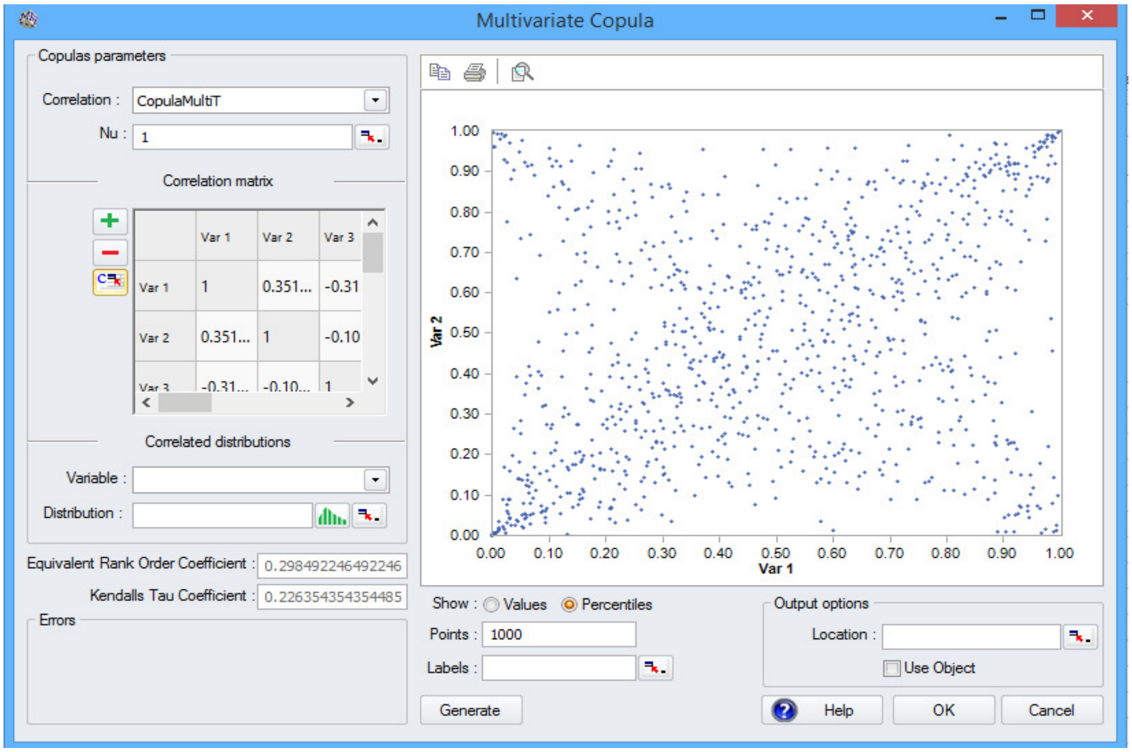

Figure 4.30: Snapshot for Multivariate Copula interface.

Different types of copulas were applied and the effect of these copulas on the reliability indexes has been investigated. For the same bridge configuration as presented in Figure 4.15 with 25 m span length and AASHTO IV standard girder, Table 4.3 shows the values of Kendall's Tau coefficient and the equivalent rank order coefficient with respect to every type of copula.

The effect of different copula types on some reliability indexes is illustrated in Table 4.4. It can be seen that the elliptical copulas (Normal and T) have higher effect on reliability indexes than the Archimedean copulas (Clayton, Frank, and Gumbel). It is also obvious that, in general, the correlation reduces the reliability index. However, for tensile stresses, the Archimedean copulas slightly increases the value of the reliability index.

Table 4.3: Value of Kendall’s tau coefficient and equivalent rank order coefficient.

Copula Type		Kendalls Tao Coefficient	Equivalent Rank Order Coefficient
Archimedean Copulas	Multivariate Clayton Copula	0.298	0.431
	Multivariate Frank Copula	0.327	0.475
	Multivariate Gumbel Copula	0.282	0.408
Elliptical Copulas	Multivariate Normal Copula	0.224	0.331
	Multivariate-T Copula	0.226	0.29

4.6.4 Results comparison (FORM vs. MCS)

The reliability analysis of the case study presented in Section 4.5 has been performed using also the Monte Carlo Simulation MCS. The MCS was performed with 100,000 cycles. The results are presented in Table 4.5 and are compared with those obtained earlier by using the FORM method. The agreement between the two methods, is investigated by measuring the percentile difference:

[4.91] Percentile difference = ABS [(result of MCS) – (result of IRB)] /(results of MCS) x 100

It has been found that the percentile difference between IRB and MCS ranges from 6% to 9.8% which reflects a good agreement between the two probabilistic methods. However MCS requires more computational efforts and longer execution time comparing to the First-Order Reliability Method (FORM).

Figure 4.31 shows a snapshot, from the developed model, related to the Monte Carlo Simulation MCS analysis.

Table 4.4: Effect of copula type on different reliability indices.

Reliability index type	Correlation condition		Reliability index value
β_{ti_mid}	No Correlation		5.020
	Estimated correlation by Copula method with different Copula types:	Multivariate Clayton	5.165
		Multivariate Frank	5.089
		Multivariate Gumbel	5.085
		Multivariate Normal	4.656
		Multivariate-T	4.564
β_{bi_mid}	No Correlation		4.108
	Estimated correlation by Copula method with different Copula types:	Multivariate Clayton	3.982
		Multivariate Frank	4.023
		Multivariate Gumbel	4.053
		Multivariate Normal	4.013
		Multivariate-T	4.071
β_{bs}	No Correlation		1.630
	Estimated correlation by Copula method with different Copula types	Multivariate Clayton	1.687
		Multivariate Frank	1.635
		Multivariate Gumbel	1.634
		Multivariate Normal	1.337
		Multivariate-T	1.382
β_{ult}	No Correlation		3.953
	Estimated correlation by Copula method with different Copula types:	Multivariate Clayton	3.756
		Multivariate Frank	3.832
		Multivariate Gumbel	3.877
		Multivariate Normal	3.806
		Multivariate-T	3.746
β_{cr}	No Correlation		2.723
	Estimated correlation by Copula method with different Copula types:	Multivariate Clayton	2.823
		Multivariate Frank	2.870
		Multivariate Gumbel	2.841
		Multivariate Normal	2.663
		Multivariate-T	2.702

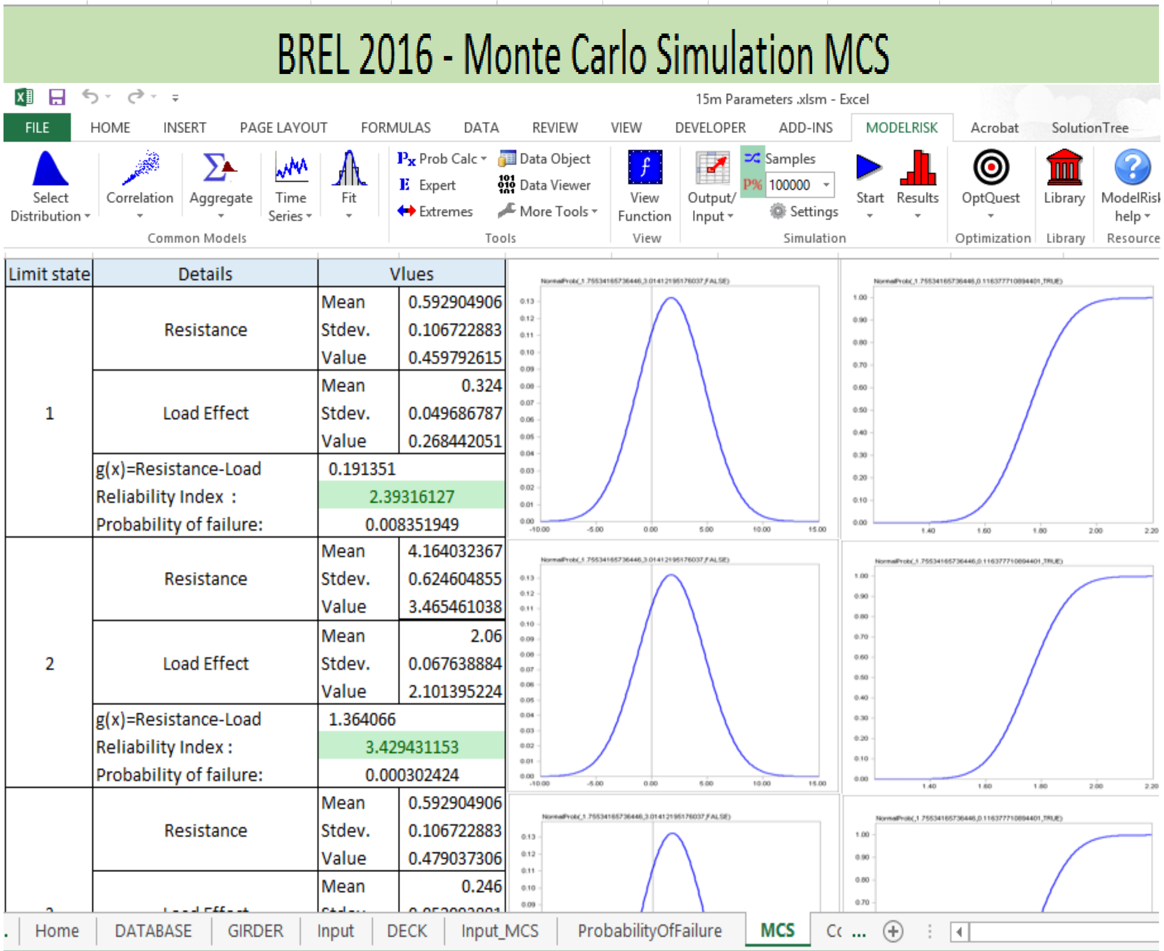

Figure 4.31: Snapshot from BREL model demonstrating the MCS analysis.

4.6.5 System Reliability

Applying the procedure detailed in Section 4.3.2, a failure mode analysis FMA has been performed using the proposed 2-D nonlinear grillage analogy algorithm GRANAL. The same case study as employed in Section 4.5 has been used with the bridge configuration modeled with a grillage mesh as illustrated in Figure 4.32.

The grillage members were classified into four groups to represent the exterior girders, interior girders, diaphragms, and deck slab. The properties of the grillage members are summarized in Table 4.6. The failure probabilities and associated reliability indexes obtained from the failure mode analysis FMA , with respect to 35 m span length, are summarized in Table 4.7.

Table 4.5: Components reliability (FORM vs. MCS)

Reliability Index	Span (m)									
	20		25		30		35		40	
	FORM	MCS	FORM	MCS	FORM	MCS	FORM	MCS	FORM	MCS
βtt_end	5.48	5.81	5.47	5.94	5.87	5.24	6.16	6.60	6.12	6.66
βbt_end	5.28	5.62	5.02	5.46	3.86	3.92	2.46	2.64	0.8	0.74
βtt_trns	5.36	5.64	5.68	6.23	5.71	5.78	6.11	6.55	5.85	5.72
βbt_trns	5.4	5.74	5.12	5.43	4.02	3.68	2.6	2.79	0.97	1.06
βtt_hrp	6.07	6.00	5.84	6.32	6.13	5.52	5.9	6.32	4.65	5.08
βbt_hrp	5.13	5.44	4.29	4.60	3.56	3.68	2.51	2.69	0.74	0.81
βtt_mid	5.97	6.23	6.12	6.58	6.16	5.54	5.8	6.22	5.24	5.14
βbt_mid	5.16	5.47	4.47	4.78	3.73	3.40	2.65	2.84	0.89	0.97
βts_g1	5.54	5.88	4.98	5.38	3.86	3.47	3.07	3.29	2.13	2.08
βts_g2	5.54	5.67	4.87	5.26	4.16	3.74	3.62	3.88	2.82	3.08
βts_g3	5.52	5.85	4.79	5.17	3.98	3.62	3.31	3.55	2.35	2.57
βts_d1	6.5	6.89	6.21	6.74	6.17	5.58	6.29	6.74	5.93	6.48
βts_d2	5.79	6.14	5.35	5.80	5.01	5.12	4.73	5.07	4.39	4.24
βbs	4.47	4.64	2.87	3.08	1.76	1.58	1.14	1.22	1.23	1.34
βftg	3.66	3.88	3.63	3.88	3.43	3.48	3.30	3.54	3.07	3.36
βult	3.70	3.92	3.72	3.89	3.76	3.38	3.72	3.99	3.74	4.09
βcr	0.98	1.06	1.30	1.40	2.00	2.08	2.23	2.39	2.06	2.25
βshr	4.08	4.32	4.00	4.32	4.20	3.78	4.24	4.55	4.18	4.57

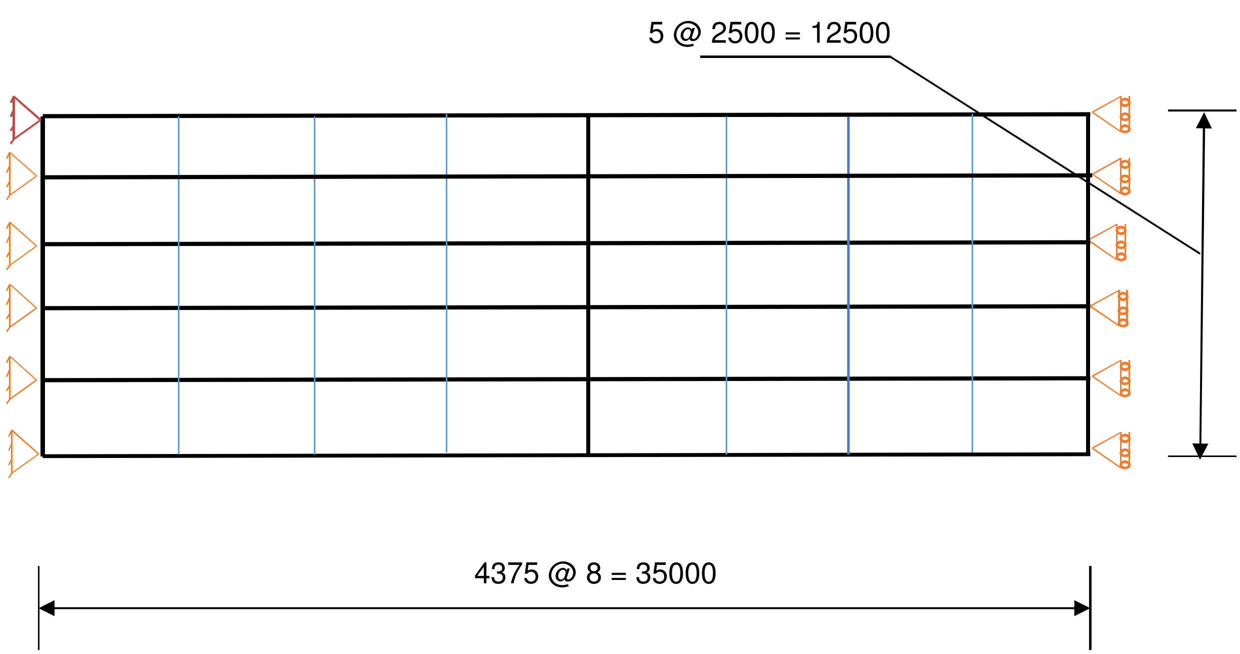

Figure 4.32 : 2-D Grillage mesh that idealizes the actual bridge configuration.

Table 4.6: Properties of grillage members

Member Group	Area (mm^2)	Moment of Inertia (mm^4)	Torsional Constant (mm^4)
Group A			
Group B	830654	2.57288E+11	4.77662E+09
Group C			
Group D			

Table 4.7: Probability of failure and reliability index of different modes of failure

Live load case	Failure Mode	Correlation Level	P_f	Reliability index, β
One truck, left lane	FM1		1.37E-07	5.14
One truck – right lane	FM2		9.44E-08	5.21
Two trucks – side by side	FM3	$\rho = 0.0$	3.73E-06	4.48
	FM4	$\rho = 0.5$	5.67E-05	3.86
	FM5	$\rho = 1.0$	0.000147	3.62

Using the improved reliability bounds IRB approach (Appendix A), the joint failure probabilities were determined, as shown in Table 4.8. The system's upper and lower bounds of probability of failure and the associated reliability indices are shown in Table 4.9.

Table 4.8: Joint failure probabilities.

	FM1	FM2	FM3	FM4	FM5
FM1	1.00	2.22E-09	6.08E-08	6.08E-09	2.02E-09
FM2		1.00	4.26E-08	2.66E-08	6.28E-09
FM3			1.00	8.02E-09	2.44E-08
FM4	Symmetric			1.00	4.88E-09
FM5					1.00

Table 4.9: System's probability of failure and reliability index

	Failure probability, P_f	Reliability index, β_{sys}
Lower bound	8.03E-08	5.24
Upper bound	1.11E-07	5.18

Figure 4.33 presents a snapshot, taken from the proposed model, showing the reliability results.

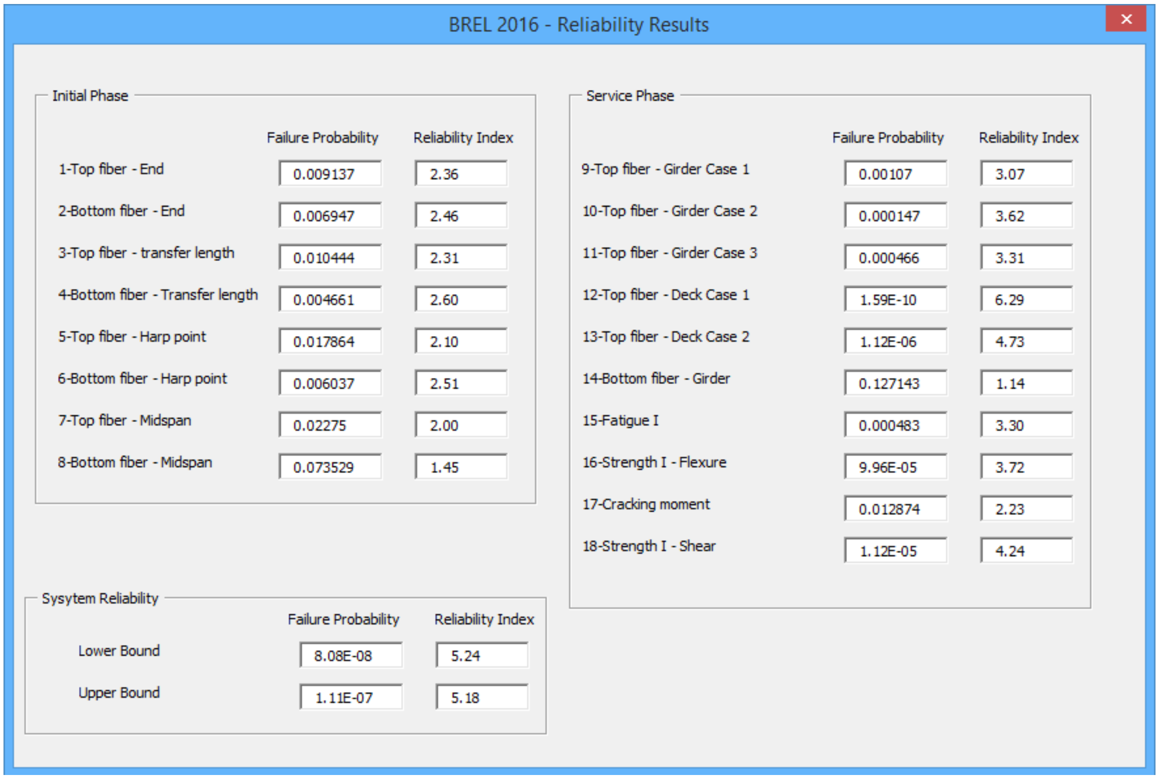

Figure 4.33: A snapshot from the proposed model showing the reliability results.

4.7 Model Validation

In this section, the accuracy of the proposed reliability model is investigated, both at the individual components' level and the overall structural system's level.

4.7.1 Component reliability indices

To validate the proposed reliability model for the individual components reliability indexes, COSSAN-X software has been employed. COSSAN-X is a comprehensive Finite Element probabilistic analysis software developed by the Institute for Risk and Uncertainty at the University of Liverpool-UK (Figure 4.34).

The bridge configuration used in the case study of Section 4.5, has been analyzed with a 3-D FE model and was probabilistically analyzed with COSSAN-X (Figure 4.35). A span length of 30 m was used. The same random variables and their statistical parameters, as shown in Table 4.2, were used and the Monte Carlo analysis with 100,000 samples has been performed. The probability of failure P_f and the corresponding reliability index β, of every limit state function, obtained from COSSAN-X software were compared with those obtained from the BREL proposed model. Table 4.10 show the results obtained from the two models. The close agreement of the results of the two models reflects the satisfactory accuracy of the proposed BREL model. However, the reliability index with respect to stress at the bottom fiber measured at end section and transfer section shows higher values measured by Cossan-X in comparison with BREL. This is due to the modeling of the boundary conditions (supports) at the nodes of the bottom fiber in the finite element model (Cossan-X). The translational displacements at these nodes were restrained while the rotational displacements were released. When the girder deflects, it tends to pull the supports. The supports resist this pulling by inducing tensile stress at the nodal support. Such tensile stress decreases the compression at the bottom fiber and, hence, increases the reliability index (Table 4.10).

4.7.2 System reliability

To examine the accuracy of the proposed algorithm for system reliability, a nonlinear FE analysis was performed with ANSYS R.16 software (Figures 4.36 and 4.37). The same bridge configuration used in the case study of Section 4.5.6, has been used. The live truck positioning followed the scenarios explained in Section 4.3.2 and for each scenario a corresponding mode of failure was assigned. Table 4.11 compares the results of the failure mode analysis FMA obtained from the proposed model GRANAL and from the ANSYS R16.0 software. Having the results of the FMA, reliability analysis with the Improved Bounds Reliability IBR analysis was conducted to obtain the lower and upper bounds of failure probabilities and the corresponding reliability indices. Comparison of these results are illustrated in Table 4.12.

Figure 4.34: COSSAN-X software from the University of Liverpool.

Table 4.10: Components reliability indices (BREL vs. COSSAN-X)

Phase	Case	BREL		COSSAN-X	
		P_f	β	P_f	β
Initial (transfer) phase	Stress at top fiber at end section	8.03E-08	2.35	9.96E-08	2.31
	Stress at bottom fiber at end section	4.43E-05	3.92	1.26E-09	4.80
	Stress at top fiber at transfer section	3.74E-09	2.27	3.12E-09	2.22
	Stress at bottom fiber at transfer section	0.000117	4.05	9.01E-09	4.84
	Stress at top fiber at harp point section	1.69E-08	2.65	1.27E-08	2.62
	Stress at bottom fiber at harp point section	0.000117	3.68	0.000153	3.62
	Stress at top fiber at midspan section	1.51E-08	2.68	1.14E-08	2.62
	Stress at bottom fiber at midspan section	0.000337	3.75	0.00027	3.71
Service phase (after losses)	Stress at top fiber of girder; Case I	0.00026	3.80	0.000313	3.76
	Stress at top fiber of girder; Case II	9.2E-05	4.20	0.000108	4.18
	Stress at top fiber of girder; Case III	0.000147	3.96	0.000165	3.98
	Stress at top fiber of deck; Case I	1.2E-08	6.20	1.07E-08	6.18
	Stress at top fiber of deck; Case II	1.53E-07	5.0	4.13E-10	4.96
	Stress at bottom fiber of girder	0.057053	2.20	0.06178	2.24
	Fatigue	0.000251	3.48	0.000313	3.44
	Ultimate bending	0.000362	3.38	0.000325	3.40
	Cracking moment	0.018763	2.08	0.017003	2.12
	Ultimate shear	7.84E-05	4.35	9.96E-05	4.32

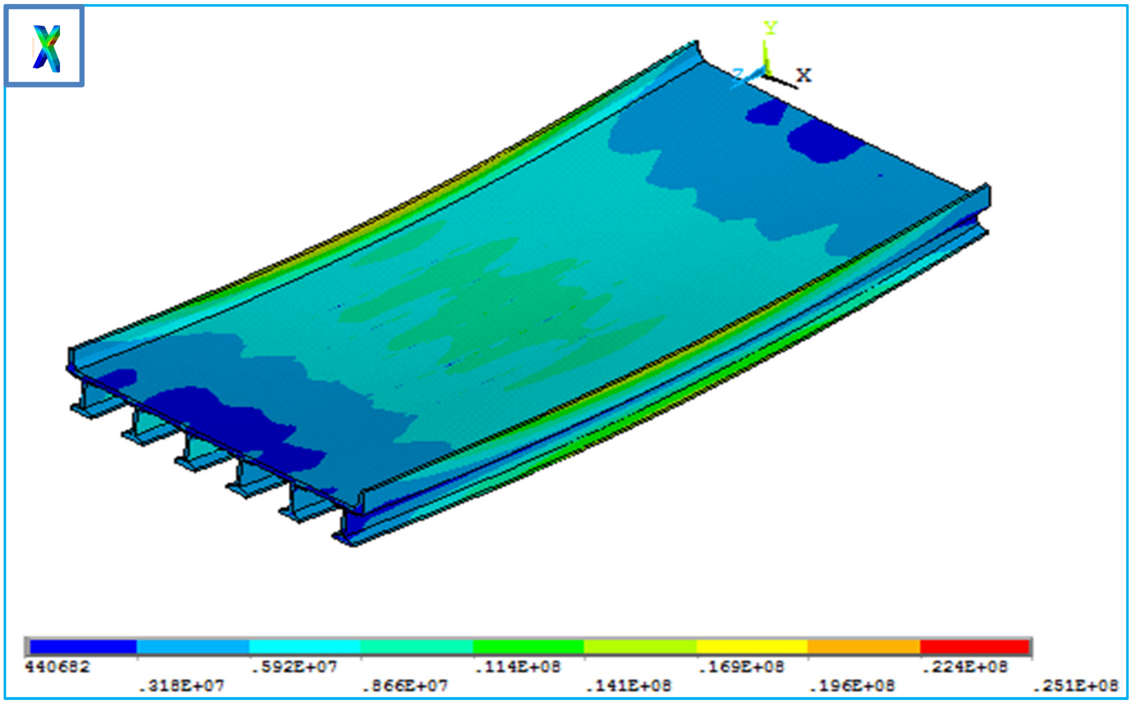

Figure 4.35: FE analysis for the bridge under study (COSSAN-X).

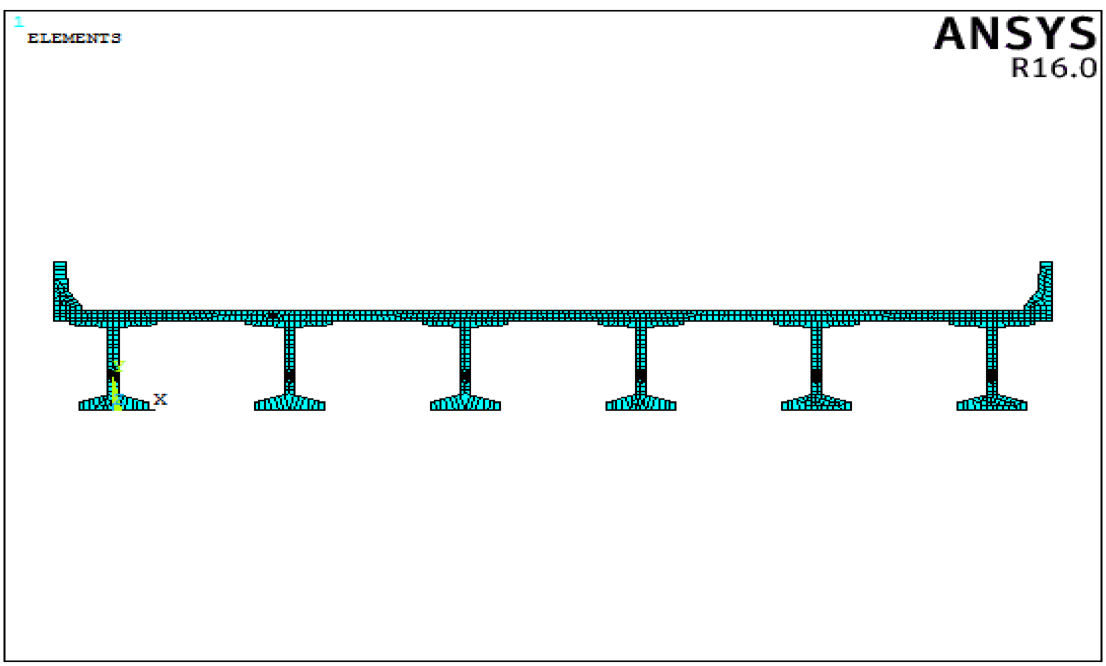

Figure 4.36: Finite element mesh (ANSYS R16.0).

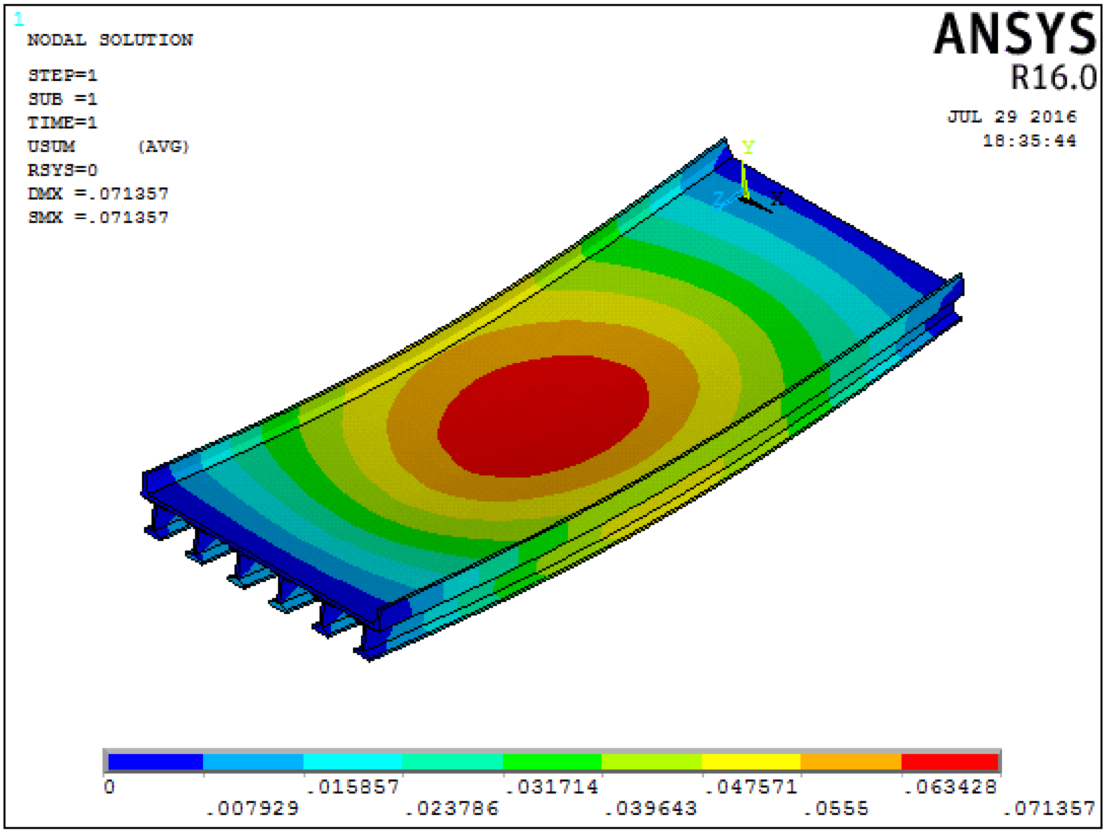

Figure 4.37: FE analysis with ANSYS R16.0 software

Table 4.11: Probability of failure and reliability index of different modes of failure

Live load case	Failure Mode	Correlation Level	GRANAL		ANSYS	
			P_f	β	P_f	β
One truck, left lane	FM1		1.37E-07	5.14	2.58E-07	5.02
One truck – right lane	FM2		9.44E-08	5.21	5.79E-08	5.30
Two trucks – side by side	FM3	$\rho = 0.0$	3.73E-06	4.48	6.5E-06	4.36
	FM4	$\rho = 0.5$	5.67E-05	3.86	7.23E-05	3.80
	FM5	$\rho = 1.0$	0.000147	3.62	0.000185	3.56

Table 4.12: System's probability of failure and reliability index

Bound	GRANAL		ANSYS	
	P_f	β_{sys}	P_f	β_{sys}
Lower bound	8.03E-08	5.24	1.23E-07	5.16
Upper bound	1.11E-07	5.18	2.58E-07	5.02

4.8 Summary

In this chapter, the reliability of prestressed girder bridges was investigated and estimated. The new statistical parameters of the random variables derived in Chapter 3 were used to obtain the updated failure probabilities and the corresponding reliability indexes. The reliability analysis considered all the limit state functions involved in the design of prestressed girder bridges, as defined by AASHTO LRFD 7th Edition 2014 code. The reliability indexes of different types of girders have been evaluated using different span lengths.

The individual components' reliability indexes were estimated using two different methods; namely, the First-Order Reliability Method FORM and the Monte Carlo Simulation MCS technique. A Visual Basic Application VBA algorithm was coded for this purpose, for which, a sample of the code is available in Appendix D. The results showed good agreement between the reliability indices obtained from FORM and MCS. The difference ranges between 6% and 9.8%.To obtain the system reliability, failure mode analysis MFA was performed using different scenarios for live load (truck) positioning for different number of loaded lanes. For this purpose, a nonlinear 2-D grillage analogy algorithm was coded with VBA. The code is presented in Appendix E. Every scenario of live load placement revealed a mode of failure with certain probability of failure and reliability index. The joint probabilities of failure modes were, then, calculated and the overall system reliability was estimated using the Improved Reliability Bounds IRB method.

In order to validate the accuracy of the proposed model, a finite element FE probabilistic analysis was conducted using COSSAN-X (developed by the University of Liverpool-UK). A shown in Table 4.10, good agreement between the results of the two models was achieved. To validate the result of the system reliability, a nonlinear progressive plastic hinge approach was required to be utilized. Therefore, a nonlinear FE analysis was conducted with ANSYS R16 software and, as shown in Tables 4.11 and 4.12, satisfactory convergence among the results obtained from the two different models was achieved.

The reliability analysis presented in this Chapter forms the basis for conducting the probabilistic design optimization of prestressed girder bridges as demonstrated in the next two Chapters.

Chapter 5

Reliability-based Design Optimization of Prestressed Girder Bridges

5.1 Introduction

During the last three decades, structural optimization has become a very inviting research field due to the advances in computational methods, availability of high-speed processors, and the need to perform cost-effective designs (Noh et al. 2011). Minimizing the weight of the structure through deterministic design optimization can reveal cost-effective solutions; however, such solutions may not be entirely safe or durable. In order to search for the best compromise between cost reduction and satisfactory safety levels, reliability-based design optimization is applied to control the structural uncertainties throughout the design process, which cannot be achieved by deterministic optimization (Chateauneuf 2007). Thus, the reliability-based optimization implements the failure probability f_p, obtained from reliability analysis, as probabilistic constraints (Thanedar and Kodiyalam 1991, Belegundu 1988, Choi et al. 1996, Chen et al. 1997, Xiao et al. 1999, Koch and Kodiyalam 1999, and Koch et al. 2000).

As explained in Chapter 2, the reliability-based design optimization approach has not been applied to prestressed girder bridges yet (Al-Delaimi and Dragomirescu 2016). As one of the novel contributions of the current research, a model was developed to perform reliability-based design optimization of prestressed girder bridges.

5.2 Formulation of Optimization Problem

In this section, the objective function, decision variables, and design constraints, related to the optimization process, are demonstrated and discussed.

5.2.1 Objective Function

In the current research, the cost of the bridge superstructure is considered as the objective function of the optimization process. For an optimal design scenario, the values of the design variables will minimize the objective function without violating the design constraints nor the target reliabilities. The proposed objective function is defined as follows (Figure 5.1):

[5.1] $$Cost = N_g\, C_g\, L + C_d V_d + C_{ps} W_{ps} + C_R W_R + C_{asph} A_{asph}$$

where, N_g = number of girders.

C_g = unit cost of precast girder ($ per meter).

C_d= unit cost of concrete in deck and diaphragms ($ per cubic meter).

C_{ps}= unit cost of prestressing strands ($ per kilogram).

C_R= unit cost of conventional reinforcement ($ per kilogram).

C_{asph}= unit cost of asphalt wearing layer ($ per square meter).

V_d= volume of concrete in deck and diaphragms (cubic meter).

W_{ps}= weight of prestressing strands (kilogram).

W_R= weight of conventional reinforcements (kilogram).

A_{asph} = area of asphalt wearing layer (square meter).

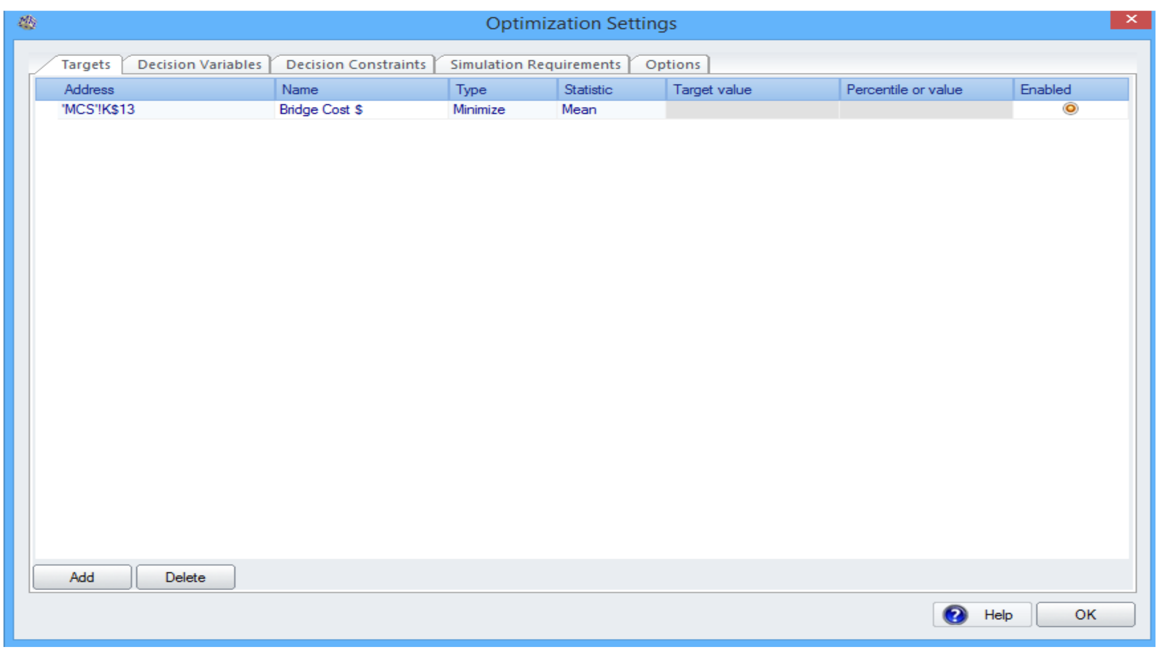

Figure 5.1: Definition of the objective function in the proposed optimization model.

5.2.2 Decision Variables (Design Variables)

The target of the design optimization process is to assign the best combination of values to the design variables in order to minimize the objective function within the constraints limits. The design variables considered in the current research are:

- Deck slab thickness.
- Number of girders.
- Girder spacing.
- Amount of prestressing steel (strands).
- Amount of non-prestressing steel (reinforcement).
- Size of diaphragm (width and depth).
- Overhang length (distance from edge of deck to the centerline of exterior girder).
- Overhang thickness.

Figure 5.2 shows a snapshot, from the proposed model, for defining the decision variables involved in the optimization process.

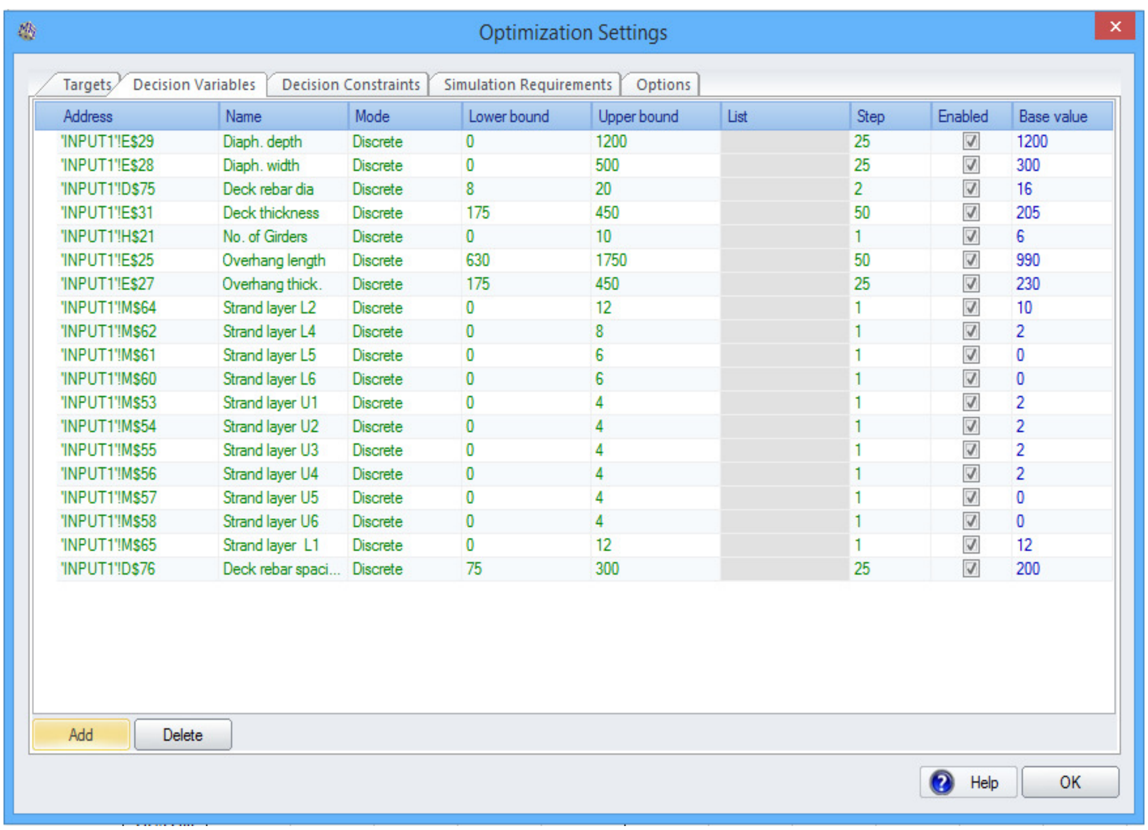

Address	Name	Mode	Lower bound	Upper bound	List	Step	Enabled	Base value
'INPUT1'!E$29	Diaph. depth	Discrete	0	1200		25	☑	1200
'INPUT1'!E$28	Diaph. width	Discrete	0	500		25	☑	300
'INPUT1'!D$75	Deck rebar dia	Discrete	8	20		2	☑	16
'INPUT1'!E$31	Deck thickness	Discrete	175	450		50	☑	205
'INPUT1'!H$21	No. of Girders	Discrete	0	10		1	☑	6
'INPUT1'!E$25	Overhang length	Discrete	630	1750		50	☑	990
'INPUT1'!E$27	Overhang thick.	Discrete	175	450		25	☑	230
'INPUT1'!M$64	Strand layer L2	Discrete	0	12		1	☑	10
'INPUT1'!M$62	Strand layer L4	Discrete	0	8		1	☑	2
'INPUT1'!M$61	Strand layer L5	Discrete	0	6		1	☑	0
'INPUT1'!M$60	Strand layer L6	Discrete	0	6		1	☑	0
'INPUT1'!M$53	Strand layer U1	Discrete	0	4		1	☑	2
'INPUT1'!M$54	Strand layer U2	Discrete	0	4		1	☑	2
'INPUT1'!M$55	Strand layer U3	Discrete	0	4		1	☑	2
'INPUT1'!M$56	Strand layer U4	Discrete	0	4		1	☑	2
'INPUT1'!M$57	Strand layer U5	Discrete	0	4		1	☑	0
'INPUT1'!M$58	Strand layer U6	Discrete	0	4		1	☑	0
'INPUT1'!M$65	Strand layer L1	Discrete	0	12		1	☑	12
'INPUT1'!D$76	Deck rebar spaci...	Discrete	75	300		25	☑	200

Figure 5.2: Snapshot showing the decision variables in the proposed optimization model.

5.2.3 Optimization Constraints

The optimization process aims to assign the best values of decision variables in order to minimize the objective function within certain constraints. In addition to the AASHTO LRFD code's requirements (which are considered as design constraints), the optimization process will be, probabilistically, controlled by a certain reliability limits which are referred to as *target reliabilities*. The component's reliability and the system's reliability should not be less than specific target reliabilities. Thus:

[5.2] $$\beta_c \geq \beta_{c\_T}$$

[5.3] $$\beta_{sys} \geq \beta_{sysT}$$

where,

β_c= computed component reliability.

β_{c_T}= target component reliability.

β_{sys}= computed system reliability.

β_{sys_T}= target system reliability.

As recommended by Nowak and Szerszen (2000), the following target reliabilities are recommended for 50-75 year bridge service life:

- For tensile stress, Service I Limit State, β_{target}= 1.25 (i.e. P_f=0.10565).
- For compressive stress, Service I Limit State, β_{target}= 3.00 (i.e. P_f=0.00135).
- For cracking moment, Stress I Limit State, β_{target}= 3.10 (i.e. P_f=0.000968).
- For tensile stress, Service III Limit State, β_{target}= 1.25 (i.e. P_f=0.10565).
- For fatigue I Limit State, β_{target}= 1.0 - 2.0 (conservatively, the upper limit will be considered in this current study, i.e. P_f=0.02275).
- For ultimate bending, Strength I Limit State, β_{target}= 3.50 (i.e. P_f=0.000233).
- For ultimate shear, Strength I Limit State, β_{target}= 3.50 – 4.0 (conservatively, the upper limit will be considered in this current study, i.e. P_f= 3.17E-05).
- For overall structural system reliability, β_{sys_target}= 4.5 (i.e. P_f=3.4E-06).

Table 5.1: Probabilistic constraints formulation related to RBDO

Phase	Load effect	Limit State	Reliability index	Optimization constraint
Initial phase (at transfer)	Stress at top fiber	Service I	β_{ti}_end	$P_f\,[g\big(\mu_i(X),\sigma_i(X)\big) > 0.24\sqrt{f'_{ci}}\,] \leq 0.10565$
			β_{ti}_trans	
			β_{ti}_harp	
			β_{ti}_mid	
	Stress at bottom fiber	Service I	β_{bi}_end	$P_f\;[g\big(\mu_i(X),\sigma_i(X)\big) > 0.60f'_{ci}] \leq 0.00135$
			β_{bi}_trans	
			β_{bi}_harp	
			β_{bi}_mid	
Service phase (after losses)	Stress at top fiber of girder – load case 1	Service I	β_{bs}_g1	$P_f\big[g\big(\mu_i(X),\sigma_i(X)\big) > 0.45f'_c\big] \leq 0.00135$
	Stress at top fiber of girder – load case 2	Service I	β_{bs}_g2	$P_f\big[g\big(\mu_i(X),\sigma_i(X)\big) > 0.40f'_c\big] \leq 0.00135$
	Stress at top fiber of girder – load case 3	Service I	β_{bs}_g3	$P_f\big[g\big(\mu_i(X),\sigma_i(X)\big) > 0.60f'_c\big] \leq 0.00135$
	Stress at top fiber of deck – load case 1	Service I	β_{bs}_d1	$P_f\big[g\big(\mu_i(X),\sigma_i(X)\big) > 0.45f'_c\big] \leq 0.00135$
	Stress at top fiber of deck – load case 2	Service I	β_{bs}_d2	$P_f\big[g\big(\mu_i(X),\sigma_i(X)\big) > 0.60f'_c\big] \leq 0.00135$
	Stress at bottom fiber of girder	Service III	β_{bs}	$P_f\big[g\mu_i(X),\sigma_i(X)\big) > 0.19\sqrt{f'_c}\big] \leq 0.10565$
	Fatigue at centre of gravity of prestressing strands	Fatigue I	β_{ftg}	$P_f\big[g\big(\mu_i(X),\sigma_i(X)\big) > (\Delta F)_{TH}\big] \leq 0.02275$
	Bending moment	Strength I	β_{ult}	$P_f\big[g\big(\mu_i(X),\sigma_i(X)\big) > Mr\big] \leq 0.000233$
	Cracking moment	Strength I	β_{cr}	$P_f\big[g\big(\mu_i(X),\sigma_i(X)\big) > Mcr\big] \leq 0.000968$
	Shear	Strength I	β_{shr}	$P_f\big[g\big(\mu_i(X),\sigma_i(X)\big) > Vr\big] \leq$ 3.17E-05

Considering the failure probabilities corresponding to these reliability indices, the probabilistic constraints considered in the current research are formulated as shown in Table 5.1. A snapshot from the proposed model for defining the optimization constraints is shown in Figure 5.3

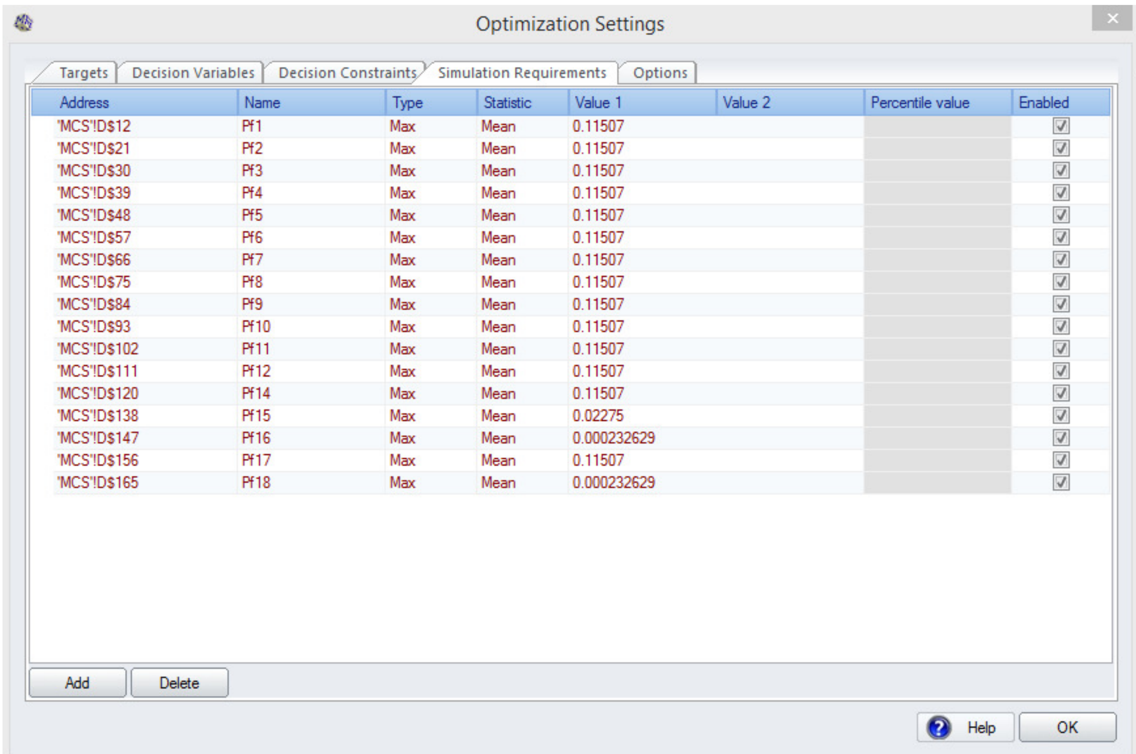

Address	Name	Type	Statistic	Value 1	Value 2	Percentile value	Enabled
'MCS'!D$12	Pf1	Max	Mean	0.11507			☑
'MCS'!D$21	Pf2	Max	Mean	0.11507			☑
'MCS'!D$30	Pf3	Max	Mean	0.11507			☑
'MCS'!D$39	Pf4	Max	Mean	0.11507			☑
'MCS'!D$48	Pf5	Max	Mean	0.11507			☑
'MCS'!D$57	Pf6	Max	Mean	0.11507			☑
'MCS'!D$66	Pf7	Max	Mean	0.11507			☑
'MCS'!D$75	Pf8	Max	Mean	0.11507			☑
'MCS'!D$84	Pf9	Max	Mean	0.11507			☑
'MCS'!D$93	Pf10	Max	Mean	0.11507			☑
'MCS'!D$102	Pf11	Max	Mean	0.11507			☑
'MCS'!D$111	Pf12	Max	Mean	0.11507			☑
'MCS'!D$120	Pf14	Max	Mean	0.11507			☑
'MCS'!D$138	Pf15	Max	Mean	0.02275			☑
'MCS'!D$147	Pf16	Max	Mean	0.000232629			☑
'MCS'!D$156	Pf17	Max	Mean	0.11507			☑
'MCS'!D$165	Pf18	Max	Mean	0.000232629			☑

Figure 5.3: Snapshot showing the optimization constraints in the proposed optimization model.

5.3 Simulation-based Optimization

Simulation is a powerful tool that can be utilized to mimic the performance of real-world systems over time (Law and McComas, 2002). Simulation can produce the output of a system based on the variations in the input to a system (Gosavi 2015).

In order to obtain optimal or best-scenario results, using simulation, requires performing a vast number of replications of experiments to try different input values or alternatives (Mawlana and Hammad, 2013). Simulation-based optimization can be defined as the process of using a heuristic (or metaheuristic) algorithm to guide the simulation analysis without the need to perform an exhaustive analysis of all the possible combinations of input variables (Carson and Maria, 1997).

The current research proposes a computer-aided model that interactively links the reliability analysis to the optimization engine. The proposed reliability and optimization model (BREL) is interactively integrated to OptQuest optimizer (OPTTEK 2012) to perform simulation-based design optimization for prestressed girder bridges. The optimization methodology consists of metaheuristic scatter search assisted by neural network accelerator. Monte Carlo Simulation MCS has been applied as a simulation technique. The flowchart, shown in Figure 5.4, illustrates how the proposed reliability-based optimization RBDO model works.

As already detailed in Chapter Four (Figure 4.13), the proposed model can utilize different types of prestressed girders in the simulation-optimization process in order to determine the optimum design scenario.

5.4 Metaheuristic optimization

When dealing with the optimization of complex systems, such as bridge structures, a course of action taking for many years has been to develop specialized heuristic procedures which, in general, do not require a mathematical formulation of the problem (Marti et al., 2013). The search strategies proposed by metaheuristic methodologies result in iterative-procedures.

During the last three decades, successful applications have been achieved through four metaheuristics approaches: (1) simulated annealing, (2) genetic algorithms, (3) tabu search and (4) scatter search. Of these, tabu search and scatter search have proved to be by far the most effective, and are at the core of the simulation optimization approach (Ólaffson (2005). When supplemented by algorithms such as neural networks in a predicting or curve fitting role, the scatter search technique has proved its efficiency and flexibility in multi-objective optimization of complex systems (Gosavi 2015).

The macros of the current model (BREL and GRANAL) are interactively integrated with the optimization engine as illustrated in Figure 5.5.

5.5 Scatter search

Scatter search aims to obtain a best-case solution for a problem that contains a set of variables particularly in multiobjective optimization problems (Nebro et al. 2008).

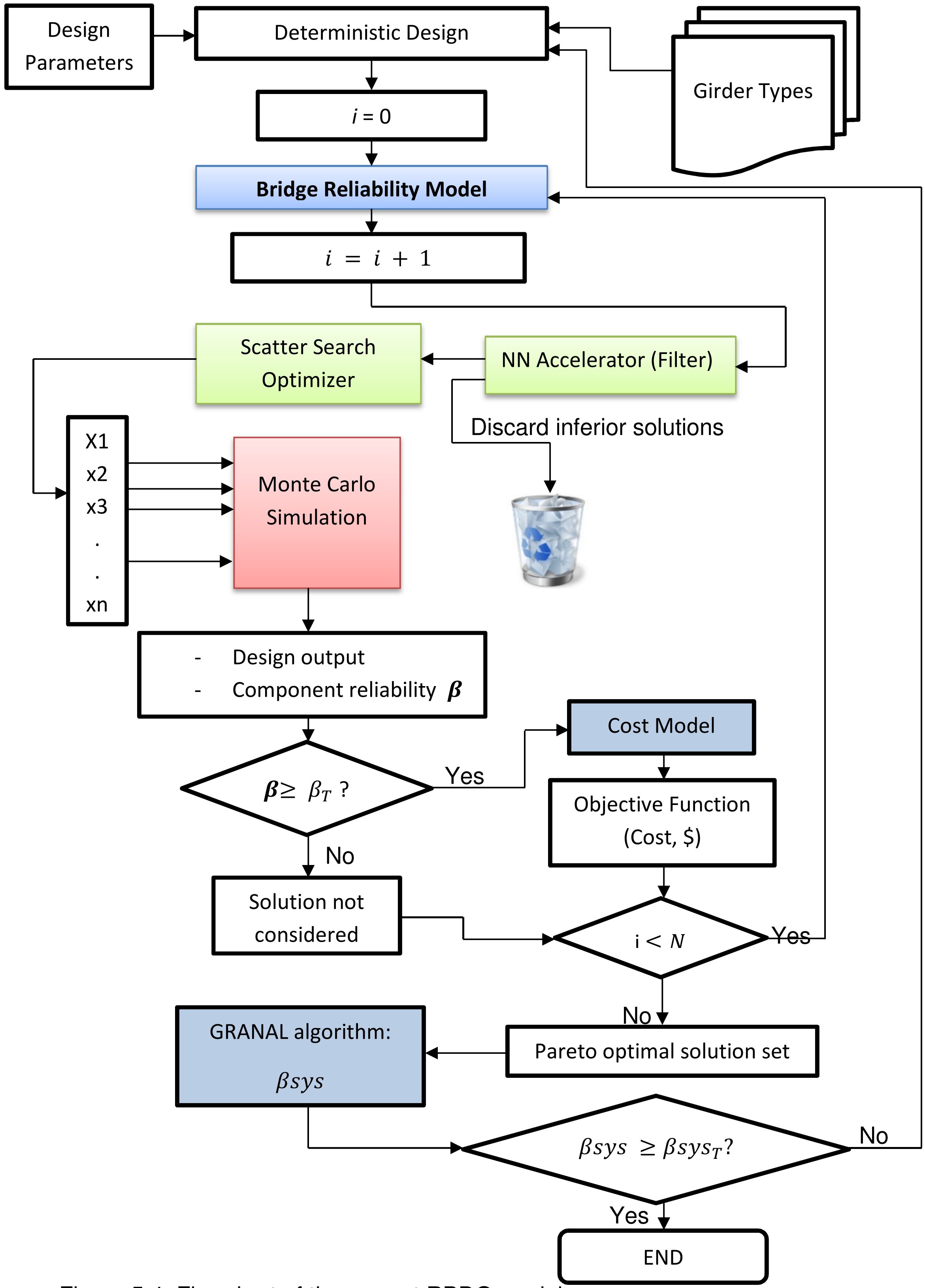

Figure 5.4: Flowchart of the current RBDO model

Let:

$\boldsymbol{Z}$ = set of variables that are bounded with upper and lower limits,

$\boldsymbol{L}$ = set of lower bounds corresponding to the vector of variables , and

$\boldsymbol{U}$ = set of upper bounds corresponding to the vector of variables $\boldsymbol{Z}$.

Hence:

[5.4] $$l_i \leq z_i \leq u_i$$

[5.5] $$z_i = \frac{u_i - l_i}{2} + l_i$$

for $i = 1, 2, \ldots, n, \quad z_i \in \boldsymbol{Z}.$

If the elements of the population are considerably different from each another, then that population is considered divers (Nebro et al. 2008). The optimizer uses a Euclidean distance measure to determine how "close" a potential new point is from the points already in the population, in order to decide whether the point is considered or discarded (Laguna, 1997).

Scatter search imposes linear constraints on every new solution $\boldsymbol{Z}$. This allows testing the feasibility of the newly generated population prior to calculating the objective function. The linear constraints can be expressed as follows:

[5.6] $$\boldsymbol{AZ} \leq \boldsymbol{B}$$

For each point, the feasibility test will examine whether the linear constraints considered by the user are satisfied. An infeasible point $\boldsymbol{Z}$ is made feasible by formulating and solving a linear programming (LP) problem (Laguna, 1997). The LP aims to discover a feasible $\boldsymbol{Z}^*$ that minimizes the absolute deviation between $\boldsymbol{Z}$ and $\boldsymbol{Z}^*$. This can be formulated as follows:

[5.7] Minimize $\boldsymbol{d}^- + \boldsymbol{d}^+$

[5.8] Subject to $\boldsymbol{AZ}^* \leq \boldsymbol{B}$

[5.9] $$\boldsymbol{Z} - \boldsymbol{Z}^* + \boldsymbol{d}^- + \boldsymbol{d}^+ = 0$$

[5.10] $\boldsymbol{L} \leq \boldsymbol{Z}^{*} \leq \boldsymbol{U}$

where $\boldsymbol{d}^{-}$ and $\boldsymbol{d}^{+}$ are negative and positive deviations from the feasible point $\boldsymbol{Z}^{*}$ to the infeasible reference point $\boldsymbol{Z}$. When constraints are not specified, infeasible points are made feasible by simply adjusting variable values to their closest bound. That is,

If $z_i > u_i$, then $z_i^{*} = u_i$ for all $i = 1, .., n$.

Similarly,

If $z_i < l_i$, then $z_i^{*} = l_i$ for $i = 1, .., n$.

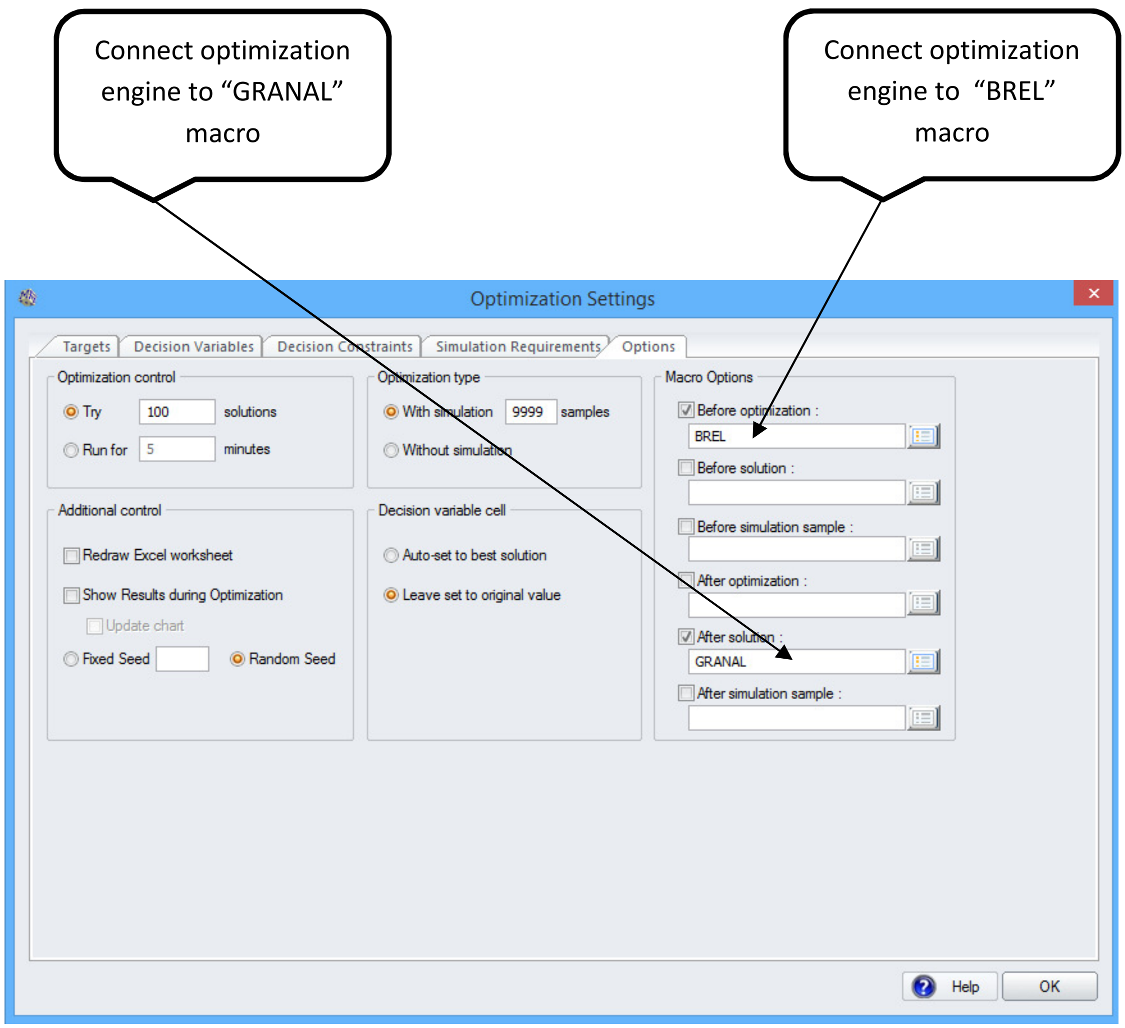

Figure 5.5: Integrating optimization engine with macros of reliability algorithms

The scatter search will apply iteration process to select the improved results. At every iteration, two reference points are chosen to generate four offspring (Glover and Laguna, 1997). Let the parent-reference points be $\boldsymbol{Z_1}$ and $\boldsymbol{Z_2}$, then the offspring $\boldsymbol{Z_3}$ to $\boldsymbol{Z_6}$ are generated as follows:

[5.11] $\boldsymbol{Z_3} = \boldsymbol{Z_1} + d$

[5.12] $\boldsymbol{Z_4} = \boldsymbol{Z_1} - d$

[5.13] $\boldsymbol{Z_5} = \boldsymbol{Z_2} + d$

[5.14] $\boldsymbol{Z_6} = \boldsymbol{Z_2} - d$

[5.15] $d = (\boldsymbol{Z_1} - \boldsymbol{Z_2}) / 3$

The selection of the parent-reference points $\boldsymbol{Z_1}$ and $\boldsymbol{Z_2}$ is biased by the evaluation of the objective function $f(\boldsymbol{Z_1})$ and $f(\boldsymbol{Z_2})$ as well as the previous search results.

5.6 Neural Network accelerator

In order to increase the efficiency and speed of the scatter search process, a neural network is embedded into the optimizer. The neural network role is to “screen out” reference points that are likely to have inferior objective function values as compared to the best known objective function value (Laguna, 1997). In other words, the neural network would act as a filter to eliminate solutions that can be predicted with certain accuracy to be inferior to the best known solution (Laguna and Marti 2002). Such filter will avoid estimating $f(\boldsymbol{Z})$ value (corresponding to a newly generated reference point $\boldsymbol{Z}$), in cases of low quality results . From successive iterations, the values of reference points $\boldsymbol{Z}$ and objective functions $f(\boldsymbol{Z})$ are collected. During the search process, the collected data points are then used to train the neural network. The system automatically determines how many data points to collect and how much training is done (Glover and Laguna, 1997).
Neural Network performs according to the following formulation:

Let:

z = a solution revealed from simulation-based optimization process. This solution will be used as input set in the simulation process (simulation engine).

$f(z)$= output obtained from the simulation engine.

$p(z, w)$= the output of the simulation as predicted by the neural network with weights w when the solution z is used as the inputs.

z^*= best-case solution revealed from the simulation-based optimization process. Thus,

[5.16] $$f(z^*) < f(z) \; \forall \, z$$

l= lower bounds set for decision variables z,

u= upper bounds set for decision variables z.

The optimization process is to minimize the objective function:

Min (z) , subject to:

[5.17] $$l \leq z \leq u$$

Parallel to the optimization-simulation problem, there is a training problem. The objective of the training problem is to determine the set of weights w and to minimize an aggregate error. The training process is utilized to a feed-forward network with a single hidden layer. Figure 5.6 shows a schematic representation of the network.

Let:

n= number of decision variables in the simulation-based optimization problem,

m= number of hidden neurons per layer,

and w_1 to w_n are the weights for all the inputs to the first hidden neuron.

Then, two activation functions for the hidden neurons shall be tested as follows:

[5.18] $$a_k = \tanh[1.5\left(w_{k(n+1)} + \sum_{j=1}^{n} w_{(k-1)(n+1)+jz_j}\right)]$$

[5.19] $$a_k = \frac{1}{1+\exp(-w_k - \sum_{j=1}^{n} w_{(k-1)(n+1)+jz_j})}$$

where, $k = 1, \ldots, m.$

Now, for the output layer, the activation function is formulated as follows:

[5.20] $$p(w, z) = w_{m(n+1)+1} + \sum_{k=1}^{n} w_{m(n+1)+k a_k}$$

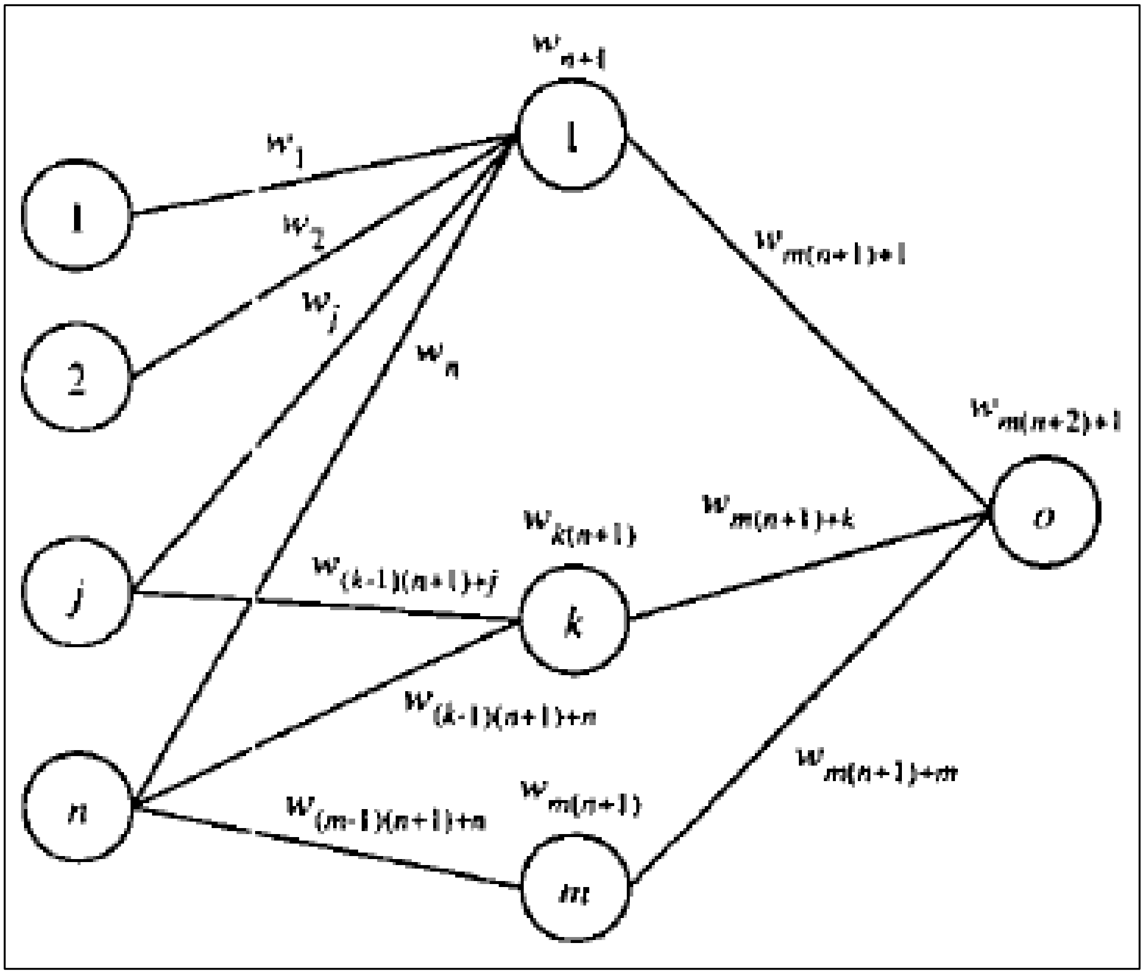

Figure 5.6: Neural network with one hidden layer and one output (Laguna and Marti 2002).

In optimization problems, specifically simulation-optimization approach, the most popular (common) error is Mean Squared Errors , MSE (Laguna and Marti 2002).
Now, Let:

ALL = a set of solution, generated from simulation-optimization, containts all feasible solutions z.

and:

TRAIN = a random sample of solutions in **ALL**.

Then,

the best-known (optimum) solution z^* ∈ **ALL**.

And:

[5.21] $|\mathbf{TRAIN}| \leq |\mathbf{ALL}|$

Accordingly, the training problem can be formulated as follows:

[5.22] Min $g(w) = \frac{1}{|\text{TRAIN}|} \sum_{z \in \text{TRAIN}} (f(z) - p(z,w))^2$

As a filter, the neural network will perform the following test, before evaluating $f(z)$:

[5.23] if $p(z,w) > f(z^*) + \propto$ then discard z.

where, ∝ accounts for the variability of the objective function values and can be calculated as follows:

[5.24] $\propto = 2\sigma_{f(z)}$

in which, $\sigma_{f(z)}$ is the standard deviation of $f(z)$ for z ∈ **TRAIN.**

In the current research, Equation 5.24 was considered a rejection criterion as recommended by Laguna and Marti (2002). Some researchers (e.g. Sharda and Rampal 1995) considered Equation 5.24 as moderate rejection criterion; and they went for a conservative definition by reducing ∝ from two to one standard deviation(s).

5.7 Cost model

To calculate the bridge cost (objective function) associated with every optimization solution (configuration), a cost model is developed, in the current study, and linked to the simulation-optimization model as shown in Figure 5.4. Following the ASTM UNIFORMAT II Standard (ASTM E2103), the bridge configuration has been divided into standard elements and work breakdown structure WBS. A thorough investigation and search have been made to collect unit prices, of the bridge elements, from previous projects and contracts. These unit prices were installed in a database developed for that purpose. For any new project, these unit prices need to be adjusted for locations and inflation rates. Figure 5.7 show the flowchart of the proposed cost model.

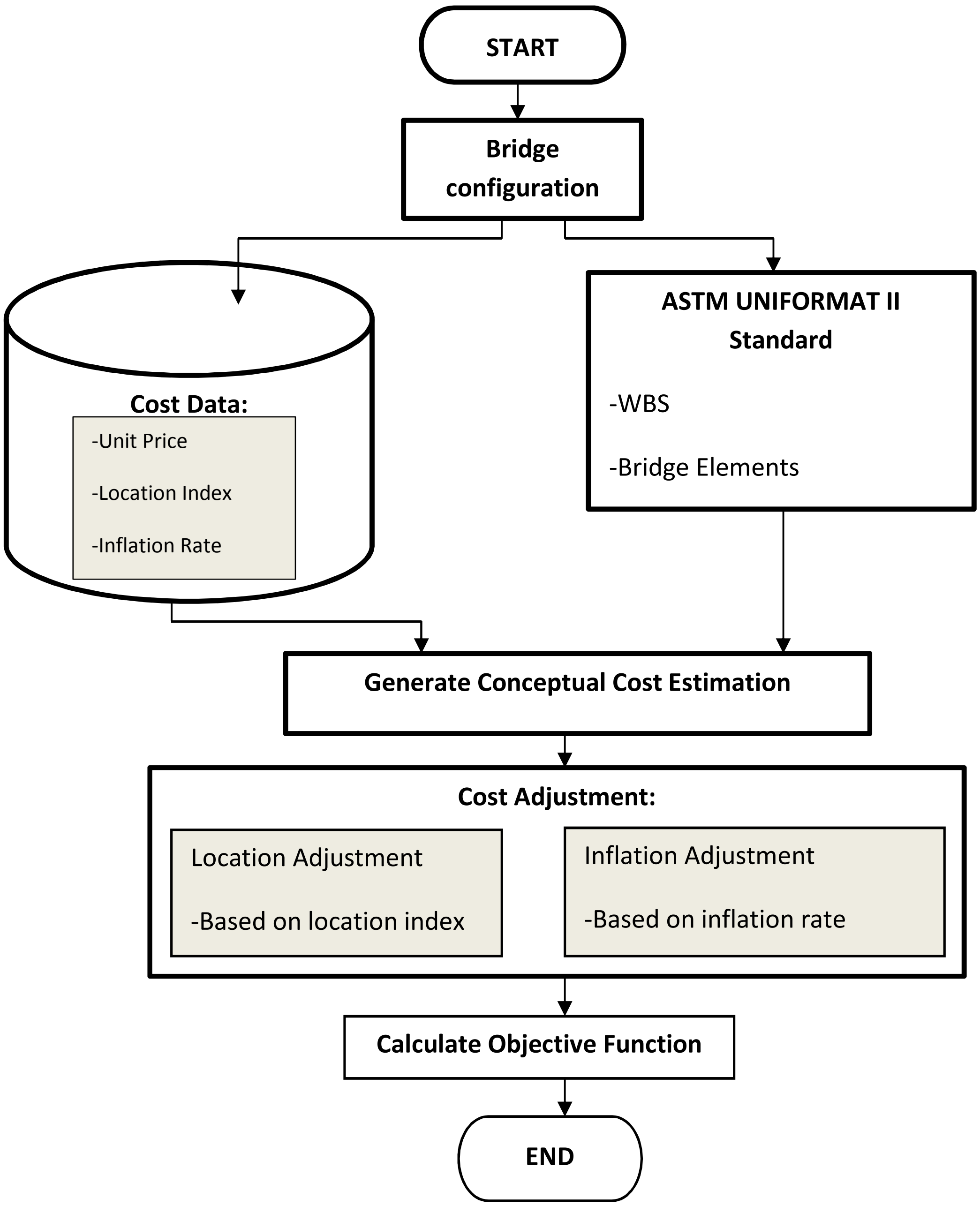

Figure 5.7: Cost model developed in the current study

5.7.1 Cost Data

Preparing a cost estimate greatly depends on the accuracy of the collected data. Thus, data collection has to be carried out prior to developing the cost model. So far no published cost data is available for bridges. Alternatively, cost data were collected from previously constructed bridge projects. The resources of the collected data were from different previously constructed bridge projects in North America. Samples of the collected cost data are illustrated in Appendix D. Using the ASTM (E2103) standards and the collected cost data, a bridge elements and components Excel spreadsheet for each type of bridge is created. These Excel spreadsheets are used to calculate the estimated conceptual cost for the project by entering the dimensions and parameters obtained from the KBS.

5.7.2 Cost adjustment

It is necessary to adjust the cost of previous similar projects for inflation rate and location so that they are suitable for the new project.

5.7.2.1 Adjustment for Location

In order to adjust the cost according to the location, R. S. Means (2012) cities indices are used for this purpose. R.S. Means adjustment for location Equation 5.25 is used as follows:

[5.25] $$C_c = C_r\left(\frac{I_c}{I_R}\right)$$

where,

C_c = cost of proposed project

C_r = cost of previous project

I_c = city index for the current project

I_R = city index of the previous project.

5.7.2.2 Adjustment for Inflation Rate

After adjusting the unit cost for location, inflation adjustment can easily be conducted by applying the inflation rate and the number of the years for which the project cost is needed.

R.S. Means adjustment for time Equation 5.26 is used to calculate the inflation adjustment as follows:

[5.26] $$F = P \times (1 + i)^n$$

Where, F = Future or present total project cost

P = past total project cost, taken from the location adjustment equation

i = inflation rate

n = number of years between the proposed project and the previous project

Figure 5.8 shows a snapshot from the proposed model.

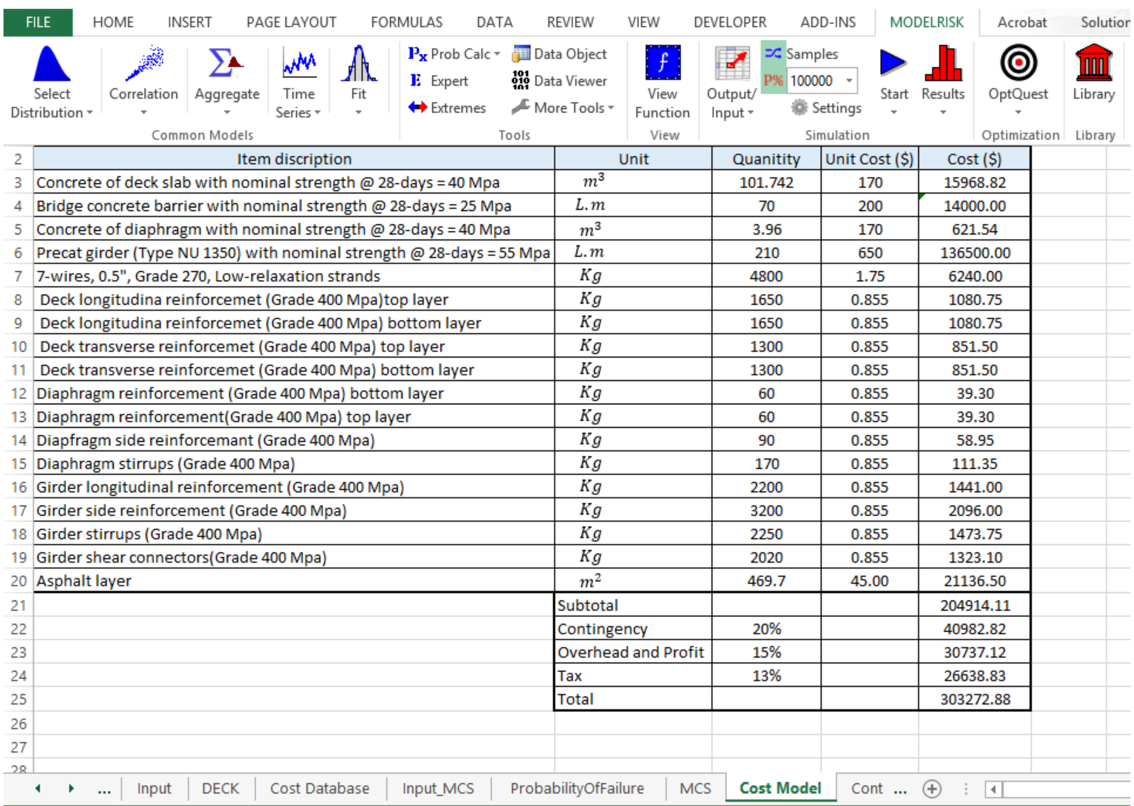

2	Item discription	Unit	Quanitity	Unit Cost ($)	Cost ($)
3	Concrete of deck slab with nominal strength @ 28-days = 40 Mpa	m^3	101.742	170	15968.82
4	Bridge concrete barrier with nominal strength @ 28-days = 25 Mpa	$L.m$	70	200	14000.00
5	Concrete of diaphragm with nominal strength @ 28-days = 40 Mpa	m^3	3.96	170	621.54
6	Precat girder (Type NU 1350) with nominal strength @ 28-days = 55 Mpa	$L.m$	210	650	136500.00
7	7-wires, 0.5", Grade 270, Low-relaxation strands	Kg	4800	1.75	6240.00
8	Deck longitudina reinforcemet (Grade 400 Mpa)top layer	Kg	1650	0.855	1080.75
9	Deck longitudina reinforcemet (Grade 400 Mpa) bottom layer	Kg	1650	0.855	1080.75
10	Deck transverse reinforcemet (Grade 400 Mpa) top layer	Kg	1300	0.855	851.50
11	Deck transverse reinforcemet (Grade 400 Mpa) bottom layer	Kg	1300	0.855	851.50
12	Diaphragm reinforcement (Grade 400 Mpa) bottom layer	Kg	60	0.855	39.30
13	Diaphragm reinforcement(Grade 400 Mpa) top layer	Kg	60	0.855	39.30
14	Diapfragm side reinforcemant (Grade 400 Mpa)	Kg	90	0.855	58.95
15	Diaphragm stirrups (Grade 400 Mpa)	Kg	170	0.855	111.35
16	Girder longitudinal reinforcement (Grade 400 Mpa)	Kg	2200	0.855	1441.00
17	Girder side reinforcement (Grade 400 Mpa)	Kg	3200	0.855	2096.00
18	Girder stirrups (Grade 400 Mpa)	Kg	2250	0.855	1473.75
19	Girder shear connectors(Grade 400 Mpa)	Kg	2020	0.855	1323.10
20	Asphalt layer	m^2	469.7	45.00	21136.50
21		Subtotal			204914.11
22		Contingency	20%		40982.82
23		Overhead and Profit	15%		30737.12
24		Tax	13%		26638.83
25		Total			303272.88
26					
27					

Figure 5.8: Snapshot, from the proposed model, for cost summary

5.8 Case study

In this Section, the applicability of the proposed model to perform reliability-based design optimization is demonstrated.

A single span, simply supported prestressed girder bridge is to be designed according to AASHTO LRFD 7th Edition (2014) code. The longitudinal profile of the bridge is shown in Figure 5.9, while, the bridge cross section is illustrated in Figure 5.10. The available information and data are as follows:

- Span (from center of bearing to center of bearing) = 30 m.
- Bridge total width = 14.20 m
- Asphalt thickness = 75 mm.
- Concrete strength (f'_{ci}) for deck = 40 MPa.
- Concrete initial strength (f'_c) for girder = 41.25 MPa.
- Concrete strength (f'_c) for girder = 55 MPa.
- Strand type: Low-relaxation, 12.70 mm, seven-wire strands.
- Ultimate strength(f_u) for strand = 1860 MPa.
- Yield strength(f_y) for strand = 1660 MPa.
- Yield strength(f_y) for reinforcement = 400 MPa.
- Modulus of elasticity of reinforcement = 200,000 MPa
- Precast standard girder: NU 1350 Girder (Nebraska University girder).

First, initial design is performed. The detailed design calculations are presented and discussed in Appendix C. This design will be referred to as “initial design” in the following sections.

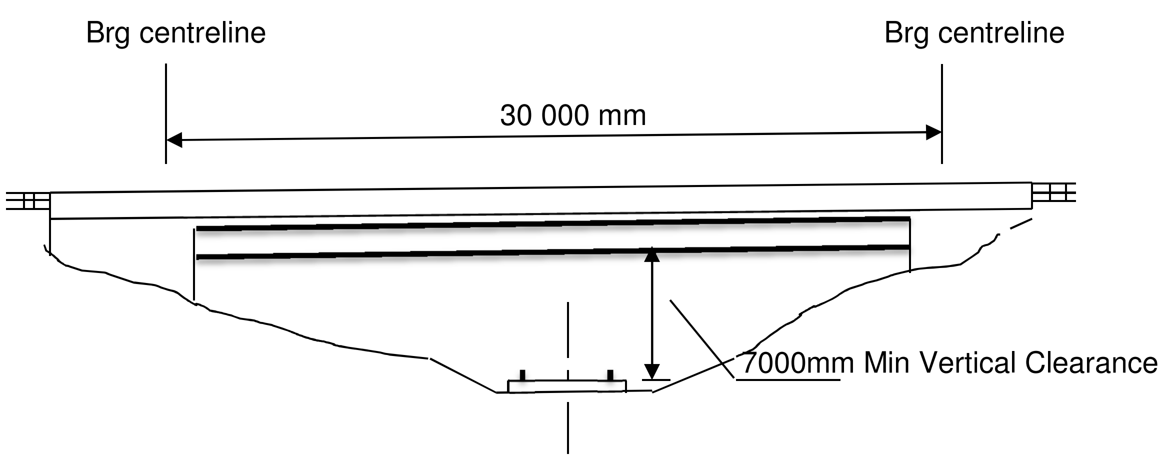

Figure 5.9: Bridge longitudinal profile.

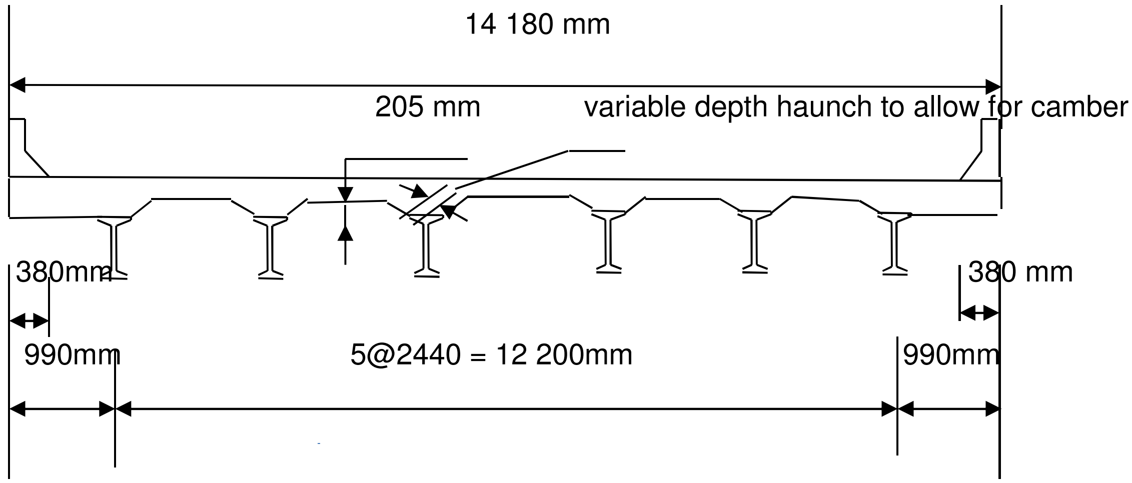

Figure 5.10: Bridge cross section.

Then, using the formulation of the optimization problem demonstrated in Section 5.2, reliability-based design optimization RBDO is performed.

In order to illustrate the importance and necessity of adopting such probabilistic optimization approach, a deterministic design optimization DDO has also been performed by removing (deactivating) the probabilistic constraints. Then, the safety levels in the optimized structure revealed from DDO was assessed by conducting reliability analysis.

Table 5.2 summarizes, the design output obtained from the initial design, deterministic design optimization DDO, and reliability-based design optimization RBDO. The bridge cost related to the initial design, DDO, and RBDO are summarized in Table 5.3. Apparently, the DDO revealed a considerable cost saving (around 28.3%), while the RBDO reduced the cost by about 15%.

Due to imposing the probabilistic constraints on RBDO, all the reliability indices are greater than the specified target reliabilities, which means that reserved safety levels in the final optimized configuration are guaranteed.

In order to evaluate the safety levels in the optimized configuration revealed from the DDO, a reliability analysis has been performed. The results of this analysis are summarized in Table 5.4, which shows some of the reliability indices (written in red) are less than the target reliabilities. This clearly indicates that the optimized structural configuration obtained from DDO failed to satisfy the target safety levels. This demonstrates the importance and necessity to adopt a probabilistic approach, rather than a deterministic approach, when performing design optimization of prestressed girder bridges.

Figure 5.11 illustrates the details of girder's non-prestressing steel (reinforcement) as referred to in Table 5.2. Figure 5.12 shows a histogram plot of the objective function (cost) related to the reliability-based design optimization RBDO of the bridge under consideration.

Table 5.2: Results of Initial Design, DDO, and RBDO

<table>
<tr><th colspan="3">Design variable</th><th>Initial Design</th><th>DDO</th><th>RBDO</th></tr>
<tr><td colspan="3">Number of girders</td><td>6</td><td>4</td><td>5</td></tr>
<tr><td colspan="3">Girder spacing</td><td>2440</td><td>3600</td><td>2900</td></tr>
<tr><td colspan="3">Deck slab thickness, mm</td><td>205</td><td>215</td><td>210</td></tr>
<tr><td colspan="3">Number of strand per girder</td><td>52</td><td>64</td><td>58</td></tr>
<tr><td rowspan="4">Area of deck reinforcement, $mm^2/_m$</td><td rowspan="2">Top layer</td><td>Longitudinal</td><td>615</td><td>1340</td><td>1005</td></tr>
<tr><td>Transverse</td><td>450</td><td>450</td><td>450</td></tr>
<tr><td rowspan="2">Bottom layer</td><td>Longitudinal</td><td>615</td><td>1340</td><td>1005</td></tr>
<tr><td>Transverse</td><td>646</td><td>646</td><td>646</td></tr>
<tr><td rowspan="5">Area of girder non-prestressing reinforcement</td><td colspan="2">Stirrups (bar # 1 in Figure 5.11)</td><td>No. 3 @ 300 mm</td><td>No. 3 @175mm</td><td>No.3 @ 200mm</td></tr>
<tr><td colspan="2">Transverse reinforcement (bar # 2 & 3 in Figure 5.11)</td><td>No. 3 @ 300 mm</td><td>No. 3 @175mm</td><td>No.3 @ 200mm</td></tr>
<tr><td colspan="2">Shear connectors (bar # 4 in Figure 5.11)</td><td>No. 3 @ 300 mm</td><td>No. 3 @175mm</td><td>No.3 @ 200mm</td></tr>
<tr><td colspan="2">Longitudinal reinforcement (bar # 5 & 6 in Figure 5.11)</td><td>10 No. 4</td><td>12 No. 14</td><td>12 No. 4</td></tr>
<tr><td colspan="2">Longitudinal reinforcement (bar # 7 in Figure 5.11)</td><td>2 x 7 No. 4</td><td>2 x 7 No. 4</td><td>2 x 7 No. 4</td></tr>
<tr><td rowspan="2">Intermediate diaphragm</td><td colspan="2">Width, mm</td><td>300</td><td>200</td><td>250</td></tr>
<tr><td colspan="2">Depth, mm</td><td>1400</td><td>1000</td><td>1100</td></tr>
<tr><td colspan="3">Overhang length, mm</td><td>990</td><td>1690</td><td>1290</td></tr>
<tr><td colspan="3">Overhang thickness, mm</td><td>230</td><td>215</td><td>210</td></tr>
</table>

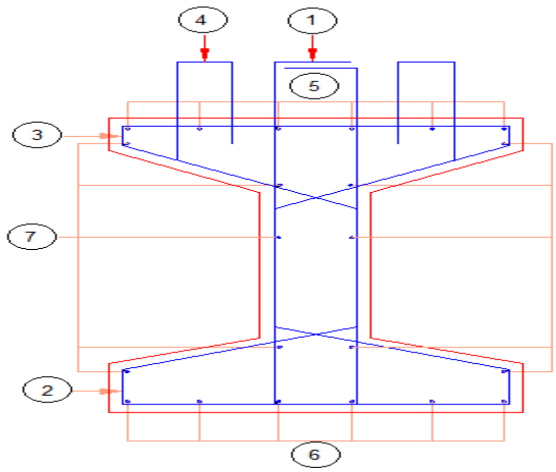

Figure 5.11: Details of girder's non-prestressing reinforcement as referred to in Table 5.2.

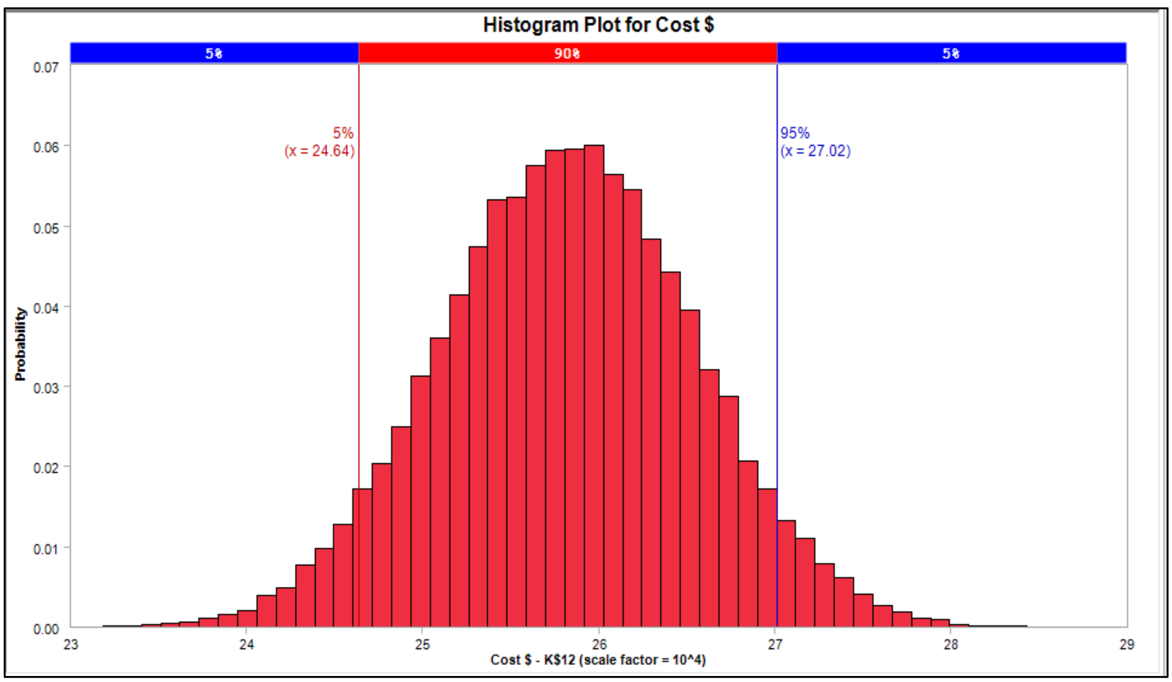

Figure 5.12: Histogram plot for the objective function (Cost $) related to RBDO.

Table 5.3: Bridge Cost as per initial design, DDO, and RBDO

Type	Cost $	Cost saving
Original Design	303640	
Deterministic Design Optimization, DDO	217835	28.3 %
Reliability-based Design Optimization, RBDO	258250	15.0 %

Table 5.4: Reliability assessment of the bridge configuration revealed from DDO

<table>
<tr><th rowspan="2">Phase</th><th rowspan="2">Load effect</th><th rowspan="2">Limit State</th><th colspan="4">Reliability index</th></tr>
<tr><th>Symbol</th><th>DDO</th><th>RBDO</th><th>β_{target}</th></tr>
<tr><td rowspan="8">Initial phase (at transfer)</td><td rowspan="4">Stress at top fiber</td><td rowspan="4">Service I</td><td>β_{ti}_end</td><td>0.78</td><td>1.48</td><td>1.25</td></tr>
<tr><td>β_{ti}_trans</td><td>0.80</td><td>1.50</td><td>1.25</td></tr>
<tr><td>β_{ti}_harp</td><td>1.20</td><td>1.54</td><td>1.25</td></tr>
<tr><td>β_{ti}_mid</td><td>1.28</td><td>1.56</td><td>1.25</td></tr>
<tr><td rowspan="4">Stress at bottom fiber</td><td rowspan="4">Service I</td><td>β_{bi}_end</td><td>3.00</td><td>3.24</td><td>3.00</td></tr>
<tr><td>β_{bi}_trans</td><td>3.10</td><td>3.28</td><td>3.00</td></tr>
<tr><td>β_{bi}_harp</td><td>2.80</td><td>3.34</td><td>3.00</td></tr>
<tr><td>β_{bi}_mid</td><td>2.92</td><td>3.32</td><td>3.00</td></tr>
<tr><td rowspan="12">Final phase (Service stage, i.e. after losses)</td><td>Stress at top fiber of girder – load case 1</td><td>Service I</td><td>β_{bs}_g1</td><td>3.06</td><td>3.40</td><td>3.00</td></tr>
<tr><td>Stress at top fiber of girder – load case 2</td><td>Service I</td><td>β_{bs}_g2</td><td>3.27</td><td>3.44</td><td>3.00</td></tr>
<tr><td>Stress at top fiber of girder – load case 3</td><td>Service I</td><td>β_{bs}_g3</td><td>3.04</td><td>3.32</td><td>3.00</td></tr>
<tr><td>Stress at top fiber of deck – load case 1</td><td>Service I</td><td>β_{bs}_d1</td><td>4.08</td><td>5.00</td><td>3.00</td></tr>
<tr><td>Stress at top fiber of deck – load case 2</td><td>Service I</td><td>β_{bs}_d2</td><td>3.88</td><td>4.12</td><td>3.00</td></tr>
<tr><td>Stress at bottom fiber of girder</td><td>Service III</td><td>β_{bs}</td><td>0.98</td><td>1.26</td><td>1.25</td></tr>
<tr><td>Fatigue at strand level</td><td>Fatigue I</td><td>β_{ftg}</td><td>2.78</td><td>2.84</td><td>2.00</td></tr>
<tr><td>Bending moment</td><td>Strength I</td><td>β_{ult}</td><td>3.44</td><td>3.58</td><td>3.50</td></tr>
<tr><td>Cracking moment</td><td>Service I</td><td>β_{cr}</td><td>2.68</td><td>3.24</td><td>3.10</td></tr>
<tr><td>Shear</td><td>Strength I</td><td>β_{shr}</td><td>3.62</td><td>4.12</td><td>4.00</td></tr>
<tr><td rowspan="2">Redundancy (System Reliability)</td><td rowspan="2">β_{sys}</td><td>Upper bound</td><td>4.12</td><td>4.84</td><td>4.50</td></tr>
<tr><td>Lower bound</td><td>4.17</td><td>4.78</td><td>4.50</td></tr>
</table>

Figures 5.13 and 5.14 show the Pareto set of optimum solutions revealed from DDO and RBDO, respectively.

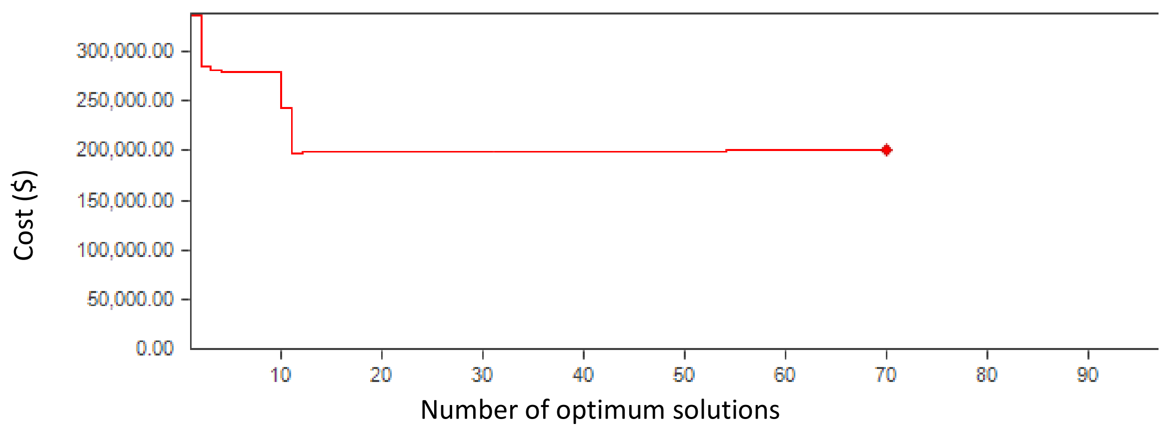

Figure 5.13: Pareto set of optimum solutions revealed from DDO

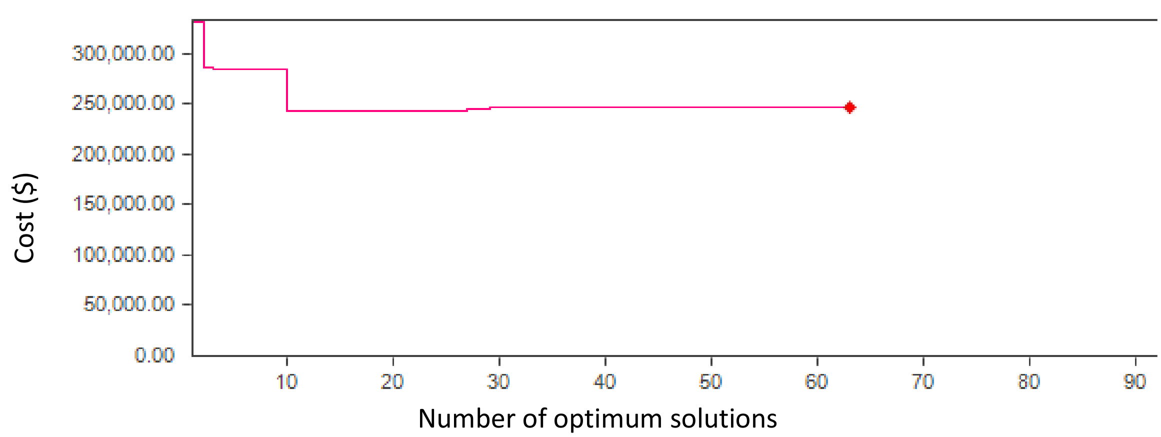

Figure 5.14: Pareto set of optimum solutions revealed from RBDO

6.8 Summary

In this chapter the details, formulation and application of the newly developed model for reliability-based design optimization of prestressed girder bridges has been presented. To cope with the complexity of structural systems like prestressed girder bridges, the simulation-based optimization approach forms a very efficient technique. An algorithm with VBA and spreadsheets was developed to integrate the world's most efficient optimization engine, OptQuest, with the proposed reliability and cost models. The simulation was performed using Monte Carlo analysis, while the optimization utilized metaheuristic scatter search with Neural Network Accelerator.

The failure probabilities corresponding to the target reliability indexes of the individual components and the entire system, were imposed as probabilistic constraints in the simulation-optimization procedure.

To precisely calculate the object function (bridge cost), a cost model was developed. For that purpose, the bridge configuration was decomposed, according to ASTM UNIFORMAT II, and list of work-breakdown-structure (WBS) was developed. Also, a comprehensive database for the unit cost for all bridge components was developed. The cost model was interactively integrated with the simulation-optimization procedure.

The applicability of the proposed model was demonstrated through a case study where a simple span prestressed girder bridge was designed according to the AASHTO LRFD 7th edition (2014). Then, using the newly developed model, the bridge design was optimized. The optimization was, first, deterministically performed (without considering the uncertainties associated with the design parameters. This deterministic design optimization (DDO) revealed 28.3 % cost saving. However, the safety levels, which have been assessed with reliability analysis, were less than the target levels for different limit states (i.e., unsafe configuration from the reliability-basis)

Then, a reliability based design optimization (RBDO) was performed. A cost saving of 15% was achieved with all reliability indexes higher than the target reliabilities (i.e., safe configuration).

The reliability-based design optimization approach imposes specific target reliabilities, as probabilistic constraints, to ensure that the design solutions perform as desired. As will be explained in the next Chapter, this approach could be further improved, from the quality point of view, by applying the Six Sigma quality concept.

Chapter 6

Six Sigma Quality with Robust Design Optimization of Prestressed Girder Bridges

6.1 Introduction

The most recent quality philosophy, also originating in a manufacturing setting, is the six sigma concept (Stamatis, 2015). The concepts of six sigma quality can be defined in an engineering design context through the relation between the concepts of design, reliability and robustness – as probabilistic design approaches (Koch et al., 2004). Within this context, design quality is measured with respect to the probability of constraint satisfaction and sensitivity of performance objectives, both of which can be related to a design "sigma level" (Vlahinos and Kelkar, 2002).

Six sigma is a quality philosophy at the highest level relating to all processes (Li et al. 2006). The term "sigma" refers to standard deviation, σ, which is a measure of dispersion of a set of data around the mean value, μ, for the respective data. This approach can be used both to describe the known variability of parameters that influence a system and as a measure of performance variability, and thus quality (Koch et al. 2004). The concepts of six sigma quality, measurement, and improvement can be related to two probabilistic design measures: reliability and robustness. The two goals in designing for quality are: (1) striving to consistently maintain performance within acceptable limits (reliability), and (2) striving to reduce performance variation and thus increase robustness (Koch 2002).

Performance variation can be characterized as a number of standard deviations from the mean performance, as shown in Figure 6.1. The areas under the normal distribution in Figure 6.1 associated with each σ-level relate directly to the probability of performance falling in that particular range (for example, $\mp 1\sigma$ is equivalent to a probability of 0.683). As illustrated in Table 6.1, quality can be measured using any "sigma level", percent variation or probability (equivalent to reliability), or number of defects per million parts (Kumar et al., 2006). In Figure 6.1, the lower and upper specification limits that define the desired performance range are shown to coincide with $\mp 3\sigma$ measured from the mean (Vlahinos and Kelkar 2002). The design associated with this level of performance variance would be considered a “3σ” design.

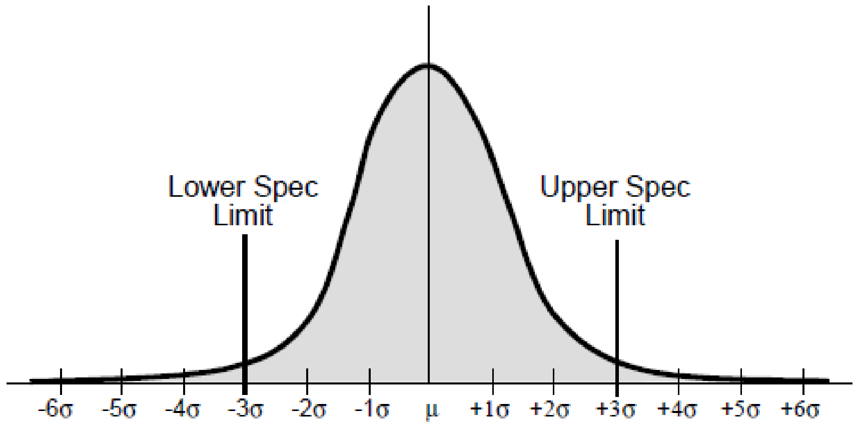

Figure 6.1: Normal Distribution, 3-σ Design (Vlahinos and Kelkar, 2002).

Table 6.1: Sigma Level as Percent Variation and Defects per Million (Koch, 2002)

Sigma Level	Percent Variation	Defects/million (short term)	Defects/million (long term)
±1σ	68.26	317,400	697,700
±2σ	95.46	45,400	308,733
±3σ	99.73	2,700	66,803
±4σ	99.9937	63	6,200
±5σ	99.999943	0.57	233
±6σ	99.9999998	0.002	3.4

To design for six sigma (DFSS), in engineering applications, performance variability is measured and, if needed, this is improved with respect to two quality goals: i) - by shifting the performance distribution relative to the constraints or specification limits (thus improving reliability) and ii) - by shrinking the performance distribution to reduce the variability and sensitivity of the design (thus improving robustness) (Banuelas and Antony 2004).These concepts of “shift” and “shrink” are illustrated in Figure 6.2. In Figure 6.2a, where the performance distribution is shifted until an acceptable level of reliability (area of distribution inside the constraint) is achieved. In Figure 6.2b, the spread of the performance distribution is shrunk to reduce the potential performance loss associated with the tails of the distribution and thus to reduce the sensitivity and improve the robustness (Banuelas and Antony 2004).

.

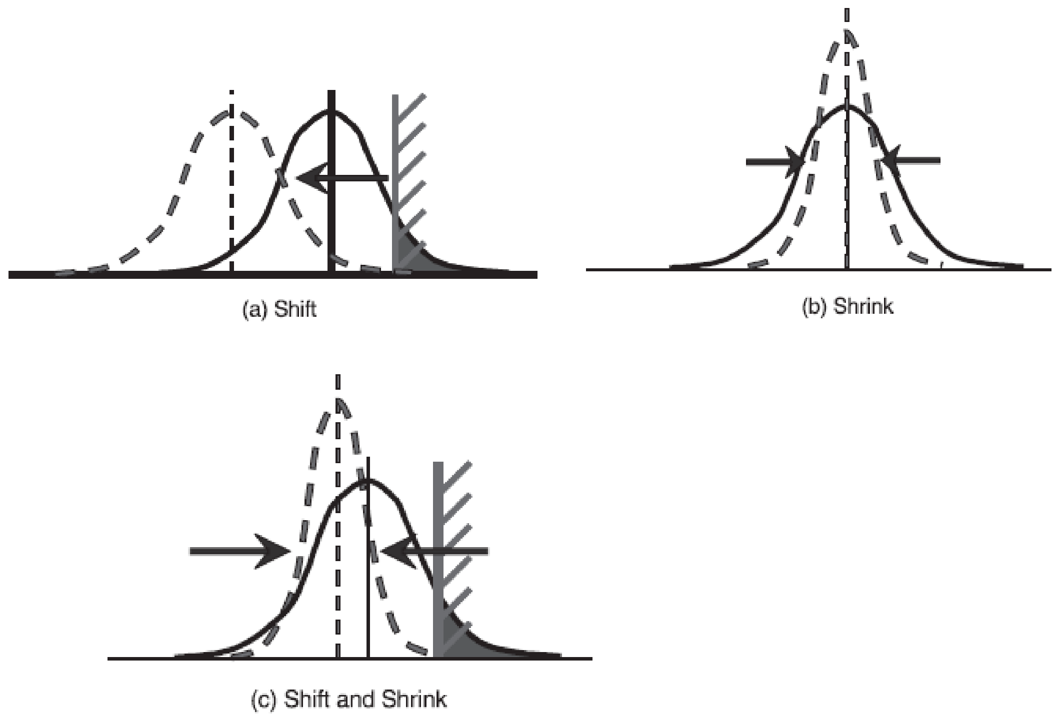

Figure 6.2: Design for six sigma: reliability “shift” and robust “shrink” (Stamatis 2015)

The ideal case in improving design quality in designing for six sigma (DFSS) is to both shift and shrink a performance distribution, as illustrated in Figure 6.2c. As shown in Figure 6.2a, while the loss of mean performance associated with the shifted distribution may be acceptable, given the increased reliability, the potential worst-case performance associated with the left tail may be undesirable. With the shrunken distribution of Figure 6.2b, the level of reduced spread possible may not be sufficient to achieve an acceptable reliability level without shifting the mean performance (Schroeder et al. 2008). In Figure 6.2c, with both shift and shrink, the reliability level is achieved, the robustness improved, and the worst-case performance was not significantly affected. This is the desired goal in implementing the *design for six sigma* DFSS.

As a unique contribution of the current research, this chapter applies the design for six sigma (DFSS) philosophy to the optimization of prestressed girder bridge design (Al-Delaimi and Dragomirescu 2016). This methodology has been utilized by formulating a six sigma-based robust design optimization that combines probabilistic concepts of structural reliability and robust design with the six sigma quality concept. The optimization model incorporates robust objective formulation, variability of input design parameters formulation, and output constraint formulation. Such approach ensures not only that the design performs as desired but also that the design consistently performs as desired.

6.2 Formulation of Optimization Problem

The robust optimization formulation combines the probabilistic elements of reliability, robust design, and six sigma quality concept. This incorporates formulation of objective robustness (minimize variation in addition to mean performance on target), defining random variables, formulation of reliable input constraints (random design variable bounds), and determining the output constraints (sigma level quality constraints or reliability constraints). In this section, the formulation for implementing six sigma-based robust optimization is discussed.

In general, the formulation for implementing six sigma-based robust optimization is given as follows:

Find the set of design variables X that:

[6.1] Minimizes: $F(\mu z(X), \sigma z(X))$

[6.2] subject to: $gi(\mu z(X), \sigma z(X)) \ \leq \ 0$

[6.3] $XL + n\sigma X \ \leq \ \mu X \ \leq \ XU \ - n\sigma X.$

where, $F(X)$ is the objective function, $gi(X)$ is the limit state function related to limit state i, and X includes input parameters that are bounded with lower limit XL and upper limit UX. Both input and output constraints are formulated to include mean performance and a desired “sigma level” (number of standard deviations, $n\sigma$), as follows:

[6.4] $\mu z \ - n\sigma z \ \geq$ Lower specification limit

[6.5] $\mu z \ + n\sigma z \ \leq$ Upper specification limit.

[6.6] $F \ = \ \sum_{i=1}^{l} [\mp \frac{w_{1_i}}{s_{1_i}} \ \mu Z_i + \frac{w_{2_i}}{s_{2_i}} \ \sigma^2 Z_i]$

where,

$\mp$: the "+" sign is used before the first term when the response mean is to be minimized and the "−" sign is to be used when the response mean is to be maximized (Banuelas and Antony 2004).

w_{1_i} and w_{2_i}: are, respectively, the weights for the mean and variance of performance response i.

S_{1_i} and S_{2_i}: are, respectively, the scale factors for the mean and variance of performance response i.

l: is the number of performance responses included in the objective function.

Here, "$n\sigma$" refers to the desired quality level (sigma level). The "six" in "six sigma" does not imply that only 6σ solutions are sought in a six sigma concept (6σ is a quality measure, six sigma is a quality improvement philosophy). A six sigma process seeks to explore the tradeoff between performance and quality and to investigate the quality levels achievable for a given design. In many cases, 6σ quality is not achievable for a given design concept, configuration, and/or set of requirements because, in many cases, the cost of achieving 6σ quality is very expensive (Schroeder et al. 2008).

The key to implementing this six sigma-based robust optimization formulation is the ability to evaluate performance variability statistics which allow the reformulation of constraints and objectives as defined in Eqs. 6.1 to 6.6 (Koch et al. 2004). Applying such optimization formulation on the design of prestressed girder bridges makes it feasible to define the objective function, decision variables, and optimization constraints.

6.2.1 Objective Function

The proposed objective function is to minimize the cost of the bridge superstructure. This objective function is treated as a random variable. Hence, the objective function is defined as follows:

[6.7] Minimize $\mu[Cost] + \sigma[Cost]$

[6.8] $Cost = N_g\, C_g\, L + C_d V_d + C_{ps} W_{ps} + C_R W_R + C_{asph} A_{asph}$

where,

N_g = number of girders.

C_g = unit cost of precast girder ($ per meter).

C_d= unit cost of concrete in deck and diaphragms ($ per cubic meter).

C_{ps}= unit cost of prestressing strands ($ per kilogram).

C_R= unit cost of conventional reinforcement ($ per kilogram).

C_{asph}= unit cost of asphalt wearing layer ($ per square meter).

V_d= volume of concrete in deck and diaphragms (cubic meter).

W_{ps}= weight of prestressing strands (kilogram).

W_R= weight of conventional reinforcements (kilogram).

A_{asph} = area of asphalt wearing layer (square meter).

As shown in Figure 6.3, the bridge cost, which was considered as the objective function in the current model, should be minimized.

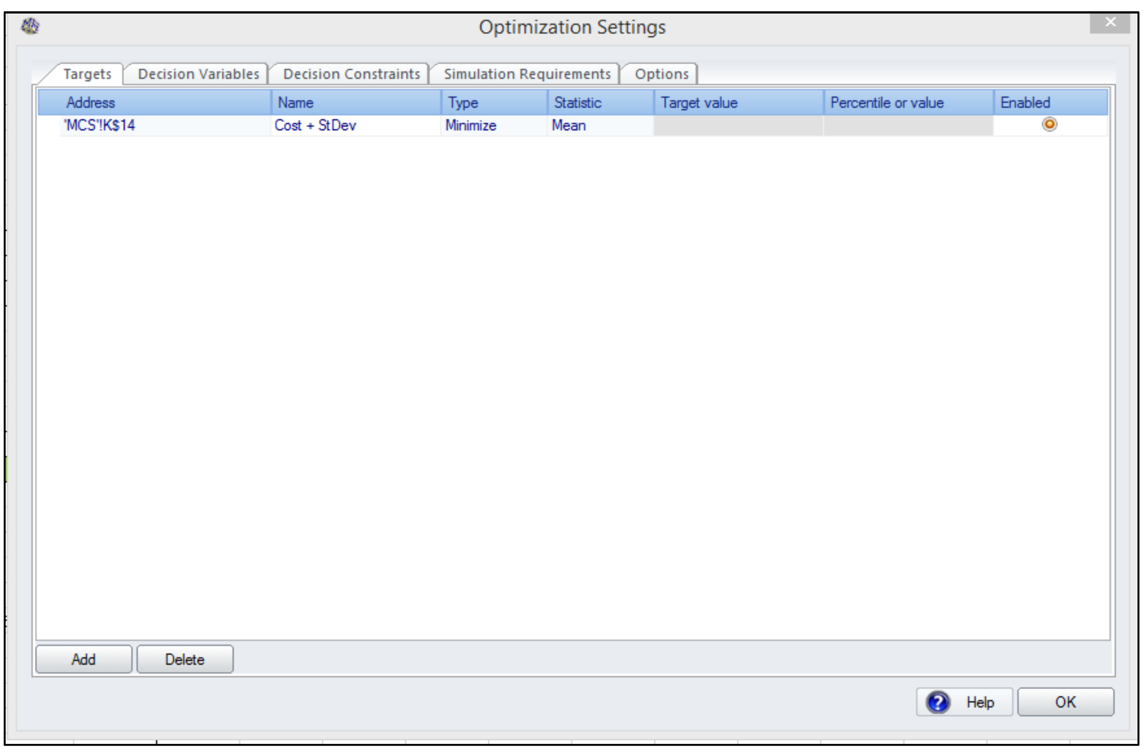

Figure 6.3: Snapshot showing the objective function (Cost $) treated as random variable.

The model interactively integrates the reliability model, the cost model, the simulation engine, and the optimization engine. The model was developed using Visual Basic Applications VBA. The details of the cost model was already demonstrated in Section 5.7.

6.2.2 Decision Variables (Design Variables)

The design optimization process aims at obtaining best combination of design variables in order to minimize the objective function within the constraints limits. As detailed in Chapter 5, the design variable variables considered in the current research are:

- Deck slab thickness.
- Number of girder.
- Girder spacing.
- Amount of prestressing steel (strands).
- Amount of non-prestressing steel (reinforcement).
- Size of diaphragm (width and depth).
- Overhang length (distance from edge of deck to the centerline of exterior girder).
- Overhang thickness.

6.2.3 Optimization Constraints

In order to formulate the optimization constraints, all limit state functions related to the design of prestressed girder bridges at the initial and final phases need, first, to be defined and formulated. Then, quality level (number of sigma) is imposed.

Table 6.2 illustrates, in detail, the formulation of the constraints of the six sigma-based robust design optimization of prestressed girder bridges. A snapshot from the developed model, is shown in Figure 6.4 presenting the optimization constraints. These constraints represents the limit state functions as defined by the AASHTO LRFD 7th Edition (2014). As already explained in Chapter 4, the current research comprehensively considered 18 limit state functions that governs the design of prestressed girder bridges.

However, it is important to decide on the desired quality level (number of sigma) prior to starting the optimization process. Figure 6.5 shows a snapshot, taken from the model, for the window from which the user can define his/her preferred quality level.

Table 6.2: Optimization constraints formulation related to DFSS

Phase	Load effect	Limit State	Optimization constraint
Initial phase (at transfer)	Stress at top fiber	Service I	$g(\mu_i(X) + n\,\sigma_i(X)) \leq 0.24\sqrt{f'_{ci}}$
	Stress at bottom fiber	Service I	$g(\mu_i(X) + n\,\sigma_i(X)) \leq 0.60f'_{ci}$
Final phase (Service stage, i.e. after losses)	Stress at top fiber of girder – load case 1 *	Service I	$g(\mu_i(X) + n\,\sigma_i(X)) \leq 0.45f'_c$
	Stress at top fiber of girder – load case 2	Service I	$g(\mu_i(X) + n\,\sigma_i(X)) \leq 0.40f'_c$
	Stress at top fiber of girder – load case 3	Service I	$g(\mu_i(X) + n\,\sigma_i(X)) \leq 0.60f'_c$
	Stress at top fiber of deck – load case 1	Service I	$g(\mu_i(X) + n\,\sigma_i(X)) \leq 0.45f'_c$
	Stress at top fiber of deck – load case 2	Service I	$g(\mu_i(X) + n\,\sigma_i(X)) \leq 0.60f'_c$
	Stress at bottom fiber of girder	Service III	$g\mu_i(X) + n\,\sigma_i(X) \leq 0.19\sqrt{f'_c}$
	Fatigue at strand level	Fatigue I	$g(\mu_i(X) + n\,\sigma_i(X)) \leq (70\ or\ 125)$
	Bending moment	Strength I	$g(\mu_i(X) + n\,\sigma_i(X)) \leq Mr$
	Cracking moment	Strength I	$g(\mu_i(X) + n\,\sigma_i(X)) \leq Mcr$
	Shear	Strength I	$g(\mu_i(X) + n\,\sigma_i(X)) \leq Vr$

*Note: for the definition of load cas1, load case2, and load case3, please refer to Table 4.1.

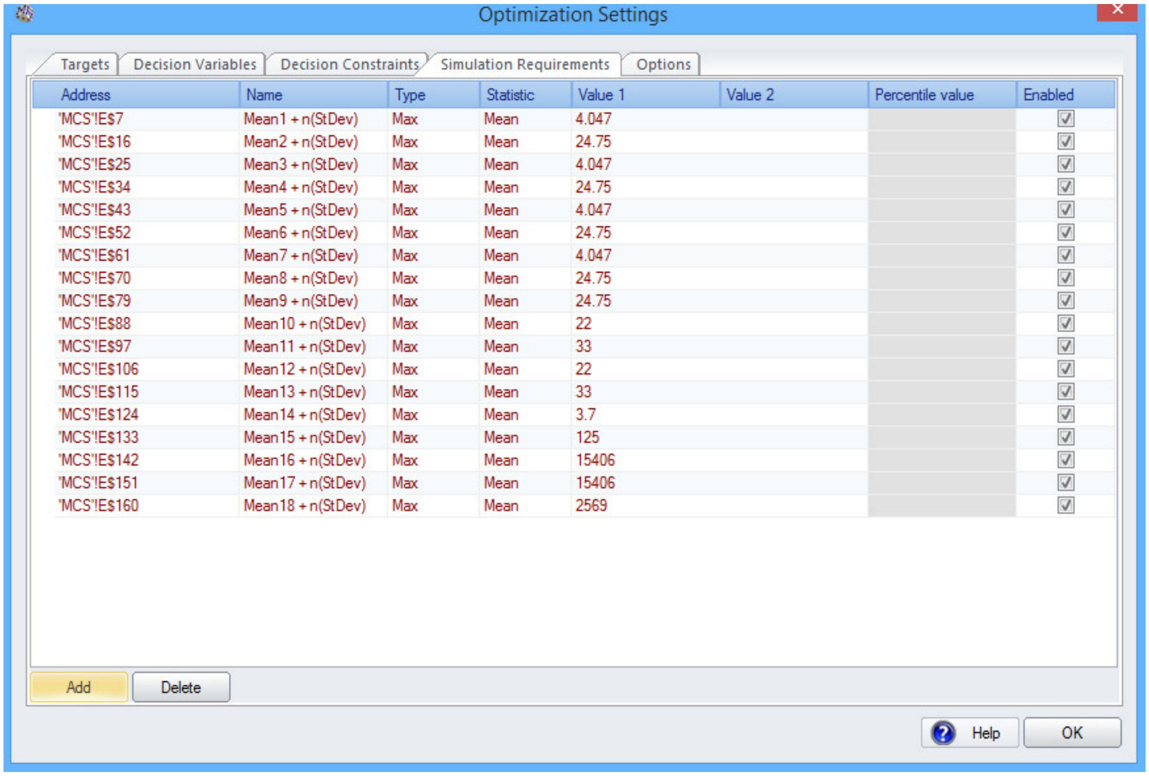

Address	Name	Type	Statistic	Value 1	Value 2	Percentile value	Enabled
'MCS'!E$7	Mean1 + n(StDev)	Max	Mean	4.047			✓
'MCS'!E$16	Mean2 + n(StDev)	Max	Mean	24.75			✓
'MCS'!E$25	Mean3 + n(StDev)	Max	Mean	4.047			✓
'MCS'!E$34	Mean4 + n(StDev)	Max	Mean	24.75			✓
'MCS'!E$43	Mean5 + n(StDev)	Max	Mean	4.047			✓
'MCS'!E$52	Mean6 + n(StDev)	Max	Mean	24.75			✓
'MCS'!E$61	Mean7 + n(StDev)	Max	Mean	4.047			✓
'MCS'!E$70	Mean8 + n(StDev)	Max	Mean	24.75			✓
'MCS'!E$79	Mean9 + n(StDev)	Max	Mean	24.75			✓
'MCS'!E$88	Mean10 + n(StDev)	Max	Mean	22			✓
'MCS'!E$97	Mean11 + n(StDev)	Max	Mean	33			✓
'MCS'!E$106	Mean12 + n(StDev)	Max	Mean	22			✓
'MCS'!E$115	Mean13 + n(StDev)	Max	Mean	33			✓
'MCS'!E$124	Mean14 + n(StDev)	Max	Mean	3.7			✓
'MCS'!E$133	Mean15 + n(StDev)	Max	Mean	125			✓
'MCS'!E$142	Mean16 + n(StDev)	Max	Mean	15406			✓
'MCS'!E$151	Mean17 + n(StDev)	Max	Mean	15406			✓
'MCS'!E$160	Mean18 + n(StDev)	Max	Mean	2569			✓

Figure 6.4: Snapshot showing the optimization constraints.

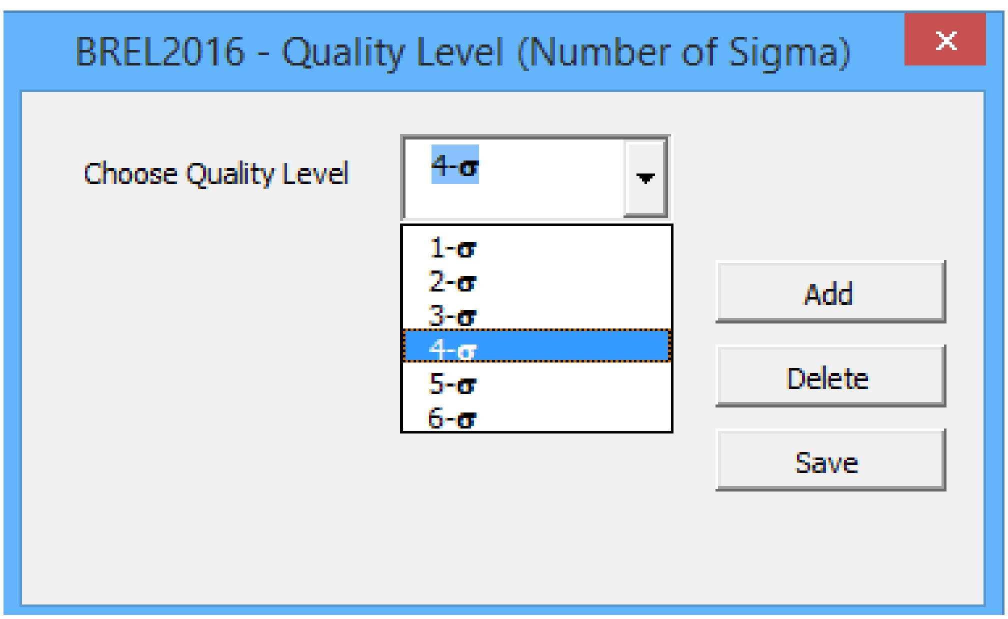

Figure 6.5: A snapshot from the proposed model for selecting quality level

6.3 Optimization Technique

Similar to the technique adopted for the Reliability-based Design Optimization RBDO (explained in Section 5.3), Simulation-optimization was applied to perform design for six sigma DFSS optimization following the formulations in Section 6.2. The simulation-optimization technique conducts iterative process.

The flowchart shown in Figure 6.6 demonstrates the proposed methodology for DFSS. This flowchart shows the interaction among the deterministic analysis, reliability model, simulation engine, and the optimization engine. The simulation engine performs Monte Carlo Analysis, while the optimization engine conducts metaheuristic scatter search with neural network accelerator (filter).

Any solution revealed from the simulation-optimization process is sent to the cost model if and only if it satisfies the probabilistic constraints. At the end of the simulation-optimization process, the model produces a report to present the details of all feasible solutions (pareto set).

6.4 Case study

For better comparison between the two different probabilistic optimization approaches developed in the current research (RBDO of Chapter Five and DFSS of the current Chapter), the same bridge example considered in Section 5.8 was utilized here. The initial design calculations are illustrated in Appendix C. The six sigma-based design optimization has been performed according the formulation presented in Section 6.2.

In this case study, different quality levels ($n\sigma$) were considered ($where, n = 1, 2, \ldots, 6$). For each quality level, simulation-based optimization was performed. A pareto of feasible solutions were obtained with respect to each quality level. In the current study, the solution that revealed the minimum objective function (bridge cost), out of the pareto set, was considered

Table 6.3 summarizes the results of the design optimization with respect to every quality level (sigma level), while Table 6.4 illustrates the value of the objective function (Cost $). As shown in Table 6.4, when the quality level increases the corresponding objective function (bridge cost) takes higher value (more expensive).

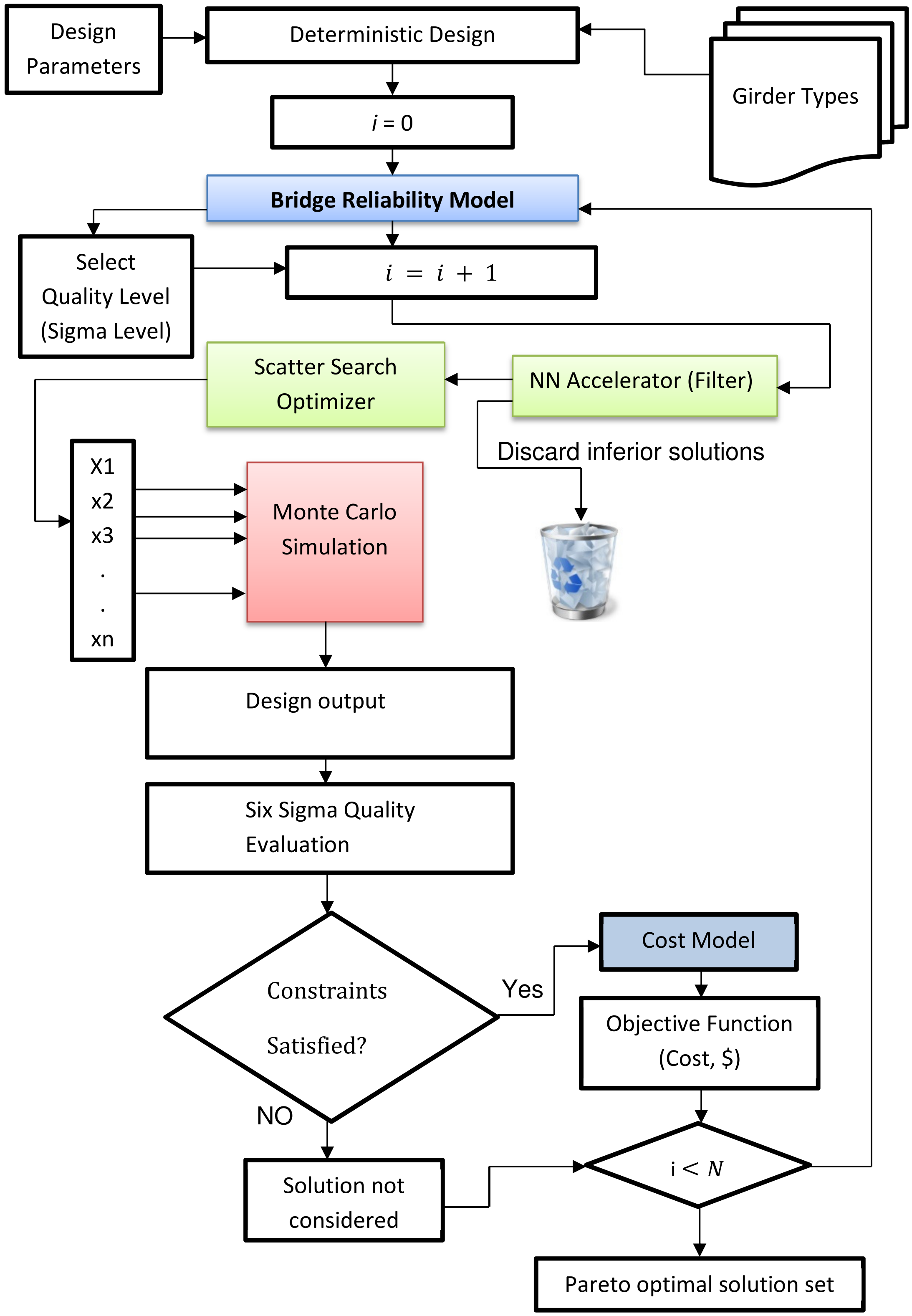

Figure 6.6: Flowchart of the DFSS model developed in the Current Study

Table 6.3: Summary of design optimization results considering different quality levels

<table>
<tr><th colspan="3" rowspan="2">Design variable</th><th colspan="6">Quality Level (Number of Sigma)</th></tr>
<tr><th>1-σ</th><th>2-σ</th><th>3-σ</th><th>4-σ</th><th>5-σ</th><th>6-σ</th></tr>
<tr><td colspan="3">Number of girders</td><td>4</td><td>5</td><td>5</td><td>6</td><td>6</td><td>7</td></tr>
<tr><td colspan="3">Girder type</td><td>NU 1350</td><td>NU 1350</td><td>NU 1600</td><td>NU1350</td><td>NU1600</td><td>NU1350</td></tr>
<tr><td colspan="3">Girder spacing, mm</td><td>3730</td><td>3080</td><td>2900</td><td>2490</td><td>2400</td><td>1490</td></tr>
<tr><td colspan="3">Deck slab thickness, mm</td><td>225</td><td>190</td><td>225</td><td>175</td><td>200</td><td>175</td></tr>
<tr><td colspan="3">Number of strand per girder</td><td>62</td><td>58</td><td>61</td><td>59</td><td>61</td><td>59</td></tr>
<tr><td rowspan="4">Area of deck reinforcement, mm^2/m</td><td rowspan="2">Top layer</td><td>Longitudinal</td><td>1340</td><td>2010</td><td>1005</td><td>895</td><td>895</td><td>670</td></tr>
<tr><td>Transverse</td><td>450</td><td>600</td><td>450</td><td>450</td><td>450</td><td>450</td></tr>
<tr><td rowspan="2">Bottom layer</td><td>Longitudinal</td><td>1340</td><td>2010</td><td>1005</td><td>895</td><td>895</td><td>670</td></tr>
<tr><td>Transverse</td><td>646</td><td>646</td><td>646</td><td>646</td><td>646</td><td>646</td></tr>
<tr><td rowspan="5">Area of girder non-prestressing reinforcement, mm^2/m</td><td colspan="2">Stirrups (bar # 1 in Figure 5.8)</td><td>No.3 @175mm</td><td>No.3 @ 200mm</td><td>No. 3 @200mm</td><td>No.3 @ 300mm</td><td>No. 3 @300mm</td><td>No.3 @ 300mm</td></tr>
<tr><td colspan="2">Transverse reinforcement (bar # 2 & 3 in Figure 5.8)</td><td>No. 3 @175mm</td><td>No.3 @ 200mm</td><td>No. 3 @200mm</td><td>No.3 @ 300mm</td><td>No. 3 @300mm</td><td>No.3 @ 300mm</td></tr>
<tr><td colspan="2">Shear connectors (bar # 4 in Figure 5.8)</td><td>No. 3 @175mm</td><td>No.3 @ 200mm</td><td>No. 3 @200mm</td><td>No.3 @ 300mm</td><td>No. 3 @300mm</td><td>No.3 @ 300mm</td></tr>
<tr><td colspan="2">Longitudinal reinforcement (bar # 5 & 6 in Figure 5.8)</td><td>12 No. 14</td><td>12 No. 4</td><td>12 No. 4</td><td>12 No. 4</td><td>12 No. 4</td><td>12 No. 4</td></tr>
<tr><td colspan="2">Longitudinal reinforcement (bar # 7 in Figure 5.8)</td><td>2 x 7 No. 4</td><td>2 x 7 No. 4</td><td>2 x 7 No. 4</td><td>2 x 7 No. 4</td><td>2 x 7 No. 4</td><td>2 x 7 No. 4</td></tr>
<tr><td rowspan="2">Intermediate diaphragm</td><td colspan="2">Width, mm</td><td>300</td><td>300</td><td>300</td><td>200</td><td>200</td><td>100</td></tr>
<tr><td colspan="2">Depth, mm</td><td>1200</td><td>1000</td><td>1000</td><td>1000</td><td>1000</td><td>800</td></tr>
<tr><td colspan="3">Overhang length, mm</td><td>1495</td><td>930</td><td>1290</td><td>865</td><td>1090</td><td>745</td></tr>
<tr><td colspan="3">Overhang thickness, mm</td><td>225</td><td>200</td><td>225</td><td>175</td><td>200</td><td>175</td></tr>
</table>

Figures 6.7 to 6.12 show the histogram plot for the objective function with respect to the quality levels from 1 to 6, respectively. The Pareto data sets related to the feasible optimum solutions, with respect to each quality level, are demonstrated in Figures 6.13 to 6.18.

Table 6.4: Objective function (Cost $) with respect to different quality levels

Quality Level	Cost, ($)
1-σ Level	218020
2-σ Level	253335
3-σ Level	268604
4-σ Level	296450
5-σ Level	313460
6-σ Level	347520

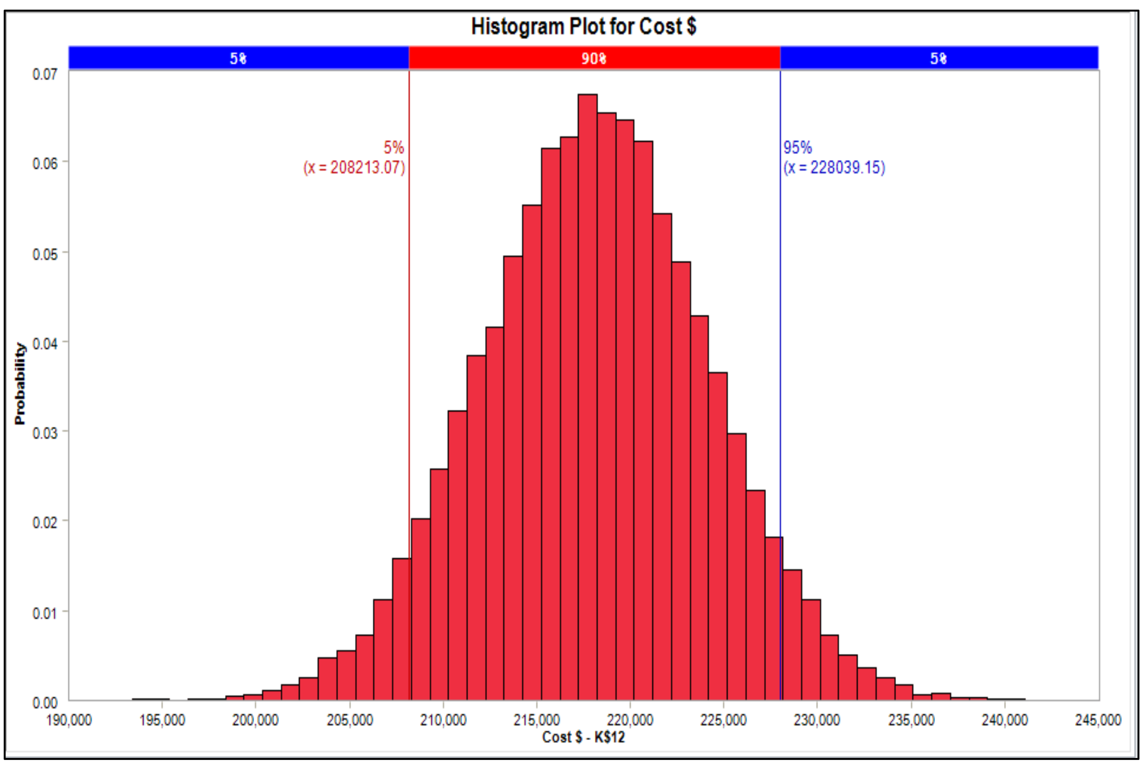

Figure 6.7: Histogram plot for objective function (Cost $) with respect to 1-$\sigma$ quality level.

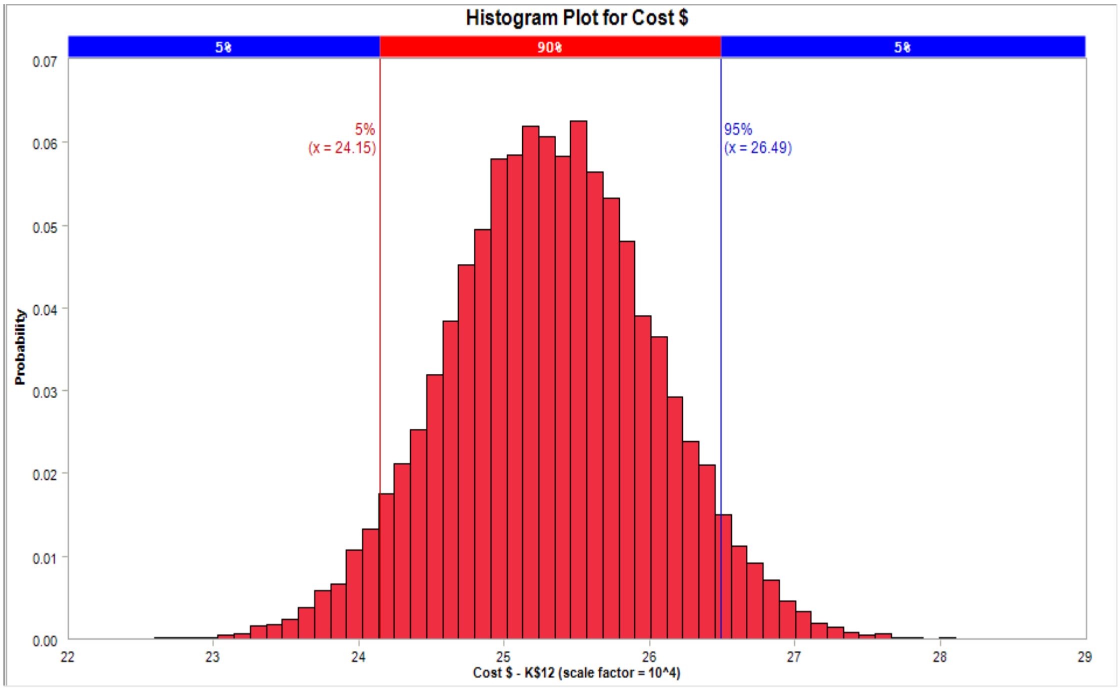

Figure 6.8: Histogram plot for objective function (Cost $) with respect to 2-$\sigma$ quality level

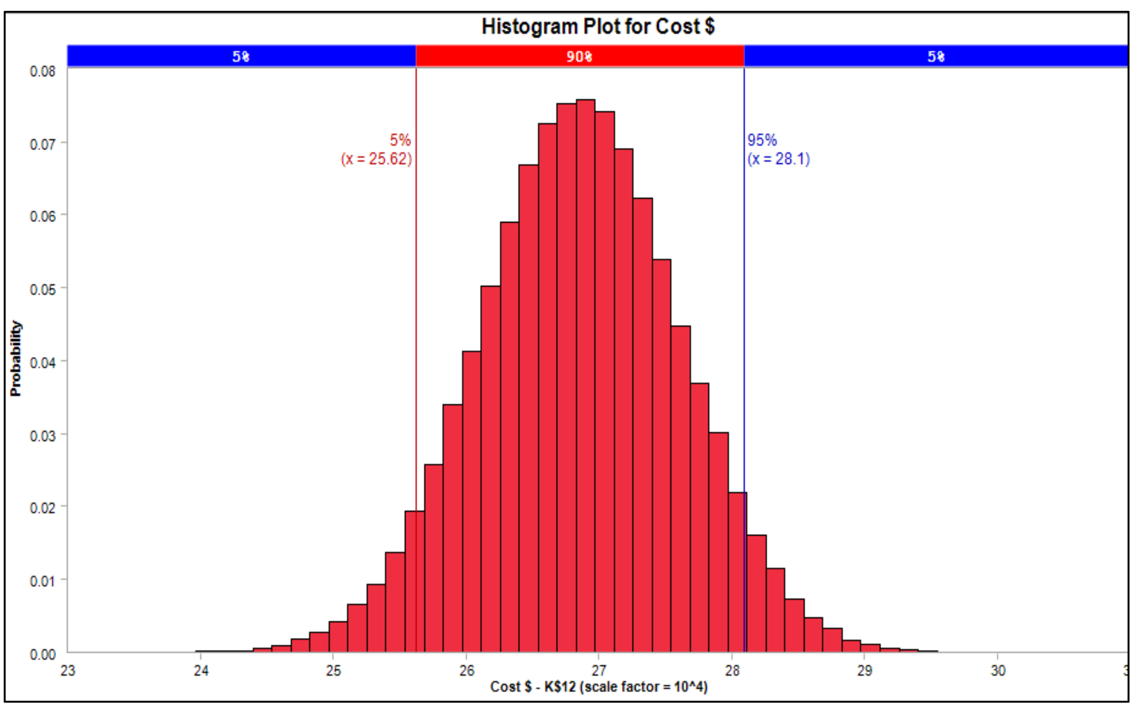

Figure 6.9: Histogram plot for objective function (Cost $) with respect to 3-$\sigma$ quality level

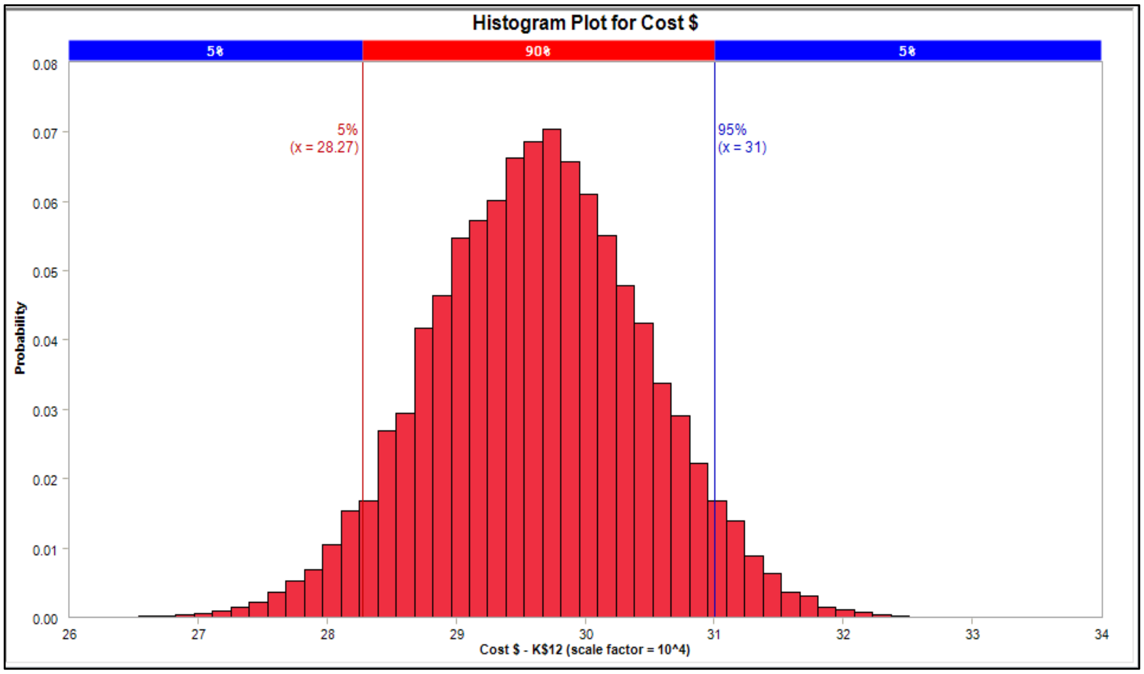

Figure 6.10: Histogram plot for objective function (Cost $) with respect to 4-$\sigma$ quality level.

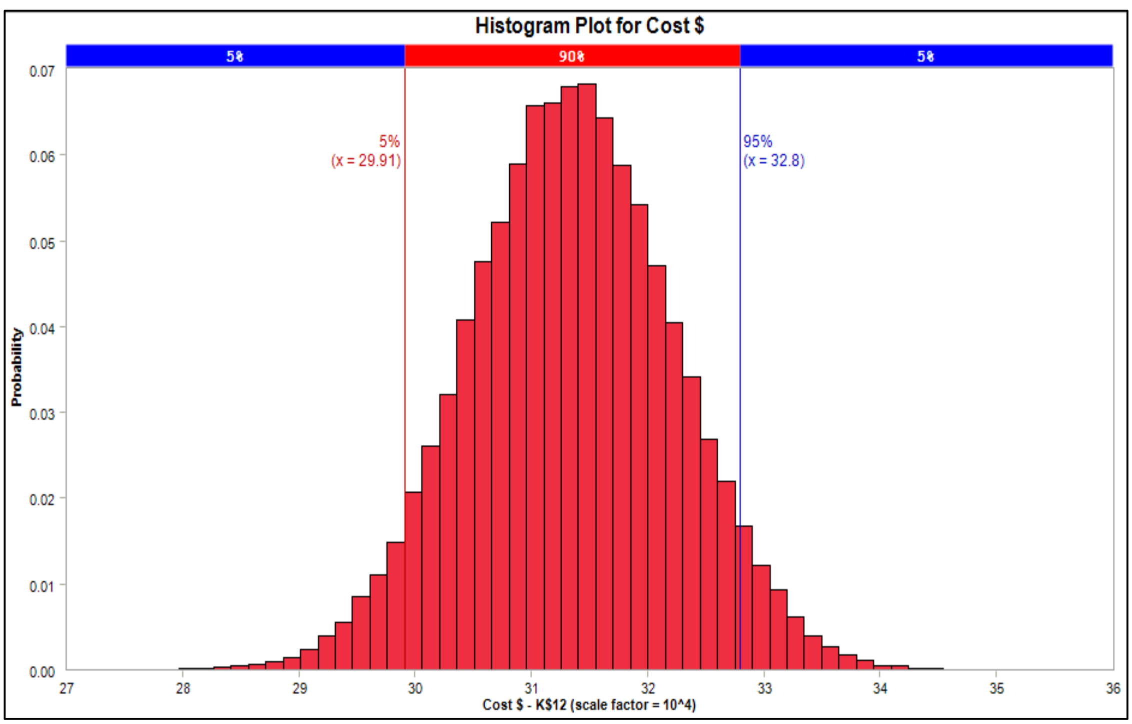

Figure 6.11: Histogram plot for objective function (Cost $) with respect to 5-$\sigma$ quality level.

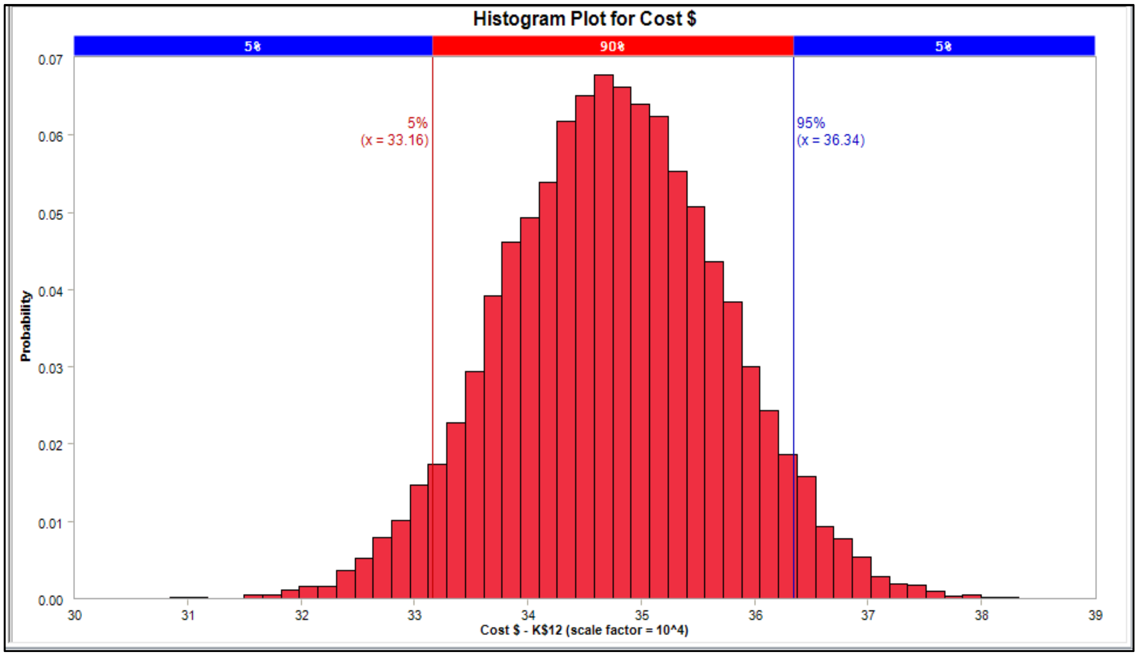

Figure 6.12: Histogram plot for objective function (Cost $) with respect to 6-$\sigma$ quality level.

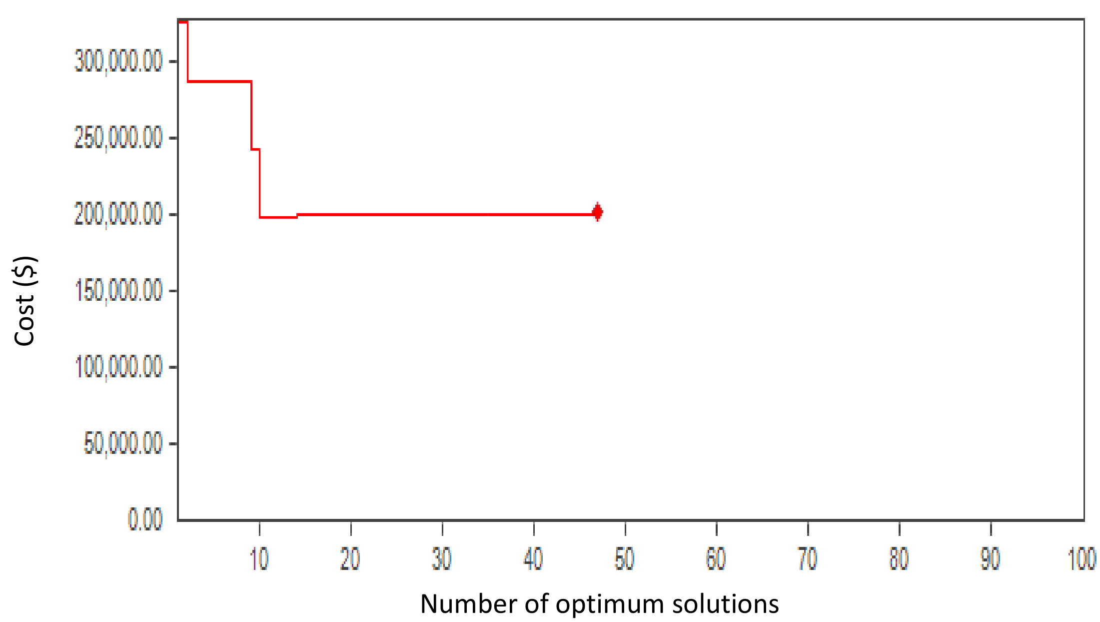

Figure 6.13: Pareto set of optimum solutions related to 1-σ quality level.

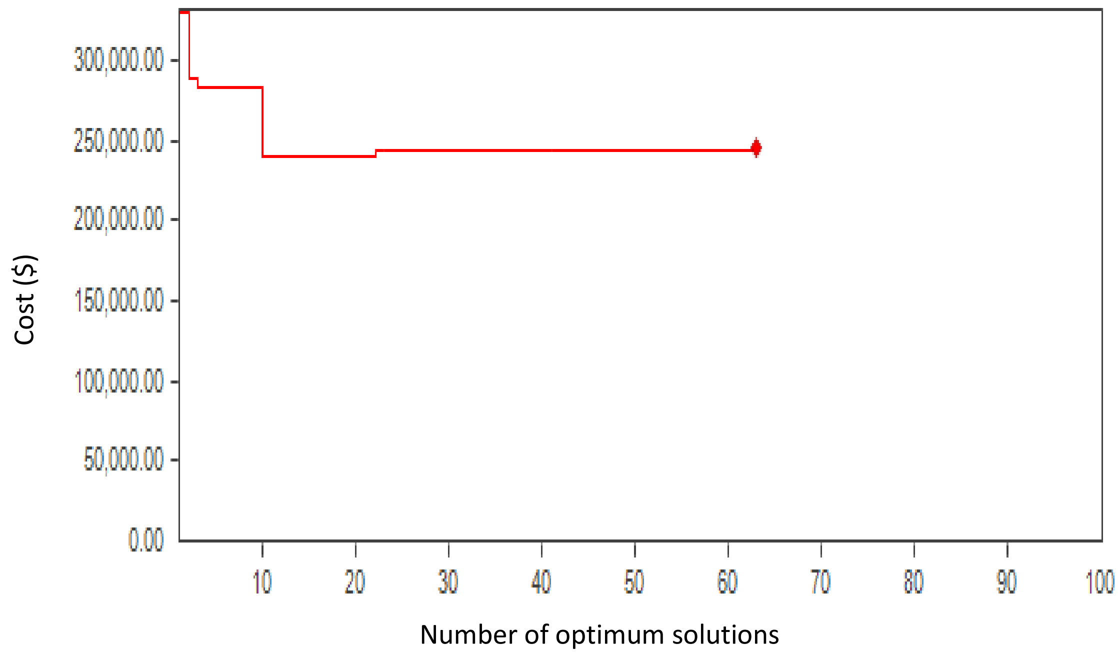

Figure 6.14: Pareto set of optimum solutions related to 2-σ quality level.

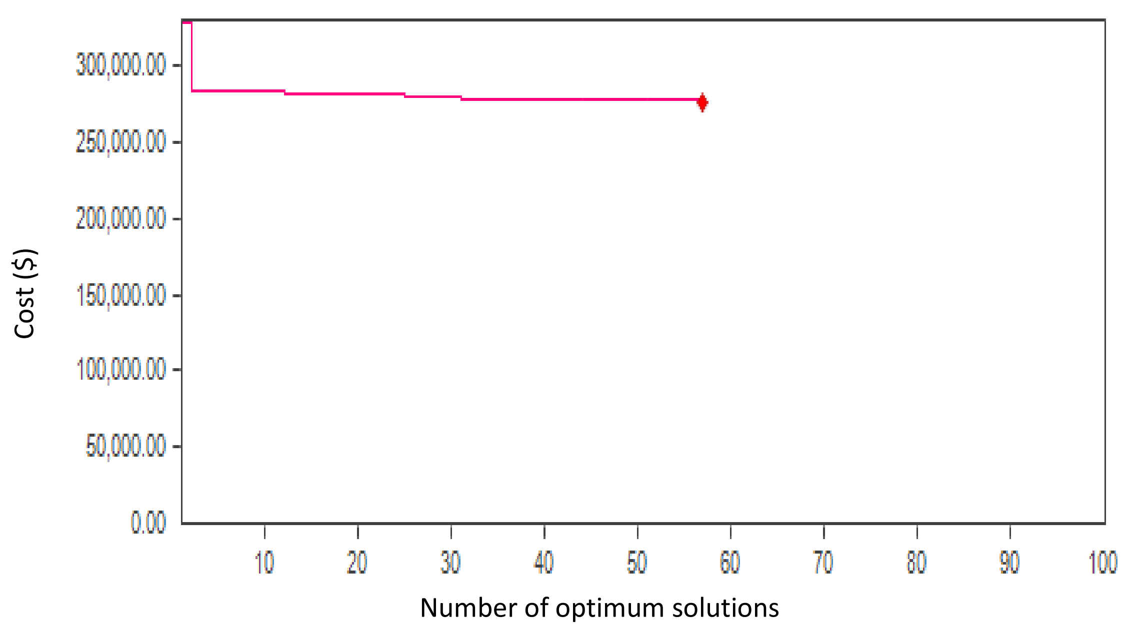

Figure 6.15: Pareto set of optimum solutions related to 3-σ quality level.

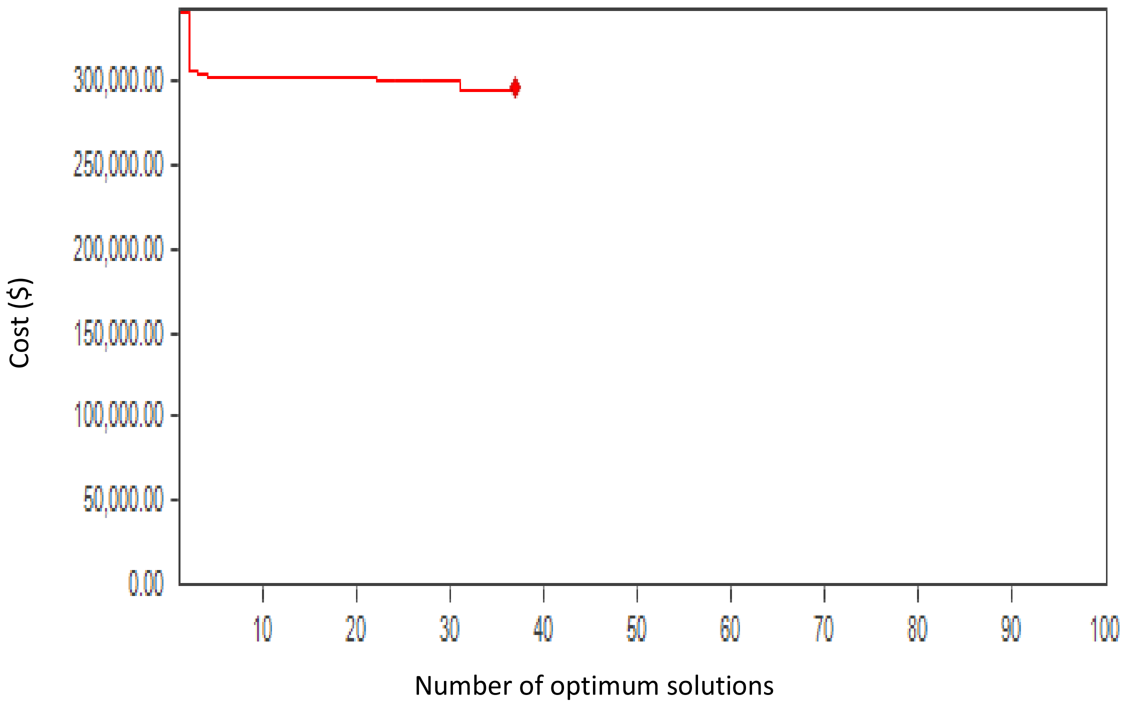

Figure 6.16: Pareto set of optimum solutions related to 4-σ quality level.

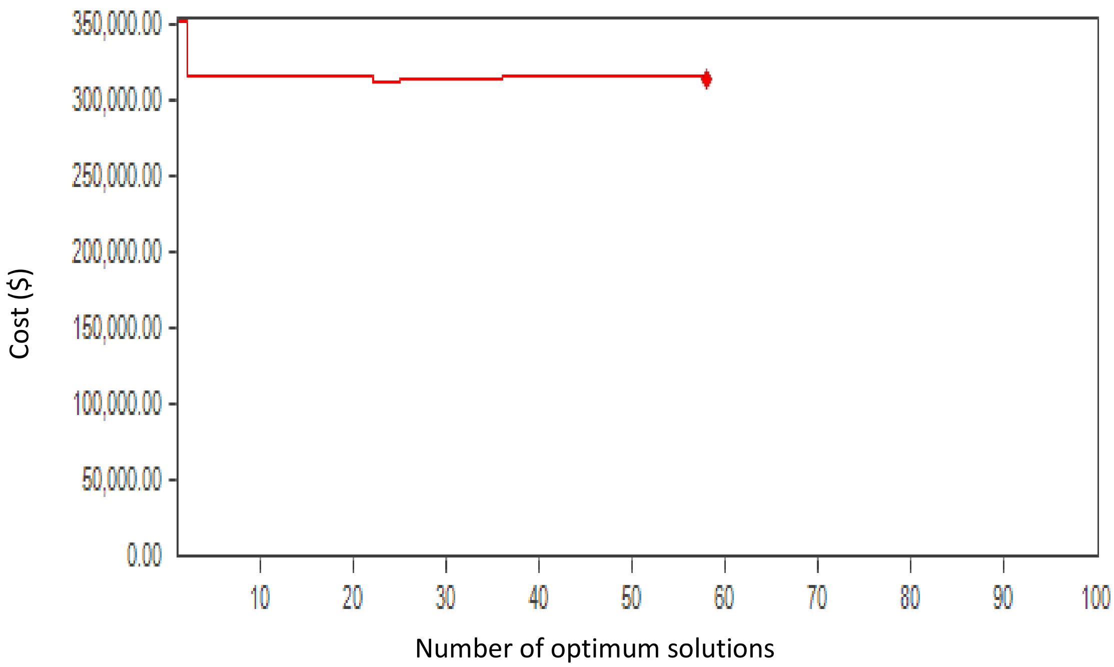

Figure 6.17 Pareto set of optimum solutions related to 5-σ quality level.

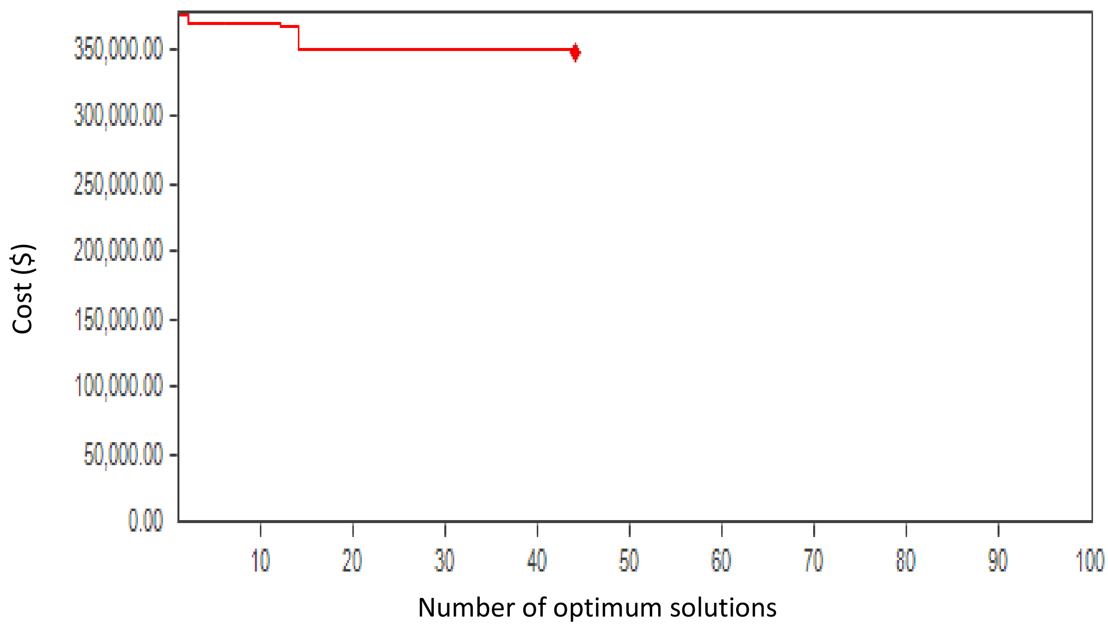

Figure 6.18: Pareto set of optimum solutions related to 6-σ quality level.

Figure 6.19 compares the value of the objective function (cost \$) as obtained by the deterministic design optimization DDO, reliability-based design optimization RBDO, and the design-for-six sigma DFSS optimization. As shown in Figure 6.19, an analogy exists between DFSS and RBDO at a quality level of 2.35σ. However, such analogy might exist at different quality levels for different structural configurations. As shown in Figure 6.19, the deterministic design optimization DDO has a quality level slightly less than 1$\boldsymbol{\sigma}$. This is mainly because of not considering the uncertainties and variation associated with the design variables. However, DDO usually reveals considerable cost saving.

Figure 6.20 compares the value of the objective function (cost) as obtained from the original (initial) design, from the reliability-based design optimization RBDO, and from the six sigma design optimization. Hence, the DDO might not be entirely safe during the expected life of the structure, although it could reveal considerable cost saving. Figure 6.20 also tells that the more quality desired the more costly the bridge will be. Based on that, it is not necessary to go to the highest levels of quality as they might be very expensive.

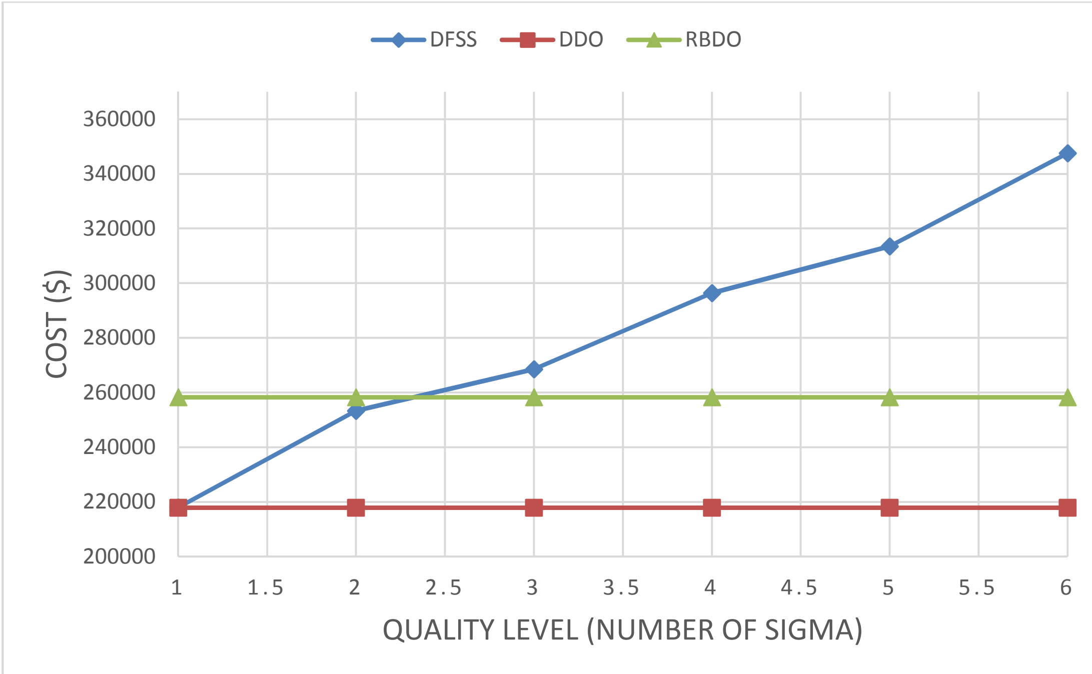

Figure 6.19: Objective function (Cost $) related to DDO, RBDO, and DFSS

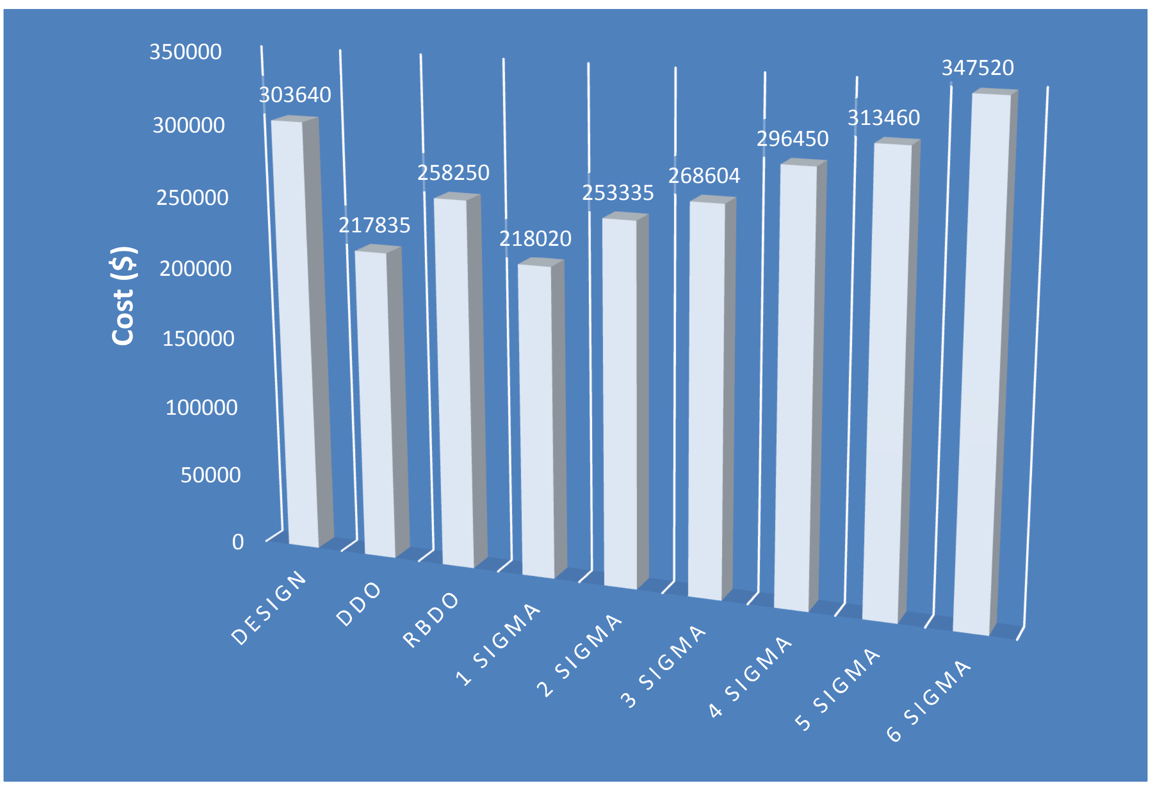

Figure 6.20: Comparing bridge cost resulted from original design and different optimization techniques.

6.5 Summary

A unique methodology was developed, in the current research, as new contribution. A design quality concept (referred to as design-for-six sigma DFSS) has been applied to produce a quality-controlled probabilistic design optimization of prestressed girder bridges. In this optimization approach, the six sigma quality concept was utilized to achieve robust design solutions. Such approach ensures not only that the design performs as desired but also that the design consistently performs as desired.

As for reliability-based design optimization RBDO (Chapter 5), simulation-optimization technique was used in for DFFS optimization. Different quality levels (number of sigmas) were used and the associated results were tabulated and compared with those revealed from the original design, deterministic optimization DDO, and RBDO. The results showed increasing cost with increasing number of sigma (quality level). DDO gives quality level slightly less than 1σ. There was an analogy between RBDO and DFSS around a quality level of 2.35σ.

Chapter 7

New Method to Select the Optimum Type of Bridge Superstructure

7.1 Introduction

The current research provides a probabilistic approach for the design optimization of prestressed girder bridges. However, the first essential step for such optimization process is to verify that a prestressed girder bridge system is the most appropriate bridge type for specific project conditions. For this purpose, a new model for deciding about the optimum bridge type is developed in the current research. The model is based on experts' decisions analysis integrated with decision tree analysis and sensitivity analysis. The client's requirements (CRs) and the design requirements (DRs) form the main variables in the optimization process. The uncertainty involved in the expert's opinion is considered and represented by an appropriate statistical distribution. The possible dependence (correlation) among the CRs and DRs is also considered.

The proposed methodology is new and original as it, for the first time, takes the uncertainties involved with the experts' opinions into consideration and models such uncertainties with an appropriate statistical distributions. Also, the proposed computer-aided model incorporates, for the first time, the decision tree analysis in selecting the optimum bridge superstructure type after performing sensitivity analysis. The sensitivity analysis investigates the influence of the independent variables (CRs and DRs) on the dependent variable (bridge type).

7.2 Client's Requirements CRs

It is the responsibility of the designer to provide a structural solution that maintains the client's requirements. In bridge design projects, the client's requirements can generally be defined as follows (Raina, 2012):

- *Cost*: for every project, the client has a specific allocated budget. The design drawings and specification of the bridge structure should be determined in such a way that it would ensure that the project can successfully be completed within the budget limits. A general rule is that the bridge with the minimum number of spans, fewest deck joints, and widest spacing of girders will reveal the most economical structure for the given project (Barker & Puckett, 2013).

- *Time*: Putting a new bridge into service and opening it to traffic are usually made according to the client's pre-planned schedule. The designer should consider this time requirement when selecting the bridge type, deciding on the design detailing, and agreeing on the project specifications.
- *Quality*: it is important that the project deliverables meet the aims and objectives for which it was undertaken. Also, the project output shall meet the durability and sustainability requirements.
- *Availability*: the project should be planed and managed, through its various phases, to assure and maintain proper accessibility to its various elements (Malekley, 2010).

7.3 Design Requirements DRs

The design processes are directly influenced by the following design requirements (Barker & Puckett, 2013):

- *Geometric Conditions*: the horizontal and vertical profiles of the road and the vertical clearance requirements form the essential geometric parameters to decide about the suitable bridge type.
- *Functional Requirements*: A properly designed bridge will reveal a structure which would function efficiently to carry present and future volumes of traffic. To maintain this requirement, decisions must be made on the number of lanes, inclusion of sidewalks and/or bike paths, provision of medians, drainage of surface water, and future wearing surface.
- *Aesthetics*: As a grade-separation structure, every bridge has a visual effect and appearance impact on the area where it exists. Bridges are long lasting structures which can stay for decades and can be viewed by thousands of people every day. An important objective, a bridge designer should consider, is to obtain a positive aesthetic response to the bridge type selected. An aesthetically-designed bridge can be achieved when uninterrupted lines, clean lines, and uncluttered appearance are provided for the bridge shape (Malekly, H. et al, 2010).

- *Constructability*: the construction and erection considerations have a great influence when choosing a bridge type. For example, the project duration and economy for precast girder bride is totally different from those of segmental box girder bridge.
- *Legal and Environmental Conditions*: Federal, governmental, provincial, and municipal regulations always exist. These regulations are usually beyond the designer control but they are real and should be taken into consideration. Among those regulations, environmental-impact limitations are usually specified by the authorities and should always be considered (FAHWA 2012).

7.4 Expert's Opinion

When insufficient data are available to describe and identify the uncertainty of a variable, one or more experts will be usually consulted to obtain their opinion with respect to such uncertainty (O'Hagan, 2006).

As explained in Chapter 2, various researchers have benefited from experts' decisions in choosing the most appropriate bridge type; Bitarafan et al.,(2013), Farkas (2011), Malekly et al., (2010), Furuta et al. (1995), Choi and Choi (1993), Hammad and Itoh (1993), and Burgoyne and Sham (1987). However, in all of those efforts, the experts' opinions were treated deterministically. In other words, the uncertainty involved in the expert opinion was not considered in the previously mention contributions. The modeller (analyst) should bear in mind the following heuristics, the expert may employ when attempting to provide subjective estimates, which are potential sources of systematic bias and errors (Vose 2008). These biases are explained in considerably more detail in Hertz and Thomas (1983) and Morgan and Henrion (1990):

- Availability: this is where experts use their recollection of past occurrences of an event to provide an estimate. It can produce poor estimates if all or part of the data are not still available.
- Representativeness: this is where the analyst focuses on an enticing detail of the problem and forget (or sometimes ignore) the overall picture.
- Adjustment and anchoring: this is probably one of the most important heuristics. Individuals will usually begin their estimate with a single value (usually the most likely value) and then make adjustments for its minimum and maximum from that first value. The estimators appear to be "anchored" to their first estimated value.

This is certainly one source of *overconfidence* and can have a dramatic impact on the validity of the model.

- Unwillingness to consider extremes: the expert will often find it difficult or be unwilling to consider conditions that would yield a variable to be extremely low or high. However, the analyst in encouraged to request opinions on such extremes in order to cover the entire range.
- Eagerness to say the right thing: sometimes, interviewees intend to provide the answer they think the interviewer wants to hear. Accordingly, it is important to avoid asking questions that are leading and never to offer a value for the expert to comment on.

From the above, it becomes obvious that the expert's opinion involve a level of uncertainty. Hence, the experts' decisions should be treated probabilistically rather than deterministically. This approach is adopted in the current research.

The variability in expert's opinion is treated, in this research, by determining a statistical distribution than can best model the expert decision. A PERT distribution is frequently used to model an expert's opinion (Vose, 2008 and O'Hagan, 2006). PERT has been adapted so that the expert need only to provide estimates of the minimum, most likely and maximum values of the variable. In this proposed model, PERT distribution has been applied to model the expert's opinion.

7.5 PERT Distribution for Modelling Expert Opinion

The PERT distribution is a version of the beta distribution and requires three parameters: minimum (a), most likely (b), and maximum (c) (these three parameters are, sometimes, referred to as pessimistic, most likely, and optimistic). For illustration, Figure 7.1 gives examples of different PERT distributions. The formulation of a PERT distribution can be demonstrated as follows (Vose, 2009):

[7.1] $$\text{PERT}(a,b,c) = \text{Beta}(\propto_1,\propto_2)^* \,(c-a)+a$$

where,

[7.2] $$\propto_1 = \frac{(\mu-a)*(2b-a-c)}{(b-\mu)*(c-a)}$$

[7.3] $$\propto_2 = \frac{\propto_1 * (c - \mu)}{(\mu\mu - a)}$$

The mean (μ):

[7.4] $$\mu = \frac{a + 4 * b + c}{6}$$

The variance (V):

[7.5] $$V = \frac{(\mu - a) * (c - \mu)}{7}$$

The probability density function $f(x)$:

[7.6] $$f(x) = \frac{(x-a)^{\propto_1 - 1} (c-x)^{\propto_2 - 1}}{B(\propto_1, \propto_2)(c-a)^{\propto_1 + \propto_2 - 1}}$$

The cumulative distribution function $F(x)$:

[7.7] $$F(x) = \frac{B_z(\propto_1, \propto_2)}{B(\propto_1, \propto_2)}$$

where,

[7.8] $$z = \frac{x-a}{c-a}$$

and $B_z(\propto_1, \propto_2)$ is an incomplete beta function.
The skewness:

[7.9] $$skewness = \frac{a + c - 2\mu}{4} \sqrt{\frac{7}{(\mu - a)(c - \mu)}}$$

and

[7.10] $$Kurtosis = 3 \frac{(\propto_1 + \propto_2 + 1)[2(\propto_1 + \propto_2)^2 + \propto_1 \propto_2 (\propto_1 + \propto_2 - 6)]}{\propto_1 \propto_2 (\propto_1 + \propto_2 + 2)(\propto_1 + \propto_2 + 3)}$$

It is obvious that the mean in Eq. (7.4) is a restriction that is assumed in order to be able to determine values for $\propto_1$ and $\propto_2$. It also shows how the mean for the PERT distribution is 4 times more sensitive to the most likely value than to the minimum and maximum values.

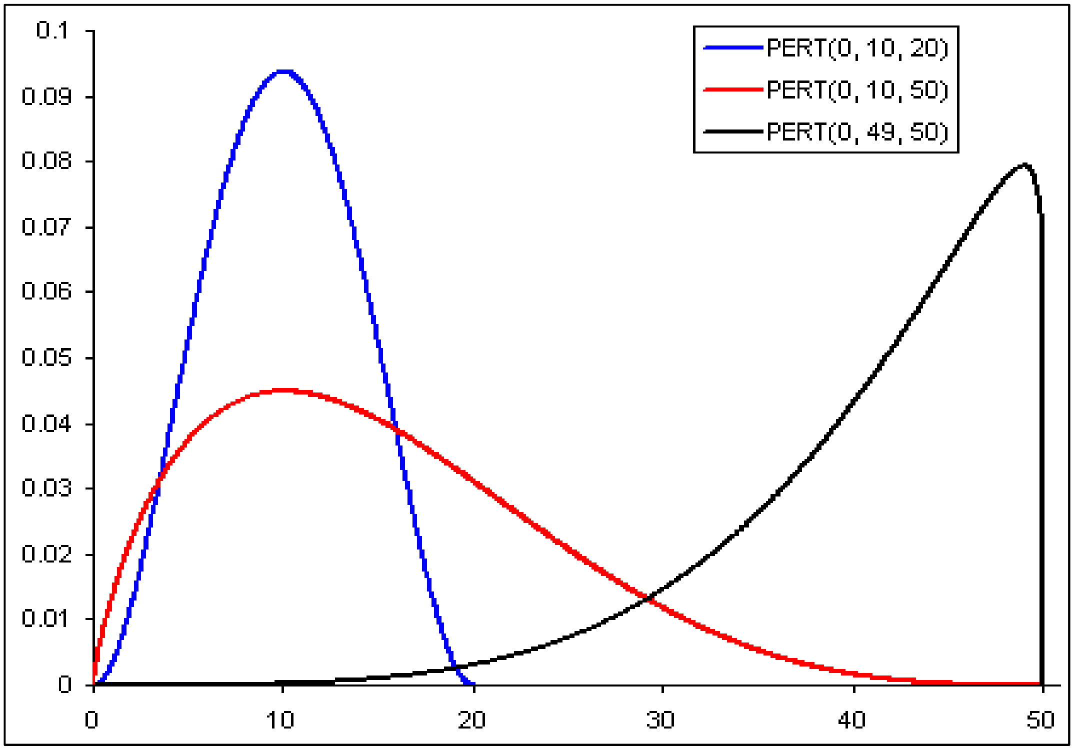

Figure 7.1: Examples of PERT distributions (Vose, 2009).

7.6 Proposed Methodology

In this section, the steps to select the optimum type of bridge superstructure, according to the proposed model, are discussed. Those steps are illustrated by the flowchart shown in Figure (7.2).

7.6.1 Define possible types of bridge superstructure

The analyst (modeler) will, first, define and list the available (possible) types of bridge superstructure from which the most appropriate type will be obtained according to the proposed optimization model. The span length plays the key role in deciding about the possible alternatives. Table 7.1 illustrates the maximum span up to which a particular type of bridge can be recommended (Raina, 2007).

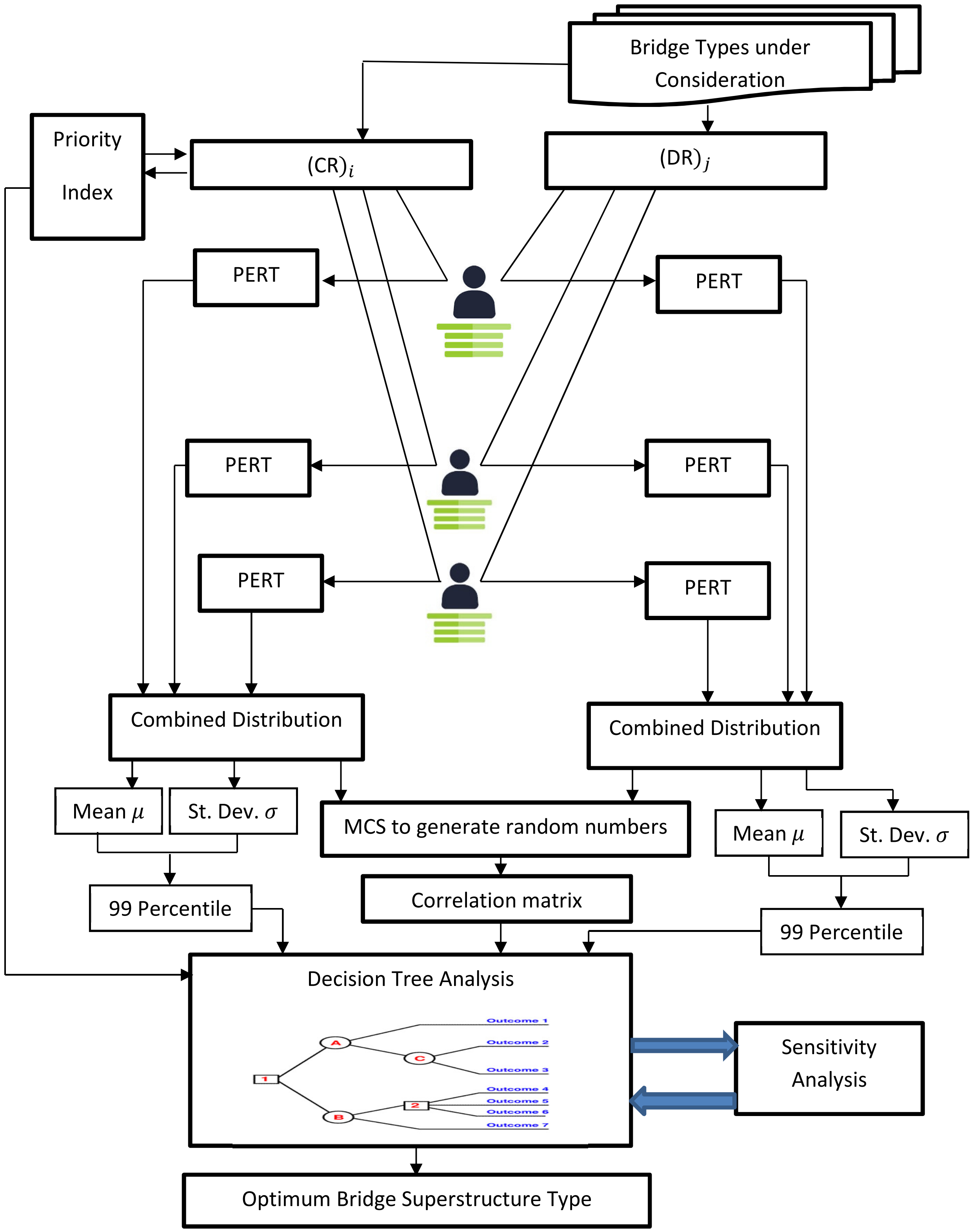

Figure 7.2: Flow chart of the proposed model

Table 7.1: Maximum span corresponding to bridge type (Raina, 2007).

Bridge Type	Maximum span (m)
Steel rolled beam bridge	10
RC portal frame bridge	15
RC Monolothic T-girder bridge	20
RC cantilever bridges with balanced type	30
Steel plate girder	30
RC filled spandrel fixed arch bridge	35
RC continuous bridge	45
RC bow-string girder bridge	45
Prestressed girder bridge	55
RC box girder bridge	65
Post-tension box girder bridge	110
RC concrete arch bridge	150
Steel truss bridge	180
Prestressed arch bridge	200
Suspension bridges	1200

7.6.2 Collect available information

The analyst shall collect all the available technical data (geometrical and geotechnical), site conditions, and information of existing structures and utilities. The longitudinal and transverse road profile should be studied carefully in order to properly decide about the vertical and horizontal clearances. All this information will be necessary for the experts to build their assessments.

7.6.3 Define CRs and DRs

The analyst will, then, define and list the client's requirements (CRs) and the design requirements (DRs) as explained earlier in sections 7.2 and 7.3, respectively.

However, although the client's requirements (CRs) are of essential importance to the client, it is still valid to ask the following question: "Are those requirements of equal priority and importance to the client in every project?". According to numerous previous projects, the answer is "No". Love and Earl (1998) conducted surveys of 41 clients and 35 consultants to obtain the experience data to be implemented in the methods and criteria for project selection. Their findings indicated that, contrary to the expectations, similar clients generally do not have similar procurements needs. Also the findings show different appropriate weighting for different needs. For this reason, Al-Delaimi and Dragomirescu (2015) suggested an *Importance Level* (IL) to scale the strength of each of the client's requirements, as illustrated in Table (7.2). In this table, linguistic terms associated with fuzzy scale (from 1 to 5) are provided to define the strength of those client's requirements. For that purpose, the analyst shall have a session of discussion with the client to define the importance of his/her requirements, accordingly. This approach is adopted in the current model.

Table 7.2: Importance levels associated with client's requirements (Al-Delaimi and Dragomeriscu, 2015)

Importance Level (IL)	Weight
Very Low	1
Low	2
Fair	3
High	4
Very high	5

The analyst will ask the client to rate the importance and priority of every client's requirement (CR) by assigning an importance level (IL) corresponding to each CR.

7.6.4 Select a team of experts

A team of experts shall carefully be selected. Every expert must have a recognized knowledge with proven professional records and achievements in the field of bridge engineering.

A one-to-one interview shall be held between the relevant expert and the analyst (modeller). In preparing for such interviews, analysts should make themselves familiar with various sources of biases and errors involved in subjective estimations. The experts, in their turn, having been informed of the interviews well in advance, should have evaluated any relevant information either on their own or in a brainstorming session prior to the interview (Vose, 2009). During the interview, the expert will be provided with a questionnaire form to fill out. The questionnaire form is that shown in Figure (7.3). The expert will treat the design requirements (DRs) and the client's requirements (CRs) as variables. The expert shall rate the suitability of every bridge type with respect to each of (DRs) and (CRs).

Bridge Type Questionnaire Form

Client's Name ……………………………………………….. Reference:
Project ……………………………………………………………… Date:
Bridge Ref. ……………………………………………………..
Expert Name …………………………………………………
Company …………………………………………………………
Position ………………………………………………………….

Please rate the suitability of the referenced bridge type with respect to the following requirements by ticking √ the appropriate score :

Requirement	Description *		0 (Not suitable at all)	1	2	3	4	5	6	7	8	9	10 Perfectly suitable
Client Requirements (CRs)	Cost	Max											
		Min											
		M.L.											
	Time	Max											
		Min											
		M.L.											
	Quality	Max											
		Min											
		M.L.											
	Availability	Max											
		Min											
		M.L.											
Design Requirements (CRs)	Geometric	Max											
		Min											
		M.L.											
	Functional	Max											
		Min											
		M.L.											
	Aesthetic	Max											
		Min											
		M.L.											
	Constructability	Max											
		Min											
		M.L.											
	Legal and Environmental	Max											
		Min											
		M.L.											

* Max= maximum, Min= Minimum, M.L. = Most Likely.

Figure 7.3: Bridge type questionnaire form.

As recommended by Karsak (2004), the expert opinion will be expressed in three scores (levels): lowest, most plausible and highest. Such three scores are in harmony to those required to build a PERT distribution (minimum, most likely, and maximum). Hence, every expert will evaluate the suitability of a bridge type to satisfy each of the DRs and CRs by providing such three levels.

As recommended by Vose (2009), the analyst should attempt to determine the expert's opinion of the maximum value first and then the minimum, by considering scenarios that could produce such extremes. Then, the expert should be asked for his/her opinion of the most likely value within that range. Determining the parameters in the order (1) *maximum*, (2) *minimum*, and (3) *most likely* will go some way to removing the "anchoring" error described in Section 7.4.

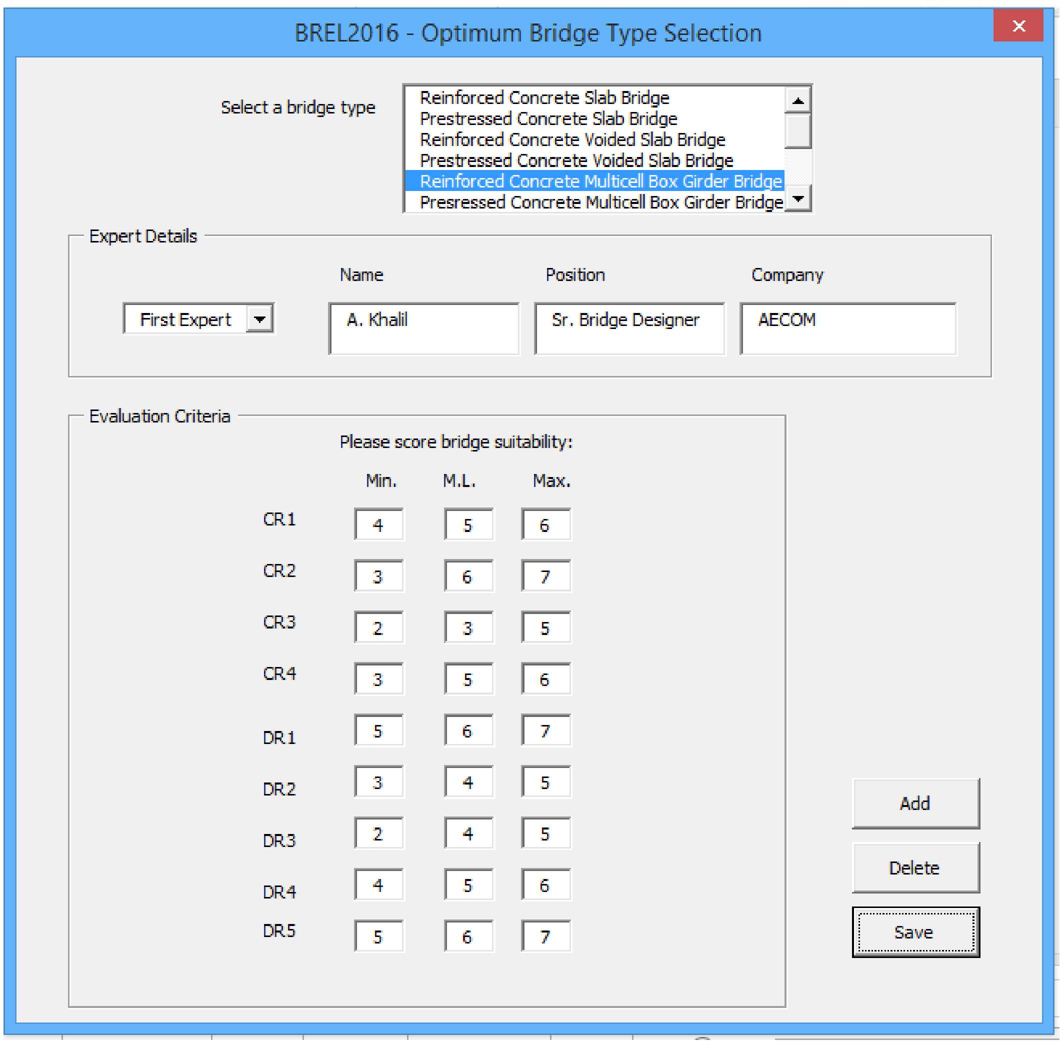

Figure: 7.4: A snapshot from the proposed model showing experts' opinions (evaluations).

The experts' evaluations (opinions) will, then, be extracted from the questionnaire form and sent to the model as shown in Figure 7.4.

7.6.5 Eliciting from expert's opinion

Once the expert has given his/her assessments as scores against the client's requirements (CRs) and design requirements (DRs), the analyst would be able to start analysing the expert's output. From the three-point estimates, a PERT distribution can be made as a statistical representation of the expert's opinion. As explained in Sections 7.2 and 7.3, four CRs requirements and five DRs exist. Hence, for each bridge type under consideration, every expert shall provide nine assessments (each with three scores: *minimum*, *most likely, and maximum*). In other words, this will result in developing nine PERT distributions per expert per bridge type.

An Excel Add-Inn, ModelRisk (Vose, 2009), has been integrated with the developed model (BREL), to model the statistical distribution of each expert. As a unique feature, though optional, the model allows appointing weights that represent the confidence level associated with each expert opinion. Figure (7.5) shows an example of the PERT distribution for the decisions of a team of four experts. The horizontal axis represents the range of values of the experts' assessments (minimum, most-likely and maximum). The vertical axis refers to the corresponding probability density function.

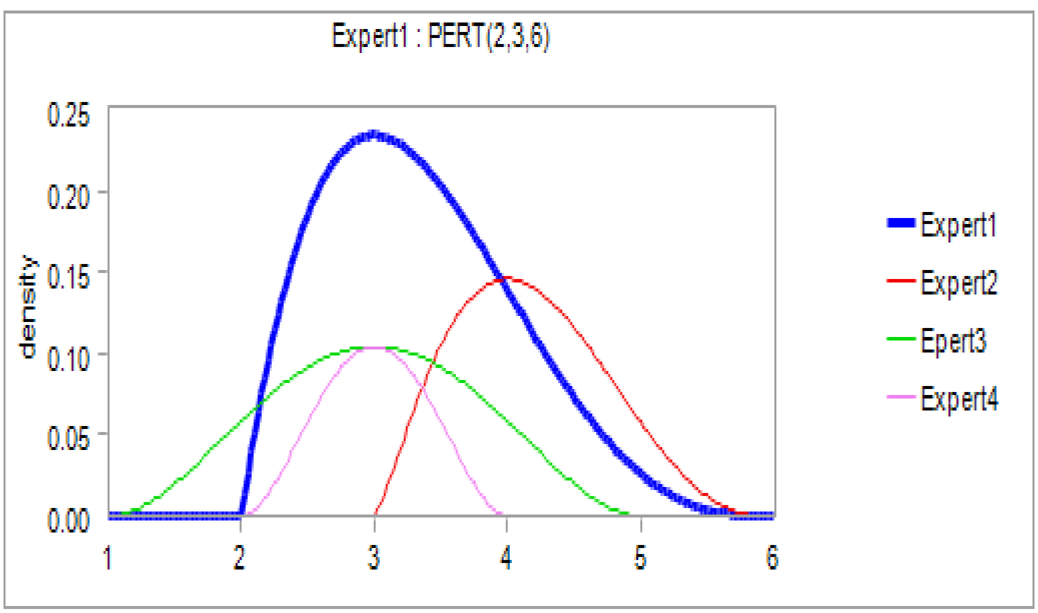

Figure 7.5: PERT distribution of the opinions of four experts

When requesting experts to model a variable with uncertainty, it can often happen that different experts independently provide different estimates. As result of that, the analyst will get a number of recognizably different distributions, one for each expert's opinion. The difference in opinion is another source of uncertainty (Jutte, 2012). This should not be discounted by, for example, taking the average of the opinions, or the largest (or smallest). Instead, the analyst needs to develop a combined distribution that reflects the range and emphasis of each opinion and the confidence in the estimators (Albert et al., 2012). Combined distribution combines these "individual" distributions into one final distribution that incorporates all the information. So, if there were four experts A, B, C and D, the density function $f(x)$ and the cumulative function $F(x)$ of the combined distribution at x are determined as follows:

[7.11] $$f(x) = \frac{[\mathrm{f}_A(\mathrm{x})*\mathrm{w}_A + \mathrm{f}_B(\mathrm{x})*\mathrm{w}_B + \mathrm{f}_C(\mathrm{x})*\mathrm{w}_C + \mathrm{f}_D(\mathrm{x})*\mathrm{w}_D]}{\mathrm{w}_A + \mathrm{w}_B + \mathrm{w}_C + \mathrm{w}_D}$$

[7.12] $$F(x) = \frac{[\mathrm{F}_A(\mathrm{x})*\mathrm{w}_A + \mathrm{F}_B(\mathrm{x})*\mathrm{w}_B + \mathrm{F}_C(\mathrm{x})*\mathrm{w}_C + \mathrm{F}_D(\mathrm{x})*\mathrm{w}_D]}{\mathrm{w}_A + \mathrm{w}_B + \mathrm{w}_C + \mathrm{w}_D}$$

where, f_A is the probability density of expert A's estimate, F_A is the cumulative function of expert A's estimate, and w_A is the weight assigned to this expert's opinion.

This technique has been adopted in the current research. Figure (7.6) shows combining three differing opinions but where expert A is given twice the emphasis of the others due to her greater experience.

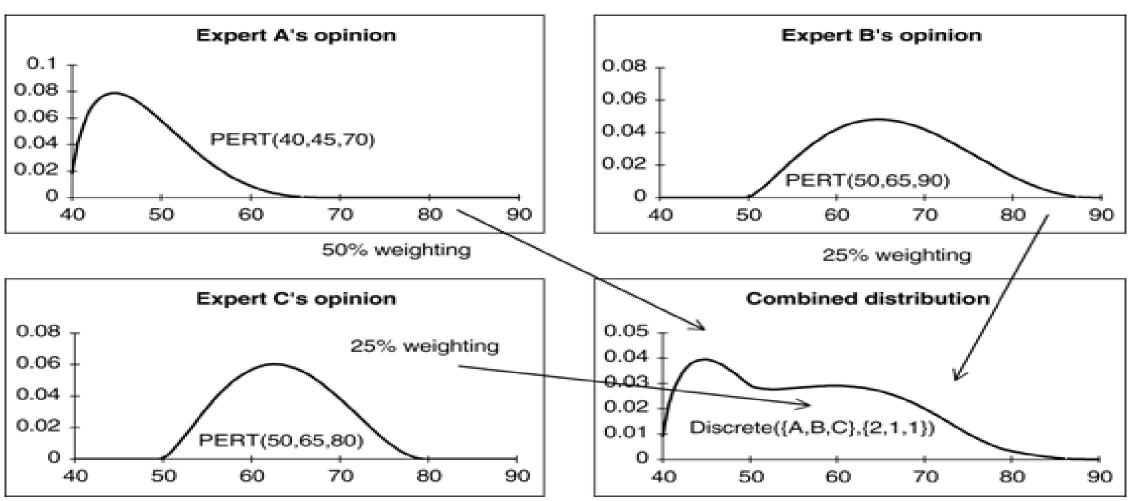

Figure 7.6: Combining opinions of three experts (Vose, 2009).

After combining the idividual distributions into one combined distribution, the model will calculate the four main statistical moments (parameters), namely: the mean, standard deviation, skweness, and kurtosis as shown in Figure (7.7) .

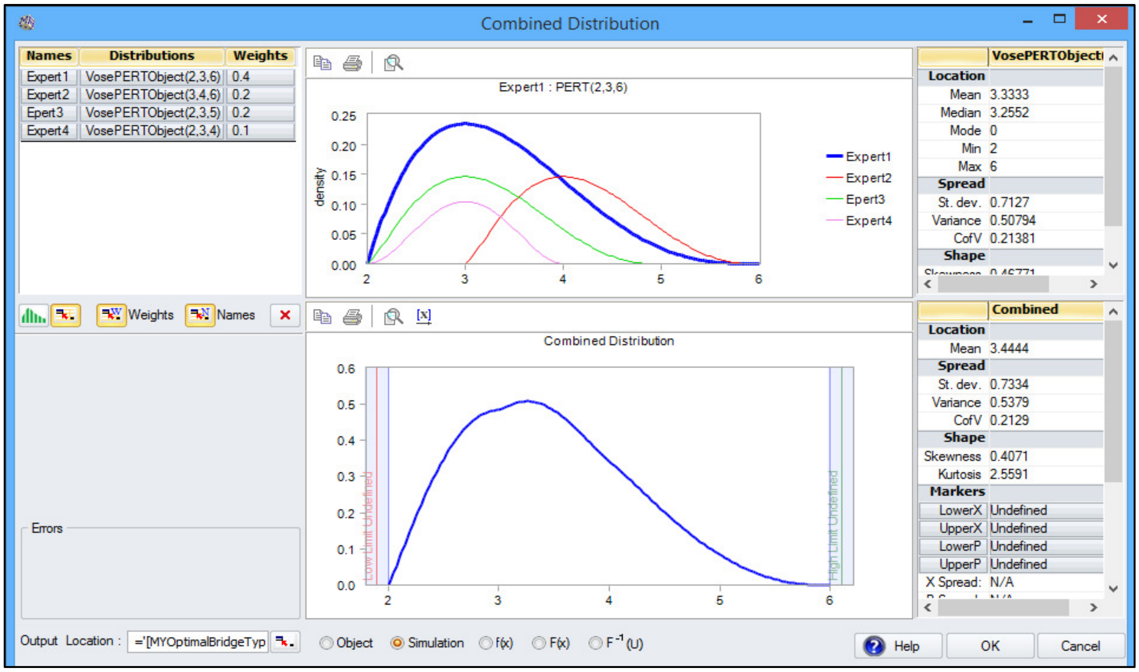

Figure 7.7: Combined distribution and its statistical parameters.

From the combined distribution related to every CR and DR, the 99% percentile P_{99} value will, then, be calculated as follows:

[7.13] $$P_{99} = [F(x)]^{-1} \qquad at\ x = 0.99$$

7.6.6 Correlation between CRs and DRs

As explained in the previous sections, the CRs and DRs have been treated as variables. The experts' opinions on these variables have been represented by statistical distributions. The possible dependency (correlation) between such distributions has also been considered in this proposed model.

Statistical distributions in a model should often be correlated to ensure that only meaningful scenarios are generated for each iteration of the model (Vose 2009). In the current model, the possible correlation between CRs and DRs has been investigated and represented in the form of a correlation matrix.

In order to develop a correlation matrix, random numbers need first to be generated. For this purpose, the Monte Carlo Simulation technique has been used to generate the random numbers.

The technique developed by Iman and Conover (1982) to generate rank order correlated input distributions has been adopted in the current model. The coefficients of the correlation matrix are called Spearman's rank correlation coefficient (also referred to as Spearman's *rho*). The correlation process is carried out on the *ranks* of the data by considering what position (rank) the data point takes in an ordered list from the minimum to maximum values, rather than the actual data values themselves (Vose 2009). Hence, it is independent of the distribution shapes of the data sets and allows the integrity of the input distributions to be maintained. Based on that, the analyst is therefore assured that the distribution used to model the correlated variables will still be replicated (Vose 2009). The correlation coefficient ρ between two variables, X_i and Y_i , can be calculated as follows::

[7.14] $$\rho = \frac{12}{n(n^2-1)} \sum_{i=1}^{n} [\, rank(X_i\,) - \frac{n+1}{2}]\, [rank(Y_i\,) - \frac{n+1}{2}\ ]$$

in which n is the number of data pairs. The resulting correlation matrix is a symmetrical diagonal one.

As recommended by Carnevalli and Miguel (2008), the correlation between CRs and DRs as well as among the DRs must be considered. Hence, two classes of correlation coefficients exisit:

- ρ_{sj} : correlation coefficient between the s^{th} CR and j^{th}DR.
- ρ_{jm} : correlation coefficient between the j^{th} and m^{th}DR.

7.6.7 Decision tree analysis

Several researchers, from different engineering fields, utilized the decision tree analysis in developing decision-making tools (McCloud et al. 1992). The current model proposes a new method to select the optimal bridge type by integrating the experts' opinions with the decision tree analysis.

The decision tree of the current model consists of a trunk, main branches, secondary branches, and twigs. The trunk represents the optimal bridge type that will be revealed as an output. Each main branch represents a bridge type. Therefore, if ten bridge types are investigated, then the model should have ten main branches. From each main (parent) branch, two secondary (baby) branches will be developed, one for the Client's Requirements (CRs) and one for the Design Requirements (DRs). From every secondary branch, a number of twigs will form out. The number of twigs represents the number of variables under consideration. As we stated earlier, we have four CRs as variables, so four twigs should fork out from the secondary branch related to the Client's Requirements. Similarly, five twigs for the DRs exist. Figure (7.8) shows a snapshot containing three main branches (every one corresponds to a bridge type). For more clarity, Figure (7.9) shows a specific main branch which represents a specific bridge type. This main (parent) branch has two secondary (baby) branches (one for the client's requirements CR which consists of four twigs and one for the design requirements DR which consists of five twigs).

The value shown on the top of the each twig of the CR represents the 99 percentile of the experts' combined distribution related to that CR $(P_{99})_{CR}$. The value shown at the bottom of that twig represent the importance level $(IL)_i$ assigned to that CR multiplied by the correlation coefficient ρ_{sj}. On the top of each twig of the DR, the 99 percentile of the expert's combined distribution related to that DR $(P_{99})_{DR}$, is shown. While, the value shown at the bottom of the twig of DR represents the correlation coefficient, ρ_{jm}, taken from the correlation matrix, is allocated.
The decision tree will, then, calculate the Expected Monitory Value (EMV) with respect to client's requirements, design requirements, and with respect to the main branch (i.e. a bridge type). The EMV with respect to (CR)$_i$ is calculated as follows:

[7.15] $$(EMV)_{CR} = (P_{99})_{CR} * (IL)_i * \rho_{sj}$$

The EMV with respect to (DR) is obtained as follows:

[7.16] $$(EMV)_{DR} = (P_{99})_{DR} * \rho_{jm}$$

Then, the EMV with respect to every bridge type is obtained as:

[7.17] $$(EMV)_{CR} + (EMV)_{DR} = \sum_{i=1}^{4} (P_{99})_{CR} * (IL)_i * \rho_{sj} + \sum_{j=1}^{5} (P_{99})_{DR} * \rho_{jm}$$

Finally, from all the bridge types under consideration, the model will chose the optimum type, which has the maximum EMV:

[7.18] $$(EMV)_{max} = [\sum_{i=1}^{4} (P_{99})_{CR} * (IL)_i * \rho_{sj} + \sum_{j=1}^{5} (P_{99})_{DR} * \rho_{jm}]_{max}$$

The bridge type with $(EMV)_{max}$ is the optimum type and the main branch, corresponding to that branch, will be shown highlighted with a blue color.

7.6.8 Sensitivity analysis

In order to investigate the influence of independent variables (CDs and/or DRs) on the dependent variables (bridge types), sensitivity analysis has been conducted. The output of such analysis will produce Tornado chart and Spider chart. These charts measure the relative sensitivities of multiple dependent variables (CRs and DRs) against a single dependent variable (bridge type).

7.7 Case Study I

In order to investigate the applicability and validity of the proposed methodology, a case study has been carried out:

The Roads and Transportation Authority, RTA, of the Government of Dubai announced a bridge project, in 2007. The project is to build a bridge crossing over the Sheikh Zayed Road in order to link Al-Barsha Quarter (East) with Al-Safouh area (West) as shown in Figure 7.10. The bridge type was selected based on a detailed, comprehensive and time-consuming *Value Engineering Analysis* (*VEA*) conducted by a well reputed consultant, PARSONS International. The design criteria, developed by the Consultant, carefully considered the client's requirements. The maximum span length was 30m (98.5 ft). The bridge has a dual-carriage way with two lanes in each direction. The two traffic directions were separated by a New-Jersey-type central median. Seven types of bridge superstructures were examined:

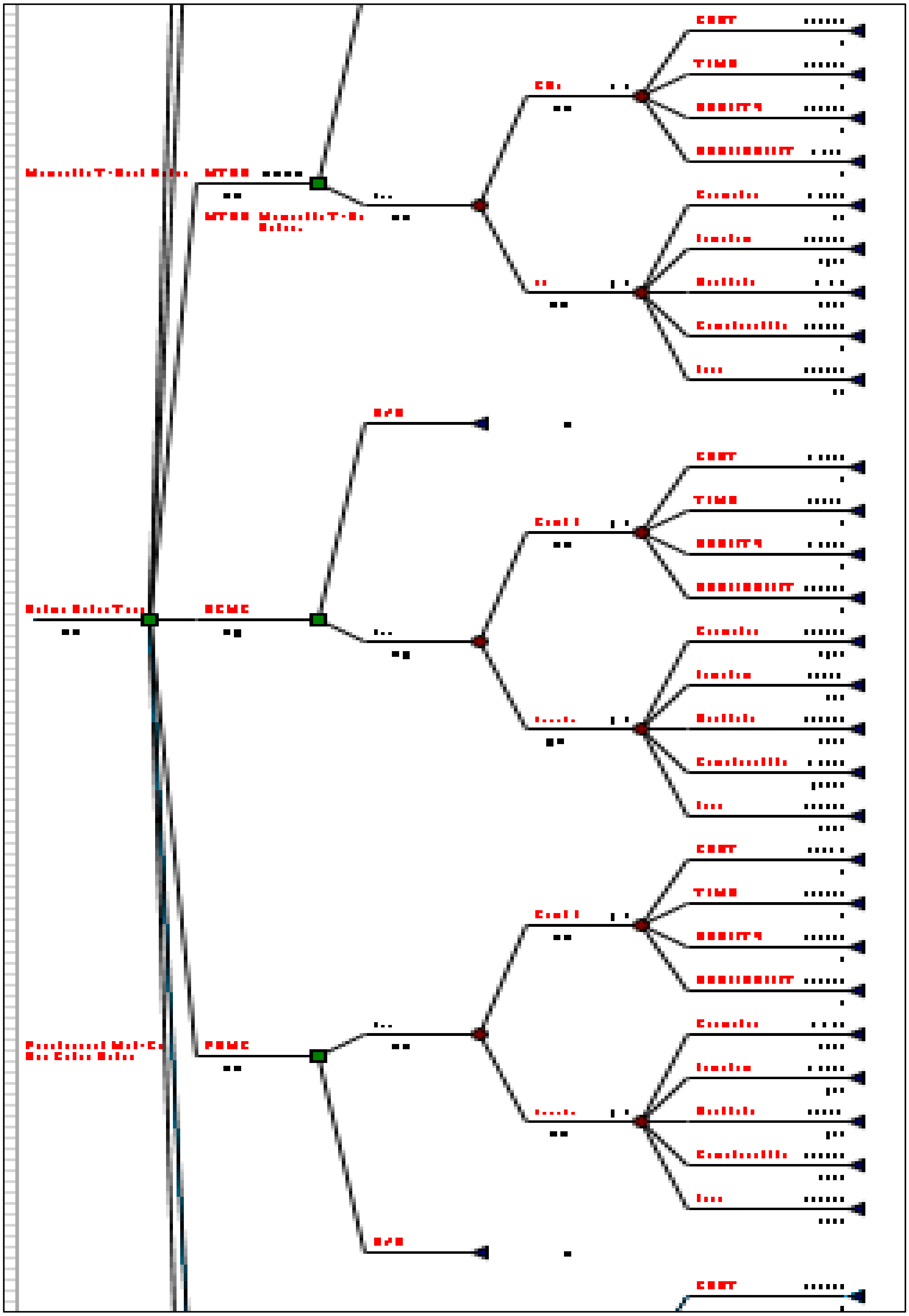

Figure 7.8: A three-branch part of a decision tree (Al-Delaimi and Dragomirescu, 2015)

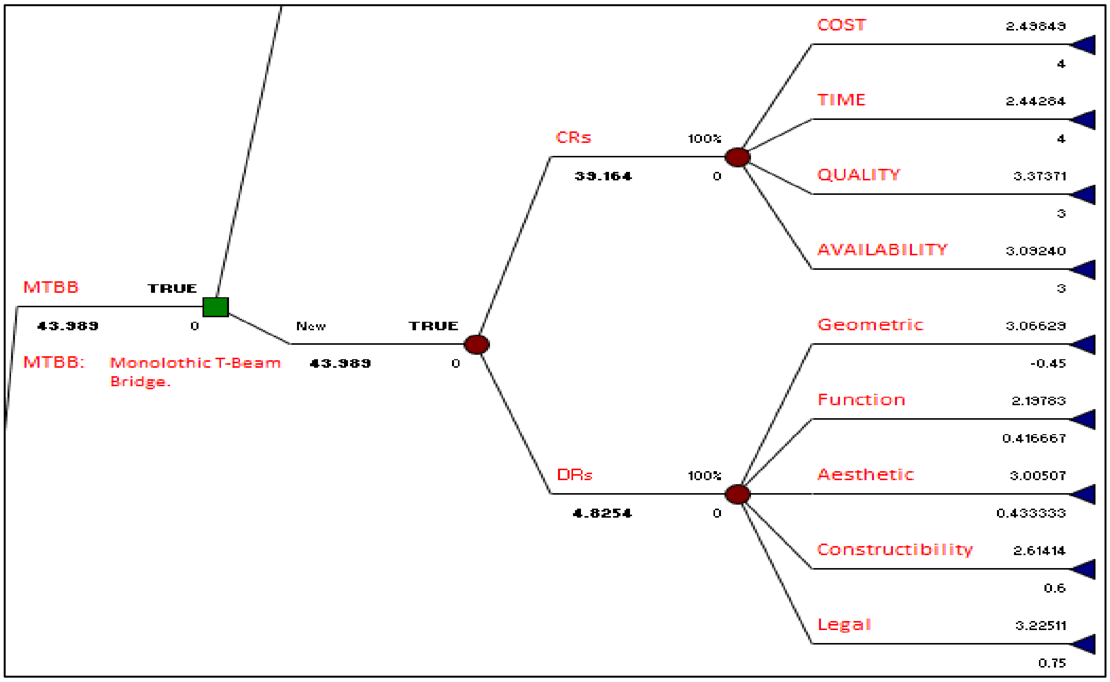

Figure 7.9: A main branch of a decision tree (Al-Delaimi and Dragomirescu, 2015)

Figure 7.10: The bridge considered for the case study (areal photo for Sheik Zayed Road, Dubai-UAE, Google map).

- Reinforced Concrete Slab Bridge (RCSB).
- Pre-Stressed Concrete Slab Bridge (PSSB)
- Monolithic T-Beam Bridge (MTBB)
- Reinforced Concrete Multi-Cell Box Girder Bridge (RCMCBGB)
- Pre-Stressed Concrete Multi-Cell Box Girder Bridge (PSMCBGB)
- Precast Prestressed Concrete Girder Bridge (PCGB)
- Steel Plate Girder Bridge (PGB)

The value engineering analysis (VEA) revealed the PSMCBGB as being the most appropriate type of bridge superstructure. The bridge was designed according to AASHTO LRFD design code. The construction of the bridge was completed in September 2009 and was opened to traffic in October 2009. The client's requirements for this specific project got the weights shown in Table 7.3.

Table 7.3: Importance levels of client's requirements related to case study I

Client's Requirements (CR)	Importance Level (IL)	Weight
Cost	Very High	5
Time	Fair	3
Quality	Very High	5
Availability	Fair	3

In order to check the validity of the proposed methodology, an assumed bridge with exactly the same conditions has been examined. With the client's consent, all the relative information have been gathered and collected. A team of four experts was consulted. This team consists of a senior Bridge designer from AECOM Consultant (Dubai office), the Head of Bridge Design Section in Hyder Consultant (Dubai office), a professor in the American University in Dubai, (AUD), who has a strong experience in bridge engineering, and the Senior Design Manager of Al-Nabooda Liang Contracting Company in Dubai. A one-to-one interview session was held with each expert separately. The questionnaire forms were filled out (one form for each type of bridge). The total numbers of forms:

(1 form per bridge type per expert) * (7 bridge types) * (4 experts) = 28 forms

The experts' score assessments were statistically analyzed and corresponding PERT distributions were developed. Combined distributions have been determined and the 99 percentile P_{99} values were obtained. Then, the correlation coefficients were calculated. After that, the model conducted the decision tree analysis. For every bridge type, the decision tree analysis revealed the corresponding Expected Monitory Value, EMV. The Maximum EMV was given to the type of prestressed concrete multi-cell box girder bridge (PSMCBGB) which is in total agreement with the findings of the value engineering analysis VEA. For the seven types of bridges under considerations, Tables (7.4) to (7.10) summarize the experts' assessments with respect to the CRs and DRs (CR1= Cost, CR2 = Time, CR3 = Quality, CR4 = Availability, DR1= Geometric conditions, DR2 = Functional requirements, DR3 = Aesthetic, DR4 = Constructability, and DR5 = Legal and environmental conditions). A PERT distribution was developed from each expert's opinion. Then the four experts' opinions were composed in one combined distribution from which the mean value would be obtained. For example, probability density function of PERT distribution for (CR1) related to RCSB type is as shown in Figure 7.11 and the combined distribution is illustrated in Figure 7.12. Similarly, the cumulative distribution and corresponding combined distribution are shown in Figures 7.13 and 7.14, respectively.

Table 7.4: Experts' scores for reinforced concrete slab bridge RCSB

	Bridge Type: RCSB											
	Expert 1			Expert 2			Expert 3			Expert 4		
	Min.	M.L.	Max.	Min.	M.L.	Max.	Min.	M.L.	Max.	Min.	M.L.	Max.
CR1	2	3	4	1	2	3	1	3	4	3	4	5
CR2	2	4	5	1	3	5	1	2	3	2	4	5
CR3	2	3	5	1	3	4	1	3	5	2	3	4
CR4	1	2	3	2	3	4	2	4	5	1	3	4
DR1	1	2	3	2	3	4	1	3	5	1	2	3
DR2	2	3	4	2	3	5	2	3	4	1	3	4
DR3	1	2	3	1	2	4	1	2	3	2	3	4
DR4	3	4	5	2	3	4	1	3	4	2	4	5
DR5	4	5	6	3	5	6	2	4	5	3	5	6

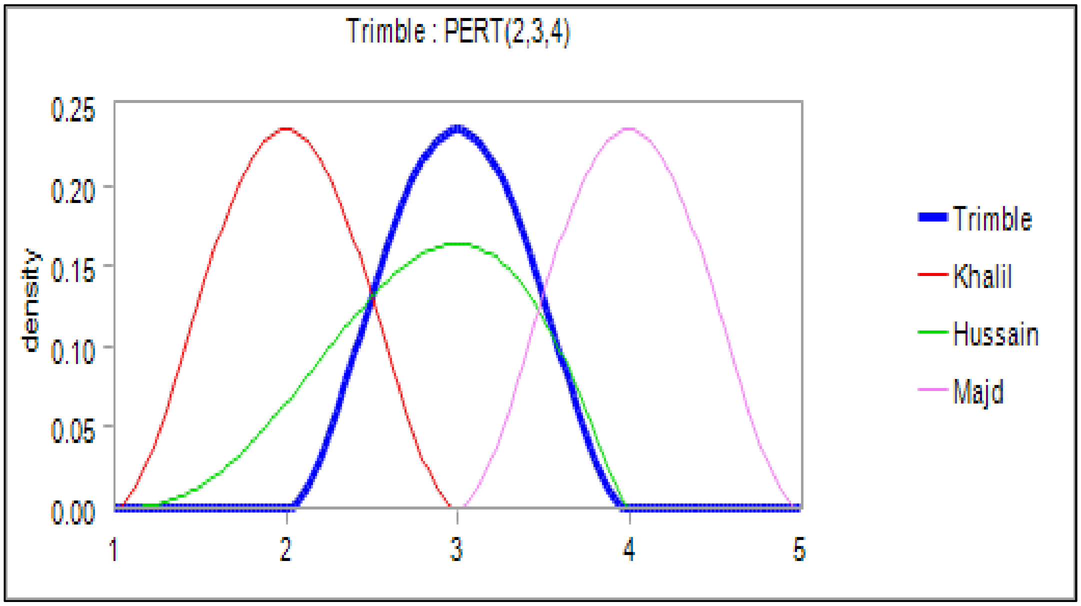

Figure 7.11: The probability density function of PERT distribution related to CD1

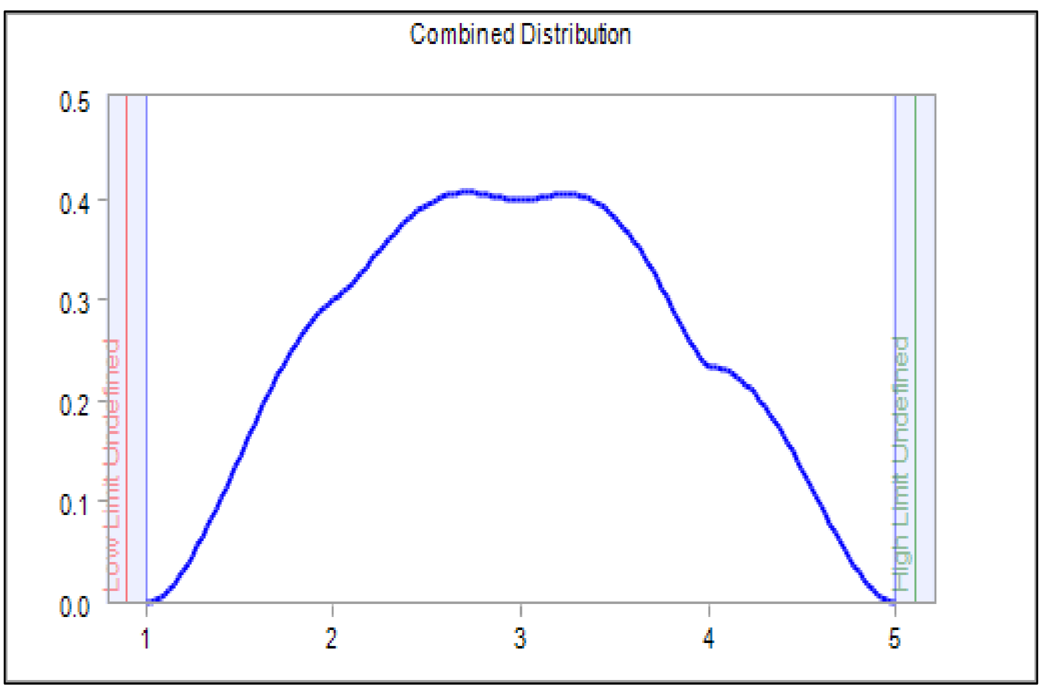

Figure 7.12: The probability density function of the combined distribution related to CD1.

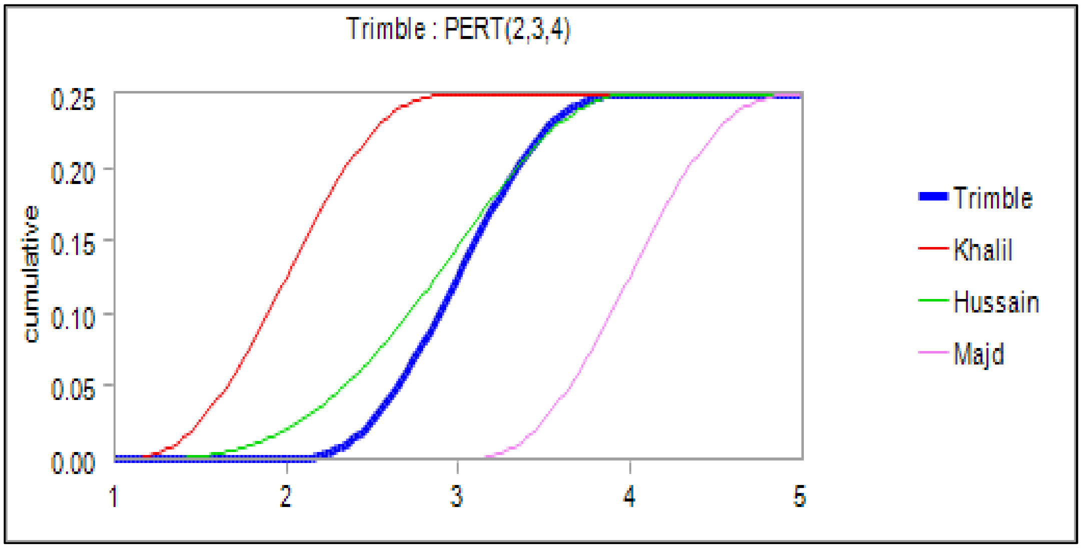

Figure 7.13: The cumulative distribution functions related to CD1.

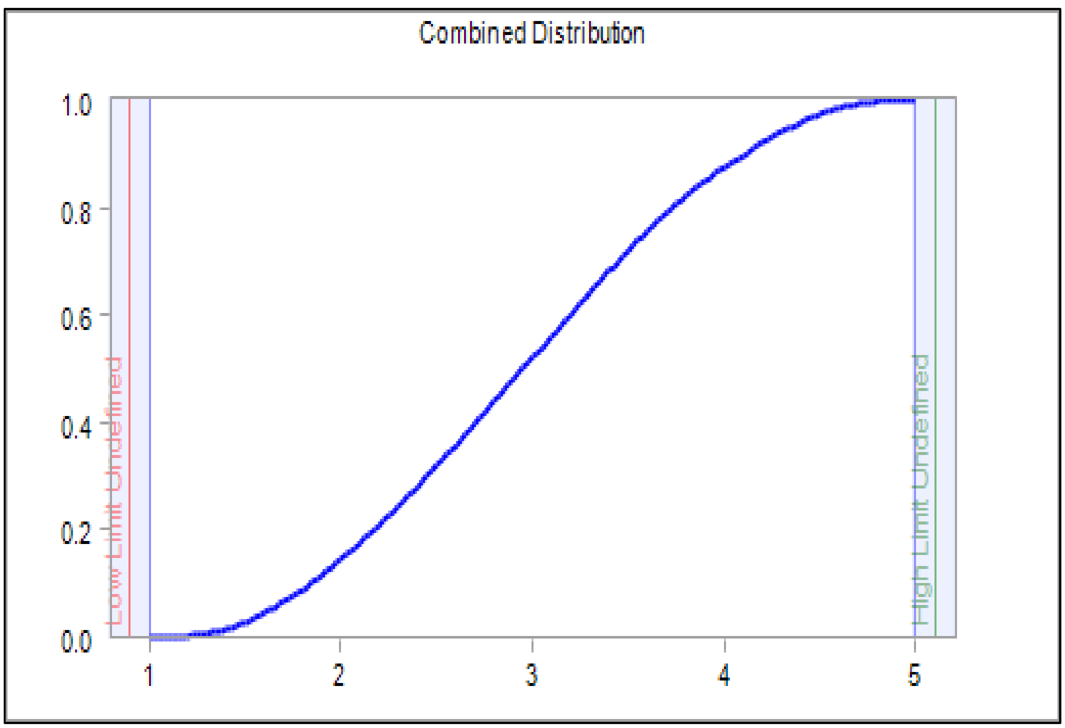

Figure 7.14: The combined cumulative distribution function related to CD1.

Table 7.5: Experts' scores for prestressed concrete slab bridge PSSB

	Bridge Type: PSSB											
	Expert 1			Expert 2			Expert 3			Expert 4		
	Min.	M.L.	Max.	Min.	M.L.	Max.	Min.	M.L.	Max.	Min.	M.L.	Max.
CR1	3	4	5	1	3	5	2	4	5	2	5	6
CR2	1	3	4	2	3	4	1	3	4	2	4	5
CR3	2	4	5	2	3	4	2	3	4	1	3	4
CR4	3	5	6	2	4	5	1	3	5	2	4	5
DR1	3	4	5	2	4	5	1	3	4	1	3	4
DR2	2	3	6	1	2	4	2	3	4	2	4	6
DR3	1	2	3	2	4	5	1	2	4	2	3	4
DR4	2	3	4	1	3	5	1	4	5	2	5	6
DR5	1	2	3	2	3	4	1	3	4	1	3	4

Table 7.6: Experts' scores for monolithic T-beam bridge MTBB

	Bridge Type: MTBB											
	Expert 1			Expert 2			Expert 3			Expert 4		
	Min.	M.L.	Max.	Min.	M.L.	Max.	Min.	M.L.	Max.	Min.	M.L.	Max.
CR1	1	2	3	2	3	4	1	2	3	1	2	3
CR2	1	3	4	2	3	4	2	4	5	2	3	5
CR3	2	4	5	1	3	4	1	3	5	1	2	3
CR4	2	3	4	2	3	5	1	2	3	2	3	4
DR1	1	2	4	1	3	5	1	2	4	2	4	6
DR2	1	3	4	2	4	5	1	3	4	1	2	3
DR3	2	4	5	2	3	4	2	3	4	2	3	4
DR4	1	2	4	1	2	4	2	3	5	1	2	4
DR5	2	4	6	1	3	5	2	3	5	2	3	5

Table 7.7: Experts' scores for reinforced concrete multicell concrete box girder bridge RCMCBGB

	Bridge Type: RCMCBGB											
	Expert 1			Expert 2			Expert 3			Expert 4		
	Min.	M.L.	Max.	Min.	M.L.	Max.	Min.	M.L.	Max.	Min.	M.L.	Max.
CR1	4	5	6	4	6	7	3	5	6	2	5	7
CR2	3	6	7	2	4	6	2	3	4	2	5	6
CR3	2	3	5	2	4	6	3	4	5	4	5	7
CR4	3	5	6	3	5	6	2	4	5	5	6	7
DR1	5	6	7	4	5	6	3	5	6	3	5	6
DR2	3	4	5	5	6	7	2	5	6	2	5	7
DR3	2	4	5	5	6	7	1	3	5	2	4	5
DR4	4	5	6	4	5	6	3	5	7	3	5	7
DR5	5	6	7	4	5	6	3	6	7	2	5	6

Table 7.8: Experts' scores for reinforced concrete multicell concrete box girder bridge PSMCBGB

	Bridge Type: PSMCBGB											
	Expert 1			Expert 2			Expert 3			Expert 4		
	Min.	M.L.	Max.	Min.	M.L.	Max.	Min.	M.L.	Max.	Min.	M.L.	Max.
CR1	7	8	9	6	8	9	6	7	8	7	8	9
CR2	3	4	6	3	5	6	4	5	6	3	4	6
CR3	2	5	6	5	6	7	5	6	7	7	8	9
CR4	4	5	7	4	5	6	5	7	8	5	6	7
DR1	6	7	8	5	6	7	5	6	8	4	5	6
DR2	4	6	7	4	6	7	5	6	8	7	8	9
DR3	7	8	9	6	8	9	5	7	8	5	7	8
DR4	4	5	7	4	5	7	5	6	7	4	6	7
DR5	7	8	9	6	8	9	6	8	9	5	6	7

Table 7.9: Experts' scores for precast prestressed girder concrete slab bridge PCGB

	Bridge Type: PCGB											
	Expert 1			Expert 2			Expert 3			Expert 4		
	Min.	M.L.	Max.	Min.	M.L.	Max.	Min.	M.L.	Max.	Min.	M.L.	Max.
CR1	4	5	6	1	2	3	2	3	4	2	3	4
CR2	7	8	9	6	7	9	5	7	8	6	8	9
CR3	6	8	9	6	7	8	6	7	9	5	7	8
CR4	7	8	9	6	8	9	5	7	9	6	7	9
DR1	2	3	4	3	4	5	5	6	7	2	5	7
DR2	2	5	6	1	3	4	1	2	3	2	3	4
DR3	2	3	5	3	4	5	3	4	5	1	3	4
DR4	6	7	9	6	8	9	6	7	9	5	7	8
DR5	2	3	4	3	4	5	2	4	5	2	4	5

Table 7.10: Experts' scores for steel plate girder bridge PGB

	Bridge Type: PGB											
	Expert 1			Expert 2			Expert 3			Expert 4		
	Min.	M.L.	Max.	Min.	M.L.	Max.	Min.	M.L.	Max.	Min.	M.L.	Max.
CR1	4	5	6	4	5	7	4	5	7	3	4	5
CR2	3	4	5	3	5	7	3	5	6	4	5	6
CR3	4	7	8	7	8	9	2	4	5	2	6	7
CR4	5	6	7	6	7	8	5	6	8	4	5	7
DR1	3	5	6	4	5	6	2	3	4	5	7	8
DR2	3	5	6	4	5	6	3	5	7	2	5	6
DR3	2	3	4	5	6	7	5	7	8	6	7	8
DR4	7	8	9	4	5	6	2	4	5	3	5	6
DR5	4	5	6	3	5	6	7	8	9	5	6	7

The values of the mean μ , standard deviation σ, and the 99 percentile P_{99} of the combined distribution corresponding to every bridge type is summarized in Table 7.11.

Table 7.11: The mean value μ of the combined distribution

Bridge Type		Client's Requirement				Design Requirements				
		CR1	CR2	CR3	CR4	DR1	DR2	DR3	DR4	DR5
RCSB	μ	2.958	3.167	3.000	2.917	2.500	3.000	2.500	3.417	4.625
	σ	0.830	0.949	0.588	0.805	0.707	0.488	0.906	0.694	0.692
	P_{99}	0.496	0.539	0.5	0.497	0.457	0.5	0.369	0.503	0.548
PSSB	μ	3.875	3.125	3.167	3.875	3.375	3.125	2.750	3.583	2.667
	σ	0.857	0.661	0.614	0.891	0.750	0.904	0.871	0.948	0.614
	P_{99}	0.526	0.484	0.467	0.521	0.525	0.466	0.468	0.45	0.52
MTBB	μ	2.250	3.208	2.917	2.792	2.833	2.875	3.208	2.417	3.333
	σ	0.575	0.640	0.869	0.630	1.004	0.829	0.560	0.702	0.769
	P_{99}	0.337	0.473	0.487	0.527	0.444	0.487	0.446	0.472	0.47
RCMCBGB	μ	5.125	4.083	4.083	4.875	5.167	4.542	6.458	5.000	5.333
	σ	0.761	1.316	0.916	0.924	0.679	1.125	0.947	0.598	0.777
	P_{99}	0.501	0.462	0.486	0.501	0.49	0.454	0.644	0.5	0.515
PSMCBGB	μ	6.458	7.667	6.167	7.708	7.750	7.708	7.375	6.875	7.417
	σ	0.947	0.679	1.285	0.596	0.643	0.596	0.750	1.838	0.948
	P_{99}	0.644	0.565	0.423	0.536	0.537	0.536	0.525	0.718	0.616
PCGB	μ	3.250	3.417	2.500	2.917	4.458	3.125	3.500	4.083	3.667
	σ	1.153	1.003	0.627	0.481	1.241	1.100	6.990	1.172	0.614
	P_{99}	0.388	0.405	0.5	0.525	0.445	0.424	0.548	0.447	0.52
PGB	μ	4.833	4.708	6.000	6.083	4.917	4.875	5.708	5.417	5.958
	σ	0.679	0.680	1.666	0.805	1.437	0.633	1.665	1.627	1.331
	P_{99}	0.51	0.505	0.536	0.503	0.512	0.526	0.683	0.328	0.395

The correlation coefficients between the statistical distributions related to CRs and DRs for the different types of bridges are summarized in Tables 7.12 to 7.18.

The decision tree for the seven bridge types under consideration is shown in Figure 7.15. For clarity, the main branches are separately shown in Figures 7.16 To 7.22. The main branch related to the optimum bridge type (prestressed multi-cell box girder bridge PCMCBGB) is distinguished by a blue color.

The expected monitory value EMV resulted from the decision tree analysis corresponding to the every bridge type is shown in Table 7.19. The maximum EMV was that corresponding to the prestressed multi-cell box girder bridge PSMCBGB. This is the same bridge type obtained from the value engineering analysis VEA conducted by the consultant (Parsons International).

Table 7.12: Correlation matrix related to RCSB.

	Correlation matrix for RCSB								
	CR1	**CR2**	**CR3**	**CR4**	**DR1**	**DR2**	**DR3**	**DR4**	**DR5**
CR1	1.000	0.167	0.050	0.017	0.233	0.217	0.350	0.067	0.017
CR2	0.167	1.000	0.100	0.367	0.450	0.167	0.217	0.367	0.417
CR3	0.050	0.100	1.000	0.383	0.633	0.567	0.217	0.050	0.217
CR4	0.017	0.367	0.383	1.000	0.083	0.233	0.300	0.383	0.367
DR1	0.233	0.450	0.633	0.083	1.000	0.833	0.083	0.083	0.017
DR2	0.217	0.167	0.567	0.233	0.833	1.000	0.133	0.517	0.083
DR3	0.350	0.217	0.217	0.300	0.083	0.133	1.000	0.417	0.850
DR4	0.067	0.367	0.050	0.383	0.083	0.517	0.417	1.000	0.400
DR5	0.017	0.417	0.217	0.367	0.017	0.083	0.850	0.400	1.000

Table 7.13: Correlation matrix related to PSSB.

	Correlation matrix for PSSB								
	CR1	**CR2**	**CR3**	**CR4**	**DR1**	**DR2**	**DR3**	**DR4**	**DR5**
CR1	1.000	0.667	0.117	0.083	0.100	0.417	0.583	0.100	0.067
CR2	0.667	1.000	0.300	0.300	0.317	0.033	0.150	0.017	0.250
CR3	0.117	0.300	1.000	0.367	0.067	0.183	0.033	0.433	0.383
CR4	0.083	0.300	0.367	1.000	0.350	0.417	0.250	0.283	0.100
DR1	0.100	0.317	0.067	0.350	1.000	0.100	0.667	0.467	0.467
DR2	0.417	0.033	0.183	0.417	0.100	1.000	0.567	0.050	0.183
DR3	0.583	0.150	0.033	0.250	0.667	0.567	1.000	0.417	0.217
DR4	0.100	0.017	0.433	0.283	0.467	0.050	0.417	1.000	0.167
DR5	0.067	0.250	0.383	0.100	0.467	0.183	0.217	0.167	1.000

Table 7.14: Correlation matrix related to MTBB.

	Correlation matrix for MTBB								
	CR1	**CR2**	**CR3**	**CR4**	**DR1**	**DR2**	**DR3**	**DR4**	**DR5**
CR1	1.000	0.167	0.483	0.383	0.467	0.383	0.033	0.367	0.050
CR2	0.167	1.000	0.050	0.600	0.167	0.600	0.150	0.000	0.017
CR3	0.483	0.050	1.000	0.350	0.167	0.317	0.100	0.883	0.452
CR4	0.383	0.600	0.350	1.000	0.050	0.067	0.150	0.600	0.075
DR1	0.467	0.167	0.167	0.050	1.000	0.200	0.633	0.017	0.109
DR2	0.383	0.600	0.317	0.067	0.200	1.000	0.383	0.217	0.176
DR3	0.033	0.150	0.100	0.150	0.633	0.383	1.000	0.100	0.293
DR4	0.367	0.000	0.883	0.600	0.017	0.217	0.100	1.000	0.427
DR5	0.050	0.017	0.452	0.075	0.109	0.176	0.293	0.427	1.000

Table 7.15: Correlation matrix related to RCMCBGB.

	Correlation matrix for RCMCBGB								
	CR1	**CR2**	**CR3**	**CR4**	**DR1**	**DR2**	**DR3**	**DR4**	**DR5**
CR1	1.000	0.417	0.400	0.383	0.100	0.000	0.117	0.500	0.500
CR2	0.417	1.000	0.617	0.150	0.367	0.100	0.367	0.633	0.450
CR3	0.400	0.617	1.000	0.100	0.400	0.100	0.783	0.583	0.033
CR4	0.383	0.150	0.100	1.000	0.300	0.133	0.267	0.117	0.217
DR1	0.100	0.367	0.400	0.300	1.000	0.500	0.133	0.233	0.317
DR2	0.000	0.100	0.100	0.133	0.500	1.000	0.317	0.167	0.000
DR3	0.117	0.367	0.783	0.267	0.133	0.317	1.000	0.333	0.017
DR4	0.500	0.633	0.583	0.117	0.233	0.167	0.333	1.000	0.417
DR5	0.500	0.450	0.033	0.217	0.317	0.000	0.017	0.417	1.000

Table 7.16: Correlation matrix related to PSMVBGB.

	Correlation matrix for PSMCBGB								
	CR1	**CR2**	**CR3**	**CR4**	**DR1**	**DR2**	**DR3**	**DR4**	**DR5**
CR1	1.000	0.250	0.067	0.150	0.217	0.133	0.217	0.150	0.033
CR2	0.250	1.000	0.250	0.383	0.783	0.067	0.700	0.433	0.567
CR3	0.067	0.250	1.000	0.383	0.167	0.133	0.383	0.383	0.133
CR4	0.150	0.383	0.383	1.000	0.183	0.050	0.633	0.117	0.100
DR1	0.217	0.783	0.167	0.183	1.000	0.167	0.817	0.300	0.883
DR2	0.133	0.067	0.133	0.050	0.167	1.000	0.000	0.200	0.400
DR3	0.217	0.700	0.383	0.633	0.817	0.000	1.000	0.133	0.500
DR4	0.150	0.433	0.383	0.117	0.300	0.200	0.133	1.000	0.233
DR5	0.033	0.567	0.133	0.100	0.883	0.400	0.500	0.233	1.000

Table 7.17: Correlation matrix related to PCGB.

	Correlation matrix for PCGB								
	CR1	**CR2**	**CR3**	**CR4**	**DR1**	**DR2**	**DR3**	**DR4**	**DR5**
CR1	1.000	0.317	0.483	0.033	0.467	0.400	0.250	0.167	0.383
CR2	0.317	1.000	0.033	0.383	0.083	0.050	0.517	0.083	0.067
CR3	0.483	0.033	1.000	0.650	0.117	0.583	0.433	0.667	0.467
CR4	0.033	0.383	0.650	1.000	0.000	0.767	0.167	0.550	0.250
DR1	0.467	0.083	0.117	0.000	1.000	0.083	0.017	0.483	0.217
DR2	0.400	0.050	0.583	0.767	0.083	1.000	0.167	0.450	0.283
DR3	0.250	0.517	0.433	0.167	0.017	0.167	1.000	0.300	0.033
DR4	0.167	0.083	0.667	0.550	0.483	0.450	0.300	1.000	0.100
DR5	0.383	0.067	0.467	0.250	0.217	0.283	0.033	0.100	1.000

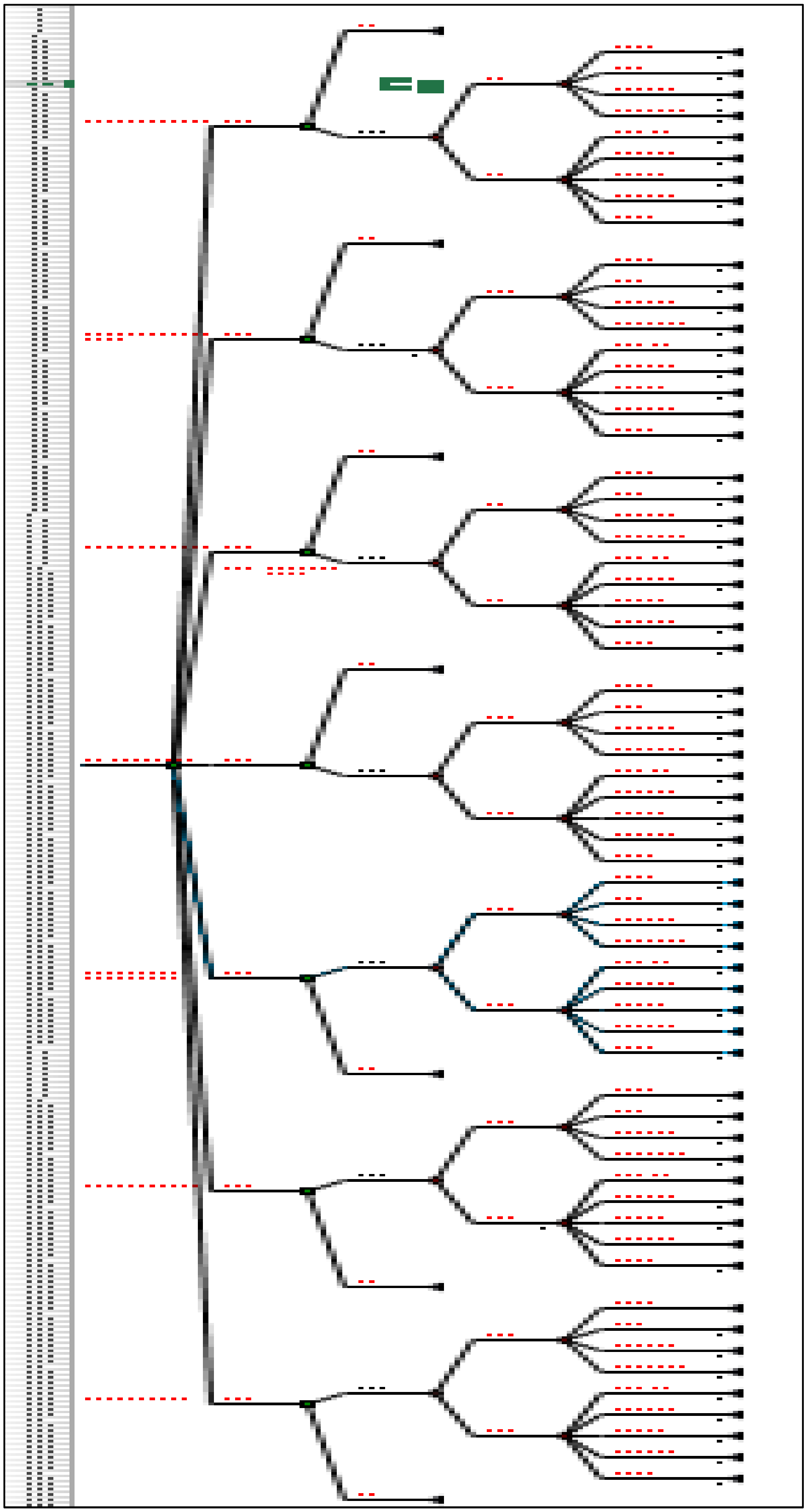

Figure 7.15 : Decision tree for seven bridge types.

Table 7.18: Correlation matrix related to PGB.

	Correlation matrix for PGB								
	CR1	**CR2**	**CR3**	**CR4**	**DR1**	**DR2**	**DR3**	**DR4**	**DR5**
CR1	1.000	0.300	0.133	0.500	0.183	0.450	0.667	0.283	0.533
CR2	0.300	1.000	0.483	0.217	0.283	0.267	0.317	0.817	0.250
CR3	0.133	0.483	1.000	0.067	0.333	0.317	0.317	0.150	0.050
CR4	0.500	0.217	0.067	1.000	0.050	0.033	0.317	0.200	0.967
DR1	0.183	0.283	0.333	0.050	1.000	0.200	0.133	0.233	0.017
DR2	0.450	0.267	0.317	0.033	0.200	1.000	0.300	0.000	0.150
DR3	0.667	0.317	0.317	0.317	0.133	0.300	1.000	0.367	0.333
DR4	0.283	0.817	0.150	0.200	0.233	0.000	0.367	1.000	0.150
DR5	0.533	0.250	0.050	0.967	0.017	0.150	0.333	0.150	1.000

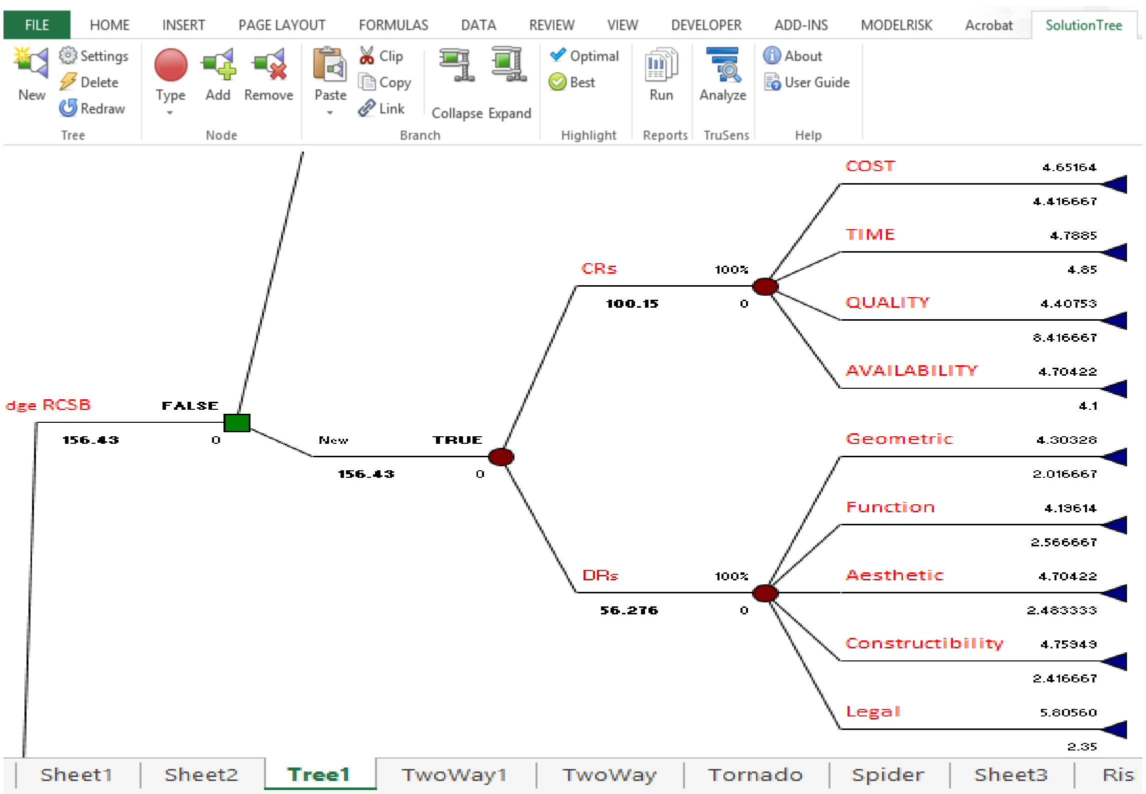

Figure 7.16: Main branch corresponding to bride type (RCSB) – Case study I

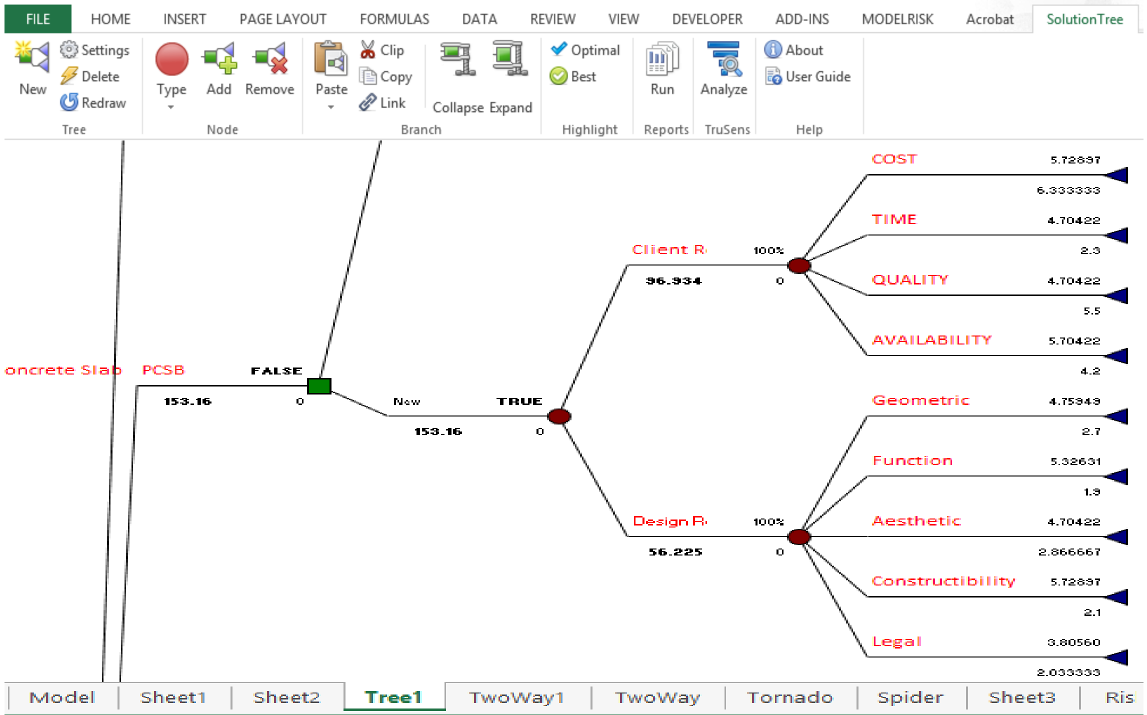

Figure 7.17: Main branch corresponding to bride type (PCSB) – Case study I

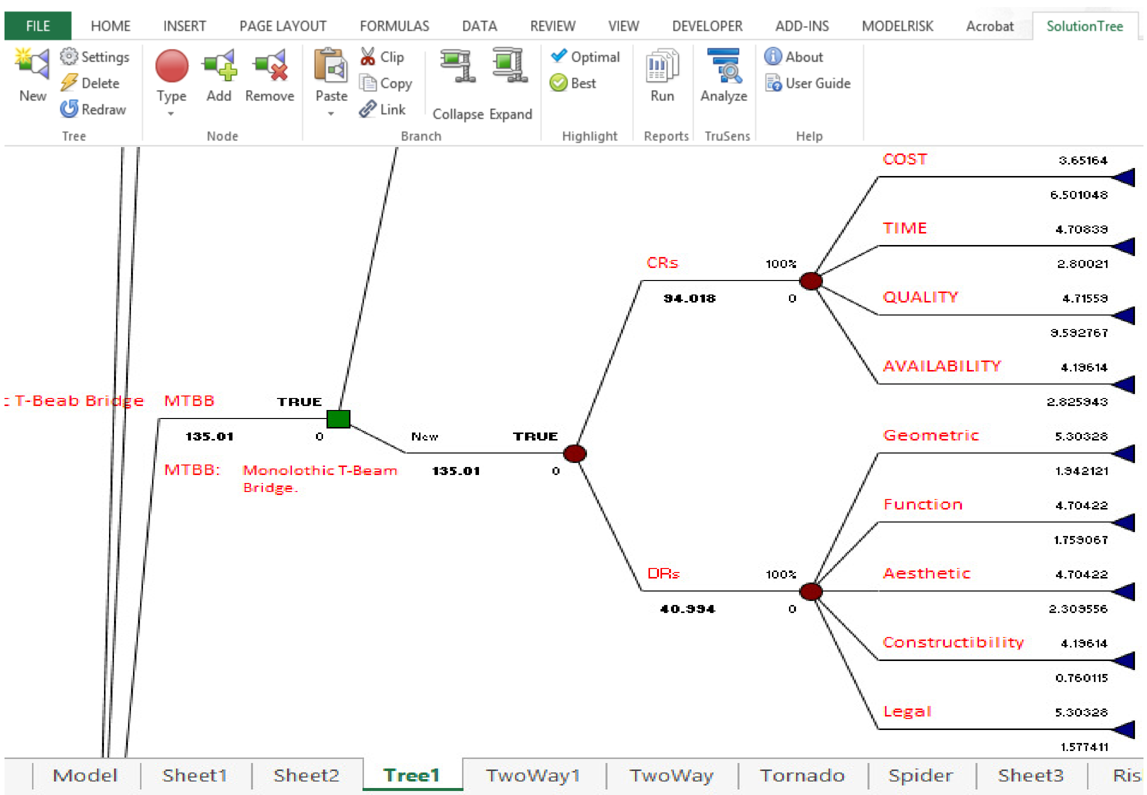

Figure 7.18: Main branch corresponding to bride type (MTBB) – Case study I

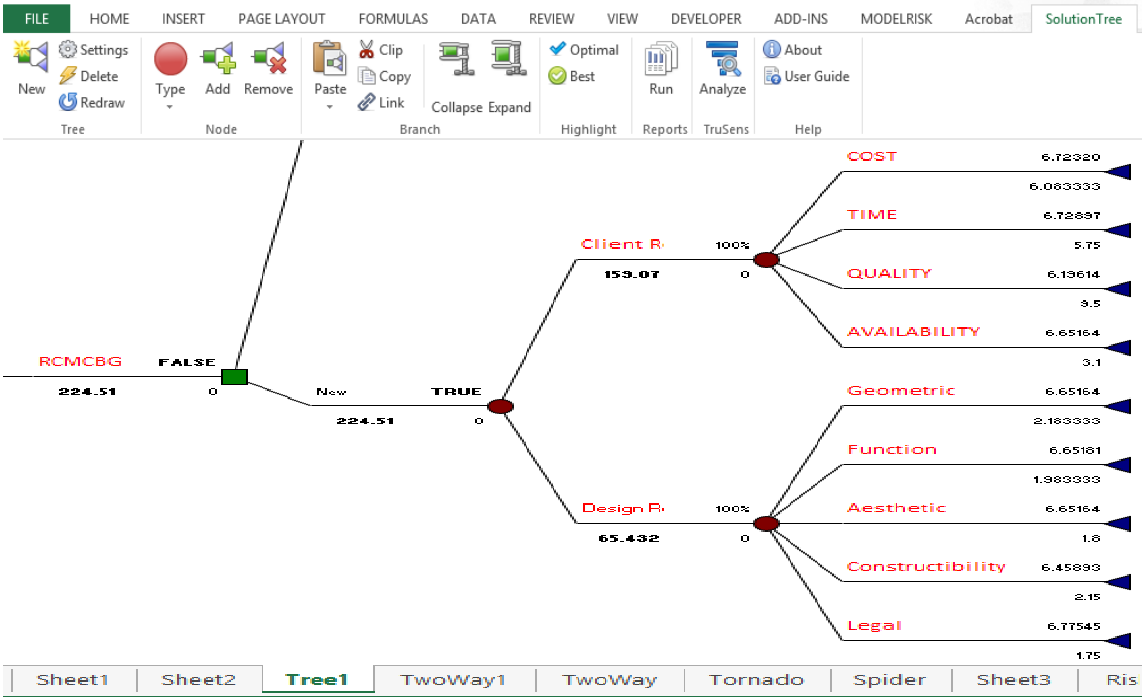

Figure 7.19: Main branch corresponding to bride type (RCMCBGB) – Case study I

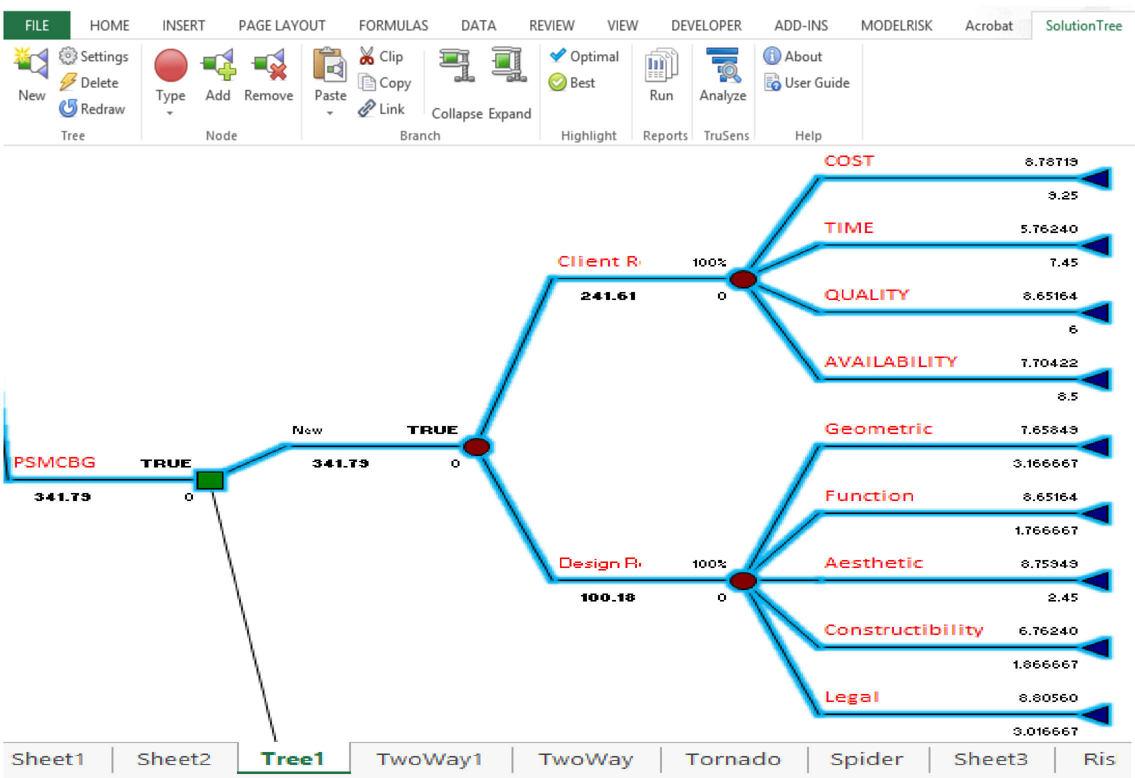

Figure 7.20: Main branch corresponding to the optimum bride type (PSMCBGB). – Case study I

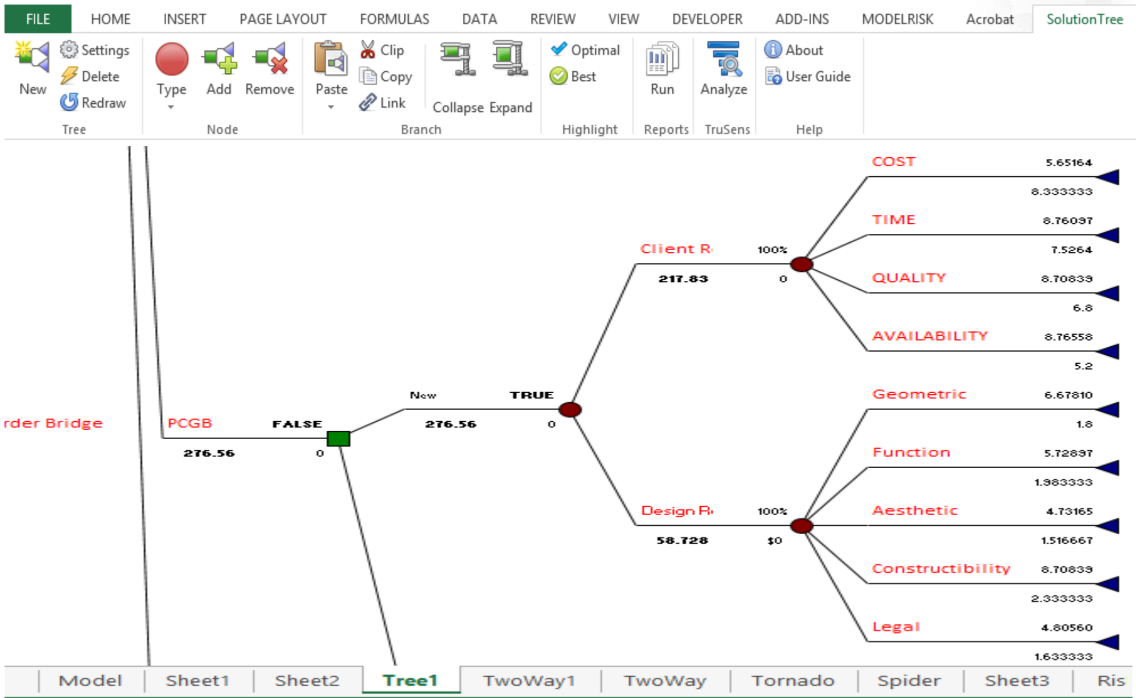

Figure 7.21: Main branch corresponding to bride type (PCGB) – Case study I

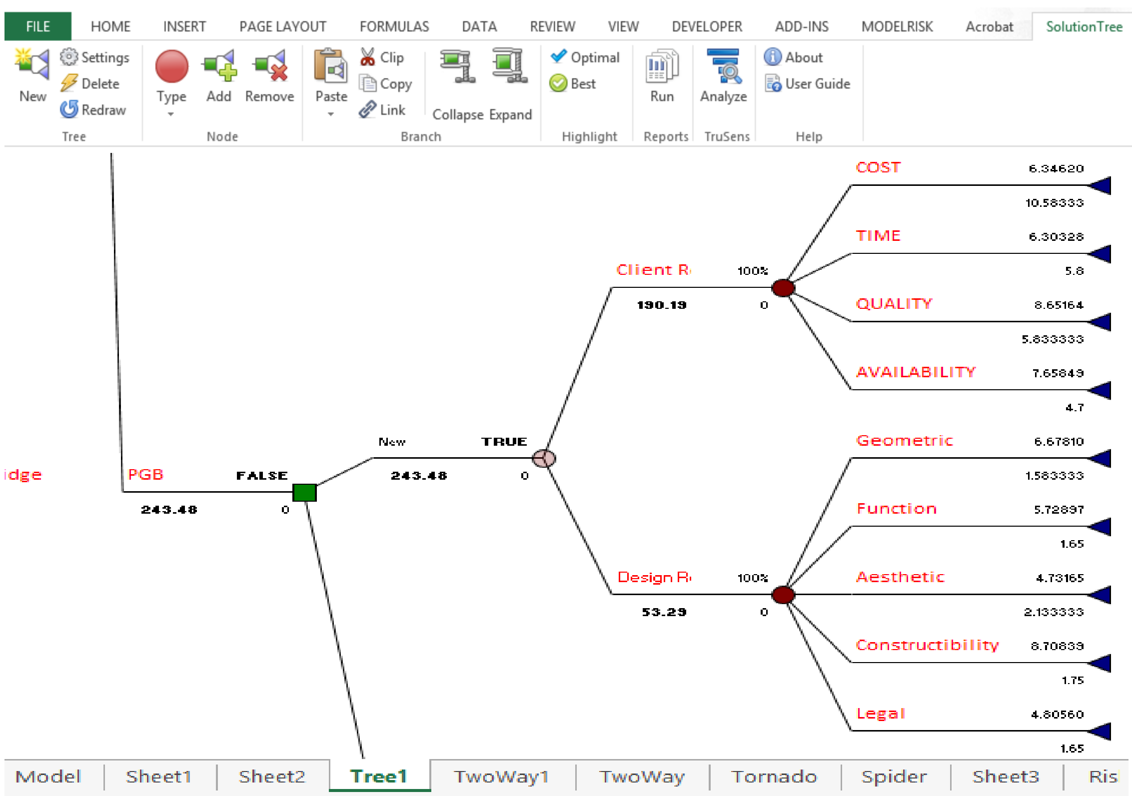

Figure 7.22: Main branch corresponding to bride type (PGB) – Case study I

Table 7.19: EMV resulted from the decision tree analysis – Case Study I.

Bridge Type	Expected Monitory Value EMV
RCSB	156.4
PSSB	153.2
MTBB	135.0
RCMCBGB	224.5
PSMCBGB	341.8
PCGB	276.6
PGB	243.5

Now, in order to investigate the influence of the independent variables (client's requirements CRs and design requirements DRs) on the dependent variable (bridge type), sensitivity analysis was conducted considering the optimum path.

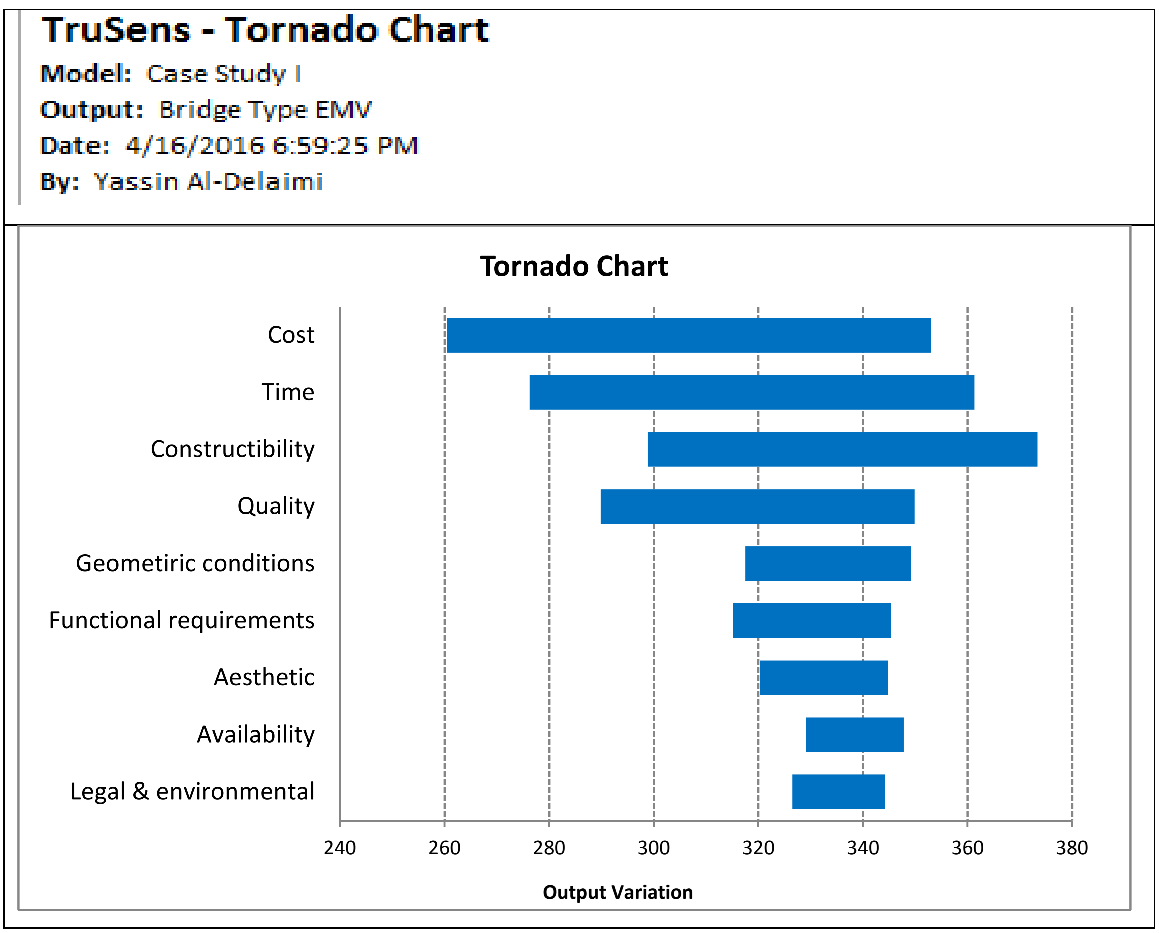

Figure 7.23: Tornado chart revealed from sensitivity analysis.

To perform such analysis, a large number of model executions (analyses) have been performed. In every time of analysis, only one variable was considered and all other variables were kept constant. The results of the sensitivity analysis were represented by a Tornado chart as illustrated in Figure 7.23 and Table 7.20.

The results of the sensitivity analysis show that the bridge type is highly sensitive to the project budget (cost), project duration (time) and constructability; eventually, this is in line with the logics of projects management.

Table 7.20: Summary of the results of sensitivity analysis

Chart Data								
Rank	Input Variable	Total Variance	Minimum			Maximum		
			Output		Input Value	Output		Input Value
			Value	Change %		Value	Change %	
1	Cost	92	261	-23.64	0.0	353	3.17	10.0
2	Time	85	276	-19.25	0.0	361	5.32	10.0
3	Constructability	74	299	-12.52	0.0	373	8.36	10.0
4	Quality	60	290	-15.16	0.0	350	2.34	10.0
5	Geometric Conditions	31	318	-6.96	0.0	349	2.11	10.0
6	Functional Requirements	30	315	-7.84	0.0	345	0.93	10.0
7	Aesthetic	24	320	-6.38	0.0	344	0.64	10.0
8	Availability	19	329	-3.74	0.0	348	1.81	10.0
9	Legal & Environmental	17	327	-4.33	0.0	344	0.64	10.0

7.8 Case Study II

In this section another case study will be considered in order to verify the applicability of the proposed model.

The results of the sensitivity analysis, performed in Section 7.7 (for case study I), gave the motivation to further investigate the effect project budget and project duration on the type of bridge superstructure. However, all the parameters of Case Study I will be kept intact; the only change will be made on the importance level of the client's requirements (specifically, cost and time). Table 7.21 shows the modified importance levels of the CRs. From this table, it is obvious that the time was given a very high priority. This means that the client's priority is to complete the project as fast as possible.

Table 7.21: Importance levels (priority) of client's requirements related to case study II

Client's Requirements (CR)	Importance Level (IL)	Weight
Cost	Very High	3
Time	Fair	5
Quality	Very High	5
Availability	Fair	3

The same steps and procedure used in Case Study I will be followed here. Figures 7.24 to 7.30 illustrate the results of the decision tree analysis related to the different bridge types. The main branch related to the optimum bridge type (prestressed girder bridge) is distinguished by a blue color.

The expected monitory value EMV resulted from the decision tree analysis corresponding to the every bridge type is shown in Table 7.22. The maximum EMV was that corresponding to the precast prestressed girder bridge PCGB. This reflects the logical fact that prestressed girder bridges are fast in construction (required less construction time compared to other bridge types).

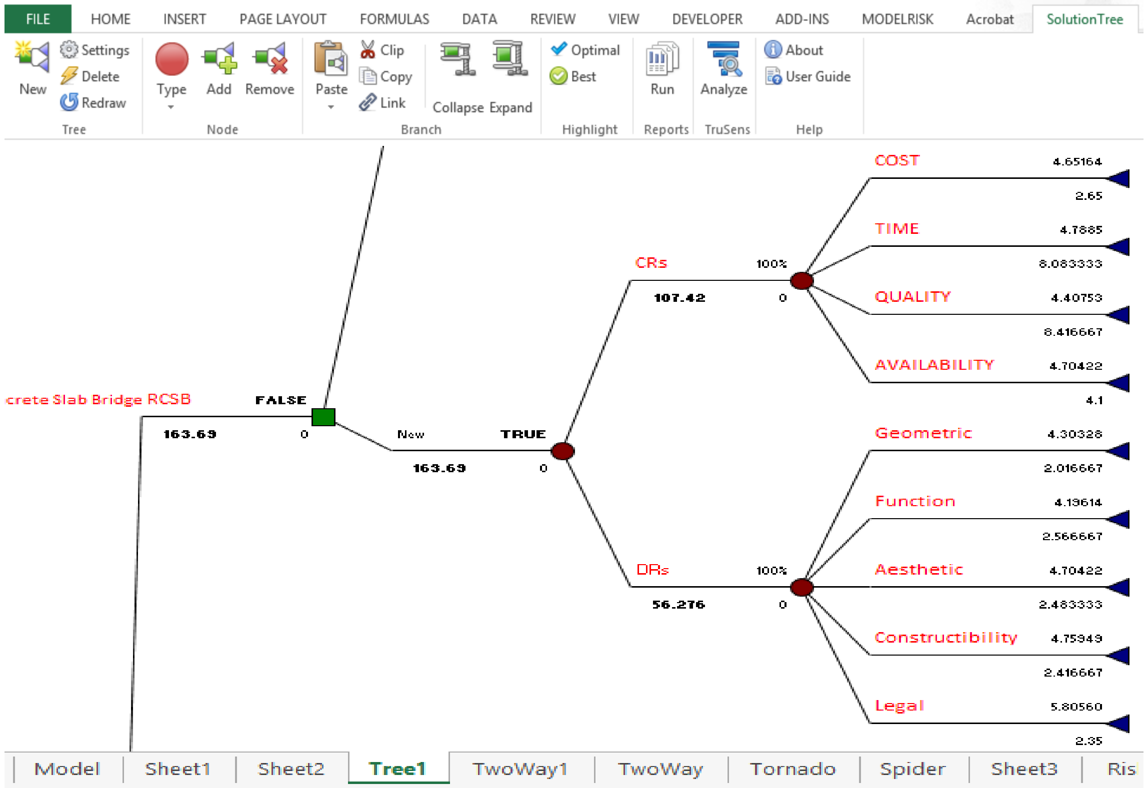

Figure 7.24: Main branch corresponding to bride type (RCSB) – Case study II

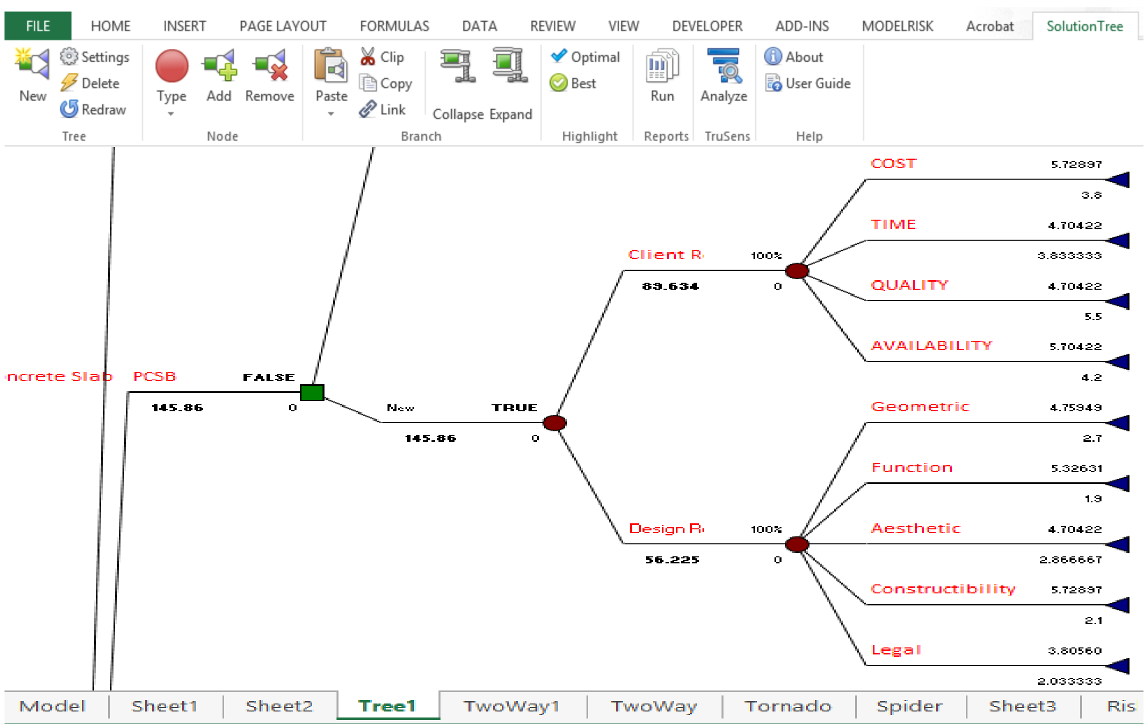

Figure 7.25: Main branch corresponding to bride type (PCSB) – Case study II

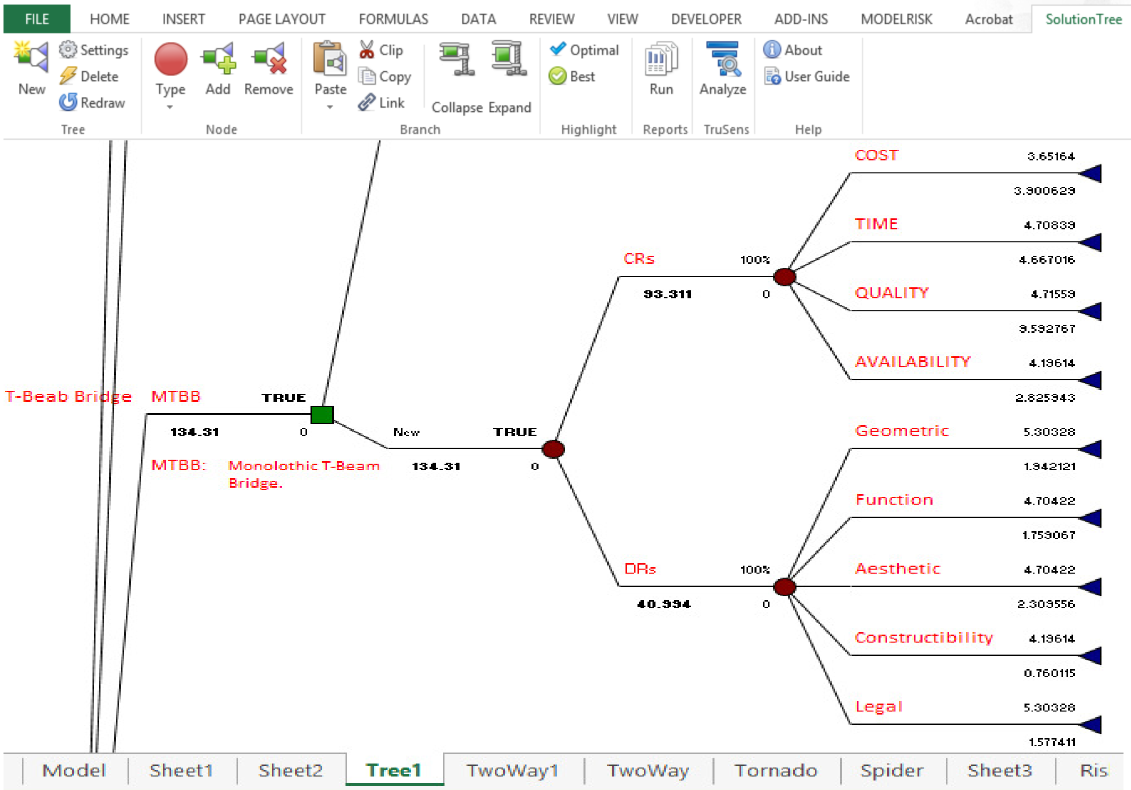

Figure 7.26: Main branch corresponding to bride type (MTBB) – Case study II

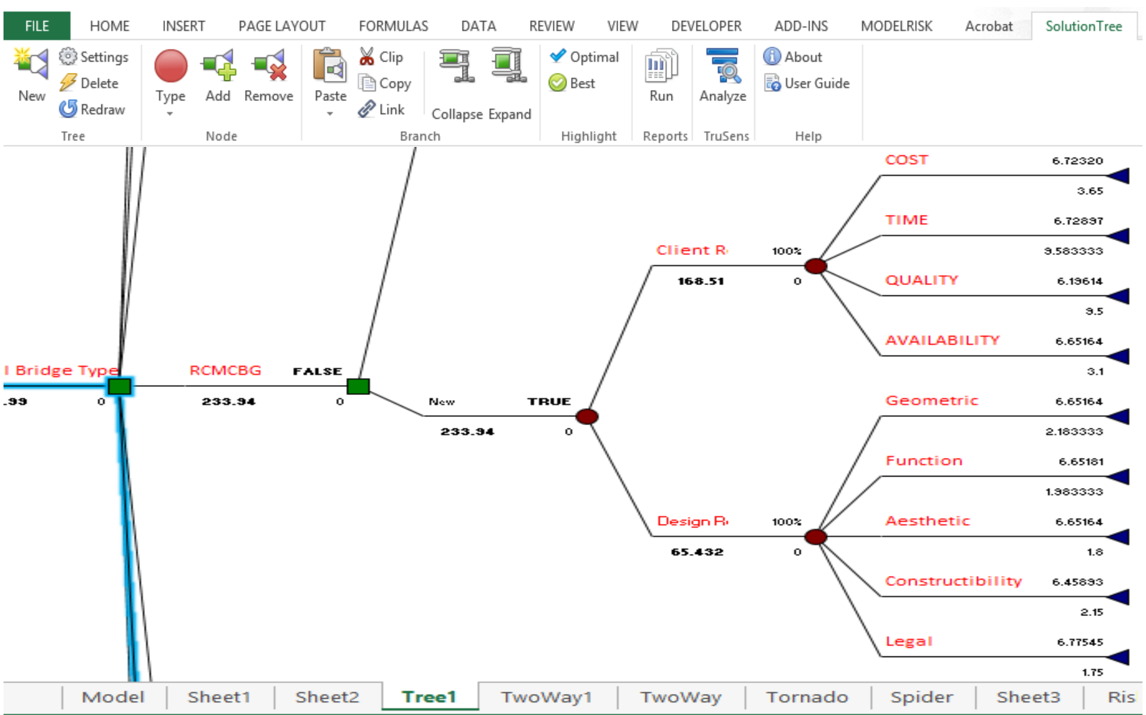

Figure 7.27: Main branch corresponding to bride type (RCMCBGB) – Case study II

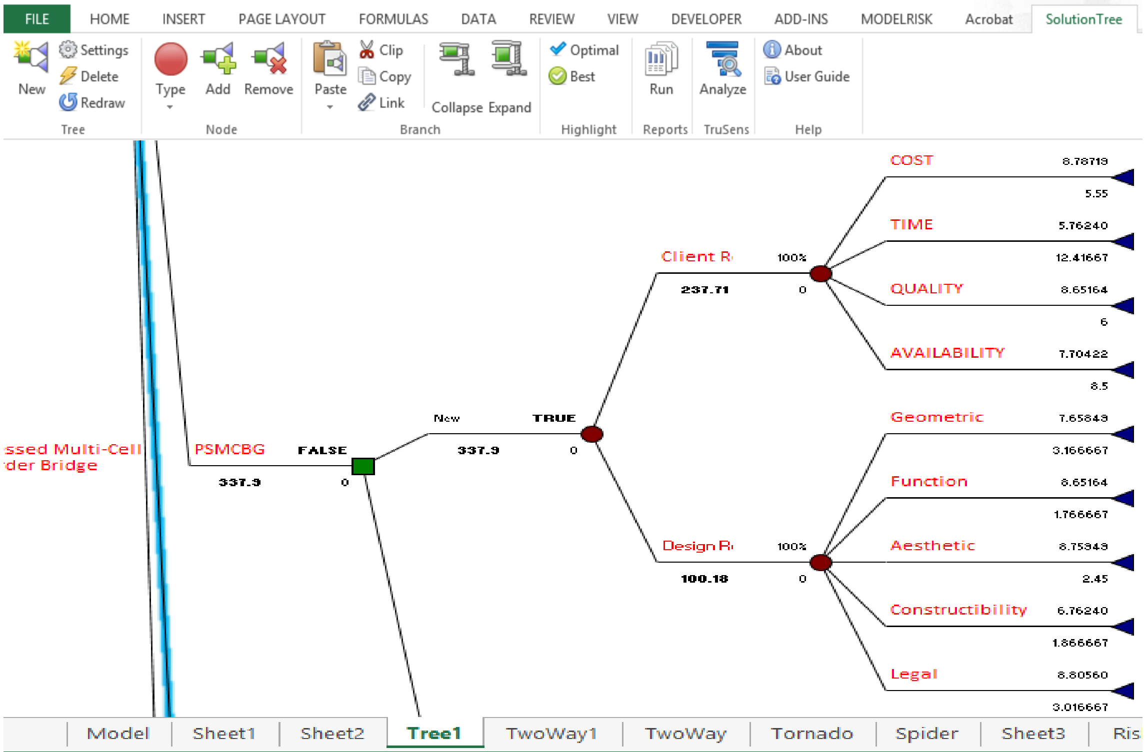

Figure 7.28: Main branch corresponding to the optimum bride type (PSMCBGB) – Case study II

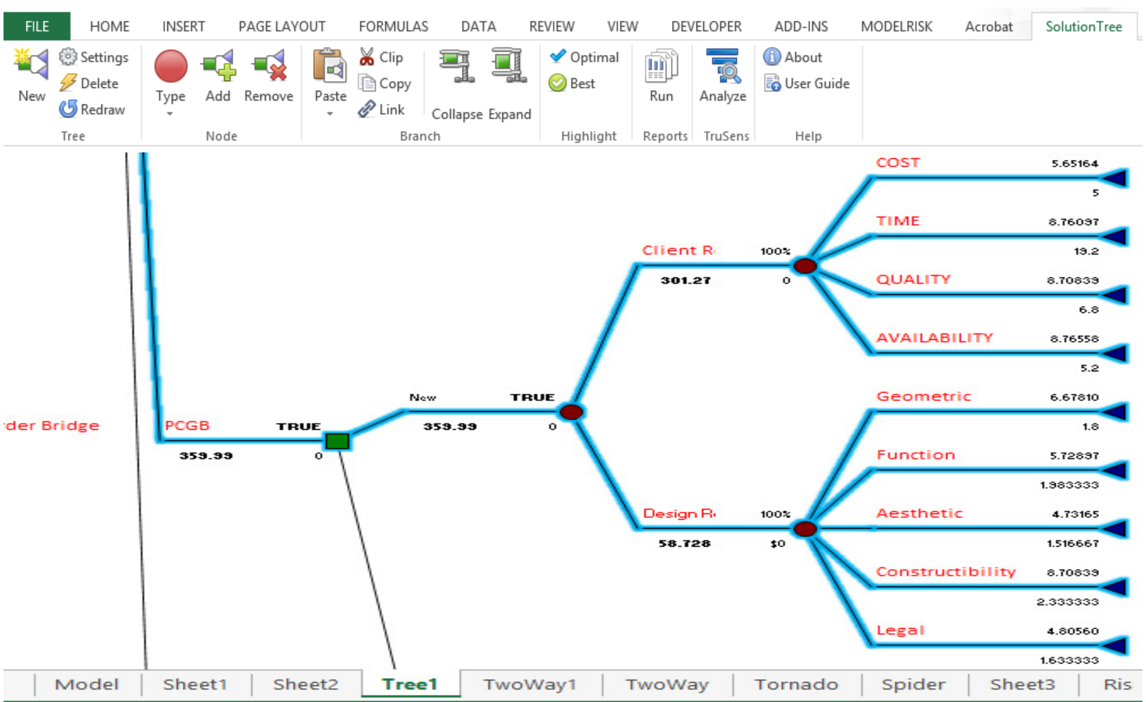

Figure 7.29: Main branch corresponding to bride type (PCGB) – Case study II

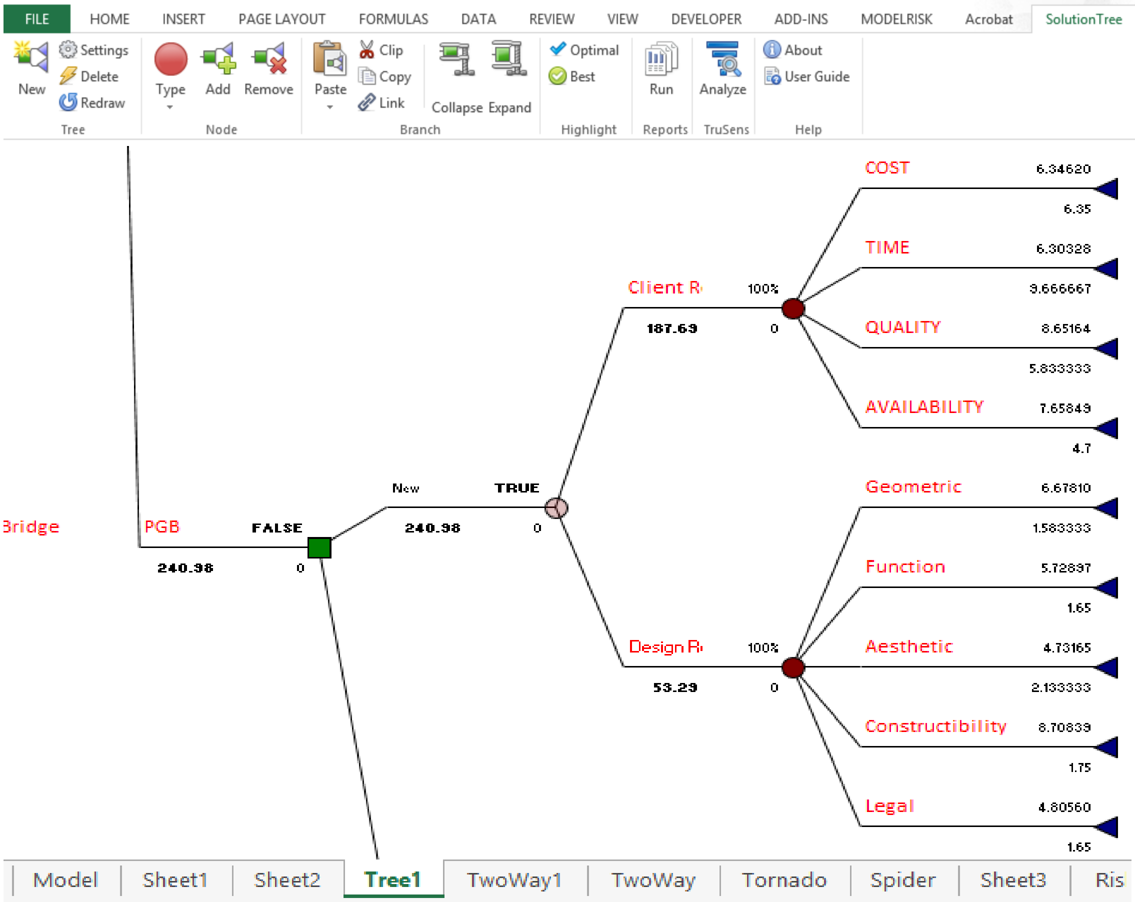

Figure 7.30: Main branch corresponding to bride type (PGB) – Case study II

Table 7.22: EMV resulted from the decision tree analysis - Case Study II.

Bridge Type	Expected Monitory Value EMV
RCSB	163.7
PSSB	145.9
MTBB	134.3
RCMCBGB	233.9
PSMCBGB	337.9
PCGB	360.0
PGB	241

7.9 Summary

The current research provides a probabilistic approach for the design optimization of prestressed girder bridges. Eventually, bridge design optimization process will only be efficient when it is applied on a properly-selected bridge type. Hence, for the current optimization model, the first essential step is to verify that a prestressed girder bridge system is the most appropriate bridge type with respect to the project conditions, requirements, and limitations. For this purpose, a new model for deciding about the optimum bridge type is developed in the current research.

The model integrates the experts' decisions with decision tree analysis and sensitivity analysis. The uncertainty associated with every expert's opinion has been statistically modeled using PERT distribution. The different opinions of different experts have been composed using a combined distribution. The client's requirements (CRs) and design requirements (DRs) were treated as the main optimization variables. The correlation between the CRs and design requirements DRs as well as among the DRs have been considered and incorporated. The statistical model is interactively linked with a decision tree that calculates an equivalent expected monitory value EMV with respect to every possible alternative. The alternative that reveals the maximum EMV represents the optimum bridge type. For the optimum solution, a sensitivity analysis was also conducted to investigate the influence of the independent variables (client's and design requirements) on the dependent variable (bridge type).The applicability of the proposed model was investigated through two case studies. The proposed model showed satisfactory performance; and the case studies revealed logical results.

Chapter 8

Summary, Conclusions, and Recommendations

8.1 Summary

The current research proposes a new efficient model that uniquely performs probabilistic-based design optimization for prestressed girder bridges. The proposed model aims to provide cost-effective design solutions with guaranteed safety levels in the optimized bridge configuration. Two different probabilistic optimization methodologies were developed: i- reliability-based design optimization, and ii- six sigma robust design optimization. The proposed model is capable of performing comprehensive reliability analysis both on the individual components level and the overall structural system level. Different reliability methods have been incorporated. The current research also proposes a new method (as part of the integrated model) for choosing the optimum bridge superstructure type by modelling probabilistically the experts' decisions and by integrating them within the decision tree analysis and sensitivity analysis.

The new friendly-user model, developed in the current research, was coded with Visual Basic Applications VBA in order to:

- derive new statistical parameters for the random variables related to the load effects and resistance,
- conduct comprehensive reliability analysis to estimate the component's failure probabilities and corresponding reliability indices by the Firs-Order Reliability Method FORM,
- estimate the overall system's reliability by conducting nonlinear failure mode analysis FMA and, by utilizing the method of Improved Reliability Bounds IRB. For this purpose, a 2-D nonlinear grillage analogy GRANAL (Grillage ANALogy) algorithm has been coded with Visual Basic Applications VBA,
- alternatively, evaluate the probability of failure and corresponding reliability indexes by Monte Carlo Simulation MCS technique,

- perform probabilistic design optimization of prestressed girder bridges with reliability-based design optimization approach, in which the failure probabilities are utilized as probabilistic constraints,
- conduct a quality-control design optimization through implementing the six sigma quality concept in order to achieve robust structural configuration,
- incorporate the Copula method in quantifying the dependency (correlation) between random variables and investigate its effect on the reliability indices, and
- to provide a decision-making tool to select the most appropriate bridge superstructure type by integrating expert decision analysis, decision tree analysis, and sensitivity analysis.

8.2 Conclusions

The following main conclusions can be drawn based on the applicability, the results and the validation of the probabilistic model developed in the current research:

1. Deterministic optimization of prestressed girder bridges could considerably reduce the cost of the bridge. However, the optimized structural configuration might not be considered as entirely safe, particularly from the serviceability point of view, as a result of not considering the uncertainties associated with the basic design variables.
2. Probabilistic optimization approaches can efficiently provide the best compromise between achieving a cost-effective design solution and guaranteeing satisfactory safety levels for the final optimized structural configuration.
3. The existing statistical parameters for the random variables related to the load effects (stresses, bending moment, shear, fatigue stress range) and resistance are no longer valid because new live load models, material coefficients, and fabrication coefficients were derived. Hence, new statistical parameters, characterizing the load effects and resistance, have been derived in the current research.
4. The available reliability analysis of prestressed girder bridges focusses only on the ultimate flexural capacity of the bridge. This can help evaluating the capacity of existing bridges. However, for the sake of reliability-based design optimization, the available reliability analysis is not enough as it should consider all limit state functions related to the design of prestressed girder bridges. On the other hand, these available reliability analyses are no longer valid as they were obtained

based on old models of load and resistance. New comprehensive reliability analysis is necessary and essential for realistically describing the safety levels of the girder bridges. The new analysis must consider all possible limit state functions based on the new statistical parameters of the load effects and resistance. This was thoroughly addressed in the current research by developing a new comprehensive reliability model that considers all limit state functions, correlation between random variables, and all possible modes of failure that could lead to system collapse (mechanism). The improved reliability bounds IRB method was employed, in the current study, to obtain the narrowest possible bounds (lower and upper bounds) for the system reliability.

5. The previous researchers focused mainly on AASHTO Girders in evaluating the reliability analysis of girder bridges. However, there are other numerous very common types of girders. In the current research, a computerized model was developed to perform comprehensive reliability analysis for any type of girder, particularly the most popular types, such as AASHTO Girders, CPCI Girders, Bulb Tee Girders, and NU Girders.
6. First-Order Reliability Method FORM provides satisfactorily accurate results for structural engineering applications. Its simple computational effort and fast processing makes it very attractive for end users and designers. However, the Monte Carlo Simulation MCS technique is still the most accurate approach for performing the reliability analysis. The new model, developed in the current research, employs both FORM and MSC methods.
7. Copulas method offers a much more flexible approach for precisely quantifying the correlation (dependency) between random variables by combining marginal distributions into multivariate distributions and offer an enormous improvement in capturing the real correlation pattern. Thus, correlation with copula is more advanced and accurate than the conventional rank-order correlation methods. As a novel contribution, the current study employed the copula functions in correlating different random variables envolved in the reliability analysis of prestressed girder bridges. Two main categories of copula functions exist; namely: Elliptical copulas (normal and T) and Archimedean copulas (Clayton, Frank, and Gumbel). Elliptical copulas, due to their mathematical formulation, have higher impact on reliability analysis than Archimedean copulas.

8. The simulation-based optimization technique offers an effective approach that efficiently copes with the complexity of structures like bridges. This technique employs a heuristic (or metaheuristic) algorithm to guide the simulation without the need to perform an exhaustive analysis of all the possible combinations of input variables. As a novel contribution, the current research developed a new model that performs probabilistic simulation-based design optimization for prestressed girder bridges. The simulation engine conducts Monte Carlo Simulation MCS while the optimization engine performs metaheuristic scatter search with neural network accelerator (filter). Both, the simulator and the optimizer are interactively integrated with a comprehensive reliability model and cost model.
9. Reliability-based design optimization provides the best compromise between achieving cost-effective solutions with guaranteed safety levels. In this approach the failure probabilities, corresponding to the target reliability indexes (both the individual components' reliability and the entire system's reliability), should be treated as probabilistic constraints in the optimization process. Employing this approach in the new model, developed in the current study forms an important contribution to the field of bridge design optimization. The reliability analysis, performed in conjunction with the design optimization procedure, represent an important advance of knowledge for the bridge engineers. The new statistical parameters for the load and resistance models were efficiently implemented in the process of selecting the appropriate safety levels of the prestressed girder bridges.
10. The six sigma quality concept can be integrated with reliability analysis and robust design. Such quality-controlled approach helps achieving design solutions which ensure not only that a structure performs as designed, but also that the structure consistently performs as designed. However, it is not necessarily to apply higher number of sigmas (e.g. 6$\boldsymbol{\sigma}$) as it might be too expensive. As a new contribution, the current study uniquely employed, formulated and applied the six-sigma based robust design optimization of prestressed girder bridges.
11. The feasibility of any bridge design is very sensitive to the bridge superstructure type. Failing to choose the most suitable bridge type will never help achieving cost-effective design alternatives. In addition to the span length, many other factors (e.g. client's requirements, design requirements, project's conditions, etc.)

affect the selection of bridge type. The current research focusses on prestressed girder bridge type. However, in order to verify whether selecting the prestressed girder bridge type, in a specific project, is the right choice, a tool for selecting the optimum bridge type was needed. Hence, the current research provides a new model for selecting the most suitable bridge type, by integrating the experts' decision analysis, decision tree analysis and sensitivity analysis. Experts' opinions and decisions form an essential tool in developing decision-making models. However the uncertainties associated with expert's decisions need to be properly incorporated and statistically modelled. This was uniquely addressed in the current study.

8.3 Recommendations for future research

The following recommendations can be considered for future research work:

1. In order to have consistent safety levels (reliability), current design codes need to be calibrated with respect to Serviceability Limit States SLS and Fatigue Limit State FLS. This required developing Live load models that represents the actual traffic, with a high degree of accuracy, by using weigh-in-motion stations. Such stations need to be installed in different provinces/states in order to have a comprehensive traffic data.
2. The probabilistic analysis performed for prestressed girder bridges can be further extended and developed to involve time-dependent reliability analysis that implements the effect of the age-related deterioration, which was beyond the scope of the current research.
3. The applicability of the probabilistic optimization approach can be further applied to other types of bridges (e.g. box girder bridges, plate girder bridges, etc.).
4. The design optimization can be further developed to involve the bridge substructure components (i.e. abutment, piers, and foundations) as considerable part of the budget is usually allocated to these components.

References

AACE International. (2005), “Cost Estimate Classification System-as Applied in Engineering, Procurement and Construction for the Process Industries,” AACE, Inc.

AASHTO (2014), "AASHTO LRFD Bridge Design Specification," 7th edition, American Association of State Highway and Transportation Officials.

Adhikari, S. (2005). Asymptotic distribution method for structural reliability analysis in high dimensions. Proceedings of the Royal Society A: Mathematical, Physical and Engineering Sciences, 461(2062), 3141–3158.

Adrian, J., (1993) “Construction Estimating an Accounting and Productivity Approach,” 2nd edition, Stipes Publishing Company.

Agarwal, A. C , and Wolkowicz, M. (1976). Interim report on 1975 commercial vehicle survey. Res. and Dev. Div., Ministry of Transp., Downsview, Ontario, Canada.

Ahmed, S. and Koo, B. (1990). Improved Reliability Bounds of Structural Systems. *J. Struct. Eng*. 1990.116: 3138-3147.

Ahmed, M., Mallick, J., & Abul Hasan, M. (2014). A study of factors affecting the flexural tensile strength of concrete. Journal of King Saud University - Engineering Sciences.

Ahsan, R., Rana, S., & Ghani, S. N. (2012). Cost Optimum Design of Posttensioned I-Girder Bridge Using Global Optimization Algorithm, 138(February), 273–284.

Akinci, B., Tantisevi, K., & Ergen, E. (2004). Assessment Of The Capabilities Of A Commercial 4D CAD System To Visualize Equipment Space Requirements On Construction Sites, Proceedings of Construction Research Congress, ASCE 2004.

Albert, I., Donnet, S., Guihenneuc-Jouyaux, C., Low-Choy, S., Mengersen, K., & Rousseau, J. (2012). Combining expert opinions in prior elicitation. Journal of Bayesian Analysis, 7(3), 503–532.

Alberto, I., Azcarate, C., Mallor, F., and Mateo, P. M. (2002). Optimization with simulation and multiobjective analysis in industrial decision-making : A case study, European Journal of Operational Research 140 (2), 373–383.

Al-Delaimi Y., and Dragomirescu E., (2015). Combining experts' decision analysis and decision tree analysis to select the optimum bridge superstructure type, Proceedings of the Canadian Society for Civil Engineers annual conference CSCE 2015, Regina, SA, Canada.

Al-Delaimi Y., and Dragomirescu E., (2016). Reliabilty-based design optimization of prestressed girder bridges, Proceedings of the 5th International Structural Specialty Conference, organized by CSCE 2016, London, Ontario Canada, (1-4) June 2016.

Al-Delaimi Y., and Dragomirescu E., (2016). Six sigma-based robust design optimization of prestressed girder bridges, EMI & PMC conference, Nashville, TN, USA (22-25) May 2016.

AI-Harthy, A. S. and Frangopol, D.M. (1994) Reliability assessment of prestressed concrete beams, ASCE. (1994), 120(1), 180–199.

Allen, D. E. (1970). Probabilistic Study of Reinforced Concrete in Bending, A C I Journal, Vol. 67, No. 12, pp. 989-993.

Allen, D. E. (1975). Limit States Design - A Probabilistic Study. Canadian Journal of Civil Engineering, 2, pp. 36-49.

Andradóttir, S., Healy, K. J., Withers, D. H., and Nelson, B. L. (1997). Proceedings of the 1997 Winter Simulation Conference ed. S. Andradóttir, K. J. Healy, D. H. Withers, and B. L. Nelson, 118–126.

Ang, A. H-S. and Cornell, C. A. (1974). Reliability Bases of Structural Safety and Design, Journal of Structural Division, ASCE, Vol. 100, No. ST9, pp.1755-1769.

ASTM Standard, (2014), "ASTM Standard Classification for Bridge Elements UNIFORMAT II (E2103)". American Standard of Testing Materials.

Ayyub, B. and Chao, R., “Uncertainty Modeling in Civil Engineering with Structural and Reliability Applications,” Uncertainty Modeling and Analysis in Civil Engineering, CRC Press, Boca Raton, FL, 1998, pp. 3-8.

Bentz E. C., Vecchio F. J., and Collins M. P. (2006). Simplified Modified Compression Field Theory for Calculating Shear Strength of Reinforced Concrete Elements, ACI Structural Journal, No. 103-S65: 614-624.

Bhattacharya B., Lu Q. and Zhong J. (2009). Reliability of redundant ductile structures with uncertain system failure criteria, Academy Proceedings in Engineering Science, 34 (6): 903-921.

Barker, R.M. and Puckett, J.A. (2013). Design of Highway Bridges, 3rd edition. John Wiley & Sons, Inc., Hoboken, New Jersey.

Bartlett F.M., Buckland P.G. and Kennedy, D.J.L. (1992). Canadian Highway Bridge Evaluation: Derivation of Clause 12 of CAN/CSA-S6-1988, Canadian Journal of Civil Engineering, 19(6):1007-1016.

Beck, A. T., & Gomes, W. J. D. S. (2012). A comparison of deterministic, reliability-based and risk-based structural optimization under uncertainty. Probabilistic Engineering Mechanics, 28, 18–29.

Belegundu A. D. (1988). Probabilistic Optimal Design Using Second Moment Criteria. Journal of Mechanisms, Transmissions, and Automation in Design 110 (3), 324–329

Billinton, R. and Allan, R. N. (2003). Reliability evaluation of engineering systems, Second edition, Springer.

Bitarafan, M., Arefi, S. L., Zolfani, S. H., & Mahmoudzadeh, A. (2013). Selecting the best design scenario of the smart structure of bridges for probably future earthquakes. Procedia Engineering, 57, 193–199.

Bø, H. S. (2014). Estimation of Reliability by Monte Carlo Simulations, M.Sc. Thesis, Norwagian University of Science and Technology, Department of Mathematical Seciences.

Boyd, S., & Vandenberghe, L. (2010). Convex Optimization. (C. U. Press, Ed.) Optimization Methods and Software (Vol. 25). Cambridge University Press.

Breitung, K. (1988). Asymptotic crossing rates for stationary Gaussian vector processes. Stochastic Processes and Their Applications, 29(3741), 195–207.

Buckland P.G. and Bartlett F.M. (1992). Canadian Highway Bridge Evaluation: A General Overview of Clause 12 of CSA Standard CAN/CSA-S6-1988, Canadian Journal of Civil Engineering, 19(6):981-986.

Burgoyne, C. J., & Sham, S. H. R. (1987). Application of expert systems to prestressed concrete bridge design. Civil Engineering Systems, 4(1), 14–19.

Butcher, N. and Demmers, L. (2003), “Cost Estimating Simplified,” Provided through the Libris Design Project, Supported by the U.S Institute of Museum and library Services.

Carnevalli, J. a., & Miguel, P. C. (2008). Review, analysis and classification of the literature on QFD-Types of research, difficulties and benefits. International Journal of Production Economics, 114(2), 737–754.

Carr, R. I. (December, 1989), “Cost Estimating Principles,” Journal of Construction Engineering and Management, Vol. 115, No. 4, ASCE, pp. 545-551.

Carson, Y., and Maria, A. (1997). Simulation optimization: methods and applications.Proceedings of the 1997 Winter Simulation Conference. San Diego: The Society for Computer Simulation.

Charette R. P. and Marshall H. E. (1999). Uniformat II Elemental Classification for Building Specifications, Cost Estimating, and Cost Analysis, US Department of Commerce Technology Administration, National Institute of Standards and Technology.

Chateauneuf A., Principles of reliability-based design optimization, Chapter 1, Structural design optimization considering uncertainties, 2007, Taylor and Francis/Balkema, Leiden.

Chen W. F. and Duan L., 2014, Bridge engineering handbook, 2nd edition, CRC Press, Taylor and Francis Group, 6000 Broken Sound Parkway NW, Suite 300, Boca Raton, FL 33487-2742.

Chen X., Hasselman T. K. and Neill D. J. (1997). Reliability Based Structural Design Optimization for Practical Applications. 38th AIAA/ASME/ ASCE/AHS/ASC, Structures, Structural Dynamics and Materials Conference, 2724–2732. Kissimmee, FL. Paper No. AIAA-97-1403

Cheng, J. (2014). Random field-based reliability analysis of prestressed concrete bridges. Ksce Journal of Civil Engineering, 18(5), 1436–1445.

Cheng, M.-Y., & Roy, A. F. V. (2010). Evolutionary fuzzy decision model for construction management using support vector machine. Expert Systems with Applications, 37(8), 6061–6069.

Cheng, M.-Y., & Wu, Y.-W. (2009). Evolutionary support vector machine inference system for construction management. Automation in Construction, 18(5), 597–604.

Cheng, M.-Y., Peng, H.-S., Wu, Y.-W., & Chen, T.-L. (2010). Estimate at Completion for construction projects using Evolutionary Support Vector Machine Inference Model. Automation in Construction, 19(5), 619–629.

Choi, C. K., and Choi, I. H. (1993). An Expert System for Selecting Types of, Computers & Structures, 48(2), 183–192.

Choi K. K., Yu X. and Chang K. (1996). A Mixed Design Approach for Probabilistic Structural Durability. 6th AIAA/ USAF/NASA/ ISSMO Symposium on Multidisciplinary Analysis and Optimization, Bellevue, WA., 785–795

Chua, D. K. H., Asce, M., & Li, G. M. (2002). RISim : Resource-Interacted Simulation Modeling in Construction, Journal of Construction Engineering and Management, 128 (3), 195–202.

Cornell, C.A. (1969). A Probability Based Structural Code, Journal o f the Demetriu, S., & Mierlus-mazilu, I. (2003). Determination of Reliability Bounds for Structural Systems, An. St. Univ. Ovidius Constanta, 11 (2), 171–182.

Cossan-X Software (2014), Institute for Risk and Uncertainty, University of Liverpool, Chadwick Building, Peach Street, Liverpool, L69 7ZF, United Kingdom, http://cossan.co.uk/software/cossan-x_developments.php

Deng, Y. (2012). Efficient Prestressed Concrete-Steel Composite Girder for Medium-Span Bridges, PhD Thesis, University of Nebraska.

Der Kiureghian, A. (1989). Measures of structural safety under imperfect sates of knowledge. Journal of Structural Engineering, 115(5), 1119–1140.

Ditlevsen, O. (1979). Narrow Reliability Bounds for Structural Systems. Journal of Structural Mechanics, 7(4), 453–472.

Ditlevsen, O., & Madsen, H. O. (2007). Structural Reliability Methods. John Wiley & Sons Ltd, Chichester.

Doriani, A. (2012). Simulation - Based 4D Modeling for Planning and Scheduling of Elevated Urban Highway Reconstruction Projects, MASC Thesis, Department of Building, Civil , and Environmental Engineering ,Concordia University, Montreal , Quebec , Canada.

Dreo J, Petrowsky A, Siarry P, and Taillard E. Metaheuristics for hard optimization. Methods and case studies. Berlin, Heidelberg: Springer; 2006.

Du, J. S., & Au, F. T. K. (2005). Deterministic and reliability analysis of prestressed concrete bridge girders: Comparison of the Chinese, Hong Kong and AASHTO LRFD Codes. Structural Safety, 27(3), 230–245.

Elderton W.P. and Johnson N.L., Systems of frequency curves, Cambridge University Press, ISBN 10: 0521073693 / ISBN 13: 9780521073691

Ellingwood, B. R. (1977). Statistical Analysis of RC Beam Column Interaction, Journal of the Structural Division, ASCE, Vol. 103, No. ST7, Proc. Paper 13061, pp. 1377-1388.

Ellingwood, B. R. (1978). Reliability Bases o f Load and Resistance Factors for Reinforced Concrete Design, NBS Building Science Series 110, Washington,D.C.

Ellingwood, B. R. (1979a). Reliability of Current Reinforced Concrete Design, Journal of the Structural Division, ASCE, Vol. 105, No. ST4, pp. 699-712.

Ellingwood, B. R. (1979b). Reliability Based Criteria for Reinforced Concrete Design, Journal of the Structural Division, ASCE, Vol. 105, No. ST4, pp.713-727.

Ellingwood, B. R. and Culver, C. (1977). Analysis of Live Load in Office Buildings, Journal of the Structural Division, ASCE, Vol. 103, No. ST8, pp.1551-1560.

Ellingwood, B. R., and Ang, A. H-S. (1974). Risk Based Evaluation of Design Criteria, Journal of Structural Division, Proceedings of ASCE, Vol. 100, ST9, pp. 1771-1787.

Ellingwood, B., Galambos, T. V., MacGregor, J. G. and Cornell, C. A. (1980). Development of a Probability Based Load Criterion fo r American NationalStandard A58, NBS Special Publication 577, Washington, D.C.

Farkas, A. (2011). Multi-Criteria Comparison of Bridge Designs. Acta Polytechnica Hungarica, 8(1), 173–191.

Feng, C.-W., & Wu, H.-T. (2006). Integrating fmGA and CYCLONE to optimize the schedule of dispatching RMC trucks. Automation in Construction, 15(2), 186–199.

Feng, C.-W., Cheng, T.-M., & Wu, H.-T. (2004). Optimizing the schedule of dispatching RMC trucks through genetic algorithms. Automation in Construction, 13(3), 327–340.

Fu, M. (2001). Simulation optimization. Proceedings of the Winter Simulation Conference, 53–61

Fu, M. C., Glover, F. W., & April, J. (2005). Simulation optimization: a review, new developments, and applications. Simulation Conference, 2005 Proceedings of the Winter, 13 pp.

Galambos, T. V. and Ravindra, M. K. (1973). Tentative Load and Resistance Factor Design C riteria for Steel Buildings, Structural Division Research Report No. 18, Washington University, St. Louis, Missouri.

Galambos, T.V ., Ellingwood, B., MacGregor, J.G ., and Cornell, C.A. (1982). Probability Based Load Criteria: Assessment of Current Design Practice, Journal of Structural Division, proceedings of ASCE, Vol.108, ST5, pp 959-977.

Ghani, S. N. (2008). "User's guide to subroutine EVOP." http://www.OptimumSystemDesigners.com

Glover F. and Laguna M., (1997), Tabu search, Kluwer Academic Publishers, Bostun.

Glover F., & Kelly, J. P. (2000). Fundamentals of scatter search, Control and Cybernetics, 29 (3), 653-684.

Goldberg D. E., Deb, K., Kargupta, H., & Harik, G. (1993). Rapid , Accurate Optimization of Di cult Problems Using Fast Messy Genetic Algorithms, IlliGal Report No. 93004, Illinois Genetic Algorithm Laboratory, University of Illinois at Urbana-Champaign, Urbana, IL 61801.

Gosavi A. (2015). Simulation-based optimization: Parametric optimization techniques and reinforcement learning, Second Edition, Springer New York-USA, ISBN 978-1-4899-7491-4 (eBook).

Halpin, D. W. (1985), "Financial and cost Concepts for Construction Management," 1st Edition, Wiley, John & Sons, Incorporated.

Hambly E. C. (1991). Bridge Deck Behaviour, Second Edition, CRC Press, ISBN-13: 978-0419172604.

Han, S. H. (1995). Application of Dcoc to optimum prestressed concrete beam design, Engineering Optimization, 25 (3), 179–200.

Hao, G., Liang, X., and Zhang, S. (2013). The new approximate calculation method for the first order reliability, Applied Mechanics, 2013, 4, 505–509.

Hasofer, A. M., and Lind, N.C. (1974). Exact and Invariant Second Moment Code Format, Journal o f Engineering Mechanics, ASCE, 100, EM I, pp. 111-121.

Hassanain M. A. and Loov R. E. (2003). Cost optimization of concrete bridge Infrastructure, Canadian Journal of Civil Engineers, 30: 841–849.

Hertz D. B. and Thomas H., 1983, Risk analysis and its applications, New York, NY: John Wiley & Sons Inc. (reprinted 1984).

Hohenbichler, B. M., & Rackwitz, R. (1989). Nonnormal dependent vectors in structural reliability, ASCE Journal of Engineering Mechanics,114(12), 2195–2199.

Hohenbichler, M. and R. Rackwitz (1983). First Order Concepts in System Reliability, Structural Safety, Vol. 1, pp. 177-188.

Holm.L, Schaufelberger J. , Griffin D. , Cole T. (2005) "Construction Cost Estimating", Process and Practices", Prentice Hall.

Hong, N. K., Chang, S. P., & Lee, S. C. (2002). Development of ANN-based preliminary structural design systems for cable-stayed bridges. Advances in Engineering Software, 33(2), 85–96.

Hong, N. K., Chang, S.-P., & Lee, S.-C. (2002). Development of ANN-based preliminary structural design systems for cable-stayed bridges. Advances in Engineering Software, 33(2), 85–96.

Hurtado J. and Barbat A. 1997. Chapter 6. Simulation methods in stochastic mechanics. In Computational stochasticmechanics in ameta-computing perspective. Editor: J.Marczyk. CIMNE. Barcelona, Spain.

Huseby, A. B., Naustdal, M., and V, I. D. (2004). System Reliability Evaluation Using Conditional Monte Carlo Methods, Statistical Research Report No. 2, Mathematical Department, University of Oslo, 1–27.

Hwang, E.-S., and Nowak, A. S. (1991). Simulation of Dynamic Load for Bridges, Journal of Structural Eng.,117(5), 1413–1434.

Iman, R. L. & Conover, W. J. (1982). A Distribution-Free Approach To Inducing Rank CORRELATION AMONG INPUT VARIABLES. Web-link:

Ismail, M., Ikhouane, F., & Rodellar, J. (2009). The Hysteresis Bouc-Wen Model, a Survey. Archives of Computational Methods in Engineering, 16(2), 161–188.

Jiang C., Zhang W., Wang B., and Han X. (2014). Structural Reliability Analysis Using a Copula-Function-based Evidence Theory Model. Computers and Structures, 143, 19-31.

Jun Y. (2007). Enjoy the joy of copulas: with a package copula. Journal of Stat Softw, 21(4):1–21.

Jutte B., 2012, Project risk management handbook, Mount Everest from Gokyo Ri, ISBN: 978-1-4691-3271-6.

Karsak, E. E. (2004). Fuzzy multiple objective decision making approach to prioritize design requirements in quality function deployment. International Journal of Production Research, 42(18), 3957–3974.

Khorasani, N. E. (2010). Sysytem-Level Structural Reliability of Bridges, MASC Thesis, Department of Civil Engineering, University of Toronto.

Kim J. B., Kim R. H., and Eberle J. R. (2013). Simplified LRFD Bridge Design, Taylor & Francis Group LLC., FL-USA.

Kim, S., and Nowak, A. S. (1997). Load distribution and impact factor for I-Girder bridges, Journal of Bridge Engineering, 2, 97–104.

Kirkpatrick, S., Gelatt, C. D., and Vecchi, M. P. (1983). Optimization by Simulated Annealing. Science, 220(4598), 671–680.

Kiureghian, A. Der, Lin, H., and Hwang, S. (1988). Second-order reliability approximations. Journal of Engineering Mechanics, 113(8), 1208–1225.

Koch P. N. and Kodiyalam S. (1999). Variable Complexity Structural Reliability Analysis for Efficient Reliability-Based Design Optimization. 40th AIAA/ASME/ASCE/AHS/ASC

Structures, Structural Dynamics, and Materials Conference, St. Louis, Missouri, 68–77. AIAA-99-1210.

Koch P.N., Wujek B. and Golovidov O. (2000). A Multi-Stage Parallel Implementation of Probabilistic Design Optimization in an MDO Framework. 8th AIAA/USAF/NASA/ISSMO Symposium on Multidisciplinary Analysis and Optimization, Long Beach, CA., AIAA-2000-4805.

Koch P.N., Yang R. J. and Gu L. (2004). Design for Six Sigma Through Robust Obtimization. Struct Multidisc Optim 26, 235–248.

Kwak, J., Choi, G., Park, N., Seo, H., and Kang, L. (2011). 4D CAD Application Examples and Directions for Development in Civil Engineering Projects, 13, 163–167.

Laguna M. (1997), Optimization of complex systems with OptQuest, Graduate School of Business Adminstration, University of Colorado, Boulder, CO 80309-0419.

Laguna M. and Marti R. (2002), Neural network prediction in a system for optimizing simulations, IIE Transaction, 34, 273-282.

Laman, J. A., and Nowak, A. S. (1996). Fatigue-load models for girder bridges, J. Struct. Eng., 122: 726–733.

Laman, J. A. (1995). Fatigue load models for girder bridges, PhD dissertation, Universiy of Michigan at Ann Arbor, Michigan-USA.

Law, A. M. and Mccomas, M. G., (2002). Simulation-Based Optimization. Optimization, Proceedings of the Winter Simulation Conference, (1), 41–44,Tuucson, USA.

Lee O.S. and Kim D.H. (2006), The reliability estimation of pipeline using FORM, SORM and Monte Carlo simulation with FAD, Journal of Mechanical Science and Technology, 20; 12: 2124-2135.

Lee, A., & Wu, S. (2005). VISCON : Computer visualization support for constructability, Proceedings of the IT Conference Vol. 10, 69–83, UK.

Lee, G., & Eastman, C. (2008). Benefits and lessons learned of implementing building virtual design and construction (VDC) technologies for coordination of mechanical , electrical , and plumbing (MEP) systems on a large healthcare project, 13 (September 2007), 324–342.

Lehký, D., Keršner, Z., & Novák, D. (2012). Determination of statistical material parameters of concrete using fracture test and inverse analysis based on FraMePID-3PB tool, Proceedings of the 5th International Conference on Reliable Engineering Computing , 261–270.

Liapi, K. A. (2003). 4D Visualization of highway construction projects 3D graphical modeling framework for visualization, Proceedings of Seventh International Conference on Information Visualization, (IV'03) 1093-9547/03, IEEE.

Lorefice, R., Etse, G., & Carol, I. (2008). Viscoplastic approach for rate-dependent failure analysis of concrete joints and interfaces. International Journal of Solids and Structures, 45(9), 2686–2705.

Lounis, Z., & Cohn, M. Z. (1993). Multiobjective Optimization of Prestressed Concrete Structures. Journal of Structural Engineering, 119(3), 794–808.

Love, P.E.D. , Skitmore, M. & Earl, G. Selecting a suitable procurement method for a building project. Construction Management and Economics (1998) **16**, 221- 233.

MacGregor, J. G., (1976). Safety and lim it states design of Reinforced Concrete,Canadian Journal of Civil Engineering, 3, pp. 484-512.

Madhkhan, M., Kianpour, a, & Harchegani, M. E. T. (2013). Life-Cycle Cost Optimization of Prestressed Simple-Span Concrete Bridges With Simple and Spliced-Girders. Iranian Journal of Science and Technology-Transactions of Civil Engineering, 37, 53–66.

Madsen H.O., Krenk S. and Lind N.C. Methods of structural safety, 2006, Dover Publications, Inc, New York.

Mahadevan S. and Halder A. (2000). Reliability assessment using stochastic finite element analysis, John Whiley & Sons.

[Mahadevan S. and Halder A. (2000). Probability, reliability and statistical methods in engineering design, John Whiley & Sons.

Mahadevan, S., Zhang, R., & Smith, N. (2001). Bayesian networks for system reliability reassessment. Structural Safety, 23(3), 231–251.

Manzoor S. and Ahmed S. (2013). Characteristics of Grade 60 and Grade 72.5 Re-bars in Pakistan. International Journal of Modern Engineering Research (IJMER),3 (2): 667-673.

Martí, J. V., & González-Vidosa, F. (2010). Design of prestressed concrete precast pedestrian bridges by heuristic optimization. Advances in Engineering Software, 41(7-8), 916–922.

Martí, J. V., Gonzalez-Vidosa, F., Yepes, V., & Alcalá, J. (2013). Design of prestressed concrete precast road bridges with hybrid simulated annealing. Engineering Structures, 48, 342–352.

Mawlana M., and Hammad A., (2013). Framework for selecting a construction scenario for bridges using simulation-based optimization, Proceedings of the Canadian Society for Civil Engineers annual conference CSCE 2013, Quebec, Canada.

Mawlana, M., Hammad, A., Doriani, A., & Setayeshgar, S. (2012). Discrete event simulation and 4D modelling for elevated highway reconstruction projects, Proceedings of the XIVth International Conference on Computing in Civil and Building Engineering, Moscow State University of Civil Engineering.

Mccahilp, B. D. F., & Bernold, L. E. (1994). Resource-oriented modeling and simulation, Journal of Construction Engineering and Management, 119(3), 590–606.

McCloud, T., Bourgouin, P. and Greenberg R (1992). Bronchogenic carcinoma analysis of staging in the mediastinum with CT by correlative lymph node mapping and sampling. Radiology;183:319.

Melchers, R. E. (1987). Structural Reliability Analysis and Prediction, John Wiley &: Sons, Toronto, Canada.

Miao, F., & Ghosn, M. (2011a). Modified subset simulation method for reliability analysis of structural systems. Structural Safety, 33(4-5), 251–260.

Miao, F., & Ghosn, M. (2011b). Modified subset simulation method for reliability analysis of structural systems. Structural Safety, 33(4-5), 251–260.

Miao, T. J., & Chan, T. H. T. (2002). Bridge live load models from WIM data. Engineering Structures, 24(8), 1071–1084.

Miles, J. C., & Moore, C. J. (1991). An expert system for the conceptual design of bridges. Computers & Structures, 40(l), 101–105.

Mirza, S. A. (1996). Reliability-based design of reinforced concrete columns. Structural Safety, 18(2-3), 179–194.

Mirza, S. A., and MacGregor, J. G.(1979). Variations in Dimensions of Reinforced Concrete Members, Journal o f Structural Division, Proceedings of ASCE, Vol.105, No.ST4, pp. 751-765.

Mirza, S. A., Kikuchi, D. K., and MacGregor, J. G. (1980). Flexural Strength Reduction Factor fo r Bonded Prestressed Concrete Beams, Journal of ACI, pp.237-246.

Mitteau J. C. (1996), Error estimates for FORM and SORM computations of failure probability, proc. Speciality Conf. Probabilistic Mechanics and Structural Reliability, Worcester, MA, ASCE, 562-565.

Morcous, G., & Akhnoukh, A. (2007). Reliability analysis of NU girders designed using AASHTO, ASCE Structures Congress: New Horizon and Better Practices,1–11.

Morgan M. G. and Henrion M., 1990, Uncertainty: a guide to dealing with uncertainty in quantitative risk and policy analysis, Cambridge, UK: Cambridge university press.

Mori, Y., & Kato, T. (2003). Multinormal integrals by importance sampling for series system reliability. Structural Safety, 25, 363–378.

Naylor T. et al. 1996, Computer simulation techniques.New York: JohnWiley & Sons, Inc, Nebro A. J., Luna F., Alba E., Dorronsoro B., Durillo J. J. and Beham A. (2008). AbYSS: Adapting Scatter Search to Multiobjective Optimization, IEEE Transactions on Evolutionary Computation, VOL. 12, NO. 4: 439-457.

Nilson, A.H., Darwin D and C.W. Dolan. (2010). Design of Concrete Structures, 14th Edition, John Wiley & Sons, Inc,.

Noch P. N. (2002). Probabilistic Design: Optimization for Six Sigma Quality. 43rd AIAA/ASME/ASCE/AHS/ASC Structures, Structural Dynamics, and Materials Conference 22-25 April 2002, Denver, Colorado.

Noh Y., Choi K. K. and Lee I. (2011). Reliability-based design optimization with confidence level under input model uncertainty due to limited test data. Struct Multidiscip Optim 43:443–58.

Nonaka, T., Clifton, R. J., & Okazaki, T. (1996). Longitudinal elastic waves in columns due to earthquake motion, Int. J. Impact Engng. 18 (96), 889–898.

Novák, D., & Lehký, D. (2006). ANN inverse analysis based on stochastic small-sample training set simulation. Engineering Applications of Artificial Intelligence, 19(7), 731–740.

Nowak, A. (2004). System reliability models for bridge structures. Technical Sciences, 52(4), 321–328

Nowak, A. S. (1993). Live load model for highway bridges. Structural Safety, 13(June 1994), 53–66.

Nowak, A. S. (1996). Calibration of LRFD bridge code, Journal of Structural Engineering, 121(8), 1245–1251.

Nowak, A. S., Park, C.-H., & Casas, J. R. (2001). Reliability Analysis of Prestressed Concrete Bridge Girders: Comparison of Eurocode, Spanish Norma IAP and AASHTO LRFD. *8th American Society of Civil Engineers Joint Conference on Probabilistic Methods and Structural Reliability*, 23(4): 331–344.

Nowak, A. S., & Rakoczy, A. M. (2012). Reliability-Based Calibration of Design Code for Concrete Structures Load and Resistance Model – General Information. 54 Congresso Brasileiro Do Concreto, (Aci 318), 1–12.

Nowak, A. S., & Rakoczy, P. (2013). WIM-based live load for bridges. KSCE Journal of Civil Engineering, 17(3), 568–574.

Nowak, A. S., & Szerszen, M. (2002). Reliability-based calibration of the design code for concrete structures, (1998), 91–99.

Nowak, A. S., and Szerszen, M. M. (1998). Bridge load and resistance models. Engineering Structures, 20(11), 985–990.

Nowak, A. S., and Szerszen, M. M. (2000). Structural reliability as applied to highway bridges. Progress in Structural Engineering and Materials, 2(2), 218–224.

Nowak, A. S., and Zhou, J. (1990). System reliability models for bridges, Structural Safety, 7, 247–254.

Nowak, A. S., and Collins K. R., 2000, Reliability of Structures, McGraw-Hill International Editions, Civil Engineering Series, Singapore, 2000

Nowak, A. S., Park, C.-H., & Casas, J. R. (2001a). Reliability analysis of prestressed concrete bridge girders: Comparison of Eurocode, Spanish Norma IAP and AASHTO LRFD. Papers Presented at the 8th American Society of Civil Engineers Joint Conference on Probabilistic Methods and Structural Reliability, 23(4), 331–344.

Nowak, A. S., Park, C.-H., & Casas, J. R. (2001b). Reliability analysis of prestressed concrete bridge girders: Comparison of Eurocode, Spanish Norma IAP and AASHTO LRFD. Papers Presented at the 8th American Society of Civil Engineers Joint Conference on Probabilistic Methods and Structural Reliability, 23(4), 331–344.

Nowak, A. S., Rakoczy, A. M., Szeliga, E., (2011). Revised statistical resistance models for R/C structural components, ACI SP honoring Andy Scanlon.

Nowak, A. S., Szerszen, M.,2012, Calibration of design code for buildings (ACI 318): Part 1&2, ACI Structural Journal, V.100, No.3, May 2003, pp.377-382.

Nowak, A.S. and Rakoczy, A.M., 2010, Statistical parameters for compressive strength of light-weight concrete, Concrete Bridge Conference, PCI, Phoenix, AZ,

Nowak, A.S. and Szersen, M.M. (2008), Reliability-based calibration for structural concrete, Phase 3, PCA R&D Seial No. 2849

O'Brien, W. J., Gau, P., Schmeits, C., Goyat, J., & Khwaja, N. (2012). Benefits of Three- and Four-Dimensional Computer-Aided Design Model Applications for Review of Constructability. Transportation Research Record: Journal of the Transportation Research Board, 2268(-1), 18–25.

O'Hagan A., 2006, Uncertain Judgements : Eliciting Experts' Probabilities, Chichester John Wiley & Sons, Ltd.

Oberkampf W.L., Deland S.M., Rutherford B.M., Diegert K.V., and Alvin K.F., 2000, Estimation of total uncertainty in modeling and simulation, Technical Report SAND2000-0824, Sandia National Laboratories, April 2000.

Ólaffson, S. 2005. Metaheuristics. Chapter 22 in Handbooks in Operations Research and Management Science: Simulation, S.G. Henderson and B.L. Nelson, eds., Elsevier.

OPTTEK System Inc. 2012, 2241 17th Street, Boulder, Colorado, USA, http://www.opttek.com/

Otero, R. P.(1993.). STIMS-MEDTOOL: Integration of Expert Systems with Systems Modelling and Simulation, Proceedings of Third International Workshop on Computer Aided Systems Theory, Las Palmas, Spain, February 22-26.

Padmanabham D., 2011, Reliability-based optimization for multidisplinary system design, VDM Verlag Dr. Muller Gmbh & Co. KG, ISBN: 978-3-639-24184-6.

Panesar D.K. and Bartlett F.M. (2006). Assessment of Precast Stringer Highway Bridges using Mean Load Method, Canadian Journal of Civil Engineering, 33(11):1359-1367.

Panesar D. K. and Bartlett, F.M. (2006). Load and Resistance Data for Precast Stringer Highway Bridges, Canadian Journal of Civil Engineering, 33(11):1368-1378.

Park, M., Kim, W.-Y., Lee, H.-S., & Han, S. (2011). Supply chain management model for ready mixed concrete. Automation in Construction, 20(1), 44–55.

Patelli, E., Pradlwarter, H. J., & Schuëller, G. I. (2011). On multinormal integrals by Importance Sampling for parallel system reliability. Structural Safety, 33(1), 1–7.

Peurifoy, R. L. and Oberlender, G. D. (2002), "Estimating Construction Costs" 5th Edition, McGraw-Hill, New York.

Pratt, D.J. (2004). "Fundamentals of Construction Estimating." 3rd edition, Delmar, Cengage Learning, USA.

Precast/Prestressed Concrete Institute (PCI). (2003). PCI bridge design manual, Chicago - USA.

Rackwitz, R. (2000). Reviewing probabilistic soils modelling. Computers and Geotechnics, 26(3–4), 199–223.

Rad, P. F. (2001), "Project Estimating and Cost Management," 1st Edition, Management Concepts, Inc.

Raina V. K., 2007, Concrete bridge practice: analysis, design and economics, 3rd edition, Shroff Publishers and Distributors Pvt. Ltd.

RAKOCZY, A.M. and NOWAK, A. S.,2012, Resistance Model of Lightweight Concrete Members, ACI Structural Journal, 2012.

Rana, S., Ahsan, R., & Ghani, S. N. (2010). Design of prestressed concrete I-girder bridge superstructure using optimization algorithm, IABSE-JSCE Joint Conference on Advances in Bridge Engineering-II, 978–984, Dhaka, Bangladesh.

Rana, S., Islam, N., Ahsan, R., & Ghani, S. N. (2013). Application of evolutionary operation to the minimum cost design of continuous prestressed concrete bridge structure. Engineering Structures, 46, 38–48.

Raphel J.M., 1984, Tensile strength of concrete, J. Am. Concr. Inst. 81 (2), 158-165

Ravindra, M. K.,Lind, N. C., and Siu, W. (1974). Illustrations of Reliability Based Design. Journalof Structural Division, ASCE, Vol. 100, No. ST9, pp. 1789-1811.

Rosenblatt, M. (1952). Remarks on a Multivariate Transformation, Annals of Mathematical Statistics, Vol. 23, pp. 470-472.

Salvadori G. and Michele C. D. (2007). On the use of copulas in hydrology: theory and practice, Journal of Hydrol Eng, 12 (4):369–80.

Schroeder R. G., Linderman K., Liedtke C. and Choo A. S. (2008). Six Sigma: Definition and Underlying Theory. Journal of Operations Management, 26, 536-554.

Schuëller, G. I., Pradlwarter, H. J., & Koutsourelakis, P. S. (2004). A critical appraisal of reliability estimation procedures for high dimensions. Probabilistic Engineering Mechanics, 19(4), 463–474.

Sharda R. and Rampal R. (1995). Neural Network and Management Science/Operations Research. Oklahoma State University, USA, http://catt.okstate/itorms/guide/nnpaper.html

Shinozuka, M. (1983). Basic Analysis of Structural Safety, Journal of Structural Division, ASCE, Vol. 3, 109.

Sirca, G. F., & Adeli, H. (2005). Cost Optimization of Prestressed Concrete Bridges. Journal of Structural Engineering, 131(3), 380–388.

Siriaksorn, A. (1980). Serviceability and Reliability Analysis o f Partially Prestressed Concrete Beams, PhD thesis, D epartm ent of M aterial Engineering, University of Illinois at Chicago Circle.

Siu, W. W. C., Parim i, S. R. and Lind, N. C. (1975). Practical Approach to Code Calibration, Journal of the Structural Division, ASCE, Vol. 101, No. ST7, pp. 1469-1480.

Song, J., & Kiureghian, A. Der. (2003). Bounds on System Reliability By Linear Programming. Journal of Engineering Mechanics, ASCE, , 129(June), 627–636.

Srinivas, V., & Ramanjaneyulu, K. (2007). An integrated approach for optimum design of bridge decks using genetic algorithms and artificial neural networks. Advances in Engineering Software, 38(7), 475–487.

Srinivas, V., & Ramanjaneyulu, K. (2007). An integrated approach for optimum design of bridge decks using genetic algorithms and artificial neural networks. Advances in Engineering Software, 38(7), 475-487.

Steinberg, E. (2010). Structural reliability of prestressed UHPC flexure models for bridge girders. Journal of Bridge Engineering, 15(February), 65–72.

Stewart, R. D., (1982). “Cost Estimating,” 1st Edition, John Wiley and Sons Inc.

Structures, B. (1995). Genetic Algorithm to Aesthetic Design. Microcomputers in Civil Engineering, 10, 415–421.

Tang X. S., Li D. Q., Zhou C. B., Phoon K. K., and Zhang L. M. (2013). Bivariate distribution models using copulas for reliability analysis. Journal of Risk and Reliability, Proc IMechE Part O, 1-14.

Tang X. S., Li D. Q., Zhou C. B., Phoon K. K., and Zhang L. M. (2013). Impact of Copulas for Modelling Bivariate Distributions on System Reliability. Structural Safety, 44, 80-90.

Thanedar, P. B. and Kodiyalam, S. (1991). Structural Optimization Using Probabilistic Constraints. AIAA/ASME/ACE/AHS/ ASC Structures. Structural Dynamics and Materials Conference, AIAA-91-0922-CP, 205–212.

Thoft-Cristensen P. and Baker M., 1982, Structural reliability theory and its applications, John Wiley &: Sons, Toronto, Canada.

Thunnissen, D. P. (2003). Uncertainty Classification for the Design and Development of Complex Systems. 3rd Annual Predictive Methods Conference, 16.

Vahdatikhaki, F., Zhang, C., Mawlana, M., and Doriani, A. (2012). Towards the smart construction site: Improving productivity and safety of construction projects using multi-agent systems, Real-time simulation and automated machine control, Proceedings of the 2012 Winter Simulation Conference C. Laroque, J. Himmelspach, R. Pasupathy, O. Rose, and A.M. Uhrmacher, eds, 3687–3698.

Vlahinos A. and Kelkar S. G. (2002). Designing for Six-Sigma Quality with Robust Optimization Using SAE. Proceedings of the 2002 SAE International Body Engineering Conference and Automotive & Transportation Technology Conference on CD-ROM (IBAT2002CD).

Vose D. (2009), Risk analysis: A quantitative guide, 3rd edition, John Wiley & Sons, Ltd., England.

Wang, J. (1999). Fuzzy outranking approach to prioritize design requirements in quality function deployment. International Journal of Production Research, 37(4), 899–916.

Westney, R. E., (1997). "The Engineer's Cost Handbook Tools for Managing Project Costs" , Marcel Dekker, Inc.

Winston, P. H., 1984, Artificial intelligence, 2nd ed., Addison-Wesley, Reading, M.A.

Wood, W. H., & Agogino, A. M. (1996). Case-based conceptual design information server for concurrent engineering. Computer Aided Design, 28(5), 361–369.

Wu, S., Chen, X., & Zhou, J. (2012). Tensile strength of concrete under static and intermediate strain rates: Correlated results from different testing methods. Nuclear Engineering and Design, 250, 173–183.

Xiao Q., Sues R. H. and Rhodes G. S. (1999). Multi-Disciplinary Wing Shape Optimization with Uncertain Parameters. 40th AIAA/ASME/ASCE/ AHS/ASC Structures, Structural Dynamics, and Materials Conference, St. Louis, Missouri,3005–3014. Paper No. AIAA-99-1601.

Xu, L., Li, Z., Li, S., & Tang, F. (2005). A polychromatic sets approach to the conceptual design of machine tools. International Journal of Production Research., 43(12), 2397–2421.

Youssef, M. a., Anumba, C. J., & Thorpe, T. (2005). Intelligent Selection of Concrete Bridge Construction Methods in Egypt. Computing in Civil Engineering (2005), 1–14.

Yuan, X.-X., & Pandey, M. D. (2006). Analysis of approximations for multinormal integration in system reliability computation. Structural Safety, 28(4), 361–377.

Zhang, H., Tam, C. M., Li, H., & Shi, J. J. (2006). Particle swarm optimization-supported simulation for construction operations, Journal of Construction Engineering and Management, (December), 1267–1274.

Zuev, K. M., Beck, J. L., Au, S.-K., & Katafygiotis, L. S. (2012). Bayesian post-processor and other enhancements of Subset Simulation for estimating failure probabilities in high dimensions. Computers & Structures, 92-93, 283–296.

Appendix A

Development of Reliability Computational Methods

A.1 Background

In the current research, different reliability methods are applied to assess the probability of failure and corresponding reliability index with respect to structural components as well as the overall structural system. For individual component's reliability, the *First-Order Reliability method* FORM is utilized, while for system reliability, the method of *Improved Reliability Bounds of Structural System* is adopted. Alternatively, the *Monte Carlo Simulation* MCS technique is also applied. In this Chapter, the development of these reliability methods is demonstrated.

A.2 First-Order Reliability Method (FORM)

In general, the limit state function can be expressed as follows (Melchers, 1987):

$$\mathrm{g}\,(\mathrm{X}) = \mathrm{g}(x_1, x_2\,, \dots \dots., x_n) \tag{A.1}$$

where x_i denote the resistance and load parameters considered as random variables, and g (.) is a function that relates these variables for the limit state under consideration. The limit state (serviceability or ultimate state) is reached when:

$$\mathrm{g}(x_1, x_2\,, \dots \dots., x_n) \leq 0 \tag{A.2}$$

Using Taylor's series, the limit state function can be expanded provided that the first order terms are maintained. Hence, Eq. (A.2) can be rewritten as follows:

$$\mathrm{g}(x_1, x_2\,, \dots \dots., x_n) \approx \mathrm{g}(x_1{}^*, x_2{}^*\,, \dots \dots., x_n{}^*) + \sum_{i=1}^{n}(x_i - x_i{}^*)(\frac{\partial g}{\partial x_i})_{x^*} \tag{A.3}$$

where, $x_i{}^*$ is the linearization point at which the partial derivatives $(\frac{\partial g}{\partial x_i})$ are evaluated.

When the linearization point is set at the mean value, this reliability method is, sometimes, referred to as *Mean-Value First-Order Second-Moment* (MVFOSM) method (Hao et al., 2013). The mean and variance of the limit state function, respectively denoted as μ_m and σ_m, are approximated by

$$\mu_m \approx \mathrm{g}(\mu_1, \mu_2, \ldots \ldots, \mu_n) \quad \text{(A.4)}$$

$$\sigma_m \approx \sum_i \sum_j (x_i - x_i{}^*) \left(\frac{\partial g}{\partial x_i}\right)_{\overline{x^*}} \left(\frac{\partial g}{\partial x_i}\right)_{\overline{x_J}} \rho_{x_i, x_j} \, \sigma_{x_i} \, \sigma_{x_j} \quad \text{(A.5)}$$

where ρ_{x_i, x_j} is the correlation coefficient and the $(\frac{\partial g}{\partial x_i})_{\overline{x^*}}$, $(\frac{\partial g}{\partial x_i})_{\overline{x_J}}$ are the partial derivatives at the mean point, $\mu_n = E(x_i) = \overline{x_\iota}$.

The accuracy of Eqs. (A.4 and A.5) depends on the effect of neglecting the higher-order terms in Eq. (A.3).

For a limit state function (M), the standardized margin G_M (which has a zero mean and a unit standard deviation) can be calculated as

$$G_M = \frac{M - \mu_m}{\sigma_m} \quad \text{(A.6)}$$

Failure occurs when $M \leq 0$; hence, the probability of failure is

$$P_f = P(M \leq 0) = F_M(0) = F_{GM}\left(\frac{-\mu_m}{\sigma_m}\right) \quad \text{(A.7)}$$

Since the reliability index $= \frac{\mu_m}{\sigma_m}$, then

$$P_f = F_{GM}\ (-\,\boldsymbol{\beta}) \quad \text{(A.8)}$$

Three shortcomings are associated with the MVFSOM:

First, if the limit state function $\mathrm{g}(.)$, inaccurate results may exist at increasing distance from the linearization point by neglecting higher-order. Secondly, the method fails to be invariant to different equivalent formation of the same problem. By other words, the reliability index $\boldsymbol{\beta}$ depends on the formulation of the limit state equation. The third shortcoming is that the probability of failure is approximated in a standardized normal space while some of the random variables have non-normal distribution.

To solve the first two drawbacks, Hasofer and Lind (1974) suggested considering the linearization problem at some point on the failure surface, as an alternative to expanding Taylor's series about the mean point. The resistance and load variables, x_i , are transformed to standardized variables with zero mean and unit variance by

$$y_i = \frac{x_i - \mu_i}{\sigma_{x_i}} \tag{A.9}$$

The reliability index β (referred to as Hasofer-Lind reliability index) represents the shortest distance from the origin to the reduced (standardized) space. Let $\alpha_i{}^*$ be the linearized unit vector normal to the limit state surface at the design point and directed towards the failure set. This unit vector can be obtained as follows:

$$\alpha_i{}^* = \left(\frac{\partial g}{\partial y_i}\right)_{y_i{}^*} \Big/ \sqrt{\sum_i \left(\frac{\partial g}{\partial y_i}\right)^2_{y_i{}^*}} \tag{A.10}$$

All the derivatives in Eq. (A.12) are evaluated at the origin (design point). The reliability index can, then, be obtained as follows:

$$G(y_1{}^*, y_2{}^*, \ldots\ldots, y_n{}^*) = 0 \tag{A.11}$$

$$\boldsymbol{\beta} = -\frac{y_i{}^*}{\alpha_i{}^*} \tag{A.12}$$

The design point (or the most probable failure point) is obtained by an iterative search approach as a sequence of projected Newton steps. The design point x^* is obtained as the limit of sequence x^0, x^1,…. . This sequence is calculated as follows:

$$x^{(m+1)} = [x^{(m)}\alpha^{(m)} + \frac{g_x(x^{(m)})}{|\nabla g_x(x^{(m)})|}]\alpha^{(m)} \tag{A.13}$$

where, $\nabla g_x(x)$ is the gradient vector of $g_x(x)$ and can be obtained as follows

$$\nabla g_x(x) = (\frac{\partial g}{\partial x_1},\ldots, \frac{\partial g}{\partial x_n})^T \tag{A.14}$$

The iteration method to find the design point is illustrated in Figure A.1.

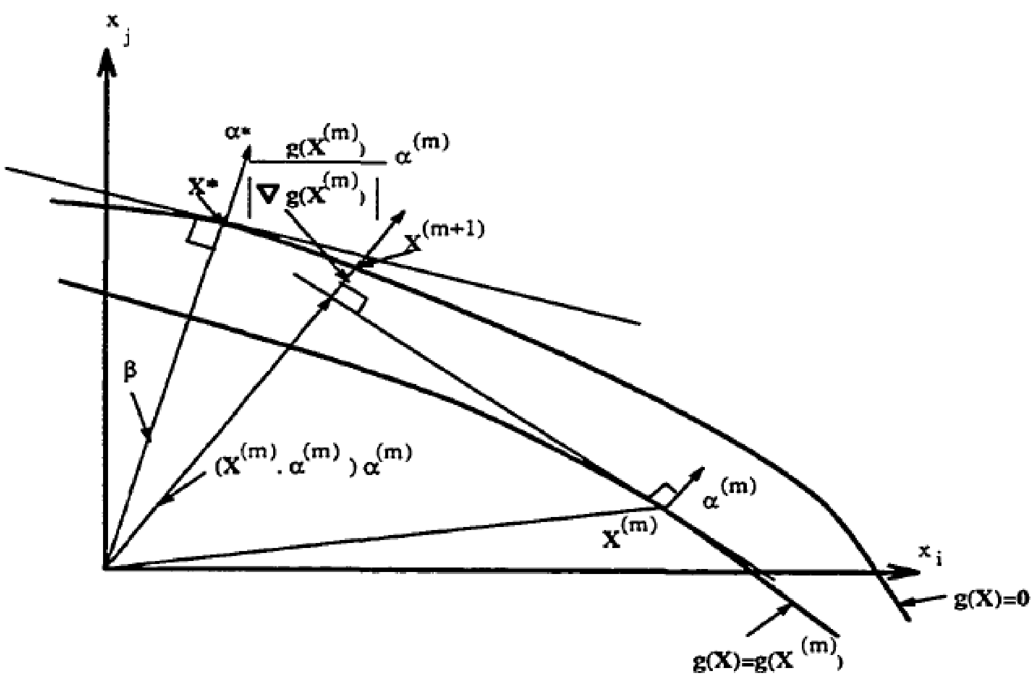

Figure A.1: Illustration of the methodology to find the design point (Rackwitz and Fiessler 1978).

The third shortcoming was overcome when Rackwitz and Fiessler (1978) suggested transforming the non-normal random variables into equivalent normal. By equating the cumulative distributions and the probability density functions of the actual distribution and the normal distribution, one can obtain the mean $\mu_x{}'$ and standard deviation $\sigma_x{}'$ of the equivalent normal variable:

$$F_x(x^*) = \Phi(\frac{x^*-\mu_x{}'}{\sigma_x{}'}) \tag{A.15}$$

$$f_x(x^*) = \frac{1}{\sigma_x{}'\sqrt{2\pi}} \exp[-0.5\ (\frac{x^*-\mu_x{}'}{\sigma_x{}'})^2]=\frac{1}{\sigma_x{}'}\varphi\{\Phi^{-1}[F_x(x^*)]\} \tag{A.16}$$

where, φ(.) denotes the standard normal probability density. Then $\mu_x{}'$ and $\sigma_x{}'$ can be calculated as follows:

$$\sigma_x{}' = \frac{\varphi\{\Phi^{-1}[F_x(x^*)]\}}{f_x(x^*)} \tag{A.17}$$

$$\mu_x{}' = x^* - \Phi^{-1}[F_x(x^*)]\,\sigma_x{}' \tag{A.18}$$

Eqs. (A.15) and (A.16) are only valid when the random variables are mutually independent. However, for cases were the variables are not mutually independent, Hohenbichler and Rackwitz (1983) recommended the application of *Rosenblatt Transformation* (Rosenblatt 1952):

$$x_1 = \Phi^{-1}[F_1(z_1)] \tag{A.19}$$

$$x_2 = \Phi^{-1}[F_2(z_2|z_1)] \tag{A.20}$$

T :

$$x_n = \Phi^{-1}[F_n(z_n|z_1, z_{2,} \ldots, z_{n-1})] \tag{A.21}$$

where $F_i(z_i|z_1, z_{2,} \ldots, z_{i-1})$ denotes the distribution function of Z_i conditional on ($Z_1 = z_i$, Z_2=z_2 , ….., Z_{i-1} =z_{i-1}) and can be calculated as:

$$F_i(z_i|z_1, z_{2,} \ldots, z_{i-1}) = \frac{\int_{-\infty}^{x_i} f_{Z_1,\ldots,Z_{i-1}}(z_1,\ldots,z_{i-1},t)d_t}{f_{Z_1,\ldots,Z_{i-1}}(z_1,\ldots,z_{i-1})} \tag{A.22}$$

Similarly, the inverse transformation can be calculated as

$$z_1 = F_1{}^{-1}((x_1)) \tag{A.23}$$

$$z_2 = F_2{}^{-1}((x_1|x_2)) \tag{A.24}$$

$\mathbf{T}^{-1}$:

$$z_i = F_i^{-1}[\Phi(x_i|z_1, z_{2,} \dots., \ z_{i-1})] \tag{A.25}$$

$$z_n = F_n^{-1}[\Phi(x_n|z_1, z_{2,} \dots., \ z_{i-1})] \tag{A.26}$$

Practically, the transformation $\mathbf{T}$ and $\mathbf{T}^{-1}$ should be calculated numerically. However, Ang and Tang (1984) suggested an approximate solution by conducting orthogonal transformation of the dependent variables into uncorrelated variables.

Let Z be a correlated vector of random variables with mean

$$\mathrm{E(Z)} = [\mathrm{E}(Z_1), \mathrm{E}(Z_2), \dots., \mathrm{E}(Z_n)\ ]^T \tag{A.27}$$

and covariance matrix

$$C_Z = \mathrm{cov}(Z_i, Z_j)_{mxn} = [\rho_{ij}\sigma_i\sigma_j]_{mxn} \tag{A.28}$$

When Z are uncorrelated, the covariance matrix will be strictly diagonal. An uncorrelated vector X and a linear transformation matrix A are now sought such that

$$X = AZ \tag{A.29}$$

or

$$\mathrm{A}^{-1}\,X = Z \tag{A.30}$$

In the case of orthogonal transformation, this implies that $\mathrm{A}^{-1} = \mathrm{A}^T$ and X are uncorrelated

$$C_x = \mathrm{cov}(X_i, X_j) \tag{A.31}$$

$$= \mathrm{cov}(X, \mathrm{X}^T) \tag{A.32}$$

$$= \mathrm{cov}(AZ, \mathrm{Z}^T \mathrm{A}^T) \quad \text{(A.33)}$$

$$= \mathrm{Acov}(Z, \mathrm{Z}^T)\mathrm{A}^T \quad \text{(A.34)}$$

$$= \mathrm{A}C_Z\mathrm{A}^T \quad \text{(A.35)}$$

To determine X as an uncorrelated vector, the matrix A which makes C_x diagonal is sought. Using standard techniques from linear algebra (e.g., based on eigenvalues and eigenvectors of C_Z), the matrix A can be obtained.

Now, the main steps to calculate structural reliabilities by the *Firs-Order Reliability Method*, FORM can be summarized as follows:

1. Define the limit state function.
2. Transform the random variables Z into uncorrelated and standardized normal variables X.
3. For random variables with non-normal distribution, determine equivalent normal mean ${\mu_{z_i}}^N$ and standard deviation ${\sigma_{z_i}}^N$.
4. Transform the limit state surface in z –space, $g(Z)$, into the corresponding limit state surface in x –space, $g(X)$.
5. Determine the gradient $\nabla g_x(X)$.
6. Determine the unit normal vector $\alpha^{(m)}$
7. Select initial design point, e.g., by setting$m = 0 , n = 0$
8. Find $g_x(X^{(m)})$,$\nabla g_x(X^{(m)})$, and $\alpha^{(m)}$.
9. Evaluate $\beta^{(m)}$= $({X^{(m)}}^T, X^{(m)})^{0.5}$
10. Determine next design point in x –space, $X^{(m+1)}$ as per Eq. (A.13)
11. Repeat steps 8 -10 until X and/or $\boldsymbol{\beta}$ stabilized.
12. A new iteration point to be calculated in z –space, $Z^{(n+1)}$

$$Z^{(n+1)} = X^{(m)}{\sigma_Z}^{(n)^N} + {\mu_Z}^{(n)^N} \quad \text{(A.36)}$$

13. Calculate new values of equivalent normal mean ${\mu_Z}^{(n)^N}$and standard deviation${\sigma_Z}^{(n)^N}$.

14. Repeat steps 8 – 12 until convergence.
15. Repeat steps 7 – 14 with using other estimation of failure point.
16. Compare $\boldsymbol{\beta}$ and select minimum $\boldsymbol{\beta}$.

The First Order Reliability, FORM, method is adopted in this current research to estimate the reliability index of the different modes of failure related to prestressed girder bridges.

A.3 Monte Carlo Simulation (MCS)

The Monte Carlo Simulation (MCS) method is, currently, considered as one of the most powerful techniques for analyzing complex systems (Ismail et al., 2009).

Monte Carlo simulation (MCS) techniques are implemented by randomly simulating a design or process, given the stochastic properties of one or more random variables, with a focus on characterizing the statistical nature (mean, variance, range, distribution type, etc.) of the responses (outputs) of interest (Koch 2004). Monte Carlo methods have long been recognized as the most equate technique for all estimations that need knowledge of the probability distribution of responses of uncertain systems to uncertain inputs. To utilize a MCS, a number of simulations cycles are generated by sampling values of random variables (uncertain inputs) using the probabilistic distributions and corresponding properties defined for each.

To apply the Monte Carlo simulation (MCS), the set of basic variables should have known or assumed probability distributions (Schueller, 2004). According to those probability distributions, a set of values of the basic random variables is generated using statistical sampling techniques. This process is repeated to generate several sets of sample data and, hence, many sample solutions can be obtained. Statistical analysis of the sample solutions is then performed (Miao and Ghosn, 2011).

Four main steps are involved in the Monte Carlo Simulation (MCS):

- Simulation of random variables.
- Using statistical sampling techniques to generate several sample data sets.
- Using the sampled data to generate solutions.
- Perform statistical analysis of the results.

The accuracy of the results obtained from the Monte Carlo simulation depends on the number of samples used. Hence, the results are not exact and are subject to sampling errors. Generally, the accuracy of the results increase as the sample size increases (Rackwitz, 2000).

Generating samples from a particular probability distribution is usually done by generating random numbers. These random numbers are treated as random variables uniformly distributed over the unit interval [0,1]. The generation of random numbers plays a key role in the generation of a set of values (realizations) of a random variable that has a probability distribution other than uniform probability law (Zuev et al., 2012).

To apply the Monte Carlo approach to structural reliability problems, the following tasks should be utilized (Svandal, 2014):

i. develop systematic methods for numerical 'sampling' of the basic random variables X.
ii. choose a suitable economical and reliable simulation technique or 'sampling strategy'.
iii. consider the effect of the complexity of calculating the limit state function $g(X)$ and the number of random variables on the simulation technique used.
iv. evaluate the number of 'sampling' required to obtain a reasonable estimate of failure probability P_f.
v. investigate the dependence between all or some of the random variables and decide how to deal with such dependency.

Let the limit state function be $g(X) = g(x_{1,}x_{2,} \dots.,x_n)$, where X is a vector of the basic design random variables. Then the failure state belongs to the region where $(X) \leq 0$, while $g(X) > 0$ represents the safe region. For every basic variable, a random sample, of values x_i , is generated numerically in accordance with its probability distribution using a random number generator. The generated sample values are then substituted in the limit state function. Then, a negative value of the limit state function means failure while a positive value means no failure. This process is repeated many times (large number of samples) in order to simulate the probability distribution of the limit state function $g(X)$. Then, the failure probability P_f can be evaluated from either of the following two methods:

- First method: the probability of failure is obtained by

$$P_f = P[g(X) \leq 0] = \lim_{N \to \infty} \frac{N_f}{N} \quad \text{(A.37)}$$

where N is the total number of simulations (trials) and N_f is the number of trials in which $g(X) \leq 0$.

The ratio N_f/N is usually very small and the estimated probability of failure is subjected to considerable uncertainty. As the variance of N_f/N depends, in particular, on the total number of simulations N, the uncertainty in estimating P_f decreases when N increases. The accuracy of Eq. (A.37) can be estimated in terms of its variance $\widehat{P_f}$. To determine the variance, assume that each simulation cycle is a Bernoulli trial with failure probability P_f. Therefore, the number of failed samples in N tests can be considered to follow a binomial distribution, which reveals the variance of the Monte Carlo method (Hurtado and Barbat, 1997),

$$\text{Var}(\widehat{P_f}) = \text{Var}(N_f/N) = (\frac{1}{N^2}) \text{ Var}(N_f) = \frac{NP_f(1-P_f)}{N^2} = \frac{P_f(1-P_f)}{N} \quad \text{(A.38)}$$

As is well known, the MCS estimator $\widehat{P_f}$ is considered unbiased (Hurtado and Barbat, 1997). Hence, the accuracy of the estimator is given by the coefficient of variation of $\widehat{P_f}$ (c.o.v. or δ), defined as the ratio of the standard deviation to the mean of $\widehat{P_f}$, given by,

$$\delta = \frac{\sqrt{\text{Var}(\widehat{P_f})}}{\widehat{P_f}} = \sqrt{\frac{1-\widehat{P_f}}{\widehat{P_f}N}} \quad \text{(A.39)}$$

- Second method: estimating the probability of failure, Thoft-Christensen and Baker (1982) suggested to start first with fitting an approximated probability distribution for $g(X)$ using the trial values. The estimated statistical moments (parameters) may be used in the fitting process. Elderton and Johnson (1969) suggested some distributions that are suitable for fitting the $g(X)$ data. The probability of failure is then obtained from

$$P_f = \int_{-\infty}^{0} f_M(m) \; dm \tag{A.40}$$

where $M = g(X)$ is a random variable representing the margin and $f_M(m)$ is its probability density function as estimated from the fitting process.

In reliability analysis and prediction, the Monte Carlo simulation method is excessively costly despite being robust to the type and dimension of the problem. In order to produce one sample in the failure domain it is necessary to generate a large number of samples lying in the safe domain. Moreover, MCS is time-consuming technique, particularly in problems with small probabilities ($P_f \leq 10^{-3}$), since it requires a large number of samples and evaluations of the systems to achieve a reasonable accuracy (Zuev et al., 2012). However, this was overcome with the development of high-speed processors, which reveal the Monte Carlo Simulation MCS technique as an attractive tool for probabilistic analysis. In this proposed research, the MCS is also adopted and utilized.

Appendix B

Simplified Modified Compression Field Theory for Shear Strength Prediction

The simplified version of the Modified Compression Field Theory MCFT is a methodology by which the shear strength of a reinforced concrete section can be conveniently estimated. This method was utilized, in Chapter Three, to derive the statistical parameters of the shear strength. For more details reference is made to Bentz et al. (2006). The shear resistance of a prestressed girder bridge is calculated assuming that the shear force is resisted only by the girder concrete and reinforcing steel (stirrups) due to the absence of draped strands.

As the section is in the flexural region of a beam, it is assumed that the clamping stresses f_z will be negligibly small, as illustrated in Figure B.1. In order for the transverse reinforcement to yield at failure, the transverse strain ε_z will need to be more than approximately 0.002, while to crush the concrete, ε_2 will need to be approximately 0.002. If ε_x is also equal to 0.002 at failure, then the maximum shear stress will be approximately $0.28f'_c$, whereas for very low values of ε_x, the shear stress at failure is determined to be approximately $0.32f'_c$.

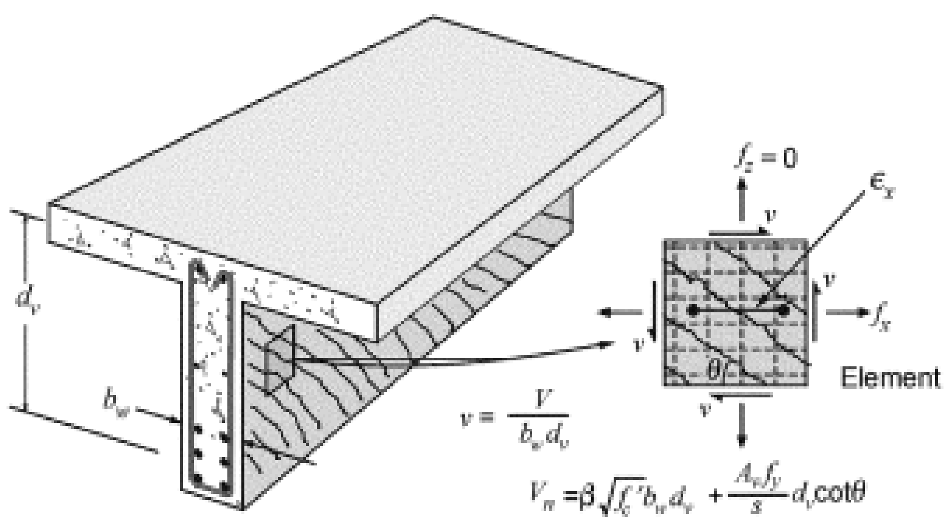

Figure B.1: AASHTO LRFD model of section of beam (AASHTO LRFD 7th Edition 2014).

For simplification, if failure occurs before yielding of the transverse reinforcement, it can conservatively be assumed that the failure shear stress be $0.25f'_c$. For failures occurring below this shear stress level, it will be assumed that at failure both f_{sz} and f_{szcr} are equal to the yield stress f_y of the transverse reinforcement (Bentz et al. 2006).

From the field theory, considering the concrete stress-strain relationship, the average principal tensile stresses in the cracked concrete f_1 can be obtained as follows (Bentz et al. 2006):

$$f_1 = 0.33\sqrt{f'_c}/(1+\sqrt{500\varepsilon_1}) \quad \text{Mpa} \tag{B.1}$$

And the shear stress on crack:

$$v_{ci} \leq \frac{0.18\sqrt{f'_c}}{0.31+\frac{24w}{a_g+16}} \tag{B.2}$$

Considering the free body diagram shown in Figure B.2, sum of forces in z-direction:

For $$\sum f_z = 0 \tag{B.3}$$

and $$f_{szcr} = f_y \tag{B.4}$$

Thus,

$$v = v_{ci} + \rho_z f_y cot\theta \tag{B.5}$$

Equation B.5 can be re-written as follows:

$$v = f_1 cot\theta + \rho_z f_y cot\theta \tag{B.6}$$

where, $\rho_z = \frac{Stirrup\ area}{Web\ area} = \frac{A_v}{b_w\, S}$ (B.7)

in which b_w is the web width and S is the spacing of the stirrups.

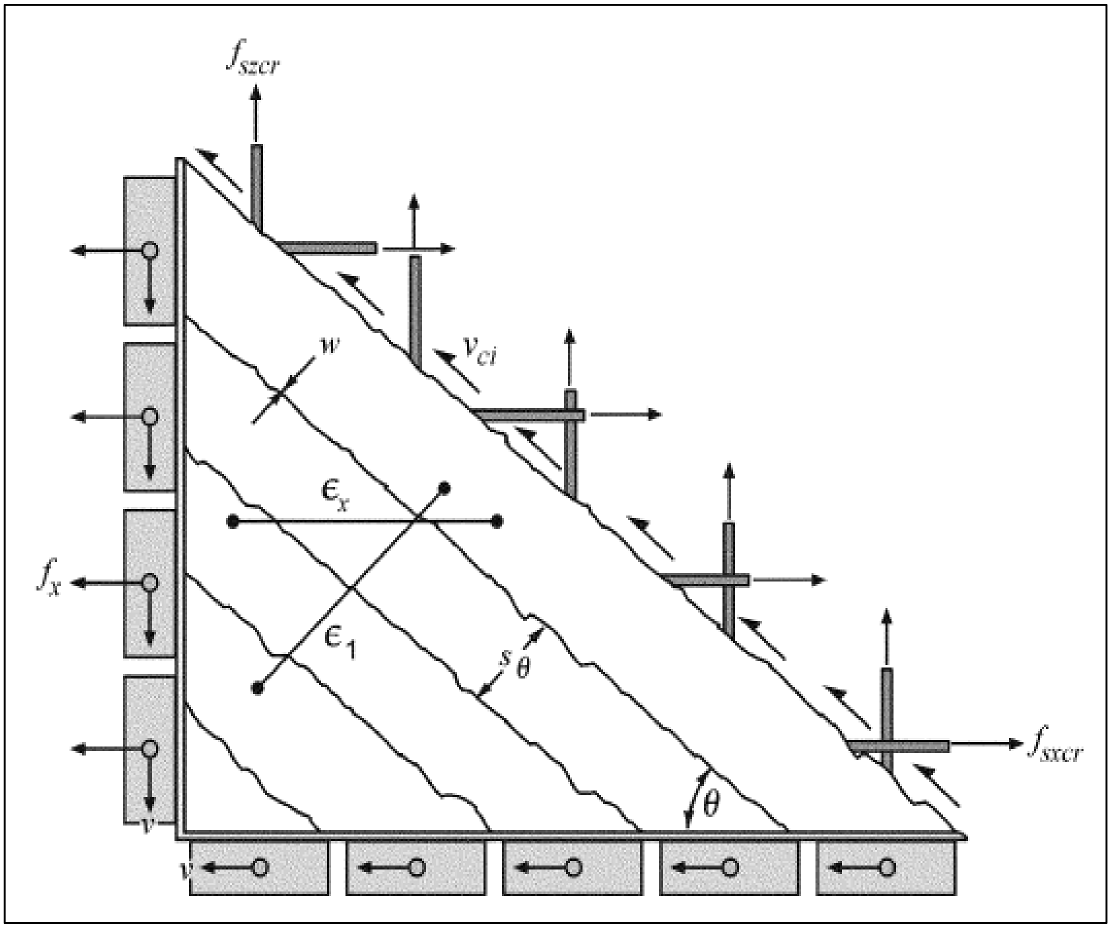

Figure B.2: Transmission of forces across cracks (Bentz et al. 2006).

Shear resistance is gained from the resistance contribution of concrete and stirrups:

$$v = v_c + v_s \quad \text{(B.8)}$$

$$v = \beta\sqrt{f'_c} + \rho_z f_y cot\theta \quad \text{(B.9)}$$

From Equation, B.1, B.6, and B.9, the value of β can be obtained as follows:

$$\beta = \frac{0.33\ cot\theta}{1+\sqrt{500\varepsilon_1}} \tag{B.10}$$

Similarly, from Equation B.2, B.5, and B.9, the value of β should satisfy

$$\beta \leq \frac{0.18}{0.31+24w(a_g+16)} \tag{B.11}$$

where,

w = crack width which is obtained as the product of crack spacing s_θ and the principal tensile strain ε_1.

a_g =maximum coarse aggregate size in mm.

For members with no transverse reinforcements, Equation B.11 can be written as follows:

$$\beta \leq \frac{0.18}{0.31+0.686\ S_{xe}\varepsilon_1/sin\theta} \tag{B.12}$$

where,

$$S_{xe} = \frac{35S_x}{a_g+16} \tag{B.13}$$

In which S_x denotes the crack spacing controlled by the reinforcement in the x-direction.

The angle

$$tan\theta = \frac{0.568+1.258S_{xe}\varepsilon_1/sin\theta}{1+\sqrt{500\varepsilon_1}} \tag{B.14}$$

Figure B.3 illustrates how Equation B.14 relates the inclination θ of the diagonal compressive stresses to the principal tensile strain ε_1 for different values of the crack spacing parameter s_{xe} (Bentz et al 2006).

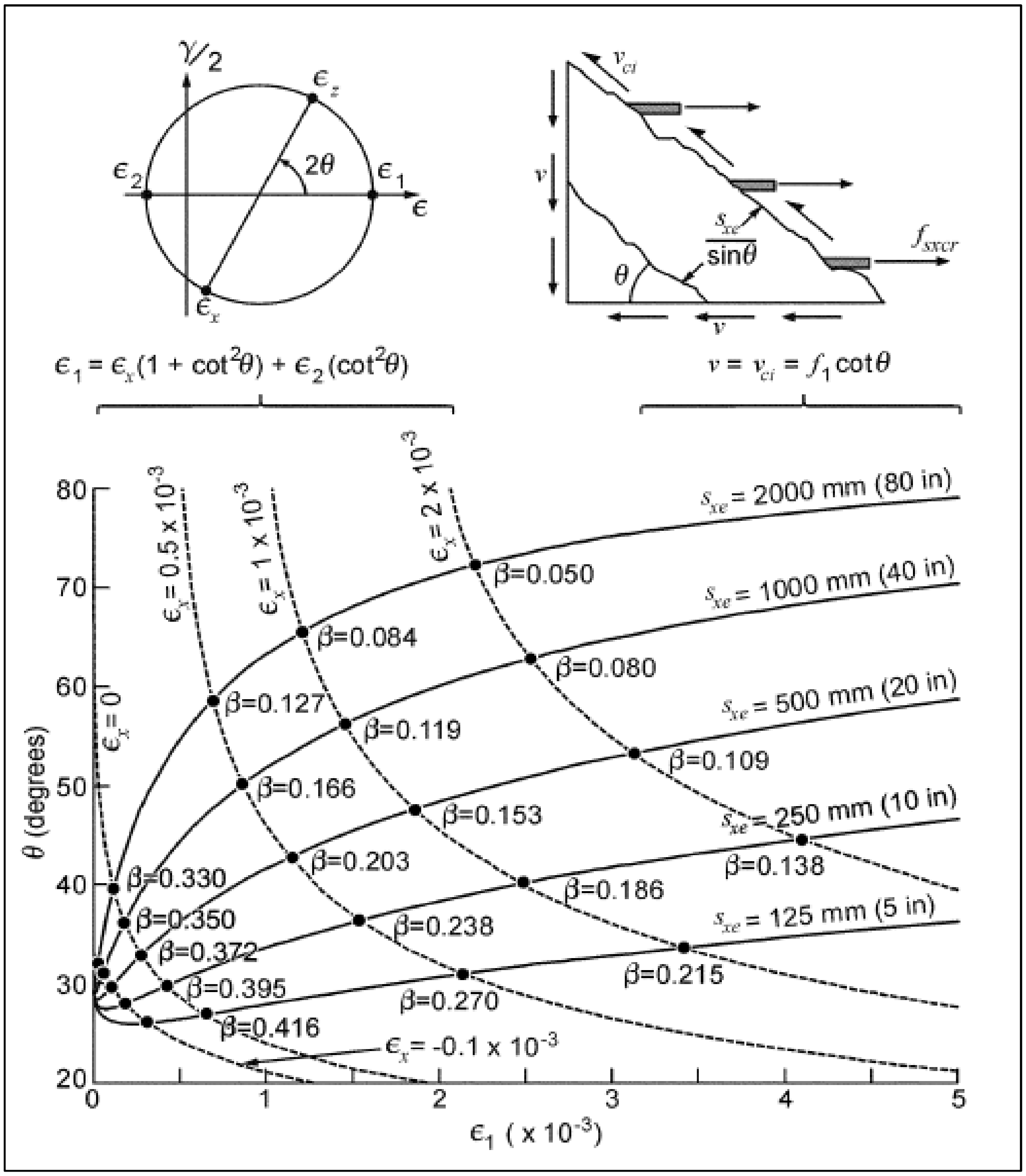

Figure B.3: Determination of beta and theta values for elements not containing transverse reinforcement (Bentz 2006).

In order to relate the longitudinal strain ε_x to ε_1:

$$\varepsilon_1 = \varepsilon_x(1 + cot^2\theta) + \varepsilon_2 cot^2\theta \quad \text{(B.15)}$$

When both f_z and ρ_z equal zero, then

$$f_2 = f_1 cot^2\theta \quad \text{(B.16)}$$

As the compressive stresses for these elements is small, it is resonably accurate to assume that

$$\varepsilon_2 = f_2/E_c \quad \text{(B.17)}$$

In which E_c is the modulus of elasticity of concrete and can be taken as $4950\sqrt{f'_c}$ in MPa. Thus, Equation B.15 can be re-written as

$$\varepsilon_1 = \varepsilon_x(1 + cot^2\theta) + \frac{cot^4\theta}{15{,}000(1+\sqrt{500\varepsilon_1})} \quad \text{(B.18)}$$

It can be seen that for all but very small values of ε_x combined with small values of s_{xe}, the simple equation gives values that are somewhat conservative.
Finally, Bentz et al. 2006 suggest Equation B.19 to calculate β and Equation B.20 to obtain the angle θ.

$$\beta = \frac{0.4}{1+1500\varepsilon_x} \cdot \frac{1300}{1000+S_{xe}} \quad \text{(B.19)}$$

$$\theta = (29\deg + 7000\varepsilon_x)(0.88 + \frac{S_{xe}}{2500}) \leq 75deg \quad \text{(B.20)}$$

Appendix C

Design of Prestressed Girder Bridge

This appendix presents the structural design of a simply supported single span prestressed girder bridge. The longitudinal profile of the bridge is shown in Figure C.1 and the bridge cross section is illustrated in Figure C.2.

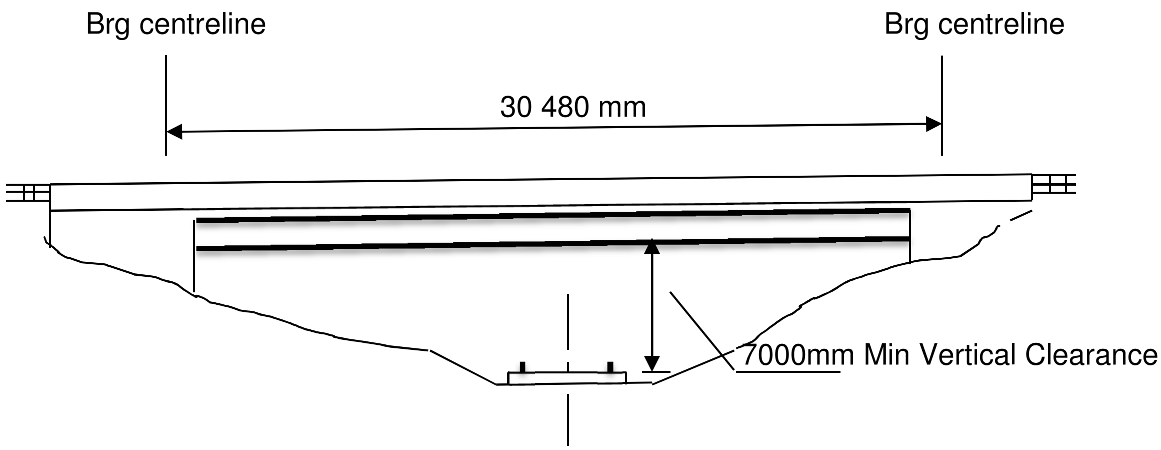

Figure C.1: Bridge longitudinal profile.

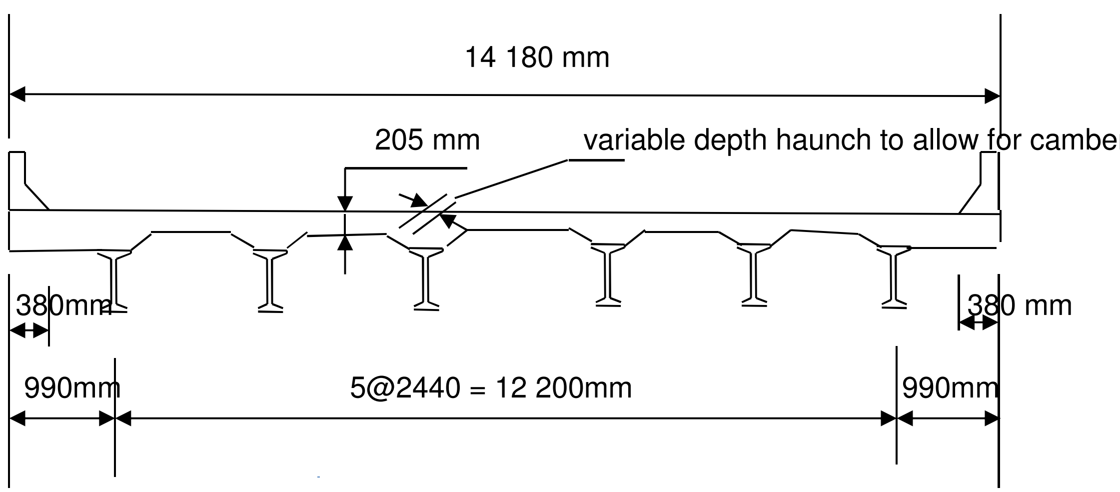

Figure C.2: Bridge cross section.

The following information is given:

- Span (from center of bearing to center of bearing) = 30 m.
- Bridge total width = 14.20 m
- Asphalt thickness = 75 mm.
- Concrete strength (f'_{ci}) for deck = 40 Mpa.
- Concrete initial strength (f'_c) for girder = 41.25 Mpa.
- Concrete strength (f'_c) for girder = 55 Mpa.
- Strand type: Low-relaxation, 12.70 mm, seven-wire strands.
- Ultimate strength(f_u) for strand = 1860 Mpa.
- Yield strength(f_y) for strand = 1660 Mpa.
- Yield strength(f_y) for reinforcement = 400 Mpa.
- Modulus of elasticity of reinforcement = 200 000 MPa
- Precast standard girder: NU 1350 Girder (Nebraska University girder).
- Design code: AASHTO LRFD 6th Edition 2012.

C.1 Check conformity of the proposed cross section to AASHTO LRFD 2012.

1.1 Check minimum thickness [A5.14.1.2.2]

Thickness of top flange (65 mm) ≥ 50 mm, OK

Thickness of web (150 mm) ≥ 125 mm, OK

Thickness of bottom flange (135 mm) ≥ 125 mm, OK

1.2 Check minimum depth (including deck) [A2.5.26.3]

h_{min}=0.045 (30 000) = 1350 mm

$<h$= 1800 + 200 = 2000 mm OK

1.3 Check effective flange widths [A.4.6.2.6.1]

The effective flange width with respect to exterior and interior girders is calculated as follows:

Effective span length = 30 000 mm.

1.3.1 Interior girders:

$$b_i \leq \begin{cases} \frac{1}{4}\ effective\ span = \frac{1}{4}\ (30\ 000) = 7500\ mm \\ 12t_s\ + \frac{1}{2}\ b_f = 12\ (200) + \frac{1}{2}\ (1225) = 3012.5\ mm \\ centre - to - centre\ of\ girders = 2440\ mm,\ \ \boldsymbol{governs} \end{cases}$$

1.3.2 Exterior girders:

$$b_e - \frac{b_i}{2} \leq \begin{cases} \frac{1}{8}\ effective\ span = \frac{1}{8}\ (30\ 000) = 3750\ mm \\ 6t_s\ + \frac{1}{4}\ b_f = 6\ (200) + \frac{1}{4}\ (1225) = 1506.25\ mm \\ width\ of\ overhang = 975\ mm,\ \ \boldsymbol{governs} \end{cases}$$

$$b_e = \frac{2440}{2} + 975 = 2\ 195\ mm$$

C.2 Design of Reinforced Concrete Deck

C.2.1 Dead load

$h_{min} = \frac{S+3000}{30} > 175\ mm$ [A9.7.1.1]

$h_{min} = \frac{S+3000}{30} = 181\ mm > 175\ mm$

Actual deck thickness: $h = 205\ mm\ > h_{min}$ OK

Weight of slab:

$w_s = 2400 * 10^{-9}\ kg/mm^3\ (9.81\ N/kg)(205mm) = 4.83 * 10^{-3}\ N/mm^2$

Weight of barrier:

$P_b = 2400 * 10^{-9}(9.81)(197\ 325\ mm^2) = 4.83 * 10^{-3}\ N/mm$

Weight of cantilever overhang 230 mm thick:

$$w_o = 2400 * 10^{-9}\ kg/mm^3\ \left(9.81\frac{N}{kg}\right)(230mm) = 5.42 * 10^{-3}\ N/mm^2$$

Asphalt wearing surface:

$$w_{DW} = 2250 * 10^{-9}\ kg/mm^3\ \left(9.81\frac{N}{kg}\right)(230mm) = 5.42 * 10^{-3}\ N/mm^2$$

Dead load analysis for deck:

$$h = 205mm,\ w_s = 4.83 * 10^{-3}\frac{N}{mm^2}\ , S = 2440\ mm.$$

$$Fixed\ End\ moment\ FEM = \mp\frac{w_s\, S^2}{12}$$

$$= \mp\frac{(4.83*10^{-3})(2440)^2}{12} = \ 2396\ N.mm/mm$$

Using influence line design aids:

Reaction: $R = w_s(net\ area\ without\ cantilever)\ S$

$$R = 4.83 * 10^{-3}(0.3928)2440 = 4.63\ N/mm$$

Moment: $M = w_s(net\ area\ without\ cantilever)\ S^2$

$$= 4.83 * 10^{-3}(0.0772)2440^2\ = 2220\ N\ mm/mm$$

$$M =\ w_s(net\ area\ with\ cantilever)\ S^2$$

$$= 4.83 * 10^{-3}(-0.1071)2440^2\ = -3080\ N\ mm/mm$$

Dead load analysis for overhang:

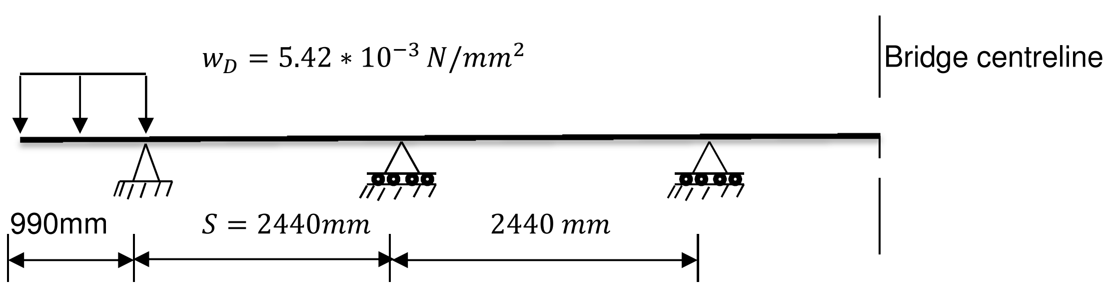

Figure C.3: Overhang dead load positioning.

The placement of dead load to produce the maximum dead load effect is shown in Figure C.3.

$h_o = 230\ mm$

$w_o = 5.42 * 10^{-3}\ N/mm^2$

$L = 990\ mm$

Reaction: $R = w_o(net\ area\ cantilever)L$

$= 5.42 * 10^{-3}\left(1.0 + 0.635\ \frac{990}{2440}\right)900 = 6.75\ N/mm$

Moment:

$M^- = w_o(net\ area\ cantilever)L^2$

$= 5.42 * 10^{-3}(-0.5000)990^2 = -2656\ N\ mm/mm$

$M^+ = w_o(net\ area\ cantilever)L^2$

$= 5.42 * 10^{-3}(0.1350)990^2 = 717\ N\ mm/mm$

Dead load analysis for overhang barrier:

The load placement to produce the maximum dead load effect is shown in Figure C.4.

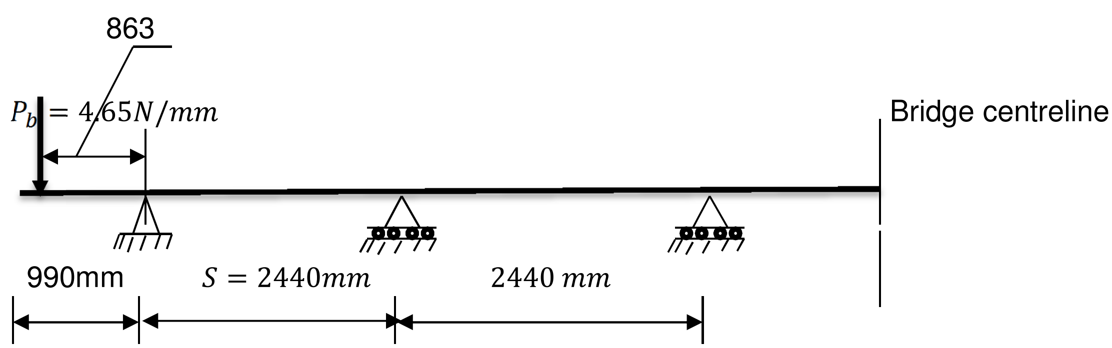

Figure C.4: Barrier dead load positioning.

Reaction: $R = P_b(influence\ line\ \ ordinate)$

$R = 4.65\left(1 + 1.27\frac{863}{2440}\right) = 6.74\ N/mm$

Moment: $M = P_b(influence\ line\ \ ordinate)\ L$

$M^- = 4.65(-0.4920)863 = -1974\ N\ mm/mm$

$M^+ = 4.65(0.2700)863 = 1083\ N\ mm/mm$

Dead load analysis for asphalt surface:

The load placement to produce the maximum load effect is shown in Figure C.5.

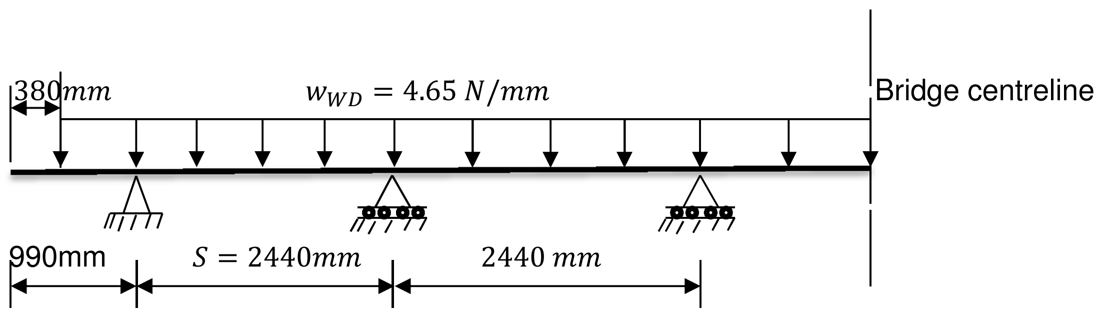

Figure C.5: Asphalt wearing surface dead load positioning.

By deducting the barrier width, the loaded cantilever length is:

$L = 990 - 380 = 610\ mm.$

Reaction: $R = w_{DW}[(net\ area\ cantileve)L + (net\ area\ without\ cantilever)S]$

$R = 1.66 * 10^{-3}[\left(1 + 0.635\frac{610}{2440}\right)610 + (0.3928)2440]$

$R = 2.76\ N/mm$

Moment: $M = w_{DW}(net\ area\ cantilever)\ L^2$

$M^- = 1.66 * 10^{-3}[(0.135)610^2 + (-0.1071)2440^2]$

$= -975\ N\ mm/m$

$M^+ = 1.66 * 10^{-3}[(-0.2460)610^2 + (0.0772)2440^2]$

$= 611\ N\ mm/mm$.

C.2.2 Live load

Deck is design according to AASHTO LRFD approximate strip method [A4.6.2.1]. Transverse strips are designed for 145 kN axel of AASHTO standard truck [A6.3.1.3.3]. In order to produce the maximum load effect, the wheel load will be positioned not closer than 300 mm from the curb face [A3.6.1.3.1].

Wheel contact area is assumed to be rectangle of 510 mm width and l length:

$$l = 2.28\,\gamma\,\left(1 + \frac{IM}{100}\right)P \qquad \text{[A3.6.1.2.5]}$$

where,

$\gamma = Load\ factor = 1.75$

$IM = Dynamic - load\ allowance = 33\%$

$P = Wheel\ load = 72.5\ kN$

Hence, $l = 2.28\ (1.75)\left(1 + \frac{33}{100}\right)72.5 = 385\ mm$

Number of design lanes, N_L:

$$N_L = INT\ \left(\frac{13\,420}{3600}\right) = 3 \qquad \text{[A3.6.1.1.1]}$$

Multiple presence factor

$$Multiple\ presence\ factor = \begin{cases} 1.20 & for\ one\ loaded\ lane \\ 1.00 & for\ two\ loaded\ lanes \\ 0.85 & for\ three\ loaded\ lanes \end{cases}$$ [A3.6.1.1.2]

The critical position of wheel load is as shown in Figure C.6.

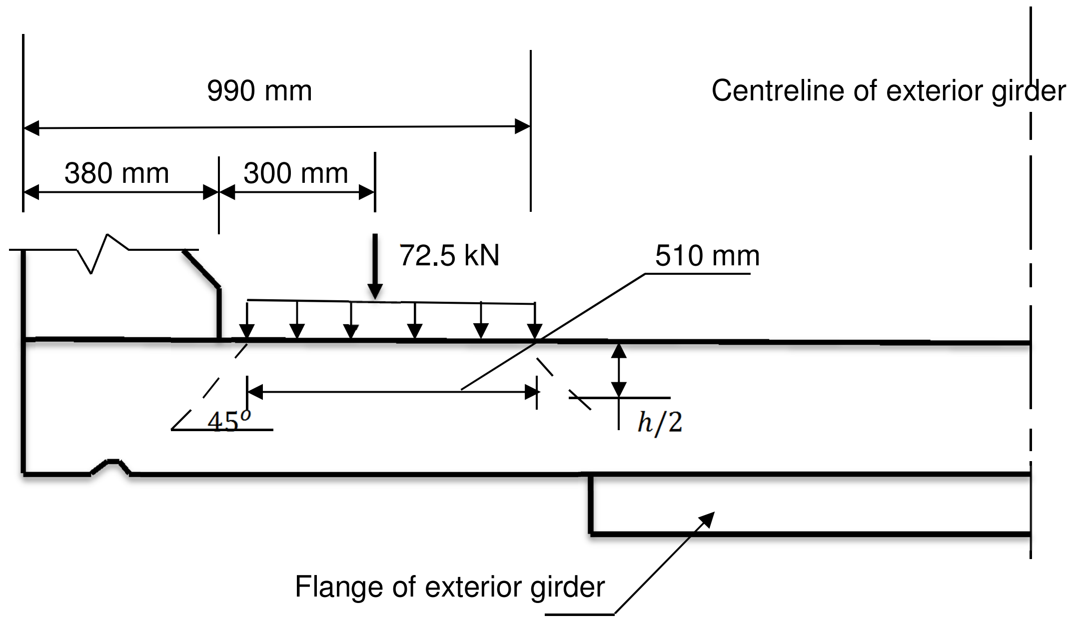

Figure C.6: Wheel load distribution on overhang

Equivalent width of a transverse strip is:

$$W_{equivalent} = 1140 + 0.833(310) = 1400mm$$ [Table A4.6.2.1.3-1]

C.2.2.1 Maximum overhang negative live load moment

$$M^- = \frac{-1.2(72.5*10^{-3})(310)}{1400} = -19\,260\ N\ mm/mm$$ = -19.26 kN m/m

C.2.2.2 Maximum positive overhang live load moment

Live load positioning to produce maximum live load positive live load is occurs close to the 0.40 point of the first interior span, as illustrated in Figure C.7.

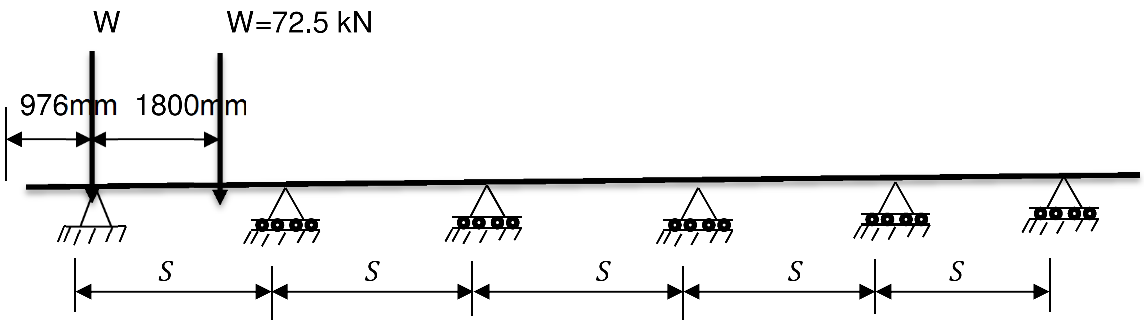

(a)

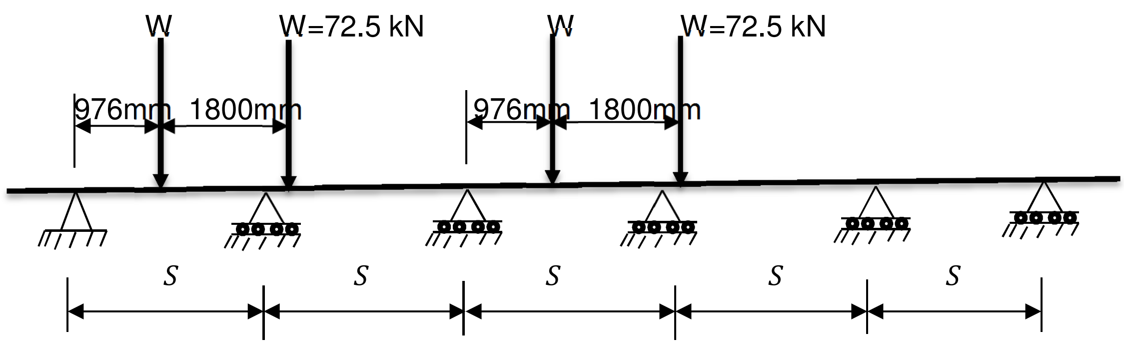

(b)

Figure C.7: position of live load for maximum positive moment. (a) One loaded lane, and (b) two loaded lanes.

Equivalent width of transverse strip:

$$W_{equivalent} = 660 + 0.55(S)$$ [Table A4.6.2.1.3-1]

$$660 + 0.55(2440) \ = 2000mm$$

- For one loaded lane:

Reaction: $R = 1.2(0.5100 - 0.0486)\frac{72.5*10^{-3}}{2000} = 20.1\ N/mm = 20.1kN/mm$

Moment: $M = 1.2(0.2040 - 0.0195)\,(2440)\,\frac{72.5*10^3}{2000}$

$$= 19\,580\ N\ mm/mm = 19.58\ kN\ m/m.$$

- For two loaded lanes:

Reaction: $R = 1.0(0.5100 - 0.0486 + 0.0214 - 0.0039)\,\frac{72.5*10^{-3}}{2000}$

$$= 17.4\ N/mm = 17.4 kN/mm$$

Moment: $M = 1.0(0.5100 - 0.0486 + 0.0214 - 0.0039)\,(2440)\,\frac{72.5*10^3}{2000}$

$$= 16\,900\ N\ mm/mm = 16.9\ kN\ m/m.$$

Thus, the case of one loaded lane will governs the design.

C.2.2.3 Maximum interior negative live load moment

The maximum negative moment at the first interior girder is usually associated with one loaded lane. The critical position of live load to produce that maximum negative moment is as illustrated in Figure C.8.

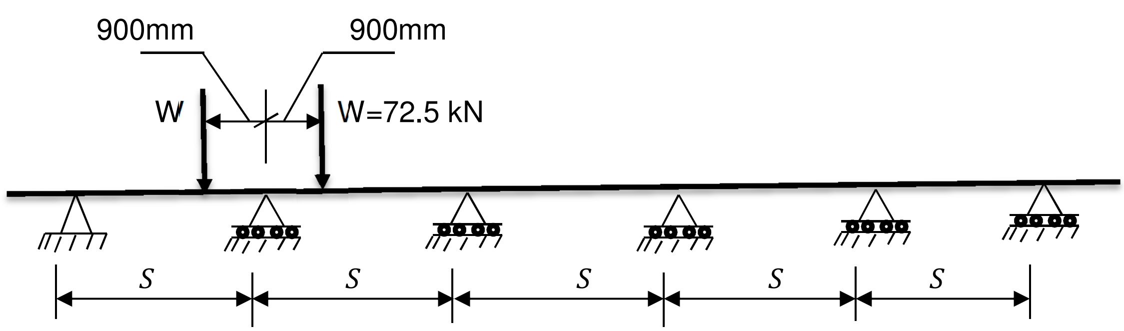

Figure C.8: Position of live load for maximum negative moment.

Equivalent width of transverse strip:

$$W_{equivalent} = 1220 + 0.25(S)$$ [Table A4.6.2.1.3-1]

$$= 1220 + 0.25(2440) = 1830mm$$

Moment: $$M = 1.2(-0.1007 - 0.0781)(2440)\frac{72.5*10^3}{1830}$$

$$= -20\,740\ N\ mm/mm = -20.74\ kN\ m/m.$$

C.2.2.4 Maximum live load reaction on exterior girder

Figure C.9 illustrate the live load placement to produce the maximum reaction on the first exterior girder.

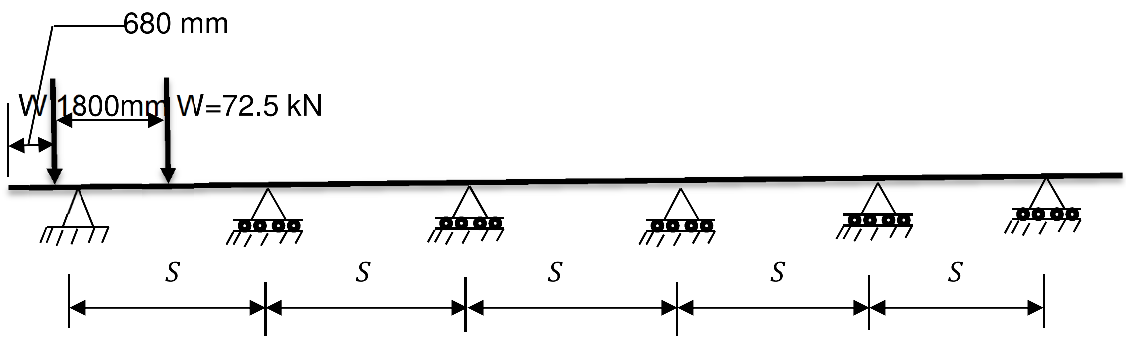

Figure C.9: Position of live load for maximum reaction at exterior girder.

Equivalent width of transverse strip:

$$W_{equivalent} = 1220 + 0.25(S)$$ [Table A4.6.2.1.3-1]

$$= 1140 + 0.833(310) = 1400\ mm$$

Reaction: $$R = 1.2(1.1614 + 0.2869)\frac{72.5*10^{-3}}{1400} = 90.0\ N/mm = 90.0kN/mm$$

C2.3 Strength I Limit State:

Load combination:

$$\eta \sum \gamma_i Q_i = \eta[\gamma_p DC + \gamma_p DW + 1.75(LL + IM)$$ [Table A3.4.1-1]

where,

$\eta = \eta_D \eta_R \eta_I \;\geq 0.95$ [A1.3.2.1-2]

$\eta_D = 0.95$, reinforcement designed to yield [A1.3.3]

$\eta_{R=}$ 0.95, continuous [A1.3.4]

$\eta_{I=}$ 1.05, operationally important [A1.3.5]

Hence, $\eta = 0.95(0.95)(1.05) = 0.95$.

$IM = 33\%$ of the live load force effect.

Critical section for M^-: $\frac{b_f}{3} < 380\ mm$ from centreline of girder [A4.6.2.1.6]

$$\frac{1255}{3} = 408\ mm\ > 380mm$$

Hence, critical section lies at 380 mm from centreline of girder.

Reaction:

$$R = 0.95[1.25(4.63 + 6.75 + 6.74) + 1.50(2.76) + 1.75(1.33)(90.0)]$$

$$= 224.5\ N/mm = 224.5\ kN/m$$

Moment:

$$M^- = 0.95[1.25(-2656 - 4013) + 1.50(-309) + 1.75(1.33)(-19\ 260)]$$

$$= -50\ 950\ N\ mm/mm = -50.95\ kN\ m/m.$$

$$M^+ = 0.95[1.25(2220) + +0.9(-1307 - 1974) + 1.50(611) + 1.75(1.33)(19\ 580)]$$

$$= 44\ 000N\ mm/mm = 44.0\ kN\ m/m.$$

C.2.3.1 Reduced negative moment:

For deck on precast I-girder, the design section is positioned at:

$$flange\ width/3\ < 380mm(from\ centreline\ of\ girder) \qquad \text{[A4.6.2.1.6]}$$

$$= 1225/3 = 408mm \quad > 380mm$$

Thus, design section lies at $x = 380mm$ from centreline of support.

As illustrated in Figure C.10, the concentrated wheel load relates to one loaded lane, while, the uniformly distributed loads are for a 1 mm wide strip.

Hence, equivalent wheel load, $W = 1.2(72\,500)/1400 = 62.14\ N/mm$

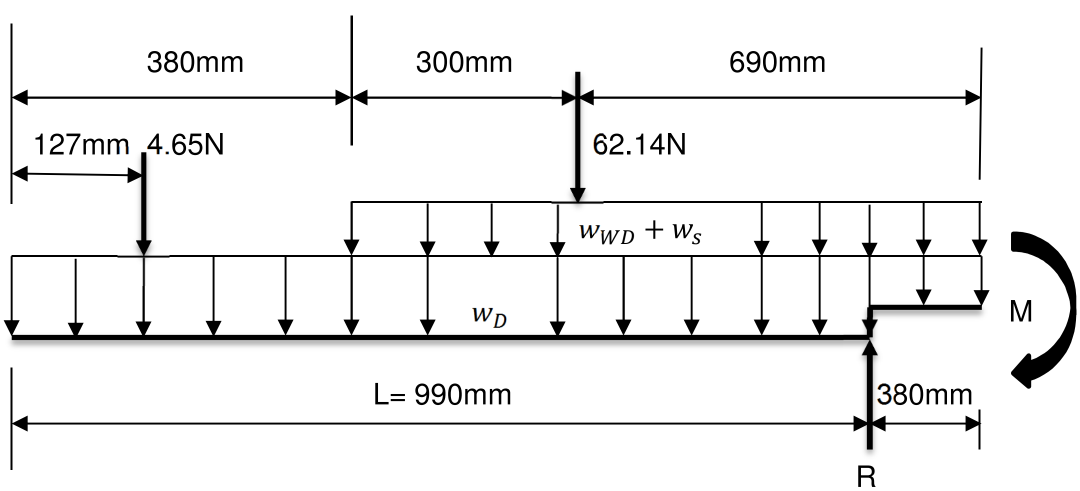

Figure C.10: Reduced negative moment at design section.

Deck:

$$M_d = -\frac{1}{2}\,w_s\,x^2 + R\,x$$

$$= -\frac{1}{2}\,(4.83 * 10^{-3}\,)(380)^2 + 4.63\,(380) = \ 1\,411\ N\ mm/mm$$

Overhang:

$$M_o = -w_o L\left(\frac{L}{2} + \ x\right) + R\,x$$

$$-(5.42 * 10^{-3})(990)\left(\frac{900}{2} + \ 380\right) + 6.75(380) = \ -2\ 130\ N\ mm/mm$$

Barrier:

$$M_b = -P_b(L + x - 127) + R\ x$$

$$= -4.65(1165 - 127) + 6.74\ (380)$$

$$= -2\ 266\ N\ mm/mm$$

Asphalt:

$$M_{DW} = -\frac{1}{2} w_{WD}(L + x - 380)^2 + R\ x$$

$$= -\frac{1}{2}(0.00166)(1165 - 380)^2 + 2.76\ (380)$$

$$= 537\ N\ mm/mm$$

Live load:

$$M_{LL} = -W(690) + R\ x$$

$$= -62.14(690) + 90.0(380)$$

$$= -8\ 677\ N\ mm/mm$$

Hence, ultimate moment is:

$$M_u = 0.95[0.9(1411) + 1.25(-2130 - 2266) + 1.50(53 + 7) + 1.75(1.33)(-8677)]$$

$$= -22\ 435\ N\ mm/mm = -22.435\ kN\ m/m$$

C.2.4 Calculate amount of reinforcement

Try bar diameter, $d_b = 14\ mm$, then area of bar, $A_b = 154\ mm^2$

Try bar spacing at 250mm.

Clear concrete cover to bottom surface = 25 mm (for positive moment)

Clear concrete cover to top surface = 60 mm (for negative moment).

Effective depth:

$$d_{pos} = 205 - 25 - 14/2 = 173mm$$

$$d_{neg} = 205 - 60 - 14/2 = 138mm$$

Moment of resistance, M_r:

$$M_r = \emptyset M_n$$

$$\emptyset M_n = \emptyset A_s f_y (d - \frac{a}{2})$$

$$a = \frac{A_s f_y}{0.85 f'_c b}$$

$$A_s \approx \frac{(M_u/\emptyset)}{f_y (jd)}$$

trial $A_s \approx \frac{M_u}{330d}$

As per AASHTO LRFD [A5.7.2.2], maximum area of reinforcement is limited by the ductility requirement of:

$c \leq 0.42d$, or

$$a \leq 0.42\beta_1 d$$

In this example:

$$\beta_1 = 0.85 - 0.05\left(\frac{2}{7}\right) = 0.836 \qquad \text{[A5.7.2.2]}$$

$$a \leq 0.35d$$

As per AASHTO LRFD, minimum reinforcement for reinforced concrete element (with no prestressing steel):

$$\rho = \frac{A_s}{bd} \geq 0.03 \frac{f'_c}{f_y}$$

$$\min A_s = \frac{0.03(40)}{400}(1)d = 0.003d\ mm^2/mm$$

Maximum spacing:

$S_{max} = \min(1.5h, 450)$ [A5.10.3.2]

$S_{max} = 1.5 * 205 = 308\text{mm}$

(a) Reinforcement for positive moment:

$M_u = 44\ kN\ m/m$, $d = 173\ mm$

Trial $A_s \approx \frac{M_u}{330d} = \frac{44\ 000}{330(173)} = 0.771\ mm^2/mm$

$minA_s = 0.003d = 0.003(173) = 0.519\ mm^2/mm,$ OK

The suggested amount of reinforcement $diameter = 14\ mm, spacing = 250mm$

So, reduce spacing to 175 mm, Then:

$A_s(provided) = 0.880\ mm^2/mm\ > 0.771mm^2/mm$ OK

Thus,

$$a = \frac{A_s f_y}{0.85f'_c b} = \frac{0.88(400)}{0.85(40)(1)} = 10.35\ mm$$

Check ductility:

$$a \leq 0.35d = 0.35(173) = 60.6\ mm$$ Ok

Check flexural capacity:

$$\emptyset M_n\ = \emptyset A_s f_y \left(d - \frac{a}{2}\right)$$

$$= 0.9(0.88)(400)\left(173 - \frac{10.35}{2}\right) = 53\ 167\ N\frac{mm}{mm}$$

$$= 53.167\ kN\frac{m}{m} > 44\ kNm/m$$ OK

(b) Reinforcement for negative moment:

$M_u = -22.44\ kN\ m/m\ ,\ d = 138\ mm$

Trial $A_s \approx \frac{M_u}{330d} = \frac{22\ 440}{330(138)} = 0.493\ mm^2/mm$

$minA_s = 0.003d = 0.003(173) = 0.519\ mm^2/mm,$ OK

Try amount of reinforcement: $diameter = 14\ mm, spacing = 250\ mm$

$A_s(provided) = 0.616\ mm^2/mm\ > 0.519\ mm^2/mm$ OK

Thus,

$$a = \frac{A_s f_y}{0.85 f'_c b} = \frac{0.616(400)}{0.85(40)(1)} = 7.25\ mm$$

Check ductility:

$$a \leq 0.35d = 0.35(138) = 48.3\ mm$$ Ok

Check flexural capacity:

$$\emptyset M_n \ = \emptyset A_s f_y \left(d - \frac{a}{2}\right)$$

$$= 0.9(0.616)(400)\left(138 - \frac{7.25}{2}\right) = 29\ 800\ N\ mm/mm$$

$$= 29.8\ kN\ m/m > 22.44\ kN\ m/m$$ OK

(c) Distribution reinforcement:

$percentage = \frac{3840}{\sqrt{S_e}} \leq 67\%$ [A9.7.3.2]

where, S_e is the effective span length [A9.7.2.3]

$S_e = 2440 - 350 = 2090\ mm$

$percentage = \frac{3840}{\sqrt{2090}} = 84\% \quad > 67\%$

dist. $A_s = 0.67(pos. A_s) = 0.67(0.88) = 0.59\ mm^2/mm$

use dia=12 mm spaced at 175 mm

Thus, dist. $A_s = 0.646\ mm^2/mm > 0.59 mm^2\ /mm$ OK

(d) Temperature and shrinkage reinforcement:

$temp\ A_s \geq 0.75 \frac{A_g}{f_y}$ [A5.10.8.2]

where, A_g: gross area, thus:

$temp\ A_s = 0.75 \frac{(205)(1)}{400} = 0.384\ mm^2/mm$

Hence, distribution reinforcement governs.

(e) Cracking control:

$tensile\ stress, f_s \leq allaowable\ tensile\ stress, f_{sa}$ [A5.7.3.4]

$f_s \leq f_{sa} = \frac{Z}{(d_c A)^{1/3}}$ [A5.7.3.4]

where, $Z = 23\ 000\ N/mm$ for sever exposure conditions

d_c = depth of concrete from extreme tension fiber to centre of closest bar $\leq 50\ mm$.

A = effective concrete tensile area per bar having the same centroid as the reinforcement.

Service I Limit State: [A3.4.1]

$M = M_{DC} + M_{DW} + 1.33 M_{LL}$

The required reinforcement for tensile stress is based on transformed elastic, cracked section properties. [A5.7.1]

Modulus of elasticity of steel, $E_s = 200\ 000\ MPa$ [A5.4.3.2]

Modulus of elasticity of concrete, $E_c = 0.043 {\gamma_c}^{1.5} \sqrt{f'_c}$ [A5.4.2.4]

$E_c = 0.043(2400 \frac{kg}{m^3})^{1.5} \sqrt{40} \quad = 31\ 975\ MPa$

Modular ratio: $n = \frac{200\ 000}{31\ 975} = 6.2$, <u>Use $n = 6$</u>

- **Positive moment:**

  $M = M_{DC} + M_{DW} + 1.33M_{LL}$

$$M^{+} = (2220) + (-1307 - 1974) + (611) + (1.33)(19\,580) = 25\,591\ N\ mm/mm$$

$= 25.591\ kN\ m/m$

Consider a 1-mm wide strip of doubly reinforced section to calculate the properties of transformed section.

$$0.5\ b\ x^2 = n\ A'_s(d' - x) + nA_s(d - x)$$

$$0.5\ (1)\ x^2 = 7\ (0.88)(53 - x) + 7(0.88)(173 - x)$$

$x = 47.7\ mm$

$$I_{cr} = \frac{bx^3}{3} + nA'_s(d' - x)^2 + nA_s(d - x)^2$$

$$I_{cr} = \frac{(1)(47.7)^3}{3} + 6(0.88)(138 - 47.7)^2 + 6(0.88)(173 - 47.7)^2$$

$= 162\,127\ mm^4/mm$

$$f_s = n\left(\frac{My}{I_{cr}}\right) = 6\left(\frac{25\,591(173 - 47.7)}{162\,127}\right) = 118.7\ MPa$$

$d_c = 33\ mm\ \leq 50\ mm$ OK

$A = 2(33)(225) = 14\,850\ mm^2$

$f_{sa} = \frac{23\,000}{(33*14\,850)^{1/3}} = 292\ MPa\ > 0.6f_y$

Thus,

$f_{sa} = 0.6\ (400) = 240\ MPa\ >\ f_s = 195\ MPa,$ OK

- **Negative moment:**

  $M = M_{DC} + M_{DW} + 1.33M_{LL}$

$$M^{-} = (-2656 - 4013) + (-309) + (1.33)(-19\ 260)$$

$$= -32\ 594\ N\ mm/mm = -32.594\ kN\ m/m.$$

$$f_s = n\left(\frac{My}{I_{cr}}\right) = 6\left(\frac{25\ 591(173-47.7)}{162\ 127}\right) = 118.7\ MPa$$

$$A = 2(50)(175) = 17\ 500\ mm^2$$

$$f_{sa} = \frac{23\ 000}{(50*17\ 500)^{1/3}} = 240.5\ MPa\ > 0.6 f_y$$

Thus,

$f_{sa} = 0.6\ (400) = 240\ MPa\ >\ f_s = 221\ MPa,$ OK

C.2.5 Fatigue Limit State:

According to AASHTO LRFD [A9.5.3], fatigue need not to be investigated for concrete decks on multi-girders.

C.3 Design of prestressed girder

Figure C.11 shows the details of NU 1350 standard girder.

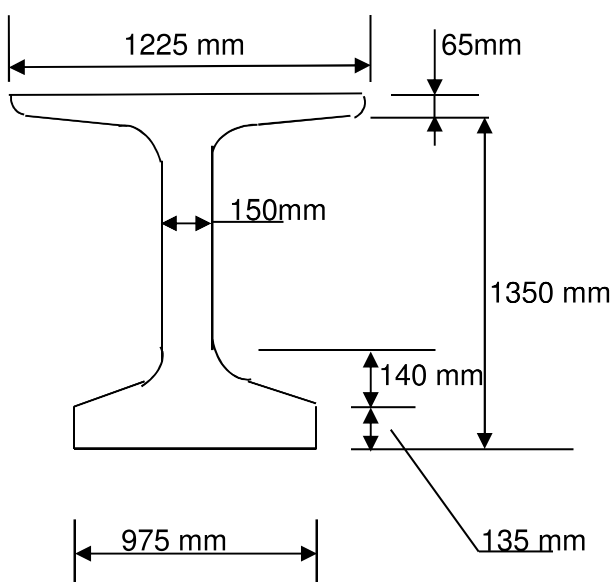

Figure C.11: Details of NU 1350 Girder

C.3.1 Number of lanes and multiple presence factor

$$N_L = INT(\frac{w}{3600})$$ [A3.6.1.1.1]

$$N_L = INT\left(\frac{13\ 420}{3600}\right) = 3$$

Multiple presence factor, m, is taken from AASHTO LRFD (Table 4.6) [A3.6.1.1.2]

Number of Loaded Lanes	m
1	1.20
2	1.00
3	0.85

C.3.2 Dynamic load allowance (Impact)

The dynamic (impact) factor is taken from AASHTO LRFD (Table4.7): [A3.6.2.1]

Component	*IM* (%)
Deck joints	75
Fatigue	15
All other	33

C.3.4 Live load distribution factor

C.3.4.1 Distribution factor for moment: [A4.6.2.2.2]

The girder stiffness factor, k_g, is calculated using AASHTO LRFD (Table 2.2).

Concrete compressive strength, f'_c, of girder = 55 MPa

Concrete compressive strength, f'_c, of girder = 40 MPa

Thus, modular ration: $n = \sqrt{\frac{55}{40}} = 1.173$

$e_g = y_{tg} + haunch + \frac{h}{2}$

$= 742 + 50 + \frac{205}{2} = 895\ mm$

$k_g = n(I_g + A{e_g}^2)$ [Table A4.6.2.2.1-1]

$= 1.173[126\ 011 + (486\ 051)(895)^2]$

$= 456.7 * 10^9\ mm^4$

$\frac{K_g}{L{t_s}^3} = \frac{456.7*10^9}{(30\ 480)(205)^3} = 1.739$

(a) Interior girders:

Using AASHTO LRFD (Table 6.5) [A4.6.2.2.2b and Table A4.6.2.2.2b-1]:

- One loaded design lane:
  Girder Distribution Factor for moment:

  $DFM = 0.06 + (\frac{S}{4300})^{0.4} (\frac{S}{L})^{0.3} (\frac{K_g}{Lt^3})^{0.1}$
  $= 0.06 + (\frac{2400}{4300})^{0.4}\ (\frac{2400}{30480})^{0.3}\ (1.739)^{0.1} = 0.450$

- Two loaded design lanes:

  $DFM = 0.075 + (\frac{S}{4300})^{0.6} (\frac{S}{L})^{0.2} (\frac{K_g}{Lt^3})^{0.1}$
  $= 0.075 + (\frac{2400}{4300})^{0.6}\ (\frac{2400}{30480})^{0.2}\ (1.739)^{0.1} = 0.523$

(b) Exterior girders:

Using AASHTO LRFD (Table 6.5) [A4.6.2.2.2d and Table A4.6.2.2.2d-1]:

- One loaded design lane:
  Use Lever Rule as illustrated in Figure C.12

  $R = \frac{P}{2}\left(\frac{650+2450}{2440}\right) = 0.635P$

  $DFM = 1.2(0.635) = 0.762$

- Two or more design lanes loaded:

  $d_e = 990 - 380 = 610\ mm$

  $e = 0.77 + \frac{d_e}{2800} = 0.77 + \frac{610}{2800} = 0.988\ < 1.0$

  Use $e = 1.0$

  $DFM = 0.671$

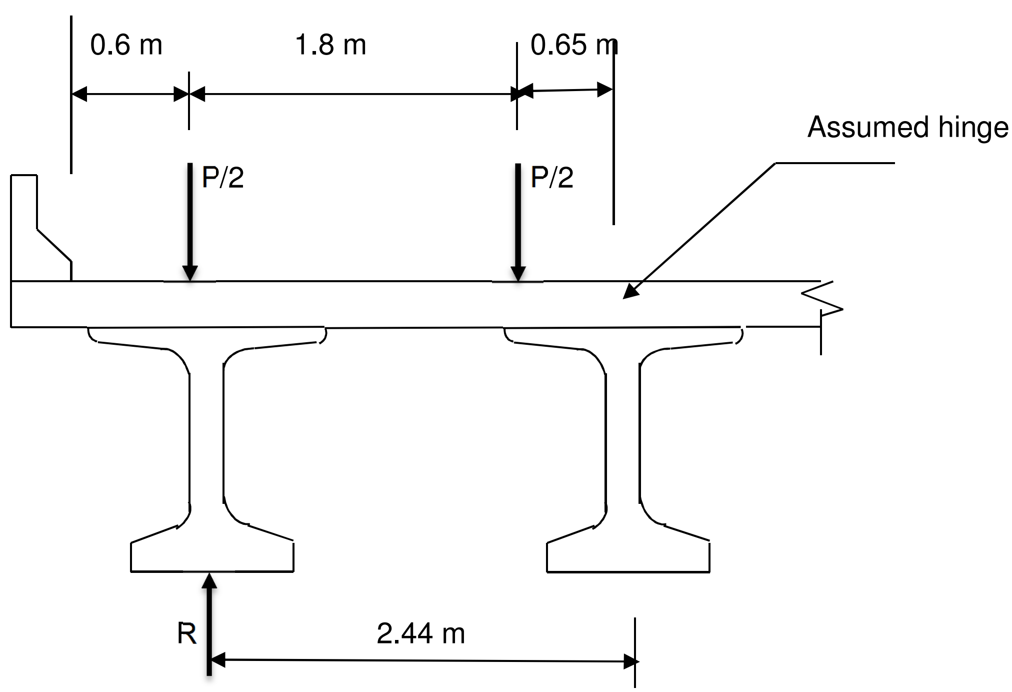

Figure C.12: definition of lever rule for an exterior girder.

C.3.4.2 Distribution factor for shear: [A4.6.2.2.3]

(a) Interior girders:

Using AASHTO LRFD (Table 6.5) [A4.6.2.2.2a and Table A4.6.2.2.2a-1]:

- One loaded design lane:
  Girder Distribution Factor for moment:

$$DFS = 0.36 + \frac{S}{7600}$$
$$= 0.36 + \frac{2440}{7600} = 0.68$$

- Two loaded design lanes:

$$DFS = 0.2 + \frac{S}{3600} - (\frac{S}{10\ 700})^{0.2}$$
$$= 0.2 + \frac{2440}{3600} - (\frac{2440}{10\ 700})^{0.2} = 0.826,$$ **governs.**

(b) Exterior girders:

Using AASHTO LRFD (Table 6.5) [A4.6.2.2.2b and Table A4.6.2.2.2b-1]:

- One loaded design lane:
  Use Lever Rule as illustrated in Figure C.12

$$R = \frac{P}{2}\left(\frac{650+2450}{2440}\right) = 0.635P$$
$$DFS = 1.2(0.635) = 0.762,$$ **governs**

- Two or more design lanes loaded:

$$d_e = 990 - 380 = 610\ mm$$
$$e = 0.6 + \frac{d_e}{3000} = 0.77 + \frac{610}{3000} = 0.803\ < 1.0$$
$$DFS = (0.803)(0.826) = 0.663$$

C.3.4.3 Calculate moments and shears

Tables C.1 and C.2 summarize the force effects for interior girder and exterior girder, respectively.

Table C.1: Summary of force effects for interior girder

Force Effect	Load Type	Distance from support					
		0	0.1 L	0.2 L	0.3 L	0.4 L	0.5 L
	Service I Loads						
M (kN m)	Girder	0	478	850	1115	1276	1328
	DC1 (including diaphragm)	0	1090	1951	2582	2947	3060
	DFM(LL+IM)	0	974	1714	2216	2518	2590
V (kN)	DC1 (including diaphragm)	395	320	245	170	75	0
	DW on composite section	62	49	37	25	12	0
	DFS(LL+IM)	441	383	327	274	223	175
Strength I Loads							
Mu (kN m)	$\eta[1.25DC + 1.5DW + 1.75(LL + IM)]$	0	3154	5594	7312	8328	8608
Vu (kN)	$\eta[1.25DC + 1.5DW + 1.75(LL + IM)]$	1291	1087	887	693	477	290

Table C.2: Summary of force effects for exterior girder

Force Effect	Load Type	Distance from support					
		0	0.1 L	0.2 L	0.3 L	0.4 L	0.5 L
	Service I Loads						
M (kN m)	Girder self-weight	0	478	850	1115	1276	1328
	DC1 (including diaphragm)	0	1038	1852	2441	2789	2900
	DC2 (barrier) on composite section	0	194	346	453	519	540
	DW on composite section	0	127	226	296	339	353
	DFM(LL+IM)	0	1106	1946	2516	2860	2941
V (kN)	DC1 (including diaphragm)	377	304	230	157	74	0
	DC2 (barrier) on composite section	71	57	43	28	14	0
	DW on composite section	46	37	28	19	9	0
	DFS(LL+IM)	407	353	302	253	206	161
Strength I Loads							
Mu (kN m)	$\eta[1.25DC + 1.5DW + 1.75(LL + IM)]$	0	3483	6167	8041	9166	9477
Vu (kN)	$\eta[1.25DC + 1.5DW + 1.75(LL + IM)]$	1274	1068	866	667	460	268

C.3.4.4 Investigate service limit state

C.3.4.4.1 Stress limits for prestressing tendons:

$f_{pu} = 1860\ MPa$, Low-relaxation 12.70mm, seven-wires strands.

$A = 98.1\ mm^2$ (Table B.2) [A5.9.3]

$E_p = 197\ 000\ MPa$ [A5.4.4.2]

Using AASHTO LRFD (Table 7.8): [A5.9.3]

At Jacking (immediately prior to transfer) $0.75f_{pu} = 0.75(1860) = 1395\ MPa$

$f_{py} = 0.9f_{pu} = 0.9(1860) = 1675\ MPa$ [AASHTO LRFD Table A5.4.4.1-1]

At service (after losses)

$f_{pe} = 0.8\ f_{py} = 0.8(1674) = 1339\ MPa$

C.3.4.4.2 Stress limits for concrete:

$f'_c = 55\ MPa$, 28-days

$f'_{ci} = 0.75\ f'_{ci} = 40\ MPa$

Temporary stresses before losses-fully prestressed components:

Allowable compressive stresses $f_{ci} = 0.6f'_{ci} = (0.6)40$

$= 24\ MPa$ [A.5.9.4.1.1]

Allowable tensile stresses $f_{ti} = 0.24\sqrt{f'_{ci}} = 0.24\sqrt{40}$

$= 1.52\ MPa$ [Table A.5.9.4.1.2-1]

Stresses at service (after losses)-fully prestressed components:

Allowable compressive stresses, *Service I Limit State* $f_c = 0.45f'_c = (0.45)55$

$= 24.75\ MPa$ [A.5.9.4.2]

Allowable tensile stresses, *Service III limit state* $f_{ti} = 0.19\sqrt{f'_c} = 0.19\sqrt{55}$

$= 1.41\ MPa$ [Table A.5.9.4.1.2-1]

Modulus of Elasticity: [C.5.4.2.4]

$$E_{ci} = 4800\sqrt{f'_{ci}} = 4800\sqrt{40} = 30\,360\ MPa$$

$$E_c = 4800\sqrt{f'_c} = 4800\sqrt{55} = 35\,600\ MPa$$

C.3.4.4.3 Preliminary choices of prestressing tendons:

Modular ratio $n_c = \sqrt{40/55} = 0.85$

$A_g = 486\,051\ mm^2$

$I_g = 126\,011 * 10^6\ mm^4$

$S_{tg} = \frac{I_g}{y_{tg}} = \frac{126011*10^6}{742} = 169 * 10^6\ mm^3$

$S_{bg} = \frac{I_g}{y_{bg}} = \frac{126011*10^6}{605} = 207.3 * 10^6\ mm^3$

$\overline{y} = \frac{(310\,726)(95)+(45325)(215)+(486\,051)(982)}{310\,726+45\,325+486\,051} = 613\ mm$

$$I_c = (126\,011 * 10^6) + (486\,051)(369)^2 + (906.5)(50)^3/12 + (45\,325)(398)^2 + (1635.4)(398)^2 + (1635.4)(190)^3/12 + (310\,726)(518)^2$$

$= 283.7 * 10^9 mm^4$

$S_{tc} = \frac{I_c}{y_{tc}} = \frac{283.7*10^9}{613} = 462.8 * 10^6\ mm^3$ (Top of deck)

$S_{ic} = \frac{I_c}{y_{ic}} = \frac{283.7*10^9}{373} = 760.6 * 10^6\ mm^3$ (Top of girder)

$S_{bc} = \frac{I_c}{y_{tc}} = \frac{283.7*10^9}{977} = 290.4 * 10^6 \ mm^3$ (Bottom of girder)

Preliminary analysis – Exterior girder at midspan:

$$f_b = -\frac{F_f}{A_g} - \frac{F_f \ e_g}{S_{bg}} + \frac{M_{dg}+M_{ds}}{S_{bg}} + \frac{M_{da}+M_L}{S_{bc}} \leq 3.71 \ MPa$$

where,

M_{dg} =moment due to self-weight of girder = 1328 kN m

M_{ds} = moment due to dead load of wet concrete + diaphragm = 1572 kN m

M_{da} = moment due to additional dead load after concrete hardens = 893 kN m

M_L = moment due to live load + impact (Service *III*) = 0.8(2941) = 2353 kN m

e_g =distance from cg of girder to centroid of pretensioned strands

=608-100 =508 mm.

$$f_b = -\frac{F_f}{486\ 051} - \frac{F_f(508)}{207.3*10^6} + \frac{2900*10^6}{207.3*10^6} + \frac{3246*10^6}{290.4*10^6} \leq 3.71 \ MPa$$

$$F_f = 4.75 * 10^{6\,N} = 4750 \ kN$$

Assume stress in strands after all losses is $0.6 f_{pu} = 0.6(1860) = 1116 \ MPa$

$$A_{ps} \geq \frac{F_f}{0.6 f_{pu}} = \frac{4.75*10^6}{1116} = 4250 \ mm^2$$

$\emptyset M_n = \emptyset\left[\left(A_{ps} * 0.95 f_{pu}\right) + A_s f_y\right](0.9h) \geq M_u$ (Collins and Mitchell 1991)

where,

$\emptyset = 1.0$

$PPR = 1.0$ (prestress ratio) [A5.5.4.2.1]

h = overall depth of composite section = 1590 mm

M_u = Strength I factored moment = 9477 kN m

$$A_{ps} \geq \frac{M_u}{\emptyset 0.95 f_{pu}(0.9h)} = \frac{9477 * 10^6}{1.0(0.95)(1860)(0.9)(1590)}$$

$A_{ps} \geq 3748\ mm^2\ < 4250\ mm^2$, Strength limit is not critical.

Try 52-12.70 mm strands. (Figure C.13)

$A_{ps} = 52(98.71) = 5133\ mm^2$

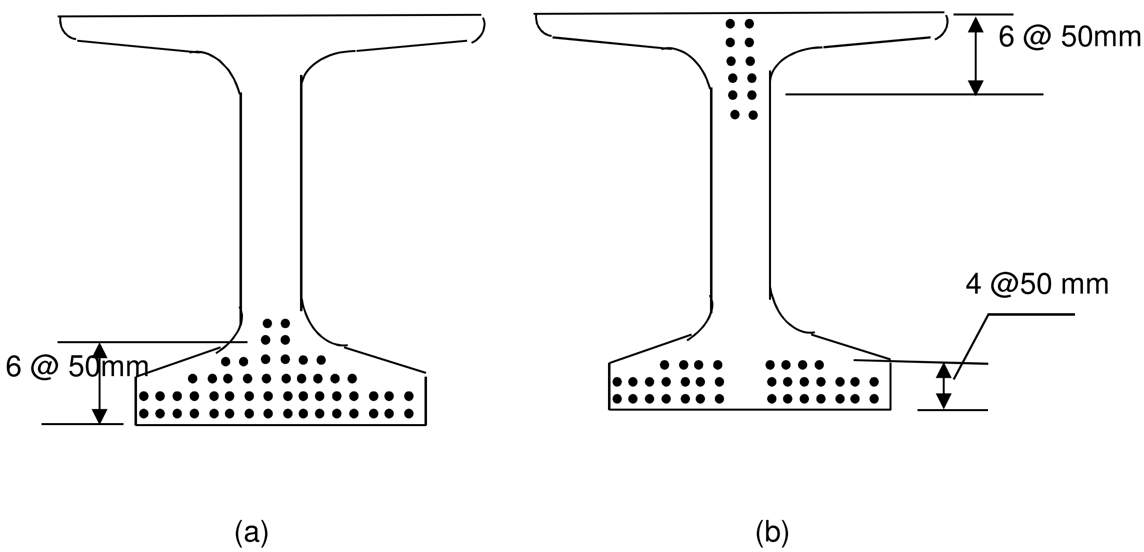

Figure C.13: Strand patterns at (a) midspan and (b) support.

<u>At midspan section</u>

$\bar{y} = \frac{6200}{52} = 119\ mm$

$e_{CL} = 608 - 119 = 489\ mm$

<u>At end section</u>

$\bar{y} = \frac{18\ 200}{52} = 350\ mm$

$e_{CL} = 608 - 350 = 258\ mm$

C.3.4.4.4 Calculate prestress losses [A5.9.5]

C.3.4.4.4.1 Elastic shortening, Δf_{pES} [A5.9.5.2.3a]

$$\Delta f_{pES} = \frac{E_p}{E_{ci}} f_{cgp}$$

where,

$$E_p = 197\,000\ MPa$$

$$E_{ci} = 4800\sqrt{40}$$

f_{cgp} =sum of concrete stresses at cg of A_{ps} due to F_i and M_{dg} at centerline

$$F_i = 0.70 f_{pu} A_{ps} = 0.70(1860)(52)(98.71 * 10^{-3})$$

$$F_i = 6683\ kN$$

$$M_{dg} = 1328\ kN\ m$$

$$f_{cgp} = -\frac{F_i}{A_g} - \frac{F_i e_{CL}{}^2}{I_g} + \frac{M_{dg} e_{CL}}{I_g}$$

$$= -\frac{6.683*10^6}{486\,051} - \frac{(6.683*10^6)(489)^2}{126011*10^2} + \frac{(1328*10^6)(489)}{126\,011*10^6}$$

$$= -21.3\ MPa$$

Thus,

$$\Delta f_{pES} = \frac{197000}{30360}(21.3) = 138.1\ MPa$$

Relaxation at transfer, $\Delta f_{pR1} = \frac{\log(24t)}{40}(\frac{f_{pi}}{f_{py}} - 0.55) f_{pi}$ [A5.9.5.4.4]

$t = 4$ days (estimated from jacking to transfer)

- *1st Iteration:*

$$f_{pi} = f_{pt} - \Delta f_{pES} = 0.74(1860) - 138.1 = 1238.3\ MPa$$

$$\Delta f_{pR1} = \frac{\log(24(4))}{40}\left(\frac{1238.3}{1674} - 0.55\right)(1238.3) = 11.6\ MPa$$

- *2nd Iteration:*

$$f_{pi} = 0.74(1860) - (138.1 + 11.1) = 1227.2\ MPa$$

$$F_i = (52)(98.71)(1.2272) = 6299.1\ kN$$

$$f_{cgp} = -\frac{6.2291 * 10^6}{486\ 051} - \frac{(6.2291 * 10^6)(489)^2}{126011 * 10^6} + \frac{(1328.6 * 10^6)(489)}{126011 * 10^6} = -19.8\ MPa$$

$$\Delta f_{pES} = \frac{197000}{30360}(19.8)128.5\ Mpa$$

$$\Delta f_{pR1} = \frac{\log[24(4)]}{40}\left(\frac{1236.8}{1674} - 0.55\right)1236.8 = 11.57\ MPa$$

- *3rd Iteration:*

$$f_{pi} = 0.74(1860) - (128.5 + 11.57) = 1236.3\ MPa$$

$$F_i = (52)(98.71)(1.2363) = 6346\ kN$$

$$f_{cgp} = -\frac{6.346 * 10^6}{486\ 051} - \frac{(6.346 * 10^6)(489)^2}{126011 * 10^6} + \frac{(1328.6 * 10^6)(489)}{126011 * 10^6} = -19.9\ MPa$$

$$\Delta f_{pES} = \frac{197000}{30360}(19.9) = 129.1\ Mpa$$

$$f_{pi} = 0.74(1860) - (129.1 + 11.57) = 1235.7\ MPa$$ OK

C.3.4.4.4.2 Shrinkage, Δf_{pSR} [A5.9.5.4.2]

$$\Delta f_{pSR} = 117 - 1.03H$$

where,

H = relative humidity; assume a value of 70%

$$\Delta f_{pSR} = 117 - 1.03(70) = 44.9\ MPa$$

C.3.4.4.4.3 Creep, Δf_{pCR} [A5.9.5.4.3]

$$\Delta f_{pCR} = 12.0 f_{cgp} - 7.0\Delta f_{cdp} \geq 0$$

where,

f_{cgp} =concrete stress at cg of A_{ps} at transfer = 19.9 MPa

Δf_{cdp} = change in concrete stress at cg of A_{ps} due to permanent loads except the load acting when F_i is applied, that is subtract M_{dg}

$$\Delta f_{cdp} = \frac{(2900 - 1328) * 10^6 (489)}{126011 * 10^6} - \frac{(540 + 353) * 10^6 (977 - 119)}{283.7 * 10^9} = -8.8\ MPa$$

Thus,

$$\Delta f_{pCR} = 12.0(19.9) - 7.0\Delta(8.8) = 177.2\ MPa$$

C.3.4.4.4.4 Relaxation, $\boldsymbol{\Delta f_{pR}}$ [A5.9.5.4.4]

$$\Delta f_{pR} = \Delta f_{pR1} + \Delta f_{pR2}$$

Δf_{pR1} = relaxation loss at transfer = 11.57 MPa

$$\Delta f_{pR2} = 0.3[138 * 0.4\Delta f_{pES} - 0.2(\Delta f_{pSR} + \Delta f_{pCR})]$$

$$\Delta f_{pR2} = 0.3[138 * 0.4(129.1) - 0.2(44.9 + 177.2)]$$

$$\Delta f_{pR2} = 12.6\ MPa$$

Thus, $\Delta f_{pR} = 11.57 + 12.6 = 24.17\ MPa$

C.3.4.4.4.5 Total losses

$$\Delta f_{pT} = (initial\ losses) + (long - term\ losses)$$

$$= (\Delta f_{pES} + \Delta f_{pR1}) + (\Delta f_{pSR} + \Delta f_{pCR} + \Delta f_{pR2}) = (129.1 + 11.57) + (44.9 + 177.2 + 12.6)$$

$$\Delta f_{pT} = 375.4\ MPa$$

C.3.4.4.5 Calculate girder stresses at transfer

$F_i = 6346\ kN$

$e_{CL} = 489\ mm$, $e_{CL} = 489\ mm$

- At midspan

$f_{ti} = -\frac{F_i}{A_g} + \frac{F_i e_{CL}}{S_{tg}} - \frac{M_{dg}}{S_{tg}}$

$= -\frac{6.346*10^6}{486051} + \frac{(6.346*10^6)(489)}{169.8*10^6} - \frac{1328*10^6}{169.8*10^6}$

$= -2.5\ MPa < 1.38\ MPa$ OK

$f_{bi} = -\frac{F_i}{A_g} - \frac{F_i e_{CL}}{S_{tg}} + \frac{M_{dg}}{S_{tg}}$

$= -\frac{6.346*10^6}{486051} - \frac{(6.346*10^6)(489)}{207.3*10^6} + \frac{1328*10^6}{207.3*10^6}$

$= -21.6\ MPa < -24\ MPa$ OK

- At end section (support)

$f_{ti} = -\frac{F_i}{A_g} + \frac{F_i e_{CL}}{S_{tg}}$

$= -\frac{6.346*10^6}{486051} + \frac{(6.346*10^6)(489)}{169.8*10^6}$

$= -3.4\ MPa < 1.38\ MPa$ OK

$f_{bi} = -\frac{F_i}{A_g} - \frac{F_i e_{CL}}{S_{tg}}$

$= -\frac{6.346*10^6}{486051} - \frac{(6.346*10^6)(489)}{207.3*10^6}$

$= -21.0\ MPa < -24\ MPa$ OK

C.3.4.4.6 Calculate girder stresses at service (after total losses)

$$f_{pf} = 0.74 f_{pu} - \Delta f_{pT} = 1376.4 - 375.4 = 1001.0\ MPa$$

$$F_f = \frac{(5133)(1001)}{10^3}$$

At mid span:

$$f_{ti} = -\frac{F_i}{A_g} + \frac{F_i e_{CL}}{S_{tg}} - \frac{M_{dg}+M_{ds}}{S_{tg}} - \frac{M_{da}+M_L}{S_{ic}}$$

$$= -\frac{5.14*10^6}{486051} + \frac{(5.14*10^6)(489)}{169.8*10^6} - \frac{(1328+1572)*10^6}{169.8*10^6} - \frac{(893+2941)*10^6}{760.6*10^6},$$ Service I

$= -17.9\ MPa < 0.45 f'_c = 24.75\ MPa,$ OK

$$f_{bi} = -\frac{F_i}{A_g} + \frac{F_i e_{CL}}{S_{tg}} - \frac{M_{dg}+M_{ds}}{S_{tg}} - \frac{M_{da}+M_L}{S_{ic}}$$

$$= -\frac{5.14*10^6}{486051} - \frac{(5.14*10^6)(489)}{207.3*10^6} + \frac{(1328+1572)*10^6}{207.3*10^6} + \frac{(893+2941)*10^6}{290.4*10^6},$$ Service I

$= 2.44\ MPa < 0.45 f'_c = 3.71\ MPa,$ OK

Hence, 52-12.70mm low-relaxation strands satisfy Service Limit State.

C.3.4.4.7 Fatigue Limit State [A5.5.3]

a) Live load moment due to fatigue truck (FTr) at mid span (Figure C.14).

$$R_a = 145\left(\frac{6.25+15.24}{30.48}\right) + 35\left(\frac{19.54}{30.48}\right)$$

$$= 124.6\ kN$$

$$M_{FTr} = [(124.6)(15.24) - (35)(4.3)]$$

$$= 1748.4\ kNm$$

Exterior girder DF: remove 1.2 multiple presence for fatigue

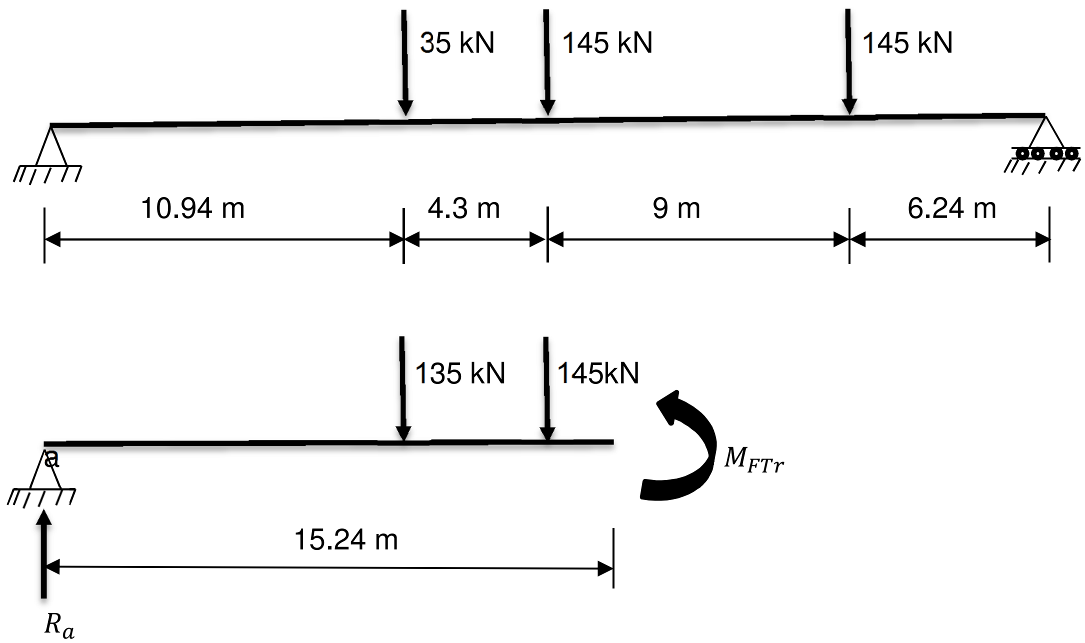

Figure C.14: Position of Fatigue truck for maximum positive moment at midspan.

DFM-fatigue $= \frac{0.762}{1.2} = 0.635$

$M_{fatigue} = 0.75(0.635)(1748.4)(1.15) = 957.6\ kN\ m$

b) Dead load moments at midspan

Exterior girder (Table C.2)

Noncomposite $M_{DC1} = 2900\ kN\ m$

Composite $M_{DC2} + M_{DW} = 540 + 353 = 2893\ kN\ m$

According to AASHTO LRFD [A5.5.3.1], fatigue does not need to be investigated if section is in compression under DL and two times fatigue load.

$$f_b = -\frac{F_f}{A_g} - \frac{F_t e_{CL}}{S_{bg}} + \frac{M_{DC1}}{S_{bg}} + \frac{M_{DC2}+M_{DW}+2M_{fatigue}}{S_{bc}}$$

$$= -\frac{5.14*10^6}{486051} - \frac{(5.14*10^6)(489)}{207.3*10^6} + \frac{2900*10^6}{207.3*10^6} + \frac{[893+2(957.6]*10^6}{290.4*10^6}$$

$= 0.94\ MPa$, (tension)

Hence, fatigue needs to be considered.

Stress range = $957.6\ kN\ m$

According to AASHTO LRFD [A5.5.3.1], cracked section properties will be used if $1.5M_{fatigue}$ and tensile stress exceeds $0.25\sqrt{f'_c}$

$$= 0.25\sqrt{55} = 1.85\ MPa$$

$$f_b = -\frac{5.14 * 10^6}{486051} - \frac{(5.14 * 10^6)(489)}{207.3 * 10^6} + \frac{2900 * 10^6}{207.3 * 10^6} + \frac{[893 + 1.5(975.6)] * 10^6}{290.4 * 10^6}$$

$= -0.71\ MPa < 1.85\ MPa$; thus:

Gross section properties will be used.

Concrete stress at cg of prestress tendons due to fatigue load

$$f_{cgp} = \frac{M_{fatigue}(977-119)}{283.7*10^9} = \frac{957.6*1^6}{330.7*10^6} = 2.9\ MPa$$

Now, calculate the stress in tension due to fatigue load (FL)

$$f_{pFL} = f_{cgp}\frac{E_p}{E_c} = (2.9)\frac{197000}{35600} = 16.0\ MPa$$

$$Stress\ range \le \begin{cases} 125\ MPa & for\ radii\ of\ curvature\ greater\ than\ 9000\ mm \\ 70\ MPa & for\ radii\ of\ curvature\ less\ than\ 3600\ mm \end{cases}$$ [A5.5.3.3]

The harped tendons are illustrated in Figure C.15

$e_{end} = 258\ mm$

$e_{CL} = 489\ mm$

$f_{pFL} = 16.0\ MPa < 70\ MPa$ OK.

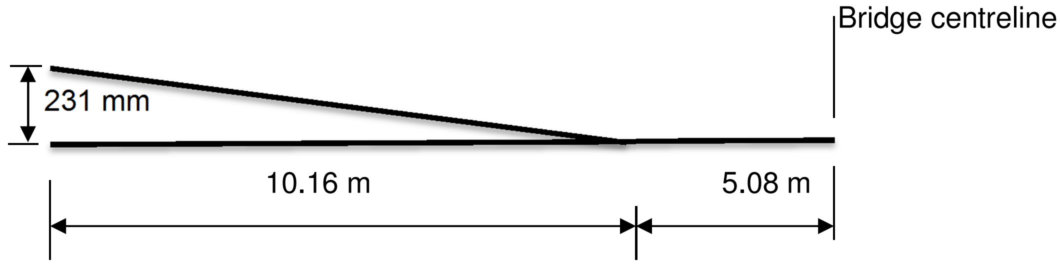

Figure C.15: Pattern of harped tendons.

C.3.4.4.8 Deflection and camber

C.3.4.4.8.1 Immediate deflection due to live load and impact

$$\Delta(x < a)x = \frac{Pbx}{6EIL}(L^2 - b^2x^2),\ b = L - a$$

$$\Delta x\left(x = \frac{L}{2}\right) = \frac{PL^3}{48EI}$$

$$E_c = 35600\ MPa,\ I_c = 283.7 * 10^2 mm^4$$

$$E_cI_c = 10.1 * 10^{15}\ N\ mm^2 = 10.1 * 10^6\ kN\ m^2$$

$$P = 35\ kN,\quad x = 15.240\ m,\quad a = 19.54\ m,\ \ b = 10.94\ m$$

$$\Delta_x^{35} = \frac{(35)(10.94)(15.24)}{6(EI)(30.48)}(30.480^2 - 10.940^2 - 15.240^2)$$

$$= \frac{18.4*10^3}{EI} = \frac{18.4*10^3}{10.1*10^6} = 0.002\ m = 2\ mm$$

$$P = 145\ kN,\quad x = \ a = 15.24\ m$$

$$\Delta_x^{145} = \frac{(145)(30.48)^3}{48(EI)}$$

$$= \frac{85.5*10^3}{EI} = \frac{85.5*10^3}{10.1*10^6} = 0.008\ m = 8\ mm$$

$$P = 145kN,\quad x = 15.240\ m,\quad a = 19.54\ m,\ \ b = 10.94\ m$$

$\Delta_x^{35} = \frac{(145)(10.94)(15.24)}{6(EI)(30.48)}(30.480^2 - 10.940^2 - 15.240^2)$

$= \frac{76.3*10^3}{EI} = \frac{76.3*10^3}{10.1*10^6} = 0.008\ m = 8\ mm$

Total deflection:-

$\Delta_{105}^{Tr} = \frac{(18.4+85.5+76.3)*10^3}{EI} = \frac{180.2*10^3}{10.1*10^6}$

$= 0.018\ m = 18\ mm$

b) Long-term deflection (Collins and Mitchell 1991)

- Due to self weight of girder at transfer

  $E_{ci} = 30\ 360\ MPa, \quad I_g = 126\ 011 * 10^6 mm^2, \quad E_{ci}I_g = 3.83 * 10^6\ kN\ m^2$

  $\Delta_{gi} = \frac{5}{384}\frac{wL^4}{EI} = \frac{5}{384}\frac{(11.44)(30.480)^4}{3.83*10^6}$

  $= 0.034\ m = 34\ mm \downarrow$

- Due to prestress at transfer for double harping point (Collins and Mitchell 1991)

  $\beta L = 0.333L$

  $\Delta_{pi} = [\frac{e_c}{8} - \frac{\beta^2}{6}(e_c - e_e)]\frac{F_i L^2}{EI}$

  $\Delta_{pi} = [\frac{489}{8} - \frac{(0.333)^2}{6}(489 - 258)]\frac{(6346)(30.480)^2}{3.83*10^6}$

  $= 88\ mm \uparrow$

  Net upward deflection (at transfer) = $88 - 34 = 54\ mm \uparrow$

- Due to deck and diaphragm on exterior girder:

  $DC1 - w_g = 24.13 - 11.44 = 12.69\ N/mm = 12.69\ kN/m$

  From diaphragm = $9.705\ kN$

  $\Delta_{DC} = \frac{5}{384}\frac{wL^4}{EI} + \frac{Pb}{24EI}(3L^2 - 4b^2)$

$$= \frac{5}{384}\frac{(12.69)(30.480)^4}{4.49*10^6} + \frac{(9.705)(10.160)}{24(4.49*10^6)}[3(30.480)^2 - 4(10.160)^2]$$

$$= 0.032 + 0.002 = 0.034\ m = 34\ mm \downarrow$$

- Due to asphalt and barrier

  $$DW + Barrier = 3.04 + 4.65 = 7.69\frac{N}{mm} = 7.69\ kN/m$$

  $$\Delta_c = \frac{5}{384}\frac{wL^4}{EI} = \frac{5}{384}\frac{(7.69)(30.84)^4}{10.1*10^6} = 0.009\ m = 9mm \downarrow$$

C.3.4.4.8.2 Long-term deflection

Table C.3, which is taken from PCI (1992), provides multipliers to approximate the creep effect. Net upward deflection:

$$\Delta_1 = 1.80(88) - 1.85(34) = 96\ mm \uparrow$$

The net long-term upward deflection is:

$$\Delta_{LT} = 2.20(88) - 2.40(34) - 2.30(34) - 3.00(9)$$

$$= 7\ mm \uparrow$$

It can be seen that, when the construction is completed, the deflection of the centre of the bridge will change. It is estimated to deflect downward from an initial upward deflection of 96 mm to a final upward value of 7 mm.

C.3.4.4.9 Check Strength Limit State

C.3.4.4.9.1 Flexure

- Stress in prestressing steel bonded tendons [A5.7.3.1.1]

  $$f_{ps} = f_{pu}(1 - k\frac{c}{d_p})$$

  $$k = 2\left(1.04 - \frac{f_{py}}{f_{pu}}\right) = 2\left(1.04 - \frac{1674}{1860}\right)$$

  $$= 0.28$$

Table C.3: suggested multipliers to be used as a guide in estimating Long-term cambers and deflections for typical members (PCI 1992)

Phase	Type	Without Composite Topping	With Composite Topping
At erection	Deflection (downward) component- apply to the elastic deflection due to the member weight at release of prestress	1.85	1.85
	Camber (upward) component- apply to the elastic camber due to prestress at the time of release of prestress	1.80	1.80
Final	Deflection (downward) component- apply to the elastic deflection due to the member weight at release of prestress	2.70	2.40
	Camber (upward) component- apply to the elastic camber due to prestress at the time of release of prestress	2.45	2.20
Prestress	Deflection (downward) – apply to elastic deflection due to superimpose dead load only	3.00	3.00
	Deflection (download) – apply to elastic deflection caused by the composite topping		2.30

Transformed section is used:

$b = 1635.4\,mm, \qquad d_p = (1350 + 50 + 190) - 119 = 1471\,mm$

$f'_c = 55\,MPa, \quad A_s = A'_s = 0$

$\beta_1 = 0.85 - \frac{55-28}{7}(0.05) = 0.657$

$c = \frac{A_{ps}f_{pu} + A_s f_y + A'_s f'_y - 0.85\beta_1 f'_c (b - b_w) h_f}{0.85 f'_c \beta_1 b_w + k A_{ps}(f_{pu}/d_p)}$

$= \frac{(5133)(1860) - 0.85(0.657)(55)(1635.4-150)(190)}{0.85(55)(0.657)(150) + 0.28(5133)(1860/1471)}$

$= 136.8\,mm$

$f_{ps} = 1860\left[1 - 0.28\left(\frac{136.8}{1471}\right)\right] = 1812\,MPa$

$T_p = A_{ps}f_{ps} = \frac{(5133)(1812)}{10^3} = 9300\,kN$

- Factored flexural resistance – Flanged section [A5.7.3.2.2]

$a = \beta_1\,c = (0.657)(136.8mm) = 89.9\,mm$

$\emptyset = 1.00$

$\emptyset M_n = \emptyset[A_{ps}f_{ps}\left(d_p - \frac{a}{2}\right) + A_s f_y\left(d_s - \frac{a}{2}\right) - A'_s f'_y\left(d'_s - \frac{a}{2}\right) + 0.85\beta_1 f'_c (b - b_w) h_f\left(\frac{a}{2} - \frac{h_f}{2}\right)]$

$$= 1.0[(5133)(1812)\left(1471 - \frac{89.9}{2}\right) + 0.85(0.657)(55)(1635.4 - 150)(190)\left(\frac{89.9}{2} - \frac{190}{2}\right)]$$

$\emptyset M_n = 12.8 * 10^9\,N\,mm = 12\,800\,kN\,m$

$M_u = 9477\,kN\,m < 12\,800\,kN\,m$ OK

C.3.4.4.9.2 Limits for reinforcement [A5.7.3.3]

- Limit of maximum reinforcement

$\frac{c}{d_p} \leq 0.42$ for $d_e = d_p$

$\frac{c}{d_p} = \frac{136.8}{1471} = 0.093 \ < 0.42$ OK

- Limit for minimum reinforcement

$$\emptyset M_n \geq \begin{cases} 1.2M_{cr} \ based \ on \ elastic \ stress \ distribution \ and \ modulus \ of \ rupture \\ 1.33M_u \ \ Strength \ I \ Limit \ State \end{cases}$$

$$M_{cr} = S_c\left(f_r + f_{cpe}\right) - M_{dnc}\left(\frac{S_c}{S_{nc}} - 1\right) \ \geq \ S_c f_r$$

$$f_r = 0.37\sqrt{f'_c} = 0.37\sqrt{55} = 2.744 \ MPa$$

$$M_{cr} = (2900 + 893 + 2353 + 648) = 6794 \ kN \ m$$

$$1.2M_{cr} = 1.2(6794) = 8\ 153 \ kN \ m$$

$$1.33M_u = 1.33(9477) = 12\ 604$$

$\emptyset M_n = 12\ 800 \ kN \ m \ > 1.2M_{cr}$ OK, also:

$\emptyset M_n = 12\ 800 \ kN \ m \ > 1.33M_u$ OK

C.3.4.4.9.3 Check shear [A5.8]

- General:

$\Phi_v = 0.9$ [A5.5.4.2.1]

$\eta = 0.95$

$V_n = V_c + V_s + V_p \leq 0.25f'_c b_v d_v$ [A5.8.3.3]

$d_e = 1471\ mm$

At centre of the girder

$$d_v = d_e - \frac{a}{2} \geq max\begin{cases}0.9d_e = 0.9(1471) = 1324mm,\ governs\\ 0.72h = 0.72(1590) = 1145\ mm\end{cases}$$ [A5.8.2.7]

$d_v = 1471 - \frac{89.9}{2} = 1426\ mm > 1324mm,$ OK

At the end of the girder

$d_e = 1590 - 350 = 1240\ mm$

$$d_v = max\begin{cases}0.9d_e = 0.9(1240) = 1116mm\\ 0.72h = 0.72(1590) = 1145\ mm,\ governs\end{cases}$$ [A5.8.2.7]

b_v = minimum web width within $d_v = 150mm$

- Contribution of prestressing strands to shear resistance:

$V_p = vertical\ component\ of\ prestressing\ force$

Transfer length = 60 strand diameters [A5.8.2.3]

= 60(12.70) = 762 mm

Critical section for shear ≥ $0.5d_v cot\theta\quad or\ \ d_v = 1145mm$ [A5.8.3.2]

$d_v >$ transfer length, hence, full value of V_p can be used.

cg of harped strands $(12) = 1350 - 175 = 1175\ mm$ from bottom of girder

$= 1175 - 119 = 1056mm\ fron\ cg\ A_{ps}$ at centreline (Figure C.16)

$\gamma = tan^{-1}\frac{1056}{10\ 160} = 5.934^o$

$F_f = 5140\ kN$

$V_p = \frac{12}{52}F_f sin\gamma = \frac{12}{52}(5140)sin5.934 = 122.6\ kN$

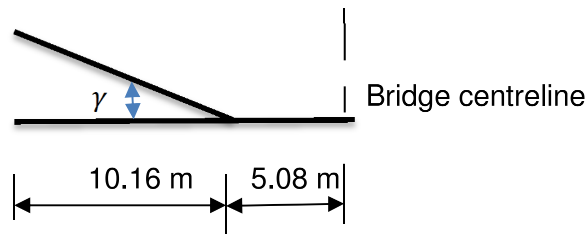

Figure C.16: Harped tendon profile

- Check shear design at distance at a distance of d_v from the support and at tenth point along the span.

Below are the calculations with respect to a distance d_v from support (Figure C.17). The results of the remaining points are shown in Table C.4.

$$d_v = 1145\, mm, \quad \xi = \frac{d_v}{L} = \frac{1145}{30\,480} = 0.0376$$

$$w = unit\ load = 1.0\,\frac{N}{mm} = 1.0\ kN/m$$

$$V_x = wL(0.5 - \xi) = w(30.480)(0.5 - 0.00376) = 14.094\, w\ \ kN$$

$$M_x = 0.5wL^2(\xi - \xi^2) = 0.5w(30.48)^2(0.0376 - 0.0376^2)$$

$$= 16.8w\ kN\ m$$

$$DC_1 = 24.13\ N/mm$$

$$DC_2 = 4.65\ N/mm$$

$$DW = 3.04\ N/mm$$

$$Ddiaph. = 9.705\ N/mm$$

$$IM = 0.33\ \%$$

$$V_{support}^{Tr} = [145\left(\frac{25.035+29.335}{30.480}\right) + 35\left(\frac{20.735}{30.48}\right)] = 282.5\ kN$$

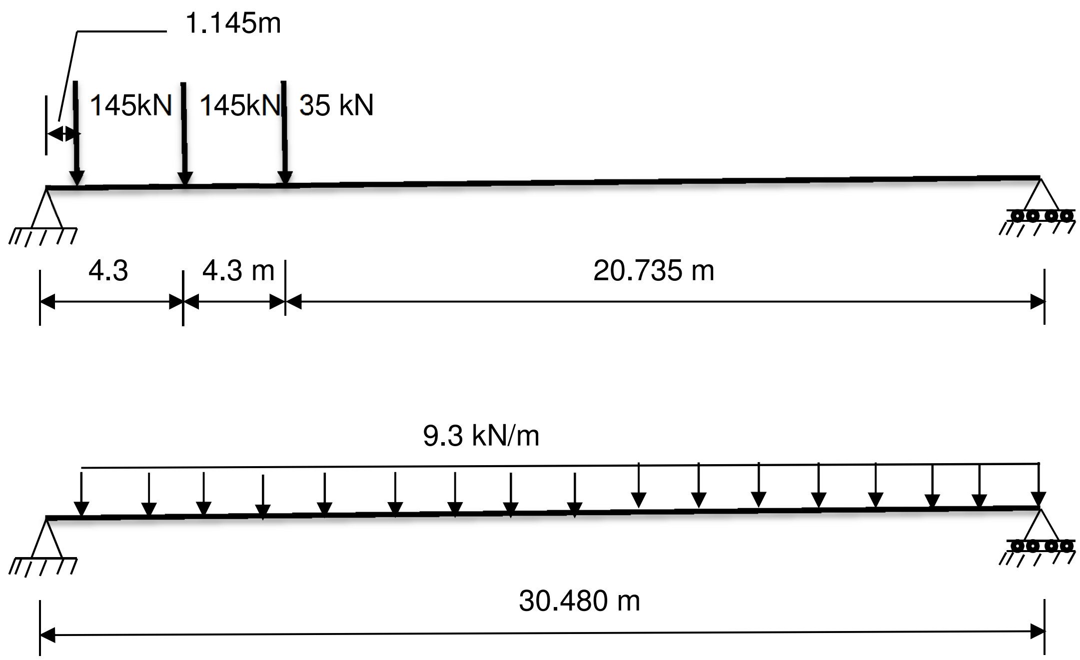

Figure C.17: Live load placement for maximum shear

$$M_{support}^{Tr} = 1.145(282.5) = 323.5\ kN\ m$$

$$V_{support}^{Ln} = \frac{1}{2}(9.3)(\frac{29.335}{30.480})^2 = 131.3\ kN$$

$$M_{support}^{Ln} = \frac{1}{2}(1.145)(29.335)(9.3) = 156.2\ kN\ m$$

$$V_u = 0.95\{1.25[(24.13 + 4.65)(14.09) + 9.705] + 1.50[(3.04)(14.094) + 1.75(0.762)[(282.5)(1.33) + 131.3]\}$$

$$= 1197\ kN$$

$$M_u = 0.95\{[1.25[(24.13 + 4.65)(16.8) + 9.705(1.145)] + 1.50[(3.04)(16.8)] + 1.75(0.762)[(323.5)(1.33) + 131.3]\}$$

$$= 1403\ kN\ m$$

$$v = \frac{V_u - \emptyset V_p}{\emptyset b_v d_v}$$

$$= \frac{(1.197*10^6) - 0.9(122.6*10^3)}{0.9(150)(1145)}$$

$$= 7.02\ MPa$$

$$\frac{v}{f'_c} = \frac{7.02}{55} = 0.128\ > 0.100$$

$$S_{max} = min \begin{cases} 0.4d_v = 0.4(1145) = 458\ mm \\ \quad 300\ mm, governs \end{cases}$$ [A5.8.2.7]

$$d_e = d_v = 1590 - 350 + \frac{1145}{10\ 160}(489 - 258) = 1266mm$$

- $1st\ Iteration$:

Let $= 30^o$, $f_{p0} \approx f_{se} = 1001\ MPa$

$$d_e = 1266\ mm$$

$$d_v = max \begin{cases} d_e - \frac{a}{2} = 122 - \frac{89.9}{2} = 1221\ mm, governs \\ 0.9d_e = 0.9(1266) = 1139\ mm \\ 0.72h = 0.72(1590) = 1145\ mm \end{cases}$$

So, $d_v = 1221\ mm$

$$\varepsilon_x = \frac{\left(\frac{M_u}{d_v}\right) + 0.5N_u + 0.5V_u cot\theta - A_{ps} f_{po}}{E_s A_s + E_p A_{ps}}$$ [A5.8.34.2]

$$= \frac{\left(1.402*\frac{10^9}{1221}\right) + 0.5(1.197*10^6)cot30 - (5133)(1001)}{(197000)(5133)}$$

$= -2.9 * 10^{-3}$ (compression)

As the strain ε_x is negative, it shall be reduced by F_ε [A5.8.3.4.2]

$$F_\varepsilon = \frac{E_s A_s + E_p A_{ps}}{E_c A_c + E_s A_s + E_p A_{ps}} = \frac{E_p A_{ps}}{E_c A_c + E_p A_{ps}}$$

where,

A_c is the area of concrete on flexural tension side of member defined as concrete below $h/2$ of member. [Fig. A5.8.3.4.2-3]

$h = 1350 + 50 + 190 = 1590\ mm$

$\frac{h}{2} = 795\ mm$

$A_c \cong (135)(975) + 2\left(\frac{1}{2}\right)(140)(412.5) + (600)(150)$

$\approx 288\ 375\ mm^2\ \ F_\varepsilon = \frac{(197000)(5133)}{(35600)(288375)+(197000)(5133)} = 0.0897$

$\varepsilon_x = (-0.0029)(0.0897) = -0.26 * 10^{-3}$

Having $\frac{v}{f'_c} = 0.128,\quad \theta = 20^0$

$cot\theta = 2.747, \beta = 2.75$

- 2nd Iteration

$\theta = 20^o$

$M_{DC1} = (24.13)(16.8 * 10^6) + (9705)(1221)$

$= 416.4 * 10^6\ N\ mm$

$e = d_p - (y_{tg} + t_s + 50)$

$= 1221 - (742 + 190 + 50) = 239\ mm$

$f_{ps} = -\frac{F_f}{A_g} + \frac{F_f\ e(y_{bc}-y_{bg})}{I_g} - \frac{M_{DC1}(y_{bc}-y_{bg})}{I_g}$

$= -\frac{5.14*10^6}{486051} + \frac{(5.14*10^6)(239)(977-608)}{126011} - \frac{(416.4*10^6)(977-608)}{126011*10^6}$

$= -8.20\ MPa$

$f_{po} = f_{se} + f_{pc}\frac{E_p}{E_c} = 1001 + 8.2\frac{197000}{35600} = 1046.5\ MPa$

$$\varepsilon_x = \frac{\frac{1.402*10^9}{1221}+0.5\left(1.196*10^6\right)(2.747)-(5133)(1046.5)}{(197000)(5133)}$$

$$= -0.0026$$

$$F_\varepsilon \varepsilon_x = 0.0897(-0.0026) = -0.23 * 10^{-3}$$

$$V_c = 0.083\beta\sqrt{f'_c}b_v d_v$$

$$= 0.083(2.75)\sqrt{55}(150)(1221) = 310 * 10^3\ N$$

$$V_s = \frac{V_u}{\emptyset} - V_c = \frac{1.196*10^6}{0.9} - 310 * 10^3 = 1.019 * 10^6\ N$$

Use stirrups with diameter = $16\ mm\ \ A_v = 2(200\ mm^2) = 400\ mm^2$,

Spacing of stirrups:

$$s \le \frac{A_v f_y d_v cot\theta}{V_s} = \frac{(400)(400)(1221)(2.747)}{1.019*10^6}$$

$$s = 526\ mm\ >\ s_{max} = 300mm$$

Check longitudinal reinforcement [A5.8.3.5]

$$A_s f_y \ge [\frac{M_y}{d_v \emptyset_f} + 0.5\frac{N_u}{\emptyset_a} + \left(\frac{V_u}{\emptyset_v} - 0.5V_s - V_p\right)cot\theta]$$

$$V_s = 1.019 * 10^6\ \left[\frac{526}{300}\right] = 1.787 * 10^6\ N$$

$$(5133)(1812) \ge \frac{1.402*10^9}{(1221)(1.0)} + \left[\frac{1.196*10^6}{0.9} - 0.5(1.1787 * 10^6) - 122.6 * 10^6\right]2.747$$

$9.301 * 10^6\ N\ > 2.007 * 10^6\ N$ OK

$$Use\ s = s_{max} = 300\ mm$$

- Summary of shear design:

Table C.4 summarizes the results of the shear design.

Table C.4: Summary of shear design

Parameter	Location					
	100.38	101	102	103	104	105
$V_u\ (kN)$	1196	1068	865	666	459	268
$M_u\ (kN\ m)$	1.4	3481	6162	8036	9159	9470
$V_p\ (kN)$	122.6	122.6	122.6	122.6	0	0
$d_p\ (mm)$	1221	1204	1334	1403	1426	1426
v/f'_c	0.128	0.102	0.0762	0.0533	0.043	0.0253
$f_{po}\ (MPa)$	1047	1049	1056	1060	1064	1066
$\varepsilon_x * 10^3$	-0.23	-0.124	0.0469	0.781	1.236	1.320
$\theta, degree$	20	23.5	27	34	38.5	39
β	2.75	5	4.4	2.3	2.1	2.1
$V_c\ (kN)$	310	584	296	246	230	230
$Req'd.V_s$	1019	603	420	442	224	209
$s\ (mm)$	526	771	999	752	1281	13482
$A_{ps}f_{ps}\ (*\ 10^6)$	2.007	3.419	5.580	6.233	6.764	6.719
$prov'd\ s\ (mm)$	300	300	600	600	600	600

C.3.4.4.9.4 Horizontal shear [A5.8.4]

$$V_{nh} = cA_{cv} + \mu\left(A_{vf}f_y + P_c\right) \leq \begin{cases} 0.25f'_cA_{cv} \\ 5.5A_{cv} \end{cases}$$ [A5.8.4]

where,

$A_{cv} =$ area of concrete engaged in shear transfer $= 1225\ mm^2$

A_{vf} = area of shear reinforcement crossing the shear plane = $2(200) = 400mm^2$

f_y = yield strength of reinforcement = $400\ Mpa$

$\begin{cases} c = cohesion\ factor = 0.7 \\ \mu = friction\ factor = 1.0 \end{cases}$ (intentionally roughened) [A5.8.4.2]

$P_c = permanent\ net\ comprehenssive\ force\ normal\ to\ shear\ plane = overhang + slab + haunch + barrier$

$= [5.37 + 5.83 + 0.61 + 4.65] = 16.46\ N/mm$

$V_{nh} = 0.70(1225) + 1.0[\left(\frac{400}{s}\right)(400) + 16.46]$

$= 873.96 + \frac{160000}{s}\ N/mm$

$V_{nh} \leq\ min \begin{cases} 0.2f'_c A_{cv} = 0.2(40)(1225) = 9800\ N/mm \\ 5.5A_{cv} = 5.5(1225) = 6740 \frac{N}{mm}, governs \end{cases}$

$\emptyset_v V_{nh} \geq\ \eta V_{uh}$

where,

V_{uh} = horizontal shear due to barrier, *FWS*, and *LL+IM*

$= \frac{V_u Q}{I_c}$

$I_c = 283.7 * 10^9 mm^2$

$Q = A\bar{y} = (1635.4)(190)(1590 - 977 - \frac{190}{2})$

$= 160.96 * 10^6 mm^3$

Strength I load combination:

$V_u = 1.25\ DC2 + 1.5\ DW + 1.75(LL + IM)$

$V_u = 1.25(71) + 1.5(46) + 1.75(407) = 870\ kN$

$\frac{\eta V_{uh}}{\emptyset_v} = \frac{0.95(493.4)}{0.9} = 520.8\frac{N}{mm} < 6740\ N/mm$

Thus,

$873.96 + \frac{160000}{s} \geq 520.8$

$s \leq \frac{160000}{873.96-520.8}\ 453\ mm$

$Use \quad s_{max} = 300\ mm$

C.3.4.4.9.5 Check details

- Anchorage zone [A5.10.10]

Let P_r = Factored resistance provided by transverse reinforcement

$P_r = \emptyset_{ca} f_y A_s \ \geq 4\%\ Factored\ prestressing\ force\ (F_{ui})$ [A3.4.3]

$\emptyset_{ca} f_y A_s \geq 0.04F_{ui} = 0.04(8.24 * 10^6) = 329.6 * 10^3\ N$

$A_s \geq \frac{329.6*10^3}{0.8(400)} = 1030\ mm^2$

Within $\frac{d}{4} = \frac{1350}{2} = 337.5\ mm$

Use U-stirrups with diameter 16mm: $\frac{1030}{400} = 2.6$

Use 3 No. dia. 16mm stirrups at 130 mm.

- Confinement reinforcement: [A5.10.10.2]

For a distance of $1.5d = 1.5(1350) = 2025\ mm$ from the end of the beam, reinforcement shall be placed to confine the prestressing steel in the bottom flange.

Use $14\ No.\ dia.\ 10mm\ at\ 150\ mm\ shaped\ to\ enclose\ the\ strands.$

C.3.4.4.9.5 Design sketch

Figure C.18 visualizes the design results.

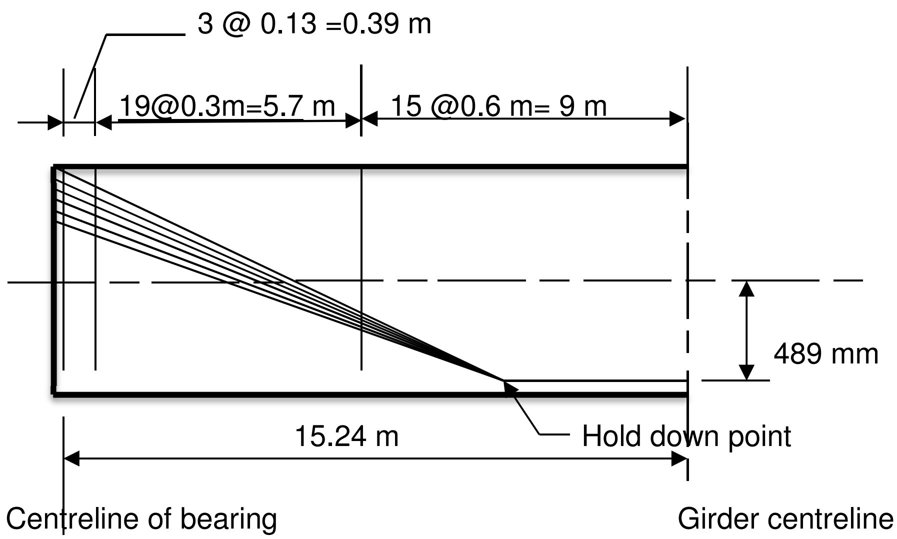

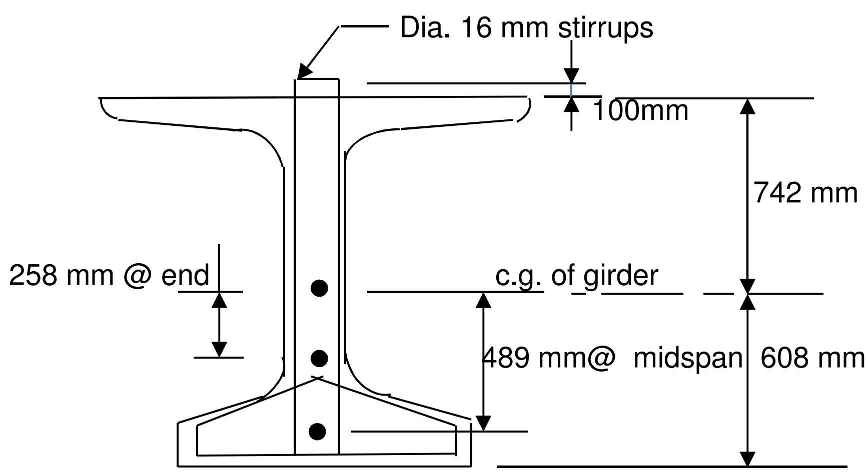

Figure C.18: Design sketch for prestressed girder.

Appendix D

Sample of BREL Macro for Component Reliability

In this Appidex, the codes of two algorithms are presented. The first code is for the reliability analysis to obtain the individual component's failure probabilityis and corresponding reliability indices. The second code is for 2-d grillage analysis reuired to obtain the system reliability.

```
Sub Clear()


  Sheets("Control").Range("S7").ClearContents
  Sheets("Control").Range("S8").ClearContents
  Sheets("Control").Range("F21").ClearContents
  Sheets("Control").Range("F22").ClearContents
  Sheets("Control").Range("D4:F21").ClearContents
  Sheets("Control").Range("K6:N9").ClearContents
  Sheets("Control").Range("I12:Z29").ClearContents
End Sub
Sub Compute()
Dim timestarted As Double
timestarted = Time
Dim t As Single
t = Timer
'code
linestatus = 10
    Sheets("Control").Range("S7").Value = "Running ..."
    '----------------------------------------------------------
    'Variable Declaration
    nv = 300
    it = 100
```

```
ic = 300
  lineout = 21
colout = 6
colver = 8
Dim grdnt()  As Double, varmn()  As Double, stdevval() As Double, alphx() As Double, X() As Double, z() As Double, xinit() As Double, cor() As Double
Dim beta() As Double, evarmn() As Double, sigma() As Double, Function() As Double, rind() As Double
Dim beta1() As Double, pl2l() As Double, pl2u() As Double, wk1() As Double, wk2() As Double, bf() As Double
Dim keyval() As Integer, kj(20) As Integer
ReDim grdnt(nv, ic)
ReDim varmn(nv, ic)
ReDim stdevval(nv, ic)
ReDim alphx(nv, ic)
ReDim X(nv, ic)
ReDim z(nv, ic)
ReDim xinit(nv, ic)
ReDim cor(ic, ic)
ReDim beta(it, ic)
ReDim evarmn(nv, ic)
ReDim sigma(nv, ic)
ReDim Function(ic)
ReDim rind(ic, 1)
ReDim beta1(it, ic)
ReDim pl2l(ic, ic)
ReDim pl2u(ic, ic)
ReDim keyval(nv, ic)
Dim i As Integer, ii As Integer, Lst As Integer, nran As Integer, im As Integer
Dim p  As Double, q As Double, a As Double, c As Double, d As Double
Dim b As Double, h  As Double, e  As Double, f As Double, eps As Double
Dim pcu As Double, pcl As Double, pdu As Double, pdl As Double
Dim sumx#, sumgr#
```

```
    '---------------------------------------------------------
colver = colver + 1

colver = colver + 1
        If Sign < 0# Then
          beta(iter, Lst) = -beta(iter, Lst)
        End If
colver = colver + 1
        'c  convergence criteria
        'c
        '
        If iter > 1 Then
          conv = Abs(beta(iter, Lst) - beta(iter - 1, Lst))

          If conv < eps Then
            beta1(itb, Lst) = beta(iter, Lst)
              Exit Do
          End If
        End If
      Loop

      If iter = it Then
        Sheets("Control").Cells(linestatus, 6).Value = "Maximum iteration reached for -iter-"
'
      End If
            For i = 1 To nran
      If keyval(i, Lst) <> 0 Then
        If itb > 1 Then
        If beta1(itb, Lst) <> 0 Then
                    conv1 = Abs(beta1(itb, Lst) - beta1(itb - 1, Lst))
          If conv1 < eps Then
```

```
End Sub

'c

'c   this program calculates equivalent mean and standard deviation for the

'c  norami distribution from the Type-I asymptotic distribution,

'c

Sub gumbel(b As Double, h As Double, a As Double, e As Double, f As Double)

    Dim alpha As Double, u As Double, pow As Double, ex1 As Double, cum As Double, dens As Double, param As
Double, phitmp As Double

    Const MAX_EXP_ARGUMENT As Double = 709.782712893

    Pi = 3.14159265

    If b = 0 Then

    e = 0

    f = 0

    Else

    alpha = Pi / (h * Sqr(6#))

    'u = b - 0.577216 / alpha

    'pow = alpha * (a - u)

    'If pow < -MAX_EXP_ARGUMENT Then

      'pow = -MAX_EXP_ARGUMENT

      'End If

         'ex1 = Exp(-pow)

    'cum = Exp(-ex1)

    'dens = alpha * Exp(-pow - Exp(-pow))

    'param = phiinv(cum)

    'phitmp = 1# / Sqr(2# * Pi) * Exp(-0.5 * param * param)

'If dens = 0 Then

'dens = 0.000000000000001

'End If

    'f = phitmp / dens

    f = Sqr(Pi * Pi * alpha / 6)

    'e = a - f * param
```

```
    e = b + 0.577216 * f
    grdnt(17, Lst) = (a * (1 - b) + c) * sigma(17, 3)
    grdnt(18, Lst) = (c * z(17, 3) / (z(16, 3) * z(18, 3))) * sigma(18, 3)
    grdnt(19, Lst) = 0#
    grdnt(20, Lst) = 0#
    grdnt(21, Lst) = 0#
    grdnt(22, Lst) = 0#
    grdnt(23, Lst) = 0#
    grdnt(24, Lst) = 0#
    grdnt(25, Lst) = 0#
    grdnt(26, Lst) = 0#

End If
'c
'c At transfer limit state for compressive stress at bottom fiber of girder at transfer length
'c
If Lst = 4 Then
            a = z(6, 4) * z(7, 4) / z(8, 4)
          b = z(9, 4) * z(8, 4) / z(10, 4)
          c = 0.00004167 * z(8, 4) * z(15, 4) * Ltr * (Lgir - Ltr) / z(10, 4)
          Load_Effect = -z(14, 4) * a * (1 + b) + z(14, 4) * c
    Function(Lst) = z(4, 4) - Abs(Load_Effect)
    grdnt(1, Lst) = 0#
    grdnt(2, Lst) = 0#
    grdnt(3, Lst) = 0#
    grdnt(4, Lst) = sigma(4, 4)
    grdnt(12, Lst) = 0#
     grdnt(6, Lst) = (a * z(14, 4) / z(6, 4) + z(7, 4) * z(9, 4) * z(14, 4) / z(10, 4)) * sigma(6, 4)
    grdnt(7, Lst) = (a * z(14, 4) / z(7, 4) + z(6, 4) * z(9, 4) * z(14, 4) / z(10, 4)) * sigma(7, 4)
      grdnt(8, Lst) = (-z(14, 4) / z(8, 4) * (a + c)) * sigma(8, 4)
    grdnt(9, Lst) = (a * z(8, 4) * z(14, 4) / z(10, 4)) * sigma(9, 4)
```

```
  grdnt(10, Lst) = (-a * z(8, 4) * z(9, 4) * z(14, 4) / z(10, 4) ^ 2 + c * z(14, 4) / z(10, 4)) * sigma(10, 4)
 grdnt(11, Lst) = 0#
 grdnt(12, Lst) = 0#
 grdnt(13, Lst) = 0#
 grdnt(14, Lst) = (a * (1 + b) - c) * sigma(14, 4)
  grdnt(15, Lst) = (-c * z(14, 4) / (z(10, 4) * z(15, 4))) * sigma(15, 4)
 grdnt(16, Lst) = 0#
 grdnt(17, Lst) = 0#
 grdnt(18, Lst) = 0#
 grdnt(19, Lst) = 0#
 grdnt(20, Lst) = 0#
 grdnt(21, Lst) = 0#
 grdnt(22, Lst) = 0#
 grdnt(23, Lst) = 0#
 grdnt(24, Lst) = 0#
 grdnt(25, Lst) = 0#
 grdnt(26, Lst) = 0#
 End If
'c
'c   At transfer limit state for tensile stress at top fiber of girder at harp-point section
'c
If Lst = 5 Then
    a = z(8, 5) * z(10, 5) / z(13, 5)
    b = z(16, 5) * z(13, 5) / z(21, 5)
    c = 0.00004167 * z(13, 5) * z(23, 5) * Lhrp * (Lgir - Lhrp) / z(21, 5)
  Load_Effect = -z(22, 5) * a * (1 - b) - z(22, 5) * c
 Function(Lst) = z(3, 5) - (Load_Effect)
 grdnt(1, Lst) = 0#
 grdnt(2, Lst) = 0#
 grdnt(3, Lst) = sigma(3, 5)
 grdnt(4, Lst) = 0#
```

```
    grdnt(5, Lst) = 0#
    grdnt(6, Lst) = 0#
    grdnt(7, Lst) = 0#
    grdnt(8, Lst) = (a * z(22, 5) / z(8, 5) - z(10, 5) * z(16, 5) * z(22, 5) / z(21, 5)) * sigma(8, 5)
    grdnt(9, Lst) = 0#
    grdnt(10, Lst) = (a * z(22, 5) / z(10, 5) - z(8, 5) * z(16, 5) * z(22, 5) / z(21, 5)) * sigma(10, 5)
    grdnt(11, Lst) = 0#
    grdnt(12, Lst) = 0#
    grdnt(13, Lst) = (z(22, 5) / z(13, 5) * (a + c)) * sigma(13, 5)
    grdnt(14, Lst) = 0#
    grdnt(15, Lst) = 0#
  grdnt(16, Lst) = (-a * z(13, 5) * z(22, 5) / z(21, 5)) * sigma(16, 5)
    grdnt(17, Lst) = 0#
    grdnt(18, Lst) = 0#
    grdnt(19, Lst) = 0#
    grdnt(20, Lst) = 0#
      grdnt(21, Lst) = (a * z(22, 5) * z(13, 5) * z(16, 5) / z(21, 5) ^ 2 - c * z(22, 5) / z(21, 5)) * sigma(21, 5)
    grdnt(22, Lst) = (a * (1 - b) + c) * sigma(22, 5)
       grdnt(23, Lst) = (c * z(22, 5) / (z(21, 5) * z(23, 5))) * sigma(23, 5)
    grdnt(24, Lst) = 0#
    grdnt(25, Lst) = 0#
    grdnt(26, Lst) = 0#
End If
'c
'c   At transfer limit state for compressive stress at bottom fiber of girder at harp-point section
'c
If Lst = 6 Then
               a = z(9, 6) * z(11, 6) / z(14, 6)
           b = z(18, 6) * z(14, 6) / z(22, 6)
           c = 0.00004167 * z(14, 6) * z(24, 6) * Lhrp * (Lgir - Lhrp) / z(22, 6)
           Load_Effect = -z(23, 6) * a * (1 + b) + z(23, 6) * c
```

```
    Function(Lst) = z(6, 6) - Abs(Load_Effect)
    grdnt(1, Lst) = 0#
    grdnt(2, Lst) = 0#
    grdnt(3, Lst) = 0#
    grdnt(4, Lst) = 0#
    grdnt(5, Lst) = 0#
    grdnt(6, Lst) = sigma(6, 6)
    grdnt(7, Lst) = 0#
    grdnt(8, Lst) = 0#
      grdnt(9, Lst) = (a * z(23, 6) / z(9, 6) + z(11, 6) * z(18, 6) * z(23, 6) / z(22, 6)) * sigma(9, 6)
    grdnt(10, Lst) = 0#
      grdnt(11, Lst) = (a * z(23, 6) / z(11, 6) + z(9, 6) * z(18, 6) * z(23, 6) / z(22, 6)) * sigma(11, 6)
    grdnt(12, Lst) = 0#
    grdnt(13, Lst) = 0#
    grdnt(14, Lst) = (-z(23, 6) / z(14, 6) * (a + c)) * sigma(14, 6)
    grdnt(15, Lst) = 0#
    grdnt(16, Lst) = 0#
    grdnt(17, Lst) = 0#
     grdnt(18, Lst) = (a * z(14, 6) * z(23, 6) / z(22, 6)) * sigma(18, 6)
    grdnt(19, Lst) = 0#
    grdnt(20, Lst) = 0#
    grdnt(21, Lst) = 0#
    grdnt(22, Lst) = (-a * z(14, 6) * z(18, 6) * z(23, 6) / z(22, 6) ^ 2 + c * z(23, 6) / z(22, 6)) * sigma(22, 6)
    grdnt(23, Lst) = (a * (1 + b) - c) * sigma(23, 6)
      grdnt(24, Lst) = (-c * z(23, 6) / (z(22, 6) * z(24, 6))) * sigma(24, 6)
    grdnt(25, Lst) = 0#
    grdnt(26, Lst) = 0#
End If
'c
'c  At transfer limit state for tensile stress at top fiber of girder at mid span
'c
```

```
If Lst = 7 Then
        a = z(8, 7) * z(10, 7) / z(12, 7)
      b = z(15, 7) * z(12, 7) / z(18, 7)
      c = 0.000010417 * z(12, 7) * z(20, 7) * Lgir ^ 2 / z(18, 7)
      Load_Effect = -z(19, 7) * a * (1 - b) - z(19, 7) * c
 Function(Lst) = z(4, 7) - (Load_Effect)
   grdnt(1, Lst) = 0#
  grdnt(2, Lst) = 0#
  grdnt(3, Lst) = 0#
      grdnt(4, Lst) = sigma(4, 7)
    grdnt(5, Lst) = 0#
  grdnt(6, Lst) = 0#
  grdnt(7, Lst) = 0#
  grdnt(8, Lst) = (a * z(19, 7) / z(8, 7) - z(10, 7) * z(15, 7) * z(19, 7) / z(18, 7)) * sigma(8, 7)
  grdnt(9, Lst) = 0#
  grdnt(10, Lst) = (a * z(19, 7) / z(10, 7) - z(8, 7) * z(15, 7) * z(19, 7) / z(18, 7)) * sigma(10, 7)
  grdnt(11, Lst) = 0#
   grdnt(12, Lst) = (-z(19, 7) / z(12, 7) * (a - c)) * sigma(12, 7)
  grdnt(13, Lst) = 0#
  grdnt(14, Lst) = 0#
   grdnt(15, Lst) = (-a * z(12, 7) * z(19, 7) / z(18, 7)) * sigma(15, 7)
  grdnt(16, Lst) = 0#
  grdnt(17, Lst) = 0#
   grdnt(18, Lst) = (a * z(12, 7) * z(15, 7) * z(19, 7) / z(18, 7) ^ 2 - c * z(19, 7) / z(18, 7)) * sigma(18, 7)
   grdnt(19, Lst) = (a * (1 - b) + c) * sigma(19, 7)
  grdnt(20, Lst) = (c * z(19, 7) / (z(18, 7) * z(20, 7))) * sigma(20, 7)
  grdnt(21, Lst) = 0#
  grdnt(22, Lst) = 0#
  grdnt(23, Lst) = 0#
  grdnt(24, Lst) = 0#
  grdnt(25, Lst) = 0#
```

```
   grdnt(26, Lst) = 0#

End If

'c

'c   At transfer limit state for compressive stress at bottom fiber of girder at mid span

'c

If Lst = 8 Then

       Let a = z(6, 8) * z(9, 8) / z(11, 8)

          b = z(15, 8) * z(11, 8) / z(17, 8)

         c = 0.000010417 * z(11, 8) * z(20, 8) * Lgir ^ 2 / z(17, 8)

  Load_Effect = -z(19, 8) * a * (1 + b) + z(19, 8) * c

   Function(Lst) = z(2, 8) - Abs(Load_Effect)

   grdnt(1, Lst) = 0#

   grdnt(2, Lst) = sigma(2, 8)

   grdnt(3, Lst) = 0#

   grdnt(4, Lst) = 0#

   grdnt(5, Lst) = 0#

      grdnt(6, Lst) = (a * z(19, 8) / z(6, 8) + z(9, 8) * z(15, 8) * z(19, 8) / z(17, 8)) * sigma(6, 8)

   grdnt(7, Lst) = 0#

   grdnt(8, Lst) = 0#

     grdnt(9, Lst) = (a * z(19, 8) / z(9, 8) + z(6, 8) * z(15, 8) * z(19, 8) / z(17, 8)) * sigma(9, 8)

   grdnt(10, Lst) = 0#

     grdnt(11, Lst) = (-z(19, 8) / z(11, 8) * (a + c)) * sigma(11, 8)

   grdnt(12, Lst) = 0#

   grdnt(13, Lst) = 0#

   grdnt(14, Lst) = 0#

     grdnt(15, Lst) = (a * z(11, 8) * z(19, 8) / z(17, 8)) * sigma(15, 8)

   grdnt(15, Lst) = 0#

   grdnt(16, Lst) = 0#

   grdnt(17, Lst) = (m * z(14, 12) / z(17, 12)) * sigma(17, 12)

   grdnt(18, Lst) = 0#

      grdnt(19, Lst) = (m * z(14, 12) / z(19, 12)) * sigma(19, 12)
```

```
   grdnt(20, Lst) = 0#

   grdnt(21, Lst) = 0#

     grdnt(22, Lst) = (n * z(14, 12) / z(22, 12)) * sigma(22, 12)

     grdnt(23, Lst) = (n * z(14, 12) / z(23, 12)) * sigma(23, 12)

   grdnt(24, Lst) = 0#

     grdnt(25, Lst) = (-z(14, 12) * (m + n) / z(25, 12)) * sigma(25, 12)

   grdnt(26, Lst) = 0#

   End If

     'c

'c   Limit state for top of deck slab under permanent and transient loads, Service I

'c

If Lst = 13 Then

         m = 0.003 / Ng * z(11, 13) * z(13, 13) * Leff_FT ^ 2 / (z(25, 13) * n_c)

         n = 0.0015 * z(16, 25) * z(17, 13) * Leff_FT ^ 2 / (z(25, 13) * n_c)

         p = 12 * z(20, 13) * z(21, 13) / z(25, 13) / n_c

         q = 12 * z(22, 13) * z(21, 13) * (1 + z(24, 13)) / (z(25, 13) * n_c)

         Load_Effect = -z(8, 13) * (m + n + p + q)

    Function(Lst) = z(4, 13) - Abs(Load_Effect)

   grdnt(1, Lst) = 0#

   grdnt(2, Lst) = 0#

   grdnt(3, Lst) = 0#

   grdnt(4, Lst) = sigma(4, 13)

   grdnt(5, Lst) = 0#

   grdnt(6, Lst) = 0#

   grdnt(7, Lst) = 0#

   grdnt(8, Lst) = (m + n + p + q) * sigma(8, 13)

   grdnt(9, Lst) = 0#

   grdnt(10, Lst) = 0#

     grdnt(11, Lst) = (m * z(8, 13) / z(11, 13)) * sigma(11, 13)

   grdnt(12, Lst) = 0#

     grdnt(13, Lst) = (m * z(8, 13) / z(13, 13)) * sigma(13, 13)
```

```
    grdnt(14, Lst) = 0#
    grdnt(15, Lst) = 0#
      grdnt(16, Lst) = (n * z(8, 13) / z(16, 13)) * sigma(16, 13)
      grdnt(17, Lst) = (n * z(8, 13) / z(17, 13)) * sigma(17, 13)
    grdnt(18, Lst) = 0#
    grdnt(19, Lst) = 0#
       grdnt(20, Lst) = (p * z(8, 13) / z(20, 13)) * sigma(20, 13)
       grdnt(21, Lst) = ((p + q) * z(8, 13) / z(21, 13)) * sigma(21, 13)
       grdnt(22, Lst) = (q * z(8, 13) / z(22, 13)) * sigma(22, 13)
    grdnt(23, Lst) = 0#
       grdnt(24, Lst) = (q * z(8, 13) / (1 + z(24, 13))) * sigma(24, 13)
        grdnt(25, Lst) = (-z(8, 13) * (m + n + p + q) / z(25, 13)) * sigma(25, 13)
    grdnt(26, Lst) = 0#
    End If
Next i
For j1 = 1 To im1
    For i = 1 To im1
        If i = j1 Then
            cor(i, i) = 1#
        Else
            cor(i, j1) = cor(j1, i)
        End If
     Next i
For i = 1 To im1
Sheets("Control").Cells(11 + j1, i + 8).Value = cor(j1, i)
Next i
Next j1
End Sub
Function GetMeanValueFromMCS(limitstaterequired As Integer) As Double
Dim myrange As Range
Dim r As Range
```

```
Dim limitstates As Integer

Set myrange = Sheets("MCS").Range("b3").CurrentRegion

Set myrange = myrange.Offset(1).Resize(, 1)

For Each r In myrange

If IsNumeric(r.Value) = True And IsEmpty(r.Value) = False Then

limitstates = r.Value

If limitstaterequired = limitstates Then

GetMeanValueFromMCS = r.Offset(2, 4)

Exit Function

End If

End If

Next r

End Function

Function GetstandarddeviationFromMCS(limitstaterequired As Integer) As Variant

Dim myrange As Range

Dim r As Range

Dim limitstates As Integer

Set myrange = Sheets("MCS").Range("b3").CurrentRegion

Set myrange = myrange.Offset(1).Resize(, 1)

For Each r In myrange

If IsNumeric(r.Value) = True And IsEmpty(r.Value) = False Then

limitstates = r.Value

If limitstaterequired = limitstates Then

GetstandarddeviationFromMCS = r.Offset(3, 4)

End If

End If

Next r

End Function

Function getmeFunction(inputvalue, Function9, Function10, Function11, Function12, Function13, Function16, Function17,
Function18, Function14) As Double

If inputvalue = 9 Then
```

```
getmeFunction = Function9


End If

If inputvalue = 10 Then

getmeFunction = Function10

End If

If inputvalue = 11 Then

getmeFunction = Function11

End If

If inputvalue = 12 Then

getmeFunction = Function12

End If

If inputvalue = 13 Then

getmeFunction = Function13

End If

If inputvalue = 16 Then

getmeFunction = Function16

End If

If inputvalue = 17 Then

getmeFunction = Function17

End If

If inputvalue = 18 Then

getmeFunction = Function18

End If

If inputvalue = 14 Then

getmeFunction = Function14

End If

End Function

Function SystemREL(Function9 As Double, Function10 As Double, Function11 As Double, Function12 As Double,
Function13 As Double, Function16 As Double, Function18 As Double, Function14 As Double, Function17 As Double, pf9
As Double, pf10, pf11, pf12, pf13, pf16, pf18, pf14, pf17)

Dim var1(5, 1) As Variant
```

```
Dim var2() As Variant

Dim var3() As Variant

Dim var4() As Variant

Dim var5() As Variant

Dim myrange As Range

Dim mystandarddeviation As String

ProbabilityOfFailure.Range("B2").Value = pf9

ProbabilityOfFailure.Range("c2").Value = pf10

ProbabilityOfFailure.Range("d2").Value = pf11

ProbabilityOfFailure.Range("b3").Value = pf12

ProbabilityOfFailure.Range("c3").Value = pf13

ProbabilityOfFailure.Range("b4").Value = pf16

ProbabilityOfFailure.Range("c4").Value = pf18

ProbabilityOfFailure.Range("b5").Value = pf14

ProbabilityOfFailure.Range("b6").Value = pf17

ProbabilityOfFailure.Range("e2").Value = pf11

ProbabilityOfFailure.Range("k2").Value = getmeFunction(ProbabilityOfFailure.Range("h2").Value, Function9, Function10,
Function11, Function12, Function13, Function16, Function17, Function18, Function14)

ProbabilityOfFailure.Range("k3").Value = getmeFunction(ProbabilityOfFailure.Range("h3").Value, Function9, Function10,
Function11, Function12, Function13, Function16, Function17, Function18, Function14)

ProbabilityOfFailure.Range("k4").Value = getmeFunction(ProbabilityOfFailure.Range("h4").Value, Function9, Function10,
Function11, Function12, Function13, Function16, Function17, Function18, Function14)

ProbabilityOfFailure.Range("k5").Value = getmeFunction(ProbabilityOfFailure.Range("h5").Value, Function9, Function10,
Function11, Function12, Function13, Function16, Function17, Function18, Function14)

ProbabilityOfFailure.Range("k6").Value = getmeFunction(ProbabilityOfFailure.Range("h6").Value, Function9, Function10,
Function11, Function12, Function13, Function16, Function17, Function18, Function14)

Set myrange = ProbabilityOfFailure.Range("a1").CurrentRegion

myrange.Copy myrange.Offset(7)

SortProbabilityOfFailure

GetMeanandStandardDeviation

 mystandarddeviation = GetstandarddeviationFromMCS(9)

End Function

Function GetFunction(limitstaterequired As Integer) As Variant
```

```
Dim myrange As Range

Dim r As Range

Dim limitstates As Integer

Set myrange = Sheets("MCS").Range("b3").CurrentRegion

Set myrange = myrange.Offset(1).Resize(, 1)

For Each r In myrange

If IsNumeric(r.Value) = True And IsEmpty(r.Value) = False Then

limitstates = r.Value

If limitstaterequired = limitstates Then

GetFunction = r.Offset(2, 2).Value

Exit Function

End If

End If

Next r

End Function

    'f = phitmp / dens

    f = Sqr(Pi * Pi * alpha / 6)

    'e = a - f * param

    e = b + 0.577216 * f

    grdnt(17, Lst) = (a * (1 - b) + c) * sigma(17, 3)

    grdnt(18, Lst) = (c * z(17, 3) / (z(16, 3) * z(18, 3))) * sigma(18, 3)

    grdnt(19, Lst) = 0#

    grdnt(20, Lst) = 0#

    grdnt(21, Lst) = 0#

    grdnt(22, Lst) = 0#

    grdnt(23, Lst) = 0#

    grdnt(24, Lst) = 0#

    grdnt(25, Lst) = 0#

    grdnt(26, Lst) = 0#


End If
```

```
            For i = 1 To nran
        If keyval(i, Lst) <> 0 Then
          If itb > 1 Then
          If beta1(itb, Lst) <> 0 Then
                  conv1 = Abs(beta1(itb, Lst) - beta1(itb - 1, Lst))
            If conv1 < eps Then
End Sub
```

Appendix E

Sample of GRANAL Macro for System Reliability

```
Sub Clear()
    Application.Calculation = xlManual
    Application.ScreenUpdating = False
Sheets("Verif").UsedRange.Delete
Sheets("Output").UsedRange.Delete
Sheets("Input").UsedRange.Delete
Sheets("Main").Range("A1:K10").ClearContents
Sheets("Main").Range("F1:K150").ClearContents
    Application.ScreenUpdating = True
End Sub
Private Sub UserForm_Initialize()
Dim i%
Set rngList = wsLoadComb.Range("LoadList")
Set rngNLC = wsLoadComb.Range("NLC")
Set rngLCTitle = wsInput.Range("LCtitle")
Set rngCombs = wsLoadComb.Range("LoadCombs")
DoEvents
NLC = wsLoadComb.Range("NLC")
Ncomb = wsLoadComb.Range("Ncomb")
'ListBox1.RowSource = "LoadComb!" & rngList.Address
For i = 1 To NLC
    ListBox1.AddItem rngList(i)
Next i
tbCurrentLoad.ControlSource = "Input!" & rngLCTitle.Address
'tbCurrentLoad.Value = rngLCTitle.Value
' initialize combinations
```

```
For i = 1 To Ncomb

   ListBox2.AddItem rngCombs(i)

   ListBox3.AddItem rngCombs(i)

Next i

End Sub

Sub TestCase()

Call Clear

testin = Sheets("Main").Cells(18, 4).Value

testout = Sheets("Main").Cells(18, 5).Value

Sheets(testin).Cells.Copy Destination:=Sheets("Input").Cells

'Sheets(testin).Range("A1:ZZ10000").Copy Sheets("Input").Range("A1:ZZ10000")

rivate Sub UserForm_Initialize()


Dim i%


wsSetup.Range("AnalysisOption") = 5

MultiPage1.Pages("PageProgress").Visible = False

Set rngList = wsTruckList.Range("TruckList")

Set rngNtrucks = wsTruckList.Range("Ntrucks")

Set rngTruckTitle = wsTrucks.Range("Trucktitle")


Ntrucks = rngNtrucks.Value


ListBox3.RowSource = "trucklist!" & rngList.Address

ListBox3.ListIndex = 0

ListBox3.Selected(0) = True

TextBoxStep.Value = wsSetup.Range("TruckStep")

CheckBox1.Value = wsSetup.Range("isBackward")


Label5.Caption = "Travel step (" & wsSetup.Range("units_length") & ") :"

TextBoxNLanes.Value = wsSetup.Range("NLanes")
```

```
Label7.Caption = wsSetup.Range("units_length")


TextBox2.Value = wsSetup.Range("TruckStep")


TextBox3.Value = wsStdTruckDB.Range("HL93_truck_impact").Value

TextBox4.Value = wsStdTruckDB.Range("HL93_lane_impact").Value

TextBox5.Value = wsSetup.Range("Nlanes").Value

Private Sub UserForm_Initialize()

With wsSetup

    LabelV.Caption = .Range("PrecisionV")

    LabelM.Caption = .Range("PrecisionM")

    LabelD.Caption = .Range("PrecisionD")

    LabelR.Caption = .Range("PrecisionR")


    ScrollBarV.Value = .Range("PrecisionV")

    ScrollBarM.Value = .Range("PrecisionM")

    ScrollBarD.Value = .Range("PrecisionD")

    ScrollBarR.Value = .Range("PrecisionR")

End With


End Sub

Call GRANAL

Private Sub SaveLoadIntoDB()

   Dim N%, LCTitle$, a, i%

   'On Error Resume Next

         LCTitle = Trim(Range("LCTitle"))

      If LCTitle = "" Then

      LCTitle = Trim(InputBox("Enter load title", "Save load", "New load"))

      Range("LCTitle") = LCTitle

   End If

      If LCTitle = "" Then
```

```
    MsgBox "Without load title data cannot be saved." & vbCr & "Please try again."
    Exit Sub
  End If
      If WorksheetFunction.CountIf(Range("LoadList"), LCTitle) > 0 Then
      a = MsgBox("Load < " & LCTitle & " > already exists. " & vbCr & _
      "Do you want to overwrite it?", vbOKCancel)
       If a = vbCancel Then Exit Sub
    Else
      ' new load
      If Range("NLC") >= 20 Then
        ' protectme
        Application.ScreenUpdating = True
        MsgBox "Maximum number of stored loadings (20)" & vbCr & " has been reached."
        Exit Sub
      End If
          End If
Function SaveTruck(truckTitle) As Boolean
' function saves current truck and returns
' TRUE if Truck is new and FALSE if existing
Dim n_new%, n_old%, n_start%, i%, vt
Dim rngDB As Range, rngAxle1 As Range
Set rngDB = Range("TruckDB")
Set rngAxle1 = Range("TruckAxle1Weight")
' verify input and calculate rows
  i = 1
  Do Until Not WorksheetFunction.IsNumber(rngAxle1.Cells(i, 1))
    i = i + 1
  Loop
  n_new = i - 1
If n_new = 0 Then
  MsgBox "Enter the weight of first axle"
  rngAxle1.Select
  End
```

```
End If
SetTruckDB truckTitle, n_old, n_start
' adjuct number of entries in the database
Select Case n_new - n_old
   Case Is > 0
      For i = 1 To n_new - n_old
         rngDB(n_start + 1).EntireRow.Insert
      Next i
   Case Is < 0
      For i = 1 To n_old - n_new
         rngDB(n_start).EntireRow.Delete
      Next i
End Select
With rngDB(n_start)
   For i = 1 To n_new
      .Cells(i, 1).Value = Range("TruckTitle")
      .Cells(i, 2).Value = rngAxle1(i, 1)
      .Cells(i, 3).Value = rngAxle1(i, 2)
   Next i
   .Cells(1, 4).Value = Range("Naxles")
   .Cells(1, 5).Value = Range("truckComm")
   .Cells(1, 6).Value = Range("truckUnits")
   .Cells(1, 7).Value = Range("truckNeglectAxles")
   .Cells(1, 8).Value = Range("truckVarSpa")
   .Cells(1, 9).Value = Range("truckMaxSpa")
   .Cells(1, 10).Value = Range("truckKT")
   .Cells(1, 11).Value = Range("TruckLaneW")
   .Cells(1, 12).Value = Range("truckKL")
   .Cells(1, 13).Value = Range("truckExcludeLane")
   .Cells(1, 14).Value = IIf(Range("truckExcludeLane") = 1, "", Range("TruckToLaneDist"))
   End With
' update load list
With WorksheetFunction
```

```
   If .CountIf(Range("truckList"), truckTitle) = 0 Then
      'new truck
      'Range("TruckList1")(Range("NTrucks") + 1) = TruckTitle
      vt = Range("TruckList")
      Range("TruckList").Offset(1).Value = vt
      Range("TruckList1") = truckTitle
      SaveTruck = True
   End If
End With
End Function
Sub SetTruckDB(TruckName, Nrows_exist%, Nstart%)
Dim rngDB As Range
Set rngDB = Range("TruckDB")
If WorksheetFunction.CountA(rngDB) = 0 Then
   Nrows_exist = 0
   Nstart = 1
   Exit Sub
End If
With WorksheetFunction
   Nrows_exist = .CountIf(rngDB, TruckName)
   If Nrows_exist > 0 Then
      Nstart = .Match(TruckName, rngDB, 0)
   Else
      Nstart = rngDB.Rows.count + 1
   End If
End With
End Sub
Sub RestoreTruck(TruckName)
Dim rngFrom As Range, rngTo As Range, N%
  N = WorksheetFunction.CountIf(Range("TruckDB"), TruckName)
   If N > 0 Then
      Set rngFrom = Range("TruckDB1").Offset(WorksheetFunction.Match(TruckName, Range("TruckDB"), 0), 1).Resize(N, 2)
      Range("TruckAxle1weight").Resize(1000, 2).ClearContents
```

```
        Set rngTo = Range("TruckAxle1weight").Resize(N, 2)
        rngTo = rngFrom.Value
            Set rngFrom = rngFrom.Offset(0, 3).Resize(1, 10) ' Comment
        Range("TruckTitle").Value = TruckName
        Range("truckComm").Value = rngFrom(1)
        Range("truckUnits").Value = rngFrom(2)
        Range("truckNeglectAxles").Value = rngFrom(3)
        Range("truckVarSpa").Value = rngFrom(4)
        Range("truckMaxSpa").Value = rngFrom(5)
        Range("truckKT").Value = rngFrom(6)
        Range("TruckLaneW").Value = rngFrom(7)
        Range("truckKL").Value = rngFrom(8)
        Range("truckExcludeLane").Value = rngFrom(9)
        Range("TruckToLaneDist").Value = IIf(rngFrom(9) = 1, "", rngFrom(10).Value)
    End If
End Sub
        Sub PerformPlasticAnalysis()
Dim i%, Nrows%, iStage%, Nreactions%, rngReactions As Range
        Application.ScreenUpdating = False
                Application.EnableEvents = False
Range("Envelope") = True
AnalysisOption = 6
Range("pa_stage0").Resize(Range("pa_Nstages") + 1, 6).ClearContents
EraseResultTables
'Range("pr_x1").Resize(10000, 9).ClearContents
'Range("pr_x1").Resize(10000, 9).ClearFormats
Select Case Range("pa_option")
  PerformProgressiveCollapse
 End Select
' restore initial conditions by eliminating all hinges
Range("PierX").Offset(2, 0).Value = SupportType
DeleteLoad sLC_incremental
If Range("pa_option") = 1 Then DeleteLoad sLC_initial
```

```
AnalysisOption = 6

Nrows = Range("pa_Nrows")

iStage = Range("pa_Nstages")

Nreactions = Range("Nsupports")

' Clean up the tables

'EraseResultTables

EraseEnvelopesResults

' copy latest results of stage analysis back into 'Results' page

wsResults.Range("DiagX1").Resize(Nrows, 5) = _

wsPlasticResults.Range("pr_x1").Offset((Nrows + 5) * iStage).Resize(Nrows, 5).Value

wsResults.Range("ReactX1").Resize(Nreactions, 3) = _

wsPlasticResults.Range("pr_x1").Offset((Nrows + 5) * iStage, 6).Resize(Nreactions, 3).Value

' rename the titles on envelope worksheet

Range("EnvX1").Offset(-2, 2) = "FINAL STAGE RESULTS"

Range("EnvX1").Offset(-2, 8) = "INITIAL STAGE RESULTS"

Range("EnvX1").Offset(-4, 0).Resize(2, 1).ClearContents

' formatting

InterpolateEnvelopes

With Range("EnvRX1").Resize(Nreactions, 3)

  .Borders(xlEdgeBottom).LineStyle = xlContinuous

  .Borders(xlEdgeRight).LineStyle = xlContinuous

  .Borders(xlEdgeLeft).LineStyle = xlContinuous

  .Borders(xlInsideVertical).LineStyle = xlContinuous

End With

With Range("EnvX1").Resize(Nrows, 5)

  .Borders(xlEdgeBottom).LineStyle = xlContinuous

  .Borders(xlEdgeRight).LineStyle = xlContinuous

  .Borders(xlEdgeLeft).LineStyle = xlContinuous

  .Borders(xlInsideVertical).LineStyle = xlContinuous

End With

With Range("EnvX1").Offset(0, 6).Resize(Nrows, 5)

  .Borders(xlEdgeBottom).LineStyle = xlContinuous

  .Borders(xlEdgeRight).LineStyle = xlContinuous
```

```
    .Borders(xlEdgeLeft).LineStyle = xlContinuous
    .Borders(xlInsideVertical).LineStyle = xlContinuous
End With
wsEnvelopes.PageSetup.PrintArea = "$A$1:$L$" & Nrows + 9
' copy initial conditions and last stage into 'Envelopes' page
wsEnvelopes.Range("EnvX").Offset(0, 0).Resize(Nrows, 5) = _
wsPlasticResults.Range("pr_x1").Resize(Nrows, 5).Value
wsEnvelopes.Range("EnvX").Offset(0, 6).Resize(Nrows, 5) = _
wsPlasticResults.Range("pr_x1").Offset((Nrows + 5) * iStage).Resize(Nrows, 5).Value
wsEnvelopes.Range("EnvRX1").Resize(Nreactions, 2) = _
wsPlasticResults.Range("pr_x1").Offset((Nrows + 5) * 0, 6).Resize(Nreactions, 2).Value
wsEnvelopes.Range("EnvRX1").Offset(0, 2).Resize(Nreactions, 1) = _
wsPlasticResults.Range("pr_x1").Offset((Nrows + 5) * iStage, 7).Resize(Nreactions, 1).Value
' Print reactions into chart worksheet
    Set rngReactions = Range("EnvRX1").Offset(0, 0).Resize(Nreactions, 3)
        With wsSetup.Range("chEnvRx1")
        .Resize(1000, 3).ClearContents
        For i = 1 To Range("Nsupports")
            .Cells(3 * i - 2, 1) = rngReactions(i, 1)
            .Cells(3 * i - 1, 1) = rngReactions(i, 1)
            .Cells(3 * i - 0, 1) = rngReactions(i, 1)
            .Cells(3 * i - 2, 2) = 0
            .Cells(3 * i - 1, 2) = rngReactions(i, 2)
            .Cells(3 * i - 0, 2) = 0
            .Cells(3 * i - 2, 3) = 0
            .Cells(3 * i - 1, 3) = rngReactions(i, 3)
            .Cells(3 * i - 0, 3) = 0
        Next i
    End With
Format_stages_of_pa_table_new
wsPlasticAnalysis.Activate
wsPlasticAnalysis.Spinners("Spinner 10").Max = Range("pa_Nstages").Value
Application.EnableEvents = True
```

```
Application.ScreenUpdating = True

End Sub

Sub PerformMomentRedistribution()

Dim i%, Nrows%, iRFmin%, iStage As Integer, Nreactions%

Dim ph As clsPlasticHinge

Dim RFmin As Double, RFsum As Double

Dim Vo, Mo, Displo, Rotationo

Dim reactR, reactD

Dim iRedundancy As Integer

Dim rngResults As Range

Dim rngReactions As Range

Dim sTemp As String

' read plastic analysis data

ReadMomentRedistributionInput

' add locations of plastic hinges into Span Table

wsInput.Activate

' calculate iRedundancy

AddPlasticHinges_to_SpanTable

 ' analyze inital load case and save the results

RestoreLoad sLC_initial

PerformStaticAnalysis

Nrows = UBound(X)

Nreactions = Range("Reactions").Rows.count

reactR = Range("Reactions").Value

reactD = Range("Reactions").Offset(0, 1).Value

PrintStageResults wsPlasticResults.Range("pr_x1"), "Stage 0 = " & Range("pa_lc1").Value, _

X, V, M, displ, Rotation

PrintStageReactions wsPlasticResults.Range("pr_x1").Offset(0, 6), reactR, reactD

' Report results of stage 0

With Range("pa_stage0").Resize(1, 8)

   .Cells(1).Value = 0

   .Cells(2).Value = Range("pa_lc1").Value

   .Cells(4).Value = WorksheetFunction.sum(reactR)
```

```
   .Cells(5).Value = WorksheetFunction.Max(displ)
   .Cells(6).Value = WorksheetFunction.Min(displ)
End With
i = 0
For Each ph In gPlasticHinges
   i = i + 1
   ph.FindX_icount X           ' find index of plastic hinge locations in array X
   ph.Mo = M(ph.iCount_in_X) ' Find initial moment in plastic hinges
      ' remove plastic hinge from the list if initial moment is opposite sign to
   ' moment specified to reduce
      If (ph.Mo > 0 And bMneg_reduction) Or (ph.Mo < 0 And (Not bMneg_reduction)) Then
      gPlasticHinges.Remove (i)
      i = i - 1
   Else
      ph.AssignYieldMoments
   End If
Next
If gPlasticHinges.count = 0 Then
   sTemp = IIf(bMneg_reduction, "positive", "negative")
   MsgBox "The load " & Range("pa_LC2") & " produces only " & sTemp & " bending moments in control points sections." & vbCr & _
   "Please alter control points location or switch analysis option to Reduce " & sTemp & " moments."
     wsPlasticAnalysis.Activate
   Application.EnableEvents = True
   End
   End If
Mo = M
Vo = V
Displo = displ
Rotationo = Rotation
CleanUpPublicDeclarations
'RestoreLoad sLC_incremental
Range("pa_Nrows") = Nrows
iStage = 0
```

```
'''''''''''''''' Start Loop Here ''''''''''''''''''''''''''''

Do While RedundancyIndex() >= 0 And iStage <= gPlasticHinges.count  ''' ********** MAIN LOOP *********

  iStage = iStage + 1

  PerformStaticAnalysis

  If Not bStable Then Exit Do

    RFmin = 10 ^ 9

  If iStage - 1 < gPlasticHinges.count Then

    ' add conditions: Initial moment shall not exceed capacity

          ' check rating factors only for active plastic hinges

                    ' keep track which plastic hinge reached its capacity

                              ' deactivate it

    i = 0 ' item counter in collection

    For Each ph In gPlasticHinges

      i = i + 1

      If Not ph.Activated Then ' dont calculate RF for activated plastic hinges

        ph.CalculateRF_mr M, bMneg_reduction  ' RF = (Mp-Mo)/Minc

        If ph.RF < RFmin Then

          RFmin = ph.RF

          iRFmin = i

        End If

      End If

    Next

        If Abs(RFmin - 10 ^ 9) <= 0.1 Then

                  Exit Do

    End If

        RFsum = RFsum + RFmin

      gPlasticHinges(iRFmin).MakeHinge

        Debug.Print "RFmin = " & RFmin

    Debug.Print "Plastic hinge at stage " & iStage & " is formed at X = " & _

      X(gPlasticHinges(iRFmin).iCount_in_X) & ". M = " & Mo(gPlasticHinges(iRFmin).iCount_in_X) + _

      RFmin * M(gPlasticHinges(iRFmin).iCount_in_X)

  Else ' all hinges are formed. Place reminder of the load

    RFmin = -RFsum
```

```
    Debug.Print "All plastic hinges formed. Placing last load = " & Round(RFmin, 3) & " of initial"

  End If

    ' calculate Mo+Mini*RFmin and print out

    For i = 1 To UBound(X)

      Mo(i) = M(i) * RFmin + Mo(i)

      Displo(i) = displ(i) * RFmin + Displo(i)

      Rotationo(i) = Rotation(i) * RFmin + Rotationo(i)

    Next i

    For Each ph In gPlasticHinges

      ph.Mo = Mo(ph.iCount_in_X)   ' update moment in plastic hinges

    Next

      For i = 1 To Nreactions

      reactR(i, 1) = reactR(i, 1) + RFmin * Range("Reactions")(i, 1)

      reactD(i, 1) = reactD(i, 1) + RFmin * Range("Reactions").Offset(0, 1)(i, 1)

    Next i


    '' ********** print this stage results  **************

    PrintStageResults wsPlasticResults.Range("pr_x1").Offset((Nrows + 5) * iStage), _

    "Stage " & iStage & " = " & 1 + Round(RFsum, 3) & " " & Range("pa_LC2"), _

    X, Vo, Mo, Displo, Rotationo

  PrintStageReactions wsPlasticResults.Range("pr_x1").Offset((Nrows + 5) * iStage, 6), _

    reactR, reactD

        Range("pa_NStages") = iStage

           ' Report stage resulst

Loop       '''' ********** END OF MAIN LOOP ************************************************

  '' ********** print this stage results  **************

  PrintStageResults wsPlasticResults.Range("pr_x1").Offset((Nrows + 5) * iStage), _

  "Stage " & iStage & " = " & Range("pa_lc1") & " + " & Round(RFsum, 3) & " " & Range("pa_lc1").Offset(1, 0), _

   X, Vo, Mo, Displo, Rotationo

Do While Application.WorksheetFunction.IsNumber(rng(1, 1))

bMneg_reduction = (Left(Range("pa_lc2").Offset(1), 1) = "N")

End Sub
```

Appendix F

Correlation with Copula

F.1 Background

In this appendix the mathematical formulation and physical charachteristic of Copula functions are presented.

Copula C is a multivariate distribution with uniformly distributed marginals U(0,1) on [0,1]. Every multivariate distribution *F* with marginals $F_1, F_2, \ldots, F_d$ can be written as (Jiang et al. 2014):

$$F(x_1, x_2, \ldots, x_n) = C(F(x_1), F(x_2), \ldots, F(x_n)) \quad \text{(F.1)}$$

The joint probability density function $f(x_1, x_2, \ldots, x_n)$ can be determine from:

$$f(x_1, x_2, \ldots, x_n) = \frac{\partial^n f(x_1, x_2, \ldots, x_n)}{\partial x_1 \partial x_2,,, \partial x_n} \quad \text{(F.2)}$$

$$= \frac{\partial^n C(F(x_1), F(x_2), \ldots, F(x_n))}{\partial x_1 \partial x_2,,, \partial x_n} \quad \text{(F.3)}$$

$$= c(F(x_1), F(x_2), \ldots, F(x_n)) \times \prod_{i=1}^{n} f_i(x_i) \quad \text{(F.4)}$$

where, $c(F(x_1), F(x_2), \ldots, F(x_n))$ is the density function for $C(F(x_1), F(x_2), \ldots, F(x_n))$ and $f_i(x_i)$ is the probability density function for (x_i).

Also, $F(x_1), F(x_2), \ldots, F(x_n)$ and the copula function $C(F(x_1), F(x_2), \ldots, F(x_n))$ is a joint distribution for the marginal distributions $F(x_1), F(x_2), \ldots, F(x_n)$.

For $u_i = F_i(x_i), i = 1, 2, \ldots, n$ in which $u = u_1, u_2, \ldots \ldots, u_n)^T \in [0,1]^n$.

Thus,

$$C(u_1, u_2, \ldots \ldots, u_n) = F(F_1^{-1}(u_1),\ F_2^{-1}(u_2),\ F_n^{-1}(u_n)) \quad \text{(F.5)}$$

where, F_1^{-1} is the inverse function of F_i.

Having $F(x_1), F(x_2), \ldots, F(x_n)$ as continuous one-variable distribution functions, Using Sklar's theorem and $u_i = F_i(x_i), i = 1, 2, \ldots, n$, all $u_i, i = 1, 2, \ldots, n$ follow a [0,1] uniform distribution, which is $C(u_{1\,,} u_2, \ldots, u_n)$ that follow [0,1] uniform distribution.

F.2 Properties of Copula $\boldsymbol{C(u_{1,}u_2, \dots, u_n)}$

Copula $C(u_{1,}u_2, \dots, u_n)$ has the following properties:

- Domain: $u_i \in [0,1], i = 1, 2, \dots, n$
- For any random variable, $u_i \in [0,1], i = 1, 2, \dots, n$ satisfies:

$$C\left(u_{1,}u_2, \dots, u_{i-1}, 0, u_{i+1}, \dots., u_n\right) = 0 \tag{F.6}$$

$$C(1, 1, \dots., 1, u_i, 1, \dots..1) = u_i \tag{F.7}$$

- If $u_1, u_2, \dots.., u_n$ are independent, then,

$$C\left(u_{1,}u_2, \dots, u_n\right) = \ u_{1,}u_2, \dots, u_n \tag{F.8}$$

- Lower and Upper bounds of a copula function $C\left(u_{1,}u_2, \dots, u_n\right)$ are deterministic, which are called Frechet bounds:

$$W\left(u_{1,}u_2, \dots, u_n\right) \le C\left(u_{1,}u_2, \dots, u_n\right) \le M\left(u_{1,}u_2, \dots, u_n\right) \tag{F.9}$$

$where,$

$$W\left(u_{1,}u_2, \dots, u_n\right) = \max(u_{1+}u_2 +, \dots + u_n - 1,0) \tag{F.10}$$

$$M\left(u_{1,}u_2, \dots, u_n\right) = min\left(u_{1,}u_2, \dots, u_n\right) \tag{F.11}$$

F.3 Copula types

Two main classes of copulas exist; namely: Archimedean copulas and elliptical Copulas.

F.3.1 Archimedean copulas

An important class of copulas - because of the ease with which they can be constructed and the nice properties they possess - are the Archimedean copulas, which are defined by:

$$C(u, v) = \varphi^{-1}(\varphi(u), \varphi(v)) \tag{F.12}$$

where, φ is the generator of the copula.

There are three Archimedian copulas in common use: the Clayton, Frank and Gumbel.

F.3.1.1 Clayton copula

The Clayton copula is an asymmetric Archimedean copula, exhibiting greater dependence in the negative tail than in the positive.

This copula is given by:

$$C_{\propto}\,(u, v) = \max([u^{-\propto} + v^{-} - 1]^{-\propto}, 0) \quad \text{(F.13)}$$

And its generator is:

$$\varphi_{\propto}\,(t) = \frac{1}{\propto}\,(t^{-\propto} - 1) \quad \text{(F.14)}$$

where,

$$\propto \in [-1, \infty)\backslash\{0\}$$

The relationship between Kendall's tau τ the Clayton copula parameter α is given by:

$$\propto = \frac{2\tau}{1-\tau} \quad \text{(F.15)}$$

Figure F.1 gives an example of Clayton copula correlation two variables.

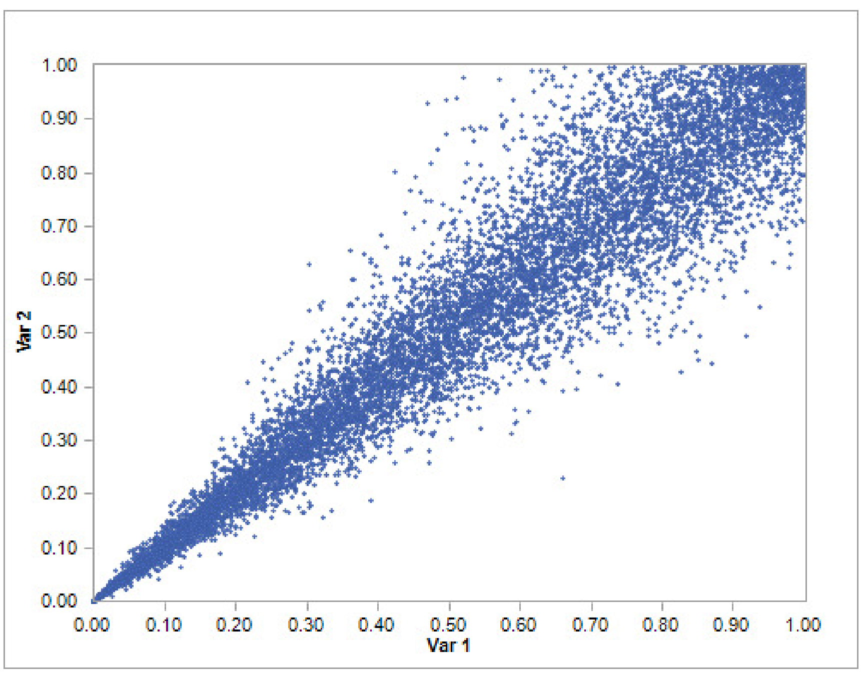

Figure F.1: Clayton copula correlation two variables.

F.3.1.2 Frank Copula

The Frank copula is a symmetric Archimedean copula given by:

$$C_{\propto}(u, v) = -\frac{1}{\propto} ln\left(1 + \frac{(e^{-\propto u}-1)(e^{-\propto v}-1)}{e^{-\propto}-1}\right) \quad \text{(F.16)}$$

And its generator is:

$$\varphi_{\propto}(t) = -ln\left(\frac{\exp(-\propto t)-1}{\exp(-\propto)-1}\right) \quad \text{(F.17)}$$

where,

$$\propto \in [-\infty, \infty)\backslash\{0\}$$

The relationship between Kendall's τ and the Frank copula parameter α is given by:

$$\frac{[D_1(\propto)-1]}{\propto} = \frac{1-\tau}{4} \quad \text{(F.18)}$$

where,

$$D_1(\propto) = \frac{1}{\propto}\int_0^{\infty} \frac{t}{e^t-1} dt \quad \text{(F.19)}$$

is a Debye function of the first kind.

Figure F.2 gives an example of Frank copula correlation two variables.

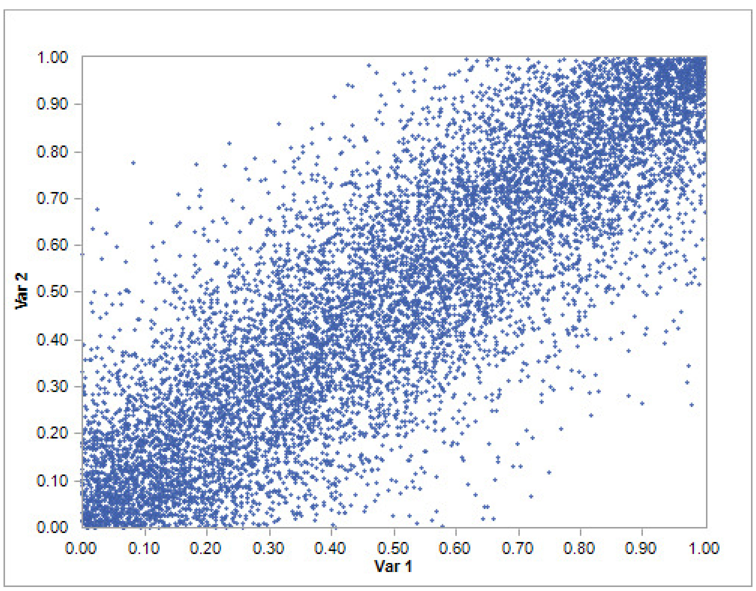

Figure F.2: Frank copula correlation two variables.

F.3.1.3 Gumbel

The Gumbel copula (a.k.a. Gumbel-Hougard copula) is an asymmetric Archimedean copula, exhibiting greater dependence in the positive tail than in the negative. This copula is given by:

$$C_{\propto}(u,v) = \exp\{-[(-\ln u\,)^{\propto} + (-\ln v\,)^{\propto}\,]^{\frac{1}{\propto}}\} \tag{F.20}$$

And its generator is:

$$\varphi_{\propto}\,(t) = -(ln\,t\,)^{\propto} \tag{F.21}$$

where,

$$\propto \in [1, \infty)$$

The relationship between Kendall's τ and the Gumbel copula parameter α is given by:

$$\propto = \frac{1}{1-\tau} \tag{F.22}$$

Figure F.3 gives an example of Gumbel copula correlation two variables.

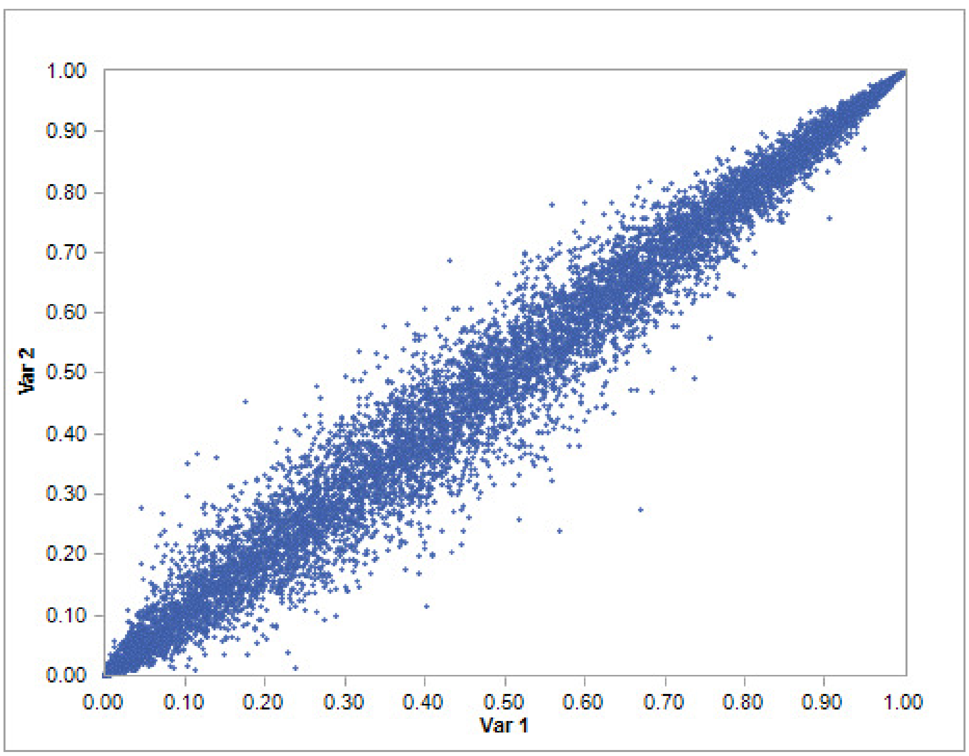

Figure F.3: Gumbel copula correlation two variables.

F.3.2 Elliptical copulas

Elliptical copulas are simply the copulas of elliptically contoured (or elliptical) distributions. The most commonly used elliptical distributions are the multivariate Normal and Student-t distributions. The key advantage of elliptical copula is that one can specify different levels of correlation between the marginals and the key disadvantages are that elliptical copulas do not have closed form expressions and are restricted to have radial symmetry (Vose 2009). For elliptical copulas the relationship between the linear correlation coefficient ρ and Kendall's tau τ is given by:

$$\rho(X,Y) = sin(\frac{\pi}{2}\tau) \qquad \text{(F.23)}$$

Two types of elliptical copulas exist; namely: The Normal and Student T copulas, which are described below.

F.3.2.1 Normal Copula

The normal copula is an elliptical copula given by:

$$C_\rho(u,v) = \int_{-\infty}^{\Phi^{-1}(u)} \int_{-\infty}^{\Phi^{-1}(v)} \frac{1}{2\pi(\rho^2)^{1/2}} \exp\{-\frac{x^2-2\rho xy+y^2}{2(1-\rho^2}\}dxdy \qquad \text{(F.24)}$$

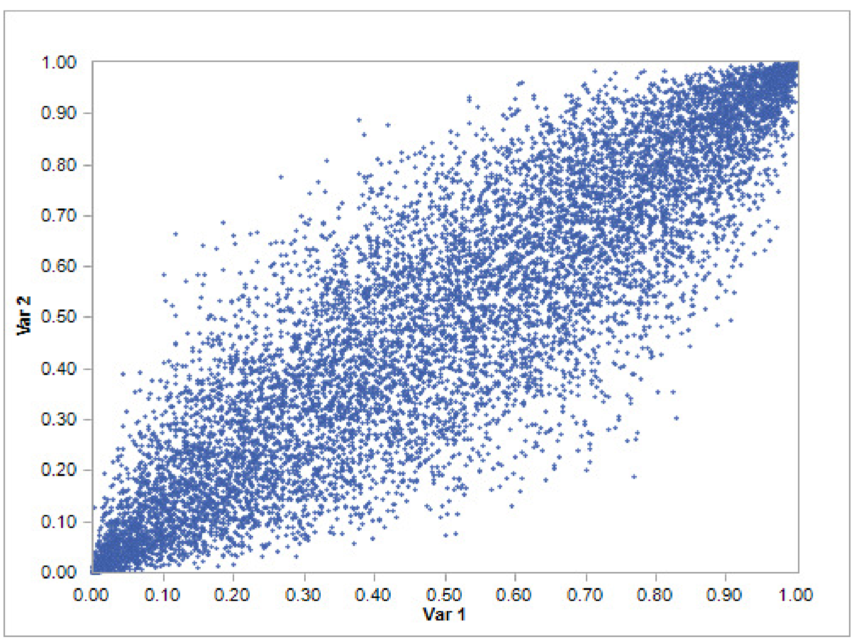

Figure F.4: Normal copula correlation two variables.

where, Φ^{-1} is the inverse of the univariate standard Normal distribution function and ρ , the linear correlation coefficient, is the copula parameter.

The relationship between Kendall's tau τ and the Normal copula parameter ρ is given by:

$$\rho(X,Y) = sin(\frac{\pi}{2}\tau) \qquad \text{(F2.5)}$$

Figure F.4 gives an example of Normal copula correlation two variables.

F.3.2.2 T copula

The Student-t copula is an elliptical copula defined as:

The normal copula is an elliptical copula given by:

$$C_\rho(u,v) = \int_{-\infty}^{\overset{-1}{t_v}(u)} \int_{-\infty}^{\overset{-1}{t_v}(v)} \frac{1}{2\pi(\rho^2)^{1/2}} \exp\{1 + \frac{x^2 - 2\rho xy + y^2}{v(1-\rho^2}\}^{-(v+2)/2} dxdy$$

where, v (the number of degrees of freedom) and ρ (linear correlation coefficient) are the parameters of the copula.

When the number of degrees of freedom n is large (around 30 or so), the copula converges to the Normal copula just as the Student distribution converges to the Normal. But for a limited number of degrees of freedom the behavior of the copulas is different: the t-copula has more points in the tails than the Gaussian one and a star like shape. A Student-t copula with n = 1 is sometimes called a Cauchy copula.

As in the normal case (and also for all other elliptical copulas), the relationship between Kendall's tau τ and the Normal copula parameter ρ is given by:

$$\rho(X,Y) = sin(\frac{\pi}{2}\tau)$$

Figure F.5 gives an example of T- copula correlation two variables.

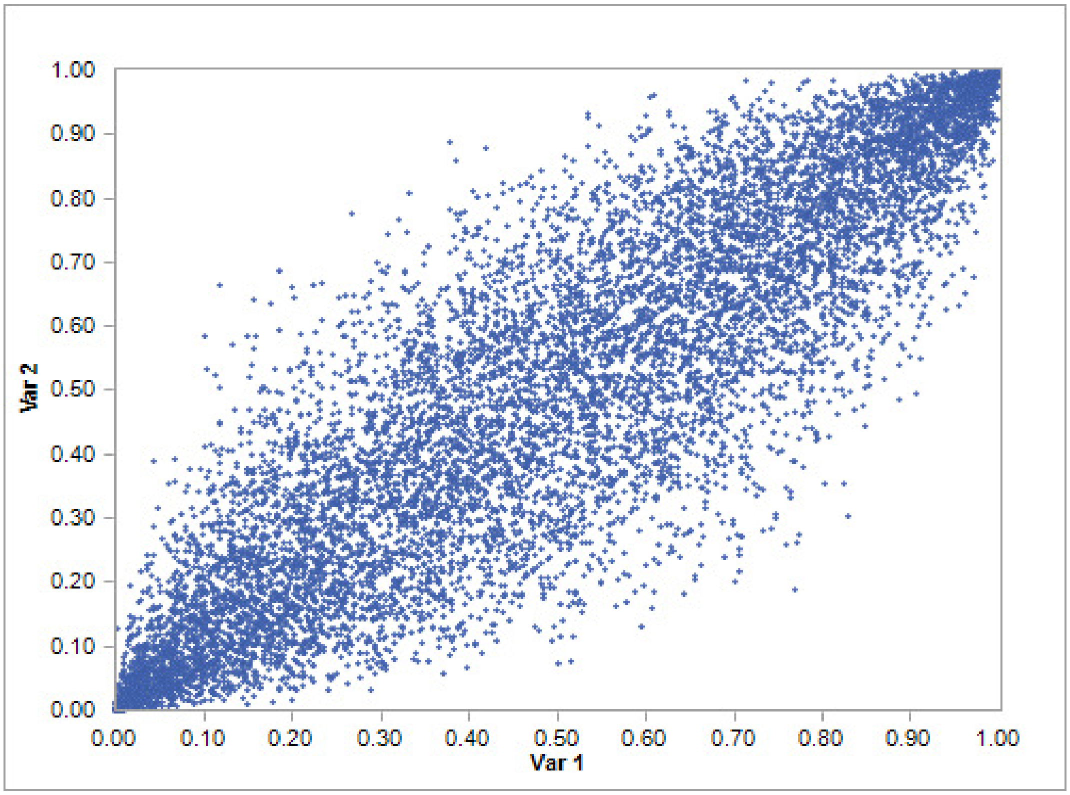

Figure F.5: T- copula correlation two variables.